UNIVERSITÉ DE GRENOBLE

THÈSE

Pour obtenir le grade de

DOCTEUR DE L'UNIVERSITÉ DE GRENOBLE

Spécialité : **Chimie Inorganique et Bio-inorganique**

Arrêté ministériel : 7 août 2006

Présentée par

Clément CAMP

Thèse dirigée par **Marinella MAZZANTI**

préparée au sein du **Laboratoire de Reconnaissance Ionique et Chimie de Coordination** du **Service de Chimie Inorganique et Biologique, INAC, CEA-Grenoble**
dans l'**Ecole Doctorale Chimie Sciences Du Vivant**

Conception et réactivité de complexes mono- et polymétalliques d'éléments f en bas degré d'oxydation

Thèse soutenue publiquement le **20 septembre 2013**,
devant le jury composé de :

Pr. F. Geoffrey N. CLOKE
University of Sussex (Rapporteur)
Pr. Polly L. ARNOLD
University of Edinburgh (Rapporteur)
Dr. Didier BOURISSOU
Université Paul Sabatier – Toulouse (Examinateur)
Dr. Olivier MAURY
Ecole Normale Supérieure de Lyon (Examinateur)
Pr. Fabrice THOMAS
Université Joseph Fourier – Grenoble (Examinateur)
Dr. Marinella MAZZANTI
CEA-Grenoble (Directrice de thèse)

Université Joseph Fourier / Université Pierre Mendès France /
Université Stendhal / Université de Savoie / Grenoble INP

THESIS

For obtaining the degree of

DOCTOR OF PHILOSOPHY OF UNIVERSITÉ DE GRENOBLE

Specialty **Inorganic and Bio-Inorganic Chemistry**

Arrêté ministériel : 7 août 2006

Presented by
Clément CAMP

Thesis directed by **Marinella MAZZANTI**

Thesis prepared in the **Laboratoire de Reconnaissance Ionique et Chimie de Coordination** du **Service de Chimie Inorganique et Biologique, INAC, CEA-Grenoble**
In the **Ecole Doctorale Chimie Sciences Du Vivant**

Design and reactivity of mono- and polymetallic complexes of low-valent f-elements

Thesis scheduled the **20 september 2013**,
in presence of :

Pr. F. Geoffrey N. CLOKE
University of Sussex (Rapporteur)
Pr. Polly L. ARNOLD
University of Edinburgh (Rapporteur)
Dr. Didier BOURISSOU
Université Paul Sabatier – Toulouse (Examinateur)
Dr. Olivier MAURY
Ecole Normale Supérieure de Lyon (Examinateur)
Pr. Fabrice THOMAS
Université Joseph Fourier – Grenoble (Examinateur)
Dr. Marinella MAZZANTI
CEA-Grenoble (Directrice de thèse)

Résumé

Au-delà de son importance dans l'industrie nucléaire, la chimie d'oxydoréduction de l'uranium retient de plus en plus l'attention des chercheurs. En effet, la capacité toute particulière des complexes d'uranium à bas degré d'oxydation à promouvoir des réductions originales par des voies inhabituelles suscite actuellement un grand intérêt, tout particulièrement leur aptitude à activer dans des conditions douces des petites molécules telles CO, CO_2, N_2, ou encore des composés aromatiques et des azotures. Les composés d'uranium, de part leurs propriétés de coordination tout à fait uniques pourraient offrir une alternative aux métaux de transition classiques pour la conception de catalyseurs. Cependant, comparativement aux métaux du bloc d, les processus polyélectroniques sont rares dans la chimie de l'uranium à bas degré d'oxidation qui est dominée par les transferts monoélectroniques. C'est pourquoi le développement de nouveaux complexes d'uranium capables de réaliser des réductions poly-électroniques est particulièrement intéressant. Le premier objectif de ce travail était d'associer à l'uranium des ligands non-innocents servant de réservoir d'électrons. Ainsi nous avons utilisé des bases de Schiff π-conjuguées pour explorer la chimie de cet élément à bas degree d'oxydation. Cela nous a permis d'isoler des complexes riches en électrons dans lesquels des électrons sont stockés sur le ligand via la formation de liaisons C-C. Ces mêmes liaisons sont rompues en présence d'agent oxydant, et les électrons sont libérés pour réaliser des transformations polyélectroniques. Ce procédé a été observé pour plusieurs bases de Schiff, permettant de moduler les propriétés des composés. Dans une seconde approche, nous nous sommes intéressés à la synthèse et à l'étude de la réactivité de nouveaux complexes d'uranium trivalent supportés par des ligands silanolates. De nouveaux composés dinucléaires d'uranium à basse valence ont été obtenus. Ces composés très réactifs décomposent spontanément en clivant des groupements tertiobutyls des ligands, conduisant à la formation de complexes d'uranium(IV). En parallèle, un complexe monoanionique mononucléaire d'U(III) a été isolé, nous permettant de comparer la réactivité de l'uranium trivalent dans différents environnements stériques et électroniques. Ces études de réactivité ont permis de stabiliser un exemple rare de dimère d'uranium ponté par un groupement CS_2^{2-} et ont mis en évidence la capacité de l'uranium trivalent à promouvoir la dismutation de CO_2 en carbonate et CO. La réaction de ces composés d'uranium trivalent vis-à-vis d'azotures organiques et inorganiques a produit de nouveaux nitrures et nitrènes d'uranium originaux. Enfin, la capacité de ces agents réducteurs puissants à transférer des électrons au toluène a permis d'isoler une famille de complexes sandwiches inversés où deux cations uranium sont liés de part et d'autre d'un cycle aromatique.

Mots-clés
uranium, réduction, bases de Schiff, ligand redox-actif, silanol, petites molécules, CO_2, azotures

Discipline
Chimie Inorganique

Laboratoire
Laboratoire de Reconnaissance Ionique et Chimie de Coordination
Service de Chimie Inorganique et Biologique, UMR-E3 CEA-UJF
Institut Nanosciences et Cryogénie, CEA Grenoble
17 Rue des Martyrs, 38054 Grenoble Cedex, France

Abstract

Beyond its importance in nuclear industry the redox chemistry uranium is attracting increasing interest because complexes of low-valent uranium can promote unusual reductive chemistry through unusual reaction pathways, including attractive examples of CO, CO_2, N_2, arenes and azides activation in mild condition. Due to the unique coordination and bonding properties of uranium, its compounds could provide an attractive alternative to transition metals for the catalytic transformation of small molecules. However, metal-based multi-electron processes remain uncommon in uranium chemistry especially in comparison with the d-block metals, the chemistry of low-valent uranium being dominated by single-electron transfers. In this context, the first aim of this project was to investigate the association of low-valent uranium to a non-innocent ligand acting as an independent electron reservoir at a same molecule. Accordingly, we interrogated the use of highly π-delocalized Schiff bases ligands for supporting low-valent uranium chemistry. This led to the isolation of electron-rich complexes which are stabilized by storing electrons on the ligands through the formation of C-C bonds. Interestingly, these C-C bonds can be cleaved by oxidizing agents and the electrons released to participate in multi-electron redox reactions. This process was observed within different Schiff-base ligand scaffolds, allowing a tuning of the properties of the compounds. The second part of this work was dedicated to the synthesis of novel trivalent uranium complexes supported by siloxy ligands and the study of their redox reactivity and coordination properties. Novel dinuclear highly-reactive low-valent uranium assemblies were developed. The study of their limited stability revealed that these compounds are spontaneously decomposing through the cleavage of ^{t}Bu groups from the supporting ligands resulting in the formation of U(IV) species. In parallel, a mononuclear trivalent uranium *ate* complex was obtained, allowing to compare the reactivity of U(III) in different steric and electronic environements. Hence we became interested in studying the redox reactivity of these compounds with different substrates including CO_2, CS_2, azides and arenes. These investigations led to the stabilization of a rare CS_2^{2-} sandwich complex of uranium, and highlited the ability of U(III) to promote reductive disproportionation of CO_2 to carbonate and CO. The reaction of these trivalent uranium siloxide species with organic and inorganic azides produced original uranium imidos and nitridos compounds with original topologies. Finally the capacity of these strongly reducing agents to transfer electrons to the toluene fragment lead to the isolation of a family of arenes inverted sandwich complexes.

Keywords
uranium, reduction, Schiff bases, redox-active ligand, silanol, small molecules, CO_2, azides

Specialty
Inorganic Chemistry

Laboratory
Laboratoire de Reconnaissance Ionique et Chimie de Coordination
Service de Chimie Inorganique et Biologique, UMR-E3 CEA-UJF
Institut Nanosciences et Cryogénie, CEA Grenoble
17 Rue des Martyrs, 38054 Grenoble Cedex, France

Acknowledgements
Remerciements

Firstly, I would like to thank all the members of my committee for accepting to review this thesis work.

I am grateful to the University of Grenoble and to the CEA-Grenoble for financial support.

My supervisor Dr Marinella Mazzanti transmitted me her passion for coordination chemistry, her rigor and her devotion to her laboratory. She has been an excellent guide throughout the journey of this PhD, challenging my ideas and supporting me until I achieve this project.

Durant ma scolarité, j'ai rencontré des enseignants qui m'ont appris à aimer les sciences et la chimie, en particulier pendant mes années de classes préparatoires et à l'Ecole Normale Supérieure de Lyon. J'ai découvert l'univers de la recherche aux côtés d'Eric Benoist lors d'un stage au SPCMIB à Toulouse : je tiens à le remercier pour cette expérience extrêmement enrichissante.

A lot of people have been extremely helpful throughout my PhD and deserve my gratitude. I would particularly like to thank Jacques Pécaut from whom I learned every secret of crystallography thanks to his great sense of pedagogy. It was a pleasure to work and spend so many time with someone always ready to run for the sake our crystals, without loosing his smile. I also want to thank Colette Lebrun, for her kindness and her great expertise of mass spectrometry. Many thanks to Lionel Dubois for his precious help for electrochemistry, Jean-François Jacquot for the magnetic measurements and for his expert advices for reaparing every single device in the lab, Pierre-Alain Bayle for NMR spectroscopy, Serge Gambarelli for EPR measurements and Vincent Artero for IR spectra and GC experiments.

I must also thank Pr Laurent Maron and his group in Toulouse who carried out the computational studies on the uranium-siloxy systems.

Un merci tout particulier à Zohra, véritable colonne vertébrale du laboratoire, dont l'efficacité n'a d'égale que la gentilesse. Nous te devons tous beaucoup.

Then of course I would like to thank all the members of the RICC group and more largely of the SCIB, past and present, for all their help, support and for making my three years in the lab so

enjoyable. A special thank to the students and colleagues with whom I shared my office, the glovebox and everyday laboratory life and who, directly or indirectly, contributed to this work : Julie, Valentin, Lucile, Biplab, Laëtitia, Gulay, Gaylord, Maria, Quentin, Oliver, Sebastiano, Yves and Lydia. Dr. Maria Augusta Antunes visited our lab for two months. It was a real pleasure and priviledge to work with her.

Victor is not a colleague for me, but a long-time friend. He introduced me to uranium chemistry and laboratory techniques. I owe him so much.

Au cours de ces trois années j'ai également eu un grand plaisir à enseigner à l'université. Dans cette mission, j'ai eu la chance d'être accompagné par une tutrice exceptionnelle, Catherine Bougault. Je tiens à la remercier très chaleureusement pour sa disponibilité et sa grande bienveillance. Un grand merci aussi à Isabelle Pernin-Wetzel ainsi qu'à l'ensemble de l'équipe enseignante, particulièrement dynamique et investie dans la préparation aux concours de l'Agrégation et du Capes de sciences physiques.

J'ai eu la chance de grandir dans une famille formidable. Maman, Papa, Emmanuel, merci pour votre soutien précieux et vos encouragements.

Enfin, il y a une personne dont la contribution est silencieuse, et sans qui pourtant rien de tout cela n'aurait été possible. Marie, merci.

Table of contents

CHAPTER I
Introduction

I.1 Purpose and Objectives of the Project

The general objective of this PhD work is to increase our fundamental understanding of the chemical properties of low-valent f-elements, and more specifically uranium. The redox chemistry of f-elements plays a crucial role in many aspects of nuclear technology including nuclear fuel reprocessing and safe disposal and in determining the mobility of actinides in the environment. Beyond its importance in nuclear industry the chemistry of low-valent f-elements could provide alternative routes to novel energy supply. A particular current interest arises from the ability of complexes of f-elements to promote small molecules (CO_2, CO, N_2) activation and atom/group transfer through unusual reaction pathways.

Activation of small molecules is an appealing goal for contemporary catalysis. Indeed, these molecules may provide renewable and harmless chemical feedstock for the production of fertilizers, fuels or commodity chemicals.[1-3] As these molecules are generally kinetically inert, their successful utilization depends on surmounting often quite significant activation barriers.[2] Furthermore, due to their thermodynamic stability, a highly negative potential is generally required to reduce them.[4, 5] To overcome this intrinsic low reactivity, fundamental research is mostly focussing on developing new catalysts that not only coordinate small molecules, but also allow them to undergo the stepwise addition of a large number of electrons. The design of such electron-rich complexes can imply low valent metallic elements,[6-10] electron-rich and/or redox active ligands[11, 12] able to reversibly store electrons, bi- or multi-nuclear microenvironments[13-16] which are very well suited to multiple electron transfer events or metal-metal bonds.[17-19]

In this context, the capacity of low-valent uranium to promote a variety of molecular activation processes[20-26] is particularly promising. The examples which will be discussed therein testify to the rich and unique reductive chemistry of uranium. Among these, numerous compounds were not yet

discovered at the start of this PhD work. This attests to the vitality of this field which is still in its infancy. A particular attention should be paid to the crucial role of the ancillary ligands in the reactivity of uranium complexes. Notably the electronic and steric properties of the ligand need to be carefully tuned. Indeed, the challenge is to create a ligand environement which can stabilize the low-valent uranium centre but maintain its high reactivity. Subtle changes in ligand architectures can bring about big differences in reactivity.[27, 28] In the recent years, some alternatives to the ubiquitous Cp ligands were proposed to explore the chemistry of low-valent uranium and although remarkable structures and reactivities were observed, such systems remain scarce. In order to improve our understanding of the properties and reactivity of this element, the synthesis and the study of new innovative well-defined systems is thus required.

Accordingly, the aim of this thesis work is to design new coordination environments allowing for exploitation of the chemical uniqueness of f-elements, more particularly uranium. These syntheses target the isolation of highly reactive mono and polymetallic complexes able to promote novel reductive chemistry, and notably activation of small molecules under controlled conditions. To this purpose, two different approaches were explored.

Low-valent uranium rarely participates in two-electron redox transformations. In the first part of this work, we explore the use of redox-active ligands with the goal of enabling multielectron processes at uranium. The objective is to use the ligand as an electron reservoir in reductive transformations. In our search for non-innocent ligands which can be associated to f-elements we have identified polydentate Schiff bases as a very convenient and synthetically versatile choice. Despite it being demonstrated that these popular chelating agents can act as redox-active ligands and electron reservoirs when combined with a range of d-block transition metals,[29-34] there are no reports for their use in low-valent f-elements chemistry. In this thesis, we will study the coordination chemistry and the redox properties of low-valent uranium with multidentate chelating Schiff bases possessing O- and N-donor atoms. With the aim of tuning the reactivity of the complexes, we will explore ligands presenting diverse denticities (tetradentate or tridentate), steric and electronic properties. This work is presented in Chapter II.

Secondly, we will focus our studies on the use of the simple tris(tert-butoxy)siloxide ligand to support trivalent uranium chemistry. Besides aryloxide derivatives, oxygen-donor ligands have been rarely associated with U(III). We reasoned that the hard and bulky $[OSi(O^tBu)_3]^-$ ligand should be able to enhance the reducing ability of U(III). Furthermore, the capability of this electron-rich ligand to adapt its coordination properties is promising for stabilizing a wide range of reaction intermediates or for accessing polynuclear assemblies. We will first study the aptitude of this siloxy ligand for

stabilizing U(III) entities. The robustness and the reactivity properties of the novel mono and polynuclear trivalent uranium compounds isolated will be then investigated. Special attention will be paid to CO_2 and CS_2 with the objective of identifying new modes of activation of these small molecules. We will also focus on the reductive transformation of inorganic and organic azides in order to explore the possibility of building novel uranium nitrido and imido architectures particularly relevant for the development of new nuclear fuels and N-atom transfer catalysts. Finally, the interaction of U(III) with aromatic systems will be investigated. The results of these studies are presented in Chapter III.

I.2 Uranium and F-elements

Since their discovery in the late 1700's, the f-elements have found a widespread use in a wide range of applications. This can mostly be imparted to their unique physico-chemical properties conferred by their chemical singularity in the periodic table. Over the past 30 years, they became indispensable in several strategic sectors of the economy, playing a key role in the rapid expansion of new technologies and being at the heart of energy-related issues and environmental stakes as for instance in nuclear power and radioactive waste reprocessing, petroleum refining catalysts, automotive catalytic converters, permanent magnets for hard disk drives and electric generators used in wind-turbines and electric vehicles, lasers, phosphors for flat panel displays and energy-efficient lighting, MRI and luminescent probes for bio-imaging. Consequently, the global demand for these elements is constantly increasing, and access to the f-elements is nowadays an economic and geopolitical imperative.[35]

I.2.1 Fundamental properties

The term f-elements refers to the 30 elements whose atoms or ions have valence electrons in f-orbitals. They can be divided into two families: the lanthanides (La-Lu) that possess *4f* valence electrons and the actinides (Ac-Lr) that possess *5f* valence electrons (Figure I.1).

57 **La**	58 **Ce**	59 **Pr**	60 **Nd**	61 **Pm**	62 **Sm**	63 **Eu**	64 **Gd**	65 **Tb**	66 **Dy**	67 **Ho**	68 **Er**	69 **Tm**	70 **Yb**	71 **Lu**
89 **Ac**	90 **Th**	91 **Pa**	92 **U**	93 **Np**	94 **Pu**	95 **Am**	96 **Cm**	97 **Bk**	98 **Cf**	99 **Es**	100 **Fm**	101 **Mb**	102 **No**	103 **Lr**

Figure I.1. F-block elements : the lanthanides (first row) and the actinides (second row). Dark shading shows unstable elements that do not occur naturally. The uranium element, which is at the center of this work, is highlighted in green.

These metallic elements, which exhibit unique characteristics, have the potential to accomplish a chemistry not possible with d-transition metals. The following summarises the properties that are of direct relevance to understanding f-elements coordination chemistry.[36-39]

These elements have large ionic radii, which give rise to high formal coordination numbers (8 and 9 being the most common) and unusual coordination geometries.[37]

The f-elements ions are hard Lewis acids.[36] As a result, they prefer to coordinate to hard bases such as fluoride or alkoxides, and have a tendency to form oxygenated compounds by hydrolysis or abstraction of oxygen. For many years, the use of these elements was disregarded for molecular activation, mostly because reactions of soft and poor ligands such as dinitrogen or carbon dioxide were not expected to occur with such hard metal ions. This assumption has proved incorrect as various coordination compounds of these two small molecules with f-elements have been reported in recent years as will be illustrated in the following sections.

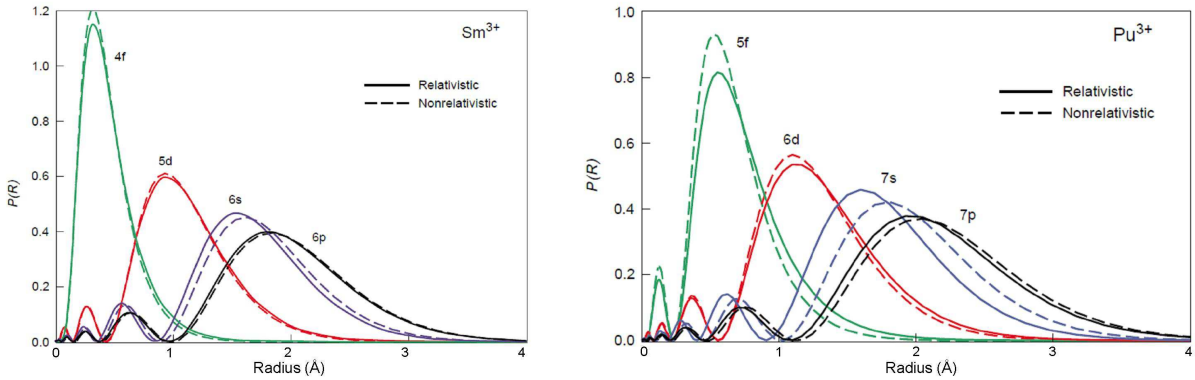

Figure I.2. Comparison of the radial extent of the electronic orbitals for the Sm^{3+} and Pu^{3+} ions.[40]

The characteristics of 4f and 5f orbitals are quite different and thus the properties induced are distinct for lanthanides and actinides.

As illustrated in Figure I.2-left, the 4f orbitals do not extend out far enough to interact to any great degree with ligand orbitals. Thus the effect of the ligand-field environment on the electronic structure of lanthanide complexes is negligible.[39] This is evidenced by the optical spectra of these species, in which the position of sharp f→f absorption bands is not affected by a change in the nature of ligands. As a result the complexes formed are held together largely by electrostatic interactions. Consequently, metal-ligand bonds are non directional, and no specific geometry is imposed in lanthanide coordination complexes. The preferences between different coordination numbers and geometries are therefore mostly ruled by the minimization of the steric repulsion between the ligands, offering the possibility for the coordination chemist to fine-tune the reactivity of these species by controlling steric factors. The coordination sphere is labile so a transition between different coordination environments can occur very easily and hence the lanthanide complexes can work as templates for catalysed reactions.[41]

In contrast, one particular feature of the early actinides elements (Th-Np) is that the radial extension of 5f and 6d atomic orbitals is increased (Figure I.2-right), leading to some overlap with ligand-based orbitals.[38, 42] Moreover, due to the energetic accessibility of metal valence electrons, these elements

display a great range of oxidation states in the early part of the series, contrary to the lanthanide elements whose chemistry is dominated by the trivalent oxidation state.[36] The combination of ligand-field effects with relativistic effects considerably complexifies the electronic structure of actinide coordination compounds. Magnetic and spectroscopic properties are thus challenging to interprete.[43] Although the actinide-ligand interaction presents some degree of covalency, the nature of the bonding is mostly ionic, and the consequences stated above for lanthanide complexes also apply for the actinide ones. The understanding of the bonding in f-element complexes remain an active domain of research notably because this might help develop selective extractants for the separation of minor actinides from lanthanides in spent nuclear fuel, the former being responsible for the radiotoxicity of the nuclear waste.[44-47]

In the end, the combination of these features induce an especially interesting and diverse chemical reactivity, opening the door to new and unique modes of activation as compared to d-block metals,[48] making f-elements complexes a very promising route for chemical transformations.

During these PhD studies I have also investigated the chemistry of lanthanides with redox-active ligands but since I predominantly investigated uranium chemistry I choose to focus the present manuscript on this element.

I.2.2 The Uranium Element

I.2.2.1 General properties

Uranium is the only actinide with thorium that occur naturally to any useful extent, with a proportion[49] of 99.27% ^{238}U and 0.72% ^{235}U, both isotopes being radioactive. Because of the interesting decay properties of the fissile ^{235}U nucleus, natural uranium is enriched in ^{235}U before being used as a fuel in nuclear power industry,[50] which is the only significant use of this element. High-purity ^{238}U depleted uranium is produced as a by-product of nuclear isotope enrichment programmes. This isotope is only weakly radioactive (half life $4.5.10^9$ years)[20] and the ^{238}U series essentially radiates α and β^- particles of weak energy[49] which are easily stopped. Working with depleted uranium is therefore safe as long as it is not inhaled or ingested, facilitating its use and studies.[51]

As previously mentioned, similarities exist between the chemical properties of this element and those of lanthanides (hard Lewis acidity, large ionic size, original coordination environments and geometries). In contrast, like d-block metals, uranium can adopt various oxidation states ranging from +II to +VI, and therefore exhibits a rich redox chemistry that can be exploited in catalytic

processes.[23] Finally, although the metal to ligand bonding in coordination complexes is mainly ionic, the uranium f-orbitals participate in bonding.[42] The result is a range of chemical reactivity that is special to uranium which only begins to be discovered.[20, 47, 52] The challenge is great, as many questions about the properties and reactivity of this unique element remain to be answered.

I.2.2.2 Survey of Oxidation states

Among the five oxidation states known for uranium (***Table I.1***), oxidation states +IV and + VI are the more stable and the more documented ones. The uranyl(VI) ion, UO_2^{2+}, is the most stable form of uranium under aerobic conditions, the low-valent ions being readily oxidized by O_2 to give the uranyl(VI) moiety. U(III), U(IV) and U(V) ions are paramagnetic while U(VI) compounds are diamagnetic. During the preparation of this manuscript, the first example of a molecular U(II) complex has been reported,[489] opening new perspective in reductive uranium chemistry.

Table I.1. Known oxidation states of the uranium element

Oxidation state	metal	U(III)	U(IV)	U(V)	U(VI)
Electronic configuration	$[Rn]7s^26d^15f^3$	$[Rn]5f^3$	$[Rn]5f^2$	$[Rn]5f^1$	[Rn]

I.2.2.2.1 U(VI)

Because of its implication in nuclear waste reprocessing and in the mobility of uranium in the environment, the coordination chemistry U(VI) has been extensively studied. The vast majority of hexavalent uranium compounds contains the linear trans dioxo $O=U=O^{2+}$ group. The uranyl(VI) UO_2^{2+} ion is extremely stable and forms a variety of mononuclear and polynuclear complexes both in aqueous or organic media.[47, 51, 53-57]

Comparatively, the number of examples of non uranyl U^{6+} compounds is extremely limited.[51, 58, 59] One example is uranium hexafluoride, which is used for the separation of uranium isotopes in the nuclear fuel cycle.

I.2.2.2.2 U(V)

Pentavalent uranium systems remain relatively rare. Several factors can explain this scarcity. First of all, U(V) compounds present a tendency to disproportionate to U(IV) and U(VI) and only the fine tuning of the coordination environment leads to the isolation of stable U(V) complexes.[60] Secondly, U(V) species are easily oxidized to U(VI) by traces of oxygen or water, rendering their isolation more challenging. Finally, until recently, there was a lack of convenient U(V) starting materials to enter this

chemistry. This situation has slightly changed over the past few years, and notably stable uranyl(V) UO_2^+ complexes have been reported.[61-66] Non-uranyl organometallic U(V) compounds are more numerous as they can be accessed by oxidation of low-valent precursors[60] (*vide infra*).

I.2.2.2.3 U(IV)

Uranium forms very stable U(IV) compounds. The U^{4+} ion is readily hydrolyzed in presence of water and oxidized by O_2, but this oxidation state has considerable importance in non-aqueous chemistry. Numerous coordination compounds have been reported, with a large palette of ligands.[38, 51]

I.2.2.2.4 U(III)

Trivalent uranium complexes are less common than their tetravalent counterparts, mostly because these strong reducing agents are stable under a more limited range of experimental conditions. In the next section the focus will be on the chemistry of U(III) species.

Due to uranium possessing such rich oxidation states diversity, it is an ideal candidate for exploring its redox reactivity. Actually, much attention is currently paid to trivalent uranium complexes, which are especially attractive prospects for small molecules activation. This chemistry lies at the very forefront of the field,[47] and requires conceiving and synthesizing novel systems in order to improve our understanding of this domain.

I.3 Molecular Chemistry of Trivalent Uranium

I.3.1 Chemical properties

Uranium in its +III oxidation state exhibits three key chemical characteristics particularly relevant for our studies.

Strong reducing potential :

Trivalent uranium species are substantial reducing agents which are exceedingly sensitive to air and moisture[67] and hence must be handled in non-aqueous solvents under an inert atmosphere of argon. Electrochemical studies show that the potential for the couple U^{4+}/U^{3+} varies depending on the ligands surrounding the metal with the reducing ability of trivalent uranium enhanced as the electron donating ability of the ligand increases,[68] and lies between -1.5 V to -2.9 V versus $[(C_5H_5)_2Fe]^{+/0}$.[24, 68-71]

Large atomic dimensions :

Trivalent uranium has an extended Van der Waals radius (1.86 Å)[22] giving rise to an unusually large palette of coordination numbers. One illustrative example is the 12-coordinate trivalent uranium complex $[^{py}Tp_2U][BPh_4]$.[72] Comparatively low coordinences can be reached with highly sterically hindered ligands, as found for instance in the emblematic tricoordinate homoleptic silylamido $[U\{N(SiMe_3)_2\}_3]$ complex.[73]

Partial covalent bonding :

As previously mentioned, the 5f orbitals are available to engage in bonding interactions with coordinating ligands.[42] Notably, trivalent uranium presents a tendency toward π and δ backbonding ligation, making possible coordination and activation of a variety of π-ligands systems.[74, 75] Thus unusual coordination modes and reactivity can be expected. However, metal-ligand bonding is still dominated by electrostatics, therefore the coordination geometry is mainly determined by steric repulsions.

I.3.2 Starting materials and synthetic routes

Exploring trivalent uranium chemistry requires convenient synthetic entries to these compounds. Given the very high reactivity of these derivatives, this is generally very challenging. Indeed, strictly inert conditions and appropriate solvents as well as stabilizing ligand system and suitable starting materials are required to avoid product decomposition. In this purpose, two main strategies are generally envisaged.

I.3.2.1 Ligand exchange route

The first approach consists in synthesising trivalent uranium complexes via ligand exchange reactions on trivalent uranium precursors. Such precursors have to be easily available and relatively stable in the desired reaction media. Currently, the THF solvated uranium triiodide $[UI_3(THF)_4]$ is the most commonly used starting material for accessing low-valent uranium derivatives.[76] The deprotonated form of the desired ligand reacts with this precursor by salt metathesis, as shown in ***Scheme I.1***. Of particular importance is the control of stoichiometry, mainly with less bulky ligands, as the strongly Lewis acidic uranium center can accommodate anionic groups in excess of the number required by its formal oxidation state, leading to ate-complexes which are generally unwanted side-products because considered unreactive.

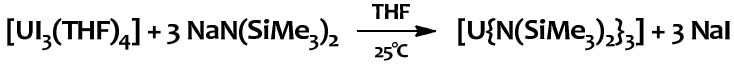

Scheme I.1. $[U\{N(SiMe_3)_2\}_3]$ preparation from the iodide salt $[UI_3(THF)_4]$ by salt metathesis.

The THF solvated uranium triiodide $[UI_3(THF)_4]$ is easily prepared by direct oxidation of uranium turnings with 1.5 equivalent of freshly sublimed I_2 in THF at 0°C (***Scheme I.2*** a).[77, 78] Average yields are usually observed for this reaction because of the formation of by-products, more probably caused by the ring-opening of THF.[79]

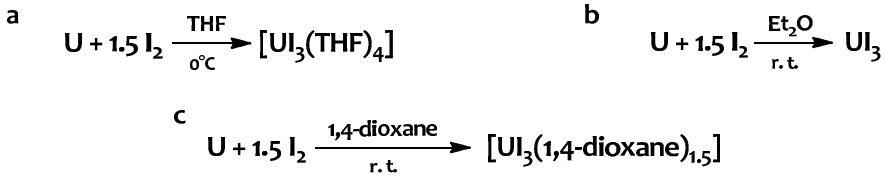

Scheme I.2.Uranium triodides syntheses a) in a THF solvated form ; b) in an unsolvated form ; c) in 1,4-dioxane solvated form.

A more convenient and efficient synthesis was reported recently for the dioxane adduct $[UI_3(1,4\text{-dioxane})_{1.5}]$.[79] The analogous THF-solvated compound can be obtained upon extraction of $[UI_3(1,4$-

dioxane)$_{1.5}$] with THF. Both 1,4 dioxane or THF ligands are readily displaced by other strong donors such as pyridine or 1,2-dimethoxyethane to access the [$UI_3(py)_4$] and [$UI_3(DME)_2$] complexes.[78, 79] The presence of solvent molecules in the coordination sphere of these three trisiodide uranium species increases the solubility of the metal center in organic solvents such as toluene or THF. Recently, a new convenient route for synthesising this starting material in an unsolvated form under mild conditions has been described.[80] This straightforward synthesis consists in oxidising uranium turnings with 1.5 equivalent of I_2 in diethyl ether at room temperature (***Scheme I.2***-b). This unsolvated starting material is preferred in some cases as solvent fragmentation with U(III) species can occur. Ring-opening of THF or ether cleavage by uranium derivatives for instance has been reported.[75, 81-84] Trisiodide uranium species do not show unusual reactivity with small molecules or solvents, but when the halides are replaced by a variety of atoms, the high reactivity of low-valent uranium becomes apparent.

In some cases, it could be useful to replace this iodide starting material with a chloride derivative as chloride anions are more coordinating, and could afford different reactivity. For instance, salt metathesis reaction between uranium(III) halides and alkaline salts of calixtetrapyrrole ligands has been shown to be strongly affected by the nature of both the halides and the alkali-metal counterions.[84] The polymeric unsolvated UCl_3 compound is poorly soluble in most common organic solvents,[85] preventing its use as a starting material. A THF-solvated uranium trichloride synthesis from the tetravalent UCl_4 compound has been described.[86] Unfortunately, this synthesis has been shown to be poorly reproducible,[87] so new synthetic ways are required in order to fully exploit this starting material.

Apart from uranium halides, other trivalent uranium precursors can be used with profit as they can lead to different solubility, coordination and reactivity properties. For instance, trivalent uranium triflate precursors which can be synthesised by three different ways[88, 89] shown in ***Scheme I.3*** have already proven to be useful.[90] By comparison with the halides, triflate ligands are less coordinating and excellent leaving groups as well as good electron-withdrawing groups. The result of these effects can be used to tune the electronic properties of the complex, whilst redox reactions involving the couple I_2/I^- are also avoided.

$$[UI_3(THF)_4] + 3\ KOTf \xrightarrow[r.t.]{MeCN} \{[U(OTf)_3].(3MeCN)\}_n + 3\ KI$$

$$[U(N(SiMe_3)_2)_3] + 3\ [pyH][OTf] \xrightarrow[r.t.]{py} [U(OTf)_3(py)_4] + 3\ NH(SiMe_3)_2$$

$$[UI_3(dme)_2] + 3\ Me_3SiOTf \xrightarrow[100°C]{dme} [U(OTf)_3(dme)_2] + 3\ ISiMe_3$$

Scheme I.3. Synthetic methodologies affording trivalent uranium triflates.

Another precursor of relative significance[76] is the easily synthesized[78] (***Scheme I.1***) highly sterically hindered $[U\{N(SiMe_3)_2\}_3]$[91] complex. The amido ligands are easily protonated and the protonolysis route was successfully utilized to access U(III) alkoxide and aryloxide species (***Scheme I.4***). As $(Me_3Si)_2NH$ is volatile, syntheses involving protonation of the homoleptic $[U\{N(SiMe_3)_2\}_3]$ with a ligand system usually results in a clean reaction with fewer undesired by-products. Indeed, this strategy circumvents the problem of *ate* complexes previously mentioned. Another benefit of this methodology resides in the fact that the ligand does not need to be deprotonated before use, so the reaction mixture is free of alkaline cations and halide anions that could interfere in the complex structure. In addition, this precursor is soluble in hydrocarbon solvents, preventing undesired reactions with oxygenated solvents. Altogether, these characteristics make this derivative of particular interest for accessing trivalent uranium species.

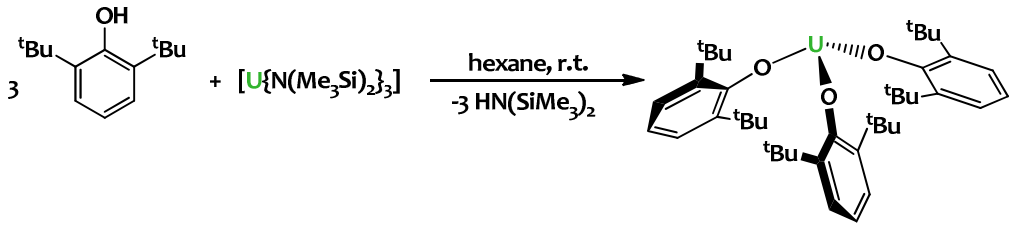

Scheme I.4. Synthesis of U(III) aryloxides by protonolysis.[92, 93]

Trivalent uranium hydride UH_3, obtained by reaction of H_2 with metallic uranium is not a practical reagent for synthetic purposes because of the low solubility of this polymeric material. In contrast, the borohydride ion BH_4^- forms a variety of covalent complexes with uranium, such as $[U(BH_4)_3(THF)_3]$ that could be used to access U(III) chemistry,[94] widening the range of trivalent precursors.

I.3.2.2 Reductive approach

A second approach to access low-valent uranium (III) compounds is via reduction of a tetravalent analogue. This synthetic pathway is particularly useful when direct metathetic replacement of ligands on $[UI_3(THF)_4]$ cannot be used (***Scheme I.5***). Indeed, the formation of uranium(IV) compounds is a common occurrence when starting from $[UI_3(THF)_4]$.[76, 95-103]

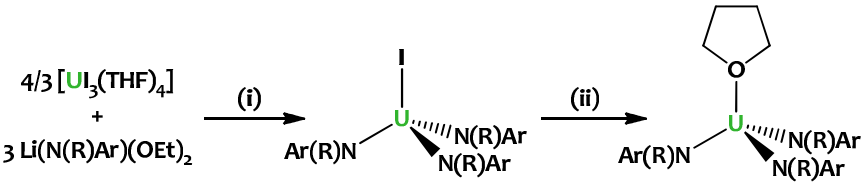

Scheme I.5. Synthesis of the $[U(THF)(NRAr)_3]$ complex. R= $C(CH_3)_3$; Ar=3,5-$C_6H_3Me_2$ (i) toluene, -90°C to 0°C, -3LiI, -"U^0", 64% yield ; (ii) 4 equiv Na/Hg (1% w:w), THF, 20min, 80% yield. The initial objective of the authors was to prepare the homoleptic amide of uranium(III) by salt metathesis with $[UI_3(THF)_4]$.

Moreover U(IV) compounds are more easily accessed[80, 104, 105] and handled than their U(III) counterparts. Reducing the tetravalent species is the key step of the process, and is generally very challenging. Because the potential for the couple U^{4+}/U^{3+} is generally very low, highly reducing agents such as alkaline metals under different forms (chunks, films, graphite intercalation compounds, mercury amalgams or naphtalenides), alkaline hydrides or carbides are required. Usually, the outcome is greatly depending on the starting material, the reducing agent and the reaction conditions. The work by Scott and coworkers[106] greatly illustrates this, as many attempts in reducing tetravalent uranium amides complexes under various conditions, afforded different results. Reduction of [UCl(NN'$_3$)] (NN'$_3$ = N(CH$_2$CH$_2$NSi^{t}BuMe$_2$)$_3$) over a potassium film does not proceed further than the mixed-valent U(III)/U(IV) dimer compound with a bridging chloride ligand (***Scheme I.6***). Even if the desired trivalent [U(NN'$_3$)] complex was achieved after fractional sublimation of this dimer, a more convenient and clean synthesis has been developed utilizing the iodide tetravalent starting material [UI(NN'$_3$)] (***Scheme I.6***). As iodide is much a poorer bridging ligand than chloride, this directly afforded the trivalent uranium complex. This reduction step is also very sensitive to the substituting groups on the amide ligands. Indeed, using SiMe$_3$ in place of Si^{t}BuMe$_2$ resulted in no reaction with potassium. In contrast, using the SiPh$_2$Me substituents lead to dark intractable products. This last example clearly illustrates the importance of the starting material utilized.

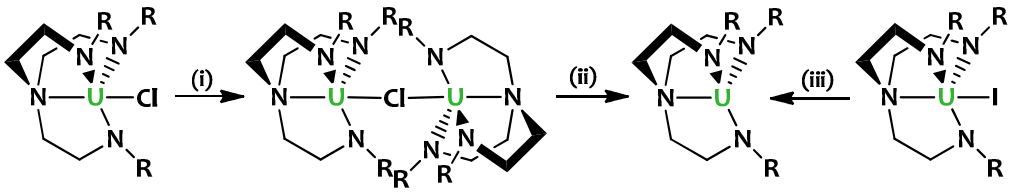

Scheme I.6. Synthesis of a triamidoamine trivalent uranium complexe. R = Si^{t}BuMe$_2$ (i) K film, pentane r.t. ; (ii) 120°C, 10^{-6} mbar, -UCl(NN'$_3$) ; (iii) K film, pentane, r.t. .

In summary, trivalent complexes can be obtained using different convenient ways. However, there is no generally applicable synthetic route and the outcome strongly depends on the choice of the reaction conditions and of the ancillary ligand(s), as a result of the strong reducing ability of U(III) and of the higher stability of U(IV) species.

I.3.3 Ligands in U(III) chemistry

The coordination chemistry of actinides has historically been dominated by aqueous synthesis, which limited the isolation of well-defined complexes. The non-aqueous coordination chemistry of uranium traces its roots back to Sir Geoffrey Wilkinson who in 1956 reported the synthesis of [Cp$_3$UCl].[107] Since then, the organometallic chemistry of uranium has been extensively investigated using

cyclopentadienyl derivatives as effective supporting ligands. The C_5Me_5 ligand is very well suited for exploring uranium chemistry as it provides steric bulk and electronic saturation necessary to form stable and isolable uranium species. Cyclopentadienyl-related ligand frameworks (***Figure I.3***) proved to be able to support the entire range of uranium oxidation states (+3 to +6), affording well-defined complexes with only a few coordination sites available for reactivity purposes. These features explain why for a long time actinide chemistry was dominated by metallocene derivatives.

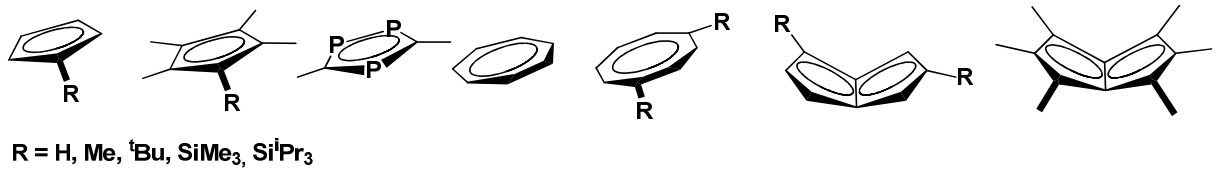

Figure I.3. Classical organouranium spectator ligands.

Accordingly, the chemistry of organouranium(III) complexes is by far the most extended.[108] In the recent years, new heteroatom-based ligand sets able to stabilize the trivalent uranium oxidation state have emerged. With the analogy to Cp in mind, carbolide, tris(pyrazolylborate) and related ligands have been utilized to investigate U(III) chemistry (***Figure I.4***).

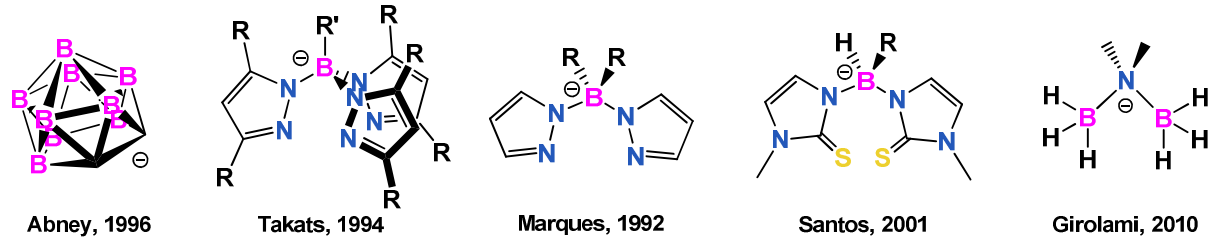

Figure I.4. Organoboron anionic ancillary ligands employed to support U(III) chemistry.[109-113]

In parallel, in view of the electropositive nature of the uranium element, several U(III) complexes of hard oxygen-donor and nitrogen-donor monodentate ligands have been obtained, including alkoxy, aryloxy, imide and silylamide derivatives (*Figure I.5*). Such hard and anionic donor ligands are particularly suited because low-valent uranium easily bind them and because they provide electron-rich environments which may enhance their reducing character. Hence these systems are still the subject of intense research.[25, 99]

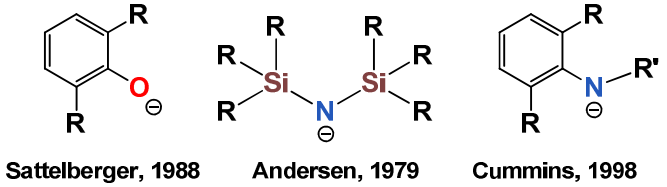

Figure I.5. Monodentate O and N-donor ligands for U(III) chemistry.[91, 92, 95]

It is only in the last decade that a broader range of ancillary ligands with various coordination modes and original topologies have been successfully implemented to stabilize U(III) (***Figure I.6***). Most of them feature hard amido or phenolate donor moieties, but more recently ligands that combine hard N or O and soft S or P donor atoms have also proved to be efficient ancillary ligands for U(III) chemistry.

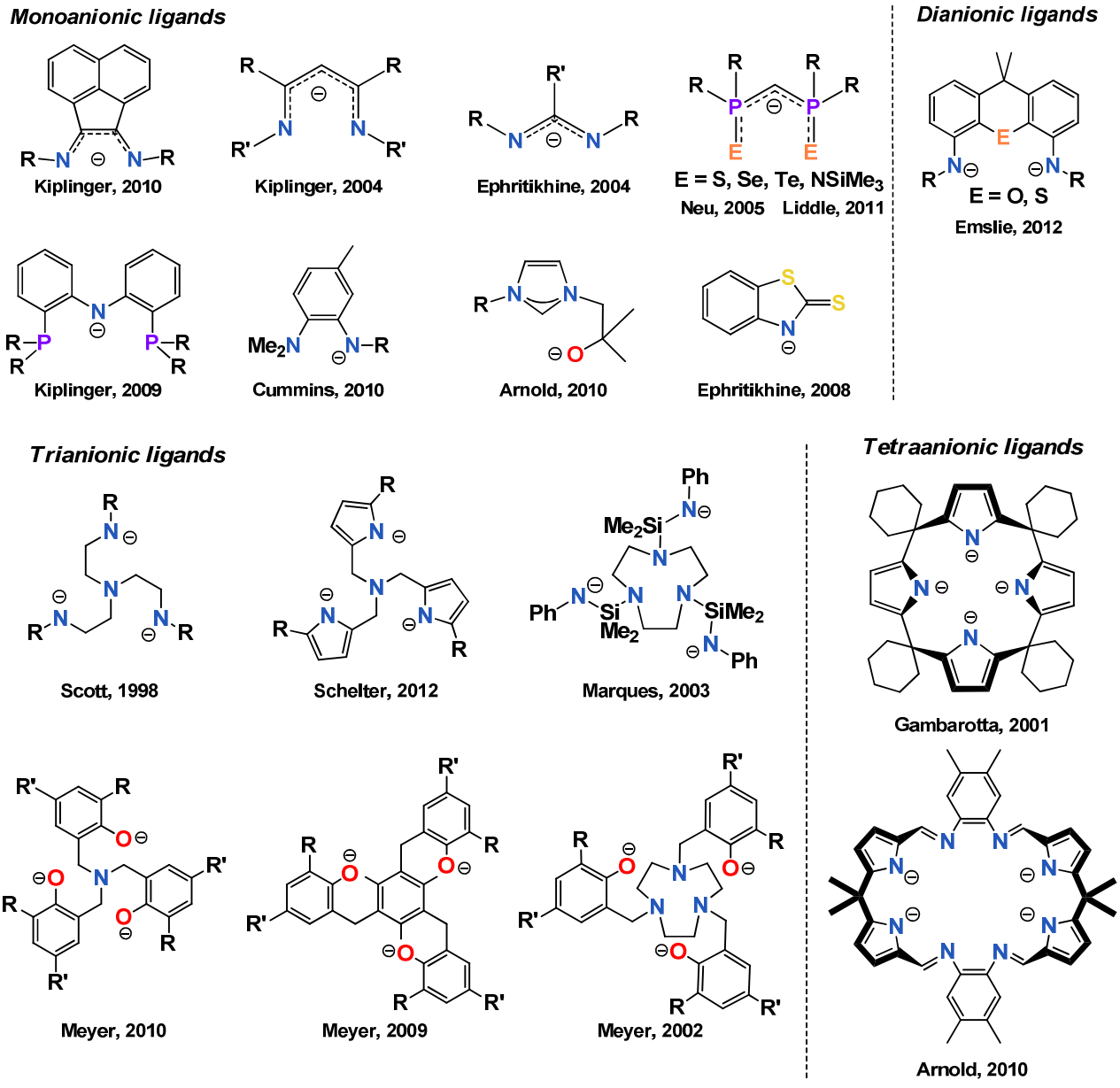

Figure I.6. Multidentate anionic ancillary ligands employed to support U(III) chemistry.[84, 98, 114-129]

A variety of nitrogen-based neutral ligands have also been used in combination with U(III) iodides (***Figure I.7***). This research was mostly directed to explore the selectivity for An(III) over Ln(III) in order to identify suitable trivalent actinide extractants for nuclear remediation.[130-137]

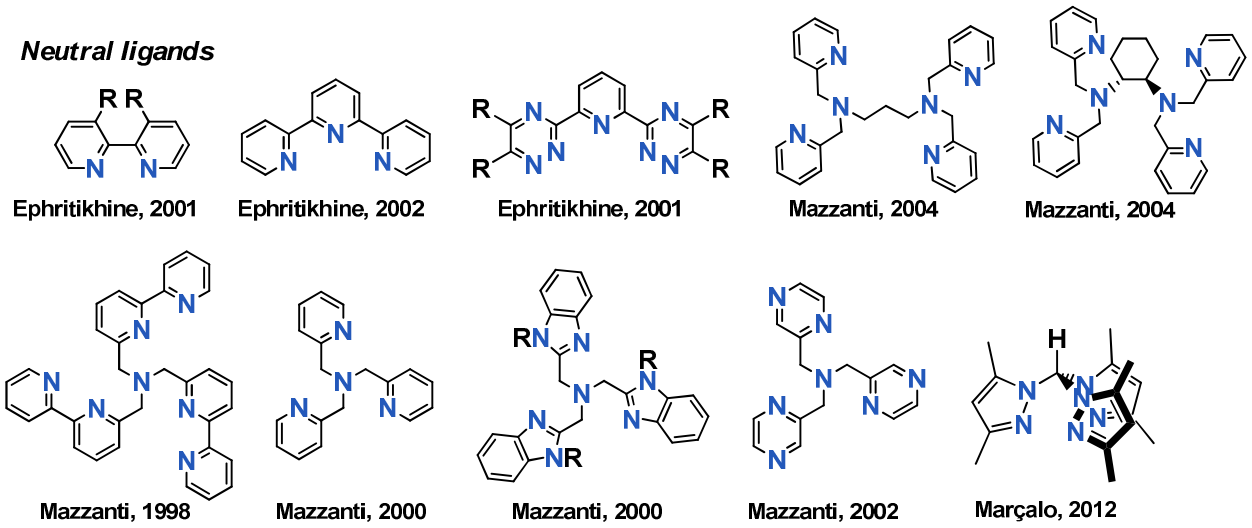

Figure I.7. Multidentate N-donor neutral ancillary ligands employed to support U(III) iodide.[130-137]

While non-cyclopentadienyl ligands are increasingly utilized to prepare stable U(III) complexes, such systems still remain limited to a few examples despite the potential for such ligands to provide access to complexes with unique and readily tunable steric and electronic properties. In addition, their properties and reactivity are just begining to be investigated, and some have been shown to support reactivity patterns and structures that are not currently available for the ubiquitous cyclopentadienyl systems. This notably lead to the characterization of rare U(III) monoalkyl[138] or ylide[139] species and allowed for the isolation of the first uranium terminal nitride[140] and a uranium complex in which a CO_2 molecule is bound in an unprecedented linear, O-coordinated η^1-CO_2 fashion.[141] These results highlight the interest of identifying novel supporting ligands capable of stabilizing U(III). Given the important role played by the geometric and electronic properties of ancillary ligands in the properties of coordination complexes, new modes of reactivity are expected.

I.3.4 Reductive reactivity of U(III) complexes

I.3.4.1 General overview

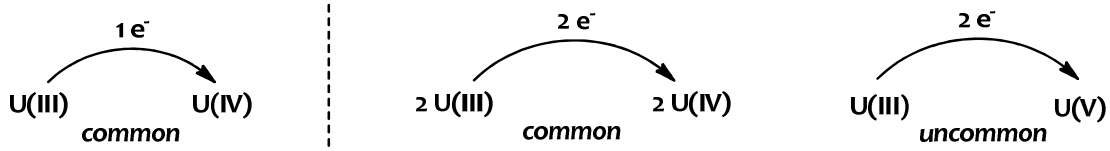

Scheme I.7. Because of the high stability of U(IV), single electron transfers are common in U(III) chemistry. Two-electron transfers to a substrate are generally achieved via the subsequent oxidation of two equivalents of U(III) to U(IV), however, U(III) to U(V) processes are also possible.

As mentioned earlier, trivalent uranium is remarkable for its unique reducing properties. Most of the time, reduction reactions with U(III) species are monoelectronic, involving the U^{4+}/U^{3+} couple.[24]

Single-electron reductions generate odd electron products that can be subsequently further reduced by a second equivalent of a trivalent uranium derivative. In addition, the possibility of trivalent uranium of affording polyelectronic reductions via the U^{5+}/U^{3+} couple witnesses of the rich reductive chemistry of trivalent uranium, making its low-valent derivatives particularly desirable. Comparatively to U(IV) complexes, pentavalent uranium systems remain relatively rare,[60] and accordingly, two-electron redox reactions from U(III) to U(V) are less common than bimolecular U(III) to U(IV) oxidations.[24, 60] Nonetheless, considerable progress has been achieved and U(V) oxos[142-145] or imidos (see section I.3.4.4.2) compounds notably can be accessed from U(III).

Characteristic examples for each transformation are given in ***Scheme I.8***.

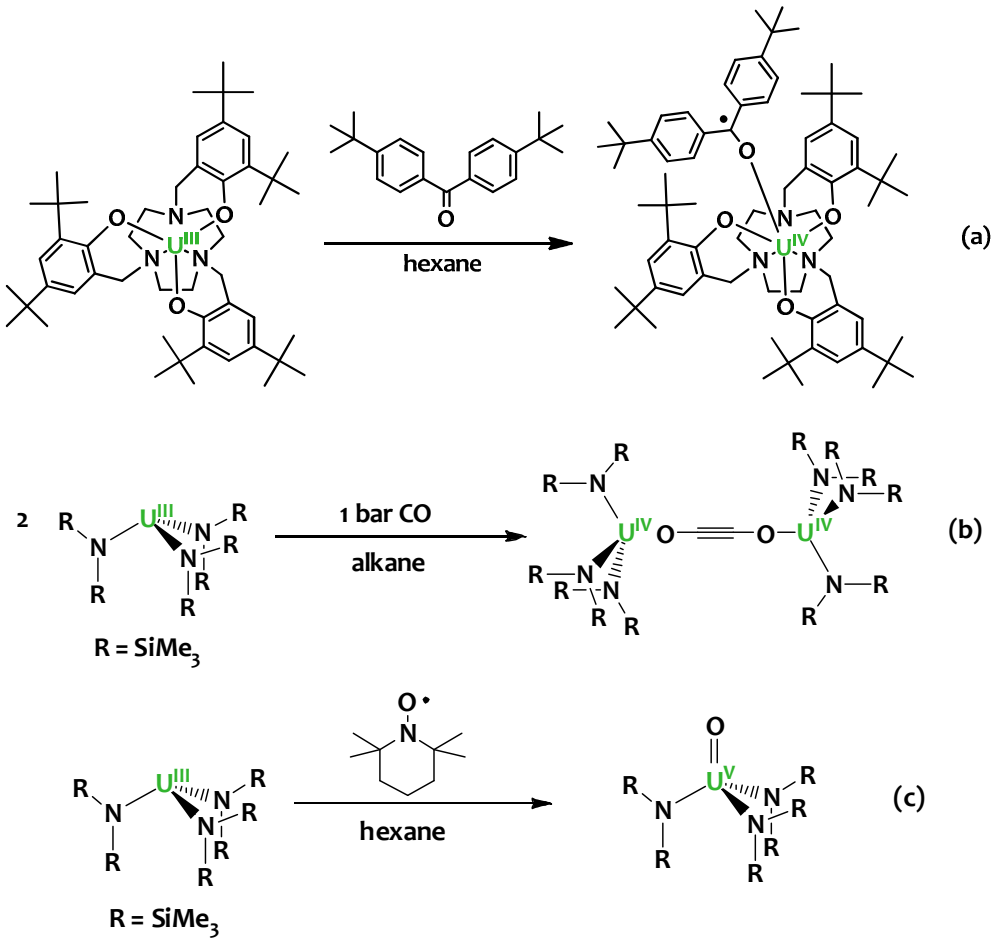

Scheme I.8 (a) Formation of a U(IV) benzophenone ketyl radical complex through a one-electron reduction of 4,4'-di-*tert*-butylbenzophenone by U(III)[146] ; (b) Formation of a U(IV)/U(IV) ynedioalte bridged complex through the concerted oxidation of two U(III) centers to U(IV)[93, 147, 148] ; (c) Formation of a U(V) terminal oxo complex through a two-electron oxidation of U(III) by TEMPO.[144]

Low-valent uranium complexes exhibit a fascinating reductive capacity, particularly in the activation of small molecules. Novel examples of reactivity including CO,[27, 93, 147, 149-156] CO_2 (see section I.3.4.2), N_2,[93, 95, 124, 157-161] NO,[153, 162] azides (see section I.3.4.4), arenes (see section I.3.4.5), and C-H activations[163] have been reported in recent years.

The ability of U(III) species to mediate molecular activation provide also synthetic routes to new functionalities and structures otherwise not attainable. Let's mention for instance the isolation of unprecedented species containing uranium-ligand multiple bonding,[164, 165] including terminal oxos,[143, 144, 166, 167] nitrides,[140, 168] chalcogenides,[167] trans bis-imides[169, 170] or the obtention of large oxo/hydroxo clusters by controlled hydrolysis or reaction with O-atom transfer reagents of U(III) precursors.[67, 90, 171, 172]

Altogether, these quite inspiring examples give a clear hint that various transformations and molecular activation processes on a broader range of substrates are yet to be discovered.

Activation of small molecules by trivalent uranium complexes has been thoroughly reviewed by several authors.[21-26] Therefore in this section we will only focus on the substrates that were studied during this PhD work. This literature review will describe the redox reactivity of U(III) complexes with heteroallenes derivatives (CO_2, COS, CS_2, N_3^-, RN_3) and with arenes.

I.3.4.2 U(III)-mediated activation of CO_2

I.3.4.2.1 General scope

The utilization of CO_2 as a carbon feedstock is an attractive objective in contemporary catalysis research, as carbon dioxide is naturally abundant, inexpensive, nontoxic and nonflammable. Furthermore, the need to reduce the accumulation of this greenhouse gas into the atmosphere requires new technologies able to reduce CO_2 emissions. Therefore the catalytic conversion of CO_2 to usable fuels or other carbon-containing chemicals may represent an interesting approach to synthetic methodologies less intensive in carbon and energy.[2, 3, 173, 174]

Nevertheless, transforming CO_2 to a useful state is a scientifically challenging problem because of the inertness of this apolar molecule. Because of the large bond enthalpy of the strong C=O double bond (532 $kJ.mol^{-1}$), CO_2 is thermodynamically stable and large energy input is required to reduce this molecule.[2, 5, 174] Furthermore, many reactions that generate carbon containing molecules from CO_2 are characterized by high activation barriers.[2, 175] Regardless, nature utilizes CO_2 as a C_1 chemical feedstock on a large scale, and [NiFe] CO dehydrogenases catalyzes the reduction of CO_2 to CO.[4] This transformation is particularly attractive as carbon monoxide is a versatile chemical precursor and can be converted to fuels via the Fischer-Tropsch process.

For the above reasons, CO_2 activation remains a major contemporary challenge in organometallic chemistry and the design of well-defined species able to activate CO_2 is a desirable target. In recent years, this field has received increasing interest and several transition metal complexes were found

to undergo CO_2 reductive transformations.[4, 174] Most of the time these species consist of low-valent metal coordination complexes allowing the stepwise addition of electrons or other reagents.[4, 174]

In this purpose, trivalent uranium species, notably because of their reducing ability and their capacity to form polarized metal-ligand bonds, have proved particularly effective to mediate CO_2 activation and reductive transformations[28] which will be described in the present section.

I.3.4.2.2 Isolation of a stabilized $CO_2^{\cdot-}$ radical species

In the quest for new ligands environments, an aminophenolate platform has been developed by the Meyer group for exploring the reactivity of trivalent uranium. In this complex, the U(III) center is tightly bound to anionic aryloxyde moieties, while the coordination to the triazacyclononane (tacn) macrocycle mainly serves to protect one side of the uranium center (***Scheme I.9***), providing a hexacoordinate complex with a single axial coordination site available for reactivity.[128, 176]

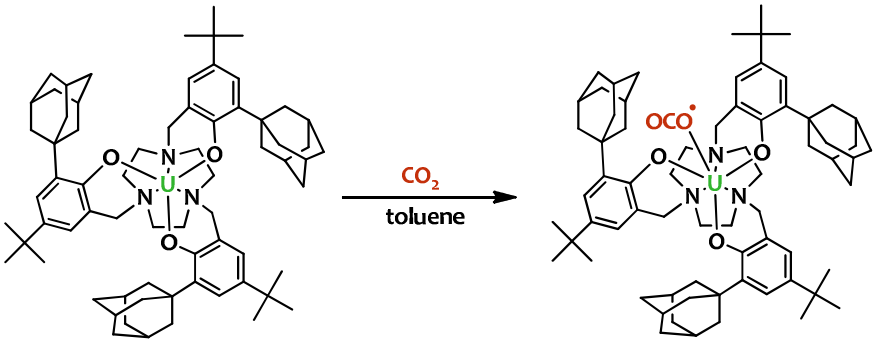

Scheme I.9. Reactivity of the U(III) triazacyclononane-anchored tris-aryloxyde complex [((^{Ad}ArO)$_3$tacn)U] with CO_2.

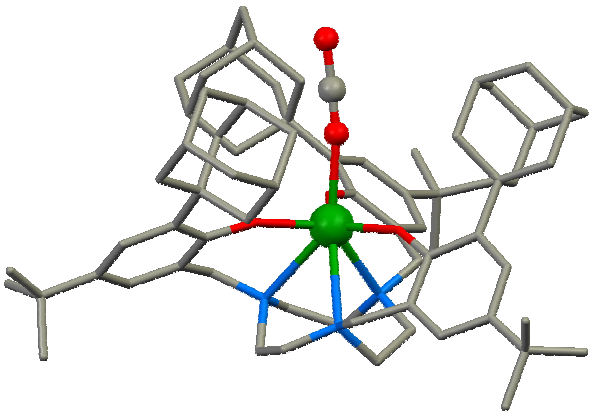

Figure I.8. Mercury diagram of the solid-state molecular structure of [((^{Ad}ArO)$_3$tacn)U(CO_2)].

The reaction of the adamantly-substituted version of this complex afforded a previously unseen end-on η^1-OCO-uranium complex[141] shown in ***Figure I.8***. The experimental data support a one-electron transfer from U to the linearly bound CO_2, thus this unusual complex is best described as a radical

anionic species (U^{IV}=O=C$^{\cdot}$-O^{-}). Meyer proposes that the linearity of the $CO_2^{\cdot-}$ reduced fragment is imposed by the sterically demanding adamantyl groups from the ligand. This study demonstrates the huge potential of U(III) derivatives as potent electron sources to interact with carbon dioxide and reduce this very stable molecule.

I.3.4.2.3 Reductive splitting of CO_2 : formation of U(IV) oxos and CO release

Exchanging the ortho adamantyl substituents on the aryloxide ligand for tert-butyl groups alters the reactivity with CO_2 and results in a two-electron reduction of CO_2 releasing CO and yielding an oxide-bridged U(IV/IV) dimeric species (***Scheme I.10***).[155] The formation of the oxo species plausibly results from the reduction of a U(IV)-$CO_2^{\cdot-}$ species by a second equivalent of U(III) to give a dinuclear CO_2^{2-}-bridged diuranium species which then eliminates CO. Compared to the previous example, the reduced steric pressure allows for dimerization.

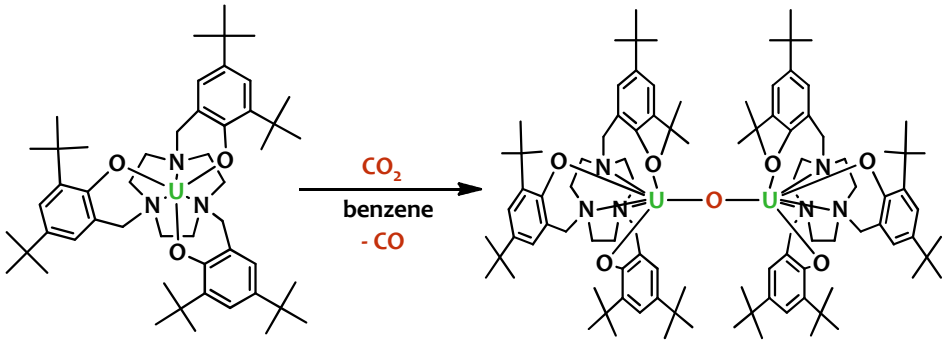

Scheme I.10. CO_2 reductive splitting promoted by the U(III) triazacyclononane-anchored tris-aryloxyde complex [((^{tBu}ArO)$_3$tacn)U].

A similar example of CO_2 reductive cleavage had been previously reported by Ephritikhine and coworkers[177] who discovered that the [U(Cp')$_3$] complex (Cp' = $SiMe_3C_5H_4$) was transformed into the oxo-bridged di-uranium(IV) (μ-O)[U(Cp')$_3$]$_2$ complex upon exposure to CO_2 (***Scheme I.11***).

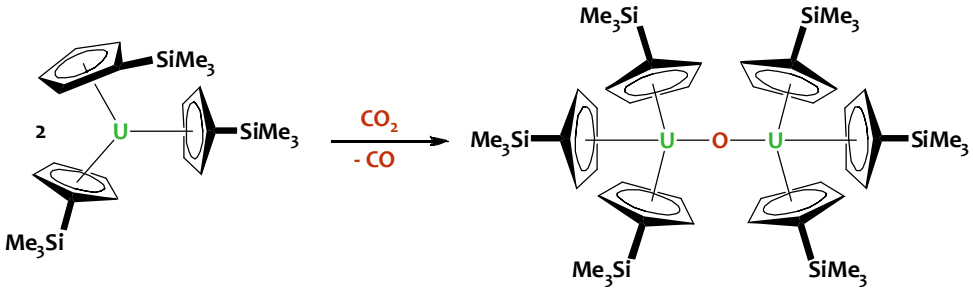

Scheme I.11. CO_2 reductive splitting promoted by the U(III) organometallic complex [U(Cp')$_3$] (Cp' = $SiMe_3C_5H_4$).

I.3.4.2.4 Reductive disproportionation

The reductive disproportionation of CO_2 involves a $2e^-$ reduction of two molecules of CO_2 to yield a carbonate CO_3^{2-} with concomitant evolution of CO (eqn (1)).

$$2\,CO_2 + 2\,e^- = CO_3^{2-} + CO \qquad (1)$$

Such behavior was observed by the Cloke group who demonstrated the ability of the mixed-sandwich U(III) compound $[U(COT^R)(Cp^{R'})]$ (R = $SiMe_3$, $Cp^{R'}$ = C_5Me_5 or C_5HMe_4) to react with CO_2 yielding CO and a U(IV) dinuclear carbonate complex $[(\mu\text{-}\eta^1\text{:}\eta^2\text{-}CO_3)\{U(COT^R)(Cp^{R'})\}_2]$ (***Scheme I.12***-top).[178] Interestingly, the authors observed that traces of the squarate complex $(\mu\text{-}\eta^2\text{:}\eta^2\text{-}C_4O_4)\{\{U(COT^R)(Cp^{R'})\}_2]$ were formed. This compound results from the reductive coupling of CO generated during the course of the reaction by the mixed-sandwich U(III) complex.[27, 151] Since a large excess of CO_2 was used, the formation of the squarate complex implies that the U(III) precursor reacts faster with CO than with CO_2. Accordingly, as shown in ***Scheme I.12***-bottom, the reaction was performed using precisely 8 equivalents of CO_2 for 10 U(III) centers, yielding one equivalent of the bridging squarate complex and four equivalents of the bridging carbonate complex.[178]

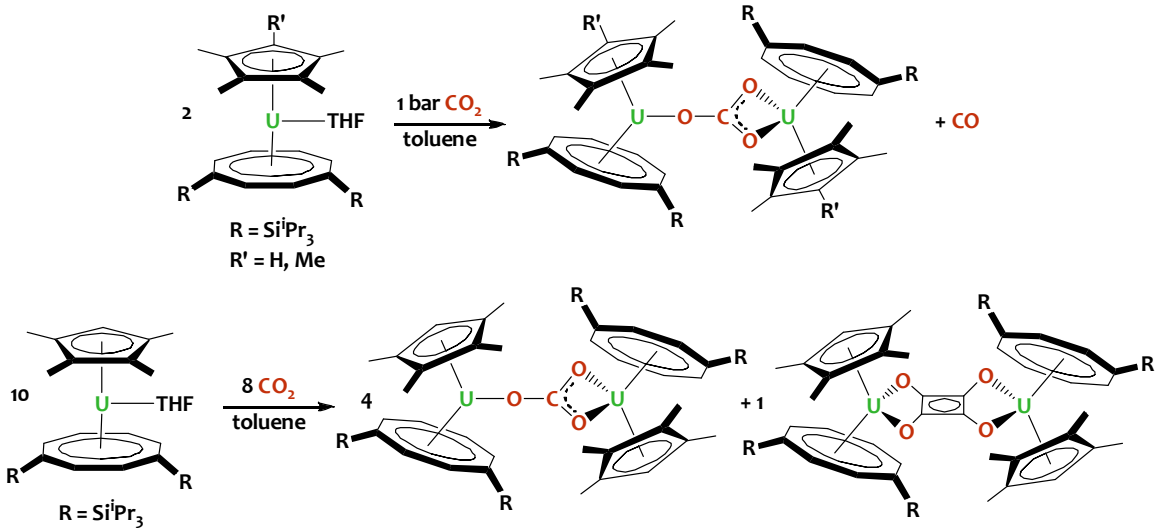

Scheme I.12. Reaction of the mixed-sandwich $[U(COT^R)(Cp^{R'})]$ (R = $SiMe_3$, $Cp^{R'}$ = C_5Me_5 or C_5HMe_4) with (top) excess CO_2 or (bottom) stoichiometric amounts of CO_2.

The Meyer group developed new aryloxide chelating ligands by replacing the tacn anchor by a mesitylene or an amine group to support U(III). Whilst the resulting complexes are structurally related to their tacn counterparts, their reactivity is remarkably different as they promote reductive disproportionation of CO_2 (***Scheme I.13***) to afford bimetallic $\mu\text{-}\eta^2\text{:}\eta^2$ or $\mu\text{-}\eta^1\text{:}\eta^2$ carbonate complexes shown in ***Figure I.9***.[126]

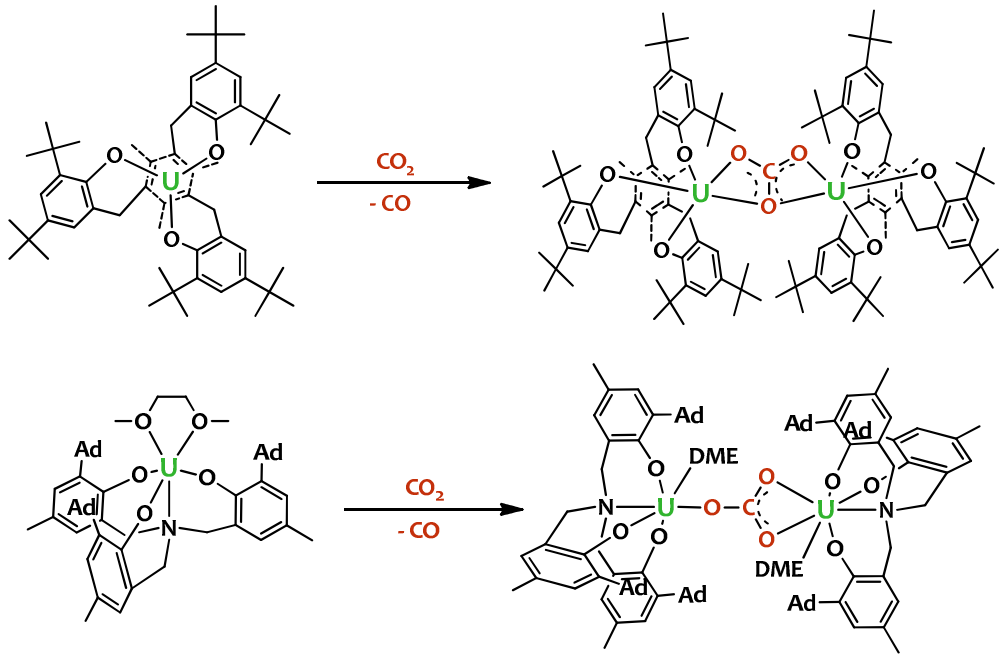

Scheme I.13. CO_2 reductive disproportionation mediated by U(III) aryloxide derivatives gives U(IV) bridging carbonate complexes with concomitant evolution of CO.

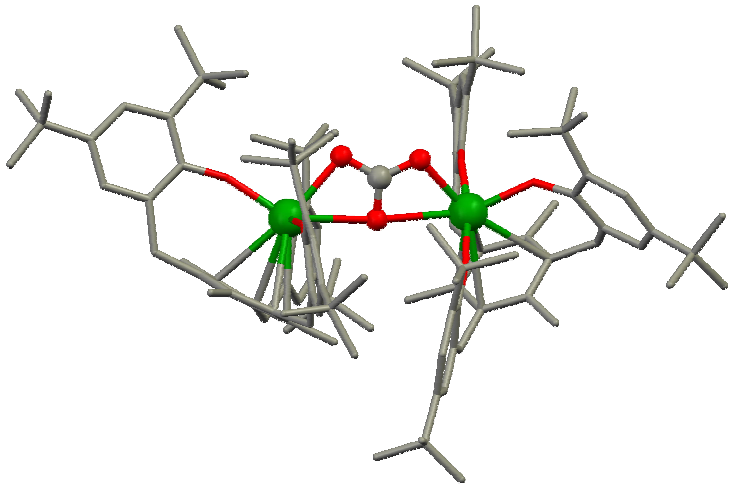

Figure I.9. Mercury diagram of the solid-state molecular structure of the bridging carbonate uranium complex [{((${}^{t\text{-Bu}}$ArO)$_3$mes)U}$_2$(μ-η^2:η^2-CO_3)].

One of the possible mechanisms for the formation of the carbonate-bridged di-uranium(IV) species involves firstly, the formation of an intermediate oxo-bridged species (similar to thoses described earlier in section I.3.4.2.3), followed by CO_2 insertion into the U(IV)-oxo bond. This hypothesis was probed by reacting the independently synthesized U(IV) bridging oxo species with CO_2, which resulted in the formation of the same carbonate species (***Scheme I.14***).[126] A DFT study performed on the reaction pathway suggests this is the correct mechanism.[179]

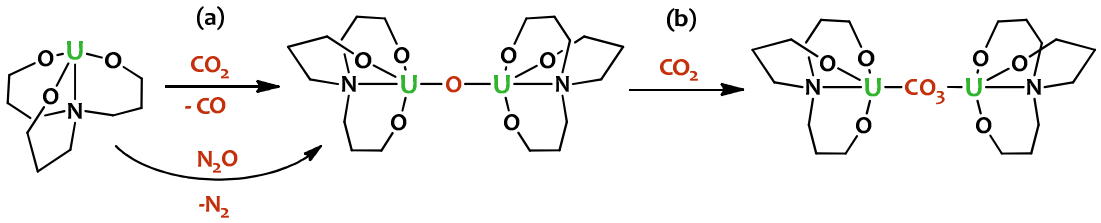

Scheme I.14. Formation of carbonate complex from CO_2 reduction through (a) reductive cleavage of CO_2 and (b) insertion of CO_2 into the intermediate oxo-bridged complex.

Interestingly, the U(IV) bridging oxo and carbonate complexes can be reduced back to U(III) using potassium graphite, eliminating K_2O and K_2CO_3.[180] However, this synthetic cycle is limited by the precipitation of an insoluble carbonate-containing tetranuclear U(IV) complex $\{[((^{Neop,Me}ArO)_3tacn)U(K_2\text{-}CO_3)]K\}_4$.[180]

Finally, it is to be noted that upon exposure to CO_2, the homoleptic $[U(OAr)_3]$ (Ar = 2,6-$^tBu_2C_6H_3$) complex is oxidized to U(IV), affording $[U(OAr)_4]$ as the major product via ligand redistribution (Scheme I.15). However, the occurrence of carbonate or oxo ligand co-products was not investigated.[71, 93] This denotes the interest of using chelating agents to avoid ligand redistribution processes.

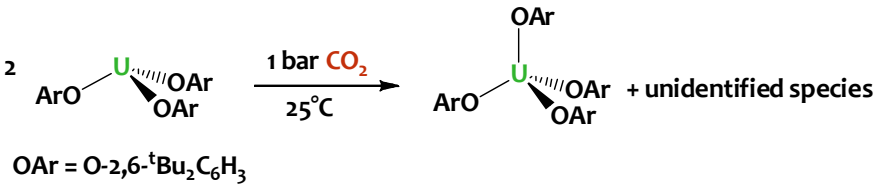

Scheme I.15. Reaction of $[U(OAr)_3]$ with CO_2.

I.3.4.2.5 Insertion into U-X bonds (X = C, N, O, S)

Insertion of CO_2 into metal-ligand bonds is a common occurrence with transition-metal complexes and several examples have been reported with U(IV) and Th(IV) species.[181-186] As discussed previously, Meyer and coworkers further demonstrated that carbonate U(IV) complexes could form through CO_2 insertion into the U(IV)-oxo metal bond[126, 179] and recently extended this study to U(IV) bridging sulfidos and selenidos complexes.[187]

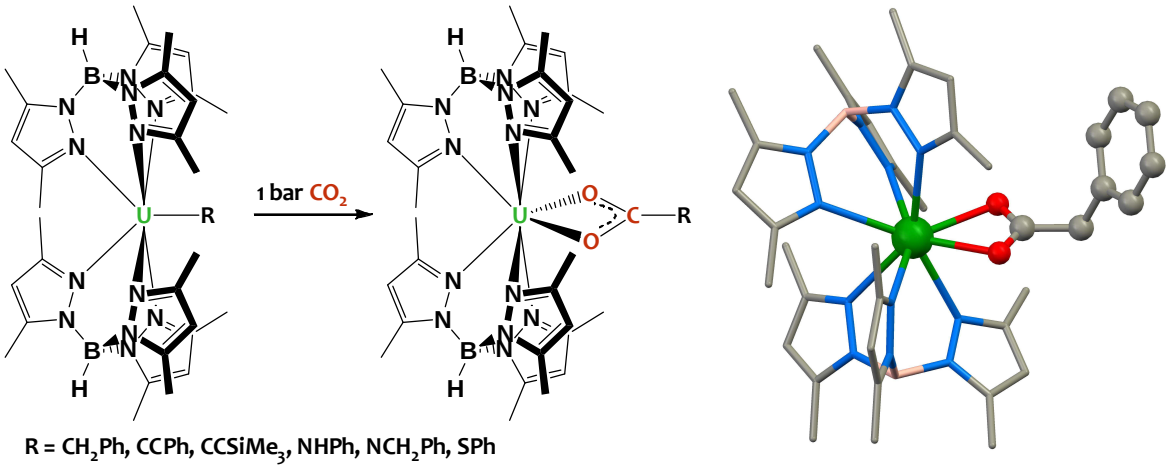

Figure I.10. (left) Formation of U(III) carboxylate derivatives from CO_2 insertion into U(III)-X bonds (X = C, N, S). (right) Mercury diagram of the solid-state molecular structure of the U(III) carboxylate complex $[U(PhCH_2CO_2)(Tp^*)_2]$ (Tp^* = hydrotris(3,5-dimethylpyrazolyl)borate).

In U(III) chemistry, CO_2 insertion into U–C, U-N and U-S bonds has been recently reported by Bart and coworkers,[138, 188] yielding rare U(III) carboxylate derivatives as depicted in ***Figure I.10***. These are unique examples upon which trivalent uranium is not oxidized by CO_2.

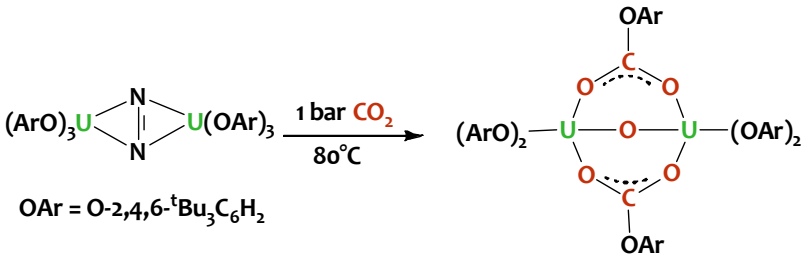

Scheme I.16. The dinitrogen U(III) complex $[\{U(OAr)_3\}_2(\mu\text{-}\eta^2\text{-}\eta^2\text{-}N_2)]$ promotes both CO_2 cleavage and insertion into the metal-ligand bonds.

Upon heating, the dinitrogen adduct $[\{U(OAr)_3\}_2(\mu\text{-}\eta^2\text{-}\eta^2\text{-}N_2)]$ (Ar = 2,4,6-^{t}Bu$_3$C$_6$H$_2$) releases the N_2 molecule and simultaneously insert two CO_2 molecules into the U-O bonds and abstract oxygen from CO_2 to yield the oxo-briged dicarbonato species $[\{U(OAr)_2\}_2(\mu\text{-}O)(\mu\text{-}O_2COAr)]$ (***Scheme I.16***).[93] CO_2 is also suspected to insert into the U-N bonds of the trivalent uranium complex $[U\{N(SiMe_3)_2\}_3]$, resulting in a carbamate species which then eliminates the isocyanate O=C=NSiMe$_3$ to give the U(IV) $[U(OSiMe_3)_4]$ complex.[93] Similar behavior was proposed for the U(III) N-heterocyclic carbene complex $[UL\{N(SiMe_3)_2\}_2]$ (L = bidentate alkoxy-tethered NHC ligand).[189] Unfortunately in both cases these species could not be crystallographically characterized.

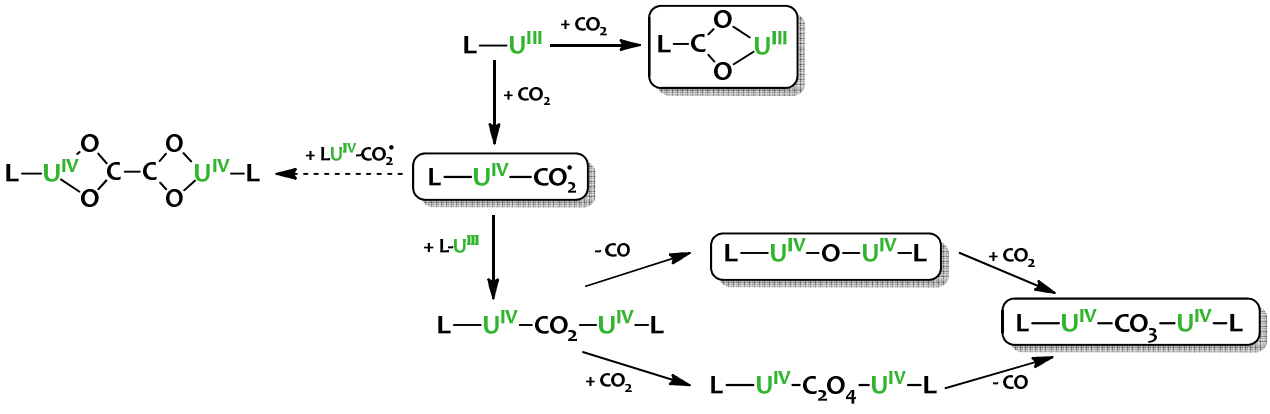

Scheme I.17. General overview of U(III)-mediated CO_2 activation.

Altogether these examples illustrate the rich CO_2 chemistry which can be achieved with uranium molecular species. ***Scheme I.17*** gives a global picture of the various possibilities offered. These studies highlight the crucial role of the ancillary ligands. Notably, the reaction with CO_2 is strongly impacted by the ligand steric and flexibility properties which control reactivity. Extremely bulky ancillary ligands prevent dimerization and result in the formation of the one-electron reduced $CO_2^{\bullet-}$ radical. Otherwise, the system undergoes a second single-electron transfer from a second U(III) center which then evolves to the formation of U(IV) bridging oxo or carbonate complex depending on the steric and flexibility features of the ligand. While it has been shown that carbonate complexes can originate from oxo species, alternative pathways, such as addition of CO_2 onto the transient U(IV)-CO_2^{2-}-U(IV) species, remain a possibility.

This chemistry remains in its early stages, and great findings can be anticipated in the near future. For instance, theory predicts that the reductive coupling of CO_2 to afford oxalates is a viable alternative.[179] The proper conditions for the formation of a preferred oxalate product from CO_2 reduction are still to be discovered. Reductive transformations of CO_2 using catalytic loadings of uranium might also be possible.

I.3.4.3 CS_2 and COS activation by low-valent uranium

The isoelectronic heteroallenes COS and CS_2 are often used as models for CO_2 reactivity. However, the C=S bonds in these molecules are much less polar compared to the C=O bonds, and these species are generally more reactive and easily reduced than their fully oxygenated analogue.

A single example of a CS_2^{2-} uranium(IV) complex was reported by Brennan and co-workers in 1986.[190] The U(IV)-U(IV) dimer $[(Cp')_3U]_2[\mu\text{-}\eta^1,\eta^2\text{-}CS_2]$ (Cp' = $SiMe_3C_5H_4$) was obtained from the reduction of

CS_2 by the U(III) complex $[(Cp)_3U]$ (Scheme I.18). This result contrasts with the reaction of the same U(III) complex with CO_2 which afforded CO and an oxo-bridged di-uranium(IV) complex, as mentioned earlier. Recent DFT studies revealed that the difference in reactivity is due to the low stability of the CS molecule compared to CO.[191]

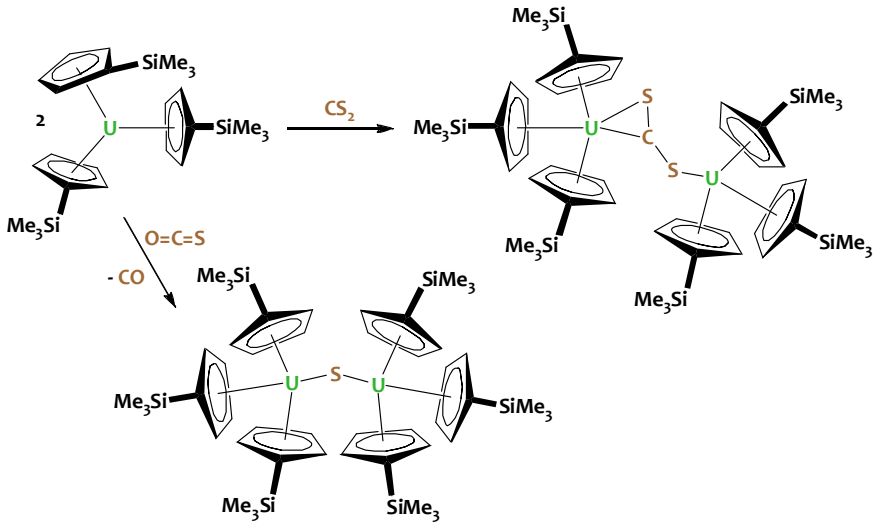

Scheme I.18. Reaction of $[U(Cp')_3]$ (Cp' = $SiMe_3C_5H_4$) with CS_2 and COS.

Comparatively, as shown in **Scheme *I.17*** and ***Scheme I.19***, the reaction of U(III) complexes with COS affords bridging sulfido U(IV) complexes.[71, 190] The reaction pathway involves the formation of a μ-COS^{2-} U(IV)/U(IV) intermediate analogous to that obtained with CS_2, which is not isolable because of the fast release of the CO molecule.[191] This suggests that the formation of CO versus CS is a higher driving force than the formation of a bridging uranium oxo molecule compared to its sulfido analogue.

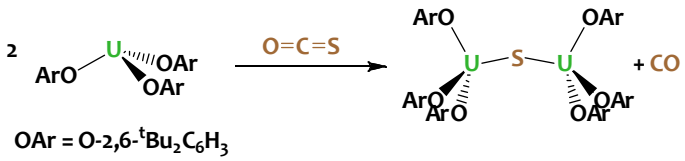

Scheme I.19. Synthesis of a sulfido-bridged U(IV) complex by reduction of COS with a U(III) aryloxide complex.

Recently, the Meyer group reported the formation of a mixture of diuranium bridged trithiocarbonate and tetrathiooxalate complexes (Scheme I.20) from the reduction of CS_2 by trivalent uranium supported by a multidentate phenolate tripodal ligand $[(^{Ad}ArO)_3N)U(DME)]$.[192, 193] These two products arise from two competitive reaction pathways : the reductive C-C coupling of two $CS_2^{\cdot-}$ radicals yielding $C_2S_4^{2-}$ and the reductive disproportionation of CS_2 involving a bridging sulfido intermediate. DFT studies indicated the CS_2^{2-} bridged U(IV)/U(IV) dimer as a reasonable

intermediate in the formation of the trithiocarbonate product. However, this intermediate was not experimentally observed.

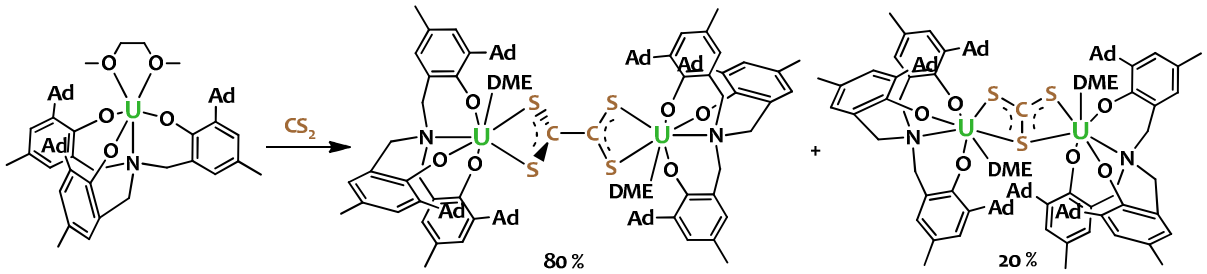

Scheme I.20. Reaction of [(^{Ad}ArO)$_3$N)U(DME)] with carbon disulfide.

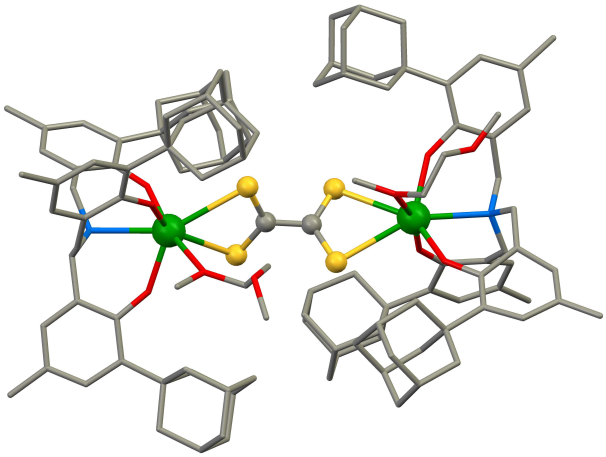

Figure I.11. Mercury diagram of the solid-state molecular structure of the tetrathiocarbonate adduct [(μ-η^2:η^2-C_2S_4){(^{Ad}ArO)$_3$N)U(DME)}$_2$].

Finally, Bart reported that insertion chemistry into the U(III)-C bond similar to that observed with CO_2 is also occurring with CS_2 **(Scheme I.21)**.[138]

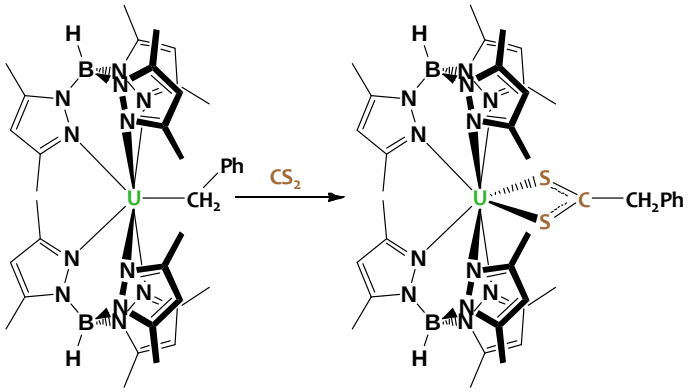

Scheme I.21. Insertion of CS_2 into the uranium-carbon bond of a trivalent uranium alkyl derivative.

I.3.4.4 Azides activation by trivalent uranium

Inorganic and organic azides can undergo two-electron reduction, resulting in the liberation of dinitrogen and formation of respectively a nitride (eqn.2) or an imide (eqn.3) ion. Therefore, a classic route to metal-imides and metal-nitrides involves the reaction of organic and inorganic azides with reducing metal complexes.[184, 194]

$$N_3^- + 2\,e^- = N^{3-} + N_2 \quad (2) \qquad\qquad RN_3 + 2\,e^- = RN^{2-} + N_2 \quad (3)$$

Nitrido and imido complexes have been the focus of numerous studies in transition metal chemistry owing to their important implication in nitrogen fixation, atom and group transfer reactions, and catalysis.[194, 195] Since the first reports in the 1980s of uranium-imido complexes[196, 197] there has been increased interest in actinide compounds containing metal-nitrogen multiple bonds.[60, 164, 165, 198, 199] The focus on such compounds has been driven by the possibility of promoting novel reactivity and catalytic transformations as a result of the larger size of actinides and of the involvement of f-orbitals in bonding.[20, 23, 26] Moreover actinide imido and nitrido complexes are particularly attractive species for gaining a better understanding of the nature of bonding in molecular actinide species,[42, 200-204] which is relevant to the problem of spent nuclear fuel reprocessing.[44-46, 136, 205] Interest in uranium nitrides also arises from the possibility of utilizing uranium nitride as an alternative nuclear fuel in generation-IV power reactors because of its higher melting point and enhanced thermal conductivity compared to the currently used uranium oxides.[206, 207] Therefore investigations on the reaction of U(III) precursors with azido derivatives offer numerous opportunities.

I.3.4.4.1 Inorganic azides

Few molecular uranium nitride complexes have been isolated thus far. In contrast to the first example of a uranium nitride, which was isolated from the dinitrogen reduction by a highly reactive "ate" complex of U(III),[157] and an octanuclear uranium nitride cluster also obtained from N_2 reduction,[160] all complexes have been obtained via the reaction of low valent uranium with inorganic azides. Photolytic activation of U(IV) azido complexes has also been investigated, but while transient nitride species are formed, decomposition through C–H bond activation prevented their isolation.[168, 208]

The nitride ion, N^{3-}, is an excellent π-donor ligand which is known to act as a bridging ligand in μ^2, μ^3 or μ^4 coordination modes resulting in the formation of polynuclear complexes. The geometry of the resulting nitride complexes is therefore strongly impacted by the ancillary ligands steric pressure, as illustrated below.

The unique polynuclear uranium complex featuring a μ^4-nitride group, $([U_4(\mu^4\text{-}N)(\mu\text{-}1,1\text{-}N_3)_8(CH_3CN)_8I_6][(Cs(CH_3CN)_3])_n$, has been isolated in our group[209] through the use of the tetravalent uranium azide complex $[U(N_3)_7Cs_3]$ as nitrogen source (***Scheme I.22***). In this azido/nitrido cluster, the μ^4-N^{3-} moiety bridges four U(IV) centers placed at the edges of a tetrahedron (Figure I.12-right). Eight end-on azide moieties bridge the uranium centers along the vertices of the tetrahedron defined by the four uranium centers. The obtention of a μ^4-nitride is most probably due to the absence of any bulky ancillary ligand in the reaction media.

$$2\,[UI_3(THF)_4] + 2\,[U(N_3)_7Cs_3] \xrightarrow[-N_2,\,-5\,CsN_3]{MeCN} \{[U_4(\mu_4\text{-}N)(\mu\text{-}1,1\text{-}N_3)_8(CH_3CN)_8I_6][Cs(CH_3CN)_3]\}_n$$

Scheme I.22. Synthesis of a nitrido/azido uranium cluster obtained by reduction of a uranium(IV) azide precursor by $[UI_3(THF)_4]$.

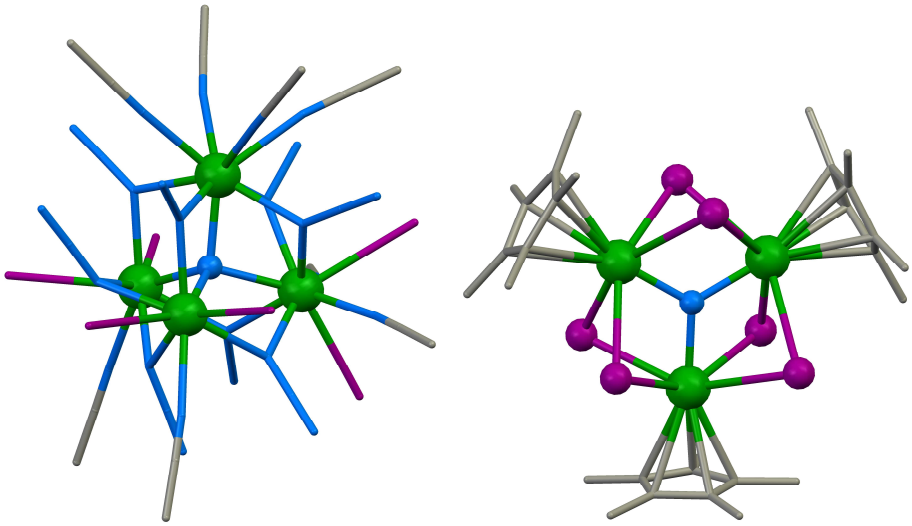

Figure I.12. Mercury diagrams of the solid-state molecular structures of the uranium nitrido clusters $([U_4(\mu^4\text{-}N)(\mu\text{-}1,1\text{-}N_3)_8(CH_3CN)_8I_6][(Cs(CH_3CN)_3])_n$ (left) and $[U(Cp^*)(\mu\text{-}I)_2]_3(\mu^3\text{-}N)$ (right).

The reaction of the U(III) precursor $[U(Cp^*)I_2(THF)_3]$ with sodium azide (Scheme I.23), reported by the Evans' group, results in the formation of the trinuclear U(IV) cluster $[\{U(Cp^*)(\mu\text{-}I)_2\}_3(\mu^3\text{-}N)]$ which features a central μ^3-nitride moiety, as highlighted in Figure I.12-right.[210] Cloke and coworkers discovered that the oxide analogue $[\{(U(Cp^*)(\mu^2\text{-}I)_2\}_3(\mu^3\text{-}O)]$ was formed upon cleavage of ethers from the same U(III) precursor.[83] These compounds have different color and NMR spectra, crystallize in different space groups, and the identity of the nitrido moiety was further confirmed by mass spectrometry and labelling experiments.[160]

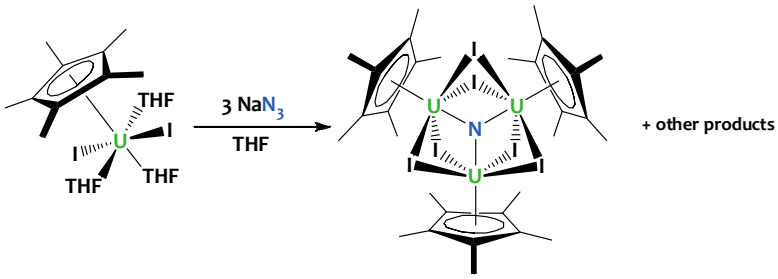

Scheme I.23. Synthesis of a uranium nitride cluster by reduction of sodium azide by the trivalent uranium complex $[U(Cp^*)I_2(THF)_3]$.

The Evans group also reported the formation of the 24-membered uranium-nitrogen ring $[(Cp^*)_2U(\mu\text{-}N)U(\mu\text{-}N_3)(Cp^*)_2]_4$ resulting from the association of nitrido and azido ligands bridging eight U(IV) cations.[211] This complex is the result of the reduction of four azide anions by eight equivalents of the U(III) complex $[U(Cp^*)_2(BPh_4)]$ (Scheme I.24). The molecular structure is composed of nearly linear U=N=U linkages associated by bidentate end-on coordinated azido ligands.

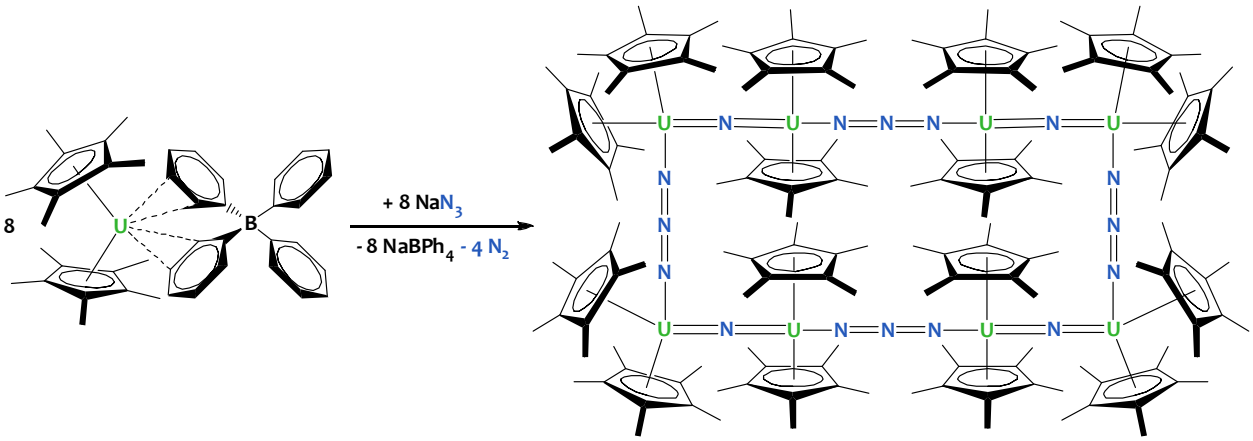

Scheme I.24. Synthesis of an octanuclear uranium nitrido/azido cluster by reduction of sodium azide with the trivalent uranium complex $[U(Cp^*)_2(BPh_4)]$.

From these three examples, one can notice that the presence of zero, one or two bulky Cp* ligands in the coordination sphere of the trivalent uranium precursors resulted in the formation of μ^4, μ^3 and μ^2 species respectively. As one could expect, the structure of nitride complexes resulting from the reduction of azides by U(III) is thus affected by the number of bulky ancillary ligands and their steric properties.

The reaction of sodium or tetrabutylammonium azide with the U(III) complex $[U(N^tBuAr)_3(THF)]$ (Ar = 3,5-$Me_2C_6H_3$) featuring three bulky amido supporting ligands yielded the dinuclear μ^2-nitride bridged uranium(IV) complex $\{(\mu^2\text{-}N)[U(N^tBuAr)_3]_2\}^-$ (***Scheme I.25***).[212] This compound features a U=N=U linear unit (***Figure I.13***) comparable to thoses found in the $[(Cp^*)_2U(\mu\text{-}N)U(\mu\text{-}N_3)(Cp^*)_2]_4$ complex described above. The presence of three bulky amides prevents the coordination of

additional N^{3-} ligands to the U(IV) cations. This dimer can be quantitatively oxidized to form the analogous U(V)/U(IV) and U(V)/U(V) complexes.[212]

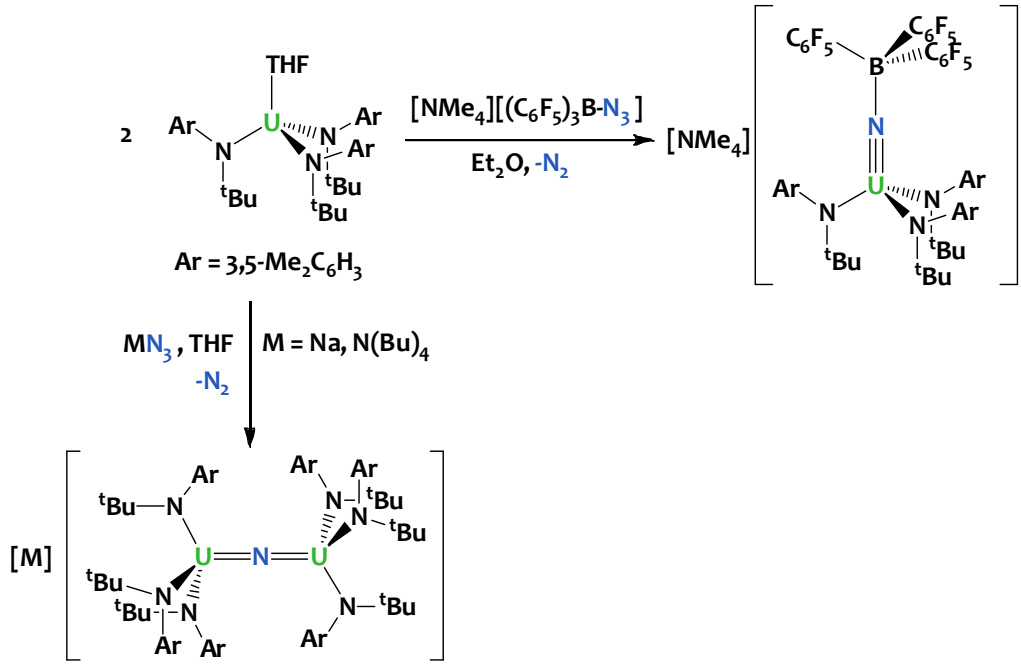

Scheme I.25. Reaction of the U(III) amido complex $[U(N^tBuAr)_3(THF)]$ (Ar = 3,5-$Me_2C_6H_3$) with azido derivatives.

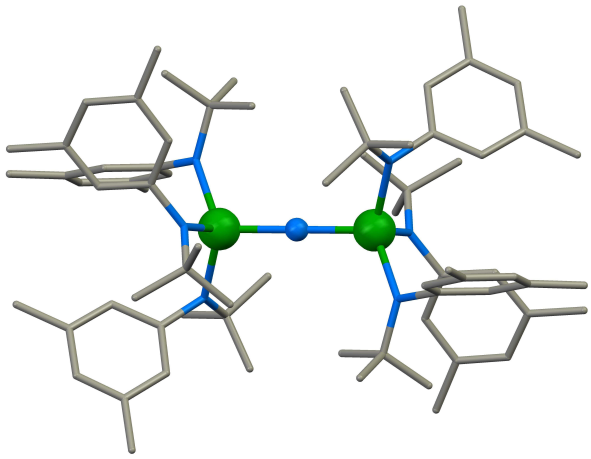

Figure I.13. Mercury diagram of the solid-state molecular structure of the linear uranium nitride dimer $\{(\mu^2\text{-}N)[U(N^tBuAr)_3]_2\}^-$.

The nitride fragments in these complexes form bridging linkages between uranium centers. These interactions might quench the potential reactivity of the uranium nitrogen bond, making the generation of a terminal uranium nitride complex an important goal.

In this effort, the Cummins group reported the synthesis of a borane-capped uranium nitride[213] obtained by reduction of the azidoborate salt $[NMe_4][(C_6F_5)B\text{-}N_3]$ by $[U(N^tBuAr)_3(THF)]$ (Ar = 3,5-

$Me_2C_6H_3$) (***Scheme I.25***). However, attempts to remove the borane protecting group were unsuccessful.

Hayton and coworkers used the more sterically crowded $[U\{N(SiMe_3)_2\}_3]$ trivalent uranium tris-silylamide presumably with the idea that a higher steric pressure could prevent dimerization. However, the reaction of $[U\{N(SiMe_3)_2\}_3]$ with sodium azide affords the dinuclear $[Na(DME)_2(TMEDA)][(NR_2)_2U(\mu\text{-}N)(CH_2SiMe_2NR)U(NR_2)_2]$ complex (***Scheme I.26***) featuring a bent UNU motif as shown on ***Figure I.14***.[214] The formation of the nitride is accompanied by the deprotonation of a $SiMe_3$ group from the silylamido ligand, a common feature for uranium[143, 147, 215, 216] and more generally f-element complexes within this ligand environment.[217]

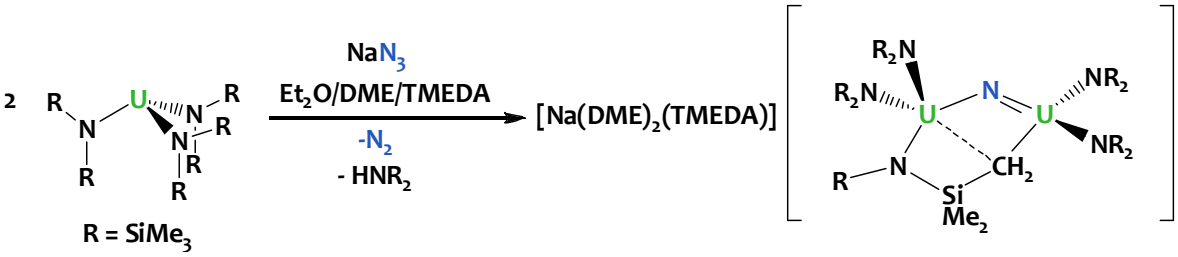

Scheme I.26. The reaction of sodium azide with $[U\{N(SiMe_3)_2\}_3]$ yields a dinuclear bridging nitride U(IV) complex.

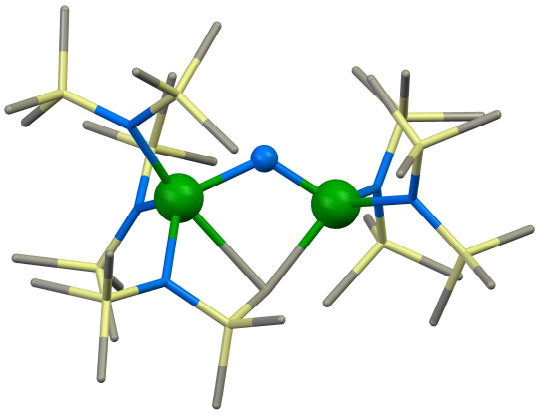

Figure I.14. Mercury diagram of the solid-state molecular structure of the anionic $[(NR_2)_2U(\mu\text{-}N)(CH_2SiMe_2NR)U(NR_2)_2]^-$ bridging nitrido complex.

In 2012 a U(V) terminal nitride was isolated by Liddle,[140] achieving the quest of a terminal UN moiety. As shown in ***Scheme I.27***, uranium(III) supported by the chelate tripodal silylamido $Tren^{TIPS}$ ligand reacts with sodium azide, yielding the sodium-bridged pentavalent uranium nitride complex $\{[Na][U(N)(Tren^{TIPS})]\}_2$. Removal of the coordinated sodium countercations was achieved by addition of 12c4 crown ether, which proved more efficient than 15c5 (***Scheme I.27***). The synthesis was performed in pyridine, a solvent which is generally avoided in U(III) chemistry since U(III) species frequently reduce this heterocycle. However, the authors discovered that the terminal nitride

complex was decomposing in ether solvent, possibly explaining why terminal nitrides were not isolated before.

Of note the reaction with the azidoborate salt $[NMe_4][(C_6F_5)B\text{-}N_3]$ did not gives the expected borane-capped nitride complex, but the U(IV) amino complex $[U(NH_2)(Tren^{TIPS})]$.[168] According to the authors, this is due to the high basicity of the terminal U(V) nitride which, in absence of stabilizing coordinated sodium atoms, abstracts hydrogens from the toluene solvent.

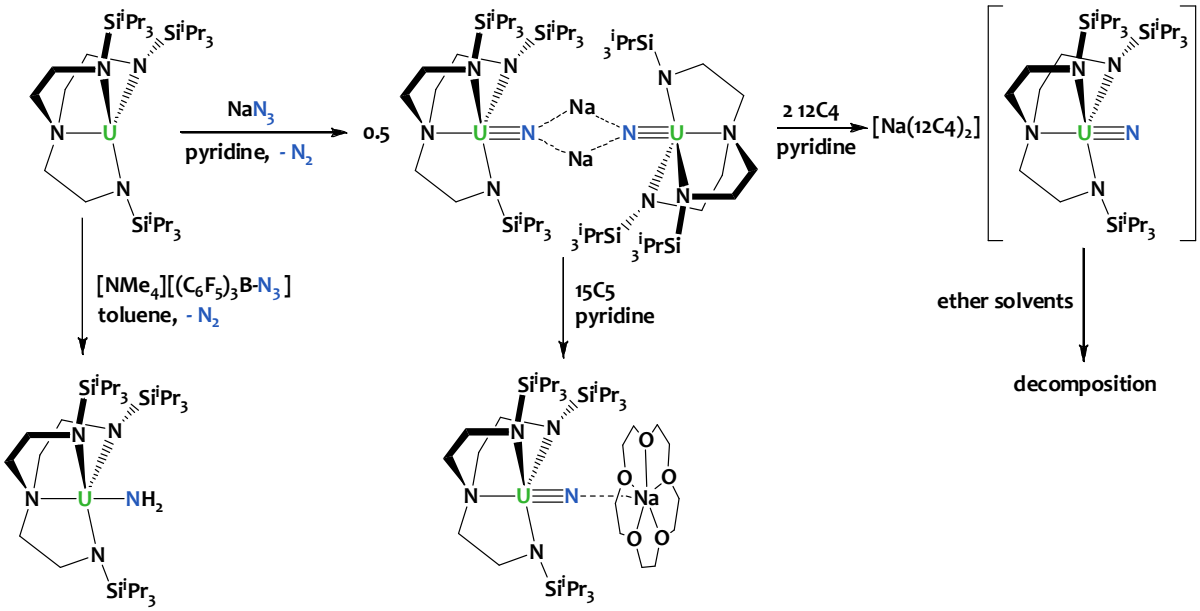

Scheme I.27. Isolation of the first terminal uranium nitride by reduction of sodium azide with the trivalent uranium complex $[U(Tren^{TIPS})]$. The reaction with the borate-capped azido derivative $[NMe_4][(C_6F_5)B\text{-}N_3]$ resuts in the formation of a U(IV) amino species.

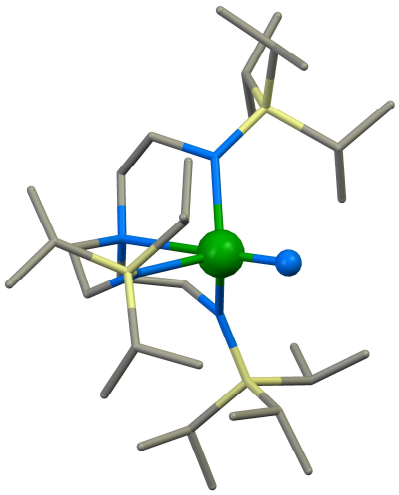

Figure I.15. Mercury diagram of the solid-state molecular structure of the U(V) terminal nitride $[U(N)(Tren^{TIPS})]^-$.

In summary, the studies detailed above reveal that the steric and electronic environments at the uranium center have a critical impact on the formation of nitrido complexes, on their geometry and stability. A careful tuning of the reaction conditions is also essential.

Finally, the reaction of U(III) complexes with inorganic azides also provides a convenient route to U(IV) azido compounds. Indeed, choosing an azide source bearing an oxidizing metal countercation results preferentially in the reduction of the later rather than of the azide ion by U(III). This strategy has been successfully utilized by the Kiplinger's group who reported that $[(Ph_3P)AuN_3]$ oxidizes the organouranium(III) complex $[U(Cp^*)_2(OAr)(THF)]$ (Ar = 2,6-(^{i}Pr)$_2$-C$_6$H$_3$) to give the U(IV) azido complex $[U(Cp^*)_2(OAr)(N_3)]$ (***Scheme I.28***).[218]

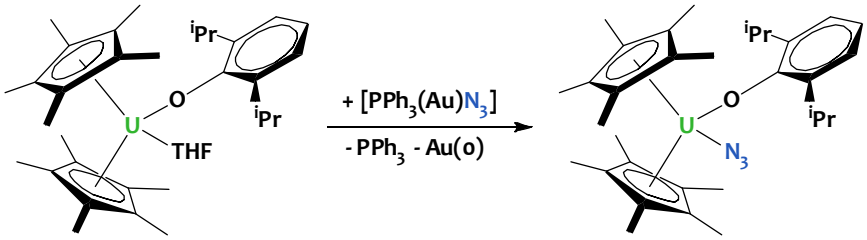

Scheme I.28. Synthesis of a U(IV) azido complex by oxidation of a U(III) precursor using the azide transfer reagent $[PPh_3(Au)N_3]$.

I.3.4.4.2 Organic azides

The reaction of U(III) complexes with organic azides proved to be an effective synthetic route to U(V) organoimidos (***Scheme I.29***). The first example was reported in 1985 by D. Andersen who showed that $[U(MeC_5H_4)_3(THF)]$ reacts with Me_3SiN_3 or PhN_3 at room temperature with evolution of dinitrogen to give $[(MeC_5H_4)_3U{=}NR]$.[197] Extending this reaction to diazidobenzene derivatives afforded the dinuclear $[(MeC_5H_4)_3U{=}N{-}(C_6H_4){-}N{=}U(MeC_5H_4)]$ pentavalent uranium compounds presenting evidence of magnetic interaction.[219] Since then, several other examples have been reported via the same synthetic strategy.[166, 168, 176, 184, 204, 220-222]

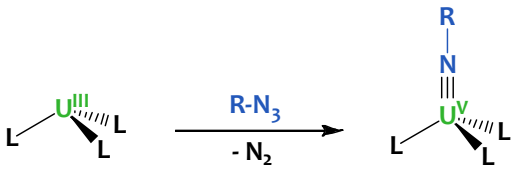

R = TMS, Ph, Mes, Ad, CPh$_3$

Scheme I.29. The reaction of organic azides with U(III) complexes generally affords U(V) organoimide derivatives.

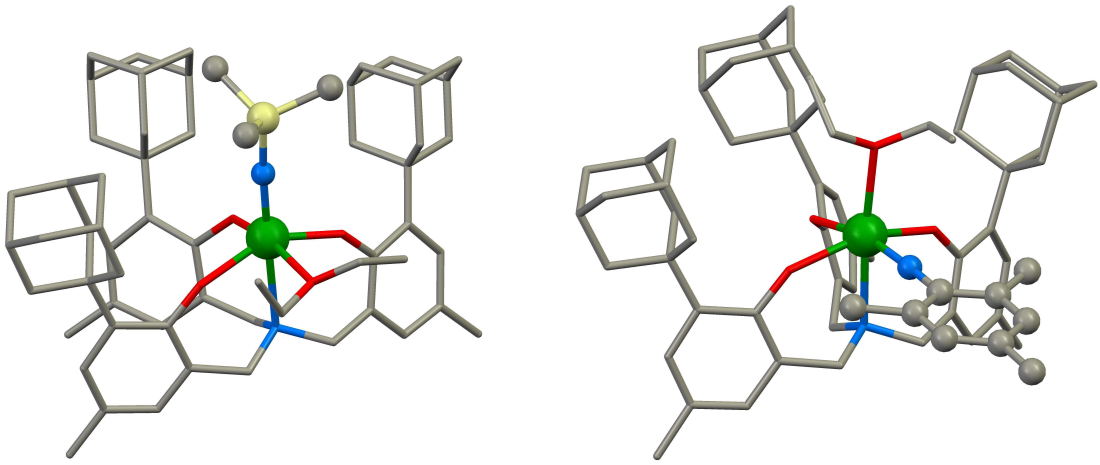

Figure I.16. Mercury diagrams of the solid-state molecular structures of U(V) terminal imido species supported by a tripodal aminophenolate ancillary ligand.

Such compounds, in which uranium is multiply bonded to a ligand, are particularly important as they provide experimental data allowing to further our understanding of the nature of the bonding in uranium complexes.[165] For instance, Meyer and co-workers have observed recently in the solid-state structure of the U(V) mesitylimide complex [((^{Ad}ArO)$_3$N)U(NMes)] (***Figure I.16***-right) that the imido ligand occupies an equatorial coordination site that is trans to an aryloxide group. This is in contrast to the analogous [((^{Ad}ArO)$_3$N)U(NTMS)] complex in which the imido ligand is classically coordinated in apical position (***Figure I.16***-left).[204] This is an interesting manifestation of the inverse trans influence phenomenon.[223]

U(V) imidos species are also particularly desirable for their reactivity. Specifically, it has been shown that these complexes could promote nitrogen-atom transfer events.[184, 221]

One possibility for the limited number of isolated U(V) imido compounds is that, depending on the supporting ligands and depending on the azide substituent, the reaction of U(III) complexes with organic azides can follow alternative pathways leading to multiple products.[26]

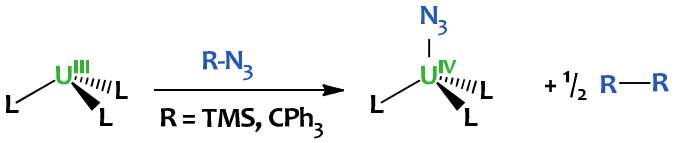

Scheme I.30. Formation of U(IV) azido complexes from homolytic cleavage of the N-R bond of organic azides mediated by U(III) species.

In several instances,[26, 176, 204] the formation of tetravalent uranium azido complexes was observed (Scheme I.30). The Meyer group has shown that the tetravalent azido complexes are the result of N-R homolytic cleavage resulting in radical elimination of a R$^{\cdot}$ group, which subsequently recombines to

form R-R. Notably, the yield of the U(IV) azido products is increased when using trityl azide because of the particular stability of the trityl radical which couples to give Gomberg's dimer.[26]

Treatment of the U(III) N-heterocyclic carbene complex $[U(L)\{N(SiMe_3)_2\}_2]$ (L = $OCMe_2CH_2\{C(NCH_2CH_2NR)\}$) with trimethylsilyl azide did not involved the conversion of U(III) to a U(V) imido complex but rather Arnold and coworkers observed addition of the silyl azide across the uranium-carbene bond (***Scheme I.31***). The resulting $[U(N_3)(L\text{-}SiMe_3)(\{N(SiMe_3)_2\}_2]$ compound is thermally unstable, and rearranges to give, among other products, the U(IV) azido complex $[U(N_3)_2(L)_2]$ where the uranium-carbene bonds have been restored.[122]

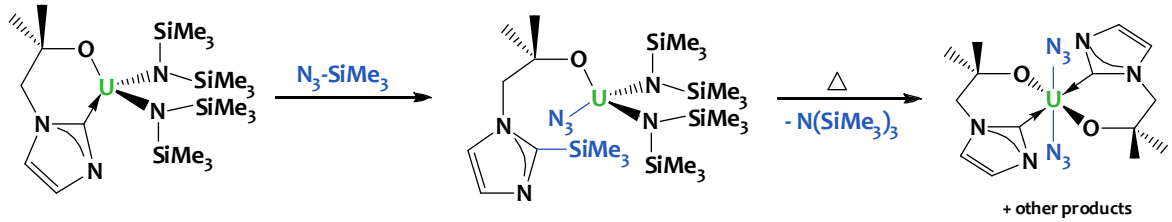

Scheme I.31. Reaction of $[U(L)\{N(SiMe_3)_2\}_2]$ (L = $OCMe_2CH_2\{C(NCH_2CH_2NR)\}$) with TMS azide.

In 2012, Bart and coworkers utilized the U(III) alkyl complex $[U(Tp^*)_2(CH_2Ph)]$ (Tp* = tris(3,5-dimethylpyrazolyl)borate) to prepare U(IV) imido complexes (***Scheme I.32***) by extrusion of 1,2-diphenyl ethane from the uranium precursor.[224] Again, the formation of U(IV) imidos contrast with the more usual two-electron oxidation of U(III) to give U(V) imido compounds. It is also to note that insertion of the azide moiety into the U-C bond rather than oxidation of the metal ion preferably occurs with U(IV) alkyls.[225]

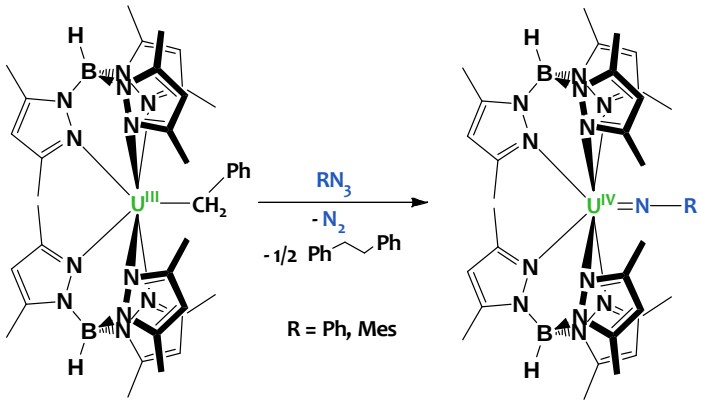

Scheme I.32. Synthesis of U(IV) imido complexes from reaction of U(III) with organic azides.

Finally, in a single occurence the reaction of a U(III) organometallic compound with organic azides produced a mixture of U(IV) and U(VI) products. The reaction of two equivalents of the *in-situ* synthesized trivalent *ate* complex $[Na][U(Cp^*)_2Cl_2]$ with RN_3 (R = Ad, Ph) yields the U(VI) cis-bis(imido) $[U(Cp^*)(NR)_2]$ and the U(IV) bis-chloride $[U(Cp^*)_2Cl_2]$ species (***Scheme I.33***).[226] The

mechanism proposed by the authors is based on previously reported reactivity of U(V) imides with U(III)[227] and involves the comproportionation of the putative U(V) intermediate ([$(C_5Me_5)_2UCl(N=R)$] with the U(III) starting complex [$(C_5Me_5)_2UCl_2$]$^-$ to afford the imido [$(C_5Me_5)_2U(N=R)$] and the bis-chloride [$(C_5Me_5)_2UCl_2$] U(IV) complexes. Further reaction of the U(IV) imido with azide yields the U(VI) cis-bis(imido) product.

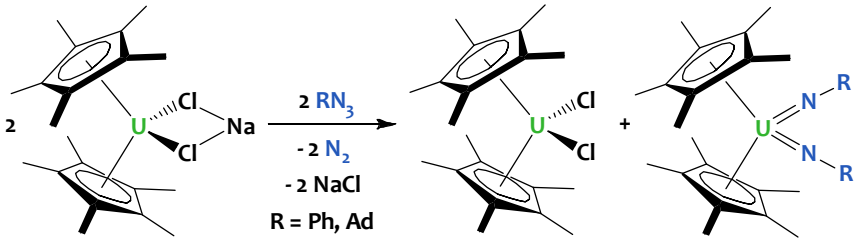

Scheme I.33. Reaction of [Na][$U(Cp^*)_2Cl_2$] with RN_3 (R = Ad, Ph).

Considering the ability of U(III) complexes to mediate azide activation, it is not surprising that this synthetic route has been explored by several groups as an entry to imidos derivatives. However, several alternative synthetic procedures are also available, including the reaction of [$UI_3(THF)_4$] with amines in presence of iodine[169, 170] or the reaction of UCl_4 with amido derivatives[228] which yielded rare U(VI) and U(V) bis(imido) complexes presenting two imido groups in a trans configurations (***Scheme I.34***). These compounds, which contain a [$U(NR)_2$] fragment isostructural of the uranyl [UO_2] motif, have so far proven elusive using the azide route.

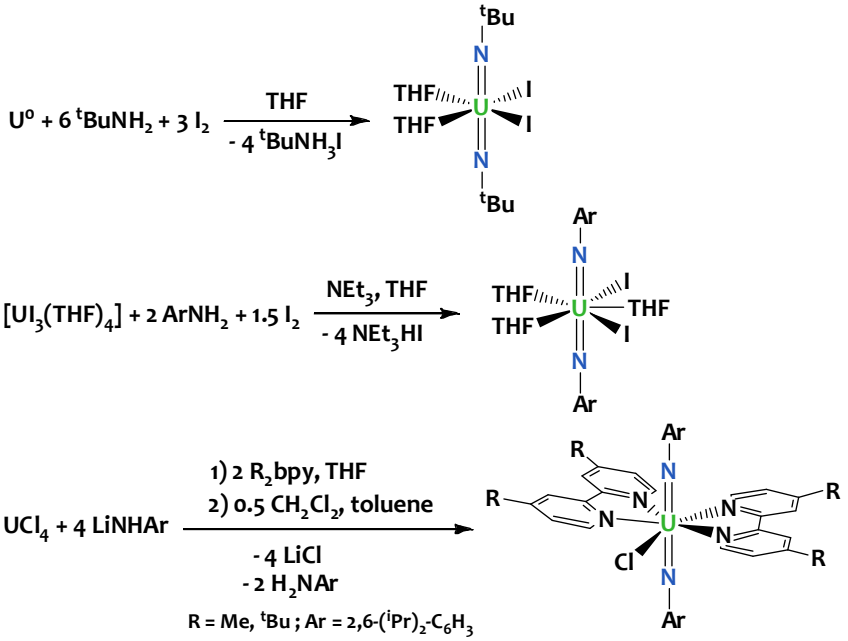

Scheme I.34. Isolation of high-valent uranium trans-bis(imido) species from low-valent uranium precursors.

I.3.4.5 Arene activation

Uranium arene complexes are rare with only a handful of low-valent uranium arene species described. The U(III) mononuclear complexes featuring piano stool half sandwich structures [(η^6-arene)U(L)$_3$] (arene = C_6H_6, $C_6H_3Me_3$, C_6Me_6 ; L = $AlCl_4$, BH_4) (***Figure I.17***-left) were obtained by refluxing [U(BH_4)$_4$] or a mixture of UCl_4, $AlCl_3$, and powdered aluminum metal in arene solvent.[229-231] A variety of polynuclear structures bridged by chloride anions were obtained using similar synthetic methodologies.[232-234] The Ephritikhine group showed that the η^6-arene unit can be displaced according to the following order of stability C_6H_6 < $C_6H_3Me_3$ < C_6Me_6, and that while these species are thermodynamically stable, the arene moiety is readily displaced by σ-donors, such as THF.[231]

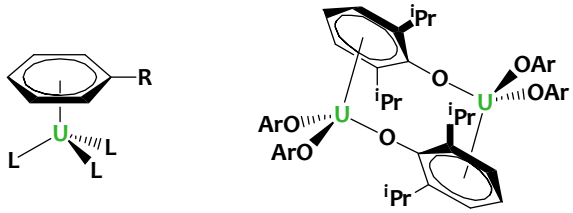

Figure I.17. Examples of coordination of arenes to U(III) centers. R = H, Me ; L = $AlCl_4$, BH_4 ; Ar = 2,6-^{i}Pr$_2$C$_6$H$_3$.

Interestingly, a η^6-arene interaction was found in the solid-state structure of the U(III) tris(aryloxide) complex [U(O-2,6-^{i}Pr$_2$C$_6$H$_3$)$_3$]$_2$ in which the arene rings of the ligand bridges the metal centers (***Figure I.17***-right).[92] This last example probably inspired the Meyer group who designed a chelate tris(aryloxide) ligand featuring a mesitylene anchor to access the uranium (III) complex [((^{t}BuArO)$_3$mes)U] presenting metal-arene interaction (***Figure I.18***).[127] In all of these compounds, the large U-C separations are in agreement with the presence of a neutral π-arene ligand bound to a U(III) center.

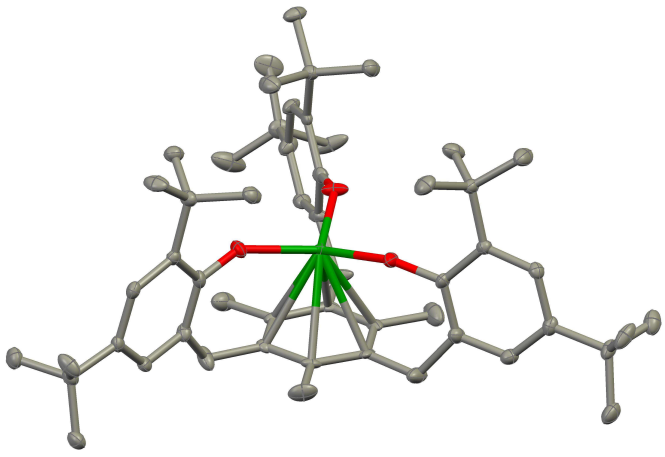

Figure I.18. Mercury diagram of the solid-state molecular structure of the uranium (III) aryloxide complex [((^{t}BuArO)$_3$mes)U] featuring metal-arene interactons.

Another class of uranium-arene compounds, known as arene inverted-sandwiches, were first reported by the Cummins group in 2000.[74] These compounds containing arenes bridging two metal ions in a -η^6:η^6 symmetrical fashion (see ***Figure I.19***) remain rare among organometallic arene complexes.[74, 118, 235-257] Most of the reported examples of diuranium inverted-sandwiches are neutral of the general formula {[UL_2]$_2$(μ-η^6:η^6-C_6H_5-R)} (L = anionic ligands including cyclopentadienyl, phenoxides, bulky amido, methanido groups ; R= H, Me).[74, 118, 252, 256, 257] Whilst benzene and toluene adducts are more common, this chemistry has also be extended to a variety of other aromatic hydrocarbons including naphthalene, anthracene, cyclooctatetraene, biphenyl, terphenyl or stilbene.[254, 255, 257]

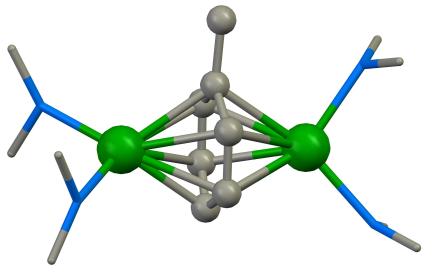

Figure I.19. Mercury diagram of the solid-state molecular structure of the inverted sandwich complex [{U(N[Ad]Ar)$_2$}$_2$(μ-η^6:η^6-C_6H_5-Me)] where Ar = 3,5-(Me)$_2$-C_6H_3. Bulky substituents are omitted for clarity.

Inverted-sandwich complexes of uranium are of particular fundamental interest due to the presence of π and δ covalent interactions between the arene and uranium d and f orbitals.[74, 118, 252, 253, 255, 257, 258] While the neutral [{UL_2}$_2$(μ-η^6:η^6-C_6H_5-R)] species are formally described as U(II), X-ray absorption near edge structure (XANES) spectroscopy and density functional theory (DFT) studies revealed that most of these complexes are best described as having a benzene (or a substituted benzene) dianion bridging two U(III) centers.

Only recently, one neutral di-uranium inverted-sandwich complex of formula [$Ts^{Xy}U$]$_2$(μ-η^6:η^6-C_7H_8) (Ts^{Xy} = HC-($SiMe_2NAr$)$_3$) has been prepared and is described as a U(V)-(toluene)$^{4-}$-U(V) complex[253] based on supporting EPR evidence.[259] The possibility of obtaining a stable 10π-electrons arene complex was first predicted by DFT studies for a barium inverted-sandwich[260] and very recently theoretical, crystallographic and spectroscopic evidence of the presence of a benzene tetra-anion with a ten-pi-electrons aromatic system have been reported for group 3 inverted-sandwich complexes.[250]

Usually, inverted-sandwich complexes are synthesized by reduction with potassium metal or similar reducing agents of uranium precursors in the presence of an arene (***Scheme I.35***) rendering rather difficult the isolation of complexes in different states of charge. Notably only one example of

inverted-sandwich complexes isolated in two states of charge by a careful control of the reduction conditions has been reported reccently.[255]

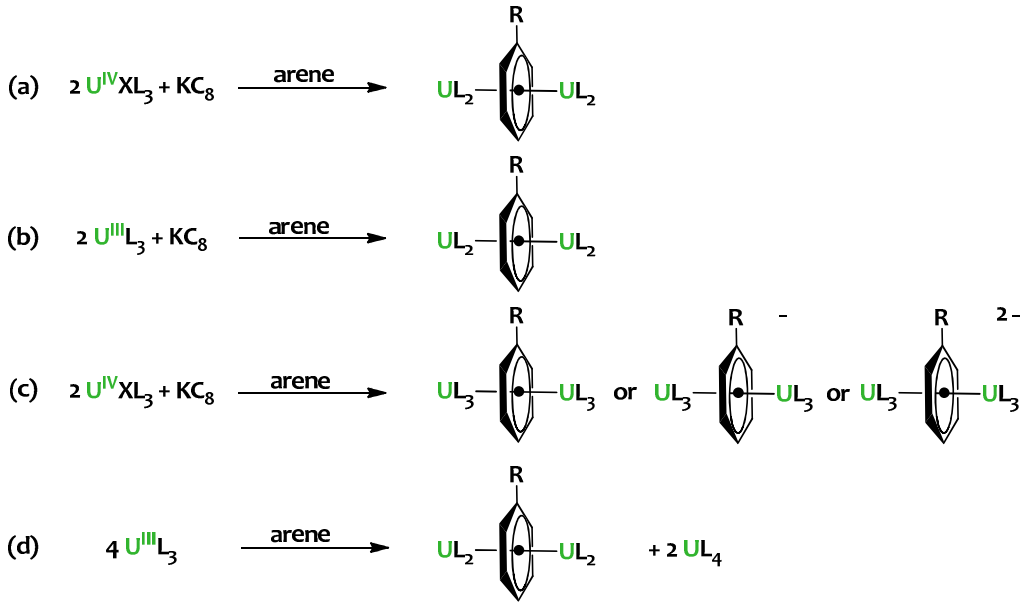

Scheme I.35. Reported syntheses of uranium arene inverted sandwiches. (a)[74, 256] ; (b)[252] ; (c)[118, 253-255, 259] ; (d)[257].

Recent advancements reported by Arnold and coworkers demonstrated that inverted sandwich complexes could be simply obtained from the reaction of U(III) complexes with arenes in absence of strong external reductants, such as KC_8.[257] The reaction takes several days to go to completion, and involves U(III) disproportionation to yield the $[\{L_2U\}_2(\mu\text{-}\eta^6\text{:}\eta^6\text{-arene})]$ molecule and a tetravalent $[UL_4]$ by-product. The mechanism, represented in ***Scheme I.36***, was proposed by the authors based on kinetic and DFT studies and involves the concerted transfer of one L bridging ligand to another UL_3 molecule concomitant with electron transfer to the arene. Addition of dihydroanthracene to trivalent homoleptic $[UL_3]$ species revealed no C-H activation, in agreement with the absence of radical species in solution, which is consistent with the cooperative activation mechanism proposed.

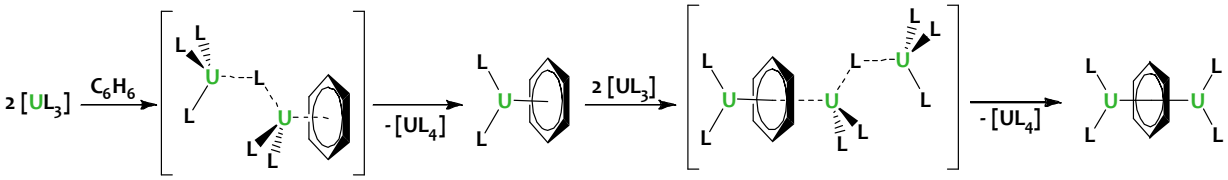

Scheme I.36. Proposed mechanism for formation of $[\{L_2U\}_2(\mu\text{-}\eta^6\text{:}\eta^6\text{-arene})]$ from UL_3 and benzene.

Besides the understanding of their electronic structure, such systems are the focus of current interest for their potential magnetic properties and reactivity. Indeed, a report from Liddle suggests that the delocalized nature of bonding in an arene bridged diuranium(III) complex provides the pathway for magnetic communication leading to single molecule magnet behavior.[43, 118, 261] Moreover,

Arnold and coworkers have shown that arene functionalization in mild conditions was possible.[257] Arene C-H activation and borylation was achieved by the addition of the borane HBBN (9-bora-9-bicyclononane) onto isolated or *in-situ* uranium inverted-sandwich arene complexes to produce H_2 and $[\{U(ODtbp)_2\}_2(\mu\text{-}\eta^6\text{:}\eta^6\text{-}C_6H_5BBN)]$ or $[\{(UODtbp)_2\}_2(\mu\text{-}\eta^6\text{:}\eta^6\text{-}C_9H_7BBN)]$ (Dtbp = 2,6-^{t}Bu$_2$C$_6$H$_3$) (***Scheme I.37***). This reaction may eventually be rendered catalytic as the functionalized naphtalene moiety can be readily displaced by a benzene molecule (***Scheme I.37***).[257] It is important to note that this could not have been possible in the presence of strong reducing agents such as KC_8 because of their incompatibility with boranes.

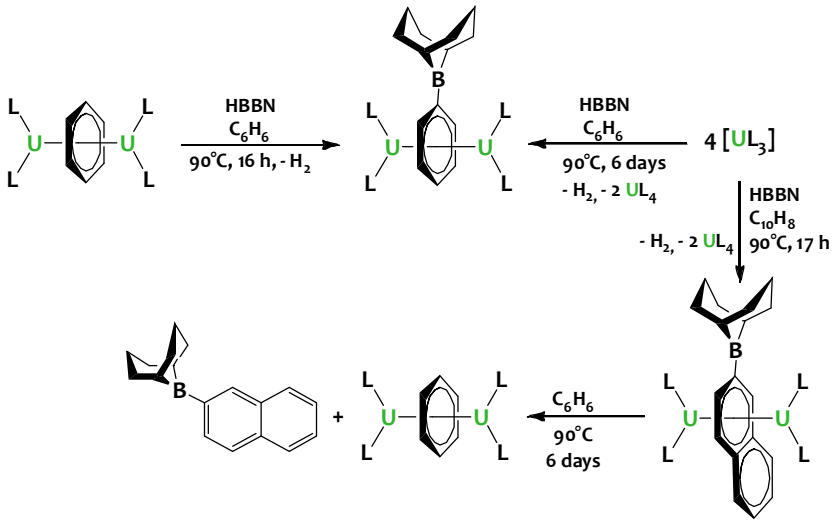

Scheme I.37. Synthesis of boryl-functionalized arenes from $[UL_3]$ (L = O-(2,6-^{t}Bu$_2$C$_6$H$_3$)).

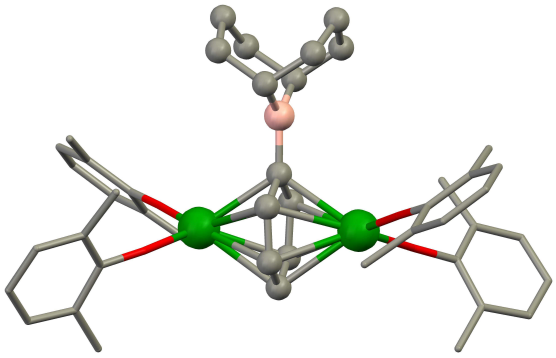

Figure I.20. Mercury diagram of the solid-state molecular structure of the functionalized arene inverted sandwich complex $[\{U(ODtbp)_2\}_2(\mu\text{-}\eta^6\text{:}\eta^6\text{-}C_6H_5BBN)]$ (Dtbp = 2,6-^{t}Bu$_2$C$_6$H$_3$). Methyl substituents from the ^{t}Bu groups are omitted for clarity.

Finally, the electrons stored on the arene fragment are available for further utilization and these species can function as U(II) synthons capable of performing rich redox chemistry which might provide new avenues to uranium mediated small molecules activation. The multi-electron reactivity of these species will be presented in the next section (I.4.3).

I.4 Ligand Non-Innocence in Uranium Chemistry

Most ligands used in coordination chemistry behave as spectator ligands and therefore do not partake in the metal-based redox chemistry of complexes. However, coordinated ligands with readily accessible oxidation states can, besides their traditional role as ancillary ligands, participate in redox processes. Metal complexes containing such ligands, known as non-innocent or redox-active ligands,[262-264] have attracted a wide range of structural, spectroscopic, magnetic, and computational studies directed to assess the valence localization. Redox events in some metalloenzymes involve ligand-based processes[265-267] and redox non-innocent ligands have become increasingly popular in d-block chemistry for the development of interesting reactivity or new catalysts[263, 268-276] including small molecule activation[11, 277-279] and industrially relevant chemical transformations.[280] They also offer new opportunities for the design of molecular switches. Accordingly this field has been expanding considerably in the last decade.

Such ligands offer a pathway for electron-rich metal centers to transfer and store electron density instead of leading to unwanted side reactions. In complexes containing redox-active ligands the metal center can access the reducing equivalents when necessary for the transformation of incoming molecules. Moreover, redox active ligands can allow the storage of a high number of electrons rendering possible multi-electron processes. This particularly applies to non-noble metals which do not have the capacity to accommodate a variable number of electrons, which is key for most catalytic transformations.[263, 281-287]

As previously mentioned, trivalent uranium preferentially reacts via the U^{4+}/U^{3+} redox couple and therefore the chemistry of low-valent uranium is dominated by single-electron transfers. Metal-based multi-electron processes remain uncommon in uranium chemistry[24, 176, 221] especially in comparison with the d-block metals, and remain mostly limited to the transformation of U(III) into U(V) imidos (see section I.3.4.4) or oxo products. In this context, the association of uranium to a non-innocent ligand acting as an independent electron reservoir at a same molecule represents an attractive alternative that should render multi-electron reactivity possible whilst affording formally low-valent oxidation state synthetic equivalents. Accordingly, in recent years ligand based redox processes have been increasingly combined with metal centered redox transfers to promote multi-electron reductions in uranium complexes. The few examples of uranium complexes supported by redox-active ligands are presented in the present section.

I.4.1 Diimines and related ligands

Diimines are popular redox-active ligands as they can access three different oxidation states when bound to metal centers (***Scheme I.38***) and therefore exhibit a rich non-innocent chemistry.[288]

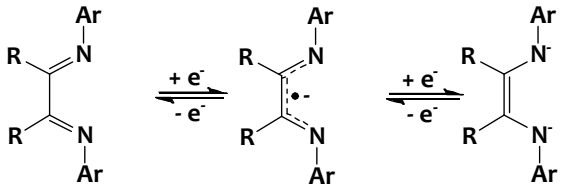

Scheme I.38. Oxidation levels of α-diimine ligands.

The association of U(IV) to the redox active ligand $(dpp\text{-}BIAN)^{2-}$ (dpp-BIAN = 1,2-bis(2,6-diisopropylphenylimino)acenaphthylene) resulted in the isolation of the [U(dpp-BIAN)$_2$] and [U(dpp-BIAN)$_2$(THF)] compounds (***Scheme I.39***).[114] Interestingly, Kiplinger and coworkers performed a series of structural, spectroscopic, magnetic, and computational studies directed to assess the valence localization. These investigations revealed that the coordination of THF results in the transfer of one electron from the $(dpp\text{-}BIAN)^{2-}$ ligand to the U(IV) center to yield a U^{III}-π^{*3} configuration in the solid-state whilst in solution the electronic configurations remain U^{IV}-π^{*4}.[114]

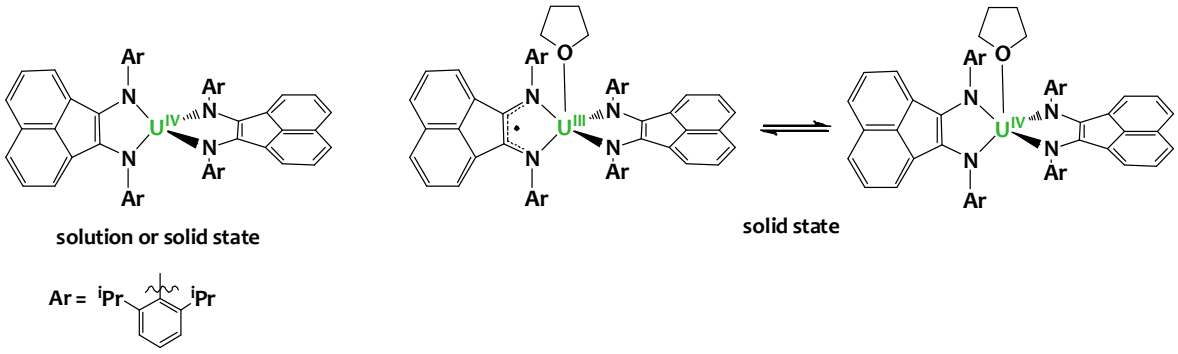

Scheme I.39. Uranium complexes of the redox-active ligand $(dpp\text{-}BIAN)^{2-}$.

Despite the reduced nature of the ligands in [U(dpp-BIAN)$_2$], reactivity studies with this compound were unfruitful because of complex decomposition. The closely-related complex [U(^{Mes}DAB^{Me})$_2$(THF)] where ^{Mes}DAB^{Me} = [MesN=C(Me)C(Me)=NMes] was prepared in 2011 by the Bart's group from the reaction of [UI$_3$(THF)$_4$] with the diimine ligand in presence of 3 equiv. KC$_8$ (***Scheme I.40***).[289] Structural and spectroscopic characterizations pointed to the presence of a uranium(IV) metal center bound to two enediamide dianionic ligands. The non-innocent behavior of the ligand backbone was evidenced by the reaction of [U(^{Mes}DAB^{Me})$_2$(THF)] with iodomethane which resulted in the alkylation of the ligand with concomitant formation of a U-I bond without change in the oxidation state of the metal.[289]

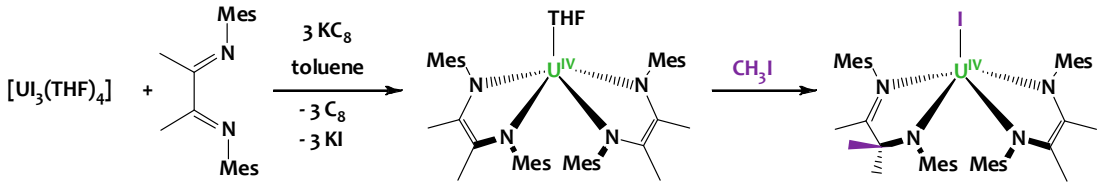

Scheme I.40. Synthesis of [U(^{Mes}DAB^{Me})$_2$(THF)] and its ability to perform activation of iodomethane.

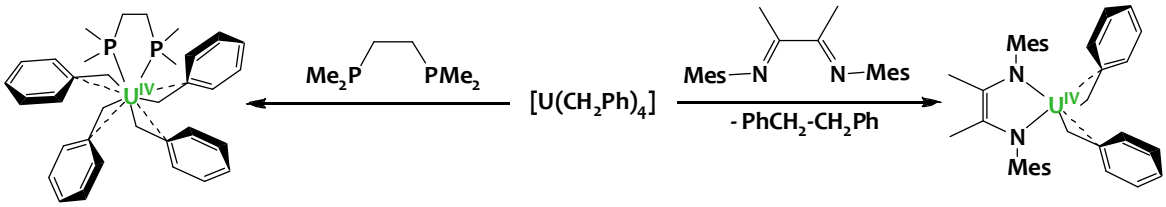

Scheme I.41. Reductive elimination at a U(IV) complex promoted by a redox-active diimine ligand.

The same diimine ligand proved able to promote C-C bond formation *via* the reductive elimination of two benzyl moieties from the U(IV) homoleptic alkyl complex [U(CH$_2$Ph)$_4$], as shown in ***Scheme I.41***.[290] The utility of the redox-active ligand, which can store two electrons on the ligand framework, was demonstrated by replacing the diimine by the redox-inactive diphosphine ligand 1,2-bis(dimethylphosphino)ethane (dmpe) which simply afforded the U(IV) adduct [U(CH$_2$Ph)$_4$(dmpe)] (***Scheme I.41***).

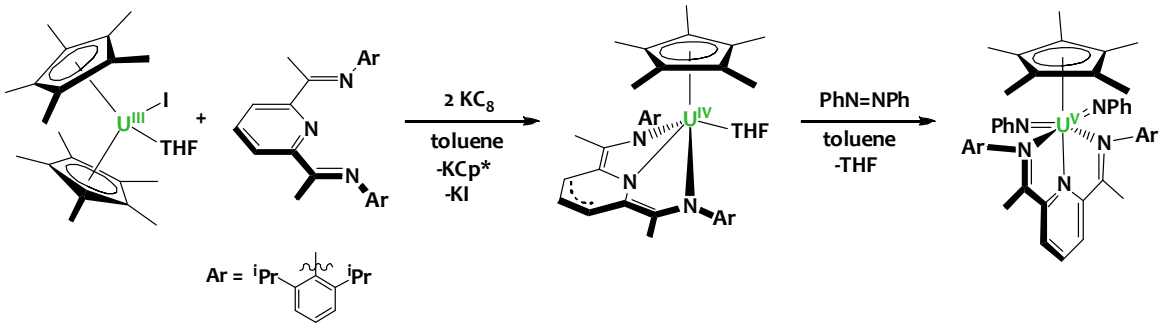

Scheme I.42. Synthesis of [U(Cp*)(PDI)(THF)] and its multi-electron reactivity with azobenzene.

Redox-active imino ligand platforms are not restricted to alpha diimines. Bart and coworkers reported the use of a tridentate pyridine(diimine) ligand (PDI) for achieving multi-electron reactions with uranium.[291] As depicted in ***Scheme I.42***, the reaction of [U(Cp*)$_2$I(THF)] with (PDI) in presence of reducing agents produces the U(IV) complex [U(Cp*)(PDI)(THF)] in which the imino ligand has been reduced to its (PDI)$^{3-}$ oxidation state. The three electrons stored on the chelate ligand together with one electron from the metal participate in the four electron reduction of azobenzene to yield the complex [U(Cp*)(PDI)(NPh)$_2$] featuring a neutral (PDI) unit.

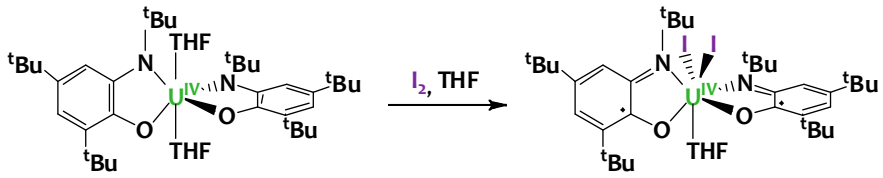

Scheme I.43. "Oxidative addition" of molecular iodine onto a U(IV) amido phenolate complex. The transformation involves the mono-electronic oxidation of two ligands without a change in the oxidation state of the metal.

Very recently, Bart also reported the reaction of a U(IV) complex featuring redox-active amido phenolate ligands with iodine[292] (***Scheme I.43***) in which halide addition occurs at the uranium with concomitant oxidation of the ligand to their radical iminosemiquinone form. Similar behavior was previously observed for the tetravalent zirconium analogue.[293]

I.4.2 Bipyridines and polypyridines

2,2'-bipyridines, a commoly utilized class of ligands in coordination chemistry, can store up to one electron to form the radical anion $(bpy)^{\bullet -}$ under strong reducing conditions. The 2,2'-bipyridine ligand is typically not reduced by U(III),[294-296] and U(III)-(bipy) complexes require an additional electron input to be converted into U(III)-$(bipy)^{\bullet -}$ species.[294, 296, 297] The bipy monoradical can thus be exploited to introduce an electron reservoir at a U(III) center, producing strong reducing agents where one additional electron is stored on the coordinated aromatic ligand. This contrasts with the examples described above, where the diimine ligands are more readily reduced than the U(IV) center.

Implimenting this strategy, the Andersen and Ephritikhine groups simultaneously reported the synthesis of the U(III) metallocene complexes $[U(Cp^*)_2(bipy^{\bullet -})]$[296] and $[U(Cp')_2(bipy^{\bullet -})]$ (Cp' = 1,2,4-$(^tBu)_3C_5H_2$)[297] featuring a radical bipyridyl ligand. As shown on ***Scheme I.44***, the Andersen group has shown that these species behave as masked forms of the low-valent $[U(Cp')_2]$ fragment and react with *p*-tolylazide and pyridine N-oxide to afford rare examples of U(IV) mono imido or oxo species respectively.[297]

More recently Bart observed similar behavior for a U(III) complex supported by hydrotris(3,5-dimethylpyrazolyl)borate) ancillary ligands with a bound radical monoanionic bipyridine unit.[294, 298]

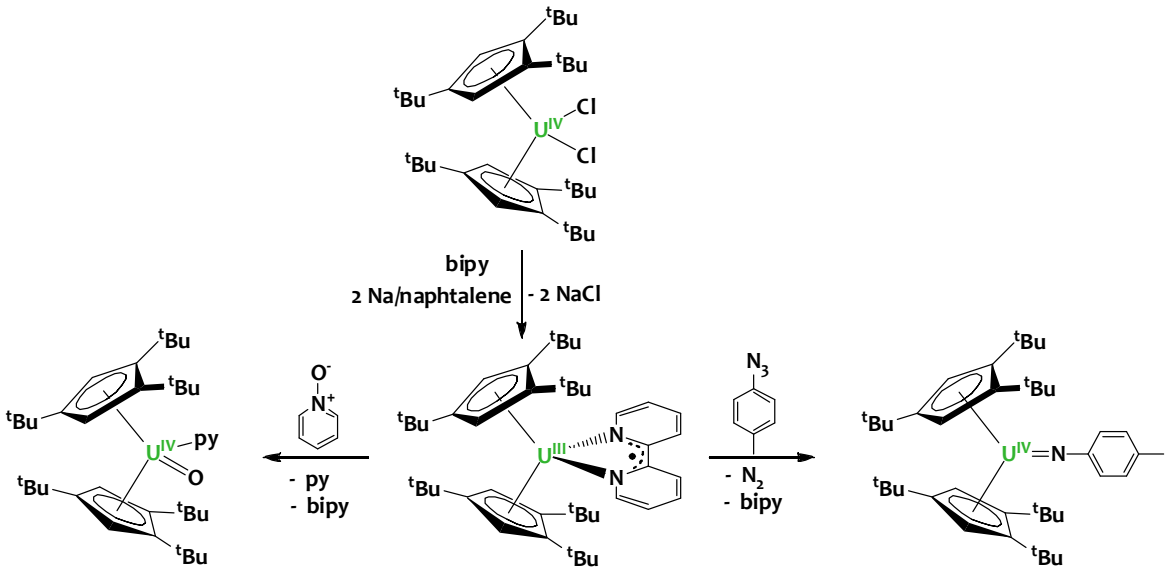

Scheme I.44. Synthesis of a U(III) complex containing a 2,2'-bipyridyl radical anionic ligand and its multi-electron redox reactivity involving both the metal and the ligand.

Likewise, the $[U(Cp^*)_2(terpy)]I$ complex featuring a terpyridine ligand can be reduced to the $[U(Cp)_2(terpy^{\bullet -})]$ form.[296] A unique series of trimetallic actinide complexes featuring terpy monoradical bridging ligands has been reported by Kiplinger.[299, 300] The redox properties of these species were investigated by cyclic voltammetry and revealed successive ligand-based $(tpy)^{\bullet -}$ to (tpy) and metal-based U(III) to U(IV) oxidation processes together with evidence of electronic interactions between the metal centers.[299, 300]

While magnetic studies seems to indicate a +III oxidation state at the uranium center in $[U(Cp)_2(terpy)]I$, the comparison with its cerium(III) analogue suggests an increased retrodonation to the terpy ligand in the case of uranium. Consistent with a notable contribution of the $[U^{IV}(Cp)_2(terpy^{\bullet -})]I$ resonance form, treatment of these complexes with Ph_3SnH resulted in hydrogen transfer to the terpyridine ligand in the uranium complex only, a behavior which has not been reported for its bipyridine counterpart.[296] Finally, in the case of the 2,4,6-tris(2-pyridyl)-1,3,5-triazine (tptz), the metal to ligand electron transfer is complete and results in the radical coupling of the azine moieties to yield the tetravalent uranium dimeric complex $[U_2I_6(tptz–tptz)(MeCN)_2]$.[301]

I.4.3 Cyclopentadienyl and arene derivatives

Another type of ligand-based redox process has been identified by Evans for the tris(pentamethylcyclopentadienl) $[U(Cp^*)_3]$ system. In this sterically crowded complex, the reactivity does not only involve a change of the metal oxidation state but is also centered on the ligand and involves a $(C_5Me_5)^{\cdot}/(C_5Me_5)^-$ redox couple according to eqn. (5).[302, 303] This process was named sterically induced reduction as the Cp* framework does not exhibit such behavior in less sterically

hindered complexes. Analogous behavior was also observed for the $[U(Cp^*)_2(BPh_4)]$ complex where the $(BPh_4)^-$ anion can formally act as a one electron reductant, as shown in eqn. (6).[304]

$$(C_5Me_5)^- = e^- + {}^1/_2\,(C_5Me_5)_2 \qquad (5)$$

$$(BPh_4)^- = e^- + BPh_3 + {}^1/_2\,(Ph)_2 \qquad (6)$$

These systems can undergo multi-electron reductions by combining ligand- and metal-based redox processes. For instance, $[U(Cp^*)_3]$ and $[U(Cp^*)_2(BPh_4)]$ can both perform a four-electron reduction of azobenzene to yield the U(VI) bis-imido derivative $[U(Cp^*)_2(NPh)_2]$ as illustrated in ***Scheme I.45***.

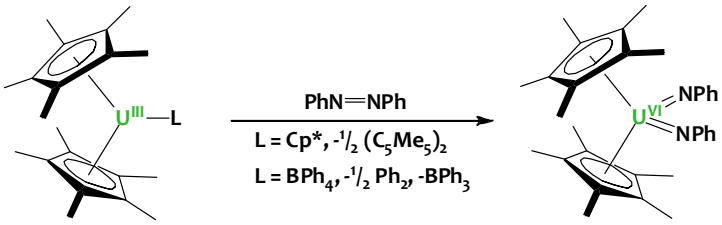

Scheme I.45. Sterically-induced reduction of azobenzene.

The $(C_5Me_5)_2$ dimerization and release upon oxidation is a limitation of the use of the popular Cp* ligand which is improperly considered as a spectator ligand in this case, preventing the possibility of restoring the original low-valent complex and therefore limiting its use in catalytic transformations.

The arene moiety in uranium arene inverted sandwich complexes, presented in section I.3.4.5, also behave as a non-innocent ligand. Indeed, the electrons stored on the arene ring are available for oxidizing substrates, releasing the original benzene or toluene unit.

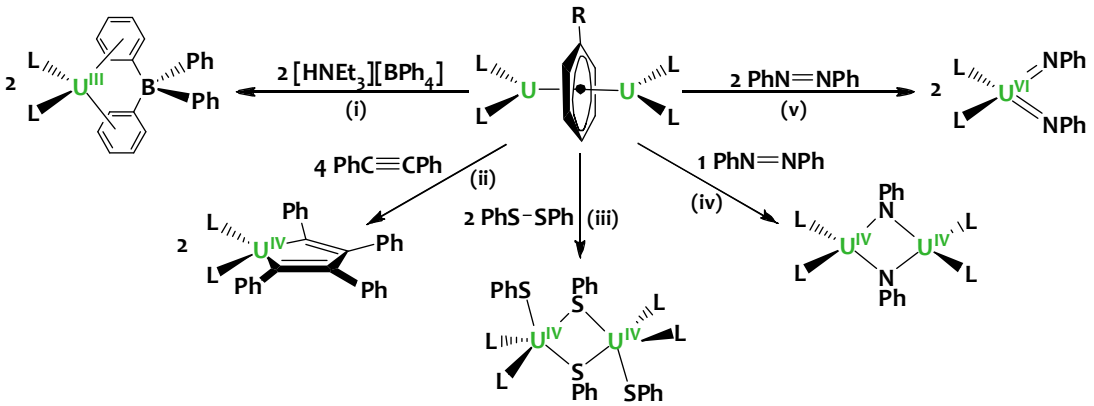

Scheme I.46. Multi-electron redox reactions of arene-inverted sandwich complexes. (i) R = H, L = Cp*, - C_6H_6, -H_2, - 2NEt_3 ; (ii) R = H, L = Cp*, - C_6H_6 ; (iii) R = Me, L = $(3,5\text{-}C_6H_5Me_2)NC(CH_3)_3$, - toluene ; (iv) R = Me, L = $(3,5\text{-}C_6H_5Me_2)NC(CH_3)_3$, - toluene ; (v) R = H, L = Cp*, - C_6H_6.

Specifically, the Cummins and Evans groups have shown that these bimetallic molecules can effect two electron (***Scheme I.46*** (i)), four electron (***Scheme I.46*** (ii), (iii) and (iv)) and up to eight electron (***Scheme I.46*** (v)) reductions of various substrates.[74, 305] As such, these systems can be considered as

U(II) synthons because these transformation mimic U(II) to U(III), U(IV) or U(VI) processes not accessible otherwise, as thus far the isolation of a molecular U(II) species remains elusive.

The multi-electron redox reactivity of uranium-arene inverted sandwiches has been recently utilized as a synthetic tool for accessing interesting homo and heteropolynuclear species. As depicted in ***Scheme I.47***-top, the uranium toluene inverted sandwich complex was implemented in the isolation of the first complex presenting an unsupported uranium-cobalt bond.[253] The Diaconescu group reported an efficient route to the formation of uranium polynuclear assemblies based on the reduction of quinoxaline from a diuranium μ-η^6:η^6-toluene complex (***Scheme I.47***-bottom) which yielded a rare parallelogram-shaped tetranuclear macrocyclic architecture.[256]

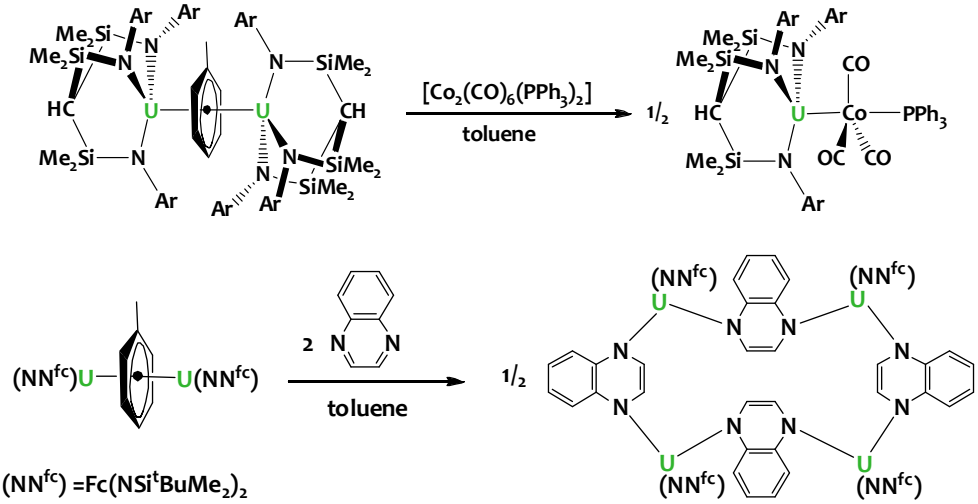

Scheme I.47. Use of the multi-electron redox reactivity of diuranium arene-inverted sandwich precursors for the synthesis of uranium-containing polynuclear species.

To summarize, non-innocent ligands are efficient tools to bring about multi-electron reactivity at uranium centers. Few systems have been investigated thus far, and whilst encouraging results were obtained, this approach remains largely unexplored. Systems that can return to their original reduced state are yet to be developed in order to allow catalytic transformations. In view of the achievements performed in this field with d-block metals, this strategy represents a promising alternative to further expand uranium chemistry.

CHAPTER II
Multielectron Redox Reactions Involving C-C Bond Formation and Cleavage in Uranium Schiff Base Complexes

II.1 Context

Schiff base ligands of the salen family (salen = N,N'-bis(salicyldiene)-ethylenediamine) are well established in the area of coordination chemistry.[306, 307] These dianionic multidendate chelating agents with O and N donor atoms have been extensively used as supporting ligands in the chemistry of d-block metals to stabilize unusual oxidation states. The popularity of these ligand frameworks resides also in their synthesis, which is easy, efficient, and requires cheap starting materials. Furthermore, the synthetic methodologies employed are highly tuneable, as substituting groups on the nitrogen atoms and on the aromatic rings can be varied, giving rise to a wide variety of salicylaldehyde derivatives, including chiral compounds which have been utilized with success in asymmetric homogeneous catalysis.[308-312] As functionalization is generally straightforward, a huge number of salen analogues are reported in the literature. The most typically studied bridging units are exemplified in **Figure II.1** but many other designs can be envisioned.

We thought that these ligands could also provide a very attractive alternative to the ubiquitous cyclopentadienyl ligand for the study of uranium chemistry. This choice has been driven by various observations. Firstly, the oxygen donor atoms of the phenolate anions provide an electron-rich environment and are capable of tightly binding with hard actinide and lanthanide cations. Secondly, by tuning steric features of these chelating ligands, it should be possible to access a wide range of structures including polymetallic ones. Thirdly, the electronics of Schiff bases can be adjusted by extending the delocalisation of π-electrons on the whole structure. The combination of these

characteristics is particularly promising for developing a coordinating platform for enhancing the redox chemistry of f-elements.

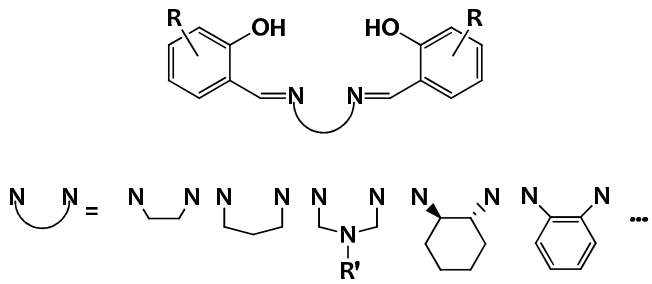

Figure II.1. Structure of Schiff base derivatives of the salen family. A trivial nomenclature for these ligands is commonly used depending on the nature of the bridging unit : salen for ethylene bridged ligands ; salophen for orthophenylene briged ligands, etc.

Furthermore, the group of Floriani has demonstrated that tetradentate ONNO Schiff base ligands can be used to promote ligand-centered redox chemistry at early transition metal centers. The ligand-based mechanism involves the reversible formation and cleavage of intraligand C-C bonds that can function as two-electron reservoirs in redox reactions. Specifically, the reduction of [$ZrCl_2$(salophen)(THF)] with magnesium affords a dinuclear species [Zr_2(cyclo-salophen)$(THF)_2$] (***Scheme II.1***) in which the original imino moieties of the ligand have been reductively coupled to form a tetra(amido) tetra(phenolate) macrocyclic ligand.[32] The electrons stored in the C-C bonds of the ligand scaffold are available for incoming oxidizing substrates. Indeed, despite a formal d^0 metal electron configuration, the complex [Zr_2(cyclo-salophen)$(THF)_2$] reacts with $PhICl_2$ to afford the original oxidative-addition-type [$ZrCl_2$(salophen)(THF)] product in which the imino moieties of the ligand are restored (***Scheme II.1***).[32]

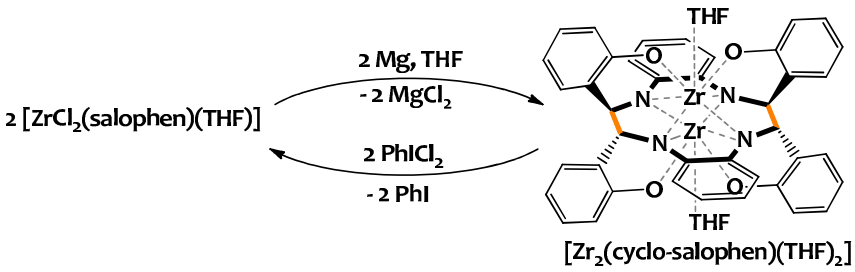

Scheme II.1. Redox-behaviour of zirconium Schiff base complexes.

As shown in ***Scheme II.2***, similar redox-active behaviour of the salophen ligand was observed for the trivalent vanadium complex [VCl(salophen)(THF)].[29] Notably, the two-electron reduction product [V_2(bis-salophen)$(THF)_2$] and the four-electron reduction product [V_2(cyclo-salophen)]$^{2-}$, featuring one and two reactive C-C bonds respectively, react with dioxygen to form the oxo-vanadium(IV) complex [OV(salophen)]. The [V_2(bis-salophen)$(THF)_2$] species also reduces phenylazide to yield the terminal phenylimido complex [PhNV(salophen)]. Multi-electron transformations allowing the

introduction of important functionalities at the vanadium center are therefore possible thanks to the cooperative redox reactivity of the metal and the Schiff base ligand electron reservoir.

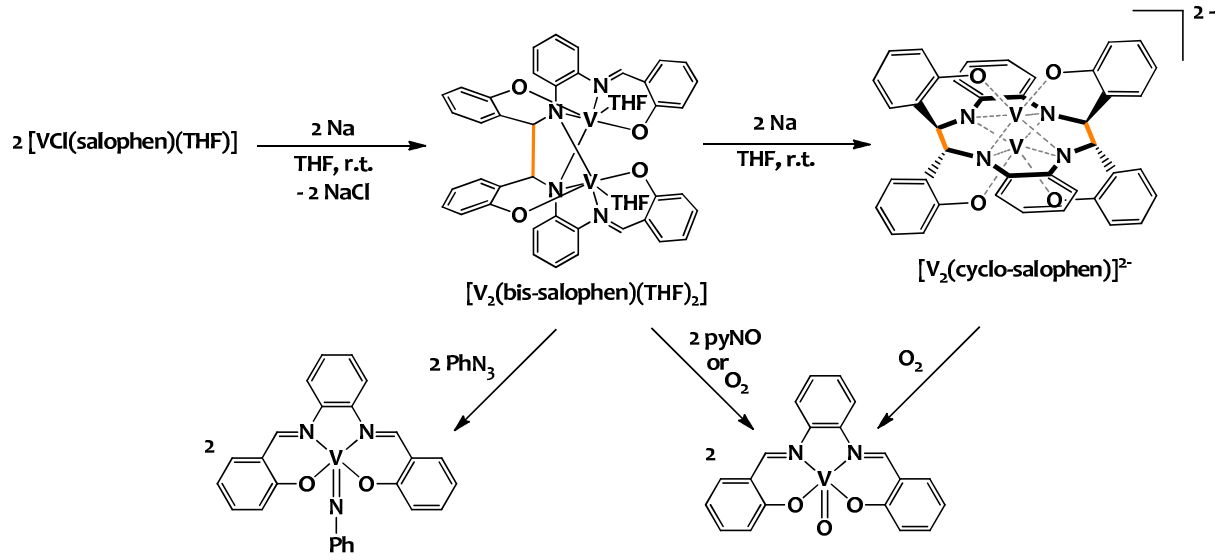

Scheme II.2. C-C bond formation and cleavage in vanadium salophen complexes.

The reduction of the niobium Schiff base complex [Nb(Cl)$_3$(^{tBu}salophen)] with magnesium also involves ligand reduction, and affords the [Nb$_2$(cyclo-^{tBu}salophen)] dimer featuring a Nb-Nb single bond (***Scheme II.3***).[31] Contrary to its vanadium analogue, using lower molar ratios niobium:reducing agents did not yielded less reduced forms. The metal centers in [Nb$_2$(cyclo-^{tBu}salophen)] can be further reduced by potassium metal to give [Nb$_2$(cyclo-^{tBu}salophen)]$^{2-}$ that contains a Nb=Nb double bond. Interestingly, metal oxidation is more favorable than the cleavage of C-C bonds, and the metal-metal bond cleavage is involved first in the reaction with iodine or diphenyldiazomethane.[31]

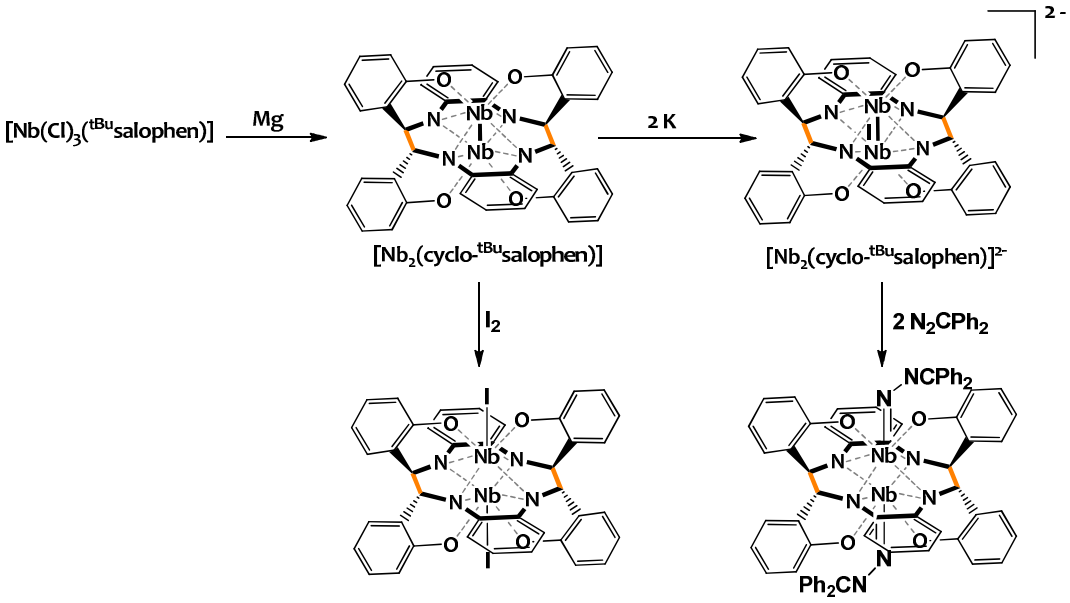

Scheme II.3. Oxidative chemistry of [Nb$_2$(cyclo-salophen)] and [Nb$_2$(cyclo-salophen)]$^{2-}$ species. The ^{t}Bu groups are omitted for clarity.

These examples illustrate the interest of using tetradentate ONNO Schiff bases to synthesize electron-rich species. Our objective is take advantage of the ligand redox activity to isolate mono and polymetallic uranium complexes able to transfer a large number of electrons to a substrate by combining a redox activity on the metal and on the ligands. The use of chemical bonds as electron reservoirs should achieve multi-electron processes at uranium and promote novel uranium reductive chemistry.

By comparison with the wealth of information available on transition metal and lanthanide complexes of Schiff bases, reports concerning the 5f elements are much less numerous. In uranium chemistry the use of these Schiff base ligands has been mostly limited to the complexation of the UO_2^{2+} ion[51, 54] especially in the search for efficient extractants of uranium from ores or other sources. Recently our group and others have shown that tetradentate and pentadentate Schiff bases are also effective ligands for the stabilization of the elusive pentavalent uranyl.[61, 63, 64, 66, 313-317]

In contrast only very few examples of U(III) and U(IV) complexes of Schiff base ligands have been reported. Mononuclear mono- and bis-ligand U(IV) species (***Scheme II.4***) have been obtained by either reacting UCl_4 or $[U(acac)_4]$ with salen-type ligands,[318-321] or via transmetallation between salen transition metal complexes and uranium salts.[322]

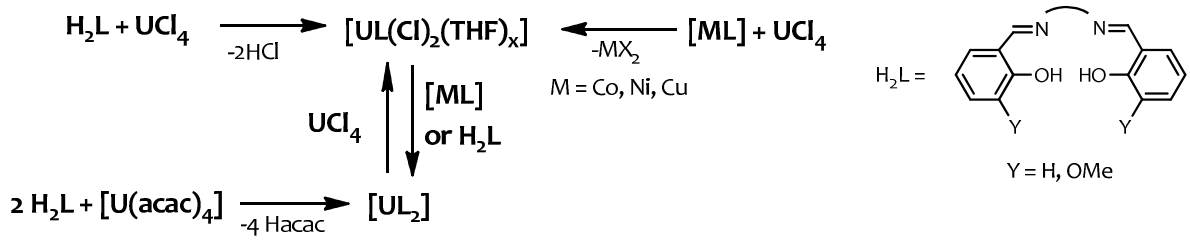

Scheme II.4. Syntheses of mononuclear Schiff base U(IV) complexes.

Polynucleating hexadentate Schiff bases have also been utilized to promote the formation of homo- and hetero-polymetallic complexes of U(IV) with 3d metals which show interesting magnetic properties.[322-326] However, to the best of our knowledge, the study of the redox reactivity of these U(IV) Schiff base complexes remain unexplored.

To date, a single occurrence of a U(III) Schiff base complex has been reported. In this recent work, Arnold and coworkers successfully used the octadentate Schiff-base pyrrole macrocycle H_4L (***Scheme II.5***) to reach the dinuclear U(III) complex $[(UI)_2L]$ which was characterized by magnetic studies.[129] In contrast the protonolysis reaction between $[U\{N(SiMe_3)_2\}_3]$ and H_4L produced the U(IV) complex [UL] (***Scheme II.5***).[327]

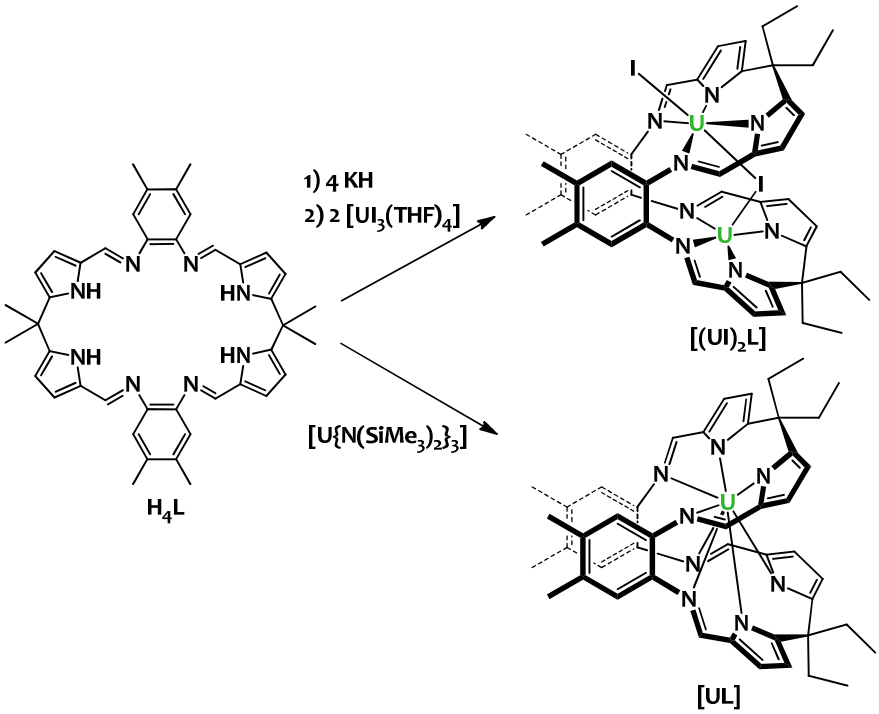

Scheme II.5. Reaction of U(III) precursors with the octadentate Schiff base pyrrole macrocycle H_4L.

The paucity of work in U(III) Schiff base chemistry is most probably due to the non-innocent behavior often observed for such ligands. As mentioned in Chapter I section I.4.1, Kiplinger[114] and Bart[289, 291] reported the ability of the π-delocalized diimine frameworks to store electrons in their conjugated π* orbitals, resulting in an increase of the oxidation state of uranium. Reduction of the imino groups of the ligand can render the isolation of well-defined complexes more challenging. However, a suitable choice of the electronic and geometric structure of the ligands should allow the isolation of stable compounds or lead to the storage of electrons on the ligand framework, as observed with early d-block metals (vide supra).

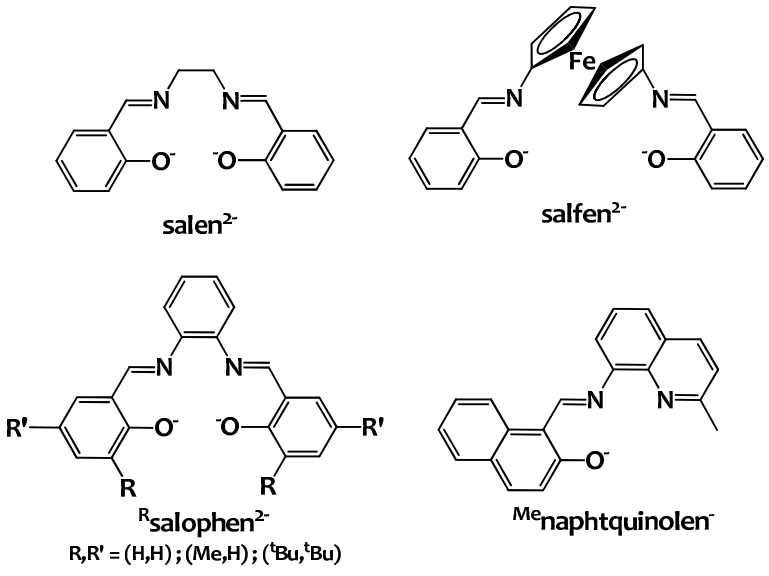

Figure II.2. List of O,N-donor polydentate Schiff base ligands used in this work.

In this chapter, we present the results obtained on the coordination chemistry of low-valent uranium with O,N-donor polydentate Schiff base ligands. Our first investigations were conducted with the tetradentate dianionic salen and ^{R}salophen ligands presented in ***Figure II.2***. We then explored the possibility of using the tetradentate salfen and the tridentate ^{Me}naphtquinolen frameworks (***Figure II.2***) as supporting ligands for uranium chemistry. These studies are presented in section II.3 and section II.4 respectively.

II.2 Synthesis and Characterization of Electron-Rich Schiff Base Uranium Complexes

II.2.1 Reaction of $[UI_3(THF)_4]$ with K_2salen

We firstly investigated the possibility of preparing electron-rich uranium salen complexes.

$$[UI_3(THF)_4] \xrightarrow[THF,\ r.t.]{K_2salen} \underset{\mathbf{1}}{[UI_2(salen)(THF)_2]} + \underset{\mathbf{2}}{[U(salen)_2]}$$

Scheme II.6. Reaction of $[UI_3(THF)_4]$ with K_2salen.

The reaction of $[UI_3(THF)_4]$ with one equivalent of K_2salen in THF produces a dark brown suspension. Analysis of the crude mixture by ^{1}H NMR (***Figure II.3***) reveals the presence of two sets of six signals assigned to $[UI_2(salen)(THF)_2]$ **1** and $[U(salen)_2]$ **2**.

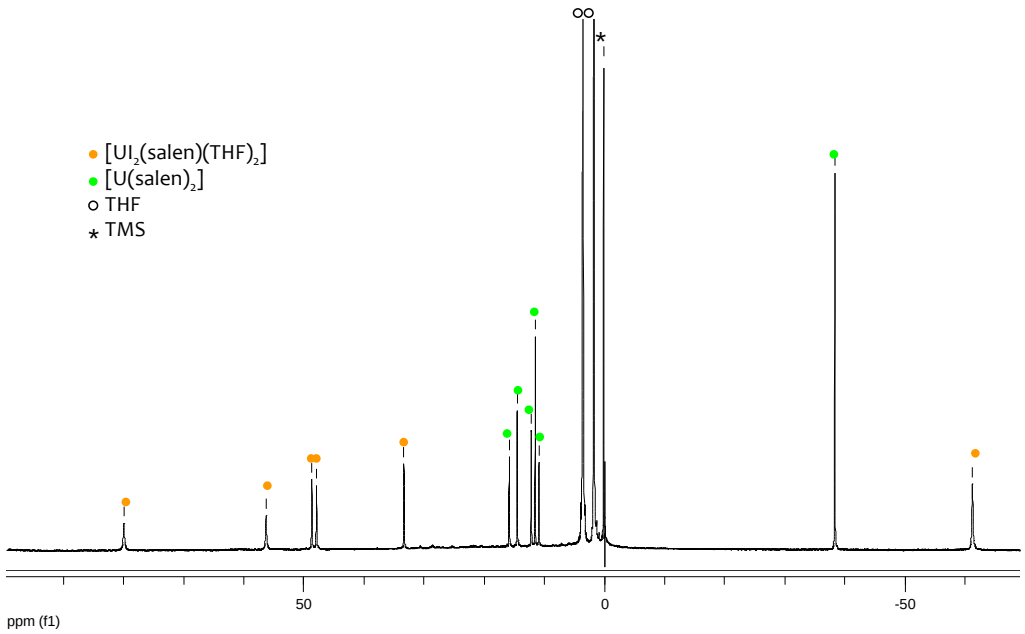

Figure II.3 ^{1}H NMR spectrum (298 K, THF-d_8, 200 MHz) of the crude mixture from the reaction of $[UI_3(THF)_4]$ with K_2salen.

These salen uranium(IV) complexes were probably formed by a disproportionation process ($4U^{III} = 3U^{IV} + U^0$) promoted by the salen ligand. Although the formation of U(0) metal could not be detected, starting from 1 equivalent of ligand *per* uranium atom, the formation of $[U(salen)_2]$

indicates that a non-salen uranium species has formed. Knowing the high chelating character of the salen ligand, it is unlikely that a uranium(IV) or uranium(III) halide is present in solution. This is also supported by a study[328] reporting ligand exchange between $[U(salen)_2]$ and UCl_4 in THF yielding $[UCl_2(salen)]$. The formation of some form of U(0) which is removed by filtration is thus a plausible alternative. An analogous behavior has been reported by several authors[76, 95-103, 254] Notably the Diaconescu group has shown that stoichiometric reaction between $[UI_3(THF)_4]$ and the dianionic ligand ferrocenediamide (NNfc) gives the U(IV) complexes $[U(NNfc)_2]$ and $[U(NNfc)I_2(THF)]$ in reproducible yields.[97] The authors indicated that the uranium(IV) complexes were presumably formed by the disproportionation of uranium(III) intermediates to U(IV) and insoluble U(0) particles. In addition, Cummins, Arnold and coworkers[95] showed that employing a stoichiometry consistent with this disproportionation increases the isolated yield of the U(IV) products.

Attempts to further reduce this reaction mixture with potassium or sodium metal were unsuccessful and no evidence of ligand reduction by U(III) was obtained for salen.

These results suggest that the salen ligand is both inappropriate to stabilize trivalent uranium and unsuited to store electrons in its π-system. Consequently, we decided to focus our studies on the salophen ligand in which the ethylene bridge has been replaced by a phenylene brige. It was anticipated that this should provide better electronic delocalization on the ligand and render the imine moieties more electron-acceptor.

II.2.2 Reaction of salophen salts with U(III) and U(IV) iodides

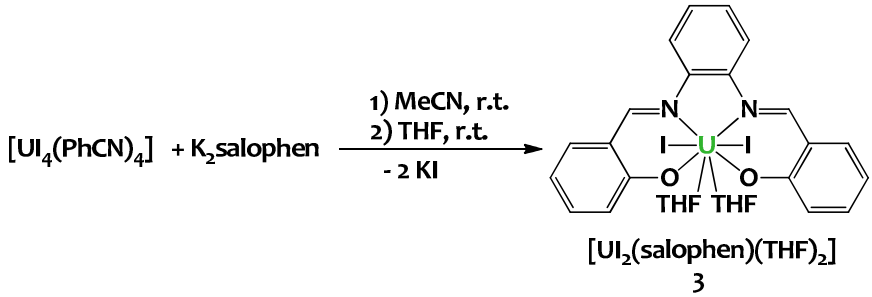

Scheme II.7. Synthesis of the heteroleptic U(IV) complex $[UI_2(salophen)(THF)_2]$ **3** by salt metathesis from the tetravalent uranium precursor $[UI_4(PhCN)_4]$.

The bis-iodide tetravalent uranium salophen complex is prepared by directly reacting the U(IV) precursor $[UI_4(PhCN)_4]$ with one equivalent of the deprotonated form of the Schiff base ligand in acetonitrile (Scheme II.7). Recrystallization in THF gives the pure complex $[UI_2(salophen)(THF)_2]$ **3** in 79% yield. The ^1H NMR spectrum for **3** exhibits seven resonances as expected for pseudo-C_2-

symmetric molecules in solution. These sharp peaks are paramagnetically shifted over a large range (-8.4 to +80.22 ppm), which is a common feature for U(IV) molecular compounds.[329]

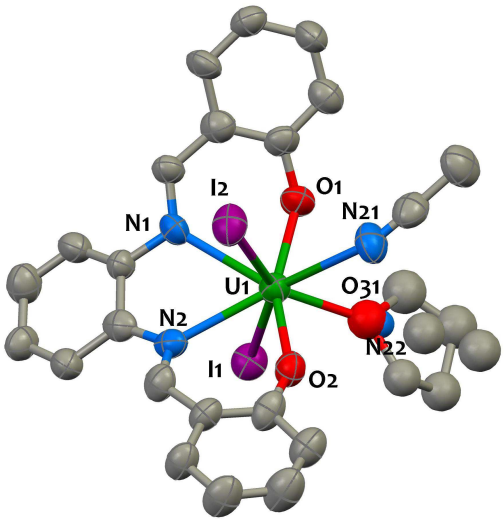

Figure II.4. Solid-state molecular structure of $[UI_2(salophen)(MeCN)_{1.5}(THF)_{0.5}]$ **3**. Hydrogen atoms are omitted for clarity. Uranium (green), iodine (purple), nitrogen (blue), oxygen (red) and carbon (grey) atoms are represented with 50% probability ellipsoids. Selected bond distances [Å]: U1-I1 3.1199(14), U1-I2 3.1464(14), U1-O1 2.153(12), U1-O2 2.128(12), U1-N1 2.610(14), U1-N2 2.590(14), U1-N21 2.631(17), U1-N22 2.60(4), U1-O31 2.30(4).

Single crystals of $[UI_2(salophen)(MeCN)_{1.5}(THF)_{0.5}]$ were obtained by slow diffusion of THF in an acetonitrile solution of the complex. The crystal structure is presented in Figure II.4 together with selected bond lengths and angles. This structure is closely related to that of $[UCl_2(salen)(THF)_2]$ reported by Floriani.[319] In both complexes, the uranium ion is surrounded by the N_2O_2 pocket of the tetradentate ligand, two halides and two solvent molecules. The coordination sphere of the metal approximates that of a dodecahedron defined by the two orthogonal trapezia O1N1N2O2⊥I1N22N21I2. Although the donor atoms of the ligand in **3** are not far from planar, the ligand as a whole is quite distorted from planarity and adopts a boat conformation.[330] The U-N and U-O bond lengths fall in the range of those observed for previously reported U(IV) Schiff bases complexes.[319-322] The U-I bond lengths are in agreement with that typically found for uranium(IV) iodide complexes.[100, 331] One solvent molecule is disordered, with a 50% occupancy rate for THF:MeCN.

We then investigated the reaction between $[UI_3(THF)_4]$ and K_2salophen with the objective of identifying new attractive precursors for performing reductive uranium chemistry.

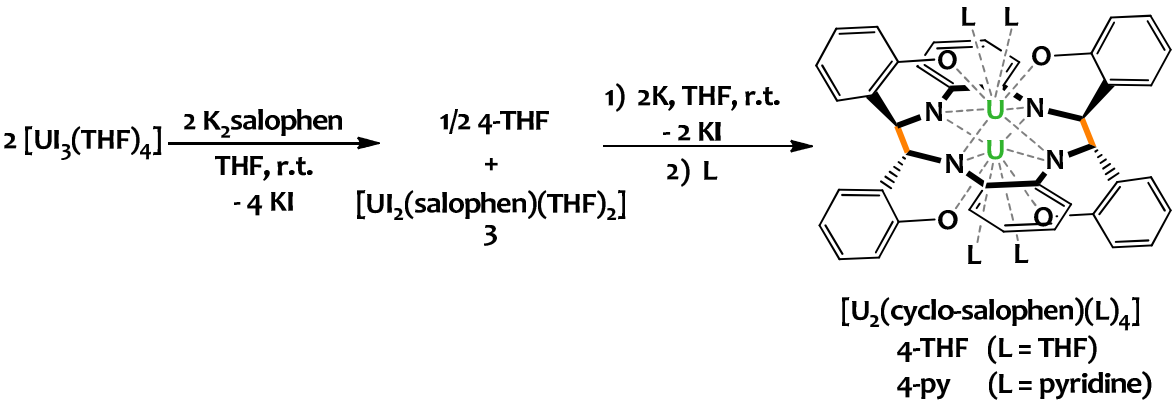

Scheme II.8. Synthesis of $[U_2(cyclo\text{-}salophen)(L)_4]$ 4-L (L = THF, pyridine).

The 1:1 reaction of $[UI_3(THF)_4]$ with the salophen potassium salt in THF produces a dark brown suspension. Analysis of the crude mixture by ^1H NMR reveals the presence of two sets of seven signals assigned to a mixture of two species (Figure II.5). One set of resonances corresponds to $[UI_2(salophen)(THF)_2]$ **3**, previously synthesized by salt metathesis from the U(IV) iodide precursor (vide supra). The second set of relatively sharp and strongly paramagnetically shifted signals corresponds to the dinuclear U(IV)-U(IV) $[U_2(cyclo\text{-}salophen)(THF)_4]$ **4-THF**. The formation of both species was confirmed by ESI-MS spectrometry.

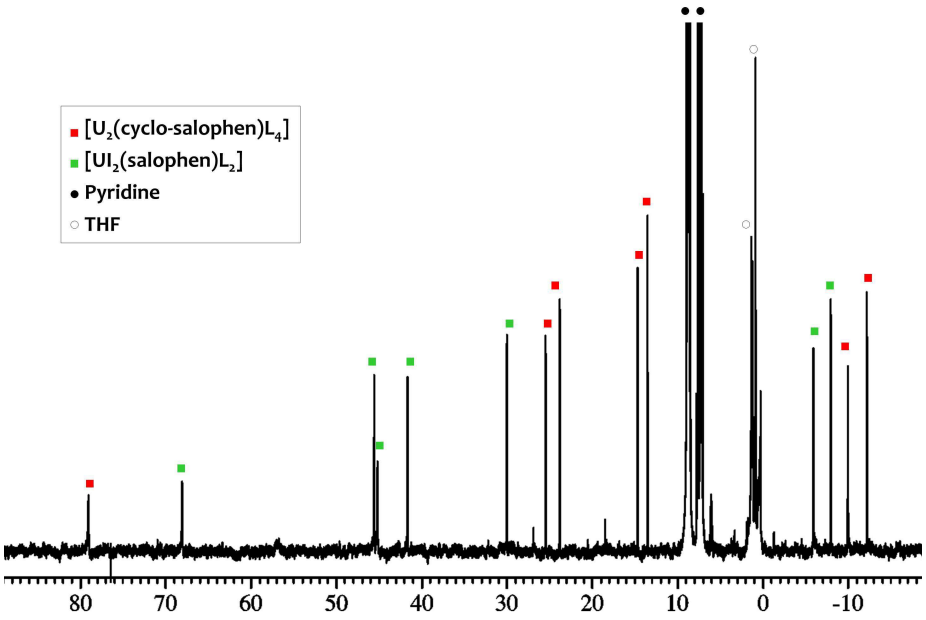

Figure II.5. ^1H NMR spectrum (298 K, pyridine-d_5, 200 MHz) of the crude mixture from the reaction of $[UI_3(THF)_4]$ with K_2salophen. L = pyridine.

Compound **4-THF** results from the reductive C–C coupling of the imine moieties of the salophen ligands. This indicates that trivalent uranium is not stabilized by the salophen ligand, but transfers one electron to the imino group of the free or U(III)-bound salophen ligand. Two electrons per uranium atom are required for the formation of a single C–C bond. Starting from trivalent uranium,

only one electron per metal center is available, and an external reducing agent is thus required to afford **4-THF** quantitatively.

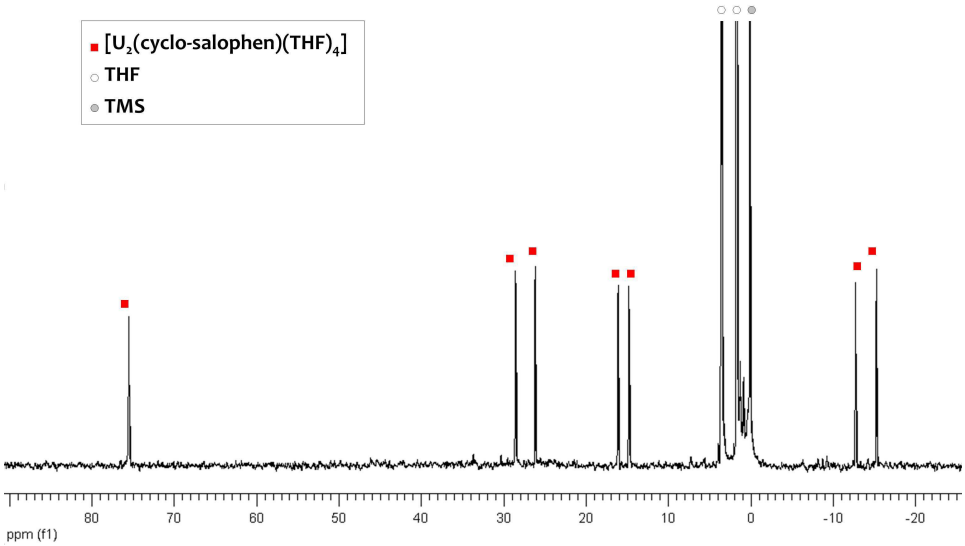

Figure II.6. ^{1}H NMR spectrum (298 K, 200 MHz, THF-d_8) of complex [U_2(cyclo-salophen)(THF)$_4$] **4-THF**.

Accordingly, [UI_3(THF)$_4$] was reacted with one equivalent of K_2salophen in THF and after four hours, the reaction mixture was subsequently reduced with one equivalent of potassium per uranium atom. Comparison of the ^{1}H NMR spectra obtained before and after reduction (***Figure II.5*** and ***Figure II.6***) shows that **3** is converted into **4-THF** upon reduction, yielding **4-THF** as the only product according to ***Scheme II.8***. Complex **4-THF** can be obtained in 86% yield from this reaction. At ambient temperature, the ^{1}H NMR spectrum for **4-THF** exhibits seven resonances, consistent with equivalent phenolate groups throughout the cyclo-salophen ligand on the NMR time-scale, indicating that the complex is in a D_{2h} arrangement in solution. The formation of compound **4-THF** was also confirmed by ESI-MS spectrometry (m/z= 1247.4 ([U_2(cyclo-salophen)(THF)$_2$]$^{+}$) and elemental analysis.

Recrystallization of **4-THF** in pyridine yields the analogous pyridinate complex [U_2(cyclo-salophen)(py)$_4$] **4-py**.

Structural data were obtained for the derivative **4-py** by single-crystal X-ray diffraction (***Figure II.7***). The structural parameters (***Table II.1***) of **4-py** point unambiguously to the presence of a U(IV) dimer complexed by the octadentate octaanionic amidophenolate macrocyclic ligand cyclo-salophen formed from the reductive C-C coupling of the two imino groups of the salophen ligands (***Figure II.7***-bottom-left). Notably the U-N bond distances (2.39 to 2.60 Å) are significantly shorter than the distances usually found in U(IV) Schiff bases complexes (usual range: 2.58-2.65 Å).[320, 321] Similarly, the C-N bond lengths (average value: 1.473(4) Å) are much longer than expected for imino moieties (usual range: 1.26-1.31 Å), in agreement with the occurrence of a reduced ligand. This is further

confirmed by the sp^3 character of the carbons involved in the C-C reductive coupling (average dihedral angle: C(1)-C(8)-C_{phenol} 110(1)°). The value of the two resulting C-C distances (1.609(5) Å), although rather long, is in the range of C-C bonds found in sterically hindered systems.[332-334] The resulting dinucleating ligand cyclo-salophen (***Figure II.7***-bottom-left) defines an almost planar 12-membered ring which holds two uranium atoms in close proximity (***Figure II.7***-bottom-right) with a U···U separation of 3.54(1) Å.

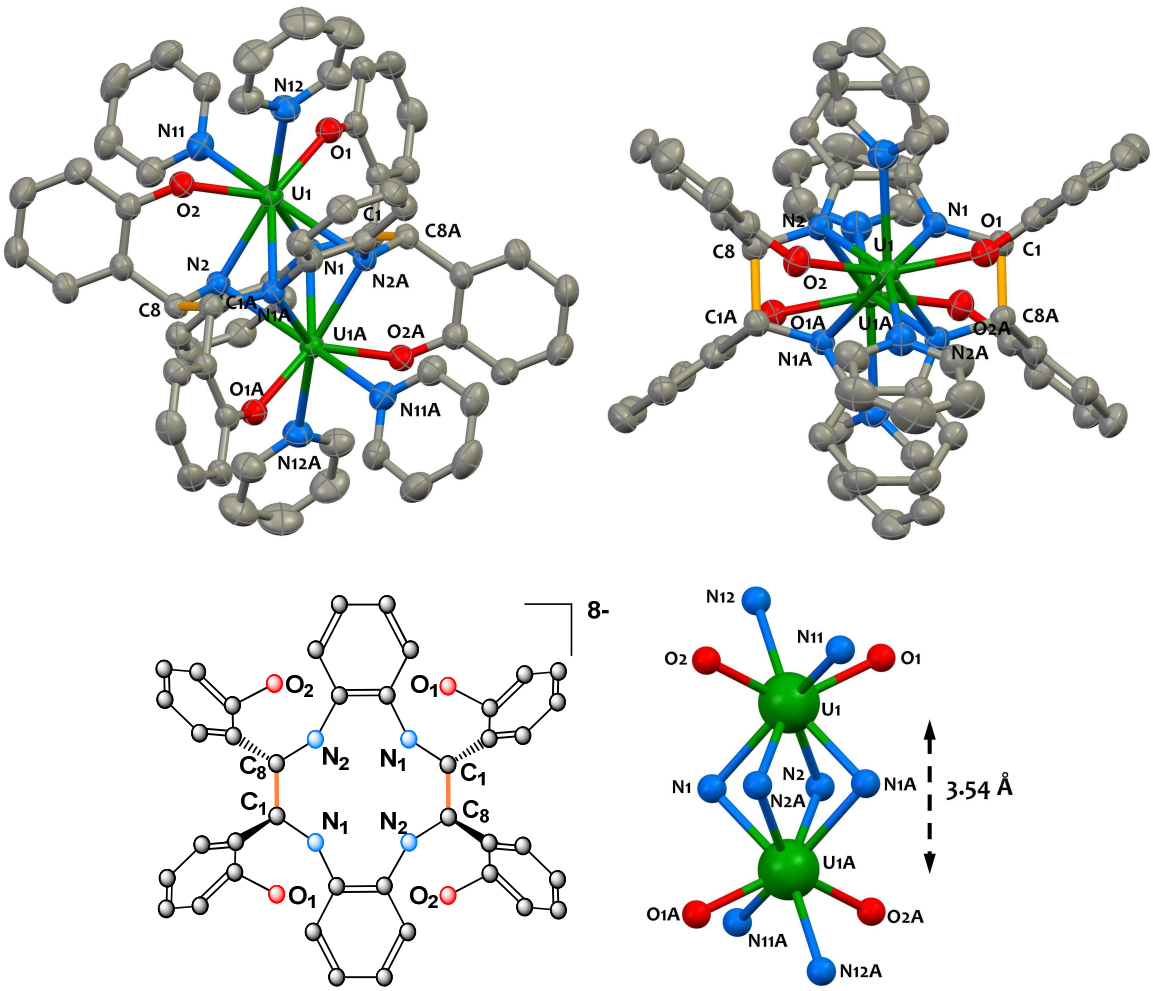

Figure II.7. Top: Side and top views of the solid-state molecular structure of [U_2(cyclo-salophen)$(py)_4$] **4-py**. Only one of the two crystallographically independent molecules is represented. Hydrogen atoms and interstitial solvent molecules are omitted for clarity. The C-C bonds bridging the two original salophen units are represented in yellow and the uranium (green), nitrogen (blue), oxygen (red) and carbon (grey) atoms are represented with 50% probability ellipsoids. Bottom: (left) Drawing and numbering scheme of the cyclo-salophen ligand. (right) View of the core of complex **4-py** showing the coordination environment of the two uranium atoms. Selected bond distances are given in ***Table II.1***.

Table II.1. Mean values of selected bond lengths [Å] in the U(IV) complex [U_2(cyclo-salophen)$(py)_4$] **4-py**. All distances are average.

Compound	U-N_{amido}	U-NA_{amido}	U-$N_{pyridine}$	U-$O_{phenolate}$	C-C_{link}	C-N_{amido}	U···U
4-py	2.2398(6)	2.57(2)	2.68(3)	2.23(1)	1.608(4)	1.473(3)	3.54(1)

A reaction sequence for the formation of **4-THF** is proposed in ***Scheme II.9*** which presents the structural consequences on the two salophen skeletons upon reduction. The formation of **4-THF** probably proceeds through the stepwise or simultaneous reduction of four imino groups by four U(III) ions to yield unstable U(IV) complexes of the corresponding radical anions which rapidly couple to form two C-C bonds. This indicates that $[UI_3(THF)_4]$ is able to reduce the imino group of the free or U(III)-bound salophen ligand. The fact that the formation of a half-reduced complex (only one salophen imino group reduced) is not observed is probably due to the high stability of the $[U(salophen)I_2(THF)_2]$ **3** by-product and because intramolecular coupling within this pre-organized system is favored. Four electrons are required to form **4-THF**, but only two electrons are available from the original U(III) centers. This explains why two additional equivalents of potassium are needed for the reaction to proceed to completion.

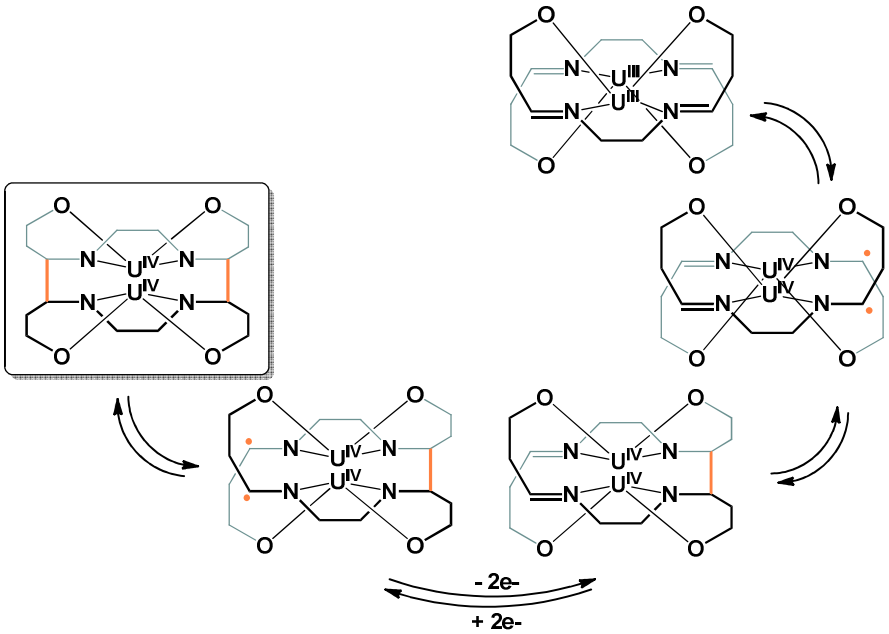

Scheme II.9. Proposed mechanism for the formation of compound **1**. Phenylene units as well as THF molecules and iodine anions in the coordination sphere of the metal have been omitted for clarity.

C-C couplings promoted by U(III) and U(IV) complexes associated, or not, with a reducing agent has been previously reported with ketones,[146, 335, 336] alkynes,[304, 337] heterocycles,[301, 338, 339] CS_2,[193] and CO[27, 147, 150-152, 154] but not for imino groups.

Such a reductive coupling of imino groups belonging to salophen ligand has precedents in literature for transition metals,[30-34] but this is the first example observed in the actinide series. Furthermore, in this case, the coupling is originated by the highly reductive trivalent uranium center which is likely to transfer one electron to the ligand. The electronic properties and the conformational characteristics of salophen probably play an important role in this phenomenon, since the maximum of electronic delocalization is assured over the three conjugated aromatic rings. Indeed, the replacement of the

phenylene bridge by an ethylene bridge has a critical impact on the outcome of the reaction and the non-innocent behaviour observed for the salophen ligand is not available for salen. As previously stated (section I.4), low-valent uranium has the ability to interact with π-conjugated non-innocent ligands to increase its oxidation state. The observed reactivity contrasts to the example of the first U(III) complex with a macrocyclic conjugated Schiff base.[129]

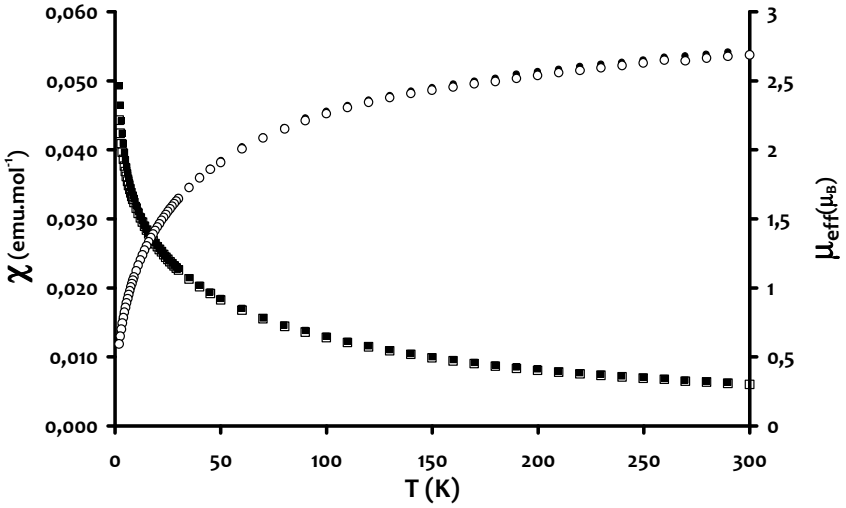

Figure II.8. Temperature-dependant SQUID magnetization data (0.5 T) for complexes **4-py** (black) and **1-THF** (white) (data per U center) plotted as χ (sqaures) and μ_{eff} (circles) versus temperature in the 2-300 K range. (X_{dia} = -6.67 × 10^{-4} emu.mol^{-1}, m=9.4 mg, M =1474.17 g.mol^{-1} for **4-py** and X_{dia} = - 6.49 × 10^{-4} emu.mol^{-1}, m=12.8 mg, M =1393.2 g.mol^{-1} for **4-THF**).

Magnetic data were collected in the temperature range from 2 to 300 K for **4-THF** and **4-py**. The similarity of the χ vs T data (***Figure II.8***) is in agreement with the presence of an analogous structure for the two complexes. The room temperature effective moments (2.68 μB for **4-py** ; 2.70 μB for **4-THF** ; values for one uranium) compare well with that measured for **4-THF** in solution using Evans method (2.74 μB), and falls in the range of the other U(IV) coordination compounds.[26, 70, 141, 340] This value is lower than the theoretical value (3.58 μ_B) calculated for a $5f^2$ ion with a full spin-orbit coupling as is commonly observed in tetravalent uranium complexes due to the crystal-field splitting of the Russel-Saunders $^3H_4$ ground term. The magnetic moments for **4-THF** and **4-py** drops off gradually with decreasing temperature due to depopulation of thermally accessible excited states. The linearity of the 1/ χ plot is characteristic of a Curie-Weiss behavior $\chi = C/(T-T_c)$ (C = 2.23 emu.K.mol^{-1}; T_c = -69 K for **4-THF ;** C = 2.24 emu.K.mol^{-1}; T_c = -74 K for **4-py**). In general, the magnetic susceptibility of U(IV) compounds displays a Curie-Weiss behavior at high temperature and temperature independent paramagnetism at low temperature.[26, 70, 209, 340-342] The complexes **4-THF** and **4-py** exhibit a deviation from this behavior. Such a deviation in U(IV) dimers with a short U-U distance could suggest the presence of a magnetic interaction between the U ions.[341]

The results obtained by the direct salt metathesis reaction between the trivalent halide precursor $[UI_3(THF)_4]$ and the potassium salt of the salophen ligand promted us to investigate other synthetic pathways.

II.2.3 Reaction of $[U\{N(SiMe_3)_2\}_3]$ with H_2salophen

We have also explored the reactivity of H_2salophen with $[U\{N(SiMe_3)_2\}_3]$[91] to access salophen uranium entities via protonolysis.[76] This strategy has been successfully used for the synthesis of stable U(III) compounds with phenoxide[92, 93, 128, 176] or alkoxide ligands,[122] and in our hands for accessing U(III) siloxide complexes (see section III.2). This starting material is generally used to circumvent the formation of undesired *ate* complexes sometimes seen with salt metathesis routes. In addition, this might prevent unwanted disproportionation processes often observed in the attempts for isolating U(III) complexes from $[UI_3(THF)_4]$.[76, 95-103]

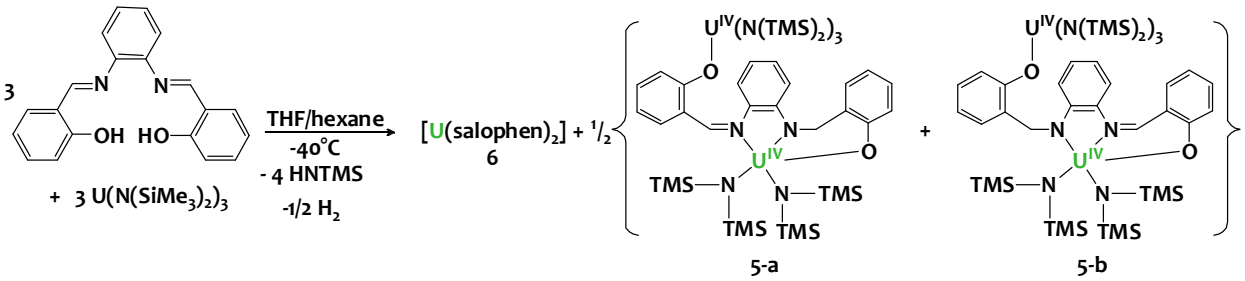

Scheme II.10. Reaction of H_2salophen with $[U(N(SiMe_3)_2)_3]$.

The ^{1}H NMR spectrum recorded in THF-d_8 for the crude reaction of $[U(N(SiMe_3)_2)_3]$ with one equivalent of the protonated salophen ligand in a THF/hexane mixture did not exhibit the presence of the characteristic resonances of $[U_2$(cyclo-salophen)$(THF)_4]$ but instead those of $[U(salophen)_2]$ **6** (see section II.2.4.1) together with a series of broad resonances between 0.0 and -10.0 ppm. The $[U(salophen)]_2$ complex could be separated from the reaction mixture upon extraction with hexane. Dark red single crystals were grown by cooling the resulting filtrate down to -40°C, allowing characterization of the other two other isomeric species $[U_2(\mu$-salophean$)\{N(SiMe_3)_2\}_5]$ **5-a** and **5-b** formed during the course of the reaction. These two compounds exhibit similar solubility and could not be separated, but possess the same molecular formula, as confirmed by X-ray diffraction studies and elemental analysis.

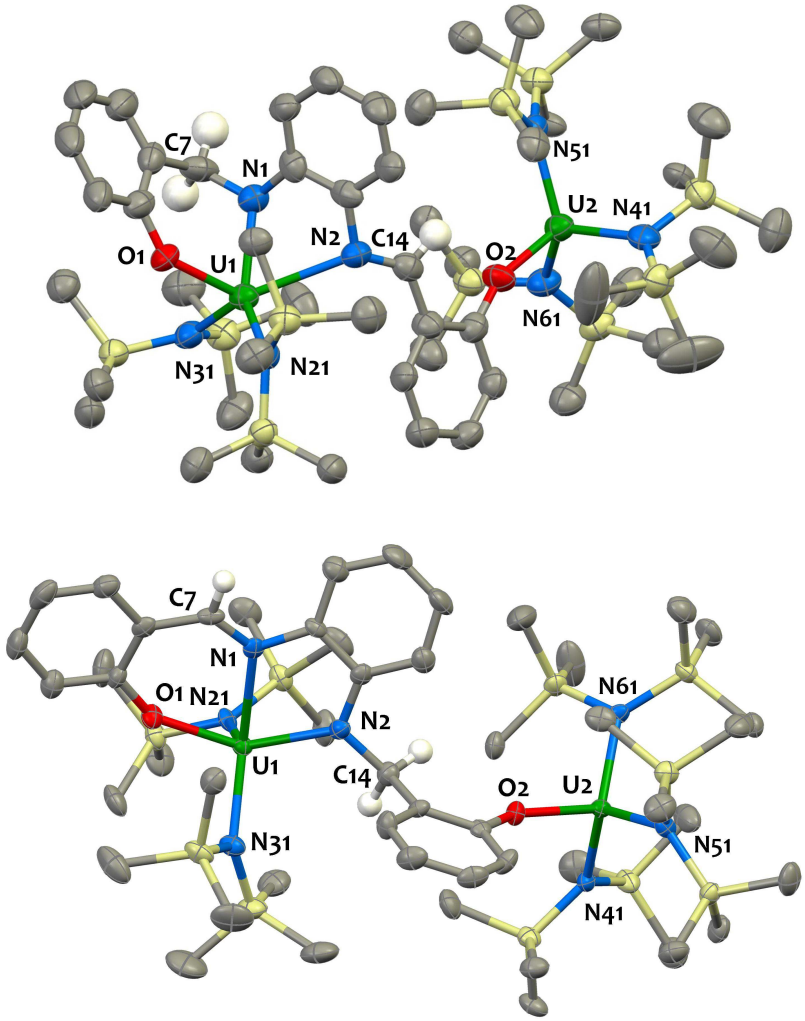

Figure II.9. Solid-state molecular structure of the two isomeric forms of $[U_2(\mu\text{-salophean})\{N(SiMe_3)_2\}_5]$ **5-a** (top) and **5-b** (bottom). Hydrogen atoms (except H7 and H14) are omitted for clarity. Uranium (green), nitrogen (blue), oxygen (red), silicon (yellow), hydrogen (white) and carbon (grey) atoms are represented with 50% probability ellipsoids. Selected bond distances [Å]: **5-a**: U1-O1 2.155(5), U1-N1 2.277(8), U1-N2 2.671(8), U1-N21 2.241(8), U1-N31 2.251(10), U2-O2 2.142(6), U2-N41 2.268(9), U2-N51 2.247(8), U2-N61 2.244(9), C7-N1 1.456(13), C14-N2 1.283(11) ; **5-b**: U1-O1 2.145(4), U1-N1 2.544(5), U1-N2 2.267(5), U1-N21 2.263(5), U1-N31 2.265(5), U2-O2 2.135(4), U2-N41 2.252(5), U2-N51 2.259(5), U2-N61 2.227(5), C7-N1 1.294(7), C14-N2 1.477(7).

The X-ray diffraction analyses revealed that two isomeric heteroleptic dinuclear complexes have formed (***Figure II.9***), in which two uranium atoms are bridged by a salophen-derived tetradentate amido-imino ligand (***Scheme II.10***). The analysis of the metrical parameters for **5-a** reveals that one moiety of the salophen has been reduced, the C7-N1 single bond distance (1.456(13) Å) being significantly longer than the C14-N2 bond length (1.283(11) Å). In addition the N1-C7-$C_{phenolate}$ bond angle (114.1(9)°) and the N2-C14-$C_{phenolate}$ bond angle (127(1)°) are in agreement with the C7 carbon possessing a sp^3 character and the C14 carbon possessing a sp^2 character. The amido character of the nitrogen atom N1 is further supported by the short U1-N1 bond distance (2.277(8) Å) compared to that of U1-N2 (2.671(8) Å). These distances are consistent with the presence of one amido group[343, 344] and one imino group.[320, 321] Overall, the U-N and U-O bond distances are in line with those reported

for other U(IV) phenolates, amido and imino complexes.[93, 161, 320, 321, 343, 344] The coordination sphere of the uranium center U1 is completed to 5 by one phenolate moiety and two hexamethyldisilylamido ligands and approximates that of a square pyramid. The second uranium atom U2 is tetracoordinated in a distorted tetrahedral fashion by a single phenolate moiety and three hexamethyldisilylamido ligands. The structural features for **5-b** are very similar to those of **5-a** except that the N2-C14 imino moiety has been reduced, as is shown by the short the C7-N1 double bond (1.294(7) Å) and the long C14-N2 one (1.477(7) Å).

The formation of [U(salophen)$_2$] **6** most probably results from the homolytic cleavage of an O-H phenol bond from the U(III) center resulting in its oxidation to U(IV) and elimination of dihydrogen. H_2 elimination is classically observed for reactions of trivalent uranium compounds with alcohols, amines or hydroxides, affording the oxidized U(IV) alkoxide, amidos or oxo complexes.[67, 127, 171, 345] In a similar fashion, the reaction between [U{N(SiMe$_3$)$_2$}$_3$] and the octadentate Schiff base pyrrole macrocycle H_4L reported by Arnold and coworkers[327] affords the U(IV) complex [UL]. However, in the latter case, [UL] is the only product of the reaction and was isolated in high yield (80%). This contrasts from our observation as no product resulting from the reduction of the Schiff base ligand was identified with the macrocyclic pyrrole platform.

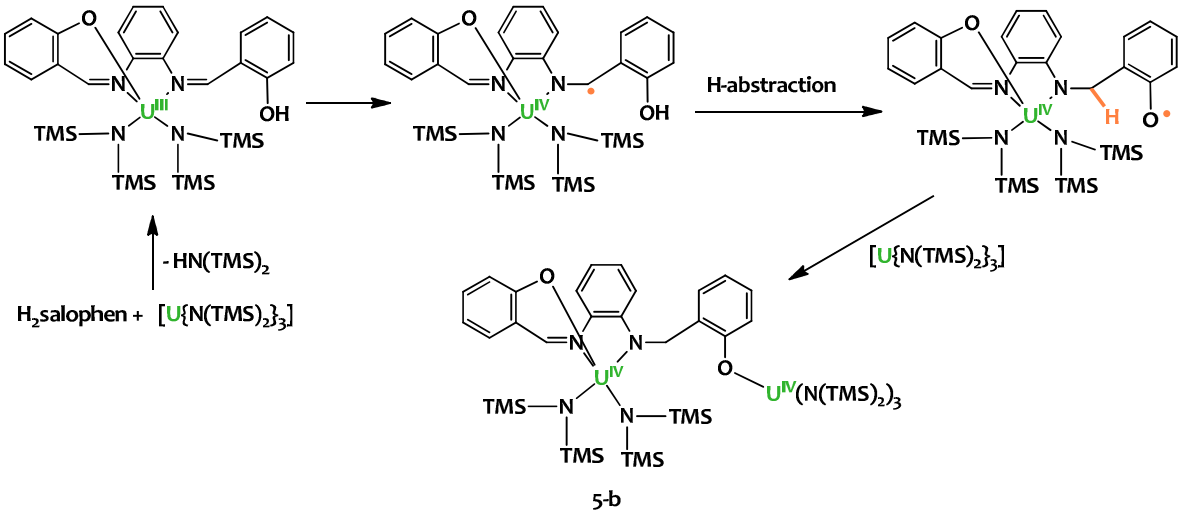

Scheme II.11. Proposed pathway for the formation of compound **5-b**.

The formation of **5-a** and **5-b** is proposed to occur via a hydrogen atom transfer mechanism depicted in ***Scheme II.11***, which involves the formation of an intermediate ligand-based radical species from the single electron transfer of the U(III) cation to the salophen ligand that rapidly abstracts an hydrogen atom from protic sources present in the reaction media instead of performing a radical coupling to yield a C-C bond as was observed in aprotic media. The hydrogen could originate from phenol moieties, which are known to be good hydrogen donors classically involved in hydrogen atom transfer processes.[346] Whilst to the best of our knowledge such uranium-mediated imine reduction

has not yet been reported, a parallel can be drawn with the U(III)-mediated reduction of benzophenone reported by Meyer and co-workers.[146] In Meyer's work, the reaction between [((^{Ad}ArO)$_3$tacn)U^{III}] and benzophenone yields the transient ketyl radical species [((^{Ad}ArO)$_3$tacn)U^{IV}(OC$^{\bullet}$Ph$_2$)] which quickly abstracts hydrogen to yield the U(IV) diphenylmethoxide complex [((^{Ad}ArO)$_3$tacn)U^{IV}(OCHPh$_2$)]. Such a mechanism is reminiscent to that proposed in ***Scheme II.11***. The source of hydrogen was postulated to occur via ligand decomposition, with a higher yield obtained in the presence of hydrogen sources such as THF, 1,4-cyclohexadiene or R$_3$SnH.[146] Interestingly, the U(IV) ketyl radical species could be stabilized by using the para-substituted 4,4′-di-*tert*-butylbenzophenone and the less sterically demanding (($^{t\text{-}Bu}$ArO)$_3$tacn) ligand. Similarly, [((^{Ad}ArO)$_3$tacn)U^{III}] reacts with diphenyldiazomethane to yield the charge-separated radical intermediate which undergo C-H activation and nitrogen insertion upon heating to produce the indazole complex [((^{Ad}ArO)$_3$tacn)U^{IV}(μ-2-3-phen(Ind))].[347] Also relevant is the reaction between [U{N(SiMe$_3$)$_2$}$_3$] and the Wittig reagent Ph$_3$P=CH$_2$ reported by Hayton and co-workers,[139] which affords the highly reactive intermediate U(III) adduct [Ph$_3$P=CH$_2$U{N(SiMe$_3$)$_2$}$_3$]. This compound in unstable at room temperature and quickly oxidizes to U(IV) to yield the carbene complex [Ph$_3$PHC=U{N(SiMe$_3$)$_2$}$_3$] along with PPh$_3$ and [CH$_3$U{N(SiMe$_3$)$_2$}$_3$] through an intermolecular H-atom transfer mechanism.

This result further confirms that trivalent uranium is not stabilized by the salophen platform, but transfers one electron to the ligand. The fate of the reaction is highly impacted by the reaction conditions, and notably by the presence of protic species in the reaction media. Indeed, while in absence of protons a reductive coupling of two imino moieties is observed, yielding C-C coupled electron-rich species, this process is quenched in presence of labile hydrogen atoms.

II.2.4 Accessing electron-rich mononuclear uranium species via intramolecular C-C coupling

II.2.4.1 Synthesis of U(IV) ^{R}salophen bis-complexes

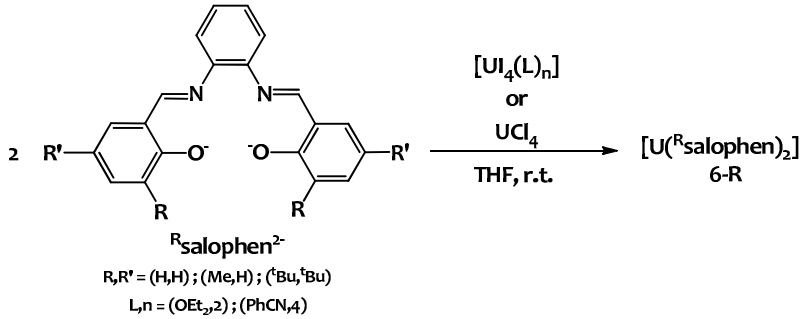

Scheme II.12. Synthesis of [U(^{R}salophen)$_2$] **6-R**.

The complexes [U(^{R}salophen)$_2$] **6-R** (R = H, Me, ^{t}Bu) are conveniently prepared from the reaction of the U(IV) halide precursors ([$UI_4(OEt_2)_2$] or [$UI_4(PhCN)_4$] or UCl_4) with two equivalents of $K_2{}^{R}$salophen in THF (***Scheme II.12***). For R = H a mixture of two bis-ligand U(IV) geometrical isomers **6-a** and **6-b** is obtained in solution, as is revealed by the two sets of 7 resonances observed in the ^{1}H NMR spectra (***Figure II.10***). The relative ratio a:b depends on the solvent, from 72:28 in THF to 86:14 in pyridine and 91:9 in acetonitrile at 25°C. The isomer distribution slightly changes upon heating in pyridine at 80°C to 82:18, but no coalescence could be observed.

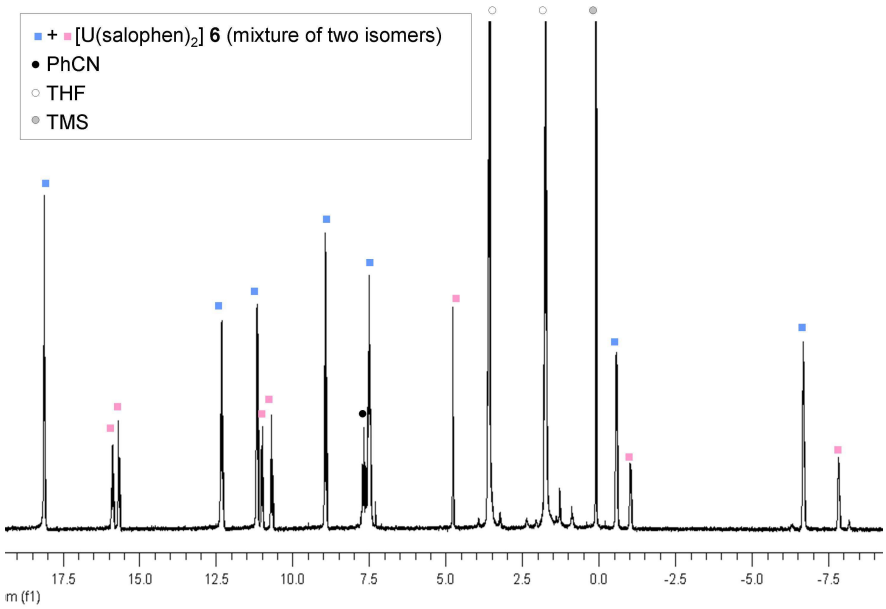

Figure II.10. ^{1}H NMR spectrum (298 K, 200 MHz) of [U(salophen)$_2$] **6** in THF-d_8 featuring a mixture of two isomeric forms **6-a** and **6-b** in solution.

Two types of isomeric structures, represented in ***Figure II.11***, have been reported for [M(salophen)$_2$] (M = Zr, Ce, Th) complexes in the solid-state;[32, 348, 349] the meridional isomer, whereby the ligands are oriented perpendicular to each other and the sandwich isomer, whereby the ligands are oriented parallel to each other. Therefore, it is probable that these are the two isomeric forms adopted in solution.

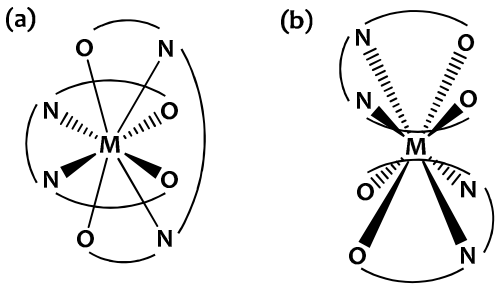

Figure II.11. Representation of the two isomeric forms of [M(salophen)$_2$] complexes. a) meridional isomer. b) sandwich isomer.

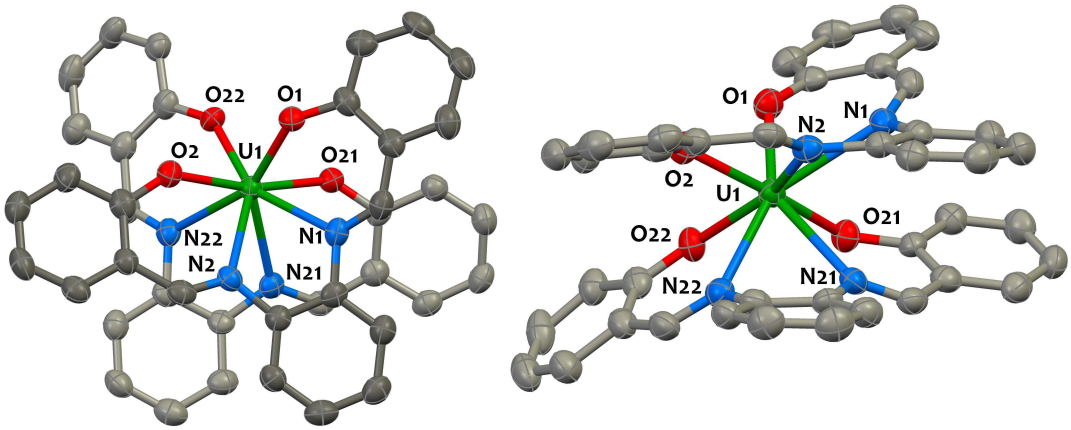

Figure II.12. Solid-state molecular structure of [U(salophen)$_2$] **6.** (left) top view ; (right) side view. Hydrogen atoms are omitted for clarity. Uranium(green), nitrogen(blue), oxygen (red) and carbon (grey) atoms are represented with 50% probability ellipsoids. Selected bond distances [Å]: U1-N1 2.623(6), U1-N2 2.645(2), U1-N21 2.629(6), U1-N22 2.578(5).

[U(salophen)$_2$] crystallizes as black blocks in the monoclinic space group $P2_1/n$. Various crystallization conditions were applied in attempts to grow single crystals of [U(salophen)$_2$], however everytime the sandwich isomer was obtained, with the equilibrium between the two isomeric forms most probably shifted towards the sole formation of this isomer in the solid-state. As shown in ***Figure II.12***, the two tetradentate Schiff base ligands adopt a boat conformation, encapsulating the uranium cation between the two convex sides of the ligands. The eight-coordinate uranium is bound by the oxygen and nitrogen atoms of two overlapping salophen ligands. The U-O and U-N bond distances are in agreement with those typically reported for tetravalent uranium complexes.[320-322] The resulting coordinating polyhedron around uranium can be described as a distorted square antiprism with the N_2O_2 cores of the Schiff bases defining the square bases of the polyhedron. The two overlapping salophen units are rotated by an angle of 49.9°, calculated from the average value of the torsion angles between O1···O2^O21···O22 and N1···N2^N21···N22.

Dissolution of the pure crystalline compound in pyridine affords a mixture of both isomers in the initial 86:14 ratio. This result suggests that the interconversion between the two isomers occurs in solution as no enrichment into one isomer was detected. These observations contrast with those for the analogous zirconium compound [Zr(salophen)$_2$], as the meridional and sandwich isomers were found to be thermally non-interconvertible.[32]

Similarly to [U(salophen)$_2$] **6,** two sets of resonances are observed in the ^{1}H NMR spectrum of [U(^{Me}salophen)$_2$] **6-Me**, confirming the presence of two isomeric forms (ratio = 73:27 in THF solution) for this complex in solution. In contrast the ^{1}H NMR spectrum recorded for complex [U(^{tBu}salophen)$_2$] **6-^{t}Bu** at 293 K displays a series of broad resonances that span the range +30 to -15 pm. This is attributed to the higher fluxionality of **6-^{t}Bu**, most probably induced by the high steric

bulk introduced by the ^{t}Bu groups. Upon cooling to 263 K, 14 sharp resonances of the same integral are observed in the ^{1}H NMR spectrum, most probably corresponding to an asymmetric complex in solution.

The electronic spectra recorded for complexes [U(^{R}salophen)$_2$] **6-R** display a similar series of absorption bands below 450 nm ($\varepsilon \geq 20000$ L.cm^{-1}.mol^{-1}, ***Figure II.14***) which are assigned to ligand-based π-π* transitions. These complexes are stable and soluble in common organic solvents such as THF, pyridine, acetonitrile, and the recorded mass spectra are in agreement with their formulation in solution.

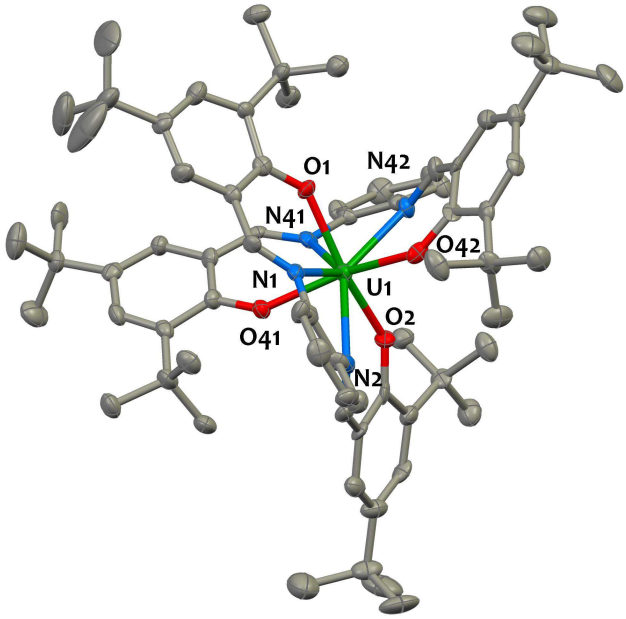

Figure II.13. Solid-state molecular structure of [U(^{tBu}salophen)$_2$] **6-^{t}Bu.** Hydrogen atoms and solvent molecules are omitted for clarity. Uranium (green), nitrogen (blue), oxygen (red) and carbon (grey) atoms are represented with 50% probability ellipsoids. Selected bond distances [Å]: U1-O2 2.236(5) ; U1-O1 2.238(4) ; U1-O41 2.243(5) ; U1-O42 2.253(5) ; U1-N2 2.555(6) ; U1-N41 2.582(6) ; U1-N42 2.585(6) ; U1-N1 2.604(6).

The solid-state structure of [U(^{tBu}salophen)$_2$] **6-^{t}Bu** is shown in ***Figure II.13***. Contrary to the structure of [U(salophen)$_2$] **6**, the ligands in **6-^{t}Bu** are arranged meridionaly. Both ligands adopt the usual boat conformation, as a result of the large size of the uranium cation, and the four coordinating atoms of each ligand are almost coplanar (mean deviation from plane : 0.019(4) Å and 0.022(7) Å). The uranium is encapsulated in the middle of the two N_2O_2 planes that are almost perpendicular to each other (89.74°), providing a distorted square antiprismatic environment to the metal. The mean U-O and U-N bond distances (2.236(7) Å and 2.58(2) Å respectively) are comparable to thoses observed in [U(salophen)$_2$] and fall within the range of thoses reported for U(IV) ONNO Schiff base complexes.[320, 321] This structure is closely related to that of [U(^{OMe}salophen)$_2$], the first homoleptic complex of uranium(IV) to be structurally characterized.[320]

II.2.4.2 Reduction studies

Although the ligands could rearrange in solution, the sandwich geometry adopted by the two ligands in the solid state structure and the short distance observed between the carbon atoms C7···C27 and C14···C34 from the imino groups of two different ligands in **2** (respectively 4.51 and 4.84 Å) suggested that the intramolecular reductive C-C coupling might be possible.

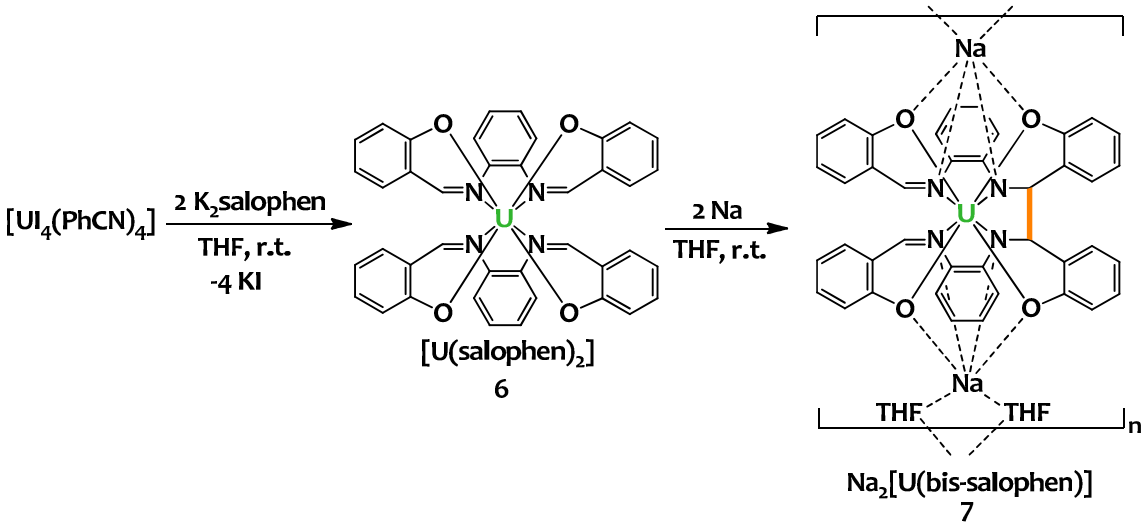

Scheme II.13. Synthesis of Na_2[U(bis-salophen)] **7**.

The reduction of [U(salophen)$_2$] **6** was successfully performed via the *in-situ* addition of two equivalents of sodium metal *per* uranium in THF (***Scheme II.13***). The reaction mixture gradually turns from brown to deep purple in 12 hours. The reduction affords the reduced complex Na_2[U(bis-salophen)] **7**, in 88% yield. Complex **7** is highly soluble in THF or pyridine, and is stable in solution over long periods of time under an argon atmosphere. The mass spectrum recorded in THF solution supports the presence of a [U(bis-salophen)]$^{2-}$ moiety with an overall di-anionic charge. The ^{1}H NMR spectrum of the complex in pyridine or THF solution at 298 K reveals the presence of 14 narrow paramagnetically shifted resonances, consistent with the presence of C_2v symmetric species in solution in agreement with the solid state structure (vide infra).

Isolation of a pure product from the reduction with potassium instead of sodium proved more difficult. The ^{1}H NMR spectrum in deuterated THF of the reaction mixture after reduction of **6** with two equivalents of potassium metal reveals an intractable mixture of products. These compounds might be different isomeric forms of K_2[U(bis-salophen)] in solution. However, given the stronger reducing ability of potassium, the presence of more reduced species is equally conceivable.

Consistent with the strong color change observed upon reduction of complex **6**, the electronic absorption spectrum of Na_2[U(bis-salophen)] **7** measured in THF solution (***Figure II.14***) displays a

series of intense absorption bands, with a new band centered at λ_{max} = 570 nm (ε = 8920 L.cm^{-1}.mol^{-1}). This absorption band is characteristic of the bis-salophen type structure and could be assigned either to a π-π* or to a charge transfer transition.

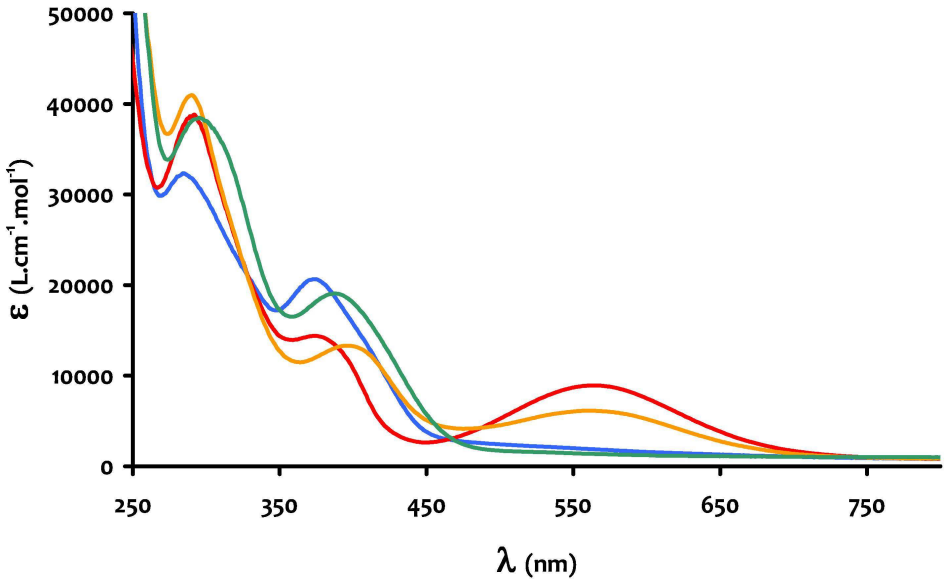

Figure II.14. UV/visible spectra (298 K) of 0.5 mM THF solutions of complexes [U(salophen)$_2$] **6** (blue line) ; Na$_2$[U(bis-salophen)] **7** (red line) ; [U(^{tBu}salophen)$_2$] **6-^{t}Bu** (green line) and K$_2$[U(bis-^{tBu}salophen)] **7-^{t}Bu** (orange line).

This absorption gives rise to the intense purple color of the complex which is reminiscent from that of conjugated ketyl radicals.[146, 350-354] C-C coupled products of triphenylmethyl[355, 356] or benzophenone ketyl[352, 357] radicals that have been reported to undergo a chemical equilibrium with their radical monomeric form. Notably, Wolczanski and coworkers reported that the absorption band at 646 nm observed in the spectrum of the head-to-tail para coupled benzophenone complex [(silox)$_3$Ti-O(Ph)$_2$C-(H)C(CH)$_2$C(CH=CH)=C(Ph)O-Ti-(silox)$_3$] was in reality due to the charge-separated ketyl radical monomeric complex in rapid equilibrium with the dimeric C-C coupled product.[352] Organotin hydrides are efficient hydrogen atom donors which are conveniently used to trap ketyl carboradicals.[146, 357, 358] Accordingly, the reaction of **7** with Bu_3SnH was carried out in order to determine if a similar equilibrium between the C-C coupled product **7** and a putative radical ligand form was occurring. However, no reaction was observed, therefore ruling out this possibility (***Scheme II.14***).

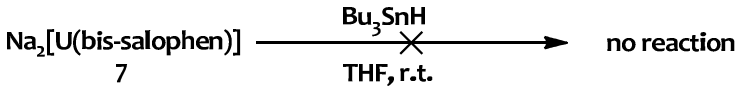

Scheme II.14. Complex Na$_2$[U(bis-salophen)] **7** does not react with tributyltin hydride.

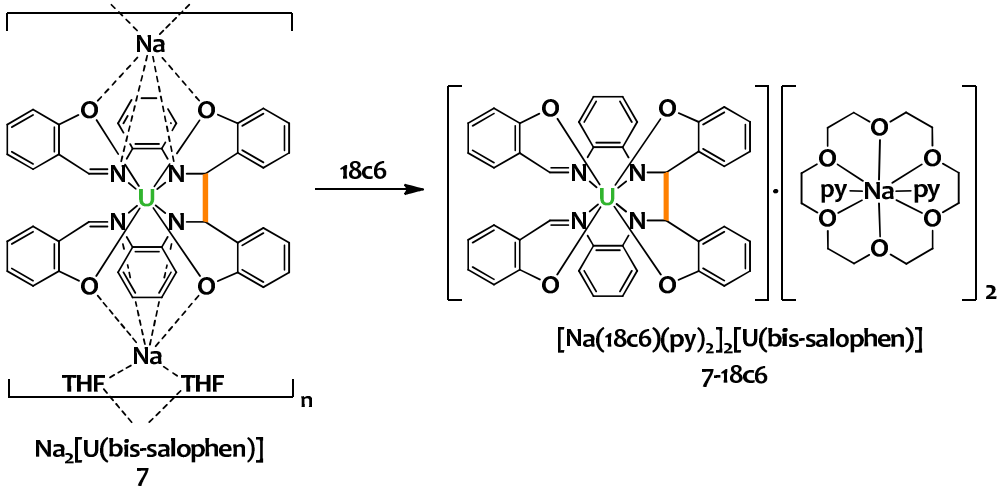

Figure II.15. Addition of 18c6 to a pyridine solution of **7** prevents the coordination of the alkali cation to the ligand and affords the ion pair [Na(18c6)(py)$_2$]$_2$[U(bis-salophen)] **7-18c6**.

Whilst the ^{1}H NMR spectrum of Na$_2$[U(bis-salophen)] **7** in pyridine solution exhibits 14 well resolved sharp resonances, addition of two equivalents of 18c6 crown ether to the NMR tube dramatically affected the ^{1}H NMR spectrum by shifting and broadening the peaks rendering the spectrum of [Na(18c6)(py)$_2$]$_2$[U(bis-salophen)] **7-18c6** hardly attributable at 25°C. Upon heating to 50°C, the resonances sharpen and 14 signals are observed for the bis-salophen ligand. The 18c6-induced changes in the ^{1}H NMR spectrum provide evidence for the coordination of sodium cations to the anionic [U(bis-salophen)]$^{2-}$ moiety in pyridine solution in absence of crown ether (***Figure II.15***). This is further supported by the solid-state structure of K$_2$[U(bis-^{tBu}salophen)] **7-^{t}Bu** (vide infra) and of the analogous lanthanide complexes K$_3$[Ln(bis-salophen)] (Ln = Nd, Tb)[359] which crystallize as 1-D coordination polymers with bridging potassium countercations in absence of crown ether.

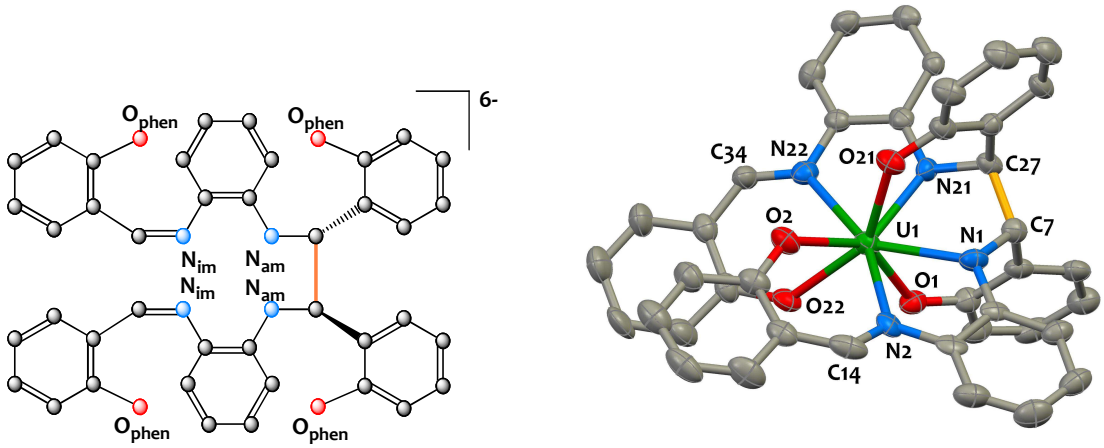

Figure II.16. Drawing of the bis-salophen ligand (right) and ellipsoid plot for the [U(bis-salophen)]$^{2-}$ anion in **7-18c6** (left). Hydrogen atoms are omitted for clarity. Uranium (green), nitrogen (blue), oxygen (red) and carbon (grey) atoms are represented with 50% probability ellipsoids. The C-C bond bridging the two original salophen units is represented in yellow. Selected bond distances are given in ***Table II.2.***

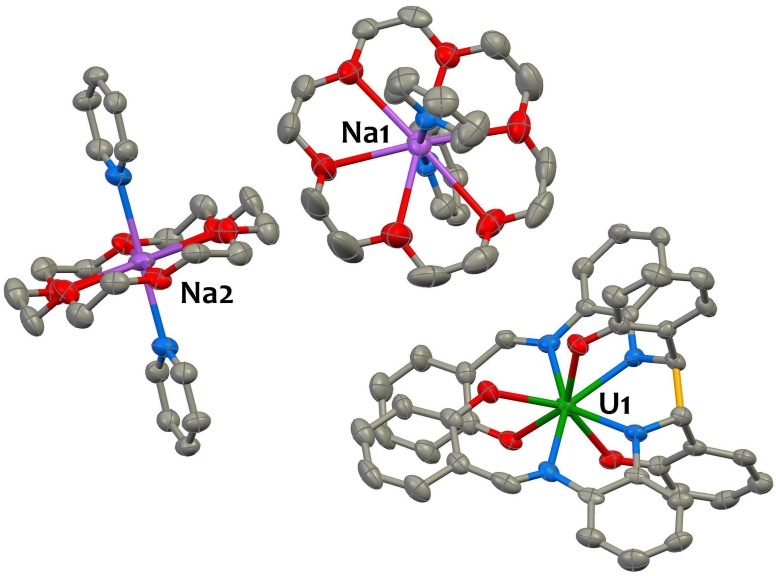

Figure II.17. Solid-state molecular structure of $[Na(18c6)(py)_2]_2[U(bis\text{-}salophen)_2]$ **7-18c6**. Hydrogen atoms and interstitial solvent molecules are omitted for clarity. The C-C bond bridging the two original salophen units is represented in yellow. Uranium (green), sodium(purple), iodine nitrogen (blue), oxygen (red) and carbon (grey) atoms are represented with 50% probability ellipsoids.

Single crystals of the complex $[Na(18c6)(py)_2]_2[U(bis\text{-}salophen)]$, **7-18c6** suitable for X-ray diffraction analysis were obtained by slow diffusion of hexane into a pyridine solution of **7** in presence of excess 18c6 crown-ether. The ion-pair structure for **7-18c6**, depicted in ***Figure II.17***, reveals unambiguously that the reduction occurs on the ligand rather than on the metal ruling out the possibility of a U(III) or U(II) species in the final mononuclear complex. Thus, the formula $Na_2[U(bis\text{-}salophen)]$ where bis-salophen is an hexa-anionic octadentate ligand (***Figure II.16***) built from the reductive coupling of imino groups from two salophen ligands, provides a good description of complex **7**.

Table II.2. Mean values of selected bond lengths [Å] in the U(IV) complexes of the ^{R}salophen ligands and the two-electron reduced bis-^{R}salophen ligand. All distances are average.

Compound	U-N_{imino}	U-N_{amido}	U-$O_{phenolate}$	C-C_{link}	C-N_{amido}	C-N_{imino}
6	2.61(3)	/	2.22(1)	/	/	1.283(8)
6-^{t}Bu	2.58(2)	/	2.236(7)	/	/	1.290(7)
7-18c6	2.624(7)	2.387(8)	2.31(1)	1.559(7)	1.46(1)	1.298(3)
7-Me-dibenzo18c6	2.61(4)	2.411(8)	2.29(2)	1.591(11)	1.47(2)	1.301(2)
7-^{t}Bu	2.618(4)	2.442(3)	2.294(3)	1.564(8)	1.456(5)	1.309(5)

The O22-N22-N21-N1-N2-02 donor atoms wrap around uranium in a helical fashion. The U(IV) cation is coordinated in a dodecahedral fashion defined by the two orthogonal trapezia O1-O22-O2-O21 and N22-N21-N1-N2. The value of the distance for the C-C bond between C7 and C27 resulting form the reductive coupling of two salophen ligand (1.559(7) Å) is 0.05 Å smaller than that observed in complex **4-py**. Bond distances and angles involving the C7, C14, C27 and C34 carbon atoms are

consistent with a sp^3 character for C7 and C27 and with a sp^2 character for carbons C14 and C34. The values of the U-N bond distances are consistent[343, 344] with the presence of two amido groups and two imino groups with the U-N_{amido} distances (U1-N1 2.393(5), U1-N21 2.380(5) Å) being significantly shorter than the U-N_{imino} distances (U1-N2 2.629(4), U1-N22 2.619(5) Å). This confirms that a partial reduction of the salophen ligands has occurred. The value of the magnetic moment (2.83 μ_B) measured using the Evans method for a THF solution of **7** is also in the range of values reported for U(IV) complexes.[114]

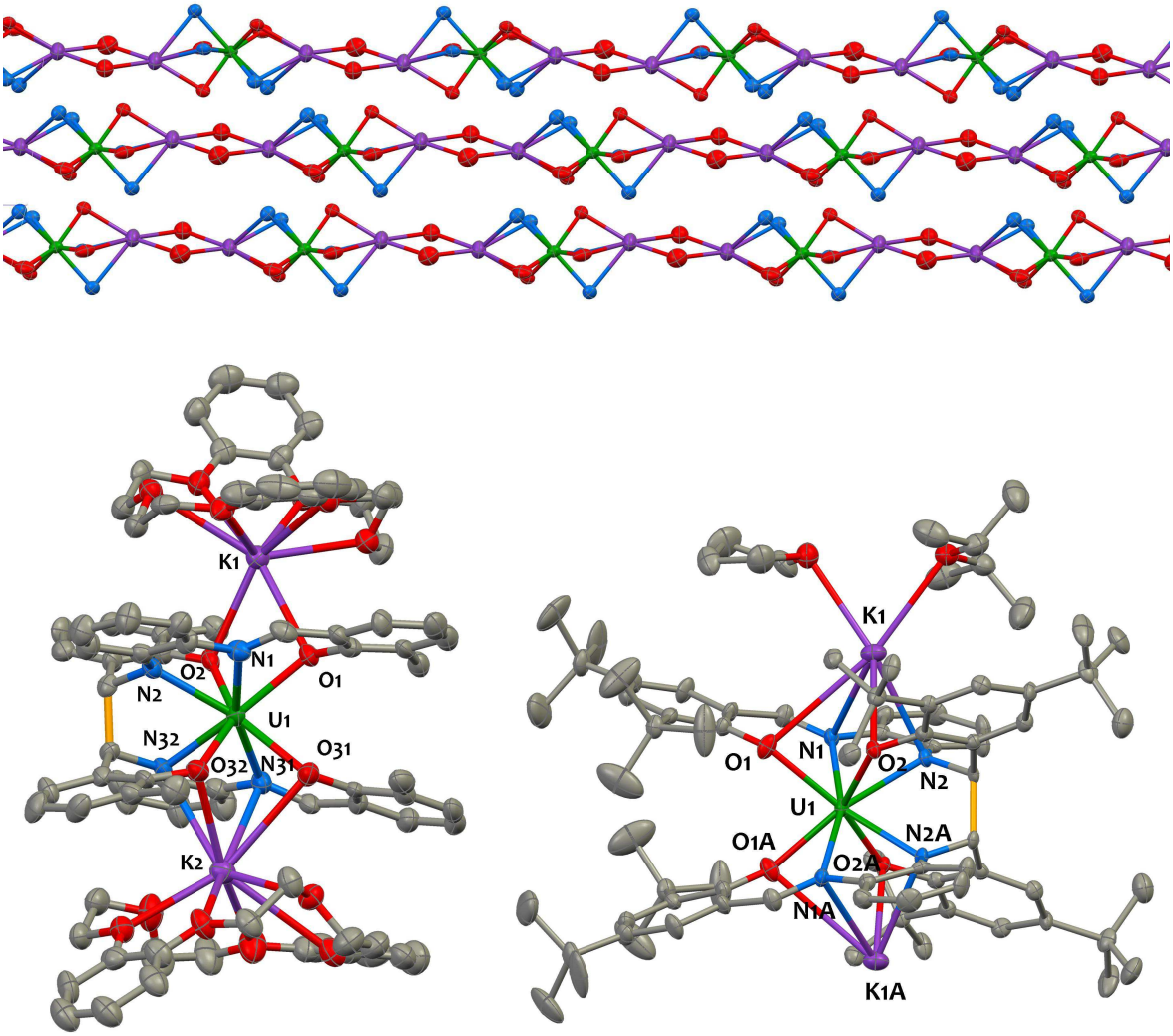

Figure II.18. Top : Mercury view of the 1-D polymeric network in **7-^{t}Bu**. Only U, K, N and O atoms are presented for clarity. Bottom : Solid-state molecular structure of [K(dibenzo18c6)]$_2$[U(^{Me}bis-salophen)] **7-Me-dibenzo18c6** (left) and K_2[U(^{tBu}salophen)$_2$].(THF).(DIPE) **7-^{t}Bu** (right). Hydrogen atoms and disorder are omitted for clarity. Uranium (green), potassium (purple), nitrogen (blue), oxygen (red) and carbon (grey) atoms are represented with 50% probability ellipsoids. The C-C bond bridging the two original salophen units is represented in yellow. Selected bond distances are given in ***TableII.2.***

In order to investigate the possible influence on the reduction reaction of the presence of bulky substituents on the salophen ligand, the reduction of the [U(^{Me}salophen)$_2$] **6-Me** and [U(^{tBu}salophen)$_2$] **6-^{t}Bu** complexes was performed with metallic potassium. In spite of the added

steric constraints, the reduction of these complexes also led to ligand reduction rather than metal reduction followed by the formation of an intramolecular C-C bond yielding the analogous [U(bis-^{R}salophen)] (R = Me **7-Me** ; R = ^{t}Bu **7-^{t}Bu**) complexes which were isolated and characterised by ^{1}H NMR, mass spectrometry and elemental analysis. The deep purple color of the complexes **7-Me** and **7-^{t}Bu** which is due to the absorption band centerd at λ_{max} = 570 nm (***Figure II.14***) characteristic of the bis-^{R}salophen ligand structure suggest ligand reduction.

Complexes **7-^{t}Bu** and **7-Me** were also characterized in the solid-state. The ^{t}Bu substituents provide higher solubility to the **7-^{t}Bu** complex compared to its **7-Me** analogue. This allowed the growth of single crystals of **7-^{t}Bu** in absence of crown ether from saturated DIPE solutions. The crystal structure of **7-^{t}Bu** consists in a 1D network of [U(bis-^{tBu}salophen)] dianions bound through K bridges, as represented in ***Figure II.18*** (top and bottom-left). This structure shows that in absence of crown ether the alkali cations remain coordinated to the Schiff bases complexes affording polymeric structures. In contrast, addition of 18c6 crown ether resulted in discrete ion pairs in the solid-state structure of [K(dibenzo18c6)]$_2$[U(^{Me}bis-salophen)] **7-Me-dibenzo18c6**. The two potassium cations in this crystal structure remain coordinated to the ligand backbone (***Figure II.18***-bottom left). Both potassiums are capped by a dibenzo18c6 molecule preventing the formation of a coordination polymeric chain analogous to those of **7-^{t}Bu**. The structural environment around uranium is fairly similar in **7-Me-dibenzo18c6** and **7-^{t}Bu**. Whilst the polydentate bis-salophen ligand in **7-18c6** wraps around uranium in a helical fashion, the uranium(IV) cation in **7-Me-dibenzo18c6** and **7-^{t}Bu** is surrounded by two N_2O_2 parallel planes from the bis-^{R}salophen (R = Me, ^{t}Bu) ligand which adopts a sandwich-derived structure. As a result, the coordination sphere of the metal approximates to that of a square antiprism. The U-N and C-N bond lengths (***TableII.2***) are in agreement with a half-reduced amido imido hexaanionic ligand. The U-N_{amido} bond lengths are much longer in **7-^{t}Bu** than in **7-18c6**, probably due to the coordination of K^+ cation to the amido moiety.

II.2.4.3 Electrochemical studies

In order to gain a better understanding of the redox properties of these uranium(IV) complexes electrochemical studies were performed. Cyclic voltammetry data were collected for complexes **7, 7-Me** and **7-^{t}Bu** in ~0.1 M [Bu_4N][PF_6] pyridine solution and are presented in ***Figure II.19***. All redox potentials are referenced against the $[(C_5H_5)_2Fe]^{+/o}$ redox couple and are given in ***Table II.3***.

The cyclic voltammogram recorded for the salophen ligand potassium salt in pyridine displays no redox processes between from 0 V to -2.5 V (***Figure II.19***, curve a). This is in agreement with the

literature value reported for the reduction potential (-2.47 V vs SCE i.e. -2.85 V vs Fc^+/Fc in DMF) of the deprotonated form of the salophen ligand.[360]

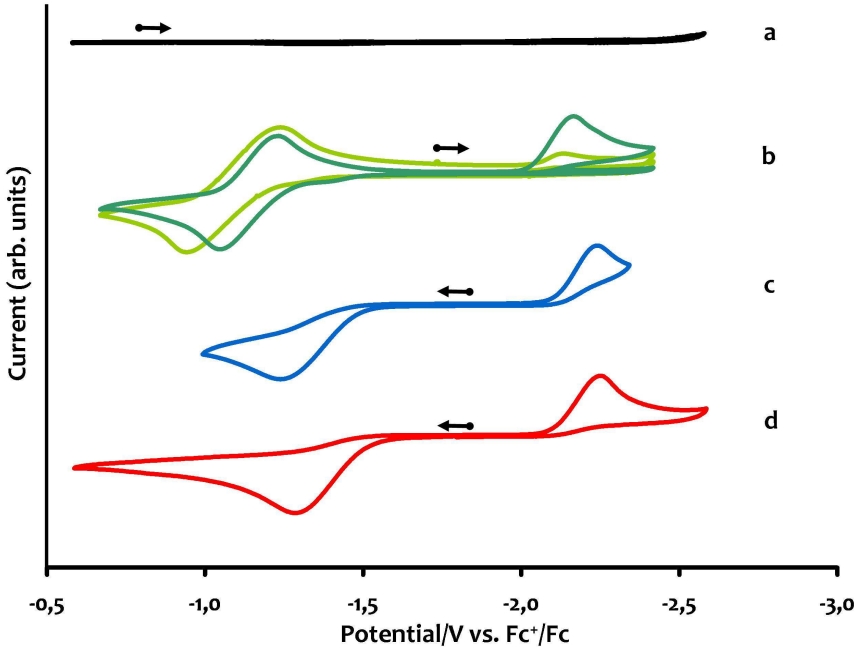

Figure II.19. Cyclic voltammograms for 10 mM solutions of (a) K_2salophen ligand, (b) Na_2[U(bis-salophen)] **7**, (c) K_2[U(bis-^{Me}salophen)] **7-Me** and (d) K_2[U(bis-^{tBu}salophen)] **7-^{t}Bu** recorded in 0.1 M $[Bu_4N][PF_6]$ pyridine solution at 100 mV/s scan rate and 5 mV/s scan rate for the dark green curve (b).

The complex Na_2[U(bis-salophen)] **7** exhibits a pseudo-reversible oxidation wave at $E_{1/2}$ = -1.14 V which corresponds to the oxidation of the bis-salophen ligand (***Figure II.19***, curve b light green). This process is associated with an irreversible reduction event at E_{pc} = -2.17 V observed when decreasing the potential from -0.6 V to -2.5 V. Indeed, this process is not observed when the voltammogram is swept initially from -1.7 V to the negative direction. Whilst the value for this reduction potential is compatible with a U(IV)/U(III) metal based reduction[24, 69, 70, 361] this process more plausibly corresponds to the reduction of the salophen ligand. Indeed a comparable process occurs for the K_3[Tb(bis-salophen)] complex for which a Tb(III) to Tb(II) reduction is unlikely to happen at this potential (vide infra). The positive shift of the reduction potential observed for the complexed Schiff base moiety (E_{pc} [U(salophen)$_2$] = -2.17 V) with respect to the ligand potassium salt (-2.85 V)[360] shows that the coordination to the electropositive uranium center facilitates the ligand reduction. Upon reducing the scan rate from 100 mV/s to 5 mV/s, the intensity for the irreversible reduction wave at -2.17 V is enhanced, and the reversibility of the wave centered at -1.14 V disminishes (***Figure II.19***, curve b dark green). Such behavior presumably arises from the occurence of a chemical process which follows the electron transfer step. In the present case, strong electronic and structural rearrangements of the bis-salophen scaffold are expected to occur upon oxidation. Notably, the cleavage of the C-C bond restoring the imino groups of the salophen ligand is likely to destabilize the

oxidized ligand form. As a result, the reduction of [U(salophen)$_2$] occurs at much lower potential (ΔEp = 1.13 V) than the oxidation of Na_2[U(bis-salophen)].

During this PhD I also carried out electrochemical studies on a series of analoguous lanthanide complexes, K_3[Ln(bis-salophen)] (Ln = Eu, Yb, Tb, Nd), in order investigate the effect of the nature of the metal ion on the redox properties of these Ln(III) complexes.[359] The study was focusssed on the four following representative elements europium, neodymium, terbium and ytterbium. These ions together with neodymium cover practically the entire range of ionic radii of the lanthanide ions (r_iNd(III)= 1.109 r_iEu(III)= 1.066 r_iTb(III)= 1.040 r_iYb(III) = 0.985).[362] Furthermore, the Ln^{III}/Ln^{II} redox potentials vary significantly in these ions (Ln^{III}/Ln^{II} reduction potentials versus NHE = -0.35 V for Eu, -1.15 V for Yb, -2.6 V for Nd and -3.9 for Tb[363, 364]). While the divalent redox state is easily accessible for Yb and Eu, Nd(II) is very difficult to stabilize and the first example of Tb(II) molecular compound was only characterized a few months ago under strong reducing conditions.[365]

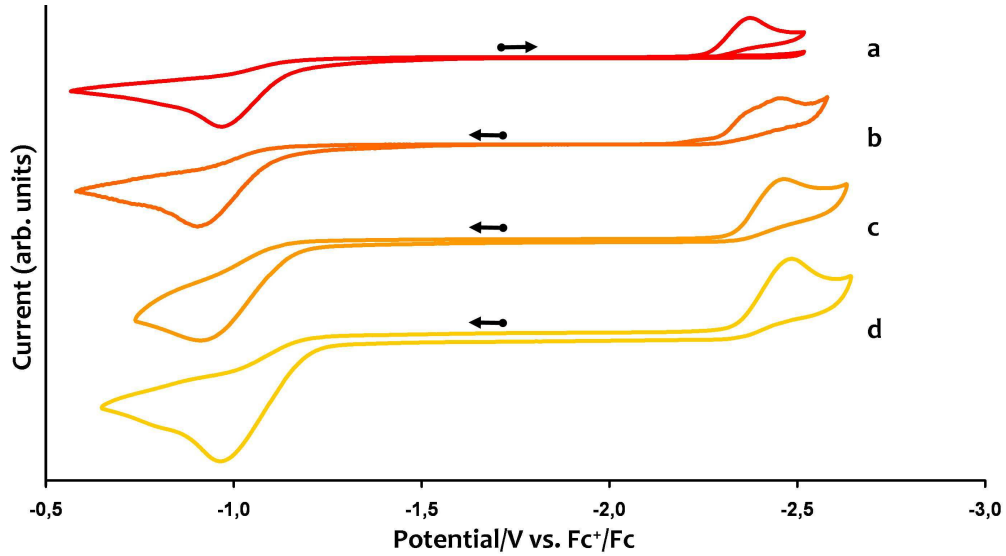

Figure II.20. Cyclic voltammograms for 10 mM solutions of a) K_3[Nd(bis-salophen)], b) K_3[Yb(bis-salophen)], c) K_3[Tb(bis-salophen)], and d) K_3[Eu(bis-salophen)] complexes recorded in 0.1 M [Bu_4N][PF_6] pyridine solution at 100 mV/s scan rate.

The cyclovoltammetric experiments show that the redox properties of the K_3[Ln(bis-salophen)] systems are very similar with irreversible oxidation and reduction processes centered at -0.94 V and -2.45 V respectively for all ions (***Figure II.20***). These results suggest that the redox properties of the ligand are not significantly affected by the polarizability and the ionic radii of the lanthanide ion which has little incidence on these ligand-centered redox processes. The similar redox behavior of all investigated lanthanide salophen complexes indicates that in every case the Schiff base ligand is reduced, and that a reduced state of the lanthanide ion is not likely to be involved in the reduction mechanism. Whilst such behavior was expected for terbium, which is unlikely to form stable divalent complexes at these potentials,[363, 366] this is more unexpected for ytterbium, and europium which can

form stable divalent complexes. However, the ligand environment plays a crucial role on the redox properties and can significantly affect the redox potential of the complexed lanthanide ions.[367] If the reduction of the europium ion would occur before the reduction of the ligand, then the electrochemical behavior should be different for Eu and Tb which is not the case. These curves are also reminiscent to thoses obtained for the Na_2[U(bis-salophen)] **7** and K_2[U(bis-^{R}salophen)] **7-R** (R = Me, ^{t}Bu) complexes (***Figure II.19***), except that spacing between the oxidation and the reduction processes in the lanthanide compounds (ΔEp = 1.5 V) is increased.

Finally from these results it appears unlikely that the mechanism of the reduction reaction would involve the reduction of the metal followed by electron transfer to the ligand. On these bases a direct reduction of the imino group assisted by the presence of the metal center is the more plausible redox pathway. The reduction of the metal center is therefore not favored within this ligand environment.

Table II.3. Voltammetric data for M_2[U(bis-^{R}salophen)] complexes (M,R = Na,H ; K,Me ; K,^{t}Bu).

Compound	E_{pa} (V)	E_{pc} (V)	ΔE_p (V)
7	-1.04	-1.24 -2.17	1.13
7-Me	-1.24	-2.24	1.00
7-^{t}Bu	-1.29	-2.25	0.96

The electrochemical properties of the K_2[U(bis-^{Me}salophen)] **7-Me** and K_2[U(bis-^{tBu}salophen)] **7-^{t}Bu** complexes were also investigated to demonstrate that the redox properties of these U(IV) complexes can be tuned by changes in the ligand architecture. Similarly to the salophen ligand, the ^{Me}salophen and ^{tBu}salophen platforms exhibit redox processes on the potential range [-2.5V ⋯ -0.5V] only when coordinated to the U(IV) ion. Two irreversible redox processes are observed for complexes **7-Me** and **7-^{t}Bu** (***Figure II.19*** curves c and d) with one irreversible oxidation wave at E_{pa} = -1.24 V and E_{pa} = -1.29 V associated with the oxidation of the bis-^{Me}salophen ligand and the bis-^{tBu}salophen ligands respectively, and one irreversible reduction wave at E_{pc} = -2.24 V and E_{pc} = -2.25 V, which is attributed to the reduction of the ^{Me}salophen ligand and the ^{tBu}salophen ligands respectively. The overall redox transformation stays irreversible at scan rates from 10 to 5000 mV/s, presumably due to the complexity of the redox events associated with the formation/rupture of the bis-^{tBu}salophen and bis-^{Me}ligands which are likely to occur faster in this case than for Na_2[U(bis-salophen)] **7**. The reason for that is unclear. Whilst spacing between the oxidation and the reduction processes is nearly constant across this series, the oxidation wave for **7-^{t}Bu** (E_{pa} = -1.29 V) is shifted negatively compared to **7** (E_{pa}= -1.04 V). These differences could originate from the different alkali countercations (Na^+ vs K^+). However, no potential shift nor change in the reversibility of the

oxidation wave of **7** is observed when the electrochemical experiment is carried out in presence of excess KPF_6, and a potential shift is also observed in the K_3[Nd(bis-^{R}salophen)] series[359] where the alkali cation is the same for every compounds. Therefore, these voltammetric data suggest that the difference derives from the nature of the ligand. The bis-^{tBu}salophen ligand platform is more readily oxidized than salophen, with the behavior of the bis-^{Me}salophen ligand platform intermediate. Hence, by varying the type and position of substituents on the ligand arms one can tune the redox properties of these uranium(IV) complexes.

II.2.5 Reactivity studies

As stated before, even if the formal oxidation state of the uranium ions in **4-THF** and **7** is +IV, these systems can be viewed as pseudo low-valent uranium species stabilized by storing two electrons in the C-C bond linking two ligand units. To couple a metal and an independent electron reservoir in the same molecule may open attractive perspectives in the design of molecules devoted to energy storage but also in the area of molecular activation. Indeed, this C-C bond may be cleaved and the two electrons released to participate in redox reactions. Consequently, the major question is: can these systems reversibly return to their original oxidation state?

In order to investigate the reducing properties of **4-THF** and **7**, we explored the reaction of these complexes with various oxidizing agents. The results obtained are reported here after.

II.2.5.1 Reactivity with oxidizing agents

A wide range of inorganic oxidizing agents are available to perform single-electron transfers in nonaqueous solutions. Amongst them, silver(I) salts are the most widely used[368] since they are commercially available, soluble in organic solvents and because the removal of the by-product of oxidation by silver(I) salts, namely silver metal, is usually straightforward.

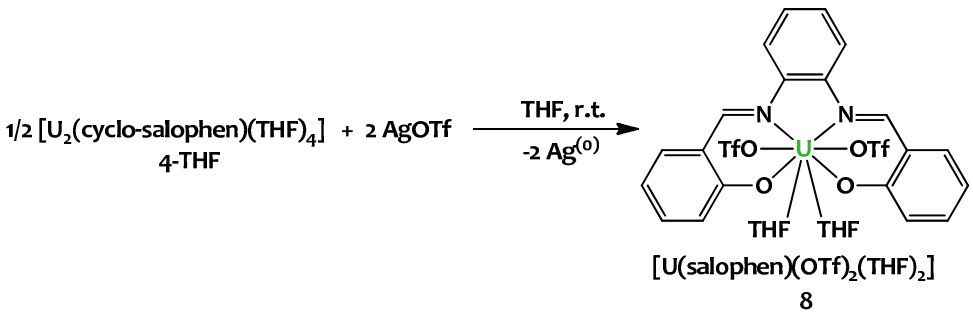

Scheme II.15. Reaction of **4-THF** with silver triflate to afford [$U(OTf)_2$(salophen)$(THF)_2$] **8**.

Addition of four equivalents of silver triflate to **4-THF** leads to the cleavage of the two C-C bonds and the disruption of the dinuclear structure to produce the mononuclear complex [U(salophen)$(OTf)_2(THF)_2$] **8**, whereby the two imino groups of the salophen ligand are restored. The formation of **8** is accompanied by the formation of black silver metal precipitate which is removed by filtration. The novel U(IV) complex **8** can be prepared in 56% yield from this reaction (***Scheme II.15***).

The solid-state structure of **8** was confirmed by X-ray diffraction. Yellow single crystals of **8** were obtained by slow diffusion of DIPE into a THF solution of the complex. The structure, which is shown in ***Figure II.21*** together with selected metrical parameters, is comparable to that of complex **3** presented in section II.2.2. The U(IV) ion is eightfold coordinated by the N_2O_2 pocket of the salophen ligand, two triflate ligands and two THF molecules and adopts a distorted dodecahedral geometry. The salophen ligand is distorted and adopts a boat conformation. The metal to ligand bond distances fall in the range of that observed for **3**. The two triflate ligands are monodentate and, as expected for a weak nucleophilic group, the U-O bond lengths of 2.326(12) and 2.412(13) Å are longer than typical U^{IV}-O bond distances (2.0-2.2 Å). These structural observations are in agreement with the few organometallic uranium(IV) triflates structures reported in literature.[369]

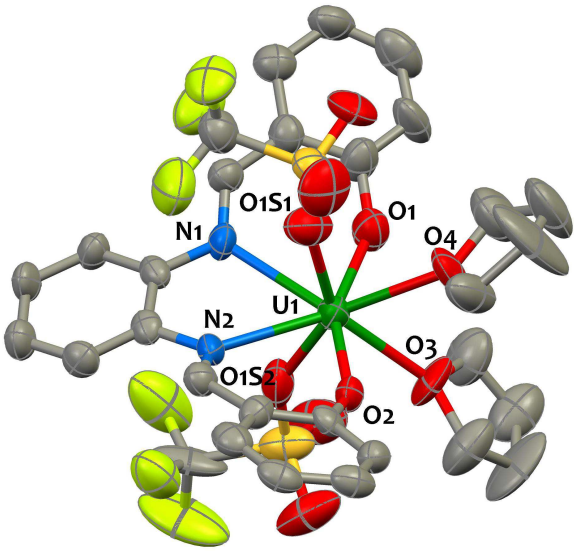

Figure II.21. Solid-state molecular structure of [$U(OTf)_2$(salophen)$(THF)_2$] **8**. Hydrogen atoms are omitted for clarity. Uranium (deep green), sulfur (yellow), nitrogen (blue), oxygen (red), fluorine (light green) and carbon (grey) atoms are represented with 50% probability ellipsoids. Selected bond distances [Å]: U(1)-O(1) 2.132(11), U(1)-O(2) 2.143(9), U(1)-O(1S1) 2.412(13), U(1)-O(1S2) 2.326(12), U(1)-O(3) 2.447(9), U(1)-O(4) 2.544(9), U(1)-N(1) 2.592(11), U(1)-N(2) 2.587(11).

This result shows that complex **4-THF** can act as a four-electron reducing agent through the cleavage of the ligand C-C bonds without undergoing a change of the oxidation state at the metal center. When the same reaction is carried out with a lower ratio of silver triflate, a mixture of **4-THF** and **8** is

obtained. This suggests a concerted breaking of the two C-C bonds in **4-THF**. The salophen ligand can therefore be regarded as a redox-active ligand able to act as an electron reservoir. Compound **4-THF** is thus a remarkable electron-rich system which behaves as a polyelectronic reducing agent, with four electrons released in total. As such, this system behaves as a synthetic equivalent of U(II), which is not chemically accessible to date.

Similarly, the reaction of complex **7** with two equivalents of the mono-electronic oxidant AgOTf or with one equivalent of the two-electron oxidant PbI_2 led to the cleavage of the C-C bond in **7,** restoring quantitatlively the original Schiff base complex **6** (***Scheme II.16***), as confirmed by ^{1}H NMR studies. The bis-salophen platform is thus able to act as reservoir of two electrons that can be involved in electron transfers.

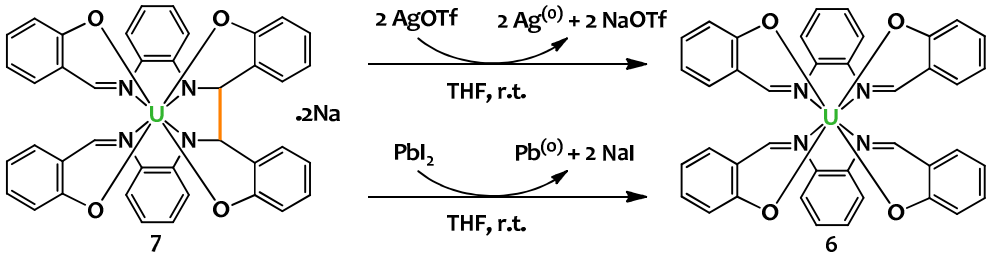

Scheme II.16. The reaction of Na_2[U(bis-salophen)] **7** with silver(I) triflate or lead(II) iodide yields [U(salophen)$_2$] **6**

Quinones are commonly used as organic two-electron oxidants. When a yellow solution containing two equivalents of 9,10-phenanthrenequinone is added dropwise to a brown solution of **4-THF**, the solution turns deep green immediately. ^{1}H NMR spectrum indicates that **4-THF** is entirely converted to give [U(salophen)$_2$] **6** as well as other unidentified U^{IV} species. The formation of [U(salophen)$_2$] from **4-THF** was also confirmed by ESI-MS spectrometry.

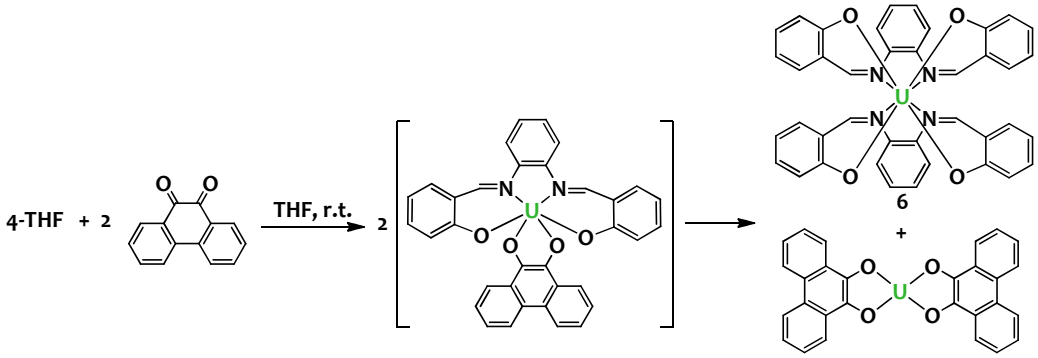

Scheme II.17. Reaction of [U_2(cyclo-salophen)(THF)$_4$] **4-THF** with 9,10-phenanthrenequinone.

Under the light of this result, it is reasonable to postulate that the four electrons stored in the C-C bonds of the uranium dimer **4-THF** are transferred to 9,10-phenanthrenequinone, which in turn is reduced to the corresponding dianion. This redox process is most probably followed by ligand

redistribution to yield [U(salophen)$_2$] **6** and a [U^{IV}(bisquinone)] complex (***Scheme II.17***). Unfortunately, attempts to isolate and crystallize this cathechol complex failed. Nevertheless, this result clearly shows that the redox behavior of the complex could be exploited with a wide range of substrates.

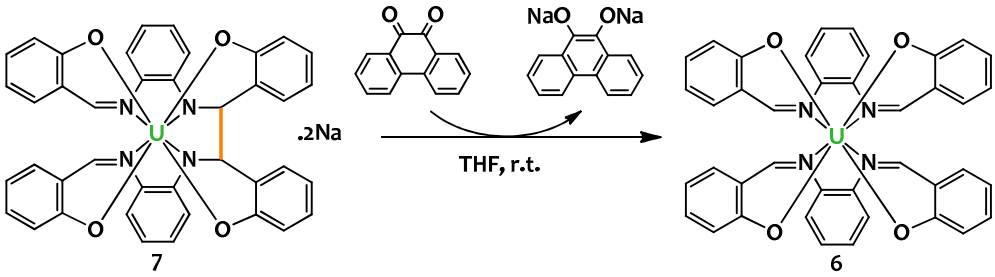

Scheme II.18. Reaction of Na$_2$[U(bis-salophen)] **7** with 9,10-phenanthrenequinone.

The reaction of **7** with one equivalent of phenantrenequinone carried out in a THF solution restores the original Schiff base complex **6** (***Scheme II.18***). The ^{1}HNMR spectrum recorded for the crude mixture exhibits the characteristic resonances of the two isomeric forms of [U(salophen)$_2$] **6-a** and **6-b**, as well as diamagnetic resonances (7.0 to 8.0 ppm) in the aromatic region attributed to the dianionic reduced form of 9,10-phenanthrenequinone. The saturated coordination sphere of the uranium in complex **7** does not allow the substrate to coordinate to uranium, hence ligand redistribution is not occurring in this case.

II.2.5.2 Reactivity with protic species

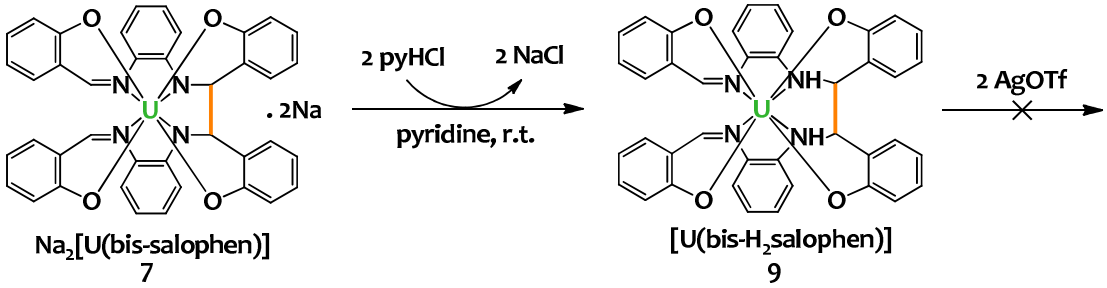

Scheme II.19. Reaction of Na$_2$[U(bis-salophen)] **7** with pyridinium hydrochloride.

We also investigated the reaction of Na$_2$[U(bis-salophen)] **7** with protic sources. In this case no electron transfer was observed but instead protonation of the highly basic amido moieties bound to the U(IV) center to give amino bonds (***Scheme II.19***). Proton NMR of the reaction mixture resulting from the addition of Na$_2$[U(bis-salophen)] **7** to two equivalents of pyridinium hydrochloride reveals the presence of the protonated complex [U(bis-H$_2$salophen)] **9**. The mass spectrometry analysis is in agreement with this formulation in solution (m/z = 869.3 [M+H]$^+$). Red needles suitable for X-ray diffraction were grown upon slow diffusion of hexane into the reaction mixture. The solid-state

structure of [U(bis-H_2salophen)] **9** is presented in ***Figure II.22*** and selected bond distances are reported in ***Table II.4***. The analysis of the structural parameters of the ligand are in accordance with the proposed structure for **9**. The C-N_{imino} bond distances (C-N_{im} = 1.298(3) Å) are within the reported range of uranium-Schiff base complexes and are in agreement with a C=N double bond. The C-N_{amino} bond distances (C-N_{am} = 1.491(6) Å) are significantly longer than C-N_{imino} bonds and correspond to C-N single bonds. Furthermore, the dissymmetry between the U-N bonds distances is opposed to that observed in Na_2[U(bis-salophen)] **7**, with shorter U-N_{imino} bonds in **7** compared to that in **9** (U-N_{im} = 2.58(1) Å in **7** and U-N_{am} = 2.66(2) Å in **9**), in agreement with the amino character of the two nitrogen atoms N2 and N22. Finally, the overall neutral charge of the complex is in agreement with a +IV charge for the uranium center supported by a tetraanionic amino/iminophenolate ligand. The length of the C-C bridging bond (1.545(7) Å) is not affected by the protonation of the complex.

Table II.4. Mean values of selected bond lengths [Å] in the U(IV) complex [U(bis-H_2salophen)] **9**. All distances are average.

Compound	U-N_{imino}	U-N_{amino}	U-$O_{phenolate}$	C-C_{link}	C-N_{amino}	C-N_{imino}
9	2.58(1)	2.66(2)	2.22(1)	1.545(7)	1.491(6)	1.298(3)

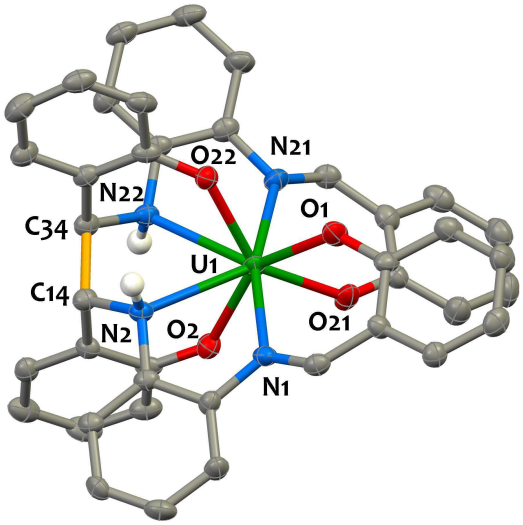

Figure II.22. Solid-state molecular structure of [U(bis-H_2salophen)] **9**. Hydrogen atoms are omitted for clarity except the amino protons. Uranium (deep green), nitrogen (blue), oxygen (red) and carbon (grey) atoms are represented with 50% probability ellipsoids.

Interestingly, when complex **9** is reacted with a solution of silver triflate (***Scheme II.19***), no reaction is observed. The electrons stored in the C-C bond are no longer available and the system loses its redox properties. This can be understood by considering that in [U(bis-H_2salophen)], the amino nitrogen is no longer conjugated with the phenylene ring. This prevents any delocalization of the electrons from the C-C bond onto the ligand backbone and thus the restoration of the original imine bonds is no

longer possible. Thus, protonation switches off the ligand centered redox reactivity in the [U(bis-H_2salophen)] complex.

II.2.5.3 Reduction of Na_2[U(bis-salophen)]

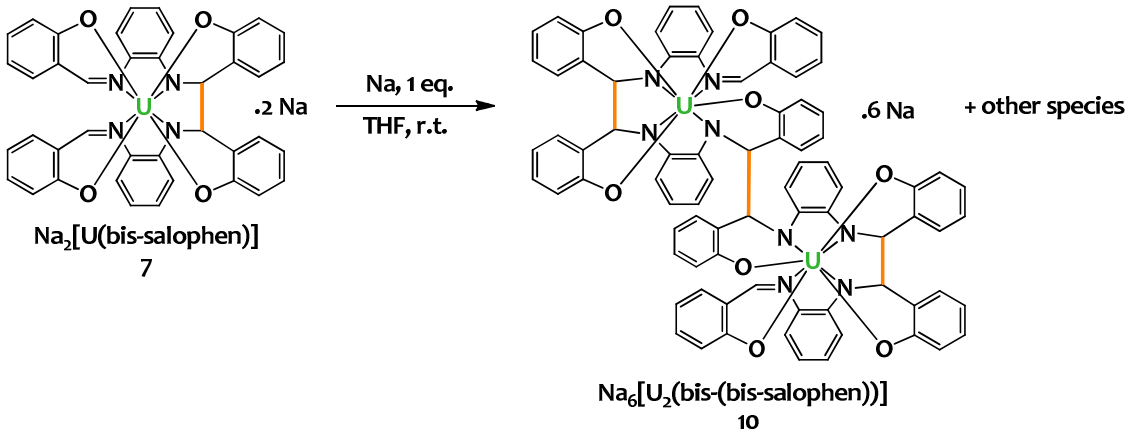

Scheme II.20. Reduction of Na_2[U(bis-salophen)] **7** with sodium dispersion.

As the ligand in Na_2[U(bis-salophen)] **7** possesses two reducible imino moieties, we decided to investigate whether this system could be further reduced. Addition of 1 equivalent of a sodium dispersion to a THF solution of **7** afforded a dark blue suspension. ^{1}H NMR reveals that several species are formed during the course of the reaction. Analysis of the crude mixture by mass spectrometry (***Figure II.23***) indicates that a new dinuclear species Na_6[U_2(bis-(bis-salophen))] **10** (m/z= [1847.2, M-Na]$^-$) is formed in solution (***Scheme II.20***).

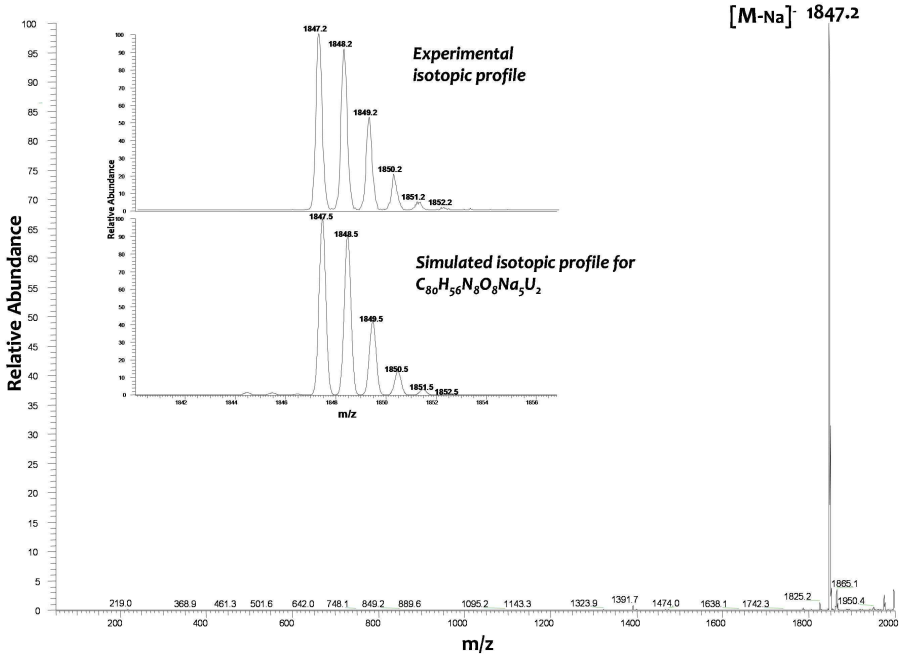

Figure II.23. ESI mass spectrum (negative ionisation mode) of complex Na_6[U_2(bis-(bis-salophen))] **10**.

This complex was crystallized in presence of dibenzo18c6. The structural analysis confirms the formation of a dinuclear complex of the general formula $\{Na_6[U_2(bis\text{-}(bis\text{-}salophen))].(py)_n\}$. The structure is composed of a separate ion pair; a $\{Na_5[U_2(bis\text{-}(bis\text{-}salophen))].(py)_6\}$ monoanion and a $[Na(dibenzo18c6)(py)_2]$ monocation. The $\{Na_5[U_2(bis\text{-}(bis\text{-}salophen))](py)_6\}^-$ unit, depicted in ***Figure II.24***, contains four peripheral Na^+ cations coordinated to phenolates moieties and pyridine solvent molecules, and a central cationic sodium which is hexacoordinated by two phenolate and four imido moieties from the ligand. The metrical parameters for the ligand backbone, reported in ***Table II.5***, are in agreement with the presence of a hexa-amido bis-imino octa-phenolate bis(bis-salophen)$^{14-}$ polydentate ligand (***Scheme II.20***). Both U(IV) ions are octacoordinated by four phenolate, three amido and one imido moieties defining a square antiprismatic coordination environment around the metals. The overall U-O and U-N bond distances are similar to those observed in **4-THF** and **7**.

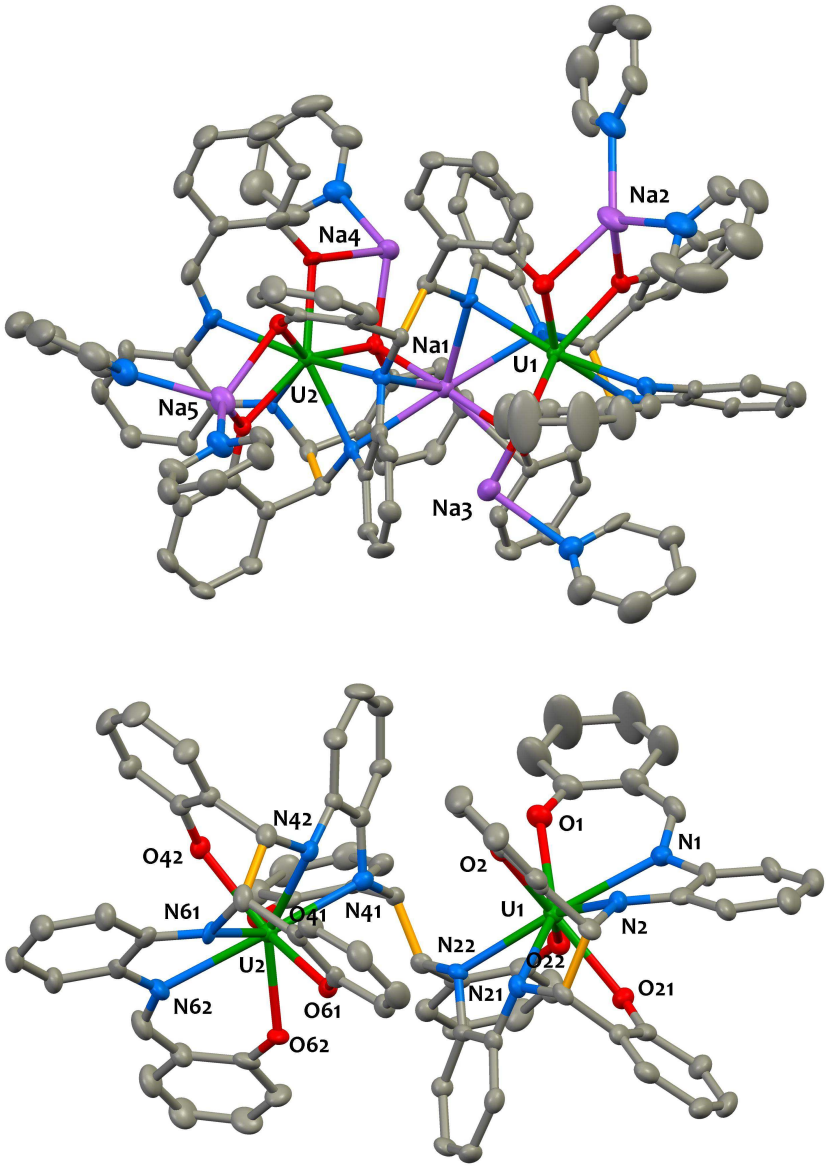

Figure II.24. Solid-state molecular structure of the $\{Na_5[U_2(bis\text{-}(bis\text{-}salophen))](py)_6\}^-$ anion in **10** with (top) and without (bottom) sodium cations and pyridine molecules. Hydrogen atoms,

[Na(dibenzo18c6)(py)$_2$] countercation and interstitial solvent molecules are omitted for clarity. The C-C bond formed by reduction of the imine moieties of the salophen ligands is represented in yellow. Uranium (green), nitrogen (blue), oxygen (red), sodium (purple) and carbon (grey) atoms are represented with 50% probability ellipsoids.

Table II.5. Mean values of selected bond lengths [Å] in the U(IV) complex **10**. All distances are average.

Compound	U-N_{imino}	U-N_{amido}	U-$O_{phenolate}$	C-$C_{link\ intra}$	C-$C_{link\ inter}$	C-N_{amido}	C-N_{imino}
10	2.63(1)	2.43(2)	2.35(3)	1.552(1)	1.544(7)	1.462(6)	1.286(5)

This complex most likely arises from the intermolecular C-C coupling of the imino moieties of two independent Na_2[U(bis-salophen)] complexes, with sodium cations possibly playing a template role in this process. Indeed, we showed that the Na^+ cations remain coordinated to the [U(bis-salophen)]$^{2-}$ anion, and as observed in the solid-state structure of K_2[U(bis-^{tBu}salophen)] **7-^{t}Bu**, the alkaline cations can bridge independent units and preorganize the system thus favoring intermolecular C-C bond formation.

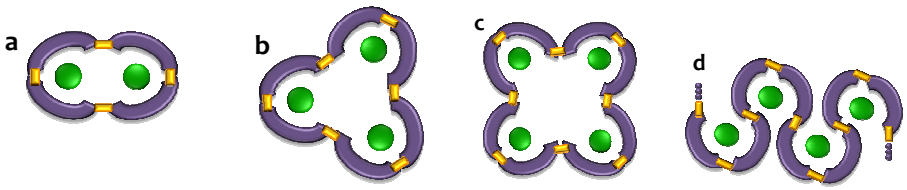

Figure II.25. Schematical representation of possible oligomeric complexes resulting from reductive coupling of imino moieties in Na_2[U(bis-salophen)] **7**. Uranium is represented as a green sphere, the ligand is represented in gray and the C-C bridging bonds in yellow.

Attempts to reduce compound **7** with two or more equivalents of sodium produces intractable mixtures of products. This could have been anticipated considering the wide variety of oligomers that could derive from Na_2[U(bis-salophen)] **7**. A combination of intra- and inter-molecular couplings could yield complex cyclic and linear polymeric structures (***Figure II.25***). A fine tuning of the reaction conditions (stoichiometry, concentration, size and charge of the countercations, solvent polarity and coordinence, type of reducing agent) is most probably necessary to favor some species and rationalize the assembly process, but so far attempts have proved unsuccessful.

We also tried to reduce compound **4-THF** under various solvent and concentration conditions using diverse reducing agents (K or Na chunks, Na dispersion, KC_8, Na/naphthalene). In every case, this produced NMR silent brown solutions. Addition of AgOTf to these solutions cleanly affords compound **8**, suggesting that one or more NMR-silent reduced species are formed. However attempts to isolate these reduced species failed in our hands.

II.2.5.4 Reactivity with metal halides acting as Lewis acids.

The reactivity of Na_2[U(bis-salophen)] **7** with metal halides can be divided into two categories. The first involves metal halides with a readily available reduced state such as silver(I) or lead(II) salts. Such species are acting as oxidizing agents and their action onto **7** has been discussed in section II.2.5.1. The second category concerns metals that are not reduced by complex **7**. In this case, the metal cation is acting as a Lewis acid. This is the purpose of the present section.

We sought to use Na_2[U(bis-salophen)] **7** as a starting material as its formulation represents a good opportunity for salt metathesis with metallic halide precursors and could provide a new synthetic route to uranium-containing bimetallic complexes. The use of cations with various charges and coordination properties could lead to the isolation of new polynuclear assemblies particularly desirable for combining the redox and magnetic properties of the two metals. Our first attempts were carried out with U(IV) halides and afforded new homobimetallic uranium complexes.

$$\underset{\mathbf{7}}{Na_2[U(\text{bis-salophen})]} + [UX_4(OEt)_n] \xrightarrow[-\,2\,NaX]{THF,\ r.t.} \underset{\mathbf{11\text{-}X}}{[U_2(\text{bis-salophen})(THF)_n]X_2}$$
$$\{X,n\} = \{I,2\}\,;\,\{Cl,0\}$$

Scheme II.21. Synthesis of $[U_2(\text{bis-salophen})(THF)_n]X_2$ **11-X** (X = Cl, I) complexes.

Addition of one equivalent of $[UI_4(OEt_2)_2]$ onto a THF solution of Na_2[U(bis-salophen)] **7** results in a strong color change from deep purple to orange, and produces the dinuclear complex $[U_2(\text{bis-salophen})(THF)_n]I_2$ **11-I** (***Scheme II.21***). Similarly, the reaction of **7** with the solvate-free uranium(IV) chloride UCl_4 in THF affords $[U_2(\text{bis-salophen})(THF)_n]Cl_2$ **11-Cl**. The ^{1}H NMR spectra for both species in THF solution display 14 shifted resonances (***Figure II.26***). The number of observed NMR features suggests that the bis-salophen ligand maintains C2 or Cs symmetry in solution on the NMR timescale. ESI/MS studies also point to the presence of a dinuclear species in THF solution (m/z = 1231.1, corresponding to the $\{[U_2(\text{bis-salophen})]I\}^+$ moiety). Unfortunately, these compounds could not be isolated as analytically pure in the solid-state, as their separation from sodium halide salts proved difficult. A strong color change from orange to deep green is observed upon dissolution of the **11-X** species in pyridine. The ^{1}H NMR spectrum recorded for **11-I** in pyridine solution is represented in ***Figure II.27***. 14 signals are recorded for this species in pyridine, similarly to what is observed in THF solution. However, the chemical shifts are strongly affected by the change of solvent. This, together with the strong solvatochromism is plausibly indicating that the solution structure of the complex in pyridine is different to that in THF. We propose that in the more dissociating pyridine solvent the halides are not coordinated to the metal while in the less polar THF solvent they remain coordinated to the uranium cations.

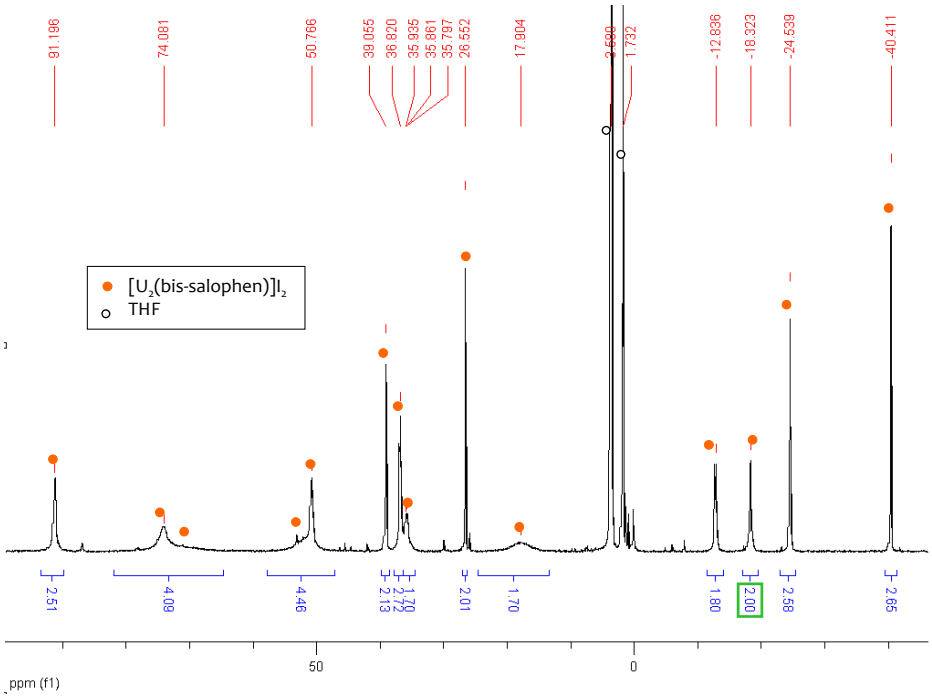

Figure II.26. ^{1}H NMR spectrum (298 K, 200 MHz) in THF-d_8 of $[U_2(bis\text{-}salophen)(THF)_n]I_2$ **11-I.**

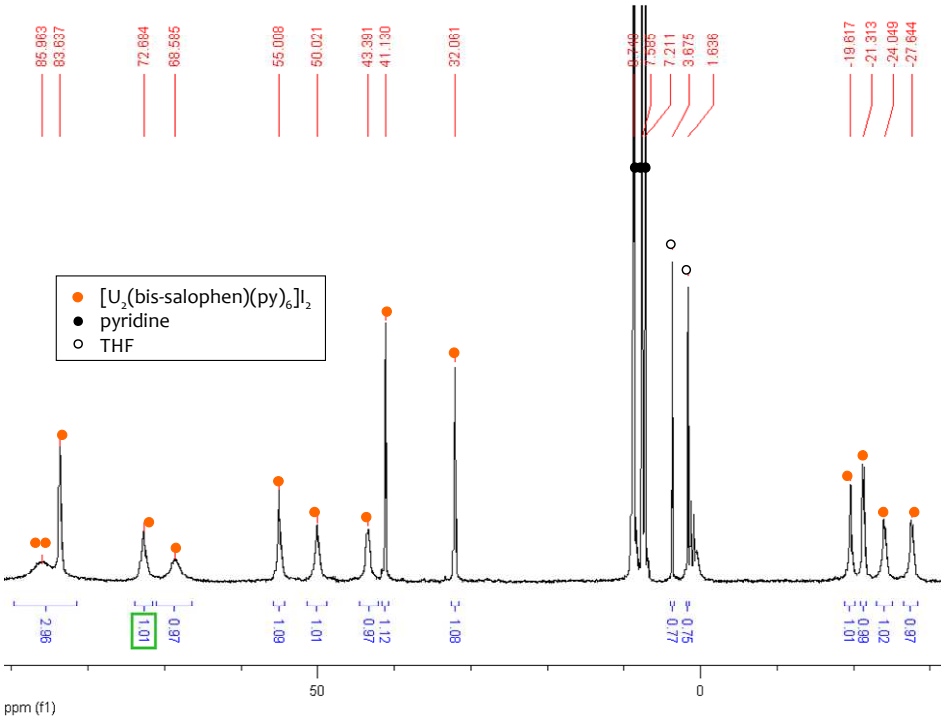

Figure II.27. ^{1}H NMR spectrum (298 K, 200 MHz) in pyridine-d_5 of $[U_2(bis\text{-}salophen)(py)_n]I_2$ **11-I.**

Single crystals were grown by slow diffusion of hexane into a pyridine solution of **11-I.** The solid-state structure consists of isolated ions pairs and the structures of the $[U_2(bis\text{-}salophen)(py)_6]^{2+}$ cation is presented in ***Figure II.28***, with selected bond distances given in ***Table II.6***. The two uraniums are encapsulated by the octadentate hexaanionic chelating ligand bis-salophen which adopts an helical structure similar to that observed in the solid-state structure of $Na_2[U(bis\text{-}salophen)]$ **7.** It is striking

that upon coordination of the second uranium center, the coordinated sodium atoms are not only removed, but the entire ligand wrapping the uranium atom in **7** is unfolded to accommodate another uranium(IV) ion. This dinuclear complex presents a pseudo-C_2 axis that passes in between the two uranium ions and the two carbon atoms C14 and C27, rendering the two halves of the bis-salophen ligand nearly identical, which is consistent with the solution NMR data. Both uranium(IV) centers are eight-coordinate and bound by two phenolate, two amido and one imino moieties from the bis-salophen ligand and three pyridine molecules in a distorted square antiprismatic fashion. The imido moieties of the ligand act as bridging units and are unsymetrically coordinated to the uranium atoms, the U1-N2 (2.4283(1) Å) and U2-N21 (2.4606(1) Å) bond distances being shorter than those of U1-N21 (2.6603(1) Å) and U2-N2 (2.6643(1) Å), analogosly to [U_2(cyclo-salophen)(THF)$_4$] **4-THF**. This results in a 4.0241(2) Å separation of the two uraniums in **11-I** (***Figure II.29***), which is significantly longer than that (3.54(1) Å) observed in the more sterically constrained complex **4-THF**. The U-N_{imino} average bond distance (2.624(7) Å) is significantly longer than the U-N_{amido} one, in agreement with the bis-salophen formulation of the ligand. Similarly, the C-N_{imino} bond distances (1.303(1) Å) are shorter than the C-N_{amido} bond lengths (1.49(1) Å), and correspond respectively to double and simple C-N bonds. Finally, the C14-C27 bond resulting from the reductive coupling of the imino bonds of the original salophen ligand is of 1.599(15) Å long and falls in the range of the C-C bond distances observed in the bis-^{R}salophen and cyclo-salophen uranium complexes.

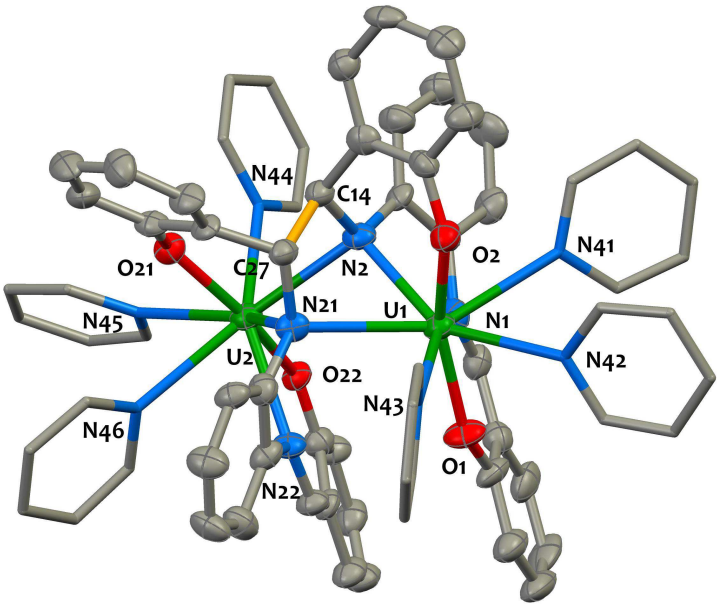

Figure II.28. Solid-state molecular structure of the cation [U_2(bis-salophen)(py)$_6$]$^{2+}$ in **11-I**. Hydrogen atoms, counteranions and solvent molecules are omitted and pyridine molecules are represented as sticks for clarity. The C-C bond formed by reduction of the imine moieties of the salophen ligands is represented in yellow. Uranium (green), nitrogen (blue), oxygen (red) and carbon (grey) atoms are represented with 50% probability ellipsoids.

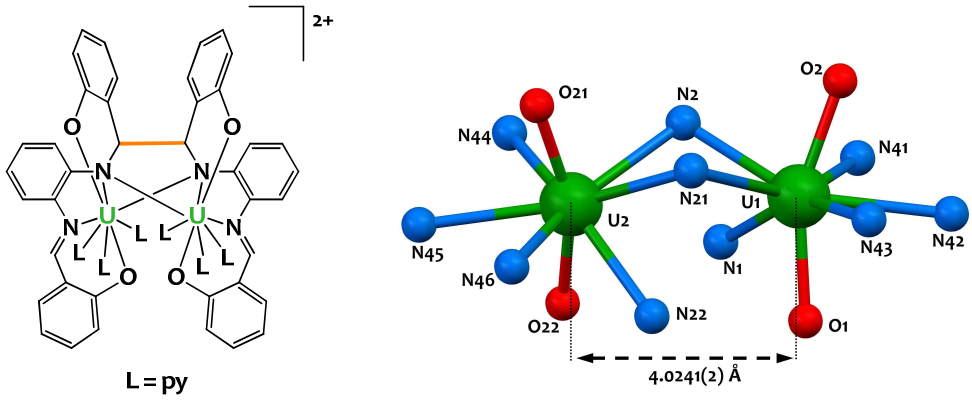

Figure II.29. Schematic representation (left) and view of the core (right) of complex $[U_2(\text{bis-salophen})(py)_6]I_2$ **11-I**.

Table II.6. Mean values of selected bond lengths [Å] in the U(IV) complex $[U_2(\text{bis-salophen})(py)_6]I_2$ **11-I**. All distances are average.

Compound	U-N_{imino}	U-N_{amido}	U-$O_{phenolate}$	C-C_{link}	C-N_{amido}	C-N_{imino}
11-I	2.55(1)	2.44(2) and 2.662(3)	2.15(1)	1.599(15)	1.49(1)	1.303(3)

As expected, the redox properties of the system are maintained. Accordingly, complex **11-I** reacts with one equivalent of iodine leading to the cleavage of the C-C bond restoring the original Schiff base structure to quantitatively yield $[UI_2(\text{salophen})(py)_2]$ **3** (***Scheme II.22***), as evidenced by ^{1}H NMR studies.

$$\underset{\textbf{11-I}}{[U_2(\text{bis-salophen})(py)_6]I_2} \xrightarrow[\text{py, r.t.}]{I_2} 2\,\underset{\textbf{3}}{[UI_2(\text{salophen})(py)_2]}$$

Scheme II.22. Oxidation of **11-I** by molecular iodine affords $[UI_2(\text{salophen})(py)_2]$ **3**.

The reduction of **11-I** was carried out in THF solution using potassium metal as a reducing agent. This afforded $[U_2(\text{cyclo-salophen})(THF)_4]$ **4-THF** in high yield, providing a second synthetic pathway for this complex (***Scheme II.23***). When looking at the overall picture, compound **11-I** could be a conceivable intermediate for stepwise formation of the cyclo-salophen structure. However, given that complex **11-I** was neither observed in the reduction of salophen by $[UI_3(THF)_4]$ nor in the oxidation of **4-THF** by AgOTf, a concerted reduction/oxidation mechanism seems more likely for the formation/cleavage of the two C-C bonds in the cyclo-salophen structure.

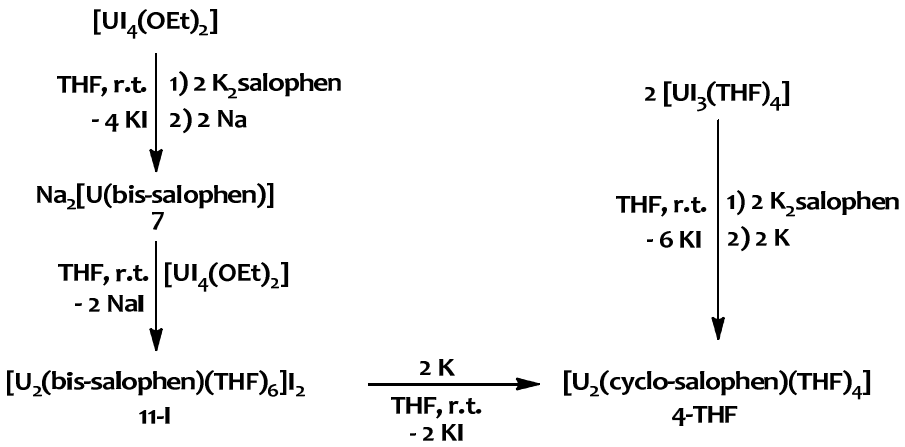

Scheme II.23. Global synthetic scheme of bis-salophen and cyclo-salophen uranium(IV) species.

It is anticipated that this rational synthetic route could be used to access original heterobimetallic complexes. Indeed, preliminary studies show that it allows the isolation of a uranium-cobalt bis-salophen complex. Heterobimetallic 5f-5f or 3d-5f compounds remain uncommon, and synthetic pathways are required to extend this chemistry. Such entities are particularly desirable from a fundamental point of view, in order to investigate the possibility of metal-metal communication with actinides. Future studies might be enriched by the possibility of constructing a family of [UM(bis-salophen)] or [UM(cyclosalophen)] species with various divalent and tetravalent cations. Furthermore, heterobimetallic 3d-5f complexes could be extremely desirable for reactivity purposes. Polymetallic species for cooperative reactivity in catalysis or related fields present an great potential which only begins to be explored[370] and heterobinuclear complexes might be ideal for inducing reactions with polarisable substrates such as CO_2.[16, 371-377]

II.3 Ferrocene-Based Chelating Schiff Base Ligands for U(IV) Chemistry

II.3.1 Context

As highlighted in the previous section (II.2), the redox properties of uranium Schiff base complexes are highly influenced by the nature of the tetradentate dianionic diimine bis(phenolate) ligand. Such ligands are very versatile[378] and offer the possibility of tuning ligand properties by changing the diimine bridging moiety. Depending on the nature of the ligand scaffold, they might provide coordination environments robust enough to stabilize U(III), or at the opposite behave as non-innocent ligands affording attractive low-valent synthetic equivalents.

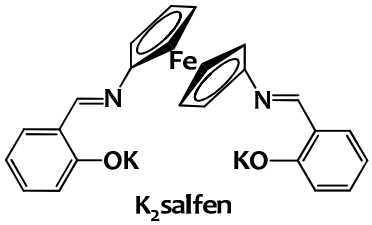

Figure II.30. Representation of K_2salfen

In this context, we decided to explore the coordination chemistry of the salfen ligand represented in ***Figure II.30***. This ONNO tetradentate ligand offers the possibility to combine the properties of ferrocene and of Schiff bases. Comparatively to the salophen platform, the length of the spacer fragment (1,1'-ferrocenyl vs 1,2-phenyl bridge) is increased, providing a larger ONNO cavity well suited for uranium. In addition, the ferrocene moiety provides a more flexible environment able to adapt the sterics and electronics features of the ligand by varying the geometry around iron. Accordingly, we envisioned that such a system was susceptible to better accommodate uranium than salophen. Moreover, the capability of the ferrocene unit to participate in redox events might increase the reactivity possibilities of the complexes.

The large number of reports mentioning tetradentate ONNO Schiff base ligands contrasts with the scarcity of studies involving the salfen ligand whose coordination chemistry remain practically unexplored. Only three reports have been published on the use of this Schiff base ligand in combination with Mg(II)[379], Zr(IV)[379], Ti(IV)[379], Ce(III)[380], Ce(IV)[381] and Y(III)[381]. In uranium chemistry, considerable interest for exploiting ferrocene-containing ligands has been raised by a recent report suggesting that magnetic coupling may occur through direct metal-metal orbital overlap between

uranium and iron in the trinuclear complex $[U(fc[NSi(^tBu)Me_2]_2)_2][BPh_4]$,[382] resulting in a strong ferromagnetic interaction between the two iron centers mediated by the uranium(IV) cation. Therefore investigations on uranium salfen compounds are particularly desirable.

Here we have investigated the ability of the tetradentate salfen ligand to form complexes with uranium in lower oxidation states.

II.3.2 Synthesis and characterization of homoleptic bis(salfen) complex of uranium

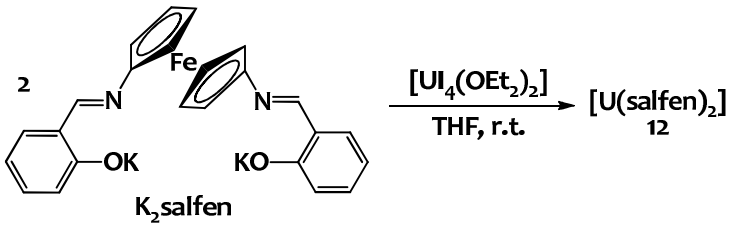

Scheme II.24. Synthesis of $[U(salfen)_2]$ **12**.

The U(IV) bis-ligand complex is easily prepared. As shown on ***Scheme II.24*** the salt metathesis reaction between $[UI_4(OEt_2)_2]$ and two equivalents of the potassium salt of the tetradentate Schiff base ligand K_2salfen in THF affords the homoleptic U(IV) complex $[U(salfen)_2]$ **12** in good yields. In solution, ^{1}H NMR spectroscopy indicates a symmetrical environment around the uranium center since a single set of seven resonances is observed in the ^{1}H NMR recorded for **12** from deuterated THF or pyridine solutions (***Figure II.32***).

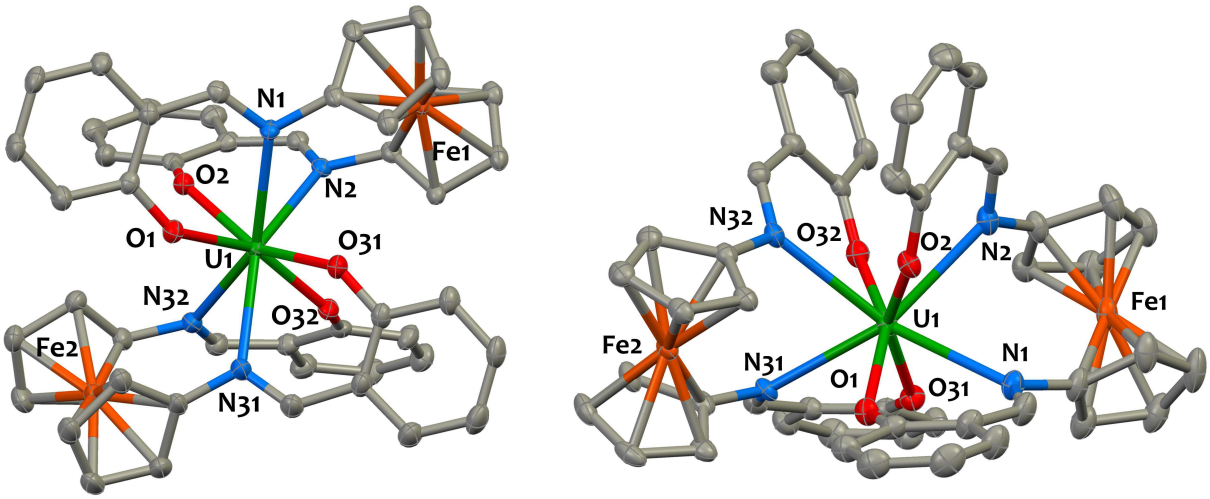

Figure II.31. Two different views of the solid-state molecular structure of $[U(salfen)_2]$ **12**. Hydrogen atoms and solvent molecules are omitted for clarity. Uranium (green), iron (orange), nitrogen (blue), oxygen (red) and carbon (grey) atoms are represented with 50% probability ellipsoids. Selected distances [Å] : U-O_{avg} 2.231(9) ; U-N_{avg} 2.664(7) ; Fe-C_{avg} = 2.041(7) ; U···Fe 4.32(1).

Single crystals of **12** suitable for X-ray diffraction studies were grown by slow diffusion of diisopropyl ether into a THF solution of **12**. The solid-state structure of **12** is represented in ***Figure II.31***. The complex crystallizes in the monoclinic $P2_1/n$ space group. The uranium cation is encapsulated between two overlapping salfen ligands which provide a N_4O_4 coordination sphere around the metal. The resulting coordinating polyhedron around uranium is best described as a distorted square antiprism with N1-O1-N31-O31 and N2-O2-N32-O32 defining the square bases of the polyhedron. Contrary to the heteroleptic mono-salfen complexes $[Ce(salfen)(O^tBu)_2]$[381] and $[Zr(salfen)(CH_2Ph)_2]$[379] where the salfen ligand adopts a planar geometry, the two N,O coordinating arms of the ligand in **12** are strongly twisted with an average angle of 73.7(7)° between the phenolate planes from a same ligand. The $U\text{-}O_{avg}$ 2.231(9) Å and $U\text{-}N_{avg}$ 2.664(7) Å bond distances are comparable to thoses in $[U(salophen)_2]$ (see section II.2.4.1) and fall in the range of thoses reported for tetravalent uranium complexes.[100, 320-322] The two ferrocene units of the ligands are almost perpendicular, as indicated by the 71.3° value for the torsion angle between the Cp centroids and the irons in **12**. Both ferrocene moieties adopt roughly eclipsed conformations, as is expressed by the small values of the N1-C1-C6-N2 and N31-C31-C36-N32 dihedral angles (16.3(3)° and 15.7(2)° respectively). The Fe-C distances average 2.041(7) Å, a classical value for ferrocene units.[97, 383] Both U···Fe separations (U1···Fe1 = 4.3087(5) Å ; U1···Fe2 = 4.3237(4) Å) have similar values and are longer than thoses (3.32 Å and 2.961 Å) respectively observed in the solid-state molecular structure of the related amido complexes $[U(fc[NSiMe_3]_2)_2]$[384] and $[U(fc[NSi(^tBu)Me_2]_2)_2][BPh_4]$.[382] This is the result of the presence of imino groups with longer U-N distances, compared to the U-N distances in the amido complexes, which maintain the uranium further apart from the ferrocenes. Such long U···Fe separation might disfavor a through-space uranium-mediated iron-iron communication.

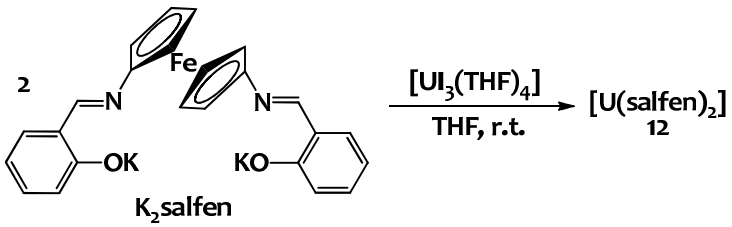

Scheme II.25. Reaction of $[UI_3(THF)_4]$ with K_2salfen.

The salfen ligand was also interrogated for the synthesis of a simple U(III) complex. Addition of 1 equiv of K_2salfen to a THF solution of $[UI_3(THF)_4]$ resulted in a rapid color change from deep blue to brown accompanied by the formation of KI precipitate. Analysis of the crude reaction mixture by ^1H NMR (***Figure II.32***) showed the formation of $[U(salfen)_2]$ **12** as the only salfen-containing species. The formation of uranium(IV) compounds is a common occurrence when starting from $[UI_3(THF)_4]$ because of its tendency to disproportionate ($4U^{III} = 3U^{IV} + U^0$).[76, 95-103] An analogous behavior was

notably observed with the salen ligand (see section II.2.1) and has been reported for the related bis(1,1'-diamidoferrocene) ligand $[K_2(OEt_2)_2]fc[NSi\text{-}(t\text{-}Bu)Me_2]_2$.[382]

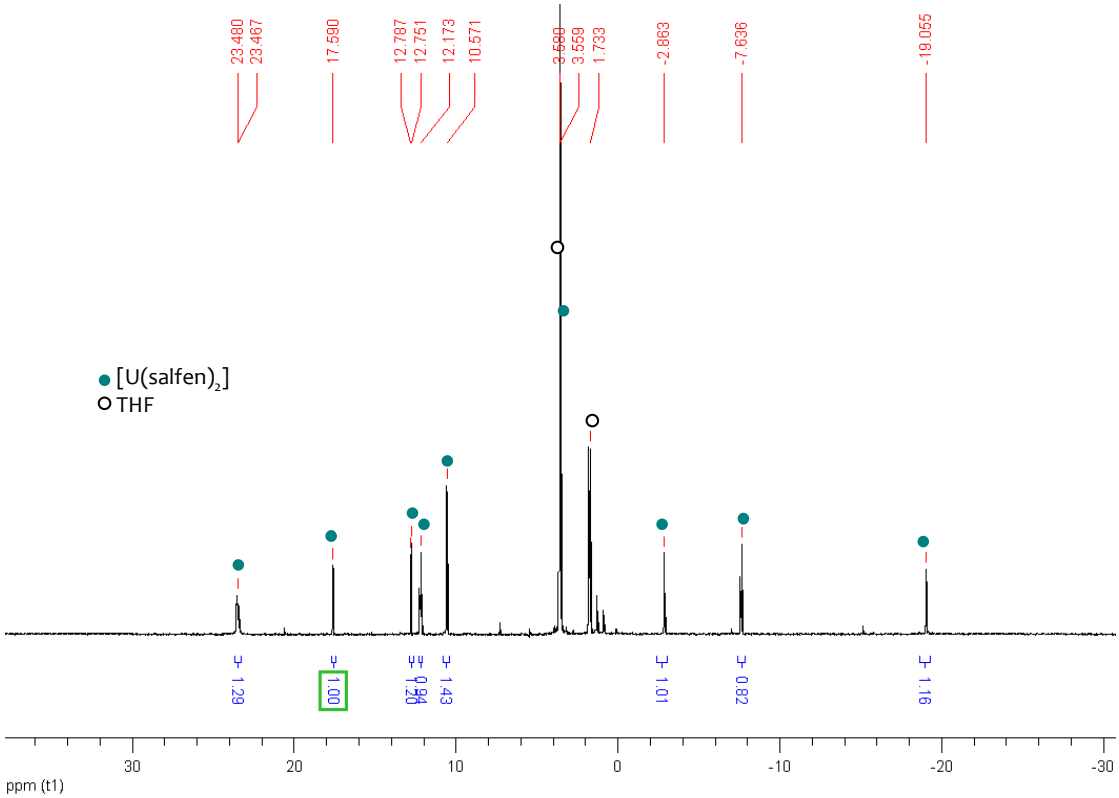

Figure II.32. ^{1}H NMR (200 MHz, THF-d_8, 298 K) of the crude mixture of the reaction of $[UI_3(THF)_4]$ with one equivalent of K_2salfen showing the resonances of $[U(salfen)_2]$ **12**.

Salt metathesis reactions of uranium iodides with salfen potassium salts show that the salfen scaffold is able to stabilize and saturate the coordination sphere of a U(IV) ion, but seems inappropriate for stabilizing its uranium(III) counterparts.

II.3.3 Electrochemical investigations

The complex $[U(salfen)_2]$ **12** possesses three different types of redox-active centers : the uranium cation, the two irons of the ferrocene moieties and the Schiff base moieties. In order to get more insights into the redox properties of the uranium(IV) bis-salfen complex, cyclic voltammetry studies were carried out.

The cyclic voltammograms recorded for $[U(salfen)_2]$ **12** are shown on ***Figure II.33***. The measurements were performed on 10 mM pyridine solutions of complexes using $[Bu_4N][PF_6]$ as supporting electrolyte. All redox potentials are referenced against the $[(C_5H_5)_2Fe]^{+/0}$ redox couple.

Complex **12** shows an irreversible reduction wave at E_{pc} = -2.49 V. This process is associated with an irreversible oxidation at E_{pa} = -1.54 V which is not observed when the voltammogram is swept initially from -2.0 V to the positive direction. A second irreversible oxidation wave of lower intensity is observed at E_{pa} = -1.10 V. Based on our studies performed on the salophen ligand (section II.2.4.3), this electrochemical signature is evocative of a reduction/oxidation feature involving the Schiff base ligand even if a U(IV)/U(III) process could also occur in this potential window.[24] Accordingly we tentatively attribute these irreversible redox waves to ligand-based processes. The reduction of salfen most likely involves the formation of C-C bonds between two reduced imino groups of the salfen ligand. Such structural and electronic rearrangements provide stabilization to the system. This results in a peak separation of ΔEp = 0.95 V for **12**, of the same order of magnitude than thoses observed in Na_2[U(bis-salophen)] and K[Ln(salophen)$_2$] (see section II.2.4.3). Compared to the salophen ligand, the reduction of salfen is less favorable (Ep_c = -2.49 V vs -2.17 V for [UL_2], L = salfen and salophen respectively).

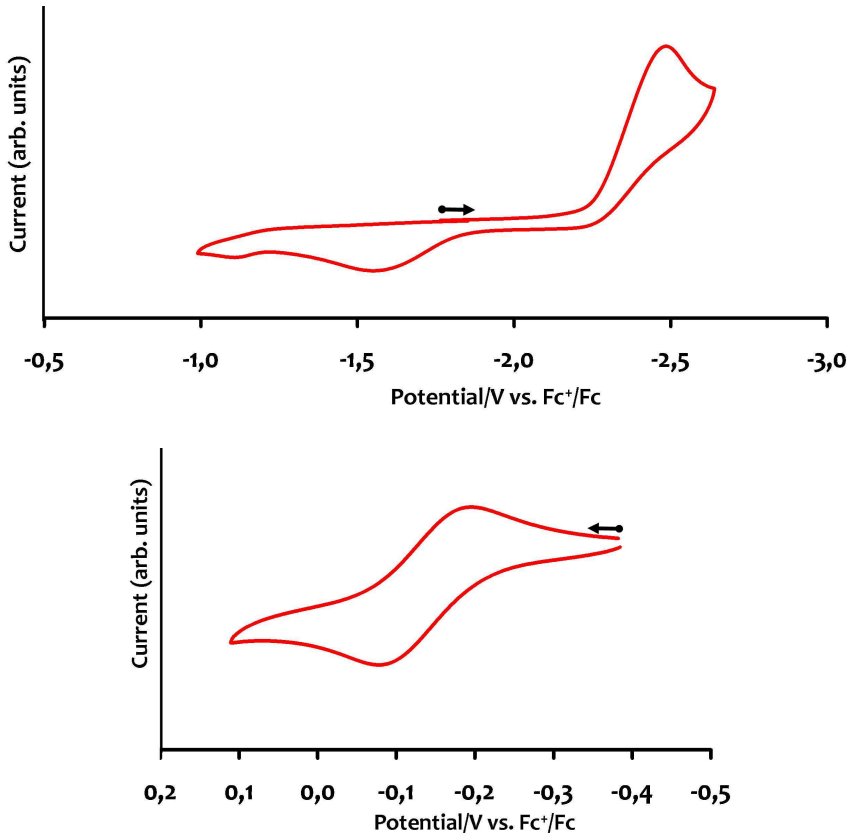

Figure II.33. Cyclic voltammograms for [U(salfen)$_2$] **12** recorded in 0.1 M [Bu_4N][PF_6] pyridine solution at 100mV/s scan rate. Top : reduction range ; bottom : oxidation range.

We also considered the electrochemical oxidation of [U(salfen)$_2$]. The cyclic voltammmogram displays a reversible feature centered at $E_{1/2}$ = -0.14 V. Although a U(V)/U(IV) event could occur at such potential[69, 203, 385] we more plausibly attribute it to a Fe(II) to Fe(III) oxidation of the ferrocene

moieties. Indeed, this potential is close to that ferrocene, and lies in between the values measured for the Fe^{2+}/Fe^{3+} process in [Ln(^{tBu}salfen)(O^{t}Bu)(X)] (Ln , X = Y , THF : $E_{1/2}$ = 0.09 V ; Ln , X = Ce, O^{t}Bu, $E_{1/2}$ = -0.28).[380] This implies that the two chemically equivalent ferrocenyl substituents from the ligands are oxidized at the same potential. Systems in which an electronic communication can occur between two ferrocene units generally display two distinct one-electron reversible waves.[382, 386, 387] Therefore it is reasonable to assume that no iron-iron communication is occurring in [U(salfen)$_2$] which is consistent with the large U···Fe separation observed in the solid state structure.

II.3.4 Reduction studies

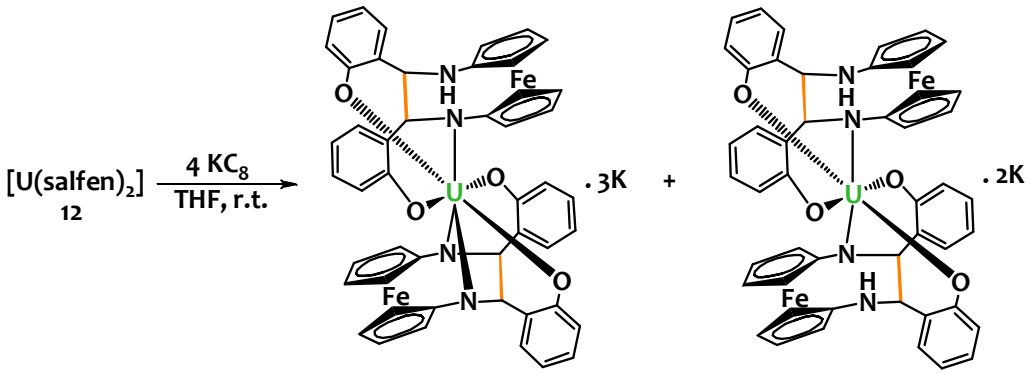

Scheme II.26. Reduction of [U(salfen)$_2$] **12**.

In order to establish if the reduced form of [U(salfen)$_2$] observed electrochemically was chemically stable, we undertook the chemical reduction of compound **12**. The reaction of **12** with potassium graphite in THF resulted in a rapid color change of the solution from orange to dark brown. Analysis of the crude mixture by ^{1}H NMR revealed that a mixture of compounds was reproducibly obtained. Best results were obtained when using 4 equivalents of KC_8 per uranium atom. The ^{1}H NMR spectrum recorded in THF for the crude reaction mixture is shown in ***Figure II.34***. It displays a series of sharp resonances paramagnetically shifted in the +40 to -30 ppm range characteristic of U(IV) complexes. Detailed analysis of the spectrum reveals that this apparently complex pattern can be decomposed into two sets of resonances corresponding to two reduced complexes identified as K_2[U(bis-Hsalfen)$_2$] **13-H$_2$** and K_3[U(bis-salfen)(bis-Hsalfen)] **13-H** (***Scheme II.26***). However, their separation proved unsuccessful, preventing their isolation in large quantities.

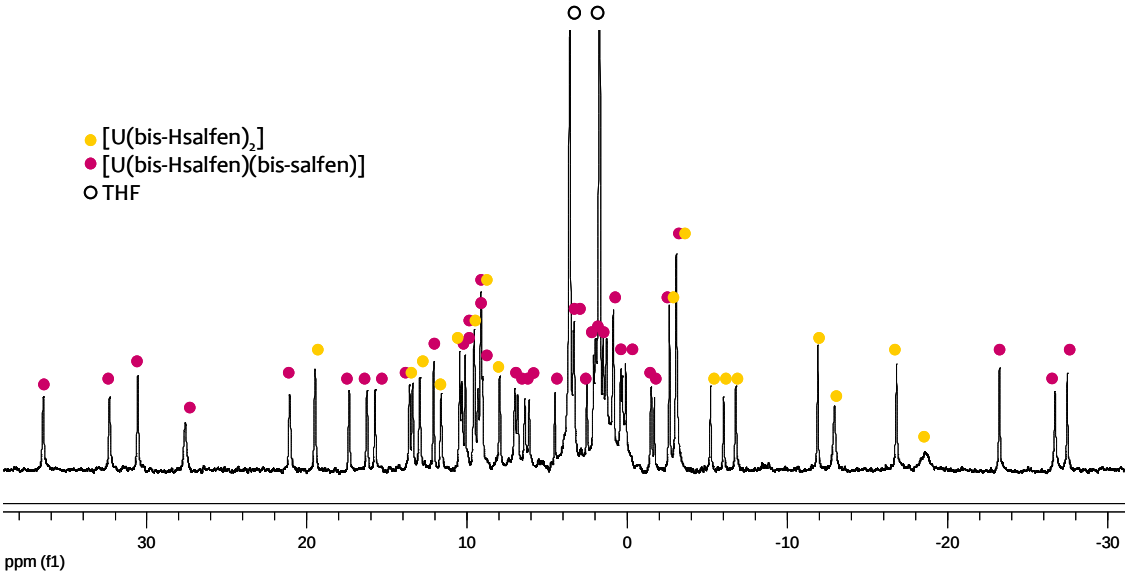

Figure II.34. ^{1}H NMR (200 MHz, THF-d_8, 298 K) of the crude reaction mixture of [U(salfen)$_2$] **12** with KC_8.

Complex K_3[U(bis-salfen)(bis-Hsalfen)] **13-H** is slightly less soluble than K_2[U(bis-Hsalfen)$_2$] **13-H$_2$,** and few crystals could be grown upon slow diffusion of DIPE into a THF solution of the complexes. While the quality of the structure is not sufficient enough to allow for a detailed discussion of the metrical parameters of the structure, it is of reasonable quality to indicate atoms connectivity. In the crystal structure of **13-H** the uranium complexes K_3[U(bis-salfen)(bis-Hsalfen)].$(THF)_n$ are connected in a 1D-coordination polymer by bridging potassium countercations with different coordination modes and geometries (***Figure II.36***). Two independent uranium complexes presenting similar features are found in the asymmetric unit. The non-equivalence of the two complexes arises from the difference in the coordination of the bridging potassium ions. The coordination environment is very similar in the two crystallographically independent uranium complexes and accordingly only the coordination sphere of U1 is shown in ***Figure II.37***.

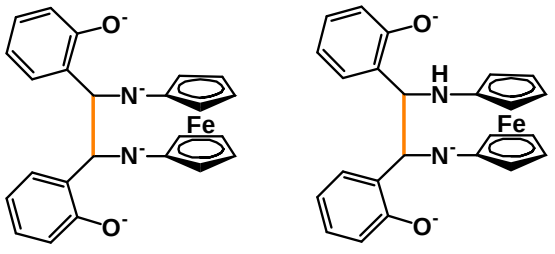

Figure II.35. Drawing of ligands bis-salfen^{4-} and bis-Hsalfen^{3-}

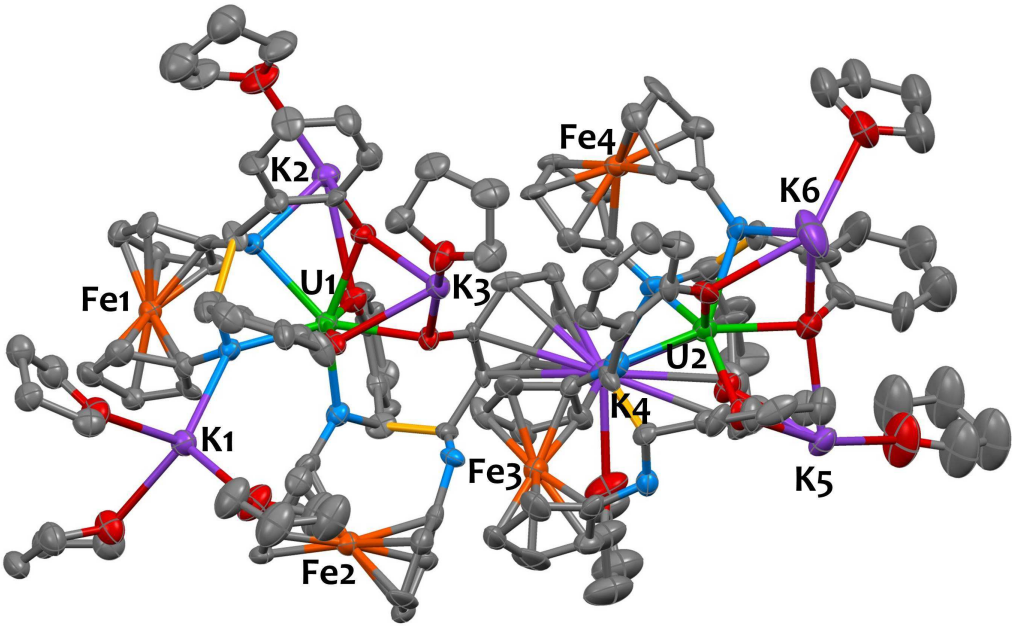

Figure II.36. Solid-state molecular structure of K_3[U(bis-salfen)(bis-Hsalfen)](THF)$_n$ **13-H**. Hydrogen atoms and non-coordinated solvent molecules are omitted for clarity. The C-C bond formed through the reductive coupling of the imino groups is represented in yellow and uranium (green), iron (orange), potassium (purple), nitrogen (blue), oxygen (red) and carbon (grey) atoms are represented with 50% probability ellipsoids.

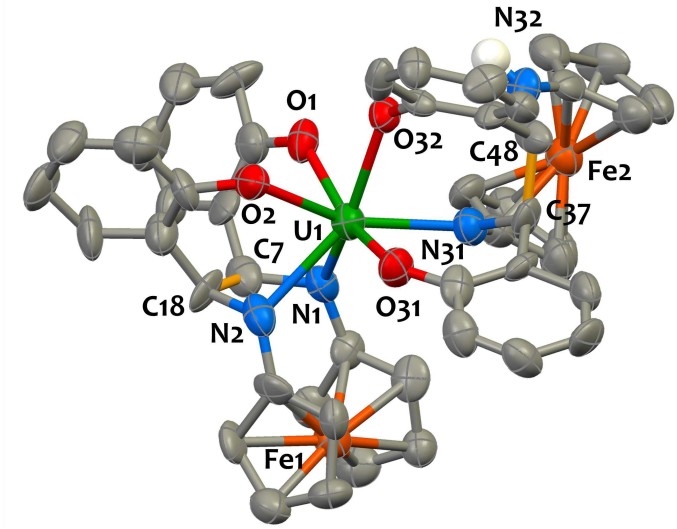

Figure II.37. Solid-state molecular structure of the [U(bis-salfen)(bis-Hsalfen)]$^{3-}$ anion from K_3[U(bis-salfen)(bis-Hsalfen)](THF)$_n$ **13-H**. Hydrogen atoms except those of the amino moiety and solvent molecules are omitted for clarity. The C-C bond formed through the reductive coupling of the imino groups is represented in yellow and uranium (green), iron (orange), potassium (purple), nitrogen (blue), oxygen (red) and carbon (grey) atoms are represented with 50% probability ellipsoids.

The uranium in **13-H** is heptacoordinated in a distorted capped trigonal prismatic arrangement. Two new C-C bonds have formed upon reduction between the imino moieties of a same salfen ligand. This results in the formation of a new bisphenolate bisamido ligand, namely bis-salfen (***Figure II.35***) and a protonated version of the same ligand, namely bis-Hsalfen (***Figure II.35***), possessing one amido group bonded to the metal (N31) and one amino group (N32) uncoordinated. The resulting

heteroleptic complex is therefore composed of a U(IV) cation coordinated by a tetraanionic bis-salfen ligand and a trianionic bis-Hsalfen ligand, which is consistent with the overall trianionic charge for the complex.

The ^{1}H NMR spectrum of **13-H** recorded in THF-d_8 at 298K (***Figure II.38***) features 37 sharp resonances over the range 36.4 to -27.5 ppm. This is in agreement with a uranium(IV) complex exhibiting a fully asymmetric solution structure, as expected for this heteroleptic species. ESI/MS studies further support the formulation of **13-H** as K_3[U(bis-salfen)(bis-Hsalfen)] in THF solution (m/z = 1201.0 corresponding to the $\{K_3[U(bis\text{-}salfen)(bis\text{-}Hsalfen)]+H\}^+$ moiety).

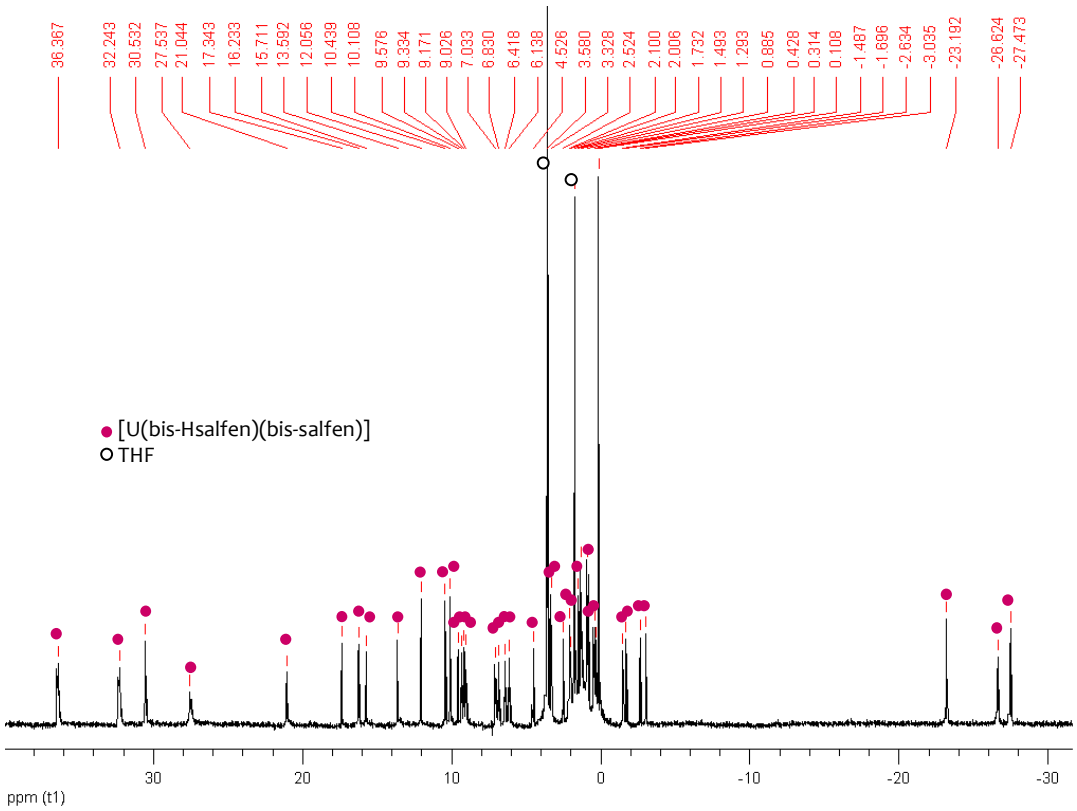

Figure II.38. ^{1}H NMR (200 MHz, THF-d_8, 298 K) of K_3[U(bis-salfen)(bis-Hsalfen)] **13-H**.

In an effort to identify the second species formed upon reduction, several crystallization attempts were undertaken. Single crystals of [K(dibenzo18c6)(py)]$_2$[U(bis-Hsalfen)$_2$] **13-H$_2$** were grown upon slow diffusion of hexane into a pyridine solution of the complex in presence of dibenzo18c6. The solid-state structure consists of an isolated ion pair and the structure of the [U(bis-Hsalfen)$_2$]$^{2-}$ anion is presented in ***Figure II.39***. Selected bond distances are given in ***Table II.7***. The uranium(IV) cation lies on a symmetry center and exhibits a pseudo-octahedral coordination with four phenolate moieties from the bis-Hsalfen ligands coordinated in the equatorial plane and two amido moieties bound in a trans configuration. This is consistent with the solution NMR data which feature 18 peaks, indicating that the two ligands are equivalent on the NMR time scale. The reduction of the salfen ligands

results in the formation of two C-C bonds of 1.586(8) Å long by coupling of two of the original imino groups. The value of the C-C bond distance is in the range of those observed in the bis-salophen and cyclo-salophen complexes presented in the previous sections. The C18-N2 and C7-N1 bond distances (1.476(6) Å and 1.461(5) Å) in **13-H$_2$** are longer than the C-N imino bond distances observed in **12** and correspond to C-N simple bonds. The U1-N2 bond distance (2.355(4) Å) is much shorter than the U-N_{imino} bond distances observed in **12**, which is consistent with an amido moiety. While N2 is strongly coordinated to the uranium cation, as expected for an amido moiety, the neutral amino nitrogen N1 remains uncoordinated to the metal center. The average value of the U-O bond distances (2.24(3) Å) is in line of those observed for U(IV) phenolate systems (see section II.2). The U···Fe separation (4.8874(9) Å) is longer than that in **12**. Finally, the overall K/U ratio is 2, in agreement with a +IV charge for the uranium. Thus, the formula $[U(bis\text{-}Hsalfen)_2]^{2-}$ where bis-Hsalfen is a trianionic tridentate ligand provides a good description of complex **13-H$_2$**.

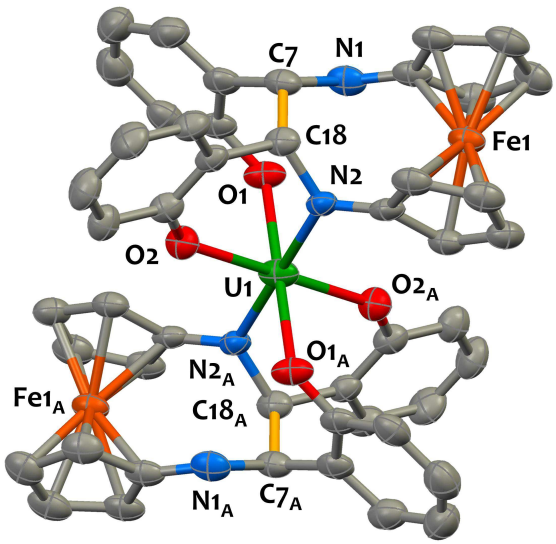

Figure II.39. Solid-state molecular structure of the $[U(bis\text{-}Hsalfen)_2]^{2-}$ anion from $[K(dibenzo18c6)(py)]_2[U(bis\text{-}Hsalfen)_2].py_5$ **13-H$_2$**. Hydrogen atoms and solvent molecules are omitted for clarity. The C-C bond formed through the reductive coupling of the imino groups is represented in yellow and uranium (green), nitrogen (blue), oxygen (red), iron (orange) and carbon (grey) atoms are represented with 50% probability ellipsoids.

Table II.7. Mean values of selected bond lengths [Å] in the U(IV) complexes **12** and **13-H$_2$**. All distances are average.

Compound	U-N	U-O	C-C_{link}	C-N	U-Fe	Fe-C
12	2.664(7)	2.231(9)	/	1.294(6)	4.316(11)	2.041(7)
13-H$_2$	2.355(4)	2.24(3)	1.586(8)	1.469(11)	4.8874(9)	2.043(13)

Mixtures of **13-H** and **13-H$_2$** were reproducibly obtained from independent syntheses. These species are respectively the mono-protonated and the di-protonated analogues of a putative $[U(bis\text{-}salfen)_2]^{4-}$ species which abstracts hydrogen from the reaction media. We already mentionned in

section II.2.5.2 that the amido moieties of the bis-salophen platform are basic. In the putative tetraanionic mononuclear $[U(bis\text{-}salfen)_2]^{4-}$ species, resulting from the 4 electon reduction of $[U(salfen)_2]$, the octaanionic environment provided at the U(IV) cation by the four phenolates and four amido groups likely results in a high electron density at the metal responsible for the unstability of the species. Unfortunately, efforts to characterize this intermediate so far proved unsuccessful in our hands. Attempts to perform the reduction in the more robust DME solvent afforded the same mixture of compounds. Similar results were obtained when replacing KC_8 by K chunks yet in this case the reduction was taking more time to go to completion and the amount of **13-H$_2$** versus **13-H** was increased. Using lower or higher quantities of potassium graphite resulted in the formation of intractable mixtures containing **13-H$_2$** and/or **13-H** together with other unidentified reduction products. Attempts to deprotonate [U(bis-salfen)(bis-Hsalfen)] **13-H** with potassium hydride also proved unsuccessful.

In summary, the reduction of $[U(salfen)_2]$ **12** affects the Schiff base ligand and affords a mixture of compounds in which C-C bonds connect the two phenolate arms of a same ligand. Such feature is not possible for the more rigid salophen ligand in which C-C coupling occurs at two separate ligands. This confirms the non-innocent behavior of the salfen ligand and the crucial role of the structure of the supporting Schiff base in the outcome of the reduction. Further work might be directed to determine the experimental conditions allowing for isolation of a uranium bis-salfen monoligand species.

II.4 Electron-Rich Uranium(IV) Complexes Supported by a Tridentate Schiff Base Ligand

II.4.1 Synthesis of ^{Me}naphtquinolen uranium(IV) complexes

II.4.1.1 Ligand design

In the previous sections, we have shown that the tetradentate Schiff base ligand salophen (salophen = N,N'-disalicylidene-o-phenylenediaminate) was behaving as a redox-active ligand able to store electrons through the reversible formation and cleavage of C-C bonds. This allowed multielectron redox reactions to occur at uranium(IV) complexes. These promising results encouraged us to investigate on new redox-active tridentate Schiff base platforms. The tridentate nature of the ligand was chosen in order to render available two coordination sites at the metal center which were not present in the Na_2[U(bis-salophen)] system. The presence of available coordination sites should allow the coordination of potential substrates to the metal center leading to a better control of the reactivity. Notably, it might favor reaction pathways involving the metal-mediated transfer of the electrons stored on the ligand to the coordinate substrate.

In our quest for suitable tridentate Schiff base ligand, we found the ^{Me}naphtquinolen (***Scheme II.27***) particularly well-matched. Based on our experience with the salophen ligand, we anticipated that one key structural criterion to maintain the redox-active properties of the ligand is that the imine moiety remains highly conjugated. In the present case, this was provided by the use of the quinoline moiety. This should in principle favor electronic delocalization onto the ligand backbone, allowing the ligand to behave as a good electron acceptor. Additionally, we decided to protect the position 2 of the quinoline by a methyl group as this particular site is prone to nucleophilic or radical attacks and could yield side products.

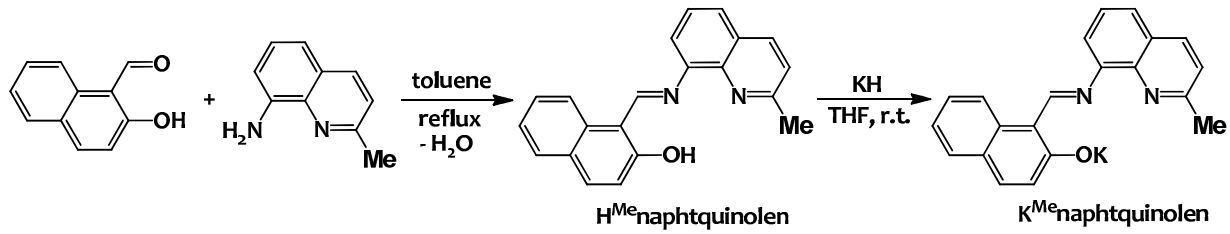

Scheme II.27. Synthesis of K-^{Me}naphtquinolen.

This new ligand was conveniently prepared by condensation between the 2-methylquinolin-8-amine and the 3-hydroxy-2-naphtaldehyde (***Scheme II.27***). Subsequent deprotonation of the phenol moiety was performed using potassium hydride under inert atmosphere.

II.4.1.2 Synthesis of $[UX_2(^{Me}naphtquinolen)_2]$ complexes

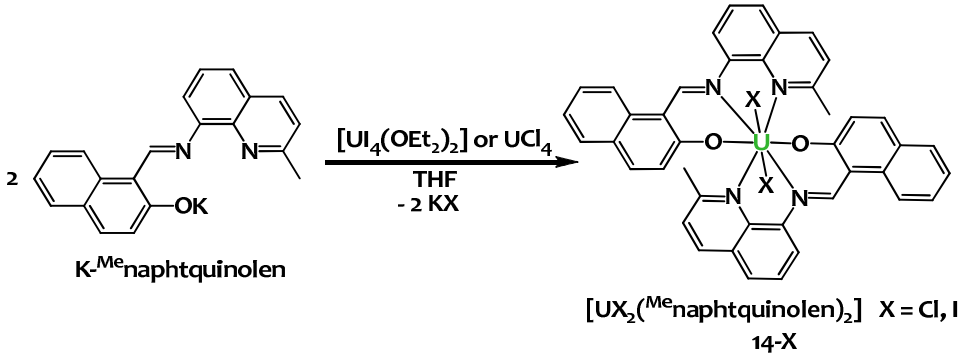

Scheme II.28. Synthesis of $[UX_2(^{Me}naphtquinolen)_2]$ **14-X** (X = Cl, I).

Proton NMR spectra of the reaction mixture of two equivalents of K^{Me}naphtquinolen and one equivalent of $[UI_4(OEt_2)_2]$ or $[UCl_4]$ in deuterated THF shows only one set of signals assigned to the heteroleptic mononuclear $[UX_2(^{Me}naphtquinolen)_2]$ **14-X** complexes (***Scheme II.28***) where X = I or Cl respectively. The solubility of **14-Cl** in organic solvents (fully soluble in THF, partially soluble in toluene) is much higher than those of **14-I** (sparingly soluble in THF, insoluble in toluene) facilitating its separation from KX salts. Accordingly, the complex $[UCl_2(^{Me}naphtquinolen)_2]$ **14-Cl** was also isolated pure in high yield.

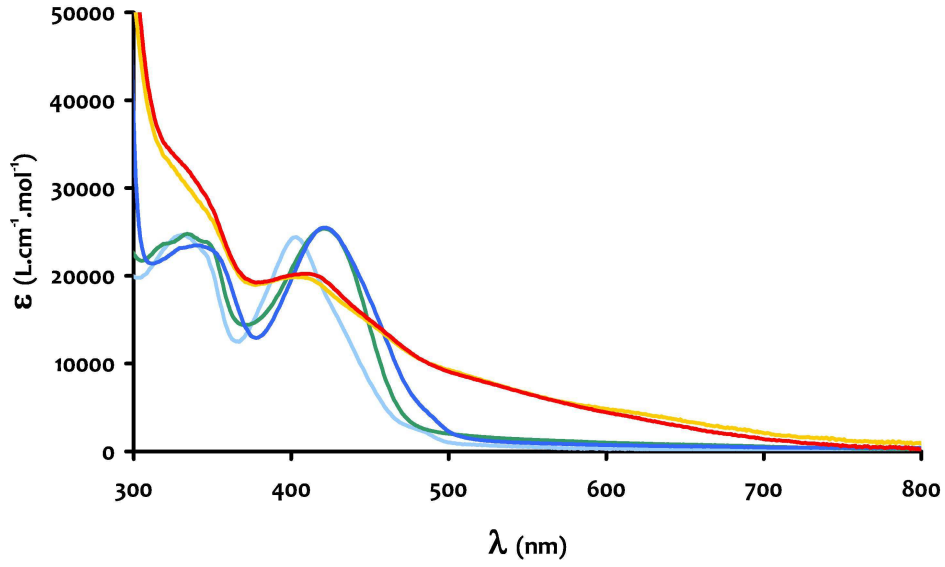

Figure II.40. UV-visible absorption spectra of 0.05 mM solutions of **14-I** (blue line), **14-Cl** (pale blue line), **15** (red line) and **16** (green line) in THF and **15** (orange line) in toluene.

The UV-visible spectra for **14-Cl** and **14-I** (***Figure II.40***) display a series of intense absorptions below 450 nm ($\varepsilon \approx 25000$ L.cm^{-1}.mol^{-1}) that we assign to ligand-based $\pi \rightarrow \pi^*$ transitions.

The X-ray structural analysis of **14-Cl** shows that the uranium atom is octa-coordinated by two ^{Me}naphtquinolen and two chloride ligands in a slightly distorted square antiprism possessing a pseudo C2 axis (***Figure II.41***). The mean values of U-O (2.20(2) Å) ; U-N (2.6(1) Å) and U-Cl (2.67(4) Å) bond distances (***Table II.8***) are in the range of thoses found in other U(IV) Schiff base complexes (see sections II.2 and II.3).[320, 321] The ^{Me}naphtquinolen ligands are strongly distorted from planarity with about 70° between the quinoline and the naphthol planes. This is most probably due to steric repulsion between the two tridentate ligands in the present coordination environment. The two ^{Me}naphtquinolen ligands are arranged perpendicular to each other with the two halide anions laying on the same face of the square antiprism. This geometry is very different from those reported for analogous tridentate ligands bound to Yb(III) or Y(III).[388] In the crystal structure of the $[L_2Ln(N(TMS)_2)]$ (Ln = Yb(III) or Y(III) L = bis(3,5-di-tert-butylsalicylidene)-8-aminoquinoline) the two tridentate Schiff bases are almost planar and bind the metal in a parallel fashion. These two binding modes are reminiscent of those observed in sandwich and meridional isomers of uranium bis-ligand complexes of tetradentate Schiff bases (see section II.2.4.1).[321]

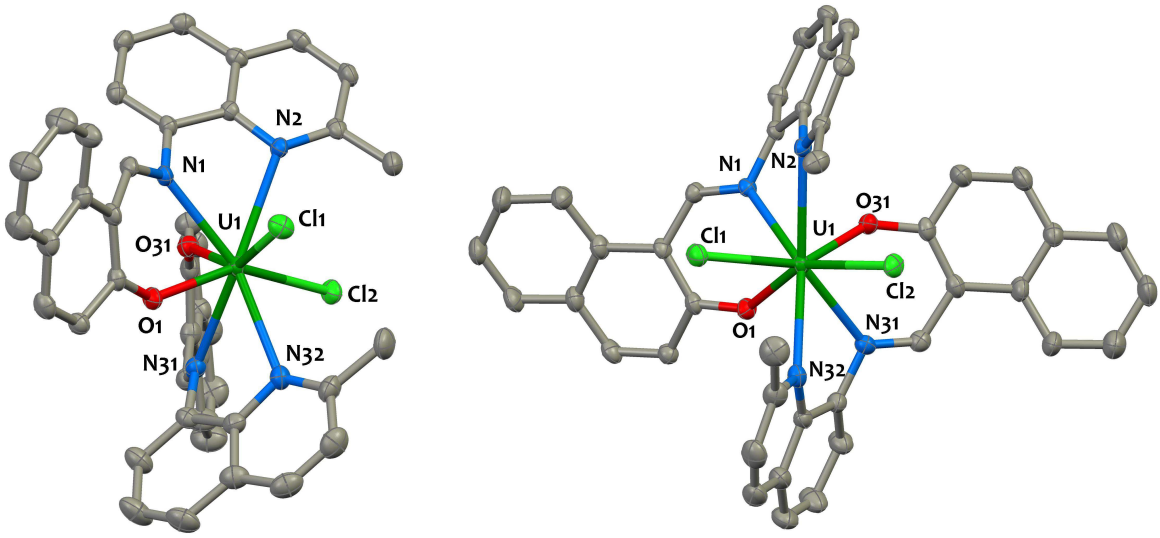

Figure II.41. Side and top views of the solid-state molecular structure of $[UCl_2(^{Me}naphtquinolen)_2]$, **14-Cl**. Hydrogen atoms and solvent molecules are omitted for clarity. Uranium (deep green), nitrogen (blue), oxygen (red), chlorine (light green) and carbon (grey) atoms are represented with 50% probability ellipsoids. Selected bond distances are given in ***Table II.8***.

II.4.1.3 Reduction of [UX_2(^{Me}naphtquinolen)$_2$] precursors : isolation of [U(μ-bis-^{Me}naphtquinolen)]$_2$

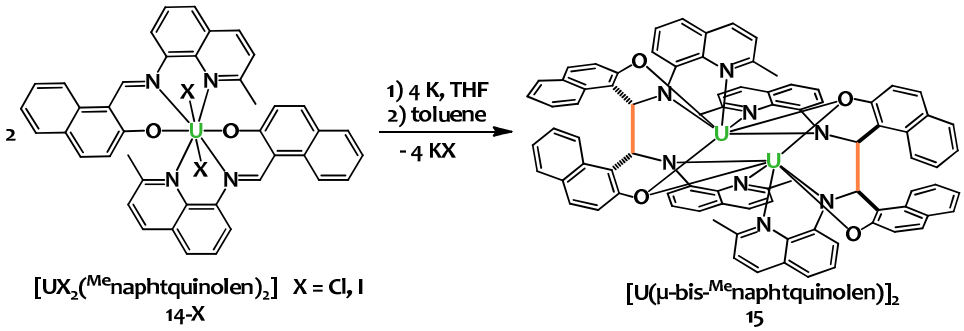

Scheme II.29. Synthesis of [U(μ-bis-^{Me}naphtquinolen)]$_2$ **15**.

The proton NMR spectrum in THF of the reaction mixture after reduction of the complex **14-I** with two equivalents of potassium (***Scheme II.29***) in deuterated THF shows the presence of two sets of 26 signals (ratio 66:34). The proton NMR in toluene of the reaction mixture after removal of THF shows the presence of only one set of 26 signals. Recrystallization from toluene affords the complex [U(μ-bis-^{Me}naphtquinolen)]$_2$ **15** pure in 67% yield.

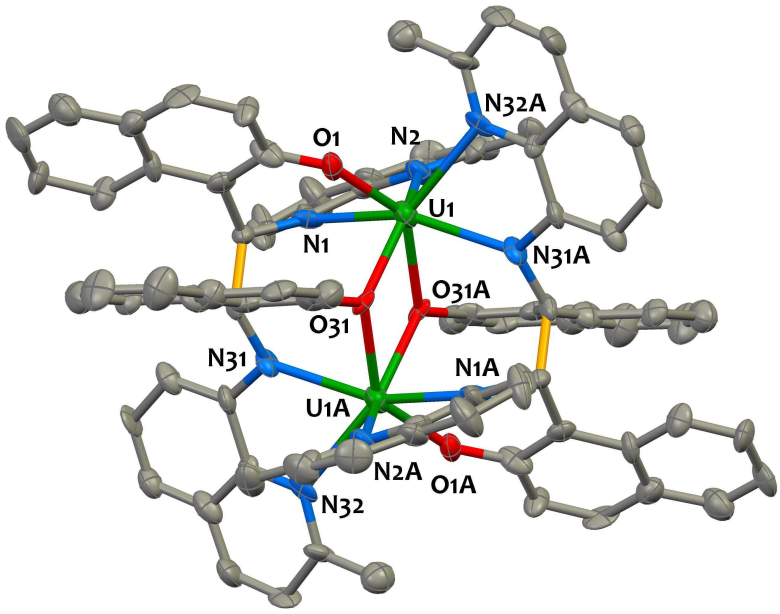

Figure II.42. Solid-state molecular structure of [U(μ-bis-^{Me}naphtquinolen)]$_2$, **15**. Hydrogen atoms and solvent molecules are omitted for clarity. The C–C bond formed by reduction of the imine moieties of the ligands is represented in yellowand the uranium (green), nitrogen (blue), oxygen (red) and carbon (grey) atoms are represented with 50% probability ellipsoids. (U1A = U1 -x+1,-y+1,-z+2). Selected bond distances are given in ***Table II.8***.

The solid state structure of **15** determined by X-ray structural studies is presented in ***Figure II.42***. It shows that the dimeric compound **15** is composed of two [U^{IV}(bis-^{Me}naphtquinolen)] complexes bridged by the phenolate oxygens of the two tetra-anionic bis-^{Me}naphtquinolen ligands. The crystal

structure is centrosymmetric, with an inversion center located halfway between the two uraniums. Each metal cation is hepta-coordinated in a distorted capped trigonal prismatic environment by the four nitrogen (mean U-N = 2.5(1) Å) and two oxygen atoms from a bis-^{Me}naphtquinolen ligand (mean U-O = 2.3(1) Å) and by a bridging phenolate oxygen form the other [U^{IV}(bis-^{Me}naphtquinolen)] complex. The two bidentate phenolate bridging ligands hold the two uranium centers in the dimer at 3.7983(8) Å apart.

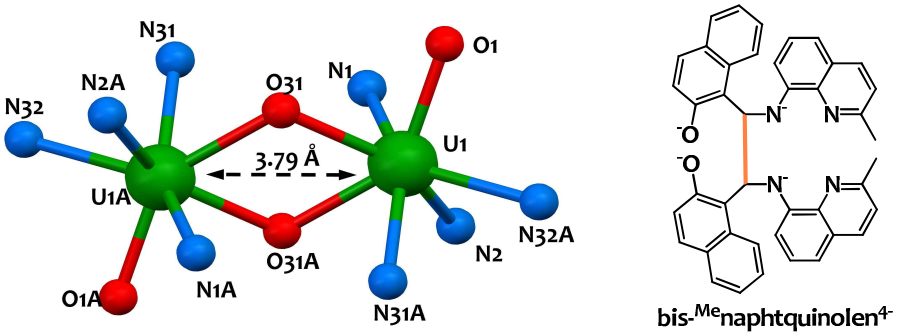

Figure II.43. View of the dinuclear core of complex [U(μ-bis-^{Me}naphtquinolen)]$_2$ **15** (right) and schematic representation of the tetranionic hexadentate ligand bis-^{Me}naphtquinolen^{4-} (left).

Table II.8. Mean values of selected bond lengths [Å] in the U(IV) complexes **14-Cl**, **15**, **16** and **17**.

Compound	U-N_{aro}	U-$N_{imino/amido}$	U-$O_{phenolate}$	U-X	C-C_{link}	C-$N_{imino/amido}$
14-Cl	2.70(3)	2.51(3)	2.204(18)	2.67(4) $_{X = Cl}$	/	1.293(2)
15	2.538(3)	2.36(2)	2.26(10)	/	1.636(14)	1.474(5)
16	2.58(7)	2.52(2)	2.227(13)	2.26(4) $_{X = O}$	/	1.294(9)
17	2.646(4)	2.55(2)	2.238(6)	1.776(3) $_{X = O}^{2-}$	/	1.292(2)

The analysis of the structural parameters of the complex clearly shows that the reduction has occurred on the imino groups of the ligands rather than on the metal ions. Notably, the two electron reduction of the ligand results in the formation of two C–C bonds, 1.636(14) Å long, by intramolecular coupling of the original imino groups. The value of the C–C bond distance in **15** is larger than those observed in the Na_2[U(bis-salophen)] **7** (1.559(7) Å) and [U_2(cyclo-salophen)$(py)_4$] **4-py** (1.609(5) Å) complexes for the C-C bonds formed after reductive coupling of the imino groups but remains in the range of reported values for C–C bond lengths in sterically congested molecules.[332-334] The C–N_{am} bond distances (mean C–N_{am} = 1.474(5) Å) of the ligand backbone are much longer than those observed in **14-Cl**, and are in agreement with the presence of two amido groups. This is further confirmed by the analysis of the values of the U–N bond distances, with the U–N_{am} distances in **15** (U–N_{am} = 2.36(2) Å) being significantly shorter than the U–N_{py} distances in **2** (U–N_{py} = 2.538(3) Å) and the U–N_{im} distances in **14-Cl** (U–N_{im} = 2.51(3) Å). This distances compares well with the U-N_{am} (2.387(8) Å) and U-N_{im} (2.624(7) Å) observed in Na_2[U(bis-salophen)] **7**. The value of the magnetic moment

(2.44 μ_B) per uranium measured using the Evans method for a toluene solution of **15** is in the range of values reported for U(IV) complexes.[30] Thus, the formula [U(μ-bis-^{Me}naphtquinolen)]$_2$ where bis-^{Me}naphtquinolen is a tetra-anionic hexadentate ligand provides a good description of this neutral complex.

Compared to the Na_2[U(bis-salophen)] **7** complex, which is only soluble in polar solvents, complex **15** is soluble in toluene. The difference in solubility can be accounted to the neutral formulation of **15**. Compound **15** is stable for weeks at room temperature in the solid state or in toluene solution under inert atmosphere. In addition to the ligand-based π-π* transitions below 450 nm, a long tail absorption extending to 750 nm is observed in the UV-visible spectrum of **15** (***Figure II.40***), responsible for its dark-brown color in solution.

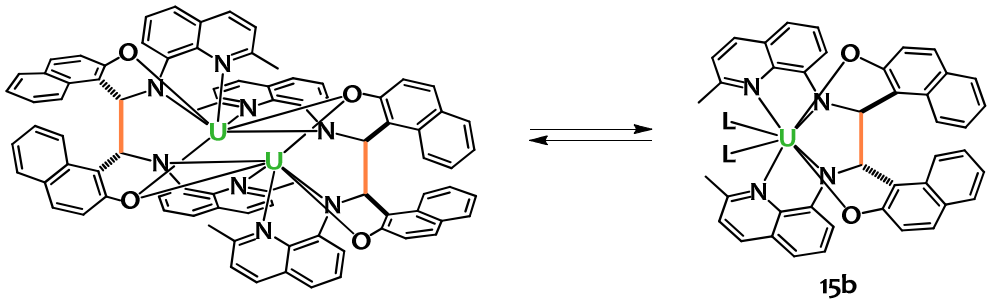

Scheme II.30. Equilibrium between the dimeric and the monomeric forms of **15** in coordinating solvents.

The proton NMR spectrum of **15** in toluene solution shows only one set of 26 signals assigned to a centrosymmetric dimeric solution species in agreement with the solid state structure of **15**. The ^{1}H NMR spectrum of **15** in deuterated THF or pyridine shows the presence of two sets of 26 resonances indicating that two forms of the complex are present in coordinating polar solvents (Figure II.44). Evaporation of the pyridine and THF solutions and dissolution of the resulting solid in toluene result again in the presence of only one species in the proton NMR spectrum. The monitoring of the ^{1}H NMR spectrum of complex **15** in pyridine solution at different times after dissolution shows that the ratio between the two isomers evolves over time, going from 3:1 after 30 minutes (***Figure II.44***), to a final stable ratio of 0.5:1 after 4 days (***Figure II.45***). The proton chemical shifts for the initially major species are close to that measured for complex **15** in deuterated toluene. This suggests that the initially major species in pyridine solution is a dinuclear complex which with time undergoes a rearrangement in pyridine solution. The second set of 26 resonances could either correspond to a solvent adduct of the dinuclear complex **15** or to a monomeric form of the complex. Pulsed-field-gradient stimulated-echo diffusion NMR spectroscopy was used to measure the diffusion coefficients of both species in pyridine solution. D is a function of the molecular weight and has been successfully used to discriminate metallosupramolecular architectures in solution.[389, 390] The values

measured in pyridine ($(D_A/D_B)^3$ = 1.63 ; M_A/M_B = 1.69) are in agreement with the presence of a mononuclear and a dinuclear complexes in solution (***Scheme II.30***). Attempts to isolate crystals of the monomeric complex from pyridine or THF were not successful.

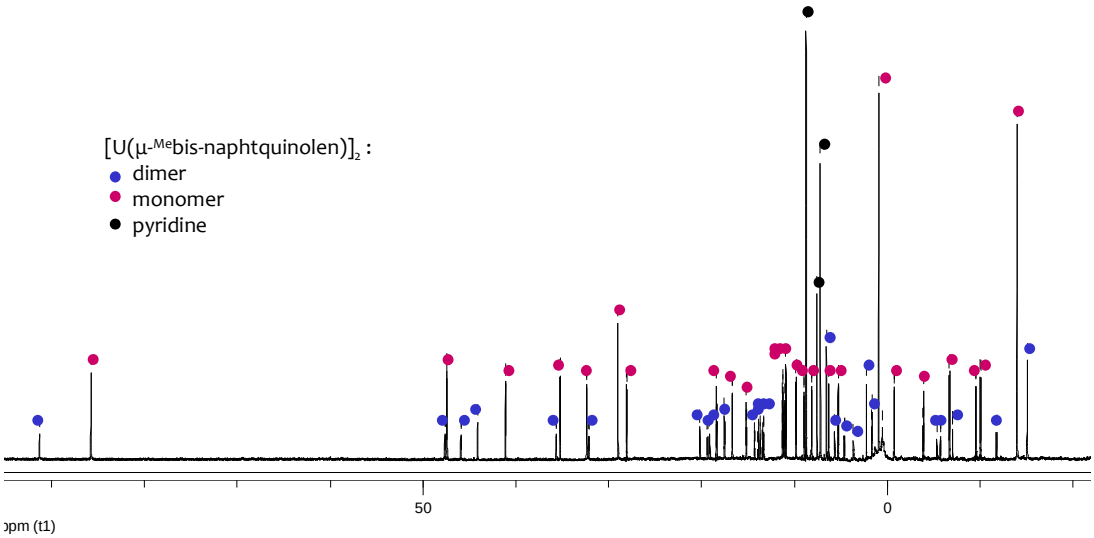

Figure II.44. ^{1}H NMR spectrum (298 K, 200 MHz) in pyridine-d_5 of [U(μ-bis-^{Me}naphtquinolen)]$_2$ **15** after 30 minutes.

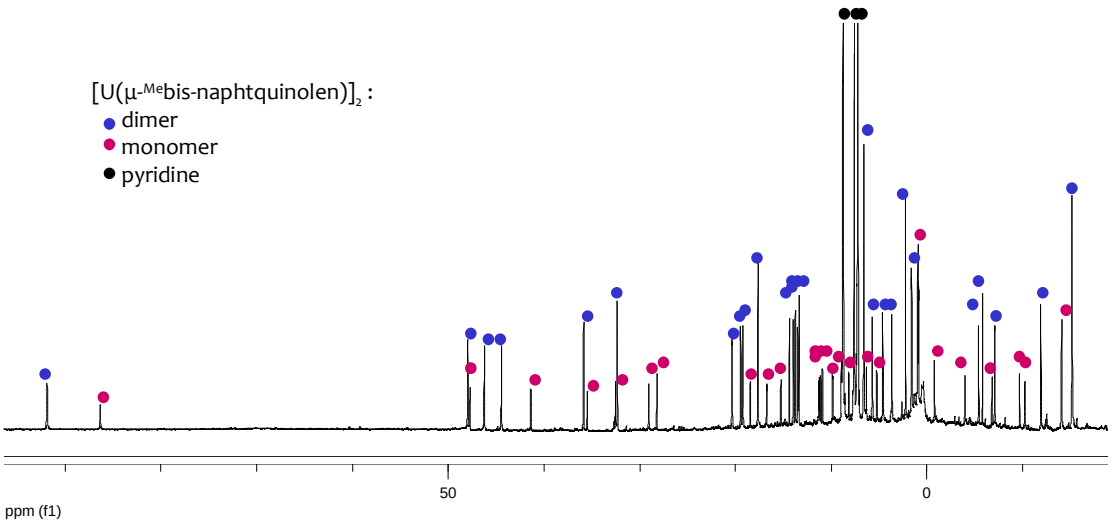

Figure II.45. ^{1}H NMR spectrum (298 K, 500 MHz) in pyridine-d_5 of [U(μ-bis-^{Me}naphtquinolen)]$_2$ **15** after 4 days.

The most probable pathway for the formation of **15** (see ***Scheme II.31***) from the reduction of **14-X** involves the reduction of the two imino group to afford two U(IV) radical anions which then undergo intramolecular C-C coupling. This produces a U(IV) complex of the new hexadentate tetranionic bis-phenolato bis-amido bis-^{Me}naphtquinolen ligand where at least two coordination sites are available at the metal center for solvent or substrate binding. In the absence of coordinating solvents this complex dimerizes through phenolate bridging to yield **15**.

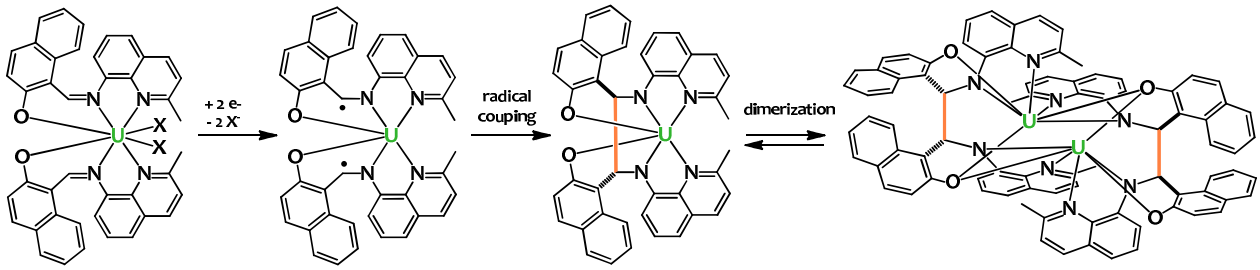

Scheme II.31. Proposed pathway to account for the formation of [U(μ-bis-^{Me}naphtquinolen)]$_2$ **15**.

Isolation of a pure product from the reduction of the chloride analogue **14-Cl** with potassium proved more difficult. Proton NMR in deuterated THF of the reaction mixture after reduction of **14-Cl** with two equivalents of potassium metal shows the presence of several sets of signals. Two sets of signals were assigned to the reduced species **15** and **15b**, the other signals remain unidentified. The presence of additional species can be explained in term of a competition of an intermolecular C-C coupling process leading to complex mixtures as a result of the presence of the more coordinating chloride ligand. Although the ligands could rearrange in solution, the conformation adopted by the two tridentate ligands in the solid state structure of the complex **14-Cl** with the two carbons of the imino groups situated at a distance of 5.995(6) Å, is not favorable to intramolecular C-C bond formation. However, proton NMR studies show that the reduction of **14-Cl** with KC_8 in THF leads cleanly to the formation of complexes **15** and **15b**. These results show that clean ligand based reduction followed by intramolecular C-C coupling is not limited to uranium complexes of tetradentate Schiff bases. However in the case of tridentate Schiff bases the choice of the halide precursor plays an important role in the outcome of the reduction reaction. Moreover, the final complex presents free coordination sites at the metal center which are not available in the previously described Na_2[U(bis-salophen)] **7** complex obtained from the intramolecular C-C coupling of two reduced imino groups from the [U(salophen)$_2$] **6** precursor.

Complex **15** provides an interesting precursor for the synthesis of more reduced species. The possibility of further reduction of the metal center in **15** was explored by electrochemical studies.

II.4.2 Redox properties

II.4.2.1 Electrochemistry studies

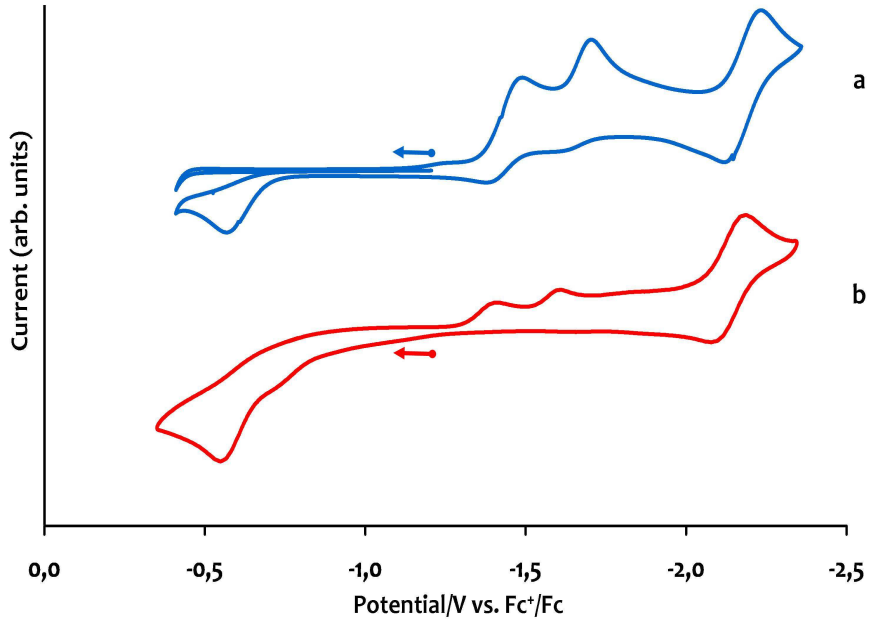

Figure II.46. Cyclic voltammogram for 10 mM solutions of a) **14-I** and b) **15** in ~0.1 M $[Bu_4N][PF_6]$ pyridine solution at 100 mV.s^{-1} scan-rate.

Cyclic voltammetry data were collected for complexes **14-I** and **15** in ~0.1 M $[Bu_4N][PF_6]$ pyridine solution and are presented in ***Figure II.46***. All redox potentials are referenced against the $[(C_5H_5)_2Fe]^{+/0}$ redox couple and are summarized in ***Table II.9***. While the free ligand in K-^{Me}naphtquinolen does not exhibits reduction process in the range -0.5 ··· -2.4 V, the voltammogram of complex **14-I** shows three distinct reduction events. A first reduction process occurs at E_{pc1} = -1.45 V and is followed by a reduction at E_{pc2} = -1.65 V. These two waves are associated with an irreversible oxidation process occurring at E_{pa} = -0.56V which is not observed when the voltammogram is swept initially from –1.2 V towards the positive direction (***Figure II.47***). These data indicate the presence of a system with a limited degree of chemical reversibility as one could expect due to the formation of the C-C bond after ligand reduction. Finally, a third reversible process is observed at $E_{1/2}$ = -2.16 V. Similar redox processes are observed on the voltammogram of the reduced species **15** which can be reversibly reduced at $E_{1/2}$ = -2.17 V and irreversibly oxidized at E_{pa} = -0.56V. The latter wave has a shoulder at -0.68 V that can be reasonably assigned to the oxidation of the monomeric form in equilibrium with the dimeric one in pyridine solution. Notably, it has been observed that the intensity of the shoulder was increasing 1 hour after dissolution of **15** in pyridine, in agreement with a higher ration monomer/dimer in pyridine solution as observed in the NMR studies. The two irreversible

reduction waves at E_{pc1} = -1.49 V and E_{pc2} = -1.70 V are not observed when the voltammogram is swept initially from -1.3 V to the negative direction and are thus associated to the reduction of the oxidation product.

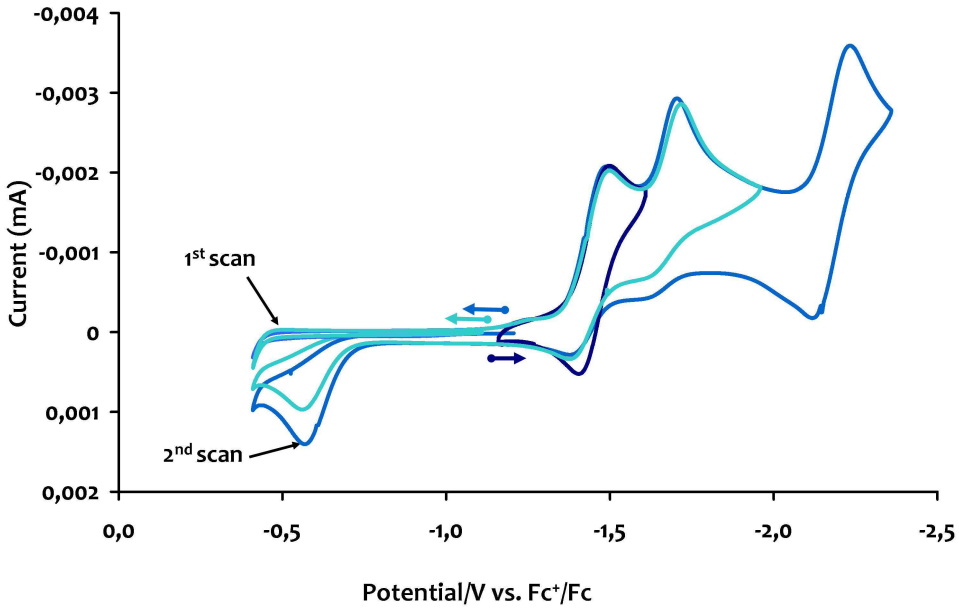

Figure II.47. Cyclic voltammograms of **14-I** in ~0.1 M $[Bu_4N][PF_6]$ pyridine solution at 100 $mV.s^{-1}$ scan-rate. The first reduction process occurring at E_{pc1} = -1.45 V is reversible. This process is followed by a reduction at E_{pc2} = -1.65 V which is associated with an irreversible oxidation process occurring at E_{pa} = -0.56 V. Indeed, this oxidation wave is not observed when the voltammogram is swept initially from –1.2 V to the positive direction.

Taking into account that both the ligand and the uranium center are electroactive species, distinguishing ligand-based and metal-based processes is critical. The values of the redox potentials of the first two reduction waves are not compatible with metal based reductions (U(IV)/U(III) and U(III)/U(II)). The pseudo-reversible reduction processes in the -1.45 ··· -1.70 V range probably correspond to two successive one electron transfers to the bis-^{Me}naphtquinolen ligand scaffold. Thus, the irreversible oxidation occurring at E_{pa} = -0.56 V corresponds to the oxidation of the bis-^{Me}naphtquinolen platform, i.e. to the oxidative cleavage of the C-C bond.

Table II.9. Voltammetric data for **14-I** and **15**.

Compound	Ligand-based waves			Metal-based wave
	E_{pa} (V)	E_{pc1} (V)	E_{pc2} (V)	$E_{1/2}$ (V)
14-I	-0.56	-1.45	-1.65	-2.16
15	-0.56	-1.49	-1.70	-2.17

Compared to the bis-salophen platform, which is oxidized at $E_{1/2}$ = -1.14 V in Na_2[U(bis-salophen)] **7** (see section II.2.4.3) the bis-^{Me}naphtquinolen ligand is more difficult to oxidize. Therefore the

reducing power of [U(μ-bis-^{Me}naphtquinolen)]$_2$ **15** is weaker than that of Na_2[U(bis-salophen)] **7**. This emphasizes that by a careful choice of the Schiff base ligand scaffold the ligand-based redox processes can be anodically shifted towards more tolerant potential windows.

The irreversibility of the ligand-based processes suggests that the electrochemical reduction is followed by a rapid chemical transformation involving the formation or cleavage of the C-C bond between two reduced imino groups. This process confers a strong stabilization to the system, as is expressed by the much lower potential required for transferring an electron to the ^{Me}naphtquinolen ligand than those required for oxidizing the bis-^{Me}naphtquinolen platform (Δ Ep =0.9 V).

The reversible wave at $E_{1/2}$ = -2.16 V corresponds to a further reduction of **15** and is attributed to a U(IV)/U(III) couple. This fits with the range of values of redox potentials reported for other U(IV)/U(III) reversible systems.[24, 69, 70, 361] This is a considerable difference with the Na_2[U(bis-salophen)] system, as in the latter, further reduction occurs at the imino moieties of the bis-salophen ligand. Future studies may be directed to identify the chemical conditions allowing the isolation of this reduced species and to investigate its reactivity.

II.4.2.2 Reactivity of [U(μ-bis-^{Me}naphtquinolen)]$_2$ with oxidizing agents

The reaction of [U(μ-bis-^{Me}naphtquinolen)]$_2$ **15** with different oxidizing substrates has been investigated to assess if the electrons stored in the C-C bond can become available. These studies were performed in collaboration with Julie Andrez which I supervized in the laboratory during her Master-2 internship.

Complex **15** can act as a multi-electron reductant when reacted with iodine, 9,10-phenanthrenequinone or molecular oxygen (***Scheme II.32***).

Proton NMR studies show that the reaction of **15** with I_2 in toluene leads to the cleavage of the C-C bond restoring the original Schiff base structure and affords the **14-I** complex demonstrating the chemical reversibility of this redox system.

Complex [U(9,10-phenanthrenediol)(^{Me}naphtquinolen)$_2$] **16** is obtained in 54% yield from the reaction of **15** with 9,10-phenanthrenequinone in toluene. The same reactivity is observed when using pyridine as solvent. The UV-visible spectrum for **16** is very similar to that of **14-I**, with two strong absorption bands centered at 420 nm and 334 nm (ε ≈ 25000 L.cm^{-1}.mol^{-1}) that we assign to ligand-based π-π* transitions. Notably, the tail absorption extending to 750 nm, characteristic of the reduced form of the ligand, is not present in **16**, in agreement with an oxidation of the ligand platform.

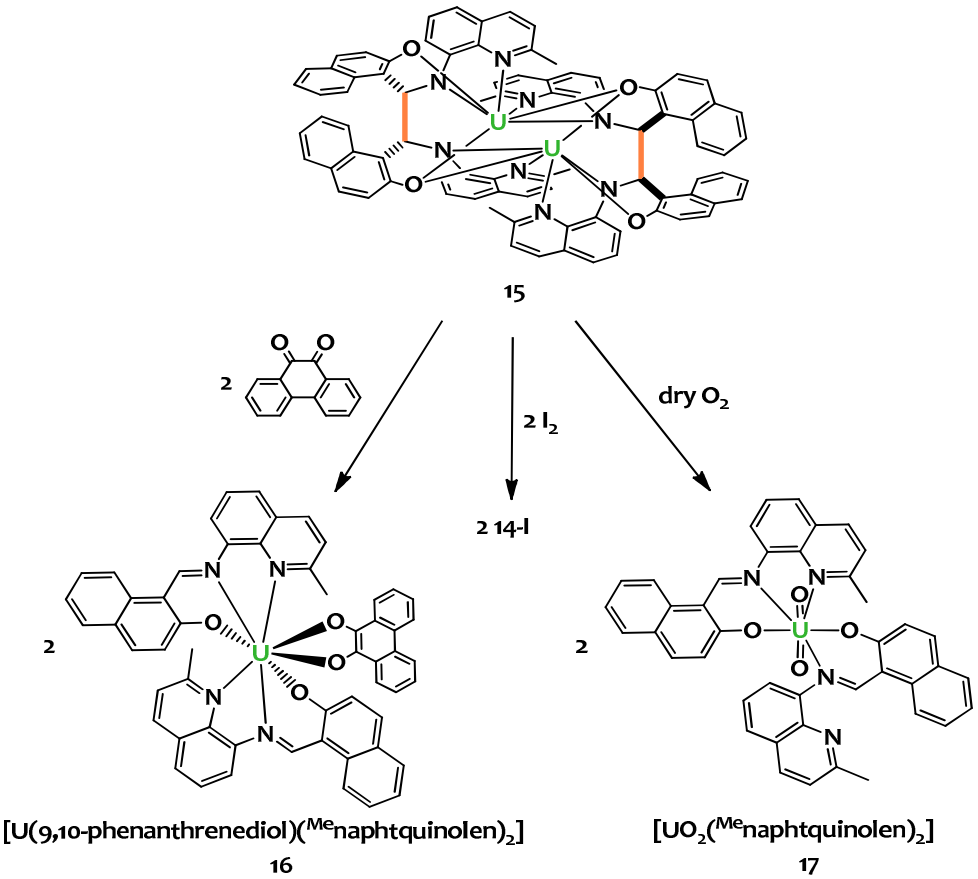

Scheme II.32. Reactivity of [U(μ-^{Me}bis-naphtquinolen)]$_2$ **15** with oxidizing agents.

Single crystals suitable for X-ray diffraction were obtained by slow evaporation of a pyridine solution of **16**, allowing its structural characterization. The molecular structure, as shown in ***Figure II.48***, consists of a C_2-symmetric complex where the uranium atom is octa-coordinated in a distorted square antiprismatic fashion by two tridentate monoanionic ^{Me}naphtquinolen ligands and one dianionic 9,10-phenanthrenediol ligand. The reduction of the quinone to its catecholate form is confirmed by the analysis of the metrical parameters for the ligand. The average U-$O_{9,10\text{-phenanthrenediol}}$ bond distances (2.26(4) Å) are relatively short, as expected for a doubly charged phenolate ligand, and are in the same range of the U-$O_{phenolate}$ moieties from the ^{Me}naphtquinolen ligand (2.23(1) Å). The C-O bond distances for this ligand (1.359(1) Å) are in agreement with the presence of simple C-O bonds. The imino moieties of the ^{Me}naphtquinolen ligands have been restored, as is illustrated by the short C-N double bond distances (1.294(9) Å) and long U-N bond distances (2.52(1) Å) which compare well with those observed in **14-Cl**. The bond distances and the overall neutral charge of the complex are in agreement with a +IV oxidation state of the uranium cation in **16**.

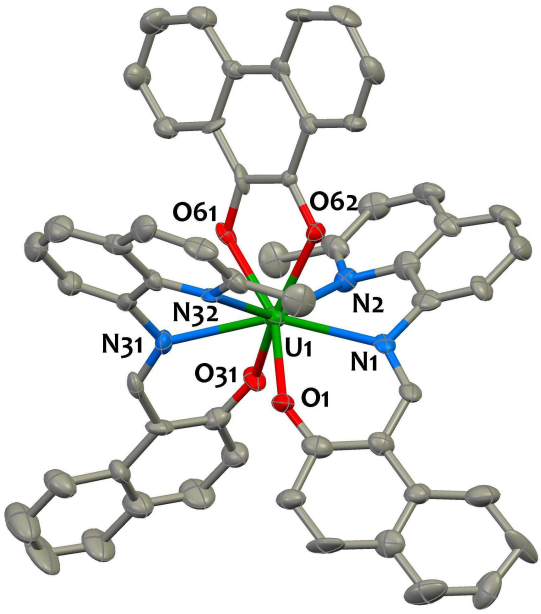

Figure II.48. Solid-state molecular structure of [U(9,10-phenanthrenediol)(^{Me}naphtquinolen)$_2$] **16**. Hydrogen atoms and solvent molecules are omitted for clarity. Uranium (deep green), nitrogen (blue), oxygen (red) and carbon (grey) atoms are represented with 50% probability ellipsoids. Selected bond distances are given in ***Table II.8.***

The reduction of 9,10-phenanthrenequinone is likely to proceed through the coordination of the substrate to the metal center and disruption of the dimeric structure of **15** followed by the cleavage of the two ligand C-C bonds. Thus each mononuclear uranium(IV) complex [U(μ-bis-^{Me}naphtquinolen)] acts as a two electrons reducing agent without undergoing a variation of the oxidation state of the metal center. The two electrons stored in each C-C bond are transferred to the substrate through a metal assisted process. In contrast to what observed for the U(IV) multi-electron redox systems based on the salophen tetradentate Schiff base, the presence of available coordination sites at the metal center allows a direct coordination of the incoming substrate to the uranium as shown by the structure of the oxidation product. This should provide a more controlled reaction pathway. Ligand redistribution, observed with [U_2(cyclo-salophen)$(THF)_4$] **4-THF**, is also avoided.

The number of transferred electrons can be increased when both the ligand and the metal are participating in the electron transfer. The reaction of a dark brown solution of **15** with excess dry oxygen in pyridine (where **15** is mostly present in its monomeric form **15-b**) proceeds instantly to give a dark red/orange solution. The ^{1}H NMR spectrum recorded for the reaction mixture shows 13 resonances in the diamagnetic region, in agreement with the presence of the new uranyl(VI) complex [UO_2(^{Me}naphtquinolen)$_2$] **17**.

The solid-state structure of **17**, determined by single crystal X-ray diffraction, is represented in ***Figure II.49***. The uranium atom has a pentagonal bipyramidal coordination provided by the two oxo groups

in axial positions and five O and N-donor atoms from two ^{Me}naphtquinolen ligands in the equatorial plane. While the first ^{Me}naphtquinolen ligand adopts a classical tridentate ONN coordination mode, as observed in **14-Cl** and **16**, the second ^{Me}naphtquinolen ligand is bound to the uranium center in a bidentate fashion by the phenolate and the imino group with the nitrogen atom from the quinoline remaining non-coordinated. Pentagonal bipyramid is the most common coordination geometry for uranyl(VI) compounds, higher coordination numbers in the equatorial plane being disfavored for steric reasons. The C-N_{im} (1.276(6) and 1.308(6) Å) bond distances from both ^{Me}naphtquinolen ligands are in the same range than thoses observed in **14-Cl** and **16**, confirming their imino character. U-N_{im}, U-N_{aro} and U-$O_{naphtol}$ mean bond distances (respectively 2.547(2), 2.646(4) and 2.238(6) Å) compare well with those reported for other uranyl(VI) Schiff base complexes.[54, 391]

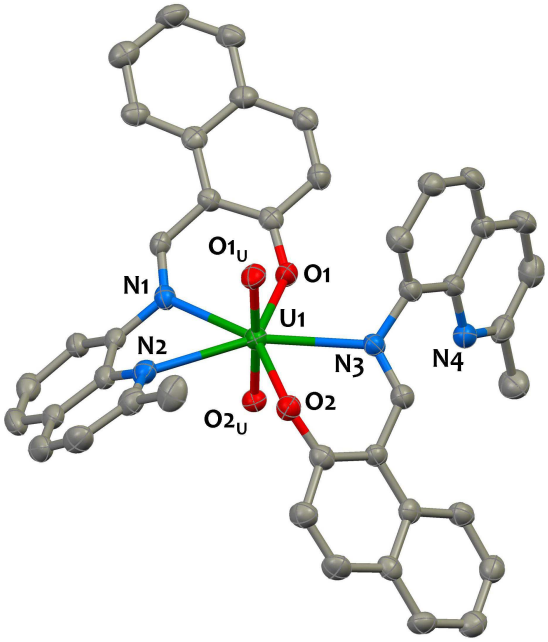

Figure II.49. Solid-state molecular structure of [UO_2(^{Me}naphtquinolen)$_2$] **17**. Hydrogen atoms are omitted for clarity. Uranium (deep green), nitrogen (blue), oxygen (red) and carbon (grey) atoms are represented with 50% probability ellipsoids. Selected bond distances are given in ***Table II.8.***

The uranyl UO_2 group in **17** is nearly linear (O–U–O angle 177.3(1)°) with uranyl bond distances (mean U–O distance 1.776(3) Å) falling in the characteristic range of seven-coordinate hexavalent uranyl complexes.[54, 391] The formation of complex **17** from **15-b** provides a rare example of a transfer of 4 electrons from a mononuclear uranium(IV) complex.

This new tridentate Schiff base ligand provides a new example of redox active ligands which enable multi-electron reductions at a U(IV) center. The reversible C-C bond formation and cleavage is not limited to salophen scaffold and controlled ligand centered reactivity can therefore be achieved with lower denticity ligands by a careful choice of the reaction condition and ligand structure.

II.5 Concluding Remarks

In summary, the work presented in this chapter represents a new example of uranium complexes with redox-active ligands. Electron-rich uranium systems have been prepared using various Schiff base ligands and multiple techniques have been used to characterize them.

These studies underline the potential of Schiff bases as supporting ligands in low-valent uranium chemistry. While both salen and salophen proved unable to stabilize trivalent uranium, only the highly-conjugated salophen ligand exhibited non-innocent behavior favoring metal-to-ligand electron transfer. This results to the reductive coupling of the imino moieties of the Schiff base to afford cyclo-salophen or bis-salophen amidophenolate octadentate chelates. Even if the formal oxidation state of the uranium ions remains +IV, it has been shown that the uranium salophen systems can store two electrons for substrate reduction in the C-C bond linking two ligand units. Indeed, reactivity studies underline the unusual ability of these kinds of systems to reversibly return to their original state. Such reduced complexes, in which the metal actually rests in a higher, stable oxidation state and the electrons for reductive transformations are available on the ligand, are prospects for performing multistep polyelectronic redox transformations. This is particularly attractive for uranium whose low-valent complexes mostly undergo single electron reduction events or eventually two-electron transfers if associated in a dinuclear complex. Therefore the possibility for a single U(IV) complex to perform polyelectronic reductions on its own is an important step forward. As such, these electron-rich molecules behave as a synthetic equivalent of U(II), which is not chemically accessible.

Besides, our results demonstrate that ligand substitution allows the tuning of the redox properties of the complexes. Furthermore, we have demonstrated that the reversible C-C bonds formation and cleavage process is not limited to the salophen framework but can be extended to other Schiff base derived ligand scaffolds.

We have shown that the reduction of [U(salfen)$_2$] leads to multiple products involving intramolecular ligand structural rearrangements. A possible continuation of this project could involve the synthesis and the reduction of a mono-ligand uranium salfen species in order to determine if the hypotethical neutral [U(bis-salfen)] complex is isolable and shows redox reactivity.

We also validated the use of the tridentate ^{Me}naphtquinolen ligand to promote multi-electron redox processes at U(IV). The redox-activity of this parlicular ligand is similar to that of salophen and

involves reversible C-C bond formation and cleavage. ^{Me}naphtquinolen bis-ligand compounds possesses free coordination sites allowing for substrate binding, a feature not possible with Na_2[U(bis-salophen)] **7**, and do not undergo ligand redistribution, contrary to [U_2(cyclo-salophen)$(THF)_4$] **4-THF**. This might result in a better control of reactivity and allow the introduction of functionalities at the uranium center. Finally, electrochemical studies suggest that the uranium centre in [U(μ-bis-^{Me}naphtquinolen)]$_2$ **15** can be reduced to U(III). Future work might be directed to isolate this species and study its reducing properties.

Given the extensive catalogue of Schiff base ligands available, numerous opportunities are therefore offered to tune the properties of these systems.

This work validates the proof of concept, and future studies should be directed to determine the full scope of reactivity of these molecules. The ligand-centered multi-electron redox reactions should offer new modes of reactivity for f-element chemistry and coul be utilized for small molecules activation. This phenomenon could also be exploited in order to achieve uranium- or lanthanide-based responsible molecular devices.[392]

Finally, a rational synthetic pathway to access bimetallic species featuring close metal-metal separation has also been developped. This versatile synthetic strategy has been successfully utilized to synthesize homobimetallic uranium species and preliminary studies show that it allows the isolation of uranium-containing heterobimetallic complexes under controlled conditions. This paves the way for further development aiming at the isolation and the study of the physicochemical and reactivity properties of a family of 3d-5f systems

CHAPTER III
Design and Reactivity of Trivalent Uranium Complexes Supported by Siloxy Ligands

III.1 Introduction

The challenge in f-elements chemistry is to place the metals in chemical environments which allow exploitation of their chemical uniqueness. Thus particular attention should be addressed to the choice of the supporting ligands. As stated in introduction, our objective is to design a coordinating environment that should enhance the reductive behavior of low-valent f elements. To this aim, the ligand must stabilize low-valent metallic species, but the degree of stabilization must be limited to maintain the high reactivity of the complex. Moreover, the ligand's geometry should be such that multimetallic reductive pathways remain accessible as most of the time each low-valent metal ion contributes one electron to the overall process.[393]

In view of the radial extension and ionic character of the f-elements, the cyclopentadienyls spectator ligands have been largely used for the stabilization of organolanthanides and organoactinides derivatives because they meet the electronic and steric requirements necessary to form stable and isolable complexes. As a result, for a long time, most studies in this area have involved organometallic complexes. Although U(III) complexes of oxygen-donor and nitrogen-donor ligands exhibit remarkable structures and unique reactivities, such systems remain limited to a very few examples.[67] Such hard and anionic donor ligands are particularly promising because low-valent f-elements easily bind them and because alkoxide and amide ligands provide electron-rich environments. Thus, combining these appealing electronic features with appropriate steric characteristics to provide kinetic stabilization may lead to powerful reducing agents.

In this context, we decided to use the bulky tris(tert-butoxy)siloxide $[OSi(O^tBu)_3]^-$ as a supporting ligand for uranium chemistry. This choice has been driven by the following observations.

Electronic features

Siloxides, like alkoxides and aryloxides, are pseudo-isolobal with oxos, imides, and cyclopentadienyl ligands in that they can all act as 1σ-, 2π- donors (***Figure III.1***).[394-396] As hard electronegative ligands, the metal-oxygen σ-bonding with electropositive metals is extremely strong primarily for electrostatic reasons. The contribution of π- covalent interaction to the bonding depends on the nature of the metal, its oxidation state and its coordination number, and will be for instance increasing to better accommodate an electron-deficient metal center.

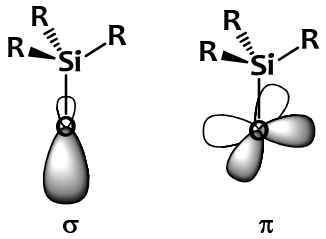

Figure III.1. Donor orbitals of the siloxy moiety.

Siloxides and alkoxides ligands are believed to electronically influence the metal center in a close manner, although the less polar Si-O bond and the small π-accepting capability of silicon is thought to slightly attenuate the donation to the metal.[395] Regardless, siloxides are generally considered as more robust than alkoxydes as the heterolytic C-O bond cleavage affording metal oxo species, which is a common limitation for accessing alcoxy complexes of electropositive metals, is unlikely to occur for a Si-O bond.

Finally, the siloxy ligand does not possess readily available redox states and should behave as an innocent spectator ligand. Therefore the $OSi(O^tBu)_3$ ligand is well-suited to promote chemistry at the low-valent metal center.

Steric aspects

The introduction of the hindered O^tBu substituents at silicon allows the tris(tert-butoxy)siloxide to act as bulky ancillary ligand (***Figure III.2***). This should in principle result in the formation of low-coordinate reactive metal centers in particular when combined with low oxidation metal centers. The importance of steric factors in determining the reactivity of metal complexes is well recognized. This is particularly critical for uranium, as compared to 3d metals, this large cation affords, as a natural consequence, compounds with high coordination numbers. Hence one can understand why the cyclopentadienyl-related ligands are popular in non-aqueous actinides chemistry.

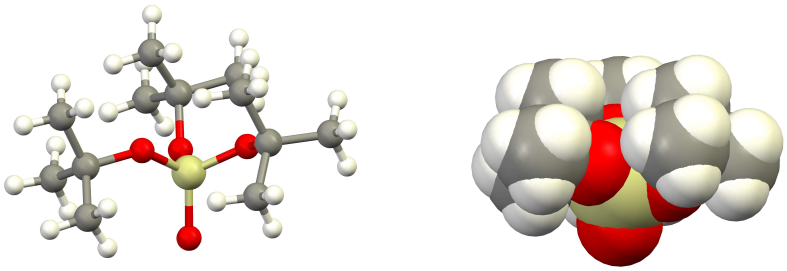

Figure III.2. Ball and stick (left) and spacefill (right) representations of $[OSi(O^tBu)_3]^-$.

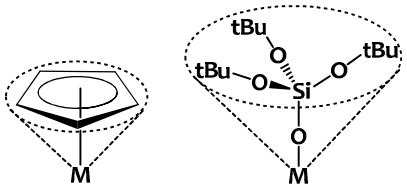

Figure III.3. Geometric modelling of the spatial distribution of ligands by a conical volume.

The Tolman's cone angle[397] is an elegant concept by its simplicity which has been conveniently used to rationalize and discuss the steric effects in organometallic compounds. Based on the analysis of 20 ligands coordinated in a monodentate fashion from 9 different crystal structures of uranium complexes presented in the next sections, we were able to estimate the Tolman cone angle[398] for the tris(tert-butoxy)siloxide ligand. The analysis of the crystallographic cone angles gives an average value 124.4°. Graphical analysis of the distribution of the cone angles as histogram is shown on ***Figure III.4***, and reveals that values are spread over a large range (115.8 ° to 136.6°). The 5° standard deviation from the mean value is usual.[398] Indeed, the cone angle can strongly vary depending on the coordination number of the metal and on the presence of other rigid or bulky ligands in the coordination sphere among other aspects. The cone angle of $[OSi(O^tBu)_3]^-$ is average, and slightly smaller than that of the cyclopentadienyl ligand which has been estimated at roughly 130°.[395]

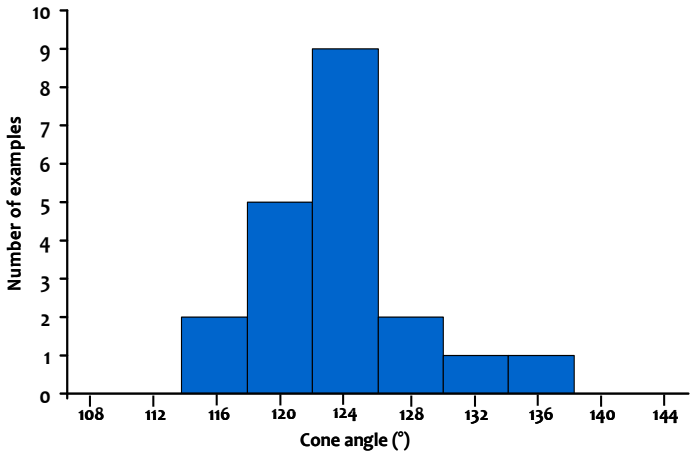

Figure III.4. Distribution of the Tolman cone angles of $[OSi(O^tBu)_3]^-$.

An alternate model has been proposed by Cavallo and coworkers to calculate the "percent buried volume" corresponding to the percent of a spherical volume occupied by a ligand.[399] Calculations are ealisly performed using a software available online,[400] and has been useful to estimate the steric bulk of phosphine, N-heterocyclic carbenes, amide, aryloxide and siloxide ligands.[161, 401] The calculations were performed using the metrical parameters of the tris(tert-butoxy)siloxide ligand from the U(IV) compound $[U(OSi(O^tBu)_3)_4]$ (*vide infra*). The calculated buried volume %Vbur = 18.2% (SambVca software parameters : sphere radius 3.5 Å, U-O distance 2.1 Å) is significantly smaller than the values obtained for the $N(SiMe_3)_3$ or the $O(2,6\text{-}^tBu\text{-}C_6H_3)$ ligands (%Vbur = 25.5 % and 25.4 % respectively), and also smaller than the value of $OSi(Mes)_3$ (%Vbur = 22.3 %).[161] However, these analyses are limited to the monodentate coordination mode of the ligand, and higher steric pressure will occur with a bidentate coordinated ligand (*vide infra*).

Besides steric aspects, the other great advantage of the O^tBu groups is to confer high solubility of the putative complexes in hydrocarbon solvents. This should in principle help the isolation of low-coordinate complexes and facilitate their handling. Moreover, several reports describe fragmentation of oxygenated solvents (Et_2O, THF, DME) in attempts to isolate low-valent uranium complexes. The possibility of replacing these coordinating solvents by the more resistant aliphatic apolar solvents (pentane, hexane) is a considerable advantage.

Another interest resides in the commercial availability of this ligands and its high tuneability that can be provided by replacing the O^tBu groups by a variety of substituents. Consequently, steric factors could be tuned to direct the synthesis of a variety of complexes by favoring monomers formation versus oligomers for instance.

Coordination chemistry

Apart from their steric role, the O^tBu substituents at silicon can act as coordinating fragments. Hence one of the particular feature of the tris(tert-butoxy)siloxide is its ability to adopt mono- or bidentate binding modes as well as its capability to act as a bridging ligand that can lead to a variety of oligomeric structures. The most common coordination modes observed for this ligand are represented in ***Figure III.5***.

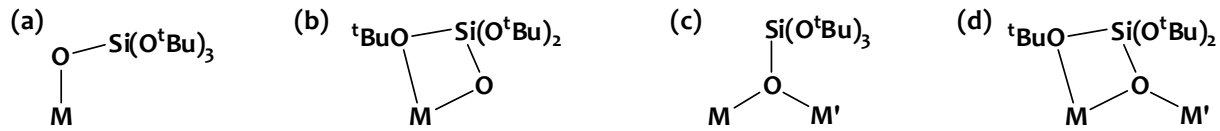

Figure III.5. Common coordination modes for the $[OSi(O^tBu)_3]^-$ ligand : (a) monodentate (terminal mode) ; (b) bidentate ; (c) monodentate bridging ; (d) bidentate bridging.

When required, as in the case of an electron-deficient center, the ligand coordination number can be increased to accommodate the metal. Conversely, the coordination number decreases to accommodate an incoming substrate. In this respect, this versatile ligand can adapt its coordination to its environment in order to meet the electronic and steric requirements of the metal centers. This property often leads to a better stabilization of reaction intermediates and as a consequence could be exploited in homogeneous catalysis. Besides, it is anticipated that the capability of the tris(tert-butoxy)siloxide to act as a bridging ligand[396, 402] should help for isolating polymetallic species. Polymetallic low-valent uranium systems are particularly desirable as they might allow multimetallic reductive pathways from a single molecule. This also offers the possibility to accommodate Lewis acidic metal centers in the direct proximity of uranium that might influence on the reactivity of the complexes. Furthermore, access to polymetallic species creates the opportunity for metal-metal interactions which could result in appealing magnetic properties.

All these characteristics are particularly attractive and accordingly, siloxide ligands have been successfully used in a variety of d-block complexes, leading notably to the isolation of active homogeneous and supported catalysts.[395, 396, 402-411]

Additionally, the development of well-defined uranium complexes containing siloxy ligands is particularly relevant for solid-state chemistry. Indeed, the team of T. D. Tilley has shown that transition metal siloxide complexes were effective soluble molecular precursors for the synthesis of silicate materials with homogeneous distribution of metal in the silica (***Figure III.6***).[412-414] Molecular uranium siloxy precursors could be used to access new original uranium silicate materials under mild and controlled conditions. The structure and chemistry of uranium silicates are notably important in spent nuclear fuel storage.[415, 416] Besides, siloxide coordination compounds can also be regarded as models for metal complexes immobilized on silica surfaces.

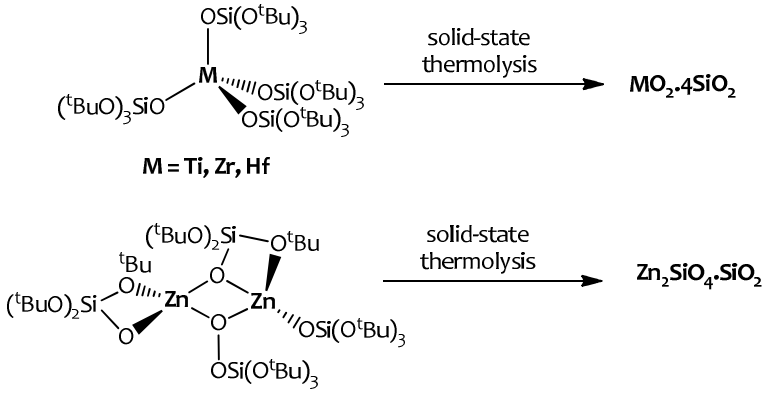

Figure III.6. Examples of molecular tris(tert-butoxy)siloxide transition metal complexes used as precursors for the synthesis of homogeneous silica materials.

These appealing features are promising for developing a coordinating platform for enhancing the redox chemistry of uranium and may thus provide an attractive alternative for the synthesis of highly reactive homoleptic U(III) complexes. Surprisingly, the use of siloxide ligands has remained extremely rare in uranium chemistry.[157, 161, 345, 406, 417, 418] The study of the coordination chemistry of uranium with tris(tert-butoxy)siloxides is presented in the next section. Preliminary investigations were conducted in the laboratory by Victor Mougel and this study was performed in continuation of his work.

III.2 Isolation of New Mononuclear and Polynuclear Low-valent Uranium Complexes Supported by Siloxy Ligands

III.2.1 Synthesis of $[U(OSi(O^tBu)_3)_2(\mu\text{-}OSi(O^tBu)_3)]_2$

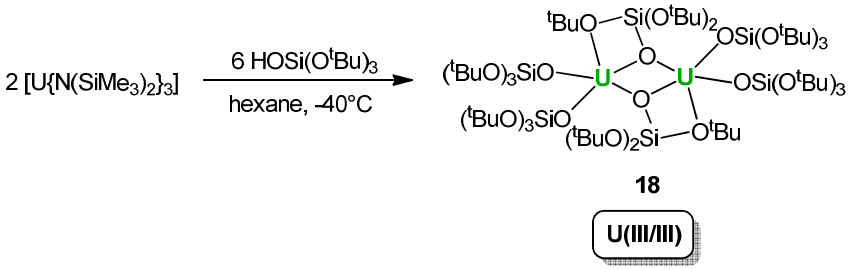

Scheme III.1. Synthesis of the U(III)/U(III) $[U(OSi(O^tBu)_3)_2(\mu\text{-}OSi(O^tBu)_3)]_2$ complex **18**.

The reaction of $[U\{N(SiMe_3)_2\}_3]$[78, 91] with 3 equivalents of tris-(tert-butoxy)silanol $HOSi(O^tBu)_3$ in hexane at -40°C results in the uranium(III) complex $[U(OSi(O^tBu)_3)_2(\mu\text{-}OSi(O^tBu)_3)]_2$ **18**, as a brown crystalline solid in 82% yield (***Scheme III.1***). This solid is exceedingly oxygen and moisture sensitive. Additionally, while this complex is stable in the solid state at -40°C for several weeks, it decomposes rapidly at room temperature in both the solid-state or in solution (see section III.2.2).

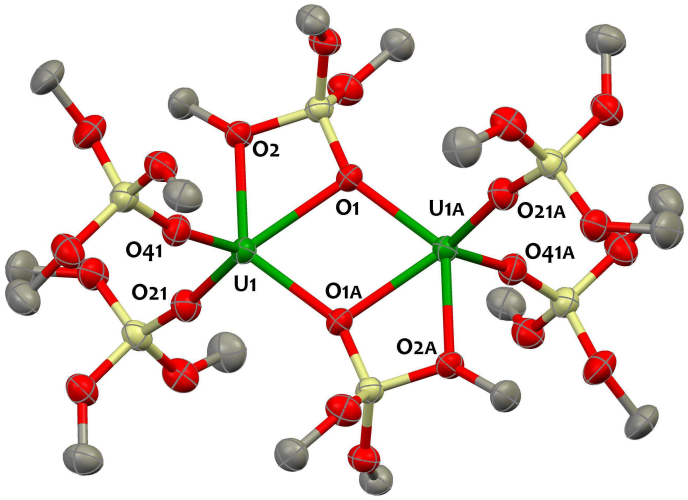

Figure III.7. Solid-state molecular structure of $[U(OSi(O^tBu)_3)_2(\mu\text{-}OSi(O^tBu)_3)]_2$ **18** crystallized from hexane. Hydrogen atoms and methyl groups (except for coordinated ^tBuO) are omitted for clarity. Uranium (green), oxygen (red), silicon (yellow) and carbon (green) atoms are represented with 50% probability ellipsoids. Selected bond distances [Å] U1-O41 2.190(3), U1-O21 2.197(4), U1-O1' 1 2.396(3), U1-O2 2.539(3), U1-O1 2.549(3).

X-ray diffraction analysis of single crystals of **18** revealed a centrosymmetric dinuclear structure in which the two uranium centers are bridged by two siloxide ligands (***Figure III.7***). Both uranium ions are coordinated in a distorted pentagonal bipyramid geometry by six oxygens from two terminal siloxide groups, two bridging bidentate siloxide ligands and from a neutral tert-butoxy group of a bridging siloxide ligand. The U-U distance is 3.9862(2) Å. The measured U-O bond lengths of the terminal siloxide (mean U-O = 2.193(4) Å) lie in the range of typical U-O distances in uranium(III) alkoxide complexes.[93,92] Longer U-O distances are observed, as expected for the bridging siloxides (U1-O1 = 2.396(3) Å and U1-O1'= 2.549(3) Å) and for the neutral tert-butoxy group (2.540(2) Å). These distances are similar to those observed for bridging siloxide in the rare reported examples of siloxide complexes of Ln(III).[419, 420] In the isostructural Sm(III) complex the Sm-O distances of the bridging siloxides are longer and those of the neutral tert-butoxy group shorter. This is probably simply the result of the larger size of the Sm(III) ion resulting in longer distances for the bridging siloxides and in a stronger interaction with the neutral tert-butoxide.

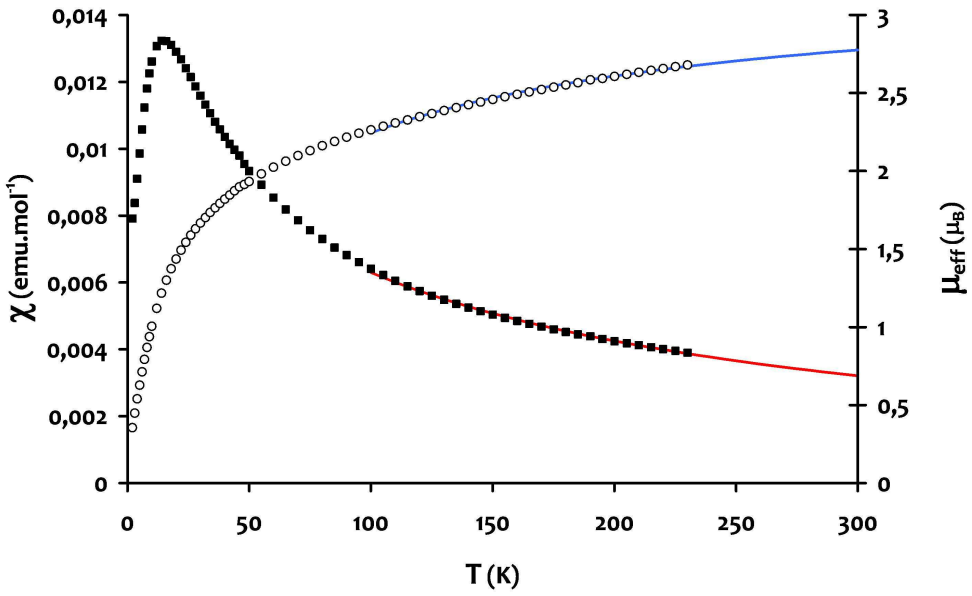

Figure III.8. Temperature-dependant SQUID magnetization data (0.5 T) for complex **18** (data per U center) plotted as χ (open circles) and μ_{eff} (black circles) versus temperature. Curie-Weiss fit : red and blue curves. Data were corrected for diamagnetism and reproducibility was checked on independently synthesized samples.

Temperature-dependent magnetic data were collected for **18** in the range 2-230 K (***Figure III.8***). Data were not collected above 230 K in order avoid the thermal decomposition of **18** (see section III.2.2). Above 100 K, compound **18** presents Curie-Weiss behavior ($\chi = C/(T-T_c)$; C = 1.31 emu.K.mol^{-1}; T_c = -108 K), as expressed by the linearity of the 1/χ curve (see appendix). The room temperature effective moment (2.78 μ_B ; value for one uranium) extrapolated from these data for **18** falls in the range of the other U(III) coordination compounds.[176, 340, 421-423] This value is lower than the theoretical value (3.62 μ_B) calculated for a $5f^3$ ion with a full spin-orbit coupling as commonly observed in trivalent uranium

complexes due to the crystal-field splitting of the Russel-Saunders $^4I_{9/2}$ ground term. The magnetic susceptibility temperature dependence below 100 K suggests the presence of an antiferromagnetic coupling of the U(III) cations with a clear maximum in the plot of χ versus T at 16 K. The presence of magnetic communication between two U(III) complexes has rarely been proposed[129, 424] and to the best of our knowledge unambiguous magnetic coupling has never been reported for U(III) molecular compounds.

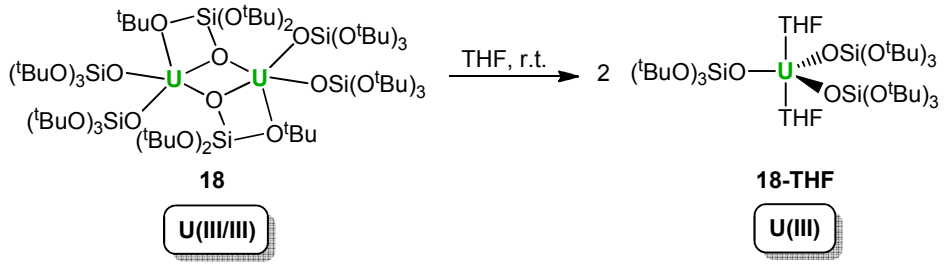

Scheme III.2. Dimeric U(III)/U(III) $[U(OSi(O^tBu)_3)_2(\mu\text{-}OSi(O^tBu)_3)]_2$ **18** complex dissociates in THF solution to yield the monommeric THF-adduct $[U(OSi(O^tBu)_3)_3(THF)_2]$ **18-THF**.

The dinuclear structure of **18** is disrupted in coordinating solvents to afford the mononuclear trivalent uranium complex $[U(OSi(O^tBu)_3)_3(THF)_2]$, **18-THF** (***Scheme III.2***), in agreement with elemental analysis and ^{1}H NMR spectroscopy. Indeed, while the ^{1}H NMR spectrum recorded for **18** in deuterated hexane shows two shifted resonances integrating respectively for 508 and 54 protons, the ^{1}H NMR spectrum of **18** in THF displays a single signal for the siloxide groups at 2.64 ppm. Such strong variation in the paramagnetic NMR data indicates a change of the structure of the complex in solution. Additionally, single crystals of **18-THF** were obtained from THF solution of **18**. Unfortunately, the quality of the X-ray diffraction studies do not allow the discussion of the metrical parameters, but they allow to confirm the presence of a mononuclear U(III) siloxide complex (***Figure III.9***).

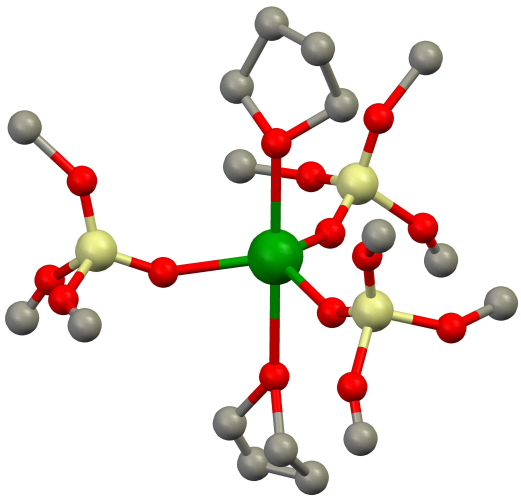

Figure III.9. Mercury diagram for $[U(OSi(O^tBu)_3)_3(THF)_2)]$, **18-THF**, crystallized from a THF/hexane mixture; Hydrogen atoms and methyl groups are omitted for clarity. Uranium (green), silicon (yellow), oxygen (red) and carbon (grey) atoms are represented with isotropic spheres.

In spite of the highly reducing character of U(III) in such an electron donor environment, complex **18** is sufficiently stable in organic solvents to investigate its reactivity, which will be presented in sections III.3, III.4 and III.5. However, this compound is extremely reactive and spontaneously decomposes at room temperature. This is central topic of the next section.

III.2.2 Decomposition of U(III) alkoxy(siloxy) complexes : a route to new polymetallic complexes of low-valent uranium

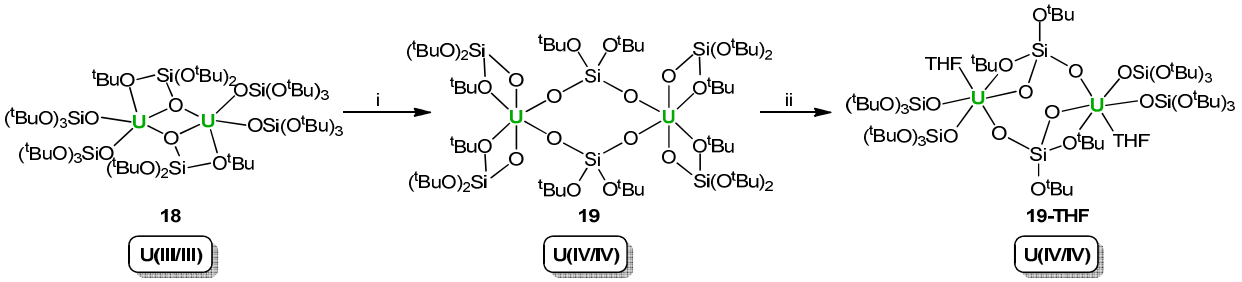

Scheme III.3. Decomposition of the U(III)/U(III) $[U(OSi(O^tBu)_3)_2(\mu\text{-}OSi(O^tBu)_3)]_2$ complex **18** i) solid state, r.t. 7 days or 80°C 30 min ; ii) THF, r.t.

The dinuclear U(III)-U(III) complex $[U(OSi(O^tBu)_3)_2(\mu\text{-}OSi(O^tBu)_3)]_2$ **18** is stable in the solid state for several weeks when stored at -40°C. However, this extremely reactive derivative spontaneously decomposes at room temperature both in the solid state and in solution. The brown/orange powder of **18** fades slowly to pale brown in 3 days at r.t., and then to pale blue/green. The process is even faster (less than 30 minutes) when the solid is heated to 80°C. The resulting product is highly soluble in hexane and can be recrystallized upon cooling a saturated solution to -40°C, to yield turquoise crystals of $[U(OSi(O^tBu)_3)_2(\mu\text{-}O_2Si(O^tBu)_2)]_2$ **19** (***Scheme III.3***). The formation of **19** from **18** involves oxidative C-O cleavage the loss of a ^{t}Bu group from a $OSi(O^tBu)_3$ ligand at each uranium center. This is probably driven by the hardness of the uranium ion and by the high stability of the final U(IV) complex. The centrosymetric X-ray crystal structure represented in ***Figure III.10*** consists of two uranium cations coordinated by two bidentate silanolate $OSi(O^tBu)_3$ ligands, and two bridging silandiolate $O_2Si(O^tBu)_2$ ligands. The U-O^- bond distance (2.17(6) Å) is shorter than in the trivalent complex **18** in agreement with a higher oxidation state for the metals in **19**.

Two resonances integrating for 108 and 36 protons attributed to the $OSi(O^tBu)_3$ and $O_2Si(O^tBu)_2$ ligands respectively are observed in the ^{1}H NMR spectrum of **19** in deuterated hexane. The ESI-MS spectrum of **19** suggest that the dimeric structure is retained both in toluene and THF solution. This contrasts with what found for **18**, which forms a mononuclear THF solvate in THF solution. The

presence of the dianionic bridging $O_2Si(O^tBu)_2$ ligands holding tightly the two uranium centers results in the isolation of dimeric species also from coordinating solvents.

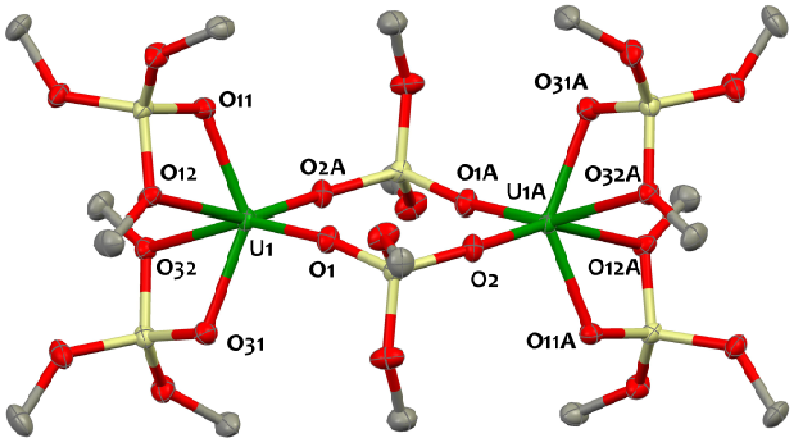

Figure III.10. Solid-state molecular structure of $[U(OSi(O^tBu)_3)_2(\mu\text{-}O_2Si(O^tBu)_2)]_2$ **19**, crystallized from a saturated hexane solution ; probability 50%. Hydrogen atoms, methyl groups and solvent molecules are omitted for clarity. Uranium (green), silicon (yellow), oxygen (red) and carbon (grey) atoms are represented with 50% probability ellipsoids. Selected bond distances [Å]: U1-O1 2.1091(18), U1-O2A 2.1249(17), U1-O11 2.2178(18), U1-O31 2.2259(19), U1-O^{tBu}_{avg} 2.621(3), A = -x+1,-y+2,-z+1.

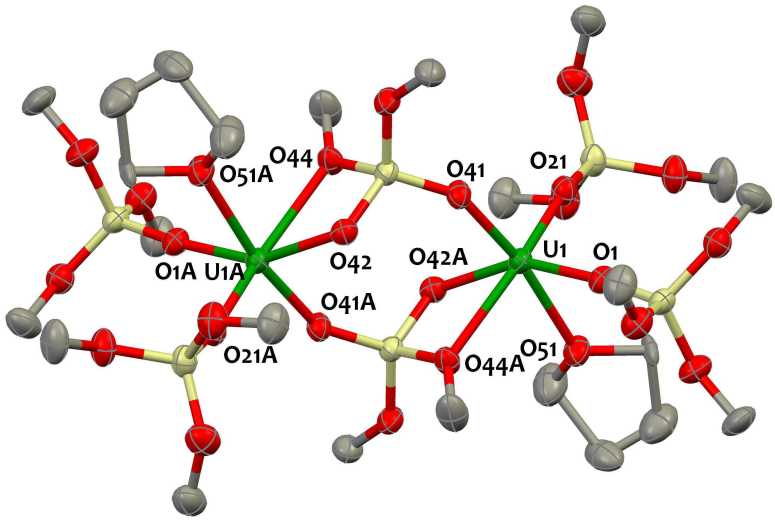

Figure III.11. Solid-state molecular structure of $[U(OSi(O^tBu)_3)_2(\mu\text{-}O_2Si(O^tBu)_2)(THF)]_2$ **19-THF**, crystallized from a saturated hexane solution in presence of THF. Hydrogen atoms and methyl groups are omitted for clarity. Uranium (green), silicon (yellow), oxygen (red) and carbon (grey) atoms are represented with 50% probability ellipsoids. Selected bond distances [Å]: U1-O21 2.126(4), U1-O1 2.166(4), U1-O41 2.206(3), U1-O42 2.207(4), U1-O51 2.513(4), U1-O44 2.551(4), A = -x+3/2,-y+3/2,-z+1.

Notably, the solid-state structure of the THF solvate **19-THF** obtained by X-ray diffraction on single crystals grown from hexane solution of **19** in presence of THF shows the occurrence of a centrosymmetric dimer (***Figure III.11***). Each U(IV) cation in **19-THF** is hexacoordinated by two $OSi(O^tBu)_3$ ligands in a terminal monodentate coordination mode, one THF molecule and two $O_2Si(O^tBu)_2$ ligands that act as tridentate bridging ligands. The comparison of the structures of **19** and **19-THF** evidences the flexibility of the weakly coordinating O^tBu moieties which can adjust to

stabilize the final compounds in both coordinating and non-coordinating solvents. Two U-O^{t}Bu bonds with the siloxy ligands are disrupted for each uranium center in **19-THF** compared to **19** to accommodate in the metal coordination sphere a molecule of THF solvent acting as a stronger donor ligand. In the coordination environment of complex **19-THF** the $O_2Si(O^tBu)_2$ ligands adopt a tridentate bridging mode, instead of the bidentate bridging mode adopted in **19**, resulting in the same uranium coordination number in **19** and **19-THF**.

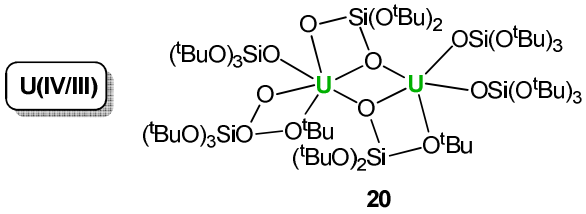

20

Figure III.12. Representation of complex **20**.

Interestingly, pale brown single crystals of the half-decomposed mixed-valent U(III)/U(IV) complex $[U_2(\mu\text{-}O_2Si(O^tBu)_2(\mu\text{-}OSi(O^tBu)_3(OSi(O^tBu)_3)_4]$ **20** (***Figure III.12***) were isolated when the decomposition reaction was stopped before completion. This complex could not be isolated analytically pure as the samples were contaminated by **18** and **19**, and its separation from the fully decomposed complex by recrystallization was unsuccessful as both species exhibit similar solubility.

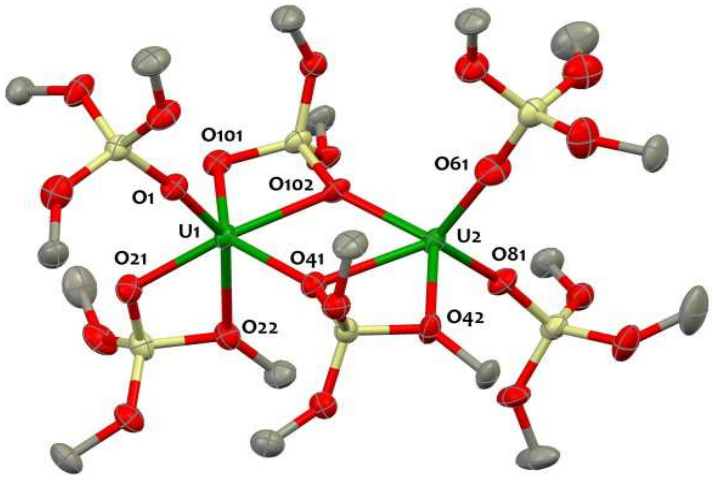

Figure III.13. Solid-state molecular structure of $[U_2(\mu\text{-}O_2Si(O^tBu)_2(\mu\text{-}OSi(O^tBu)_3(OSi(O^tBu)_3)_4]$ **20**. Hydrogen atoms, methyl groups and solvent molecules are omitted for clarity. Uranium (green), silicon (yellow), oxygen (red) and carbon (grey) atoms are represented with 50% probability ellipsoids. Selected bond distances [Å]: U1-O1 2.124(5), U1-O21 2.200(5), U1-O101 2.158(5), U1-O102 2.461(5), U1-O41 2.290(5), U1-O22 2.664(5), U2-O61 2.148(5), U2-O81 2.197(5), U2-O41 2.703(5), U2-O102 2.330(5), U2-O42 2.505(5), U1···U2 3.9944(2).

The molecular structure of **20** is illustrated in ***Figure III.13***, together with selected bond lengths. The dinuclear structure features two uranium centers coordinated by five $OSi(O^tBu)_3$ monoanionic ligands and one $O_2Si(O^tBu)_2$ dianionic ligand that derives from the original ligand which has lost one

^{t}Bu group. The two uranium atoms in **20** are non-equivalent. U1 is hexacoordinated by six oxygens from one terminal monodentate, one bidentate and one bidentate-bridging monoanionic $OSi(O^{t}Bu)_3$ ligands, and by one bidentate-bridging $O_2Si(O^{t}Bu)_2$ dianionic ligand and U2 is pentacoordinated by six oxygens from two terminal monodentate and one bidentate-bridging monoanionic $OSi(O^{t}Bu)_3$ ligands, and by one bidentate-bridging $O_2Si(O^{t}Bu)_2$ dianionic ligand. The U···U distance (3.9944(2) Å) is of the same range as that in **18** (3.9862(2) Å).

Complex **20** is intermediate between the fully reduced U(III)/U(III) **18** and the fully oxidized U(IV)/U(IV) **19** complexes and provides a rare example of a mixed-valent U(III)-U(IV) complex.[424, 425]

The analysis of the volatile components in the final decomposition reaction mixture by ^{1}H NMR and ^{13}C NMR spectroscopy revealed the presence of isobutene as the major volatile decomposition product of the reaction together with resonances corresponding to alkane products. Elimination of isobutene from tert-butoxyde has been recently reported for U(VI) alkoxy derivatives.[59] A few cases of activation and reduction of ethers by trivalent uranium to yield oxo complexes are also documented.[83, 84, 157] The elimination of isobutene from d-block metals complexes containing $OSi(O^{t}Bu)_3$ ligands has been reported in the thermolysis of siloxy complexes leading to metal silicates and several pathways have been proposed including heterolytic or homolytic cleavage and γ-H activation.[409, 410, 413, 414, 426-428] However, the mechanism of the thermolysis of d-block metal siloxides has not been fully elucidated and decomposition intermediates have not to the best of our knowledge been isolated.

In order to get some more insights into the reaction mechanism, DFT studies (B3PW91) were carried out by the group of Pr. Laurent Maron. I have decided to present these results as they provide insights into the mechanism of the transformation.

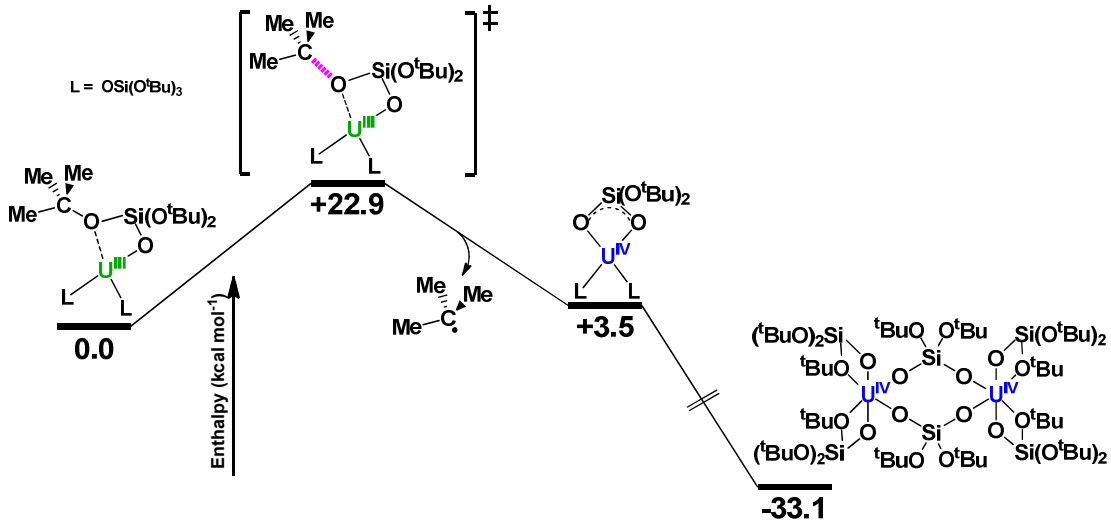

Figure III.14. Enthalpy energy computed profile for the degradation of complex **18**.

According to the experimental observations where the degradation occurs at both uranium centers, the calculations were conducted on a monomeric form of the complex. Three different decomposition pathways were considered and among all three, the ^{t}Bu radical dissociation has been found to be the energtically most favourable one (***Figure III.14*** and see appendix for the other computed profiles). The homolytic cleavage of the O-^{t}Bu bonds occurs with a kinetically accessible barrier (22.9 kcal.mol^{-1}). The formed ^{t}Bu radical can then extract an hydrogen from another ^{t}Bu radical to lead to the formation of a molecule of isobutene and one molecule of isobutane, in line with the experimental observations and lack of H_2 detection. A radical mechanism was also proposed for the diethyl ether cleavage by the trivalent uranium compound $[U(Cp^*)I_2(THF)_3]$ affording the trimetallic oxo species $[\{(U(Cp^*)(\mu^2\text{-}I)_2\}_3(\mu^3\text{-}O)]$.[83]

Preliminary studies of the decomposition of complex **19** at higher temperature show the formation of an insoluble material and of H_2O, $HOSi(O^{t}Bu)_3$ and isobutene similarly to what observed in the decomposition of d-block transition metals. Further studies should be directed to characterize the materials obtained from this decomposition. Low-valent uranium silicates are found in natural occurring minerals[429, 430] and the high temperature synthesis of few U(IV) and U(V) silicates has been reported.[415, 431, 432] The thermolysis of 2 might provides a low temperature route to homogeneous uranium silicates with tailored properties.

III.2.3 Synthesis of a dinuclear heteroleptic U(III)-U(III) siloxy complex

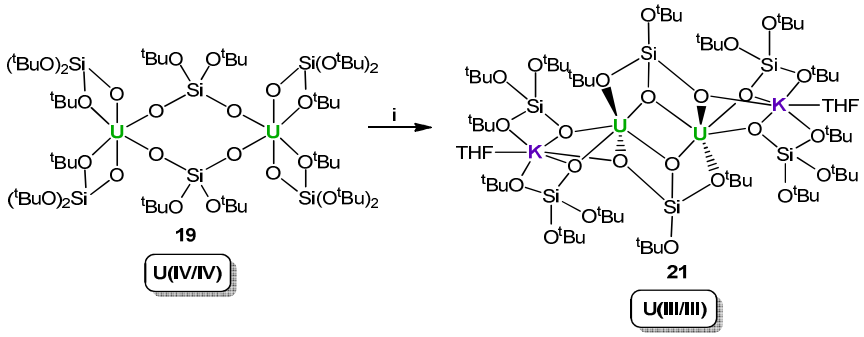

Scheme III.4. Synthesis of the U(III)/U(III) $[K(THF)U(OSi(O^{t}Bu)_3)_2(\mu\text{-}O_2Si(O^{t}Bu)_2)]_2$ complex **21** i) 2.5 KC_8, THF, r.t. 2 hours.

Complex **19** provides an attractive precursor for accessing heteroleptic dinuclear reduced species bearing silonolate and silandiolate ligands. Accordingly, the reduction of **19** was performed in THF using KC_8 as a reducing agent. This afforded the new U(III)-U(III) complex $[K(THF)U(OSi(O^{t}Bu)_3)_2(\mu\text{-}O_2Si(O^{t}Bu)_2)]_2$ **21** in high yield as depicted in ***Scheme III.4***. The ESI-MS spectrum is in line with the presence of a dinuclear species in solution. Consistent with the strong color change observed upon

reduction of **19** (pale blue) into **21** (dark brown), the UV-visible absorption spectrum for **21** displayed in ***Figure III.15*** exhibits a strong transition centered at 436 nm (ε = 2360 $L.cm^{-1}.mol^{-1}$). This band is very similar to that observed in the UV-visible spectrum of **18** and is characteristic of Laporte-allowed f→d transitions observed in U(III) complexes.[85, 127, 347, 433]

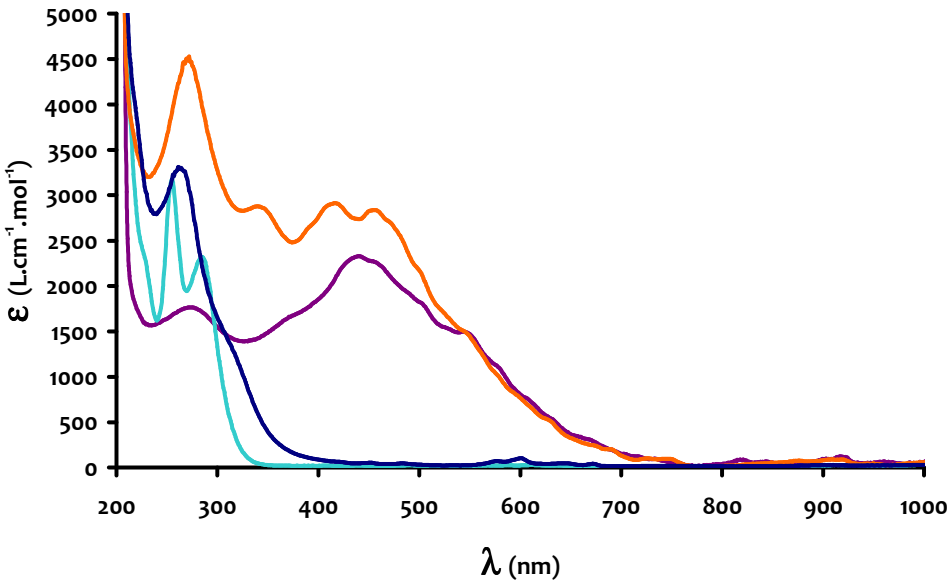

Figure III.15. UV-visible absorption spectra of solutions of **18** (orange line), **19-THF** (dark blue line) and **21** (purple line) in THF and **19** (pale blue line) in hexane.

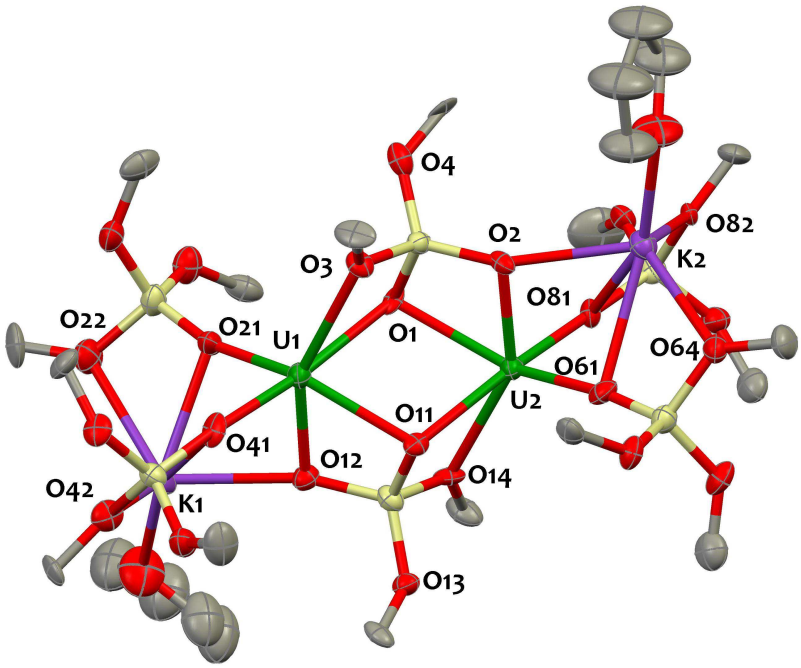

Figure III.16. Solid-state molecular structure of $[K(THF)U(OSi(O^tBu)_3)_2(\mu\text{-}O_2Si(O^tBu)_2)]_2$ **21**, crystallized from a saturated THF/DIPE solution. Hydrogen atoms, methyl groups and solvent molecules are omitted for clarity. Uranium (green), potassium (purple), silicon (yellow), oxygen (red) and carbon (grey) atoms are represented with 50% probability ellipsoids. Selected bond distances [Å]: U1-O21 2.281(8), U1-O41 2.284(9), U1-O(2 2.373(9), U1-O1 2.425(9), U1-O11 2.489(8), U(1)-O(3) 2.742(10), U2-O61 2.257(9), U2-O81 2.275(9), U2-O2 2.364(8), U2-O11 2.451(8), U2-O1 2.507(8), U2-O14 2.755(10), U1···U2 3.9619(9).

Single crystals suitable for X-ray diffraction were grown upon cooling to -40°C a saturated THF:DIPE solution of **21.** The solid-state structure (***Figure III.16***) shows the presence of a dimeric complex where two $O_2Si(O^tBu)_2$ are bridging in a $\eta^2:\eta^2$ fashion the two uranium cations in close proximity (U···U separation = 3.9619(9) Å). The coordination sphere of each uranium is completed to 6 through the coordination of two $OSi(O^tBu)_3$ ligands. Both potassium cations are held in the structure through their coordination to the siloxy ligands

Complex **21** is the first example of a U(III) complex containing both siloxide and silandiolate ligands whose dinuclear structure is maintained in THF, and provides a new precursor for reactivity studies. In an attempt to form a putative mixed-valent U(III)-U(IV) complex, the reduction of **19** with a single equivalent of reducing agent was investigated. However, the ^{1}H NMR analysis of the crude mixture showed only the presence of the resonances of **19** and **21**.

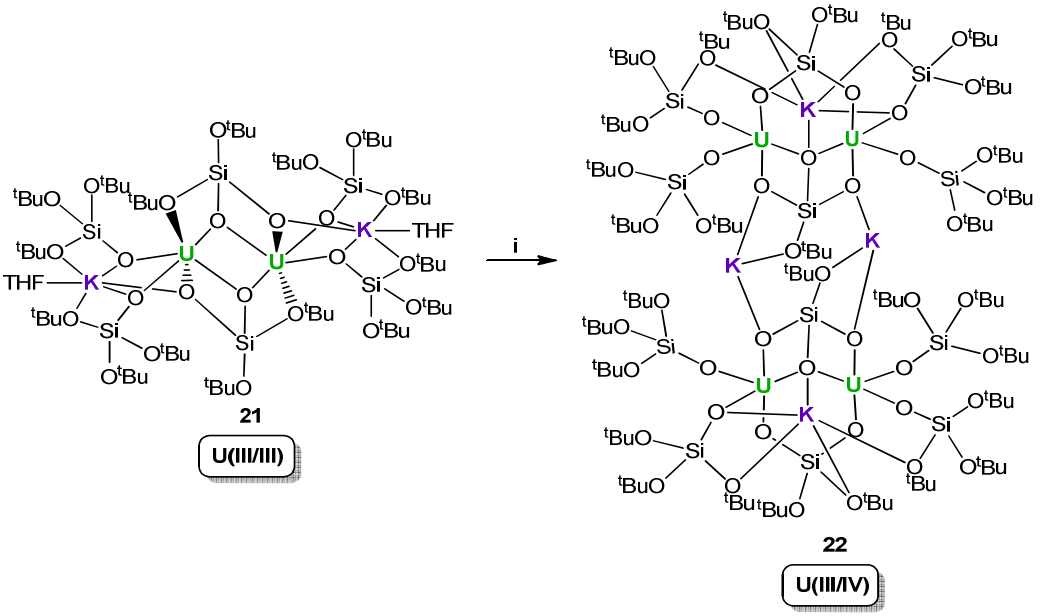

Scheme III.5. Decomposition of the U(III)/U(III) $[K(THF)U(OSi(O^tBu)_3)_2(\mu\text{-}O_2Si(O^tBu)_2)]_2$ complex **21** i) solid-state, 80°C, 2 hours.

Similarly to **18**, the U(III)-U(III) complex **21** is unstable at room temperature, and decomposes in THF solution over a period of 1 week. Decomposition also occurs in the solid-state, and purple-brown sample of **21** affords a green solid when heated to 80°C within 2 hours. The solid can be recrystallized from hexane to yield a new tetranuclear complex $[K_2U_2(OSi(O^tBu)_3)_4(O_2Si(O^tBu)_2)(O_3Si(O^tBu))]_2$ **22** which results from the elimination of a ^{t}Bu group of a bridging $O_2SiO^tBu_2$ ligand in **21 (*Scheme III.5*)**.

The solid-state structure of **22** is shown on ***Figure III.17***. The centrosymmetric structure consists of two dinuclear uranium complexes bridged by two potassium cations which are coordinated to the siloxide ligands yielding a tetramer. In each dimeric moiety the two uranium cations are bridged by a trianionic O_3SiO^tBu ligand coordinated in a $\mu\text{-}\eta^2:\eta^2$ fashion and a dianionic $O_2SiO^tBu_2$ ligand

coordinated in a μ-η^1:η^1 fashion to the uraniums. The U···U separation (3.8393(5) Å) is the shortest of all the dinuclear uranium siloxide systems described earlier. The coordination sphere of both uraniums is completed by the coordination of two $O_2SiO^tBu_2$ ligands. Overall, each uranium cation is pentacoordinated by five oxygen atoms in a distorted square pyramid environment with O81, O91, O92 and O41 for U1 and O21, O93, O82 and O91 for U2 defining two square bases linked by the O91 summit, and two terminal silanols O1 and O61 lying in apical positions.

The global entity, composed of four K^+ cations, two trianionic, two dianionic and four monoanionic siloxide ligands indicates a U(III)/U(IV) mixed-valence for complex **22**.

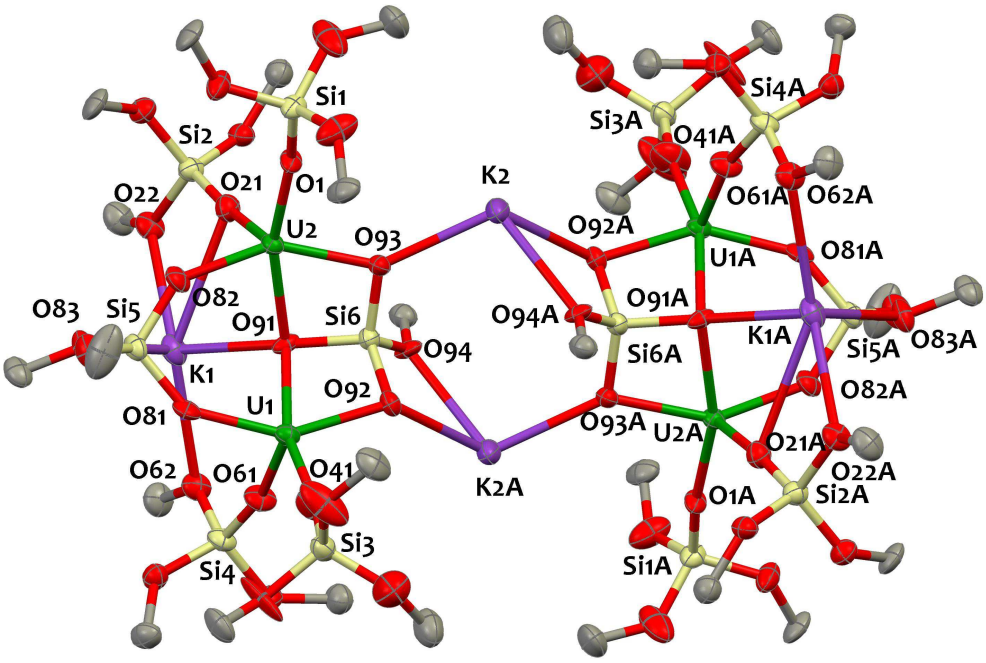

Figure III.17. Solid-state molecular structure of $[K_2U_2(OSi(O^tBu)_3)_4(O_2Si(O^tBu)_2)(O_3Si(O^tBu))]_2$ **22**, crystallized from a saturated hexane solution. Hydrogen atoms and methyl groups are omitted for clarity. Uranium (green), silicon (yellow), oxygen (red) and carbon (grey) atoms are represented with 50% probability ellipsoids. Selected bond distances [Å]: U(1)-O(81) 2.108(6), U(1)-O(41) 2.155(6), U(1)-O(61) 2.186(5), U(1)-O(92) 2.292(5), U(1)-O(91) 2.430(5), U(2)-O(82) 2.130(6), U(2)-O(1) 2.169(5), U(2)-O(21) 2.189(5), U(2)-O(93) 2.294(6), U(2)-O(91) 2.417(5), U(1)-U(2) 3.8392(5), A = -x+1,-y+1,-z+1.

The ^{1}H NMR spectrum for **22** displays two resonances integrating for 54 protons assigned to the ^{t}Bu moieties of the $OSi(O^tBu)_3$ ligands, and three resonances integrating each for 9 protons, and corresponding to the ^{t}Bu moieties of the bridging $O_2Si(O^tBu)_2$ and $O_3Si(O^tBu)$ ligands (***Figure III.18***). This NMR pattern is in agreement with a Cs symmetric structure for **22** in solution. The UV-visible spectrum for **22** (see appendix) displays a series of sharp absorption bands in the visible region of weak intensity, characteristic of f→f transitions, with a maximum at 601 nm (ε = 105 $mol^{-1}.L.cm^{-1}$) in line with the pale blue color of the complex.

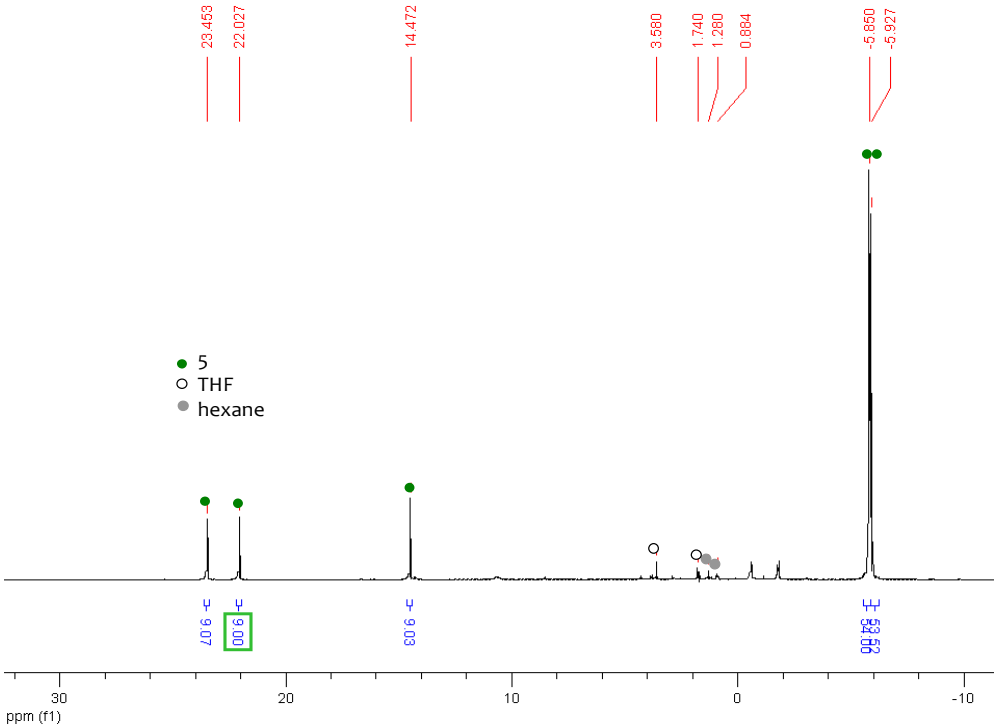

Figure III.18. ^{1}H NMR spectrum (298 K, 200 MHz) in THF-d_8 of **22**.

Complex **22** is the first example of a low valent uranium complex containing a trianionic siloxide and is of interest both for reactivity and magnetic studies.

In summary, the intramolecular C-O bond cleavage presented here extends the range of reactivity which may be achieved with trivalent uranium supported by electro-donating ligands and provides a controlled route to polymetallic heteroleptic complexes that are difficult to obtain from other synthetic ways. These compounds are the first examples of characterized molecular complexes from the decomposition reaction of siloxy complexes. The structure of these molecular decomposition products provide important unprecedented information on the molecular intermediates involved in the formation of metal silicate materials from molecular precursors. The structure of such intermediates is likely to play a key role on the final stoichiometry and homogeneity of ceramic materials. The isolated compounds also provide interesting precursor for accessing new uranium ceramics relevant for spent nuclear fuel storage and catalysis. This also points out the particular care required in the design of ligands able to substantially enhance the reactivity of U(III) but must be sufficiently robust to avoid ligand non-innocent behavior.

III.2.4 Synthesis of mononuclear uranium siloxy complexes

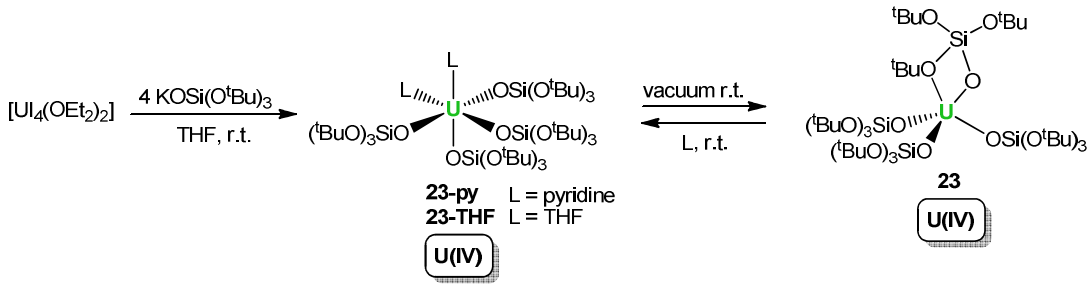

Scheme III.6. Synthesis of U(IV) mononuclear siloxy complexes.

The reaction of $[UI_4(OEt_2)_2]$ with 4 equiv of the potassium salt of tris-tertiobutoxysilanol $KOSi(O^tBu)_3$ in THF affords, after recrystallization from hexane and drying in vacuum, the uranium(IV) homoleptic complex $[U(OSi(O^tBu)_3)_4]$ **23**, as a pale lilac solid in 88% yield (***Scheme III.6***). This compound is fully soluble in polar solvents (THF, pyridine) and in hydrocarbon solvents (hexane, toluene). In non-coordinating solvents, the complex crystallizes as a solvent-free homoleptic complex. The structure, represented in ***Figure III.19***, is disordered across the plane of symmetry of the C2/m space group. In the solid-state, one siloxide ligand adopts a bidentate coordination mode, while the three other siloxide ligands are coordinated in a terminal monodentate fashion. The uranium is thus pentacoordinated by the four siloxide ligands. The U-O^- bond distances (U-O^-_{avg} 2.13(4) Å) are similar to that (U-O^-_{avg} 2.135(4) Å) observed in the previously reported U(IV) homoleptic phenolate complex $[U(OAr)_4]$ (Ar = 2,6-^{t}Bu-C_6H_3).[434]

Single crystals obtained from saturated pyridine solutions of $[U(OSi(O^tBu)_3)_4]$ were analyzed by X-ray diffraction and revealed that this homoleptic structure is not retained in coordinating solvent. The crystal structure of the pyridine adduct $[U(OSi(O^tBu)_3)_4(py)_2]$ **23-py**, set out in ***Figure III.20***, shows that the uranium center is hexacoordinated by four terminal monodentate silanol ligands and two pyridine molecules bound in a *cis* fashion. The uranium atom in **23-py** adopts a distorted octahedral geometry. The *cis*-isomer is most likely favored versus the *trans* one for steric reasons, as indicated by the higher value of the O-U-O average angle (99(2)°) versus the O-U-N one (78.4(4)°). The U-O^- bond distances (U-O^-_{avg} 2.177(12) Å) lie in the usual range of what is observed in other U(IV) alkoxide[93, 345, 434, 435] and siloxide (see above) compounds. Again, the structure of complexes **23** and **23-py** highlight the ability of the $OSi(O^tBu)_3$ ligand to adapt its coordination mode to its environment, allowing the stabilization of the low-coordinate uranium in both coordinating and non coordinating solvents. Upon drying *in vacuo*, the blue powder of $[U(OSi(O^tBu)_3)_4(THF)_2]$ **23-THF** and the green powder of $[U(OSi(O^tBu)_3)_4(py)_2]$ **23-py** is turning lilac, restoring the solvent-free $[U(OSi(O^tBu)_3)_4]$ **23** complex.

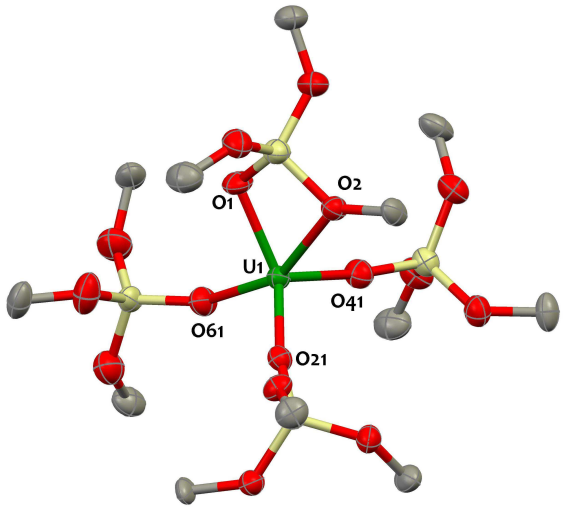

Figure III.19. Solid-state molecular structure of $[U(OSi(O^tBu)_3)_4]$ **23** crystallized from toluene. Disorder, hydrogen atoms and methyl groups are omitted for clarity. Uranium (green), silicon (yellow), oxygen (red) and carbon (grey) atoms are represented with 50% probability ellipsoids. Selected bond distances [Å]: U1-O1 2.193(6), U1-O2 2.551(6), mean U1-$O_{terminal}$ 2.112(9).

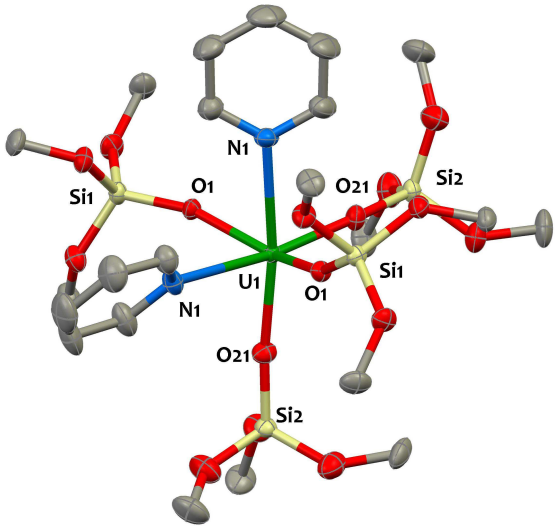

Figure III.20. Solid-state molecular structure of $[U(OSi(O^tBu)_3)_4(py)_2]$ **23-py** crystallized from pyridine. Disorder, hydrogen atoms and methyl groups are omitted for clarity. Uranium (green), silicon (yellow), nitrogen (blue), oxygen (red) and carbon (grey) atoms are represented with 50% probability ellipsoids. Selected bond distances [Å]: U1-O_{avg} 2.177(12), U1-N1 2.630(3).

A single proton resonance is observed in the ^{1}H NMR spectrum of **23** in deuterated hexane or toluene solutions. This implies that on the NMR time scale every ^{t}Bu groups are equivalents in solution in non-coordinating solvents. The ^{1}H NMR spectrum of **23-py** in deuterated pyridine exhibits a chemical exchange process with a coalescence temperature of 313 K. Below 313 K, a slow exchange regime is occurring, resulting in the appearance of two well resolved resonances on the spectrum integrating for 54 protons each. This is in agreement with a *cis*-isomer form for the $[U(OSi(O^tBu)_3)_4(py)_2]$ **23-py** complex in solution (the *trans*- isomer would give a single resonance), in line with the solid-state structure. At high temperatures, a fast-exchange between the two non-equivalent ligand positions

results in an averaging of the signal. Consequently, the ^{1}H NMR spectrum recorded for **23-py** at 353 K displays a single sharp resonance at 3.0 ppm.

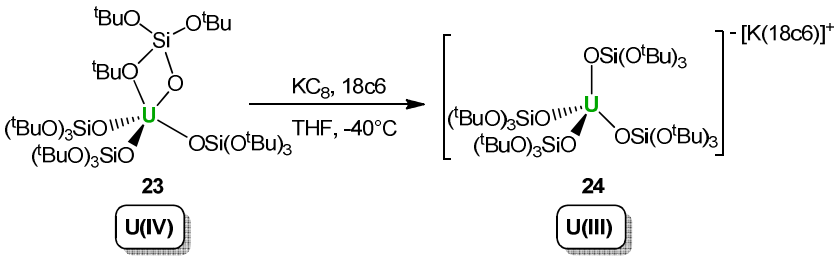

Scheme III.7. Synthesis of [K(18c6)][U(OSi(O^{t}Bu)$_3$)$_4$] **24**.

Complex **23** was successfully reduced by adding potassium graphite into a THF solution of **23** in the presence of 18c6 crown ether. The uranium(III) ate complex [K(18c6)][U(OSi(O^{t}Bu)$_3$)$_4$] **24** was isolated pure in 69% yield (***Scheme III.7***). Complex **24** is slightly soluble in hexane and toluene, and fully soluble in THF. Contrary to the dinuclear neutral complexes **18** and **21**, compound **24** is stable at room temperature, and does not decompose when heated to +80°C for 2 hours.

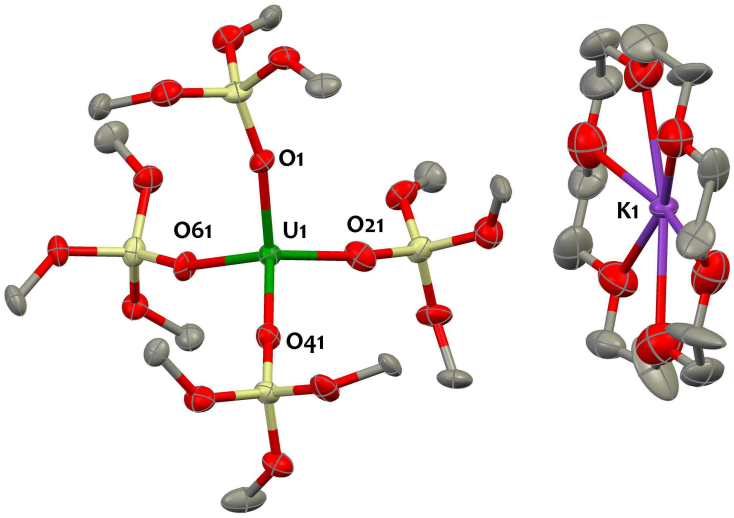

Figure III.21. Solid-state molecular structure of [K(18c6)][U(OSi(O^{t}Bu)$_3$)$_4$] **24** crystallized from toluene. Hydrogen atoms, methyl groups and solvent molecules are omitted for clarity. Uranium (green), potassium (purple), silicon (yellow), oxygen (red) and carbon (grey) atoms are represented with 50% probability ellipsoids. Selected bond distance [Å]: U1-O$_{avg}$ 2.228(17).

Single crystals of **24** were grown from saturated toluene solutions. The X-ray diffraction analysis revealed an ion-pair structure composed of a K(18c6) cation and of a [U(OSi(O^{t}Bu)$_3$)$_4$] anion (***Figure III.21***). The uranium ion is coordinated in a tetrahedral geometry by four terminal siloxide groups. The measured U-O bond lengths of the terminal siloxide (mean U-O = 2.228(17) Å) are longer than what is observed in the U(IV) silanol starting complex and is in the range of typical U-O distances in uranium(III) siloxide (vide supra) and alkoxide complexes.[93, 345, 435] The difference in the coordination mode adopted by one of the siloxide ligand in the U(III) complex **24**, with respect to the homoleptic

U(IV) complex **23** (monodentate versus bidentate) is probably the result of the difference in electron density but could also just be a crystallization effect. The U(III) cation is larger in size than the U(IV) and thus it should favor higher coordination numbers but the higher electron-rich character of the U(III) oxidation state might disfavor the coordination of the butoxide group.

Temperature-dependant magnetic data were collected for **24** in the range 2-230 K (***Figure III.22***). The room temperature effective moment (2.54 μ_B) extrapolated from these data for **24** falls in the range of the other U(III) coordination compounds.[176, 421-423] This value is lower than the theoretical value (3.62 μ_B) calculated for a $5f^3$ ion with a full spin-orbit coupling as commonly observed in trivalent uranium complexes. This is attributed to the crystal-field splitting of the Russel-Saunders $^4I_{9/2}$ ground term. The effective magnetic moment temperature dependency also supports the assignment of a trivalent oxidation state for **23**. The data show a monotonic drop in the effective moment as the temperature is lowered, decreasing to 1.54 μ_B at 2 K. This decrease is attributed to the thermal depopulation of the crystal field levels of the $^4I_{9/2}$ ground multiplet and is typically observed in U(III) complexes.[43, 340, 423, 436] The low-temperature value of the magnetic moment is in agreement with a doublet ground state, and falls in the range reported for other U(III) systems.[176, 436]

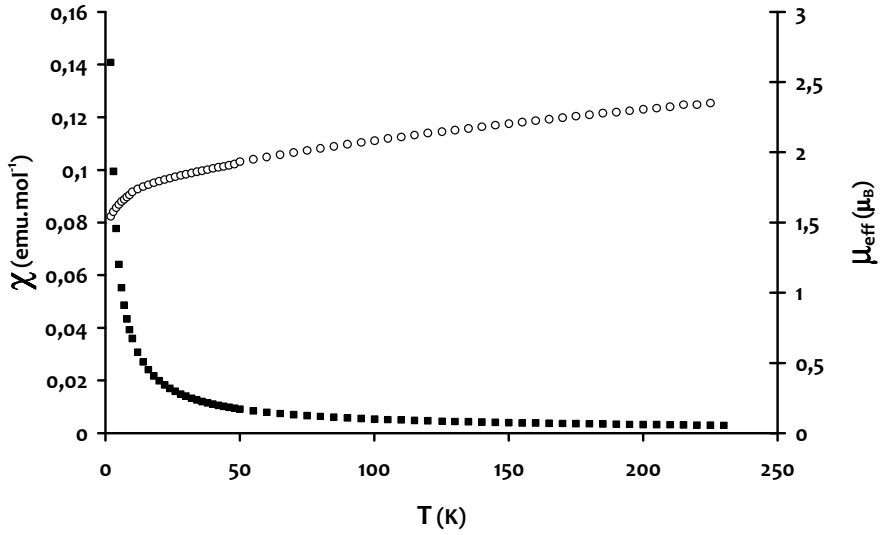

Figure III.22. Temperature-dependant SQUID magnetization data (0.5 T) for complex $[K(18c6)][U(OSi(O^tBu)_3)_4]$ **24** plotted as χ (black squares) and χT (white circles) versus temperature (2-230 K).

The proton NMR of **24** in THF and toluene solution shows the presence of one signal for the siloxide protons and one signal for the 18c6 protons in agreement with the presence of S_4 symmetric solution species. The UV-visible absorption spectrum of **24** recorded from THF solution (***Figure III.23***) displays a broad band centered at λ = 366 nm (ε = 3420 $L.cm^{-1}.mol^{-1}$). This absorption, which is responsible for the orange color of the complex, is attributed to a $5f^3 \rightarrow 5f^26d^1$ transition, a classical feature of U(III)

complexes[85, 127, 347, 433] which is also observed in the spectra of **18** and **21** (vide supra). A series of less intense (ε < 150 L.cm^{-1}.mol^{-1}) sharp resonances that we assign to 5f→5f transitions are spread over the entire recorded range above 500 nm. Such transitions are commonly observed in uranium complexes. In comparison, the spectrum recorded for complex **23-THF** (Figure 5) exhibits much weaker (ε < 50 L.cm^{-1}.mol^{-1}) 5f→5f transitions, with a maximum centered at λ = 608 responsible for the pale blue-green color of the complex.

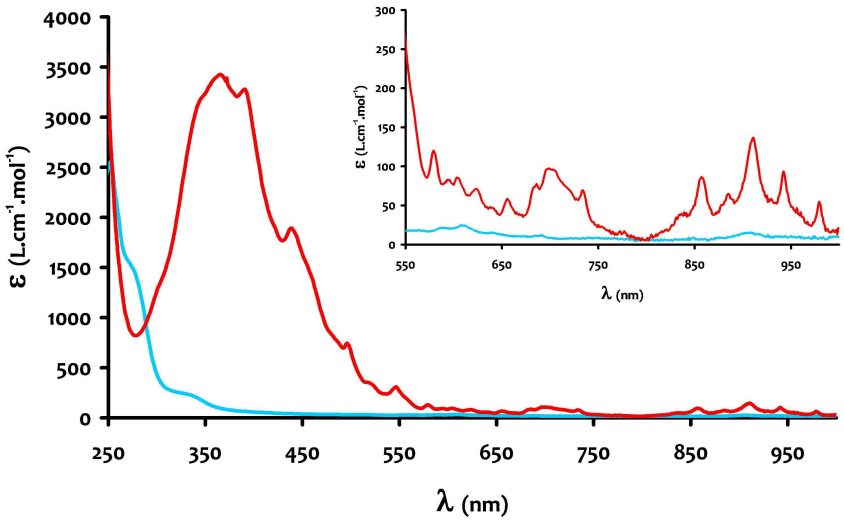

Figure III.23. UV/visible spectrum (298 K) of a THF solution of complex **23-THF** (blue line) and of complex **24** (red line). Insert : Zoom on the 550 – 1000 nm wavelength zone.

Anionic U(III) complexes are rare compared to their neutral analogues and mostly limited to cyclopentadienyl and cyclooctatetraenyl derivatives.[24, 437] Other examples of *ate*-salt complexes of U(III) have been reported with calix[4]tetrapyrrole and bulky silylamido ligands.[157, 361, 438] In spite of some very interesting reactivity in the activation of dinitrogen observed for the U(III) complex of a tetranionic calix[4]tetrapyrrole ligand the reactivity of *ate* complexes of U(III) supported by electron donor ligands has been little explored, mostly due to the general belief that such compounds will result in a saturated coordination sphere and limited reactivity. We have reasoned that the higher overall charge of the *ate* complex **24** with respect to the neutral complex **23** should result in a higher reactivity of the U(III) center. Furthermore the more crowded coordination environment of **24** might provide useful in reactivity studies.

The *ate*-salt complex **24** and the previously described neutral analogue complex [U(OSi(O^{t}Bu)$_3$)$_2$(μ-OSi(OtBu)$_3$)]$_2$ **18,** provide interesting systems for investigating the effect of charge and steric bulk in the redox properties and reactivity of U(III) complexes.

III.2.5 Redox properties

Although the high reducing character of trivalent uranium species is well recognized and is expressed by its rich reductive chemistry, potential measures of the $U^{(IV)}/U^{(III)}$ couple by electrochemical techniques remain rare. This can mostly be imparted to the high reactivity of these species that are unstable towards most common solvents and electrolytes, rendering electrochemical studies highly challenging.[24] Potentials for the $U^{(IV)}/U^{(III)}$ couple subsequently vary depending on the supporting ligands environment, and spans the range -1.5 V to -2.9 V versus $[(C_5H_5)_2Fe]^{+/0}$.[24, 69, 70] As for d-block metal complexes, the ligand platform is playing a crucial role in the stabilization of the +III oxidation state. Therefore a comprehensive understanding of the factors influencing the stabilization of low-valent uranium might result in the development of more stable and/or reactive systems. Electrochemical data of uranium complexes are hence particularly desirable.

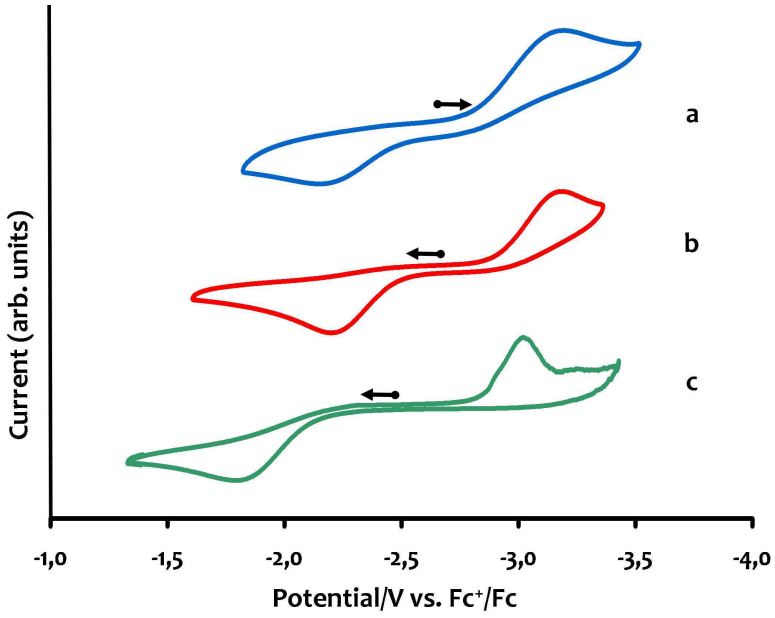

Figure III.24. Cyclic voltammograms of $[U(OSiO^tBu_3)_4(THF)_2]$ **23-THF** (a), $[K(18c6)][U(OSiO^tBu_3)_4]$ **24** (b) and $[U(OSiO^tBu_3)_3(THF)_2]$ **18-THF** (c) complexes in ~0.1 M $[Bu_4N][PF_6]$/THF solution at 100 mV/s scan rate.

Accordingly, the redox properties of $[U(OSiO^tBu_3)_3(THF)_2]$ **18-THF**, $[U(OSiO^tBu_3)_4(THF)_2]$ **23-THF** and $[K(18c6)][U(OSiO^tBu_3)_4]$ **24** were probed using cyclovoltammetry. Data were collected in ~0.1 M $[Bu_4N][PF_6]$ THF solution and are presented in ***Figure III.24***. All redox potentials are referenced against the $[(C_5H_5)_2Fe]^{+/0}$ redox couple and are summarized in ***Table III.1***. The voltammograms of the U(III) complexes **18-THF** and **24** both display an oxidation process at E_{pa} = -1.80 V and E_{pa} = -2.15 V respectively attributed to the $U^{(IV)}/U^{(III)}$ couple. This oxidation is associated with a reduction event occuring at E_{pc} = -3.02 V and E_{pc} = -3.18 V respectively for **18-THF** and **24**. This wave, which is not observed when the voltammogram is swept initially to the negative direction, corresponds to the

reduction to U(III) of the electrochemically generated U(IV) species. The voltammogram recorded for **23-THF** is very similar to that of **24** and exhibits an irreversible uranium-based reduction wave at E_{pc1} = -3.19 V, and an irreversible oxidation wave at E_{pa} = -2.18 V. This confirms that the reduction process at -3.19 V is indeed due to the $[U(OSiO^tBu_3)_4(THF)_2]/[U(OSiO^tBu_3)_4(THF)_2]^-$ couple.

Table III.1. Summary of redox data for complexes $[U(OSiO^tBu_3)_3(THF)_2]$ **18-THF**, $[U(OSiO^tBu_3)_4(THF)_2]$ **23-THF** and $[K(18c6)][U(OSiO^tBu_3)_4]$ **24** in ~0.1 M $[Bu_4N][PF_6]$ THF solutions. All values are reported in volts versus $[(C_5H_5)_2Fe]^{+/o}$.

Compound	E_{pa}	E_{pc}	ΔE_p	$E_{1/2}$
18-THF	-1.80	-3.02	1.22	2.41
23-THF	-2.18	-3.19	1.01	2.69
24	-2.15	-3.18	1.03	2.67

$\Delta E_p = E_{pc} - E_{pa}$; $E_{1/2} = (E_{pc} + E_{pa})/2$.

The observed redox behavior of these complexes provides direct insight into the influence of the ligation of a fourth siloxy ligand to the $[U(OSiO^tBu_3)_3]$ core. Indeed, compared to **18-THF**, the $U^{(IV)}/U^{(III)}$ couple for the ate-complex **24** is shifted to more negative potentials (destabilized) by ~0.4 V, therefore pointing to a greater electron density at the metal center provided by the four siloxy ligands. This is consistent with the greater stabilization of U(IV) in presence of a fourth ligand, in line with the electrochemical study of homoleptic U(IV) chloride complexes which indicates that the reduction potential becomes more cathodic when the number of halide ligands bound to uranium increases.[87] Very recently, Schelter also observed that the potential for the $U^{(IV)}/U^{(III)}$ couple in $[U\{N(SiMe_3)_2\}_4]$ was shifted by -0.8 V compared to that of $[U\{N(SiMe_3)_2\}_3]$.[361] Consequently $[U(OSiO^tBu_3)_4]^-$, and more generally U(III) homoleptic ate complexes are stronger reducing agent than their respective neutral analogues and should exhibit enhanced reactivity.

Furthermore, the value for the reduction potential of complex **23-THF** ($E_{1/2}$ = 2.7 V) is lower than what reported for the homoleptic $[U\{N(SiMe_3)_2\}_4]$ system (-2.05 V in CH_3CN vs $[(C_5H_5)_2Fe]^{+/o}$),[361] and the observed oxidation potential for **18-THF** is significantly more negative than the values reported for the reversible one electron reduction process in the homoleptic tris-aryloxide and tris-amido complexes of U(III) ($E_{1/2}$ = -1.22 V and – 1.24 V in THF vs $[(C_5H_5)_2Fe]^{+/o}$ for $[U(OAr)_3]$ (OAr = 2,6-di-tert-butylphenoxide) and $[U\{N(SiMe_3)_2\}_3]$ respectively).[71] This confirms the capability of the tris(tert-butoxy)siloxide siloxide ligand to enhance the reducing power of U(III).

The cause for irreversibility remains unclear. A possible explanation would be that the electron transfer is coupled to a chemical reaction. Such mechanistic feature is commonly observed for electroactive metal complexes where changing the oxidation state triggers a structural rearrangement reaction. In this case, if the scan rate is sufficiently fast, such chemical reaction

should have no significant effect, and the electron transfer should become reversible. Yet, such behavior was not observed, the overall redox transformation remaining irreversible in the scan-rate range 10 to 10000 $mV.s^{-1}$. This could be because the rearrangement process is extremely fast. However in absence of scan-rate effects on the voltammograms, no firm conclusion of the cause of irreversibility can be drawn.

In summary, several U(III) and U(IV) siloxy species were synthesized and characterized. The trivalent uranium complexes are of particular interest for their reducing properties and accordingly we explored their reactivity with heteroallenes (CO_2, CS_2, N_3^-) and arenes. This is the subject of sections III.3, III.4 and III.5.

III.3 Reactivity with C-1 Heteroallenes CO_2 and CS_2

To investigate the potential of these new U(III) precursors in reductive chemistry we have explored their reaction with the C1 substrates CS_2 and CO_2.

III.3.1 Reactivity with CS_2

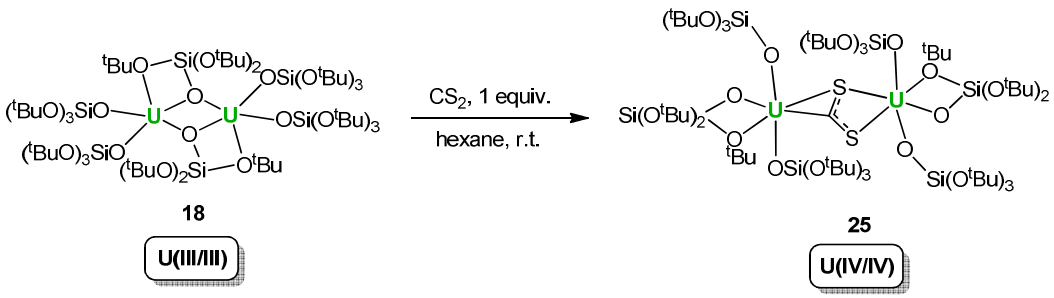

Scheme III.8. Reduction of CS_2 by $[U(OSi(O^tBu)_3)_2(\mu\text{-}OSi(O^tBu)_3)]_2$ **18**.

The addition of stoichiometric amounts of carbon disulfide to the trivalent uranium complex **18** (***Scheme III.8***) results in an immediate color change of the hexane solution from brown to yellow. NMR studies of the reaction mixture show that a reaction product is selectively formed even in the presence of an excess of CS_2. The highly soluble product can be isolated analytically pure form from a saturated solution of hexane in 53% yield. Crystallization from toluene yields crystals of $[\{U(OSi(O^tBu)_3)_3\}_2\{\mu\text{-}\eta^2(C,S):\eta^2(S,S)CS_2\}]$ **25**, suitable for X-ray diffraction studies. The X-ray diffraction analysis shows the presence of a uranium(IV) dimer that features a reduced CS_2^{2-} group bridging in a rare[439] $\mu\text{-}\eta^2(C,S1):\eta^2(S1,S2)$ binding mode (Scheme 2).

The most important feature of this structure (***Figure III.25***) is the geometry of the coordinated carbon disulfide. The CS_2^{2-} ligand binds the two crystallographically equivalent U(IV) centers, which are 5.406(2) Å apart, in a $\mu\text{-}\eta^2(C,S1):\eta^2(S1,S2)$ fashion. Both uranium ions are six coordinated with four coordination sites occupied by two oxygens from two terminal siloxides and two from a bidentate siloxide ligand. The mean $U\text{-}O_{siloxide}$ distance of 2.11(5) Å and a $U\text{-}O_{tBu}$ distance of 2.642(3) Å are in the range of previously reported U(IV) alkoxide and siloide U-O distances.[93, 434] The structure is centrosymmetric with the CS_2^{2-} unit disordered across the symmetry center with an occupancy factor of 0.5. Compared to free CS_2 (C-S = 1.560(3) Å),[440] the C-S distances in **25** are strongly asymmetric, the C1-S1 bond length (1.748(11) Å) being significantly longer than the C1-S2 one (1.594(12) Å).

Furthermore, the S1-C1-S2 angle of 131.6(8)° indicates a significant deviation from linearity. These structural data are in agreement with those reported for CS_2 complexes of transition metals and suggest the presence of a reduced CS_2.[190] The mean value of the U-S distances (2.85(2) Å) and the value of the U-C distance (2.546(13) Å) compare well with those found in the single example of a CS_2 uranium(IV) complex, reported by Brennan and co-workers (U-S at 2.792(3) and U-C at 2.53(2) Å).[190] The U(IV)-U(IV) dimer $[(RC_5H_4)_3U]_2[\mu\text{-}\eta^1,\eta^2\text{-}CS_2]$ was obtained from the reduction of CS_2 by the U(III) complex $[(RC_5H_4)_3U]$ (see section I.3.4.3). However, the coordination mode of CS_2 is significantly different in this complex with C-S bonds also highly asymmetric but shorter (1.426(2) Å) for the η^2CS than for the η^1CS (1.83(2) Å).

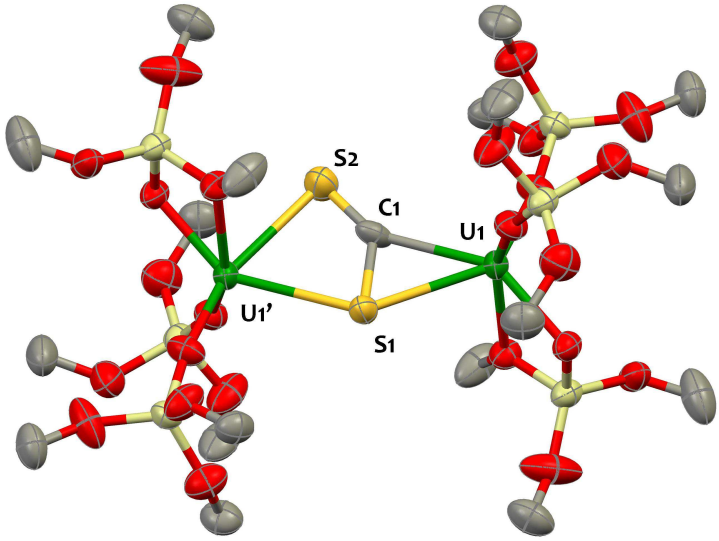

Figure III.25. Solid-state molecular structure of $[\{U(OSi(O^tBu)_3)_3\}_2\{\mu\text{-}\eta^2(C,S):\eta^2(S,S)CS_2\}]$ **25**, crystallized from toluene. Hydrogen atoms, methyl groups, solvent molecules and disorder are omitted for clarity. Uranium (green), silicon (light yellow), sulfur (yellow), oxygen (red) and carbon (grey) atoms are represented with 50% probability ellipsoids. Selected bond distances [Å] U1-C1 2.546(13), U1-S1 2.835(3) U1'-S2 2.843(3), U1'-S1 2.872(3), U1···U1' 5.4056(5).

Recently, Lam *et al.* reported the formation of a mixture of a trithiocarbonate complex and a tetrathiooxalate complex from the one- and two-electron reduction of CS_2 by the trivalent uranium complex of a multidentate phenolate $[(^{Ad}ArO)_3N)U(DME)]$ (see I.3.4.3).[192] DFT studies indicated the CS_2^{2-} bridged U(IV)/U(IV) dimer as the most reasonable intermediate in the formation of the final products. However, this intermediate was not experimentally observed. An analogous intermediate $[(^{Ad}ArO)_3N)U(\mu\text{-}CO_2^{2-})]$ was also identified by DFT studies for the reduction of carbon dioxide by the same complex to yield the final carbonate product $[(^{Ad}ArO)_3N)U(\mu\text{-}\eta^1:\eta^2CO_3^{2-})]$.[193]

DFT studies were performed on compound **25**, and are presented in section III.3.3.

III.3.2 Reactivity with CO_2

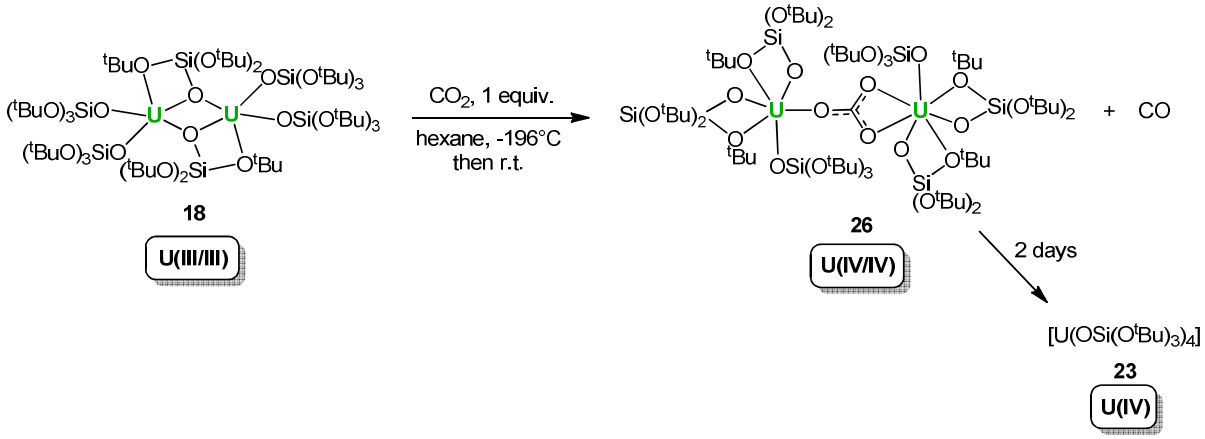

Scheme III.9. CO_2 reductive disproportionation mediated by $[U(OSi(O^tBu)_3)_2(\mu\text{-}OSi(O^tBu)_3)]_2$ **18.**

The interesting reactivity of the siloxide complex **18** with CS_2 incited us to investigate the reaction with carbon dioxide. Treating a dark brown suspension of trivalent uranium complex **18** in hexane with 1 equivalent of carbon dioxide for 6 hours resulted in a slow color change accompanied by CO evolution to yield a light green solution. The presence of free CO was identified by ^{13}C NMR and from the reaction with vanadocene. Volatiles were removed *in vacuo* and the resulting green residue was recrystallized from toluene at -40°C to afford the dinuclear uranium(IV) carbonate complex $[\{U(OSi(O^tBu)_3)_3\}_2(\mu\text{-}\eta^1\text{:}\eta^2CO_3)]$ **26,** in 33% yield (***Scheme III.9***). Monitoring of the reaction with stoichiometric amounts of CO_2 by proton NMR shows the presence of only one additional product (minor at first) which was identified by ^1H NMR and X-ray diffraction studies as the U(IV) complex $[U(OSi(O^tBu)_3)_4]$ **23.** The proton NMR of the reaction mixture after six hours shows that all the starting complex **18** is transformed into complexes **26** and **23** in a 2.5:1 ratio. Proton NMR studies of a toluene solution of complex **26** over longer periods of time (1-3 days) show that complex **26** decomposes in presence or absence of CO_2 to yield **23.** These results indicate that complex **26** undergoes slow ligand redistribution affording complex **23,** a process which requires also the formation of a unidentified U(IV) carbonate complex.

The molecular structure of **26** shows the presence of a dimeric complex with a carbonate anion bridging two uranium(IV) cations in a $\mu\text{-}\eta^1\text{:}\eta^2$ fashion at a U···U distance of 6.2600(2) Å (***Figure III.26***). Each uranium atom is coordinated by a terminal siloxide oxygen, (U-O = 2.09(1) Å), two siloxide oxygens (U-O = 2.18(1) Å) and two tert-butoxide oxygens (U-O = 2.67(6) Å) from two siloxide ligands coordinated in a bidentate fashion. These distances are in the range of previously reported U(IV) alkoxide U-O distances.[93, 434] The bridging carbonate binds the two uranium centers in a $\mu\text{-}\eta^1\text{:}\eta^2$

fashion with a shorter distance for the η¹-bound carbonate oxygen (U1-O121 = 2.25(2) Å) and two equivalent longer distances for the remaining carbonate oxygens (U2-O122 = U2-O123 = 2.404(2) Å).

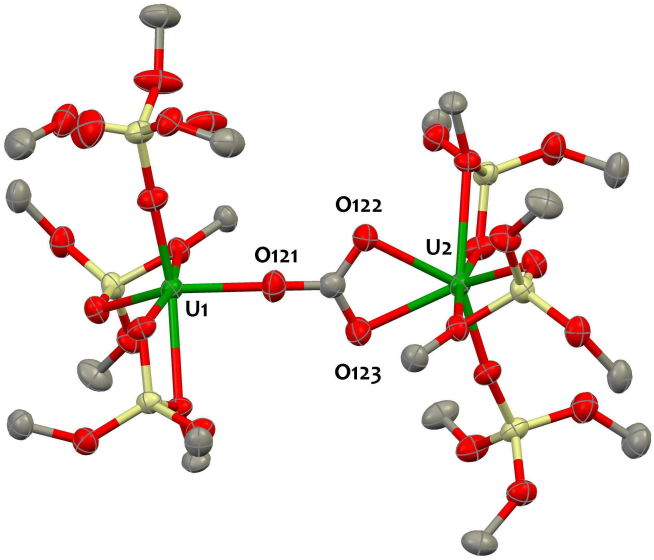

Figure III.26. Solid-state molecular structure of [{U(OSi(O^{t}Bu)$_3$)$_3$}$_2${μ-η^1:η^2-CO$_3$}] **26**, crystallized from toluene. Hydrogen atoms and methyl groups are omitted for clarity. Uranium (green), silicon (yellow), oxygen (red) and carbon (grey) atoms are represented with 50% probability ellipsoids.

The C-O distances observed within the carbonate unit are nearly equivalent, with a mean C-O value of 1.28(1) Å. A similar carbonate binding mode with comparable U-O and U-U distances was observed in the dimeric U(IV) carbonate complexes [(η-Cp^R)(η–C$_8$H$_6${Si^{i}Pr$_3$-1,4}$_2$)U]$_2$[μ-η^1,η^2-CO$_3$] and [(^{Ad}ArO)$_3$N)U(μ-η^1:η^{2}CO$_3^{2-}$)] obtained respectively by the groups of Cloke[178] and Meyer[126] (see introduction section I.3.4.2.4) from the reaction of the respective U(III) complexes with CO_2. The slow transformation of **18** into the carbonate complex **26** is accompanied by CO evolution and no other reaction intermediates were observed.

The reactivity of **18** contrasts with that reported for simple uranium tris(aryloxides) with carbon dioxide for which no carbonate adducts were isolated and multiple reduction and insertion products were identified (see section I.3.4.2.4).[93] This can be ascribed to the different electronic and steric properties of the siloxide supporting ligand and indicate the interest of siloxide as alternative ancillary ligand in U(III) chemistry.

III.3.3 Mechanistic insights

DFT calculations were carried out by the group of Pr. Laurent Maron on these systems in order to gain further insights into the reactivity of the siloxide complex **18** with CS_2 and CO_2. I have decided to present there results as they provide insights into the mechanism of these transformations. They

used the same methodology than previously developed in the study of the reaction of U(III) with heteroallenes has been used.[179, 191, 192]

The computed Gibbs free energy profile for the reactivity between complex **18** and CS_2 indicates that the bimetallic CS_2 adduct **25**, observed experimentally, is the most stable product (see ***Figure III.27***). Complex **25** is predicted to have a μ-η^2:η^2 coordination of CS_2 in good agreement with the experimental observation. As also demonstrated[191] for $[Cp'_3U]$ ($Cp' = MeC_5H_4$), the lack of reactivity of the bimetallic complex, with respect to sulfido and thiocarbonate formation, is purely thermodynamic. Indeed, the transformation of complex **25** to form a bridging sulphido complex is computed to be endergonic by 14.5 kcal.mol^{-1} (16.8 kcal.mol^{-1} for the full system). Similarly the formation of a thiocarbonate complex is also predicted to be an endergonic process either from the sulphido intermediate (almost 2.1 kcal.mol^{-1} for both systems) or from the bimetallic intermediate **25** (16.6 kcal.mol^{-1} and 19.0 kcal.mol^{-1} respectively). This is associated to the low stability of the generated CS molecule.[441]

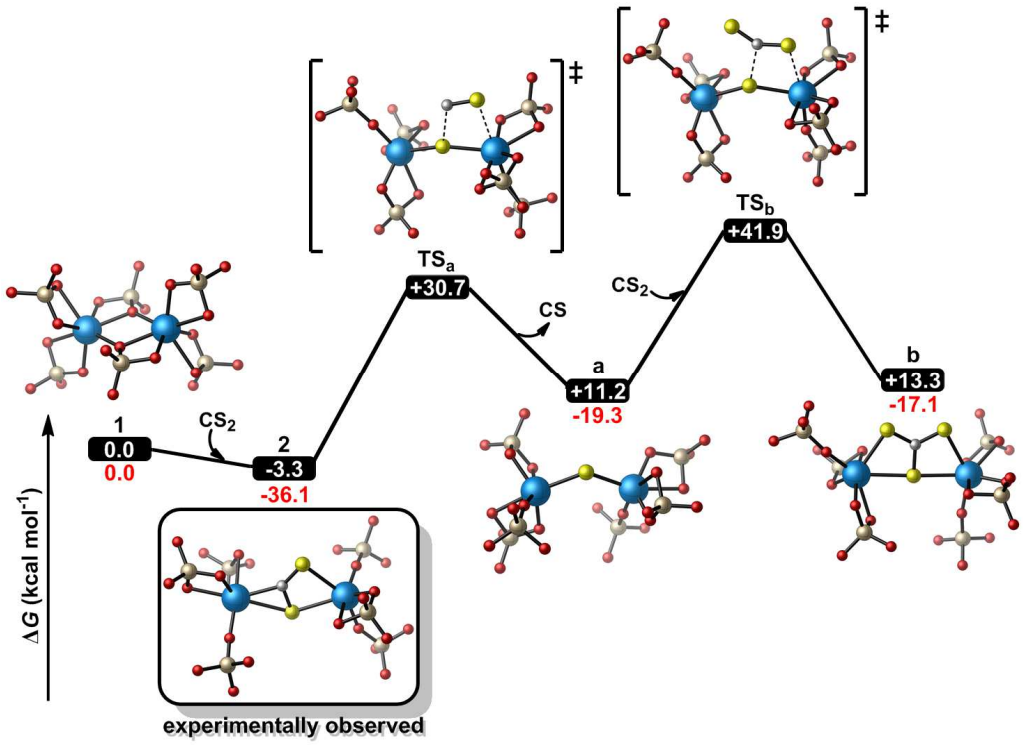

Figure III.27. Gibbs Free energy computed profile for the reactivity of CS_2 with **18**. The values are given in kcal.mol^{-1} and the red values apply for the full system.

The formation of a tetrathiooxalate complex from **25** has also been investigated (see ***Figure III.28***) and is predicted to be exergonic (8.0 kcal.mol^{-1}). However, the reaction barrier for the formation of this complex from **25** has been computed to be 33.8 kcal.mol^{-1} (very close to the barrier for the CS release). The height of the barrier is probably the result of combined electronic and steric factors introduced by the electron-rich, bulky siloxide ligands. Thus, any further reactions from the bimetallic

complex **25** are either thermodynamically or kinetically unfavorable which explains the experimental observation of the complex **25** as the only product.

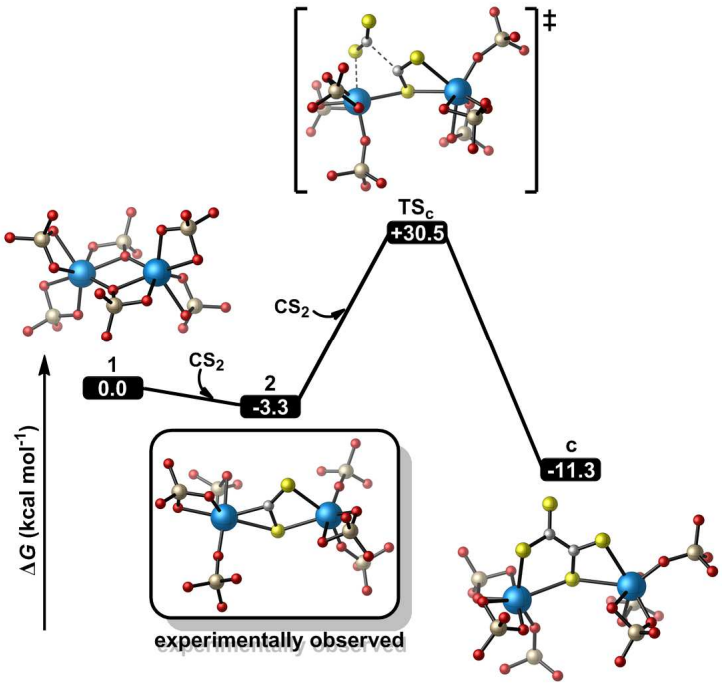

Figure III.28. Gibbs Free energy computed profile for the formation of a tetrathiooxalate from the reactivity of CS_2 with **25**. The values are given in kcal.mol^{-1}.

The Gibbs free energy profile of the reaction between complex **18** and CO_2 has also been computed and is represented on ***Figure III.29***. Two pathways were considered, namely the reaction through the formation of an oxo intermediate or the addition of a second CO_2 molecule onto the U(IV)-(CO_2^{2-})-U(IV) reaction intermediate.[442] In both cases, the reaction involves the preliminary formation of the highly stable bimetallic $(CO_2)^{2-}$ complex. The second pathway is found to be the most favorable kinetically with an overall barrier of 14.5 kcal.mol^{-1}, whereas the overall barrier for the oxo pathway is 23.8 kcal.mol^{-1}. This reaction mechanism has never been reported to date in U(III) chemistry as so far only a reaction mechanism involving the formation of an oxo intermediate was proposed by Castro et al.[191] The oxo pathway is probably prevented in our system by the coordination environment provided by the siloxides which can act as bidentate ligands. The concerted mechanism involves the reaction of a CO_2 molecule with the bimetallic complex to yield a transient 6-membered ring intermediate. From this intermediate, a spontaneous release of CO is observed (0.1 kcal.mol^{-1} barrier) leading to the formation of the observed carbonate.

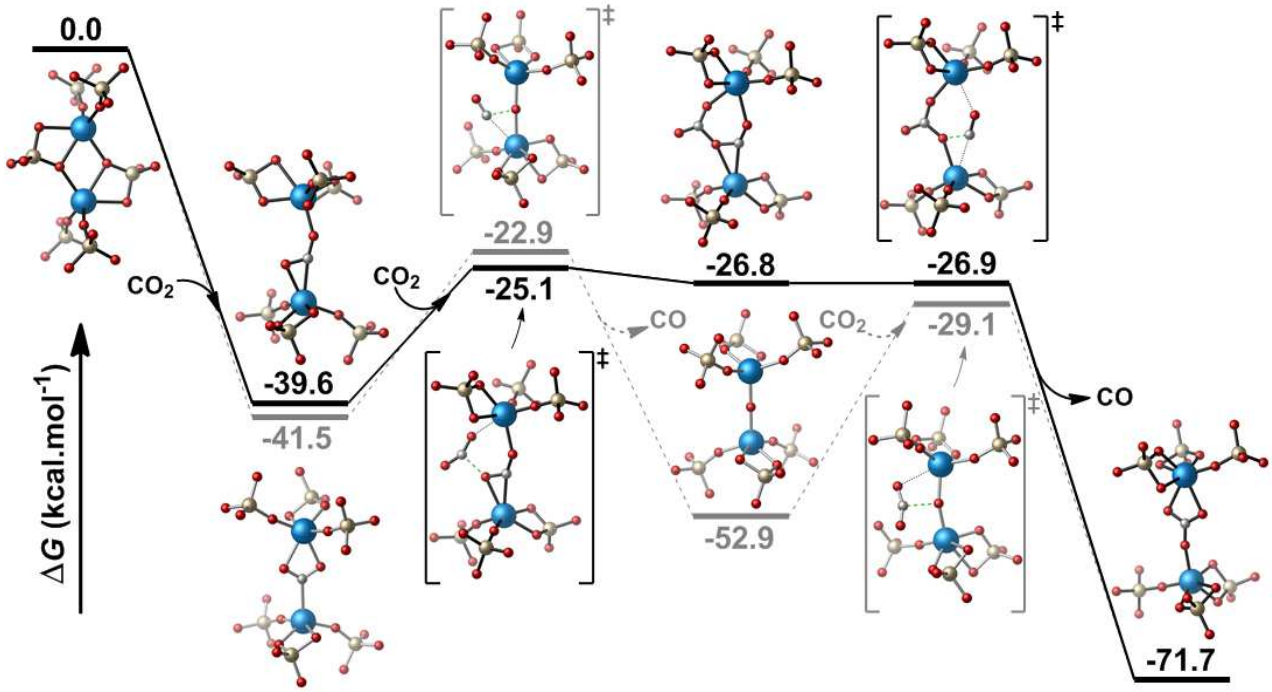

Figure III.29. Gibbs Free energy computed profile for the reactivity of CO_2 with **18.** The values are given in kcal.mol^{-1}.

III.4 Reactivity with azides

The current interest in nitride and imido complexes of high-valent uranium generated by their potential application in nitrogen transfer chemistry prompted us to investigate the reactivity of the highly reactive siloxide complexes presented in section III.2 with organic and inorganic azides.

As mentioned in introduction, differing steric and electronic environments at the uranium center have a critical impact on the formation of nitrido and imido complexes, on their geometry, stability and reactivity. For example the optimal tuning of the steric and electronic environment has been the key to the recent isolation of the first uranium complexes containing a terminal nitride.[140, 168] However, only a very limited number of studies have explored the effect of different steric environments in similar ligand systems.[26, 204, 443]

In this section we investigate the reactivity of two U(III) systems presenting a different number of alkoxy(siloxide) ligands, the neutral tris-siloxide dimer $[U(OSi(O^tBu)_3)_2(\mu\text{-}OSi(O^tBu)_3)]_2$ **18** and the monomeric *ate* complex $[K(18c6)][U(OSi(O^tBu)_3)_4]$ **24** with azido derivatives. The study presented in the next two sections will be divided into two categories: organic and inorganic azides.

III.4.1 Imides formation from the reaction of U(III) siloxides with organic azides

III.4.1.1 Reaction of $[U(OSi(O^tBu)_3)_2(\mu\text{-}OSi(O^tBu)_3)]_2$ with adamantyl azide

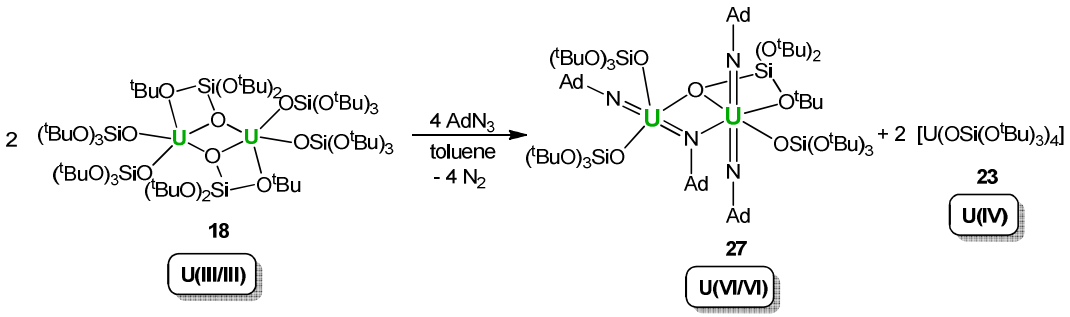

Scheme III.10. Reaction of $[U(OSi(O^tBu)_3)_2(\mu\text{-}OSi(O^tBu)_3)]_2$ **18** with adamantyl azide.

The reaction of the neutral U(III) siloxide complex $[U(OSi(O^tBu)_3)_2(\mu\text{-}OSi(O^tBu)_3)]_2$ **18** with adamantyl azide (one equivalent per uranium atom - ***Scheme III.10***) leads to the immediate formation of the U(IV) complex $[U(OSi(O^tBu)_3)_4]$ **23**, and of the dinuclear bis(imido) complex of uranium(VI) $[U_2(NAd)_4(OSi(O^tBu)_3)_4]$ **27**, in a 2:1 ratio, as shown by ^{1}H NMR.

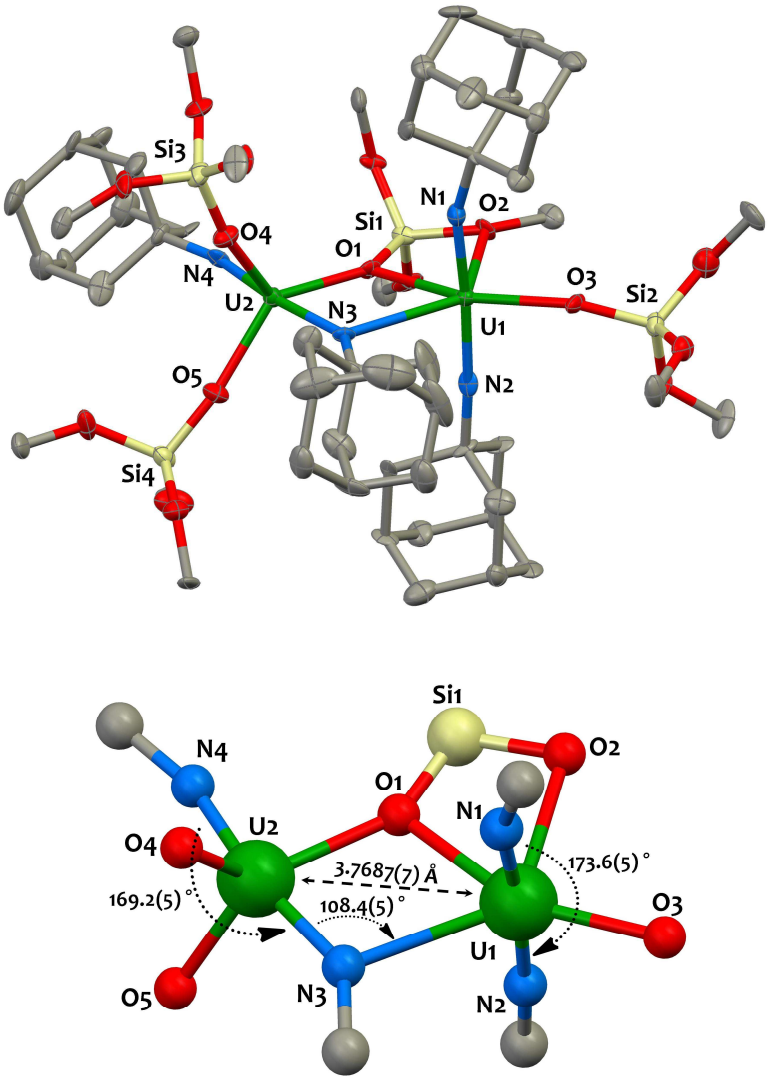

Figure III.30. (Top) Solid-state molecular structure of $[U_2(NAd)_4(OSi(O^tBu)_3)_4]$ **27** crystallized from hexane. Hydrogen atoms and methyl groups are omitted for clarity. Uranium (green), silicon (yellow), nitrogen (blue), oxygen (red) and carbon (grey) atoms are represented with 50% probability ellipsoids. Selected bond distances [Å] and angles [deg]: U-O_{avg} 2.20(2), U=N_{avg} 1.937(7), U2-N3 = 1.957(10), U1-N3 = 2.661(12), U1-N3-U2 =108.4(5), N1-U1-N2 = 173.6(5), N3-U2-N4 =169.2(5) ; (Bottom) detail of the bis(imido) cation-cation core in **27**.

Complex **27** crystallizes from hexane solution in the monoclinic space group $P2_1/n$, and its solid-state molecular structure is represented in ***Figure III.30***. The dinuclear complex contains a cation-cation interaction[444] between two $[U(NAd)_2]^{2+}$ units (U1-N3-U2 angle = 108.4(5)°). The two $[U(OSi(O^tBu)_3)_2(NAd)_2]$ moieties are also held together by a bridging siloxide with a U···U separation of 3.7687(7) Å. Both $[U(NAd)_2]^{2+}$ motifs are nearly linear (N1-U1-N2 angle = 173.6(5)° ; N3-U2-N4 angle = 169.2(5)°) and can be seen as nitrogen analogues of the UO_2^{2+} moiety. The U=N imido bond distances for the terminal imido groups are short (U=N_{avg} = 1.89(5) Å), in agreement with a multiple uranium-nitrogen bonding, and fall in the range of those reported for U(VI) imido complexes.[170, 202, 226, 228, 305, 445-449] The U=N bond distance of the imido group (U2-N3 = 1.957(10) Å) involved in the cation-cation interaction is, as expected, longer than those of the terminal imido groups but significantly

shorter than the U1-N3 bond length (2.661(12) Å), in agreement with the formulation proposed. The arrangement of the two imido groups is not planar (see ***Figure III.30***-bottom) with N4U2N3U1 and N1U1N2N2 planes almost perpendicular at 85.23°. This differs from the previously reported cation-cation complexes of pentavalent uranyl which all show a T-shaped or diamond shaped coplanar arrangement[65, 66, 315, 317, 450, 451] and is probably due to the presence of the bulky substituent on the imido nitrogen. The coordination geometry of U2 is best described as a distorted trigonal bipyramid with three $OSi(O^tBu)_3$ ligands occupying the equatorial plane. U1 is hexacoordinated in a highly distorted octahedral geometry by two adamantyl imidos in trans position, one terminal monodentate siloxy ligand, one bridging bidentate siloxy ligand and one bridging imido ligand.

While cis-bis(imido) complexes of U(VI) have been known since 1992,[226, 305, 445, 446, 452] only in 2005 the first example of stable U(VI) trans-bis-imido complexes, $[U(NR)_2I_2(THF)_2]$, were prepared from the reaction of uranium metal or $[UI_3(THF)_4]$ with iodine and alkyl- or arylamines.[169, 170] A few other examples of U(VI) trans-bis(imido) complexes in different ligand environments have been prepared in the past few years[202, 228, 305, 447-449] which have shown interesting reactivity.[169, 443, 453] Compound **27** provides a new example of uranium(VI) trans-bis(imido) complex and the first one showing a cation-cation interaction between the two imido groups. Examples of dinuclear bis(imido) complexes are rare in uranium chemistry[227, 450] and they all present a diamond-shaped geometry. Cation-cation interaction between uranyl groups is found in several recently reported uranyl(V) complexes,[64, 317, 451] but only rarely observed in uranyl(VI) complexes.[64, 454, 455]

The formation of the complexes **27** and **23** from the reaction of **18** with adamantyl azide could be the result of the disproportionation of an unstable U(V) bis(imido) intermediate (***Scheme III.11***). While the disproportionation reaction of uranyl(V) to yield uranyl(VI) and U(IV) species in aqueous or organic media[61, 64, 451, 456-458] has been the subject of high interest in past and more recent years, to the best of our knowledge there are no previous reports of the disproportionation of uranyl(V) imido complexes.

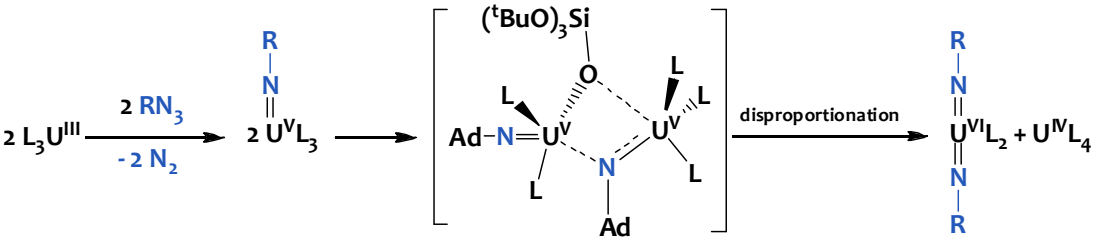

Scheme III.11. Plausible route to account for the formation of **27** and **23** from the reaction of **18** with adamantly azide. L = $OSi(O^tBu)_3$.

However, one example of the formation of a U(VI) imido complex and of a U(IV) complex from the reaction of U(III) with organic azides has been reported.[226] The mechanism proposed by the authors

is based on previously reported reactivity of U(V) imides with U(III)[227] and involves the comproportionation of the U(V) intermediate $[(C_5Me_5)_2UCl(N=R)]$ with the U(III) starting complex $\{Na[(C_5Me_5)_2UCl_2\}$ to afford the imido $[(C_5Me_5)_2U(N=R)]$ and the bis-chloride $[(C_5Me_5)_2UCl_2]$ U(IV) complexes. Further reaction of the U(IV) imido with azide yields the U(VI) cis-bis(imido) product. A similar mechanism could also be invoked for the formation of **27** and **23** from **18** as alternative to the disproportionation route. Subsequent work might be directed to further investigate this reactivity.

III.4.1.2 Reaction of $[K(18c6)][U(NSiMe_3)(OSi(O^tBu)_3)_4]$ with organic azides

We have also studied the reaction of the *ate*-salt complex **24** with organic azides in order to investigate how the increased steric bulk and the difference in charge and redox potential influence the outcome of the reaction with respect to complex **18**. The reaction of complex **24** with trimethylsilyl and adamantyl azides in toluene proceeds quickly at room temperature with a color change from orange to dark brown to afford the uranium(V) imido complexes, $[K(18c6)][U(NSiMe_3)(OSi(O^tBu)_3)_4]$ **28-TMS** and $[K(18c6)][U(NAd)(OSi(O^tBu)_3)_4]$ **28-Ad** which were isolated pure in 48 % and 66 % yield respectively (***Scheme III.12***). **28-TMS** and **28-Ad** provide new examples of stable U(V) mono(imido) complexes.

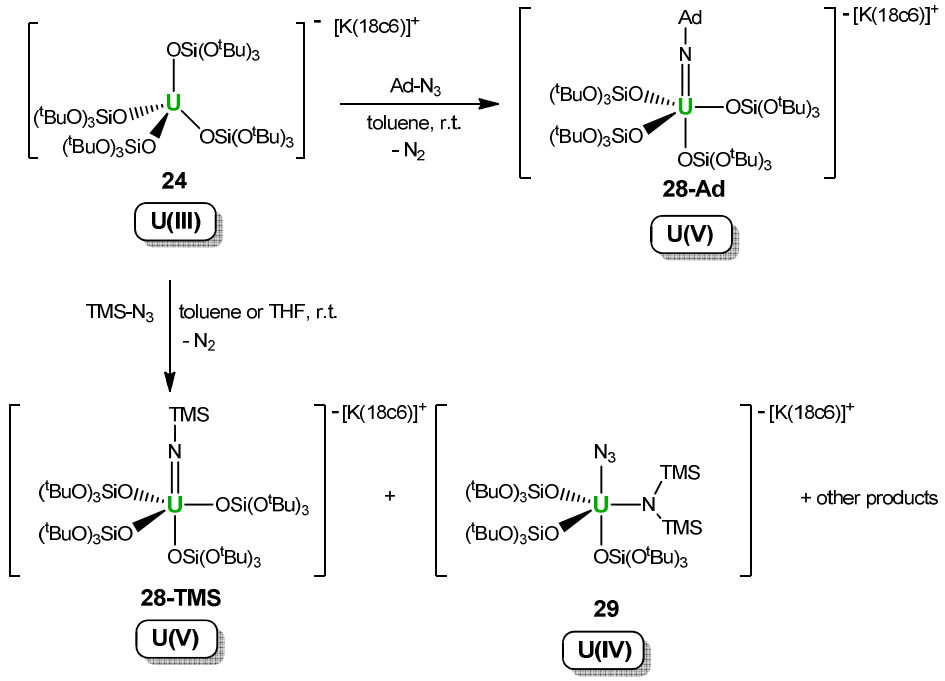

Scheme III.12. Reaction of $[K(18c6)][U(OSi(O^tBu)_3)_4]$ **24** with organic azides.

These anionic heteroleptic complexes are highly soluble in toluene and are stable in solution for several days. The ^1H NMR spectra of both compounds are in agreement with a C_3-symmetry for the

complexes in solution with respectively one and four proton resonances for the $SiMe_3$ and the adamantyl groups. The UV-visible spectra of both complexes (see appendix) display a broad unresolved band in the UV-visible region attributed to charge transfer transitions. In addition, a weaker f→f transition is observed around 910 nm. The value of the magnetic moment per uranium, measured at 298 K using the Evans method for a toluene solution of **28-TMS** (2.12 μ_B) and **28-Ad** (2.34 μ_B) is close to the calculated effective magnetic moment at room temperature for a U(V) $5f^1$ complex (2.54 μ_B) and is similar to the value reported for other U(V) imido complexes.[176, 184]

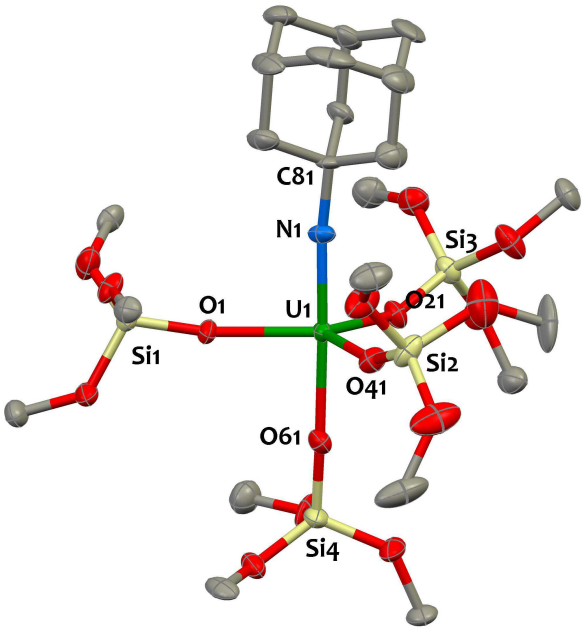

Figure III.31. Solid-state molecular structure of the anion in $[K(18c6)][U(NAd)(OSi(O^tBu)_3)_4]$ **28-Ad** crystallized from hexane. [K(18c6)] countercation, hydrogen atoms, methyl groups and solvent molecules are omitted for clarity. Uranium (green), silicon (yellow), nitrogen (blue), oxygen (red) and carbon (grey) atoms are represented with 50% probability ellipsoids. Bond distances [Å]: U1-O_{avg} 2.20(2), U1-N1 1.937(7).

Structural data for both compounds were obtained by X-ray diffraction analysis. In both complexes, the uranium cation is pentacoordinated in a distorted trigonal bipyramid geometry by three monodentate siloxy ligands in the equatorial plane and one monodentate siloxyde ligand and a trimethylsilyimido or a adamantylimido ligand, in **28-TMS** and **28-Ad** respectively, in the axial position (***Figure III.31*** and ***Figure III.32***). The short U-N bond distances, respectively of 1.889(11) Å for **28-TMS** and 1.937(7) Å for **28-Ad** lie in the lower side of the range of U=N distances (1.89 to 2.12 Å) in previously reported U(V) imido complexes.[60, 176, 184, 197, 203, 204, 220, 228, 447] The U-N-R (R = $SiMe_3$, Ad) angles (163.4(5)° and 172.3(5)°) are close to linearity. The short U=N bond distance and the linear U-N-R angle are structural features characteristic of a strong π-interaction between the two donating lone pairs of the nitrogen atom and the f-orbitals of the uranium cation and are indicative of the multiple bonding between the imido moiety and the uranium center.[164, 165]

The U-O bond distances in **28-TMS** (U-O_{avg} = 2.16(2) Å) and **28-Ad** (U-O_{avg} = 2.20(2) Å) are in the same range than that of **24** (U-O_{avg} = 2.228(17) Å). In both complexes, the U-O bond distances for the siloxide group opposite to the amido group (2.130(7) Å for **28-TMS** and 2.180(6) Å for **28-Ad**) are slightly shorter than the U-O distances observed for the three siloxide ligands in the equatorial plane (average U-O_{eq} bond distance 2.173(9) Å for **28-TMS** and 2.21(2) Å for **28-Ad**). This is expected as the axial position is less sterically constrained than the equatorial ones, allowing a closer approach of the sterically hindered tris(tert-butoxy)siloxide axial ligand. Additionally this could be further amplified by an inverse trans influence interaction which typically occurs in high-valent U(V) and U(VI) systems bearing multiply bonded imido and oxo ligands.[204, 223, 459]

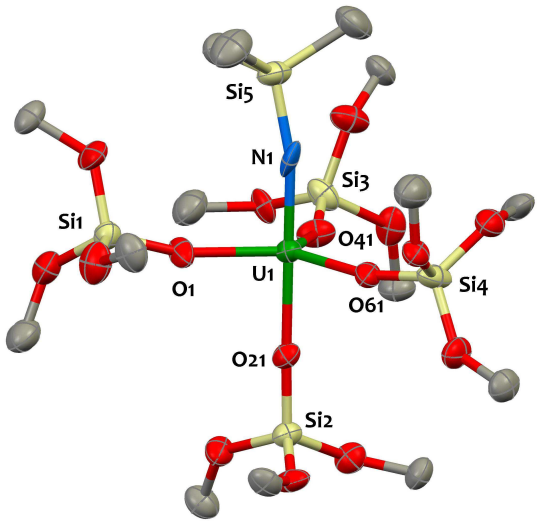

Figure III.32. Solid-state molecular structure of the anion in [K(18c6)][U(NSiMe$_3$)(OSi(O^{t}Bu)$_3$)$_4$] **28-TMS** crystallized from toluene. [K(18c6)] countercation, hydrogen atoms, disordered atoms, methyl groups and solvent molecules are omitted for clarity. Uranium (green), silicon (yellow), nitrogen (blue), oxygen (red) and carbon (grey) atoms are represented with 50% probability ellipsoids. Selected bond distances [Å]: U1-O_{avg} 2.16(2), U1-N1 1.889(11).

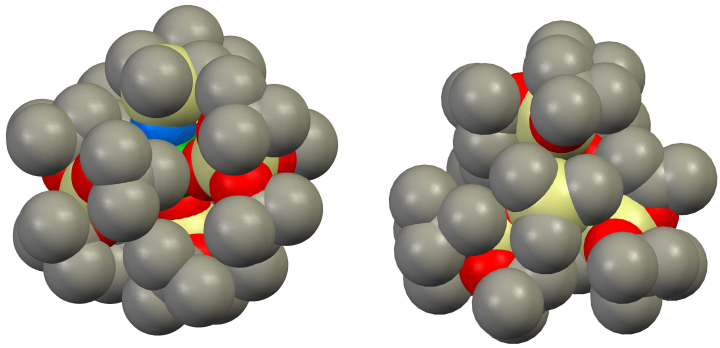

Figure III.33. Space-filling representations of the anion in [K(18c6)][U(NSiMe$_3$)(OSi(O^{t}Bu)$_3$)$_4$] **28-TMS** crystallized from toluene. [K(18c6)] countercation, hydrogen atoms and solvent molecules are omitted for clarity.

A probable reason for the limited number of isolated U(V) imido compounds[60] is that, depending on the supporting ligands and on the azide substituent, the reaction of U(III) complexes with organic azides can follow alternative pathways leading to multiple products.[26, 176, 184, 204, 222]

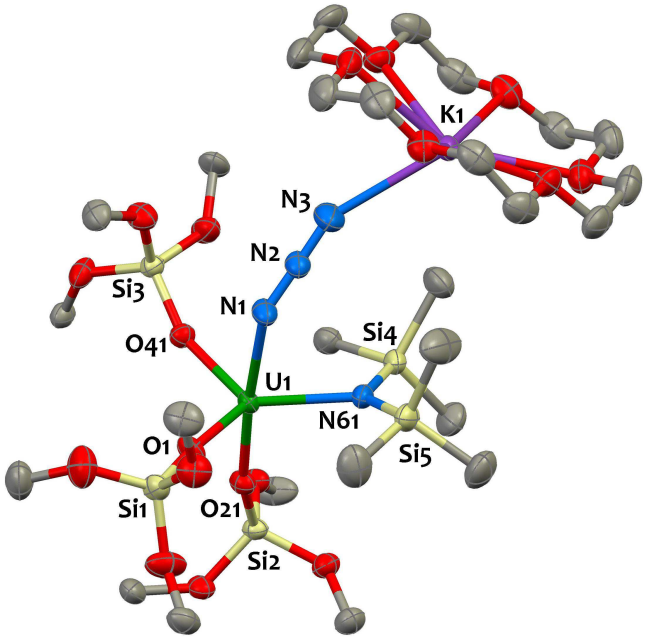

Figure III.34. Solid-state molecular structure of [K(18c6)][U(N_3){N($SiMe_3$)}$_2${OSi(O^tBu)$_3$}$_3$], **29** crystallized from toluene. Hydrogen atoms, methyl groups from OSiO^tBu ligands and solvent molecules are omitted for clarity. Uranium (green), silicon (yellow), potassium(purple), nitrogen (blue), oxygen (red) and carbon (grey) atoms are represented with 50% probability ellipsoids. Selected bond distances [Å]: U1-O_{avg} 2.146(8), U1-N61 2.330(4), U1-N1 2.409(4), N1-N2 1.184(5), N2-N3 1.157(6).

Notably, the imido complex **28-TMS** is isolated in low yield (48%) and the ^{1}H NMR spectrum of the reaction mixture of **24** with trimethylsilyl azide shows the presence of several byproducts. After separation of pure **28-TMS** from the reaction mixture, few crystals of the azido-amido complex [K(18c6)][U(N_3){N($SiMe_3$)$_2$}{OSi(O^tBu)$_3$}$_3$] **29** were obtained from the concentrated mother liquor. The solid-state structure (***Figure III.34***) shows that the uranium cation in **29** is pentacoordinated in a distorted trigonal bipyramid fashion by one azido ligand in the apical position, three monodentate siloxy ligands, and one silylamido ligand in the equatorial plane. The silylamido ligand and the azido ligand are found in a cis-arrangement (N61-U1-N1 angle: 80.93(13)°). The silylamido ligand introduces steric bulk in closer proximity of the uranium cation, forcing the two siloxide ligands occupying the equatorial plane to be in close proximity, as is shown by the smaller value of the O1-U1-O41 (105.45(12)°) angle compared to the O1-U1-N61 (125.67(13)°) and O41-U1-N61 (125.88(12)°) ones. The azido ligand adopts a bent coordination geometry (U1-N1-N2 = 135.7(3)°, N1-N2-N3 = 178.7(3)°) pointing in the direction of the silylamido ligand as highlighted in ***Figure III.34***. The U1-N61 (2.330(4) Å) distance is shorter than the U1-N1 one (2.409(4) Å), in agreement with a lower negative charge density on N1 resulting from charge delocalization on the azido moiety.

The isolation of an U(IV) azido-amido complex from the reaction of U(III) with an organic azide is unprecedented and is probably the result of the high reactivity of the nucleophilic imido complex **28-TMS** with TMS-N_3 which should lead to new interesting imido-group transfer chemistry.[26] The different reactivity observed with TMS-N_3 compared to that with Ad-N_3 and leading to the formation of **29** could arise from the higher stability of the silicon-based trimethylsilyl radical compared to the carbon-based adamantyl radical in a possible radical transfer pathway.[26]

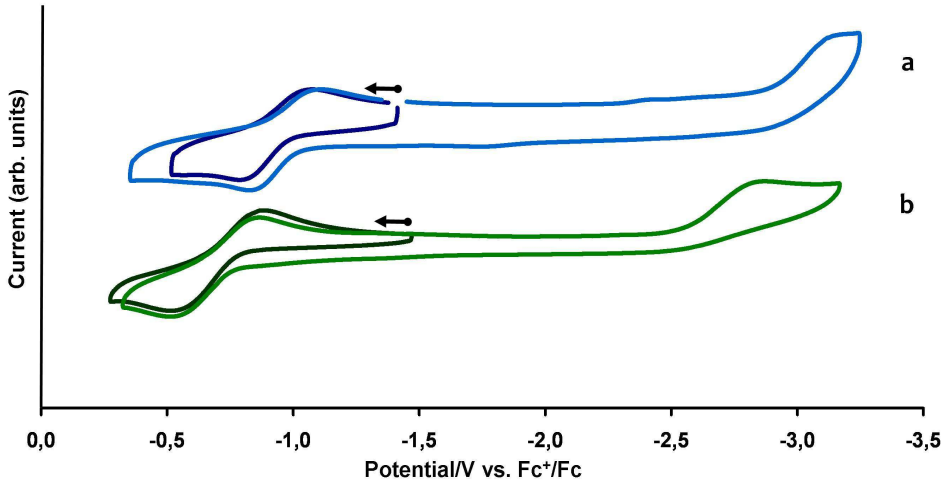

Figure III.35. Cyclic voltammograms for 2 mM solutions of a) **28-Ad** and b) **28-TMS** recorded in 0.1 M $[Bu_4N][PF_6]$ THF solution at 100 mV.s^{-1} scan rate.

The redox properties of **28-TMS** and **28-Ad** in THF solution were investigated by electrochemistry. The cyclovoltammetric curves recorded for the U(V) imidos in THF solution, represented on ***Figure III.35***, show that it is possible to oxidize them to U(VI) imidos. The U(VI)/U(V) process is reversible, and occurs at $E_{1/2}$ = -0.7 V and -1.0 V versus the Fc^+/Fc couple respectively for **28-TMS** and **28-Ad.** The +0.3 V shift in potential indicates that the N-Ad ligand favors the +VI oxidation state due to the higher electron-donor character of the adamantyl group. An irreversible reduction process is observed at E_{pc} = -2.9 V and -3.2 V vs the Fc^+/Fc couple respectively for **28-TMS** and **28-Ad,** and is attributed to the reduction to U(IV). The separation between uranium oxidation and reduction processes in both systems is similar (ΔE = 2.2 V).

To our knowledge, electrochemical studies of U(V) imidos is limited to the complexes of the general formula $[U(Cp)_2(NAr)(X)]$ (Ar = 2,4,6-$^tBu_3$-C_6H_2, 2,6-$^iPr_2$-C_6H_3 ; X = F, Cl, Br, I) reported by Kiplinger et al.[203] These species exhibit much higher potential (range: 0.11 V to -0.19 V) for the U(VI)/U(V) couple. The lower value for the oxidation of the U(V) imido observed with the siloxide ligands versus the Cp and halide ones is in agreement with the stronger electron-donating character of the siloxide ligands and with the anionic character of the complexes **28-TMS** and **28-Ad**. The observed U(VI)/U(V) redox potential compares well with those reported for homoleptic U(V) ate complexes bearing highly

electron-rich ligands $[UL_6]^-$ (L = O^tBu, CH_2SiMe_3, NC_5H_{10}, $N{=}C^tBuPh$)[58, 448, 460-462] ranging from -1.12 V, to -1.52 V versus the Fc^+/Fc couple.

These preliminary studies suggest that these monomeric anionic U(V) imido compounds are attractive precursors for exploring the chemistry of high valent uranium.

The observed high reactivity of the *ate* complex **24** with organic azides prompted us to investigate the possibility of obtaining nitrido complexes in this novel ligand environment from the reaction of **24** with inorganic azides.

III.4.2 Nitride formation from the reaction of U(III) siloxides with cesium azide

III.4.2.1 Reaction of $[K(18c6)][U(NSiMe_3)(OSi(O^tBu)_3)_4]$ with CsN_3

The reaction of $[K(18c6)][U(OSi(O^tBu)_3)_4]$ **24** with cesium azide in THF at -40°C proceeded in 24 hours to afford a complex mixture of compounds. From this mixture two types of crystals, pale blue/green and brown diamond-shaped plates, formed at -40°C. X-ray diffraction studies show the presence of the U(IV) azido complex $[K(18c6)U(N_3)(OSi(O^tBu)_3)_4]$ **30** and of the di μ-nitrido diuranium(V) complex $[KU(\mu\text{-}N)_2(OSi(O^tBu)_3)]_2$ **31** (***Scheme III.13***).

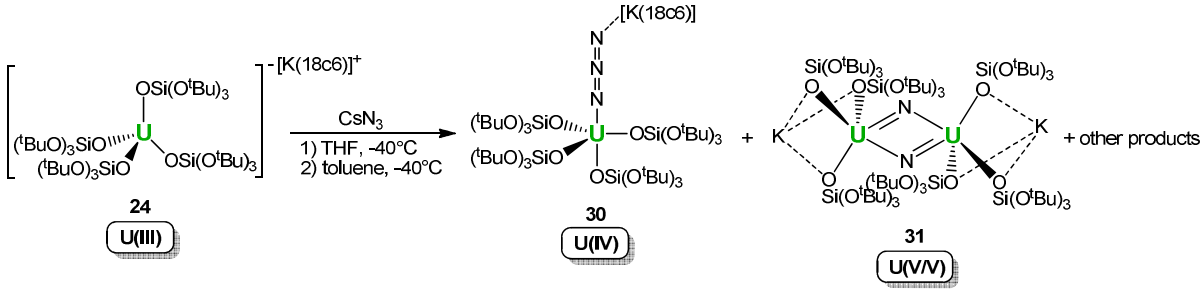

Scheme III.13. Reaction of $[K(18c6)][U(OSi(O^tBu)_3)_4]$ **24** with cesium azide.

The structure of **31** is shown in ***Figure III.36*** together with selected metrical parameters. The molecule has a crystallographically imposed symmetry center in between the two uranium cations. The most interesting feature in the structure of **31** is the presence of two nitrido atoms bridging two uranium centers in a diamond-shaped geometry. Only one example of diamond-shaped U_2N_2 nitride has been previously reported for a diuranium mixed valent complex U(V)/U(IV) isolated from dinitrogen reduction.[157] However, complex **31** is the first example of a U_2N_2 core obtained from the reaction of U(III) with azides.

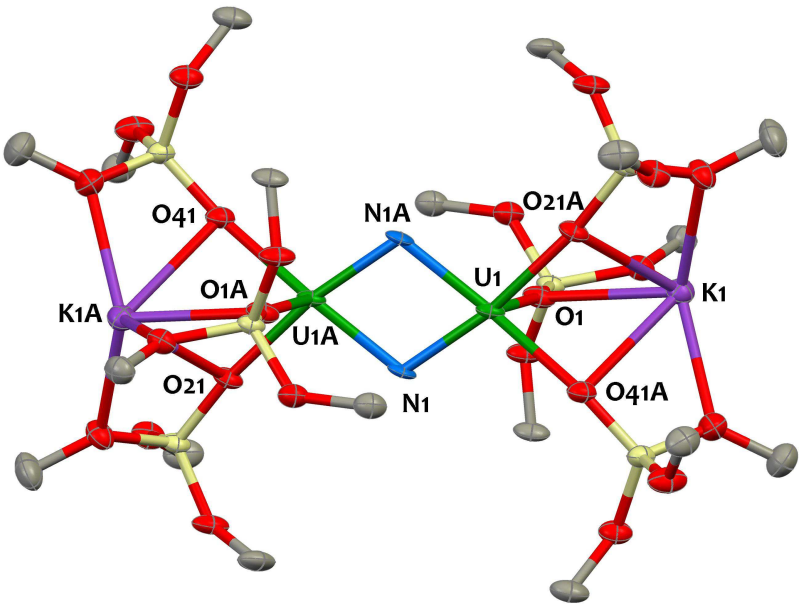

Figure III.36. Solid-state molecular structure of $[KU(\mu\text{-}N)(OSi(O^tBu)_3)_3]_2$ **31** crystallized from toluene. Hydrogen atoms, methyl groups and solvent molecules are omitted for clarity. Uranium (green), silicon (yellow), nitrogen (blue), potassium (purple), oxygen (red) and carbon (grey) atoms are represented with 50% probability ellipsoids. Selected bond distances [Å] and angles (deg): U1-O_{avg} 2.23(3), U1-N1 2.022(5), U1-N1A 2.101(6), U1-U1A 3.2960(6), N1-N1A 2.479(8), U1-N1-U1A 106.1(2).

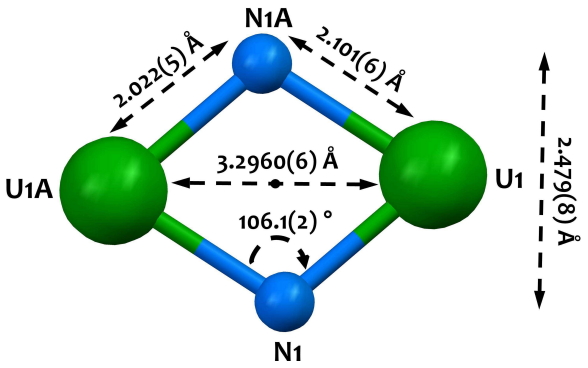

Figure III.37. $U_2(\mu\text{-}N)_2$ core view and metric parameters from the crystal structure of **31**.

The overall neutral charge of the complex is consistent with a formal +V oxidation state for each uranium cation, coordinated to six monoanionic siloxide ligands and two trianionic nitrido ligands in a distorted square pyramid geometry. The U_2N_2 core in **31** is planar (***Figure III.37***), with a N1···N1A separation of 2.479(8) Å ruling out the presence of a chemical bond between the two nitrogen atoms. The U···U separation is 3.2960(6) Å. The short U-N bond distances (2.101(6) and 2.023(5) Å) indicate a multiple bond character and are similar to the values of U-N bond distances reported for other nitride bridged uranium compounds.[157, 211] All the metrical parameters including the U-N-U angles (106.1(2)°) in **31** in the U_2N_2 core (***Figure III.37***) are similar to those observed in the U2N2 core of the U(IV)/U(V) complex supported by a calix[4]tetrapyrrole ligand[157] although a shorter U···U distance is found in **31** (3.2960(6) Å in **31** and 3.355(6) Å in $[\{K(dme)(calix[4]tetrapyrrole)U\}_2(\mu\text{-}NK)_2]$-$[K(dme)_4]$)[157] as expected given the higher oxidation state of the uraniums in **31.** A similar U2N2

diamond-shaped core is also observed in four reported examples of dinitrogen (μ-η^2:η^2-N_2) bridged diuranium complexes[93, 124, 161, 463] but with metrical parameters compatible with the presence of a bridging diazenido ligand.

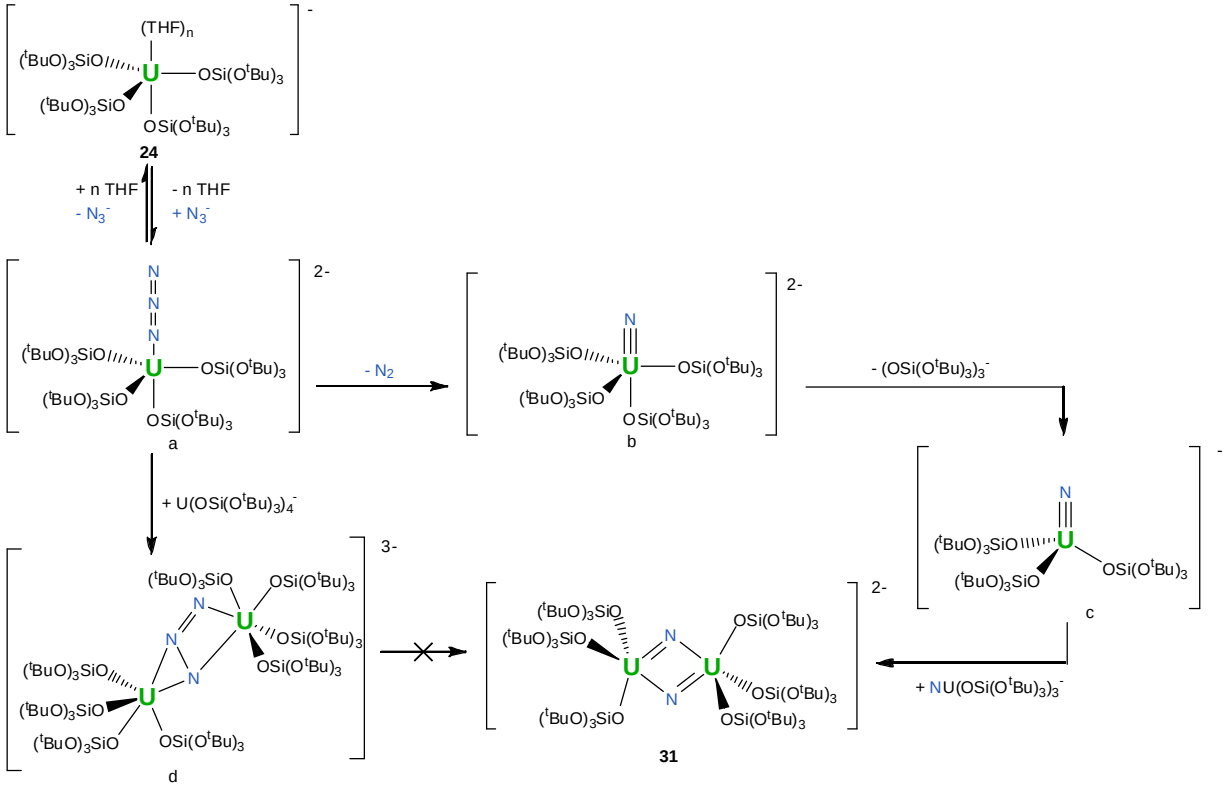

Scheme III.14. Possible pathway for the formation of **31**.

The formation of this unprecedented U(V)/U(V) complex is likely to occur through a highly reactive U(V) terminal nitrido intermediate supported by the crowded environment provided by the four siloxides by elimination of N_2 from a U(III) azido intermediate (***Scheme III.14***). The highly charged tetrakis siloxide terminal nitride will then afford the dinitrido complex through the loss of one siloxide ligand. An alternative intermediate involving a diuranium complex with a bridging azide ligand is less probable. Attempts to prepare complex **31** pure in significant amounts failed, preventing further characterization of this complex. Attempts to trap a transient terminal nitride were also unsuccessful. This is in line with the high reactivity demonstrated by the elusive uranium nitride intermediate [UN{N(SiMe$_3$)$_2$}(C$_5$Me$_5$)$_2$] which engages in intramolecular C-H bond activation yielding the U(IV) amido complex [(C$_5$Me$_5$)(C$_5$Me$_4$CH$_2$NH)U{N(SiMe$_3$)$_2$}].[208] A recently isolated terminal U(V) nitride also shows an extreme reactivity and its isolation and solution stability are very dependent on the experimental conditions, and notably decomposes in ether solvennts.[140] The high reactivity of complex **24** with TMSCl, pyridine or [B(C$_6$F$_6$)]$_3$ prevents their use for trapping a possible terminal nitrido intermediate.[140, 194, 213]

Pale blue/green crystals of the U(IV) complex $[K(18c6)][U(N_3)(OSi(O^tBu)_3)_4]$ **30** were also obtained from the reaction mixture, allowing its structural characterization. The structure, illustrated on ***Figure III.38***, shows that the uranium atom is pentacoordinated in a distorted trigonal bipyramid geometry by four siloxy ligands and one azido ligand in axial position. The U-O bond distances ($U\text{-}O_{avg}$ 2.162(16) Å) are in the range of thoses reported for other U(IV) siloxy systems. The $U\text{-}N_{azido}$ bond distance in **30** (2.351(7) Å) is shorter than that observed in **29** (2.409(4) Å) but falls within the range of distances reported for uranium azide complexes (2.219(6)-2.564(12) Å).[464] Overall, bond distances are in agreement with a +IV oxidation state for the metal, so as the pale blue/green color of the compound which is typical for U(IV) complexes with this ligand platform.

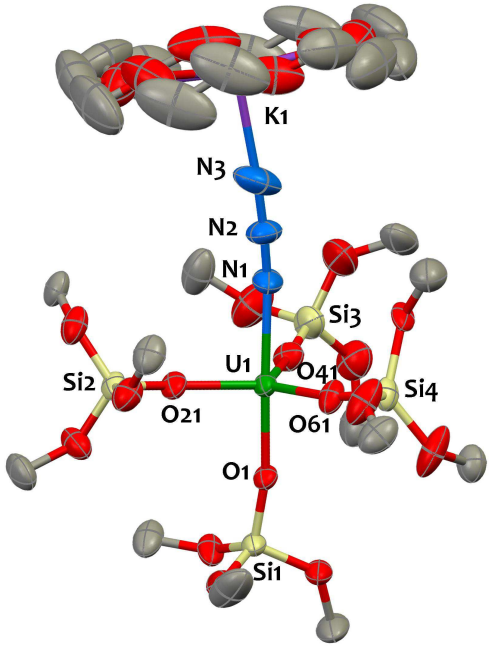

Figure III.38. Solid-state molecular structure of $[K(18c6)U(N_3)(OSi(O^tBu)_3)_4]$ **30** crystallized from toluene. Hydrogen atoms, disordered atoms, methyl groups and solvent molecules are omitted for clarity. Uranium (green), silicon (yellow), nitrogen (blue), oxygen (red) and carbon (grey) atoms are represented with 50% probability ellipsoids. Selected bond distances [Å]: $U1\text{-}O_{avg}$ 2.162(16), U1-N1 2.351(7), N1-N2 1.180(9), N2-N3 1.226(11).

While azido ligands typically adopt bent coordination orientations as is the case in **29**, the azido ligand in **30** adopts an almost linear coordination mode (U1-N1-N2 = 167.9(7)°, N1-N2-N3 = 176.2(11)°). This structural feature is rare[176, 464] and is probably the result of the high steric hindrance in **30** where the azido ligand is encapsulated into a cylindrical cavity defined by the ^{t}Bu groups of the ligands (***Figure III.39***).

Attempts to synthesize complex **30** from the reaction of $[U(OSi(O^tBu)_3)_4]$ **23** with KN_3 and 18c6 were unsuccessful. Indeed, analysis by ^{1}H NMR of the crude reaction mixture showed that multiple products have formed and most probably correspond to ligand redistribution products.

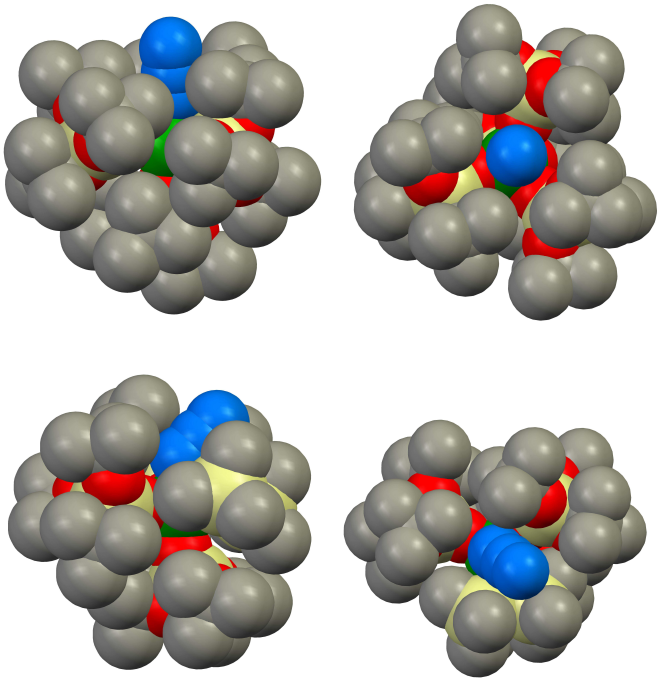

Figure III.39. Comparison of space-filling representations for the U(IV) azido complexes $[K(18c6)U(N_3)(OSi(O^tBu)_3)_4]$ **30** (top) and $[K(18c6)U(N_3)(NSiMe_3)_2(OSi(O^tBu)_3)_3]$ **29** (bottom) crystallized from toluene. [K(18c6)] cation, hydrogen atoms and solvent molecules are omitted for clarity.

III.4.2.2 Reaction of $[U(OSi(O^tBu)_3)_2(\mu\text{-}OSi(O^tBu)_3)]_2$ with CsN_3

Since in the final complex **31** only three coordinated siloxide ligands are bound to the uranium center, we have also investigated the reactivity of the tris-siloxide U(III) complex previously reported.

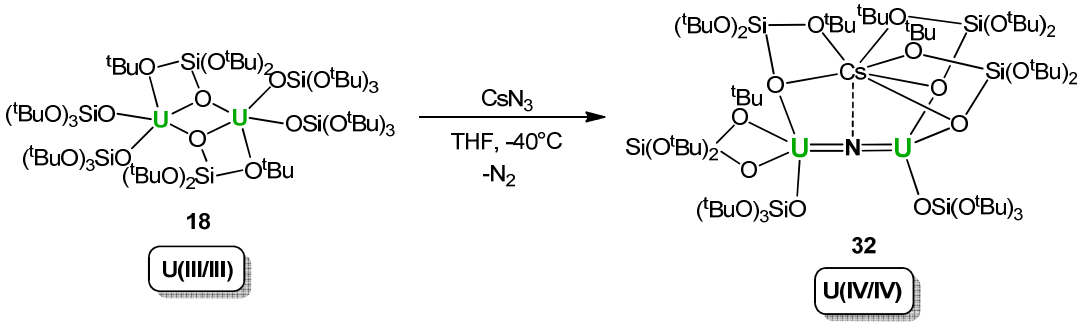

Scheme III.15. Synthesis of the dinuclear uranium(IV)/uranium(IV) nitride $Cs\{(\mu\text{-}N)[U(OSi(O^tBu)_3)_3]_2\}$ **32**.

The reaction of $[U(OSi(O^tBu)_3)_2(\mu\text{-}OSi(O^tBu)_3)]_2$ **18** with cesium azide was performed in THF at -40°C. The reaction proceeds in 24 hours to afford the complex $[Cs(\mu\text{-}N)\{U(OSi(O^tBu)_3)_3\}_2]$ **32** in 47 % yield (***Scheme III.15***). This compound is soluble in THF, toluene, and hexane, and is crystallized upon cooling a saturated toluene solution to -40°C. The crystal structure determined by X-ray studies is presented in ***Figure III.40***. It consists of a heterotrinuclear (U,U,Cs) complex. Two uranium(IV) cations are held together by a bridging nitrido N^{3-} ligand in a nearly linear fashion (U-N-U angle, 170.2(3)°) and with short U-N nitride bond distances (U1-N1 2.058(5) Å, U2-N1 2.079(5) Å) in

agreement with the presence of a multiple U=N bond. These values are close to those observed for the two other reported uranium nitrides containing the linear U=N=U fragment (U=N distance ranging from 2.05 to 2.09 Å and U-N-U angle ranging from 160 to 175 °).[211, 212]

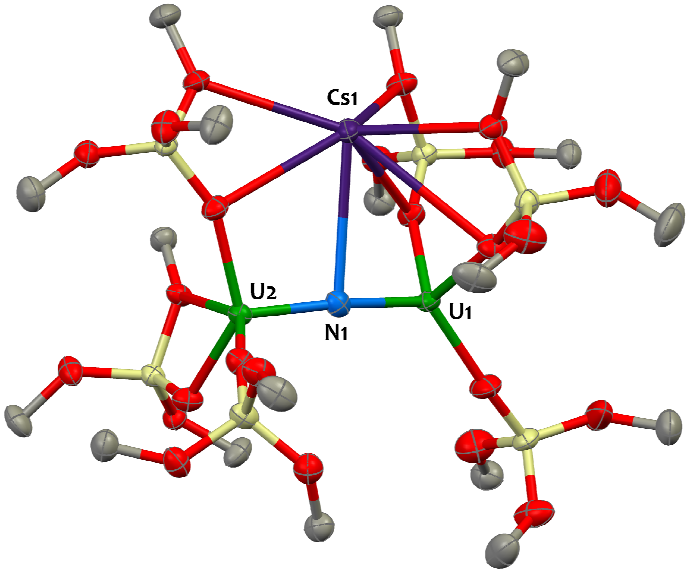

Figure III.40. Solid-state molecular structure of Cs{(μ-N)[U(OSi(O^{t}Bu)$_3$)$_3$]$_2$} **32**, crystallized from a saturated hexane solution. Hydrogen atoms and methyl groups are omitted for clarity. Uranium (green), silicon (yellow), cesium(purple), nitrogen (blue), oxygen (red) and carbon (grey) atoms are represented with 50% probability ellipsoids. Selected bond distances [Å] and angles (deg): U1-N1 2.058(5), U2-N1 2.079(5), U1-O$^-_{avg}$ 2.183(14), U2-OtBu 2.713(4), U2-O$^-_{avg}$ 2.19(3).

Uranium nitride complexes remain rare and complex **32** is only the second example of a dinuclear uranium nitride complex featuring a linear U(IV)-N-U(IV) motif. The closely related dinuclear anionic U(IV)-N-U(IV) complex [(μ-N){U(N(^{t}Bu)Ar)$_3$}$_2$]Na has been previously obtained from the reaction of the tris-amido complex [(THF)U(N(^{t}Bu)Ar)$_3$] (Ar = 3,5-Me$_2$C$_6$H$_3$) with sodium azide.[212] The main difference between the structure of the later anionic nitride complex and that of complex **32** is the neutral character of complex **32** and its heterometallic structure.[212] Notably, a cesium cation is held in the structure through the coordination of three siloxy ligands which act as bridging bidentate μ-η^2 ligands. This cesium cation lies at the exact apical position of the nitride ligand (U1-N1-Cs1 angle: 86.6(1)°), pointing at the 2p$_z$ filled orbital of the N^{3-} ligand, with a Cs-N distance of 3.393(4) Å. The coordination of the alkaline cation by the siloxide ligands results in a disymmetric structure. While U1 is coordinated by one terminal siloxide and two siloxides bridging the U and Cs centers, U2 is coordinated by a terminal siloxide ligand, a siloxide ligand bridging the U and Cs centers and a third one acting as a bidentate O$^-$/O^{t}Bu ligand. Thus U1 is tetracoordinated in a pseudotetrahedral geometry while U2 is pentacoordinated in a distorted square pyramidal environment. The mean value for the U-O$^-$ bond distances (U-O$^-_{avg}$ = 2.19(3) Å) are in the range of those observed in other U(IV)-siloxide complexes. This, together with variable-temperature magnetic moment

measurements (see below) confirm the U(IV)-N^{3-}-U(IV) formulation for the complex. This compound slowly decomposes in THF solution at room temperature over 1 week.

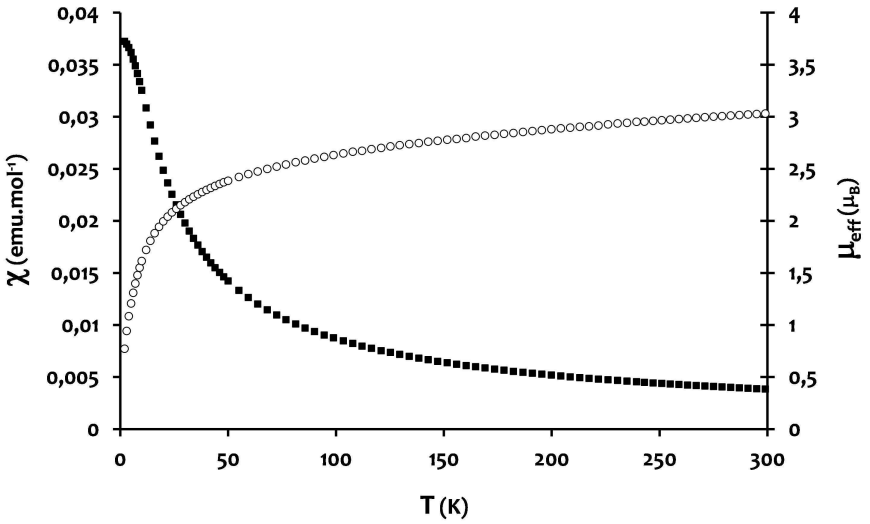

Figure III.41. Temperature-dependant SQUID magnetization data (0.5 T) for complex **32** (data per U center) plotted as χ (open circles) and μ_{eff} (black squares) versus temperature. Data were corrected for diamagnetism.

Magnetic data were collected in the temperature range from 2 to 300 K for **32**. The room temperature effective moment (3.03 μB value for one uranium) falls in the range of the other U(IV) coordination compounds.[26, 70, 340, 465] This value is lower than the theoretical value (3.58 μ_B) calculated for a $5f^2$ ion with a full spin-orbit coupling as commonly observed in tetravalent uranium complexes due to the crystal-field splitting of the Russel-Saunders $^3H_4$ ground term. The magnetic moments for **32** drops off with decreasing temperature due to depopulation of thermally accessible excited states and tends to zero at low temperatures (0.77 μ_B at 2K), a behavior consistent with U(IV) which has a singlet ground state.[141] The inflexion observed at low temperature for the χ plot could be either due to temperature independent paramagnetism often seen for U(IV) ions,[70] or to a magnetic interaction between the uranium ions.

The formation of this linear nitride could involve a mononuclear nitride or an azido bridged dinuclear complex as intermediates (***Scheme III.16***). The later intermediate is supported by the outcome of the reaction of the U(III) complex **18** with the isoelectronic CS_2 molecule which affords the dinuclear complex U(IV)-$(CS_2)^{2-}$-U(IV) complex (see section III.3.1). The different outcome of the reaction with CsN_3 for the complexes **18** and **24** clearly underlines the importance of the coordination environment in determining the structure of the final product. The isolation of the bis-nitride U(V) dimer suggests that it might be possible to find conditions leading to mononuclear nitrides using siloxides as supporting ligands. Moreover the isolation of the heterotrimetallic complex **32** provides a nice precursor for heteropolymetallic nitrido systems.

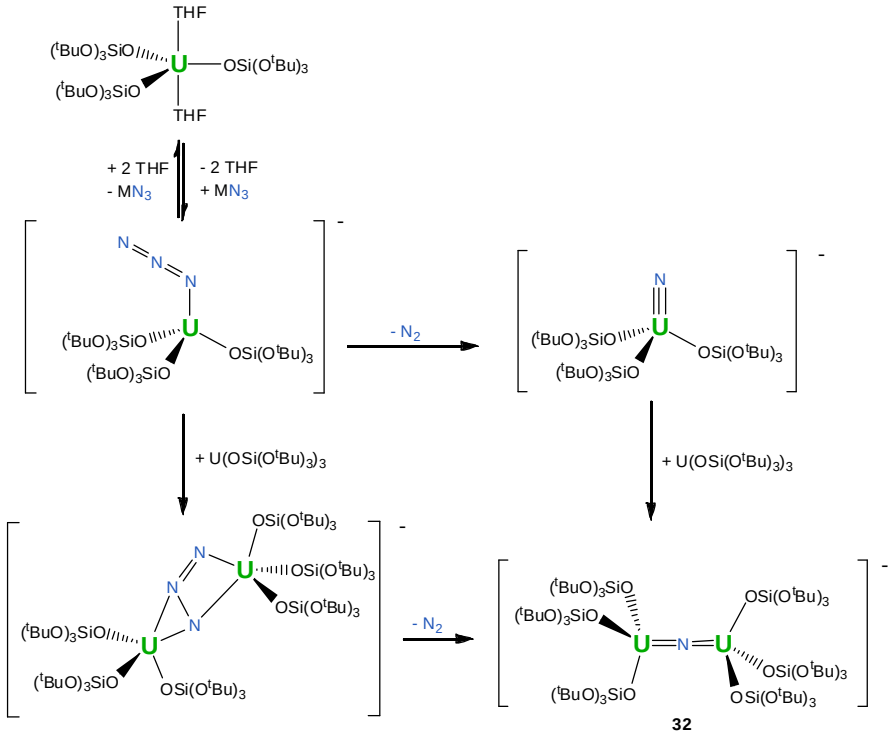

32

Scheme III.16. Possible pathways for the formation of **32**.

III.5 Reactivity with arenes

III.5.1 Isolation of a family of three toluene-bridged diuranium inverted-sandwich complexes

Further indication of the high reactivity and the interest of the dinuclear U(III) complex $[U(OSi(O^tBu)_3)_2(\mu\text{-}OSi(O^tBu)_3)]_2$ **18** in the study of uranium-mediated small molecule activation is the isolation of the inverted sandwich complex $[U(OSi(O^tBu)_3)_3(\mu\text{-}\eta^6,\eta^6\text{-toluene}]_2$ **33** from the reaction of **18** with toluene in hexane (***Scheme III.17***).

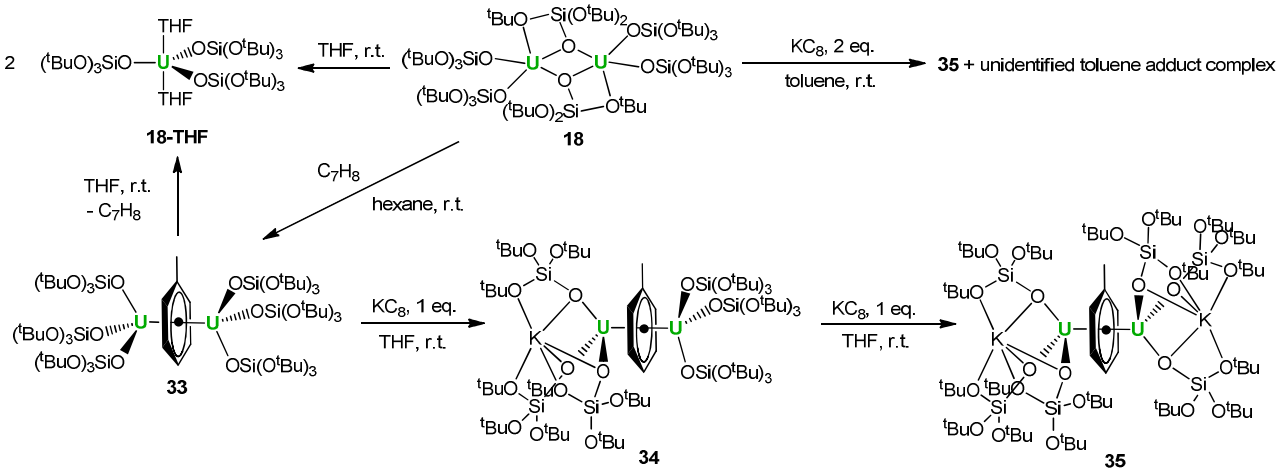

Scheme III.17. Synthesis of the inverted-sandwich complexes **33**, **34** and **35**.

33 is insoluble in toluene and hexane but can be solubilized in THF. The proton NMR of complex **33** in deuterated THF solution shows highly shifted resonances for the toluene protons (***Table III.2***) in agreement with the presence of the inverted-sandwich complex in solution. A single peak for the siloxide ligand is observed as expected for a C_3 symmetric species in solution. This complex is thermally resistant in the solid state when heated to 70°C for 2 hours. However, proton NMR studies show that the toluene adduct **33** decomposes in THF affording the $[U(OSi(O^tBu)_3)_3(THF)_2]$, **18-THF** complex (Scheme 2). Dissociation starts immediately after dissolution of **33** in THF and is complete after 12 hours. The displacement of the arene moiety by THF has precedents in U(III)-arene compounds,[231] but to the best of our knowledge has not been reported for diuranium inverted-sandwich complexes.

Structural studies of complex **33** (see below) suggest the presence of uranium in a higher oxidation state and of a reduced toluene moiety. Thus, in the presence of THF which can coordinate the metal center, the electrons stored in the reduced toluene are transferred back to the uranium center

promoting the release of the coordinated toluene and affording **18-THF**. This process is reminiscent of the reversible intramolecular electron transfer driven by the coordination of THF previously reported by Kiplinger and coworkers in a systems associating U(III) to the redox active ligand $(dpp\text{-}BIAN)^{2-}$ (dpp-BIAN = 1,2-bis(2,6-diisopropylphenylimino)acenaphthylene) (see section I.4.1). The coordination of THF results in the transfer of one electron from the $(dpp\text{-}BIAN)^{2-}$ ligand to the U(IV) center to yield a U^{III}-π^{*3} configuration.[114]

As discussed in introduction, recently reported diuranium inverted-sandwich complexes were formed through the reduction of uranium complexes with potassium metal or similar reducing agents or through U(III) disproportionation (see section I.3.4.5). The unprecedented formation of complex **33** from the spontaneous reduction of toluene in the absence of a strong reducing agent (potassium) demonstrates the novel reactivity of the low-valent uranium complex **18**.

Reduction of complex **33** with one equivalent of potassium graphite in THF affords (***Scheme III.17***), after work up and recrystallization from toluene, black crystals of the mixed-valent toluene-bridged diuranium complex $[K\{U(OSi(O^tBu)_3)_3\}_2(\mu\text{-}\eta^6\text{:}\eta^6\text{-}C_7H_8)]$ **34**. A few mixed-valent diuranium complexes have been structurally characterized[64, 157, 212, 424, 425, 466-468] with only one example of mixed valent inverted-sandwich complex.[255] Such species are attractive for the study of the possible presence of valence delocalization in uranium systems.[300, 468]

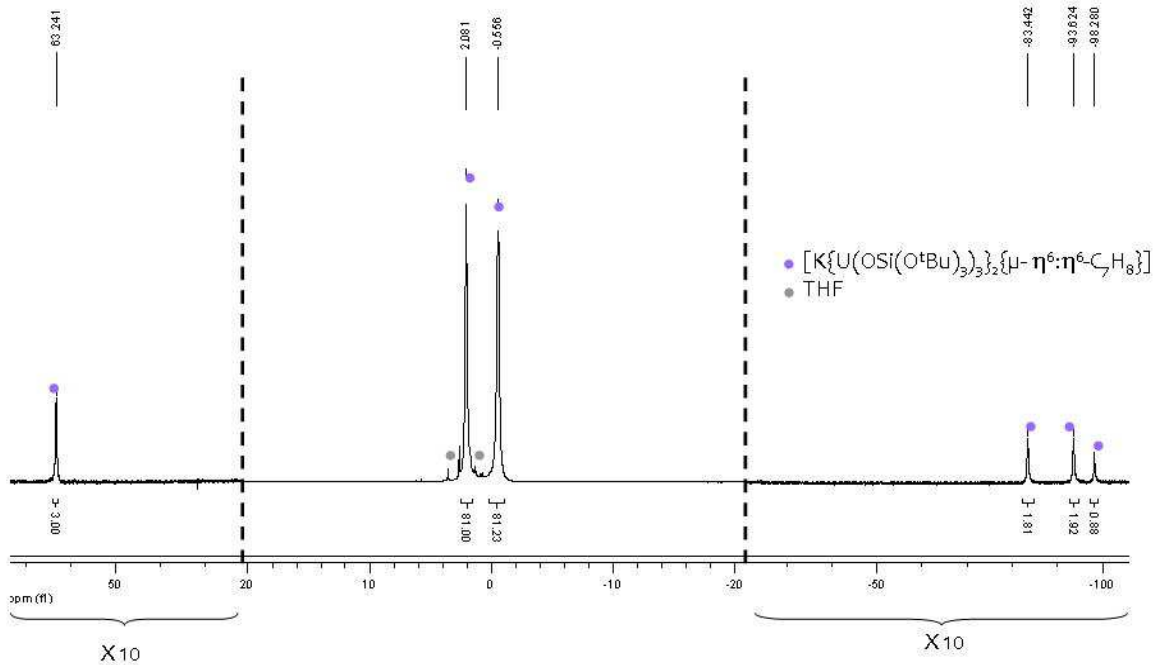

Figure III.42. ^{1}H NMR spectrum (298 K, 200 MHz) in THF-d_8 of **34**.

Table III.2. ^{1}H NMR chemical shifts (ppm) for the toluene moiety in deuterated THF solutions of complexes **33, 34, 35** and **35-18c6**.

Compound	CH_3	$H_{aro(o/m)}$		$H_{aro(p)}$
33	82.9	-112,7	-122,4	-137,9
34	63.3	-83,5	-93,7	-98,4
35	16.7	-76,3	-76,8	-72,2
35-18c6	19.8	-80.4	-80,6	-74,5

The fully-reduced complex $[K_2\{U(OSi(O^tBu)_3)_3\}_2(\mu\text{-}\eta^6\text{:}\eta^6\text{-}C_7H_8)]$ **35** is obtained when using two equivalents of potassium graphite under similar reaction conditions (***Scheme III.17***). Contrary to what was observed for **33,** the reduced arene complex **35** is stable in THF solution up to one week. Two resonances are observed in the ^{1}H NMR spectrum in deuterated THF solution for the siloxide ligand in **34** (***Figure III.42***), in agreement with the presence of an asymmetric dimeric complex in solution, while a single resonance is observed for the siloxide ligand in the ^{1}H NMR spectrum of **33** and **35** in deuterated THF solution. These results indicate that the coordination of the potassium counterion by three $OSi(O^tBu)_3$ ligands observed in the solid state (see next section) is maintained in solution. Interestingly, four well-resolved proton resonances for the toluene moiety assigned to the methyl group, ortho/para and meta protons are observed in the ^{1}H NMR spectra (THF-d_8, 200 MHz, 298 K) of complexes **33**, **34** (***Figure III.42***) and **35**. The comparison of the chemical shifts (***Table III.2***) for the arene moiety in each complex shows a clear decrease in the range of chemical shifts from **33** to **35**. The methyl resonances decrease from 82.9 in **33** to 16.7 ppm in **35**. Similarly the resonances for the aromatic protons span the range -112.7 to -137.9 ppm in **33** and are decreased to -72.2 to -76.8 ppm in **35**.

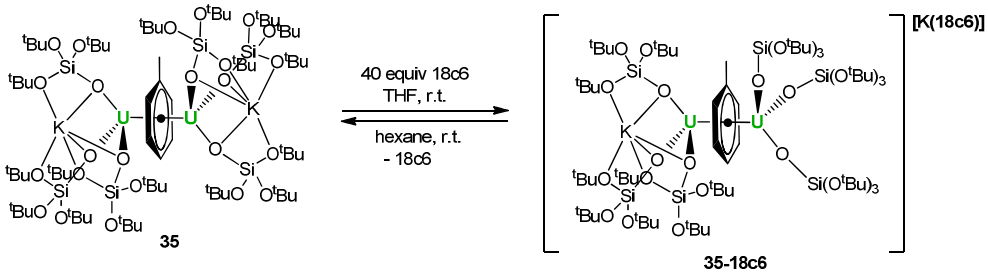

Scheme III.18. Reaction of **35** with 18c6, affording **35-18c6**.

The presence of two coordinated potassium counterions in the solution structure of **35** was confirmed by reacting it with 18c6 crown ether. The proton NMR spectrum of the resulting reaction mixture shows the appearance of a new set of signals with two resonances for the siloxide ligands in agreement with the presence of an asymmetric solution structure (***Figure III.43***). This indicates the formation of the new solution species $[K(18c6)][K\{U(OSi(O^tBu)_3)_3\}_2(\mu\text{-}\eta^6\text{:}\eta^6\text{-}C_7H_8)]$ **35-18c6** where one

potassium cation is no longer coordinated to the siloxides in solution (***Scheme III.18***). A strong excess of 18c6 (40 eq.) is necessary to fully convert **35** into **35-18c6**, confirming that the K^+ cations in **35** are strongly coordinated by the O_6 pocket formed by the three silanol ligands. Even in the presence of a large excess of 18c6 only the new set of signals assigned to **35-18c6** is present in the NMR spectrum indicating that one potassium cation remains coordinated to one set of three siloxide ligands. The four characteristic resonances of the coordinated arene observed in the ^{1}H NMR spectrum of **35-18c6** (***Table III.2***) have chemical shifts close to those of in **35** supporting the proposed formulation of **35-18c6**. This indicates the presence of a similar electronic structure in the two species. Single crystals for **35-18c6** could not be obtained from THF. When the THF is removed and the residue dissolved in hexane, only black crystals of **35** are obtained suggesting that the original structure is restored in hexane even in the presence of 18c6.

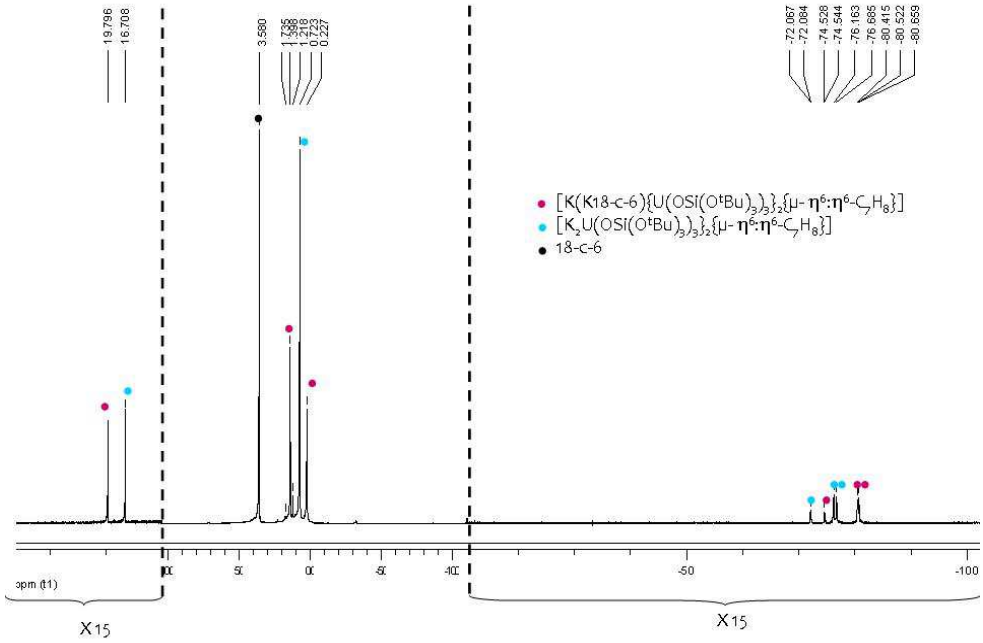

Figure III.43. ^{1}H NMR spectrum (298 K, 200 MHz) of **35** in THF-d_8 after addition of 8 equivalents of 18c6, showing its partial conversion into **35-18c6**.

We have also explored the possibility of isolating **35** directly from the reduction of the U(III) precursor **18**. However, the treatment of **18** with two equivalents of potassium graphite in toluene afforded a mixture of two products (***Scheme III.17***). The ^{1}H NMR spectrum of the crude mixture shows the formation of **35** together with another unidentified species that exhibits 4 shifted resonances most probably corresponding to a coordinated toluene fragment. Complex **35** can be isolated by using this method after re-crystallisation in 40% yield.

In the previously reported uranium inverted-sandwich systems the presence of δ back-bonding from the uranium center to the π* orbitals of the arene ligand has been established.[74, 252, 253, 255, 257, 258] Such

δ back-bonding interactions are most likely present in the complexes **33, 34** and **35,** resulting in the transfer of electron density to the arene fragment.

III.5.2 Structural comparisons

The crystals and molecular structures of complexes **33, 34** and **35** were determined by X-ray crystallography and they are presented in ***Figure III.44***. In the three structures, the uranium atoms are both coordinated by three $OSi(O^tBu)_3$ ligands in a monodentate terminal fashion and by a planar $\mu\text{-}\eta^6\text{:}\eta^6$-bridging toluene molecule perpendicular to the pseudo-C_3 axis of the molecule. The three structures differ in their state of charge resulting in the presence of one and two potassium counterions in the structures of **34** and **35** respectively. In complex **34** the potassium cation is coordinated by six oxygen atoms of three bridging bidentate $\mu\text{-}\eta^2$ siloxides bound to the same uranium center. In complex **35** each crystallographically equivalent $\{U(OSi(O^tBu)_3)\}$ moiety binds a potassium cation through three bridging bidentate $\mu\text{-}\eta^2$ siloxides.

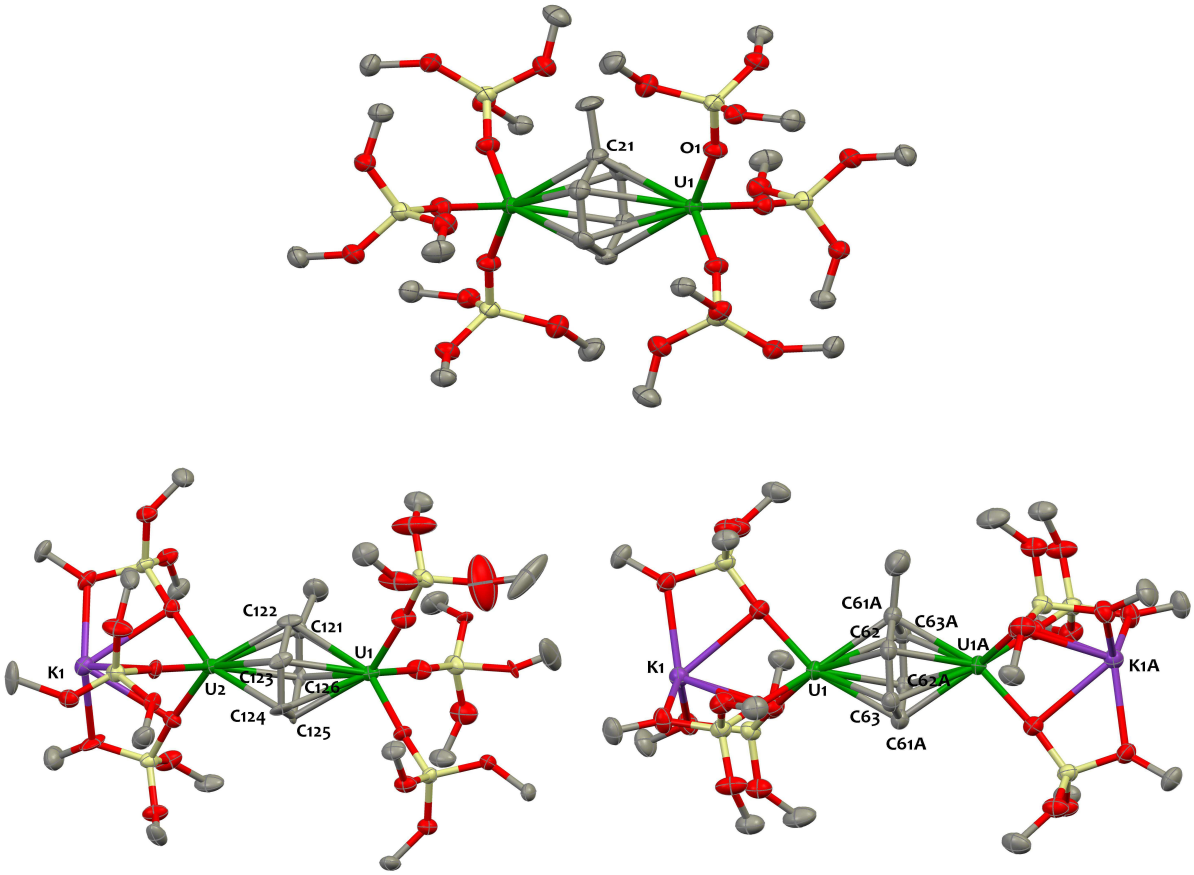

Figure III.44. Solid-state molecular structures of the inverted-arene sandwich complexes. (top) $[\{U(OSi(O^tBu)_3)_3\}_2(\mu\text{-}\eta^6\text{:}\eta^6\text{-}C_7H_8)]$ **33** ; (bottom-left) $[K\{U(OSi(O^tBu)_3)_3\}_2(\mu\text{-}\eta^6\text{:}\eta^6\text{-}C_7H_8)]$ **34** ; (bottom-right) $[K_2\{U(OSi(O^tBu)_3)_3\}_2(\mu\text{-}\eta^6\text{:}\eta^6\text{-}C_7H_8)]$ **35**. Hydrogen atoms, methyl groups, solvent molecules and disorder are omitted for clarity. Uranium (green), potassium (purple), silicon (yellow), oxygen (red) and carbon (prey) atoms are represented with 50% probability ellipsoids.

Table III.3. Bond distances [Å] in complexes **33-35**.

Compound **33**		Compound **35**		Compound **34**			
U(1)-O(1)#1	2.117(2)	U(1)-O(41)	2.233(2)	U(1)-O(41)	2.110(8)	U(2)-O(61)	2.179(8)
U(1)-O(1)#2	2.117(2)	U(1)-O(1	2.242(2)	U(1)-O(1)	2.139(9)	U(2)-O(101)	2.183(8)
U(1)-O(1)	2.117(2)	U(1)-O(21)	2.245(3)	U(1)-O(21)	2.140(8)	U(2)-O(81)	2.185(8)
U(1)-O_{avg}	2.117(2)	U(1)-O_{avg}	2.240(6)	U(1)-O_{avg}	2.130(17)	U(2)-O_{avg}	2.182(3)
U(1)-C(21)#3	2.689(3)	U(1)-C(62)	2.589(4)	U(1)-C(125)	2.602(9)	U(2)-C(124)	2.624(11)
U(1)-C(21)#4	2.690(3)	U(1)-C(63)#1	2.595(3)	U(1)-C(123)	2.626(12)	U(2)-C(123)	2.626(11)
U(1)-C(21)#5	2.690(3)	U(1)-C(61)#1	2.597(4)	U(1)-C(122)	2.630(12)	U(2)-C(126)	2.629(10)
U(1)-C(21)#1	2.695(3)	U(1)-C(61)	2.615(4)	U(1)-C(121)	2.644(10)	U(2)-C(121)	2.659(11)
U(1)-C(21)#2	2.695(3)	U(1)-C(62)#1	2.617(3)	U(1)-C(124)	2.657(13)	U(2)-C(125)	2.660(9)
U(1)-C(21)	2.695(3)	U(1)-C(63)	2.621(3)	U(1)-C(126)	2.669(11)	U(2)-C(122)	2.674(13)
U(1)-C_{avg}	2.693(4)	U(1)-C_{avg}	2.607(14)	U(1)-C_{avg}	2.64(2)	U(2)-C_{avg}	2.65(2)
C-C_{avg}	1.432(3)	C-C_{avg}	1.456(8)	C-C_{avg}	1.439(17)		
U···U	4.5596(3)	U···U	4.3259(3)	U···U	4.4313(3)		

In ***Table III.3*** are reported the most relevant structural parameters for complexes **33, 34**, and **35**. The toluene C-C bond distances in complexes **33-35** are comparable and are slightly longer (0.04 Å - 0.06 Å) than what found in free toluene.[469] They are also longer than the mean value of the C-C distance reported for the potassium bound toluene radical anion (1.398(2) Å).[243] Such distances are similar to those observed in other systems containing reduced arenes (arene^{2-} or arene^{4-}).[118, 250] While these data suggest a certain degree of electron delocalization from the uranium center on the arene ring, they cannot be used alone to determine the net charge of the toluene moiety.

The mean value of the U-C bond distances in these systems is considerably shorter than those found in U(III)[92, 231, 234] and U(IV)[232, 233] complexes of neutral arenes (~2.93 Å), in agreement with an anionic formulation for the toluene moiety. The value for the U-C_{avg} bond distance in **33** (2.693(4) Å) is longer (ca. ~0.1 Å) than what reported for the neutral arene bridged complexes $[L_2U]_2(\mu\text{-}\eta^6\text{:}\eta^6\text{-}C_6H_5\text{-}R)$ (L= C_5Me_5, bulky amido, methanide, iodide and aryloxide ; R= H, Me) [74, 118, 252, 257] usually formulated as U(III)-(tol^{2-})-U(III) systems, but compares well with those observed in the neutral triamido $[Ts^{Xy}U]_2(\mu\text{-}\eta^6\text{:}\eta^6\text{-}C_7H_8)$ (Ts^{Xy} = HC-($SiMe_2NAr)_3$) complex (2.676(15) Å) described as a U(V)-(tol^{4-})-U(V) system.[253, 259] Several organouranium(V) complexes have been reported[60] with U-C (cyclopentadienyl) distance ranging from 2.73 -2.76 Å and significantly shorter distances are observed in a cycloheptatrienyl sandwich complex of U(V) (2.53(2) Å).[470] The values for the U-C_{avg} bond distance in **34** (2.65 Å) and in **35** (2.607 Å) are similar to those reported for monoanionic and dianionic arene complexes.[255]

The arene is nearly planar in all complexes with a mean deviation from the plane of 0.003 Å in **33**, 0.018 Å in **34** and 0.015 Å in **35**. The deviation of the bridging aromatic ring can be used as an indicator

of the degree of reduction of bridging arene. For example, in the complexes $[(C_5H_5)_2U]_2(\mu\text{-}\eta^6\text{:}\eta^6\text{-}C_6H_6)$ and $[\{(Me_3Si)_2N\}(C_5Me_5)U]_2(\mu\text{-}\eta^6\text{:}\eta^6\text{-}C_6H_6)$ described as U(III)-(tol^{2-})-U(III) species, the benzene adopts a chair conformation in agreement with the presence of an antiaromatic reduced arene dianion.[252, 305] The presence of a planar arrangement of the carbon atoms in the arene ring in complexes **33**, **34** and **35** is compatible with the presence of a 10 pi-electron aromatic system.[250] However, the distorsion from planarity is not always observed in systems where structural and spectroscopic data have been interpreted in term of the presence of an arene dianion.[118, 254, 255]

Some significant differences in the metal-ligand bond distances are found across the series. The U-$O_{siloxide}$ average bond distance in **33** is shorter by 0.12 Å than that in 3**5**. In contrast, the U-C average bond distance is shortened by 0.09 Å in the reduced complex **35**. Due the presence of the potassium cations in **35** the structural comparison with **33** is not straightforward, but the observed shortening of the U-C bond lengths in the reduced complex is in agreement with an increased δ back-bonding interaction to the arene moiety from the metal center. Although the error on the distances is higher in the crystal structure of complex **34,** the values of the U-C and U-$O_{siloxide}$ average bond distances in complex **34** are intermediate between thoses of **33** and **35**.

III.5.3 Solid-State Magnetic Susceptibility

Magnetic data of uranium compounds are generally difficult to analyze due to the lack of accurate theoretical models. The effective magnetic moments reported at room temperature for either U(III), U(IV) or U(V) complexes display very large ranges rendering difficult the assignment of the metal oxidation state.[26, 60, 340] Moreover, examples of unambiguous magnetic coupling between uranium ions in molecular systems remain very limited[43, 65, 219, 315, 451, 471] although such interactions are at the origins of the single molecule magnet behavior recently reported for few multinuclear U(III) and U(V) complexes.[66, 118, 313]

Temperature-dependent magnetic data were also collected for the three arene inverted-sandwiches.

The room temperature magnetic moment for **33** (1.35 μ_B; value for one uranium ; ***Figure III.45***-a) is much lower compared to what is theoretically expected for a U^{3+} (3.62 μ_B; $^4I_{9/2}$ ground term) or a U^{4+} free ion (3.58 μ_B; $^3H_4$ ground term) ; and also lower than what is more commonly observed in U(III) and U(IV) complexes.[26, 43, 146, 167, 176, 340, 347, 422, 423, 472] This value, even if lower than the theoretical one expected for a free U^{5+} ion (2.54 μ_B ; $^2F_{5/2}$ ground term) compares better with the values of magnetic moments reported for U(V) systems.[58, 60, 63, 184, 203, 219, 462] The effective magnetic moment for **33** shows

a steady decrease when the temperature is lowered to reach a value of 0.31 μ_B (value for one uranium) at 2 K, a temperature response characteristic of $5f^1$ systems.[63, 144, 462, 473]

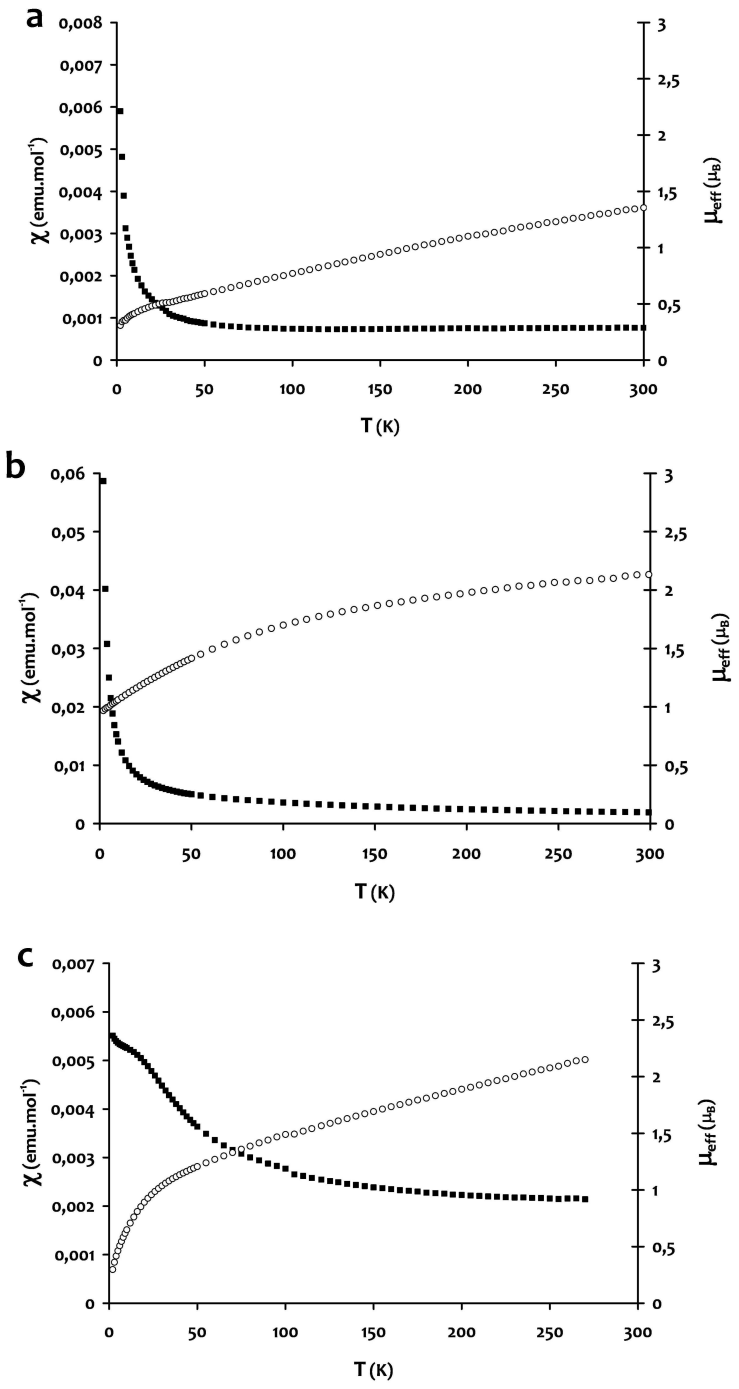

Figure III.45. Temperature-dependant SQUID magnetization data (0.5 T) for complexes **33** (a), **34** (b) and **35** (c) (data per U center) plotted as χ (open circles) and μ_{eff} (black squares) versus temperature. Data were corrected for diamagnetism and reproducibility was checked on independently synthesized samples.

The value of the magnetic moment for **35** at 300 K (2.23 μ_B ; value for one uranium) is much higher than the one of **33** and is consistent with the values reported for molecular U(IV) compounds.[26, 70, 340,

[465] This value drops off gradually with decreasing temperature to 1.26 μ_B at 50 K. Below 25 K the magnetic susceptibility of complex **35** shows a temperature-independent paramagnetism (TIP) behavior (***Figure III.45***-c). A TIP only behavior is typically observed in molecular U(IV) compounds [26, 70, 209, 340, 342] and therefore the overall magnetic behavior of **35** could be consistent with two $5f^2$ uranium ions.

The average μ_{eff} for **34** at 300 K (2.13 μ_B ; value for one uranium) is in between the values observed for the complexes **33** and **35,** as anticipated for a mixed-valent complex with $5f^1$ and $5f^2$ centers behaving as independent paramagnets. The magnetic moment decreases with the temperature to reach 0.97 μ_B *per* U center at 2K. The magnetic susceptibility do not shows evidence of TIP but it could be masked by the U(V) paramagnetism.

In the end, the recorded magnetic data do not allow a clear assignment of the electronic structure in each arene bridged complex, but the overall magnetic behavior could be consistent with the electronic descriptions proposed for related systems in litterature. Future studies involving DFT and/or XANES investigations might be fruitful to further elucidate the nature of the electronic structure of these species.

III.5.4 K^+-induced reactivity

The considerable difficulty in removing coordinated potassium suggests that its presence could have an important effect in the reduction process. This prompted us to investigate the reaction of **33** with potassium triflate.

Complex **33** reacts quickly in the presence of one equivalent of potassium cations to yield the monoanionic analogue **34** (***Scheme III.19***). The reaction was performed in THF in the presence of 0.67 eq. of potassium triflate. The ^{1}H NMR spectrum recorded for the reaction mixture clearly shows the presence of **34**. A second signal at 1.58 ppm which is integrating for 81 protons is attributed to the ^{t}Bu moieties in $[U(OSi(O^tBu)_3)_3(OTf)(THF)_2]$ **36**.

The presence of both species was confirmed by single-crystal X-ray diffraction. The structure of **36** is represented in ***Figure III.46***. The three siloxide ligands in **36** are coordinated in a η^1 terminal fashion in a *fac* arrangement. The coordination sphere of the U(IV) cation is completed to 6 through the coordination of a triflate anion and two THF solvent molecules within a distorted octahedral geometry. The U-$O_{triflate}$ (2.421(13) Å) and U-$O_{siloxide}$ (2.129(8) Å) average bond distances are in the range of those reported for U(IV) complexes.

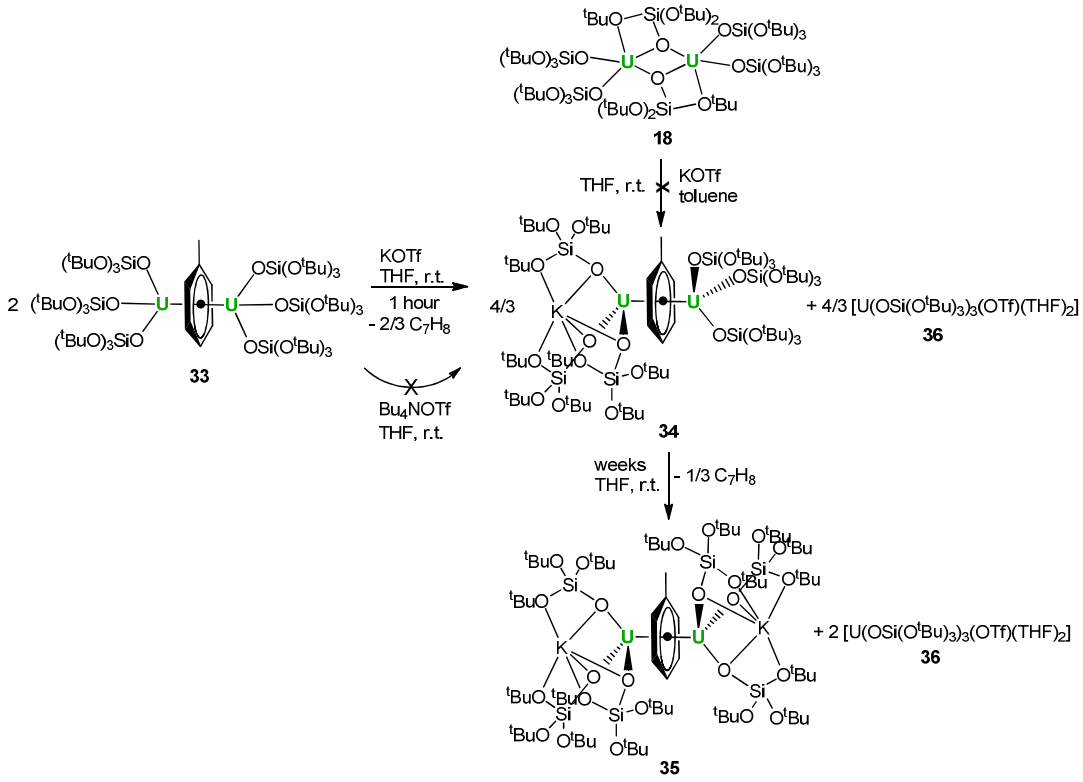

Scheme III.19. K^+-induced disproportionation of **33**.

The crucial role of the coordination of potassium cations in the disproportionation was also probed by replacing KOTf with Bu_4NOTf. Indeed, no conversion of **33** into **34** when using Bu_4NOTf, ruling out a possible effect of the triflate anion and confirming the role of potassium in this transformation.

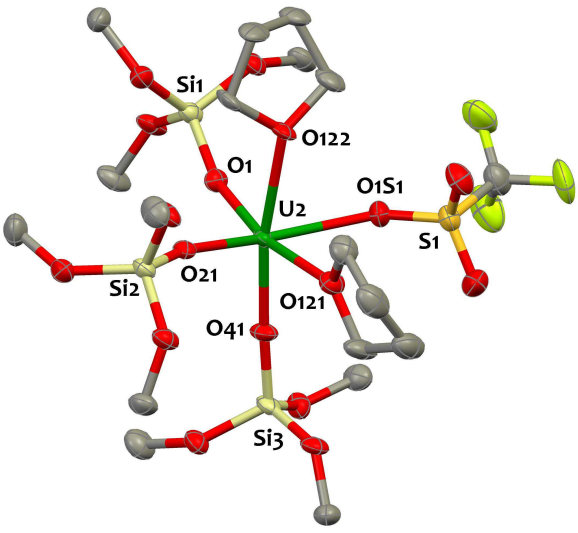

Figure III.46. Solid-state molecular structure of $[U(OSi(O^tBu)_3)_3(OTf)(THF)_2]$ **36**. Hydrogen atoms, methyl groups and solvent molecules are omitted for clarity. Uranium (dark green), fluorine (pale green), silicon (pale yellow), sulphur (dark yellow), oxygen (red) and carbon (prey) atoms are represented with 50% probability ellipsoids Selected bond distances [Å]: U-$O_{siloxide}$ 2.129(8), U-O_{OTf} 2.421(13), U-O_{THF} 2.47(2).

Monitoring the reaction of **33** with two equivalents of KOTf by ^1H NMR shows that while the first step of the reaction yielding **34** is fast (less than 1 hour at room temperature), **34** slowly reacts with

another potassium cation to afford **35**. The second step of the reaction is obviously kinetically slow (more than 4 weeks at room temperature to reach completion). Performing the reaction with an excess (20 eq.) of KOTf does not accelerate the reaction.

Knowing that the toluene moiety in **33** is readily displaced by THF, a conceivable mechanism could involve first the disruption of the toluene adduct to form the reactive fragment $[U(OSi(O^tBu)_3)_3(THF)_2]$ **33-THF** that would react with KOTf. However, when $[U(OSi(O^tBu)_3)_3(THF)_2]$ is exposed to KOTf in presence of toluene, no reactivity is observed. This is in agreement with the fact that the reactive species involved in this process is the toluene-bridged complex **33**.

The conversion of state charge promoted by addition of alkali ion is, to the best of our knowledge, unprecedented in the chemistry of μ-η^6:η^6-arene bridged di-metal complexes. For instance J. Arnold and coworkers[251] have very recently reported a different behavior for a di-niobium inverted arene sandwich in the presence of protons. Protonation of the neutral complex $[Nb(BDI)(N^tBu)(C_6H_6)]$ (BDI = N,N′-diisopropylbenzene-β-diketiminate) affords the mono- and dicationic μ-η^6:η^6-benzene complexes which are stable and show the same $4d^2$ electronic configurations. The reaction of the sterically crowded complex $[\{(C_5H_5)_2U\}_2(\mu\text{-}\eta^6\text{:}\eta^6\text{-}C_6H_6)]$ with $KN(SiMe_3)_2$ reported by Evans and coworkers[252] results in the displacement of two cyclopentadienyl groups by two amido ligands again without any significant change in the complex stability or the electronic structure.

III.6 Concluding remarks

The work presented in this chapter focused on the preparation of low-valent uranium complexes supported by the $OSi(O^tBu)_3$ ligand. Two different synthetic routes have been investigated : the protonolysis reaction between $[U\{N(SiMe_3)_2\}_3]$ and the protonated ligand resulted in the isolation of a dimeric U(III)/U(III) complex **18** while a stable homoleptic *ate* U(III) tetra-siloxide complex **24** has been prepared by reduction of its U(IV) analogue.

We have demonstrated that the trivalent uranium centers promotes the reductive C-O bond cleavage of the $OSi(O^tBu)_3$ ligand, providing a novel controlled route to polymetallic heteroleptic complexes that could hardly be obtained by using other synthetic ways. The structure of these molecular decomposition products provide important unprecedented information on the molecular intermediates involved in the formation of metal silicate materials from molecular precursors. Preliminary investigations on the magnetic properties of these polynuclear complexes reported here show that interesting magnetic couplings can be achieved, and more detailed investigations should be undertaken to deternine the exact role played by the ligand and the intermetallic distance in the U···U magnetic communication. Given the potential of U(III) complexes to behave as single molecule magnets,[422, 423, 472, 474, 475] interesting behavior can be anticipated. Moreover, the isolated compounds provide interesting precursors for accessing novel uranium ceramics.

The U(III) siloxy complexes proved to be efficient reducing agents able to promote the activation of several small molecules. The reaction of **18** with heteroallenes CS_2 and CO_2 leads to the isolation of a rare CS_2 sandwich complex of uranium and to the reductive disproportionation of CO_2 to carbonate and CO, respectively. This highlights the interest of $OSi(O^tBu)_3$ as supporting ligand in low-valent uranium chemistry. Particularly, DFT studies have shown that the formation of the carbonate complex **26** involves the addition of a second CO_2 molecule onto a U(IV)-CO_2-U(IV) intermediate followed by CO elimination instead of the formation of a bridging oxo intermediate, contrary to what observed with polyphenolate ligands. This is ascribed to the particular properties of the siloxy ligand, and notably its ability to adopt monodentate or bidentate coordination modes.

The reactivity of **18** and **24** with organic and inorganic azides lead to the formation of very different products. Notably, while the reaction of the U(III) tetrakis-siloxide with organic azides affords novel examples of stable U(V) imido complexes, the same reaction with the tris-siloxide U(III) complex leads to the isolation of a dimeric bis(imido) complex of U(VI) featuring trans-imido groups. The formation of trans-bis(imido) species from the azide route is unprecedented, and is likely to result

from the disproportionation of an unstable U(V) imido intermediate as supported by the isolation of a U(IV) by-product. A very different outcome is also observed in the reaction of the U(III) tris- and tetrakis- siloxide complexes with CsN_3. A clean reaction occurs with the U(III) tris-siloxide complex leading to a heterometallic nitride bridged diuranium(IV) complex. In contrast the reaction of the U(III) tetrakis-siloxide leads to the isolation of a rare di-nitrido bridged di-uranium(V) complex which is likely to form through a terminal nitride intermediate. These results show that the siloxide ligands provide a versatile tool to prepare novel mononuclear and polynuclear species containing uranium-nitrogen multiple bonds. The different outcome of the reaction of the U(III) tris and tetra- siloxide complexes with organic and inorganic azides demonstrate the important role of the steric environment in stabilizing U(V) imido species. Future studies might be directed to investigate the reactivity of these systems and to determine the reaction conditions and the starting materials required to cleanly reach terminal nitride species.

Complex **18** can also promote the spontaneous reduction of toluene leading to a new type of di-uranium inverted sandwich complex $[\{U(OSi(O^tBu)_3)_3\}_2(\mu\text{-}\eta^6\text{:}\eta^6\text{-}C_7H_8)]$ **33** supported by 3 siloxide ligands per U center. This parent arene-bridged complex is selectively reduced using stoichiometric amounts of KC_8 to its monoanionic and dianionic analogues. This offered us the possibility of comparing the properties of a family of uranium inverted-sandwich complexes in three states of charge. Moreover, the addition of K^+ cations to these arene-inverted complexes promoted their unprecedented disproportionation. Even if electron density is transferred to toluene, it is important to keep in mind that these species are substantial reducing agents and the full scope of reactivity of these arene-inverted sandwich compounds needs to be explored.

CHAPTER IV
General Conclusion and Perspectives

The global objective of this work was related to the development of novel electron-rich f-elements systems presenting original reductive properties. Keeping this idea in mind during this PhD work, we have designed and synthesized several low-valent and low-valent synthetic equivalents of uranium complexes, and we have studied their coordination properties and their redox reactivity. This work contributed to a better understanding of the fundamental chemical properties of low-valent uranium.

Firstly, we have shown that novel multi-electron redox chemistry can take place at themodynamically stable U(IV) centers through the use of redox-active Schiff base ligands. Indeed, we have used the ability of these ligands to store/release two electrons via the reversible formation/cleavage of C-C bonds to promote two- and four- electron reductions. We demonstrated that the non-innocent behaviour of Schiff bases is not restricted to the salophen platform, but can also occur at various imino frameworks. We notably utilized a tridentate ligand to open coordination sites at the uranium center for a better control of reactivity of the bound substrate. As such, the electron-rich molecules synthesized during this PhD behave as synthetic equivalents of U(II), which is not chemically accessible. This methodology has also been sucessfully extended to the Ln^{3+} ions in order to bring redox events at these redox-inactive electrophilic metal centers.[359]

These systems offer numerous future possibilities. The association of the unique properties of the electrophilic U(IV) center with an independent electron reservoir in the same molecule may open attractive perspectives in the molecular design of reducing agents. The possibility of building a wide range of analogous systems from the catalogue of available Schiff bases is particularly appealing for future reactivity studies. This approach could be fruitful for the design of species able to activate small molecules and should offer new modes of reactivity for f-element chemistry.

In addition, the reversible storage of electrons within these species could also be used to develop molecular-based electronic materials. Systems which can undergo reversible intramolecular C-C bond

formation are of high current interest for the development of molecular responsive devices. Notably those molecules, which are able to switch reversibly between two stable redox states, are potential candidates for memory applications or for the development of "on-off" luminescence switching systems.

Finally we have built an effective synthetic route to homo- bimetallic complexes. These studies could be extended to hetero-bimetallic species, offering the possibility to incorporate transition metal ions in f-elements complexes. This synthetic method paves the way for further structural, magnetochemical and reactivity investigations on heterobimetallic complexes.

In the second part, we have demonstrated that siloxides can act as very efficient supporting ligands in the reductive chemistry of uranium. Novel mononuclear and polynuclear low-valent uranium complexes were isolated and characterized and evidence of a rare magnetic coupling between two U(III) centers was obtained. We have established that U(III) promoted the reductive C-O bond cleavage of the O^tBu groups from the ligand, providing a novel controlled route to polymetallic heteroleptic complexes. These compounds could provide an original synthetic route for the preparation of uranium silicate materials presenting homogenous uranium distribution relevant for catalysis and nuclear fuel storage. Future studies could also be directed to investigate the magnetic properties of these multinuclear species.

These reducing uranium complexes are capable of CO_2 activation and reduction forming carbon monoxide and carbonate, highlighting the potential of these derivatives for small molecule activation.

Furthermore, the reductive capacity of the trivalent uranium siloxide species isolated during this work allowed the synthesis of original high-valent uranium nitrides and imides featuring uranium-nitrogen multiple bonding. The difference in steric demand and charge results in a very different outcome of the reactivity between U(III) and azides and show that the siloxide ligands provide a versatile tool to modulate the steric and electronic environment of low-valent uranium. Future studies might be directed to identify the conditions for the isolation of novel mononuclear and polynuclear nitride species and study the N-atom transfer chemistry of the newly isolated uranium imidos complexes.

Additionally, novel uranium arene inverted sandwich complexes in three different oxidation states were isolated and the unprecedented cation-mediated conversion of the state of charge of these uranium arene species was observed. Multiple opportunities are offered for investigating the reactivity properties of these electron-rich arenes complexes.

Overall, these results indicate the interest of siloxide as alternative ancillary ligand in U(III) chemistry and the reactivity patterns observed during this PhD work should encourage future development aiming at expanding the scope of substrate activation of these U(III) siloxide complexes. The overall electron-releasing properties and the steric bulk of the $(R)_3SiO^-$ groups can be easily tuned by a suitable choice of the substituents and thus opens the exploration of new possibilities in uranium chemistry.

CHAPTER V
Experimental Section

V.1 General Considerations

Unless otherwise noted, all manipulations were carried out at ambient temperature under an inert argon atmosphere using Schlenk techniques and an MBraun glovebox equipped with a purifier unit. The water and oxygen level were always kept at less than 0.1 ppm. Glassware was systematically dried in oven overnight at 130°C followed by 3 vacuum/argon cycles before use. Reductions or syntheses involving U(III) compounds were performed using glass-covered stirring bars.

Starting materials. Unless otherwise noted, reagents were purchased from commercial suppliers and used without further purification. Molecular sieves were activated upon heating at 200°C under high vacuum. The solvents were purchased from Aldrich in their anhydrous form, conditioned under argon and vacuum distilled from K/benzophenone (diisopropyl ether, DME, dioxane, toluene, pyridine and THF) or sodium dispersion (hexane) or CaH_2 (acetonitrile and benzonitrile) and degassed by three freeze-pump-thaw cycles. The deuterated solvents were purchased from Eurisotop and prepared identically, except pyridine-d_5 which was degassed by three freeze-pump-thaw cycles and further dried over 3 Å molecular sieves and cyclohexane-d_{12} and hexane-d_{14} which were degassed by three freeze-pump-thaw cycles and stored over potassium. All reagents were dried under high-vacuum (10^{-7} mBar) for 5 days prior to use. The $[Bu_4N][PF_6]$ electrolyte, 9,10-phenanthrenequinone and dibenzo18c6 were purified by recrystallization in toluene and dried under high vacuum prior to use. I_2 was sublimed prior to use. Dry dioxygen was prepared upon storing an O_2 atmosphere upon P_4O_{10} for one week prior to use. $(^tBuO)_3SiOH$ was purchased from ABCR chemicals and sublimed prior to use. Depleted uranium turnings were purchased from the "Société Industrielle du Combustible Nucléaire" of Annecy (France). $[UI_3(THF)_4]$ was prepared either from the direct reaction of uranium metal with iodine in THF,[78] or by hot extraction of $[UI_3(1,4\text{-dioxanne})_{1.5})]$[79] with THF. $[U\{N(SiMe_3)_2\}_3]$[78] ; $[UCl_4]$[104] ; $[UI_4(PhCN)_4]$[105] and $[UI_4(OEt_2)_2]$[80] ; were prepared according to the published procedures.

Caution: *Depleted uranium (primary isotope ^{238}U) is a weak α-emitter (4.197 MeV) with a half-life of 4.47×10^{9} years. Manipulations and reactions should be carried out in monitored fume hoods or in an inert atmosphere glovebox in a radiation laboratory equipped with α- and β-counting equipment.*

Caution: *Because of their potentially explosive character, all reactions involving azido compounds should be carried out with care, in small quantities and using appropriate protection.*

V.2 Characterizations

Elemental analyses were performed under argon by Analytische Laboratorien GMBH at Lindlar, Germany.

UV-visible measurements were carried out with a Varian Cary 50 Probe spectrophotometer in quartz cells (optical path lengths: 1 mm) adapted with Young valves.

FTIR spectra were recorded with a Perkin Elmer Spectrum 100 Series FTIR spectrophotometer from KBr pellets.

Mass spectra were acquired on a LXQ-linear ion trap (Thermo Scientific, San Jose, CA,USA), equipped with an electrospray source in a THF solution which was prepared and filtered on microporous filters in the glove-box and maintained under argon until injection in the spectrometer. Electrospray full scan spectra, in the range of *m/z* 50 –3000 amu, were obtained by infusion through fused silica tubing at 2 – 10 µL min^{-1}. The LXQ calibration (*m/z* 50-2000) was achieved according to the standard calibration procedure from the manufacturer (mixture of caffeine/MRFA and Ultramark 1621). The LXQ calibration (*m/z* 2000-4000) was performed with ES tuning mix (Agilent). The temperature of the heated capillary of the LXQ was set to the range of 180 – 220 °C, the ion spray voltage was in the range of 1 – 3 kV with an injection time of 5-100 ms. The experimental isotopic profile was compared in each case to the theoretical one.

^{1}H NMR experiments were carried out using NMR tubes adapted with J. Young valves. ^{1}H NMR spectra were recorded on Bruker 200 MHz and 500 MHz and Varian Mercury 400 MHz spectrometers, at various temperatures. NMR chemical shifts are reported in ppm with solvent as internal reference. Abbreviations used for describing multiplicity and shape of the NMR signals are : s (singulet), d (doublet), t (triplet), m (multiplet) and br (broad).

Diffusion coefficients measurements were performed by NMR using a Pulsed-Field Gradient STimulated Echo (PFGSTE) sequence, using bipolar Gradients, at 298 K and no spinning was applied

to the NMR tube.[476, 477] The following BPP-LED (Bipolar Pulse Pair – Longitudinal Eddy-current Delay) pulse sequence was applied:

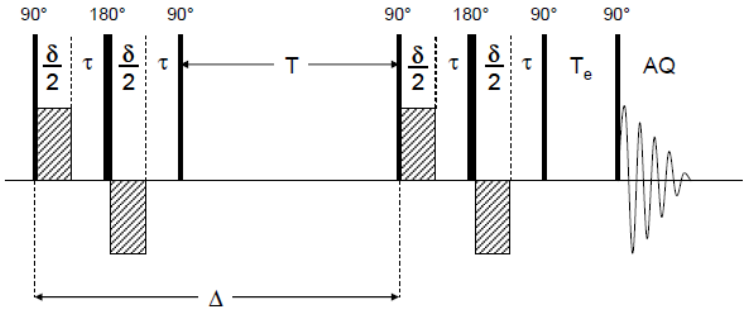

δ= 2 ms. τ = 0.5 ms.

The diffusion times T were optimized at 100 ms. The evolution of the pulsed-field gradient during the NMR diffusion experiments was established in 10 steps, applied linearly between 5.4 and 29.7 G.cm^{-1}. In the present sequence the intensity of the signal is given by the following equation:[478]

$$I(q) = I(0)\exp\left[-Dq^2\left(d - \frac{\delta}{3} - \frac{\tau}{2}\right)\right]$$

with q = γ.δ.g and D : diffusion coefficient (m².s^{-1}), Δ: time between the two gradient pulse sequences (s), δ : bipolar gradient duration (s), τ : pulse separation delay (s), γ : magnetogyric ratio of the observed nucleus (s^{-1}.T^{-1}) and finally g : gradient strength (T.m^{-1}). The diffusion coefficient is then the slope of the line obtained by plotting ln(I/I0) against $q^2(\Delta - \delta/3 - \tau/2)$.

The coefficient is a function of the molecular weight (*M*) and can been conveniently used for discriminating metallosupramolecular architectures in solution. The values of the measured coefficient diffusion can be used to estimate the solution molecular weight using the following equation:[389]

$$M_A/M_B = (D_A/D_B)^3$$

Static magnetic properties were measured in the temperature range 2 K to 240-300 K using a Quantum Design MPMS-XL 5.0 Superconducting Quantum Interference Devices (SQUID) susceptometer with Ultra-Low Field Capability ±0.05 G for the 5 T magnets. Continuous Low Temperature Control/Temperature Sweep Mode (CLTC) - Sweep rate: 0.001 - 10 K/min. During the course of the PhD studies, two types of sample holders were used. The samples **4-THF** and **4-py** were prepared in the glovebox by pressing crushed crystalline or powder samples into an aluminium container which was then introduced in a 5 mm Suprasil-Quartz tube and transferred in the SQUID using Schlenk techniques. In a second time, we found more convenient and get better results when

the samples were prepared in the glovebox by pressing crushed crystalline or powder samples into a 5 mm Suprasil-Quartz tube. Few drops of cyclohexane were added into the tubes to avoid sample torquing. Compounds **33-35** were also measured without cyclohexane but no torquing was observed. The quartz tube was then flame-sealed under reduced pressure and transferred in the SQUID machine. The contribution to the signal from the empty sample holder were measured independently and subtracted from the total signal. The resulting data were corrected for the diamagnetic contribution using tabulated Pascal's constants.[479] Susceptibility data were recorded on independently synthesized samples to insure data reproducibility. The purity of each sample was checked by elemental analysis and ^{1}H NMR spectroscopy. The value of the magnetic moment in solution was determined using the Evans method[480] upon measuring the difference in chemical shift of the protons from the solvent (THF or toluene) between a solution containing a paramagnetic complex in known concentration and a solvent reference (in absence of paramagnetic solute) accomplished by introducing a sealed capillary containing pure solvent in the NMR sample tube.

Electrochemical Methods. Cyclic voltammetry data were carried out at room temperature in an argon-filled glovebox described above. Data were collected using a Princeton Applied Research Model 273 potentiostat or a Biologic SP-300 potentiostat connected to a personal computer. All samples were 2 to 10 mM in complex with 0.1 M $[Bu_4N][PF_6]$ supporting electrolyte in pyridine or THF solution. The experiments were carried out with a platinum disk (d = 5 mm or d = 1 mm) or a vitrous carbon disk (d = 1 mm) working electrode, a platinum wire counterelectrode and an Ag/AgCl reference electrode. The experiments were repeated on independently synthesized samples in order to assess the reproducibility of the measurement. Potential calibration was performed at the end of each data collection cycle using the ferrocene/ferrocenium $[(C_5H_5)_2Fe]^{+/0}$ couple as an internal standard.

X-ray Crystallography Diffraction data were taken using a Oxford-Diffraction XCallibur S kappa geometry diffractometer (Mo-Kα radiation, graphite monochromator, λ = 0.71073 Å). To prevent evaporation of co-crystallised solvent molecules the crystals were coated with light hydrocarbon oil and the data were collected at 150 K. The cell parameters were obtained with intensities detected on three batches of 5 frames. The crystal-detector distance was 4.5 cm except for **7** where the distance was 8.0 cm. The number of settings and frames has been established taking in consideration the Laue symmetry of the cell by CrysAlisPro Oxford-diffraction software. The data were collected for 1° increments in ω with a different exposure time for each crystal depending on the intensities measured during the first three batches of 5 frames. Unique intensities detected on all frames using the Oxford-diffraction CrysalisPro Red program were used to refine the values of the cell parameters. The substantial redundancy in data allows empirical absorption corrections to be

applied using multiple measurements of equivalent reflections with the ABSPACK Oxford-diffraction program. The structures were solved by direct methods using the SHELXTL 6.14 or Superflip[481] package and refined using SHELXTL 6.14 or OLEX2[482]. Figure graphics were generated using MERCURY 2.3 supplied with Cambridge Structural Database.[483] All non-hydrogen atoms were found by difference Fourier syntheses and refined on F^2. Hydrogen atoms were fixed in the ideal position except for the cases below. For **4-py** and **12** hydrogen atoms were found by Fourier synthesis and refined except for pyridine or THF solvent molecules which were fixed in the ideal positions. For **7-^{t}Bu** hydrogen atoms were fixed in the ideal position except hydrogens of the aromatic rings of the ligand which were found by Fourier synthesis and refined. For **14-Cl** hydrogen atoms were found by Fourier synthesis and refined except for methyl groups which were fixed in the ideal position. For **23-py** the hydrogen atoms from the pyridine and the Si1 silanol moieties were found by Fourier synthesis and refined. Details of the data collection and crystal parameters are given in appendix.

V.3 Syntheses

Tetradentate Schiff base ligands were prepared by the condensation of 1,2-ethylenediamine (**H_2-salen**), 1,2-phenylenediamine (**H_2-^{R}salophen**) or 1,1'-diaminoferrocene (**H_2-salfen**) with the corresponding salicyalaldehyde derivatives (1:2 stoichiometric ratio) in ethanol under reflux according to earlier procedures.[379, 484]

H-^{Me}naphtquinolen

The ligand was prepared by a modified literature procedure.[485, 486] A solution of 2-methylquinolin-8-amine (1.0 g, 6.32 mmol, 1 equiv) and 3-hydroxy-2-naphtaldehyde (1.1 g, 6.39 mmol, 1.01 equiv) in 30 mL of anhydrous toluene was stirred in a Dean Stark set-up at 110°C during 2 days. Then the solvent was removed under vacuum giving an orange-brown solid. This solid was suspended in 100 mL cyclohexane and heated to reflux. Toluene was added dropwise until most solid was soluble and the temperature was raised to maintain the reflux. A hot filtration was carried out to remove the black insoluble impurities and the mixture was cooled down to room temperature, affording red crystals that were filtered and dried under vacuum to give H-^{Me}naphtquinolen (1.38 g, 4.42 mmol, 70 % yield). ^{1}H NMR (200 MHz, $CDCl_3$, 298 K): δ = 15.8 (br s, 1H, OH), 9.3 (d, 1H), 8.1 (d, 1H), 8.0 (d, 1H), 7.7-7.4 (m, 7H), 7.3-7.2 (m, 1H), 6.9 (d, 1H), 2.9 (s, 3H, CH_3). ^{13}C NMR (50 MHz, $CDCl_3$, 298 K): δ = 182.3 (C=N), 159.3 (C_{aro}), 145.9 (C_{aro}), 139.5 (C_{aro}), 139.3 (C_{aro}), 136.6 (C_{aro}), 136.0 (C_{aro}), 134.5 (C_{aro}), 129.5 (C_{aro}), 128.4 (C_{aro}), 127.2 (C_{aro}), 126.9 (C_{aro}), 126.7 (C_{aro}), 125.7 (C_{aro}), 124.1 (C_{aro}), 123.6 (C_{aro}), 122.3 (C_{aro}), 118.4 (C_{aro}), 113.2 (C_{aro}), 8.0 (C_{aro}), 25.9 (CH_3). ESI-MS : m/z = 313.2 [$M+H^+$].

The potassium salts of the Schiff base ligands were prepared as previously described[487] by addition of KH to a THF solution of the corresponding Schiff base. The resulting K_2salen (cream), **K_2salophen** (yellow), **K_2^{Me}salophen** (yellow), **K_2^{tBu}salophen** (orange), **K_2salfen** (red) and **K^{Me}naphtquinolen** (orange) salts were obtained in 65-95% yield.

K_2salen ^{1}H NMR: (200 MHz, dmso-d_6, 298K): δ = 3.53 (s, 2H), 5.75 (m, 1H), 6.03 (m, 1H), 6.70 (t, 1H), 7.27 (d, 1H), 8.55 (s, 1H).

K_2salophen ^{1}H NMR (200 MHz, THF-d_8, 298 K): δ = 8.4 (s, 2H, N=C*H*), 7.2 (s, 2H), 7.1 (s, 2H), 7.0 (s, 2H), 6.8 (s, 2H), 6.4 (s, 2H), 6.1 (s, 2H).

K_2^{Me}salophen ^{1}H NMR (200 MHz, pyridine-d_5, 298 K): δ = 8.6 (s, 2H), 7.3-7.1 (m, 8H), 6.5 (t, 2H), 2.3 (s, 6H).

K_2^{tBu}salophen ^{1}H NMR (200 MHz, pyridine-d_5, 298 K): δ = 8.6 (s, 2H), 7.6 (s, 2H), 7.3-7.1 (m, 6H), 1.7 (s, 18H), 1.5 (s, 18H).

K_2salfen ^{1}H NMR (200 MHz, THF-d_8, 298 K): δ = 8.9 (s, 2H, N=C*H*), 7.5 (d, 2H), 7.2 (t, 2H), 7.0 (d, 2H), 6.5 (t, 2H), 4.5 (s, 4H, C_5H_4N), 4.2 (s, 4H, C_5H_4N).

K^{Me}naphtquinolen ^{1}H NMR (200 MHz, pyridine-d_5, 298 K): δ = 9.7 (s, 1H, HC=N), 8.6 (d, 1H), 8.0 (d, 1H), 7.7 (m, 2H), 7.5-7.7 (m, 3H), 7.3-7.0 (m, 4H), 2.5 (s, 3H, CH_3).

KOSi(^{t}BuO)$_3$ was prepared upon reaction of (^{t}BuO)$_3$SiOH (1.636 g, 6.2 mmol, 1 equiv) with one equivalent of KH (248 mg, 6.2 mmol, 1 equiv) in THF (10 mL). After 24 hours stirring, the mixture was filtered and the filtrate was taking to dryness. The resulting white powder was collected and dried for 3 hours to give KOSi(^{t}BuO)$_3$ (1.460 g, 4.8 mmol, 78 % yield). ^{1}H NMR (400 MHz, THF-d_8, 298 K): δ = 1.3 (s, 27H). ^{1}H NMR (200 MHz, toluene-d_8, 298 K): δ = 1.4 (s, 27H). ^{1}H NMR (200 MHz, pyridine-d_5, 298 K): δ = 1.5 (s, 27H).

Reaction of K_2salen with [UI_3(THF)$_4$]

A solution of [UI_3(THF)$_4$] (50.0 mg, 0.055 mmol, 1 equiv) in THF (3 mL) was added to a solution of K_2salen (19.0 mg, 0.055 mmol, 1 equiv) in 3 mL THF. This suspension was stirred at room temperature for 12 h before filtration. The resulting dark greenish brown solution was analyzed by ^{1}H NMR (200 MHz, THF-d_8, 298 K). The proton spectrum displays two sets of resonances corresponding to [UI_2(salen)(THF)$_2$] **1** : δ = 79.95 (s, 2H), 56.27 (s, 2H), 48.67 (s, 2H), 47.88 (s, 2H), 33.33 (s, 2H), -61.19 (brs, 4H) and [U(salen)$_2$] **2** : δ = 15.81 (s, 4H), 14.52 (s, 4H), 12.18 (s, 4H), 11.53 (s, 4H), 10.89 (s, 4H), -38.32 (brs, 8H). Attempts to further reduce this reaction mixture with alkali metal afforded intractable dark brown/green suspension. Compounds **1** and **2** can be prepared from the reaction of

$[UI_4(PhCN)_4]$ with 1 or 2 equivalents of K_2salfen respectively using similar protocols than for the salophen analogues **3** and **6**.

$[UI_2$(salophen)$(THF)_2]$ 3

A solution of $[UI_4(PhCN)_4]$ (272.1 mg, 0.235 mmol, 1 equiv) in acetonitrile (2 mL) was added to a yellow suspension of K_2salophen (92.2 mg, 0.235 mmol, 1 equiv) in 8 mL of acetonitrile. This suspension was stirred at room temperature for 20 min to yield a clear dark red solution. The solution was filtered and the filtrate was overlayered with 4 mL THF. After 2 days, 174 mg of red brown crystals of $[UI_2$(salophen)$(THF)_2]$ **3** were collected by filtration (0.183 mmol, 79% yield). ^{1}H NMR (200 MHz, pyridine-d_5, 298 K): δ = 80.22 (s, 2H), 46.16 (s, 2H), 45.74 (s, 2H), 42.18 (s, 2H), 30.36 (s, 2H), 3.65 (s, THF), 1.60 (s, THF), -6.19 (s, 2H), -8.24 (s, 2H). Anal. Calcd for **3**: $C_{28}H_{28}I_2N_2O_4U$: C, 35.46; H, 2.98; N, 2.95. Found: C, 35.25; H, 3.13; N, 3.02.

$[U_2$(cyclo-salophen)$(THF)_4]$ 4-THF

A solution of $[UI_3(THF)_4]$ (100.0 mg, 0.110 mmol, 1 equiv) in THF (16 mL) was added to K_2salophen (43.3 mg, 0.110 mmol, 1 equiv) and the reaction was stirred at room temperature for 4 hours. The resulting brown suspension was added onto potassium chunks (4.3 mg, 0.110 mmol, 1 equiv) and stirred overnight. The dark brown mixture was filtered to remove KI, and the filtrate was evaporated to dryness under vacuum to yield **4-THF** (65.9 mg, 86% yield). ESI-MS : m/z = 1247.4 ($[U_2$(cyclo-salophen)$(THF)_2]^+$). Anal. Calcd for **4-THF**: $U_2C_{56}H_{60}O_8N_4$: C, 48.28; H, 4.34; N, 4.02. Found: C, 47.90; H, 4.53; N, 4.16. Re-crystallization of **4-THF** from a saturated THF solution with additional pyridine afforded red single crystals of **4-py** suitable for X-ray diffraction. ^{1}H NMR (200 MHz, pyridine-d_5, 298 K): δ = 69.0 (s, 4H), 25.7 (s, 4H), 24.0 (s, 4H), 14.8 (s, 4H), 13.6 (s, 4H), -10.28 (s, 4H), -12.5 (s, 4H).

Reaction of H_2salophen with $[U\{N(Si(Me)_3)_2\}_3]$

A cold (-40°C) solution of H_2salophen (44.8 mg, 0.142 mmol, 1 equiv) in THF (2 mL) was added to a cold (-40°C) solution of $[U\{N(Si(Me)_3)_2\}_3]$ (101.8 mg, 0.142 mmol, 1 equiv) in hexane (2 mL) and the reaction mixture was stirred at -40°C for 15 minutes and then at room temperature fo 2 hours, affording a deep brown suspension. The ^{1}H NMR of the crude mixture showed the presence of $[U(salophen)_2]$ **6** together with a series of broad peaks is the ppm region {0 ; -10}. The characteristic resonances of complex $[U_2$(cyclosalophen)$(THF)_4]$ **4-THF** were not detected. The crude mixture was evaporated to dryness and the resulting solid was extracted with 2 mL hexane and centrifuged to remove the $[U(salophen)_2]$ **6** complex as a brown solid (41.0 mg, 0.047 mmol, 33 %). The red hexane supernatant was concentrated to 0.4 mL, filtered and cooled to -40°C. Single crystals of **5-a** and **5-b** formed in one night (42.2 mg, 0.026 mmol, 19 %). Two types of red single crystals were identified and

characterized through X-ray diffraction, but the two compounds could not be separated because of their similar solubility. Anal. Calcd for $U_2C_{50}H_{105}O_2N_7$: C, 37.69; H, 6.64; N, 6.15. Found: C, 37.99; H, 6.38; N, 6.29. The ^{1}H NMR spectrum of complexes **5-a** and **5-b** is composed a series of broad unattributable peaks in the ppm region {0 ; -10}.

[U(salophen)$_2$] 6

A solution of [$UI_4(PhCN)_4$] (50 mg, 0.043 mmol, 1 equiv) in THF (8 mL) was added to K_2salophen (33.9 mg, 0.086 mmol, 2 equiv) and the reaction mixture was stirred at room temperature overnight. The resulting dark brown suspension was filtered. The resulting solution was evaporated (1 mL) and *n*-hexane was added to yield a brown solid. Recrystallization of this solid by slow diffusion of hexane into a pyridine solution afforded dark brown single crystals suitable for X-ray diffraction. (25 mg, 67% yield). The proton NMR spectrum of THF solutions of **6** shows the presence of two isomers, meridional (with the two ligands oriented perpendicular to each other) and sandwich (where the two ligands are oriented parallel to each other). ^{1}H NMR (200 MHz, pyridine-d_5, 298 K): isomer **6-a**: δ = 18.3 (s, 4H), 12.3 (t, 4H), 11.3 (d, 4H), 9.0 (t, 4H), 7.9 (d, 4H), -0.3 (m, 4H), -6.3 (m, 4H). Isomer **6-b**: δ = 16.1 (t, 4H), 16.0 (d, 4H), 11.1 (d, 4H), 10.8 (t, 4H), 4.9 (s, 4H), -1.0 (m, 4H), -7.8 (m, 4H). ESI-MS : m/z = 867.5 ($M+H^+$) ; m/z = 889.5 ($M+Na^+$) ; m/z = 905.4 ($M+K^+$). Anal. Calcd for **6**: $UC_{40}H_{28}O_4N_4$: C, 55.43; H, 3.26; N, 6.46. Found: C, 55.10; H, 3.39; N, 6.56.

[U(^{Me}salophen)$_2$] 6-Me

A solution of $K_2{}^{Me}$salophen (100.0 mg, 0.229 mmol, 2 equiv) in THF (6 mL) was added to [$UI_4(OEt_2)_2$] (102.7 mg, 0.115 mmol, 1 equiv) and the reaction mixture was stirred at room temperature overnight. The resulting deep brown suspension was filtered to remove KI, the deep brown filtrate was reduced to 2 mL and layered with 10 mL hexane. The resulting suspension was filtered and the deep brown filtrate was evaporated *in vacuo* to give [U(^{Me}salophen)$_2$] as a deep brown powder (82 mg, 77% yield). ESI-MS : m/z= 922.5 ([M]$^+$), 961.3 ([M+K]$^+$), 1882.9 ([M_2+K]$^+$). ^{1}H NMR (200 MHz, THF-d_8, 298 K): Isomer a: δ = 18.4 (s, 2H), 12.8 (m, 2H), 11.3 (d, 2H), 8.8 (t, 2H), 5.3 (s, 6H), 0.2 (m, 2H), -5.3 (m, 2H). Isomer b: δ = 16.1 (d, 2H), 11.4 (d, 2H), 10.7 (t, 2H), 3.3 (s, 6H), 0.0 (m, 2H), -1.8 (m, 2H), -8.9 (m, 2H). Ratio isomer a:b : 30:70. ^{1}H NMR (200 MHz, pyridine-d_5, 298 K): Isomer a : δ = 18.6 (s, 2H), 12.8 (m, 2H), 11.4 (d, 2H), 8.9 (t, 2H), 5.5 (s, 6H), 0.3 (m, 2H), -5.2 (m, 2H). Isomer b : δ = 16.3 (d, 2H), 11.6 (d, 2H), 10.9 (t, 2H), 3.6 (s, 6H), 0.3 (m, 2H), -1.7 (m, 2H), -8.7 (m, 2H). Ratio isomer a:b : 27:73. ^{1}H NMR (200 MHz, CD_3CN, 298 K): Isomer a : δ = 18.2 (s, 2H), 12.6 (m, 2H), 11.1 (d, 2H), 8.8 (t, 2H), 5.3 (s, 6H), 0.3 (m, 2H), -5.4 (m, 2H). Isomer a : δ = 16.2 (d, 2H), 11.5 (d, 2H), 10.9 (t, 2H), 3.0 (s, 6H), -0.2 (m, 2H), -1.9 (m, 2H), -8.9 (m, 2H). Ratio isomer a:b : 20:80. Anal. Calcd for [U(^{Me}salophen)$_2$].(0.05KI): $C_{44}H_{36}N_4O_4K_{0.05}I_{0.05}U$: C, 56.76; H, 3.90; N, 6.02. Found: C: 57.27; H, 3.93; N, 6.07.

[U(^{tBu}salophen)$_2$] 6-^{t}Bu

A solution of K_2 ^{tBu}salophen (98.1 mg, 0.158 mmol, 2 equiv) in THF (4 mL) was added to UCl_4 (30.0 mg, 0.079 mmol, 1 equiv) and the reaction mixture was stirred at room temperature overnight, affording an orange suspension. The solvent volume was reduced to 1 mL and the mixture was filtered to remove KCl. The filtrate was evaporated to dryness, affording **6-^{t}Bu** as an orange/brown solid. (70.6 mg, 68% yield). ESI-MS : m/z = 1314.9 ([M+H]$^+$). ^{1}H NMR (400 MHz, THF-d_8, 298 K) was hardly attributable as broad signals were obtained for this species. ^{1}H NMR (400 MHz, THF-d_8, 263 K): δ = 32.4 (s, 2H), 25.9 (s, 2H), 20.8 (s, 2H), 12.1 (s, 18H), 6.7 (s, 18H), 4.2 (s, 2H), 3.3 (s, 2H), 1.9 (s, 2H), -1.02 (s, 18H), -1.6 (s, 2H), -2.5 (s, 2H), -4.8 (s, 2H), -12.8 (s, 2H), -13.4 (s, 18H). Anal. Calcd for [U(^{tBu}salophen)$_2$] **6-^{t}Bu**: $C_{72}H_{92}N_4O_4U$: C, 65.73; H, 7.05; N, 4.26. Found: C: 65.39; H, 7.00; N, 4.37.

Na_2[U(bis-salophen)] 7

From [$UI_4(PhCN)_4$] : A solution of [$UI_4(PhCN)_4$] (63.4 mg, 0.055 mmol, 1 equiv) in THF (8 mL) was added to K_2salophen (42.9 mg, 0.109 mmol, 2 equiv) and the reaction was stirred at room temperature overnight. The resulting brown solution was filtered to remove KI and the filtrate was added onto sodium chunks (2.5 mg, 0.109 mmol, 2 equiv). The mixture was stirred overnight, affording a dark purple solution. The reaction was filtered and the solvent volume was reduced to 2 mL. 8 mL of hexane were added and the mixture was stirred overnight, to afford **7** as a purple solid. (43.1 mg, 86% yield). Single crystals of **7-18c6** suitable for X-ray diffraction were obtained by slow diffusion of hexane into a pyridine solution of **7** with excess 18c6.

From [$UI_4(OEt_2)_2$] : A suspension of K_2salophen (351.3 mg, 0.895 mmol, 2 equiv) in THF (10 mL) was added to [$UI_4(OEt_2)_2$] (400.0 mg, 0.447 mmol, 1 equiv) and the reaction mixture was stirred at room temperature overnight. The resulting brown suspension was added onto sodium chunks (20.6 mg, 0.895 mmol, 2 equiv). The mixture was stirred overnight, affording a dark purple suspension. The mixture was filtered to remove NaI and the filtrate was concentrated to 4 mL, affording a first crop of microcrystalline solid that were collected and dried in vacuo. The purple filtrate was layered with 30 mL hexane. In 1 hour, purple crystals were collected and dried under vacuum to afford Na_2[U(bis-salophen)] **7** as a crystalline purple solid. (combined yied : 359 mg, 88% yield). ESI-MS : m/z = 867.3 (MH^-). ^{1}H NMR (200 MHz, THF-d_8, 298 K): δ = 40.6 (d, 2H), 16.1 (t, 2H), 8.8 (t, 2H), 7.6 (t, 2H), 4.0 (d, 2H), 3.8 (t, 2H), 2.5 (d, 2H), 2.2 (s, 2H), -0.1 (d, 2H), -2.2 (t, 2H), -4.6 (t, 2H), -10.8 (d, 2H), -11.7 (s, 2H), -15.6 (d, 2H). ^{1}H NMR (200 MHz, pyridine-d_5, 298 K): δ = 35.8 (d, 2H), 14.9 (t, 2H), 9.2 (t, 2H), 8.7 (t, 2H), 6.2 (d, 2H), 4.8 (t, 2H), 4.6 (d, 2H), 3.7 (s, 2H), 1.1 (d, 2H), -0.9 (t, 2H), -3.4 (t, 2H), -5.0(s, 2H), -7.5 (d, 2H), -13.9 (d, 2H). Anal. Calcd for **7**: $UC_{40}H_{28}O_4N_4Na_2$: C, 52.64; H, 3.09; N, 6.14. Found: C, 52.31; H, 3.20; N, 6.32

Addition of 18c6 (9.5 mg, 0.036 mmol, 2 equiv) to pyridine (0.5 mL) solution of Na_2[U(bis-salophen)] (16.4 mg, 0.018 mmol, 1 equiv) gave a purple solution. The ^{1}H NMR (200 MHz, pyridine-d_5, 298 K) recorded for this solution shows the presence of several broad resonances hardly attributable. Upon heating to 50°C, the resonances sharpens and 14 signals of equal intensity are observed : ^{1}H NMR (200 MHz, pyridine-d_5, 323 K): δ = 34.4 (br s, 2H), 14.7 (br s, 2H), 9.7 (t, 2H), 9.4 (br s, 2H), 8.7 (br s, 2H), 5.8 (br s, 2H), 5.2 (t, 2H), 3.8 (br s, 2H), 2.1 (d, 2H), -0.5 (t, 2H), -3.0 (br s, 2H), -3.2 (d, 2H), -6.1 (br s, 2H), -13.4 (t, 2H).

Addition of 2 equiv Bu_3SnH to a THF solution of Na_2[U(bis-salophen)] **7** resulted in no reaction, as confirmed by ^{1}H NMR studies.

Reduction of [U(salophen)$_2$] with potassium

A suspension of K_2salophen (49.5 mg, 0.126 mmol, 2 equiv) in THF (10 mL) was added to [$UI_4(OEt_2)_2$] (54.37 mg, 0.061 mmol, 1 equiv) and the reaction mixture was stirred at room temperature for 12 hours. The resulting brown suspension was added onto potassium chunks (4.8 mg, 0.126 mmol, 2 equiv). The mixture was stirred for 12 hours, affording a dark purple suspension. The mixture was filtered to remove KI, yielding a purple THF solution. Analysis of the crude mixture by ^{1}H NMR showed the presence of a mixture of two unidentified species.

K_2[U(bis-^{Me}salophen)] 7-Me

A solution of $K_2{}^{Me}$salophen (150.0 mg, 0.330 mmol, 2 equiv) in THF (12 mL) was added to [$UI_4(OEt_2)_2$] (147.7 mg, 0.1651 mmol, 1 equiv) and the reaction mixture was stirred at room temperature overnight. The resulting deep brown solution was added onto potassium chunks (12.9 mg, 0.330 mmol, 2 equiv). The mixture was stirred overnight, affording a dark purple solution with white precipitate. The mixture was filtered to remove KI, and the filtrate concentrated and overlayed with hexane. The resulting suspension was filtered and the purple solid recovered and dried under vacuum. (151 mg, 91% yield) K_2[U(bis-^{Me}salophen)] **7-Me**. Single crystals suitable for X-ray diffraction were grown by slow evaporation of a pyridine/hexane saturated solution of the complex in presence of 2 equiv of dibenzo18c6. ESI-MS : m/z= 923.3 ([M-2K+H]$^-$) ^{1}H NMR (200 MHz, THF-d_8, 298 K): δ = 17.9 (s, 2H), 16.0 (s, 2H), 13.1 (s, 2H), 10.0 (s, 2H), 7.6 (s, 2H), 7.0 (s, 2H), 5.7 (s, 2H), 5.4 (s, 6H), 5.0 (s, 2H), 2.6 (s, 2H), 1.8 (s, 2H), -2.3 (s, 2H), -6.7 (s, 6H), -13.2 (s, 2H). Anal. Calcd for K_2[U(bis-^{Me}salophen)] **7-Me** : $C_{44}H_{36}N_4O_4K_2U$: C, 52.79; H, 3.62; N, 5.60. Found: C: 53.08; H, 3.90; N, 5.59.

K_2[U(bis-^{tBu}salophen)] 7-^{t}Bu

A solution of $K_2{}^{tBu}$salophen (98.1 mg, 0.158 mmol, 2 equiv) in THF (12 mL) was added to UCl_4 (30 mg, 0.079 mmol, 1 equiv) and the reaction mixture was stirred at room temperature overnight. The

resulting orange suspension was added onto potassium chunks (6.2 mg, 0.158 mmol, 2 equiv). The mixture was stirred overnight, affording a dark purple suspension. The mixture was filtered to remove KCl, and the filtrate was dried under vacuum to afford a purple solid (91 mg, 81% yield). Single crystals suitable for X-ray diffraction were obtained from a saturated diisopropylether solution of K_2[U(bis-^{tBu}salophen). ESI-MS : m/z = 1315.6 ([M-2K+H]$^-$) ^{1}H NMR (200 MHz, THF-d_8, 298 K): δ = 22.4 (s, 2H), 20.5 (s, 2H), 15.0 (s, 2H), 11.3 (s, 2H), 8.3 (s, 2H), 5.8 (s, 2H), 2.4 (m, 2H), 2.1 (s, 18H), 2.0 (s, 18H), 1.5 (s, 2H), -3.6 (m, 2H), -4.9 (s, 18H), -14.2 (m, 2H). Anal. Calcd for K_2[U(bis-^{tBu}salophen)].(0.3KCl) $C_{72}H_{92}N_4O_4K_{2.3}Cl_{0.3}U$: C, 61.07; H, 6.55; N, 3.96. Found: C: 60.98; H, 6.22; N, 3.78.

[U(salophen)(OTf)$_2$(THF)$_2$] 8

A THF (4 mL) solution of AgOTf (14.8 mg, 0.057 mmol, 4 equiv) was added dropwise to a brown solution of [U_2(cyclo-salophen)(THF)$_4$] (20 mg, 0.014 mmol, 1 equiv) in THF (4 mL). Immediately, a black precipitate of metallic silver formed. The mixture was stirred overnight and then filtered. The yellow filtrate was concentrated, precipitated with hexane and the yellow product [U(salophen)(OTf)$_2$(THF)$_2$] **8** was collected by filtration and dried under vacuum. Recrystallization by slow diffusion of diisopropylether into a THF solution afforded green crystalline needles suitable for X-ray diffraction. (28.6 mg, 56 % yield). ESI-MS : m/z = 773.1 ([U(salophen)(OTf)]$^+$) ; m/z = 701.5 ([U(salophen)(OTf)(THF)]$^+$). ^{1}H NMR (200 MHz, THF-d_8, 298 K): δ = 79.2 (s, 2H), 44.9 (s, 2H), 39.8 (s, 4H), 29.4 (s, 2H), -5.8 (s, 2H), -8.2 (s, 2H). Anal. Calcd for [U(salophen)(OTf)$_2$(THF)$_2$] **8**: $C_{30}H_{30}N_2O_{10}F_6S_2U$: C, 36.22; H, 3.04; N, 2.82; S, 6.45. Found: C, 35.86; H, 3.52; N, 2.98; S, 6.36.

Reaction of [U_2(cyclo-salophen)(THF)$_4$] 4-THF with 9,10-phenanthrenequinone

A THF (0.5 mL) solution of 9,10-phenanthrenequinone (2.9 mg, 0.014 mmol, 2 equiv) was added to a stirring THF (4 mL) solution of [U_2(cyclo-salophen)(THF)$_4$] **4-THF** (10 mg, 0.007 mmol, 1 equiv). Immediately, the solution turned deep olive green. The mixture was stirred for 12 hours before NMR analysis. The ^{1}H NMR spectrum (200 MHz, THF-d_8, 298 K) recorded for the crude reaction mixture showed that a mixture of compounds had formed, among which the characteristic resonances of [U(salophen)$_2$] **6** could be identified. The presence of [U(salophen)$_2$] **6** was confirmed by ESI-MS analysis.

Reaction of Na_2[U(bis-salophen)] 7 with AgOTf

A 2.7.10^{-3} mol.L^{-1} THF-d_8 (1 mL) solution of Na_2[U(bis-salophen)] **7** (24.7 mg, 0.027 mmol, 1 equiv) was prepared. 0.05 mL hexane was added as internal reference. This solution was poured on AgOTf (13.9 mg, 0.054 mmol, 2 equiv). Immediately, the solution turned deep brown and a black precipitate of metallic silver formed. The mixture was stirred 1 hour before filtration and NMR analysis. The ^{1}H NMR

spectrum (400 MHz, THF-d_8, 298 K) shows that the isomeric mixture of compound [U(salophen)$_2$] **6** is restored. The concentration of [U(salophen)$_2$] estimated by ^{1}H NMR integration using hexane as internal reference ($2.4.10^{-3}$mol.L^{-1}) is consistent with a quantitative transformation of Na_2[U(bis-salophen)] **7** into [U(salophen)$_2$] **6** after addition of AgOTf. ESI-MS: m/z = 866.6 ([U(salophen)$_2$]$^+$).

Reaction of Na_2[U(bis-salophen)] 7 with PbI_2

To a 0.5 mL THF solution of Na_2[U(bis-salophen)] **7** (10.0 mg, 0.011 mmol, 1 equiv) was added a 0,5 mL THF suspension of PbI_2 (5.1 mg, 0.011 mmol, 1 equiv). The reaction mixture was stirred 16 hours, affording a dark brown suspension. The mixture was filtered to remove NaI salts and Pb(0) and the brown filtrate was analyzed by ^{1}H NMR. The spectrum (200 MHz, THF-d_8, 298 K) displayed the characteristic resonances of the isomeric mixture of compound [U(salophen)$_2$] **6**.

Reaction of Na_2[U(bis-salophen)] 7 with 9,10-phenanthrenequinone

A THF (1 mL) solution of 9,10-phenanthrenequinone (2.5 mg, 0.012 mmol, 1.1 equiv) was added to Na_2[U(bis-salophen)] **7** (10 mg, 0.011 mmol, 1 equiv). Immediately, the solution turned deep olive green. The mixture was stirred 15 minutes before NMR analysis. The ^{1}H NMR (200 MHz, THF-d_8, 298 K) showed the characteristic resonances of [U(salophen)$_2$] **6** as well as diamagnetic resonances (7.0 to 8.0 ppm) in the aromatic region attributed to the dianionic reduced form of 9,10-phenanthrenequinone.

[U(bis-H_2salophen)] 9

A pyridine solution (2 mL) of pyridinium hydrochloride (11.1 mg, 0.096 mmol, 2 equiv) was added onto a pyridine solution (2 mL) of complex Na_2[U(bis-salophen)] **7** (44.1 mg, 0,048 mmol, 1 equiv). Immediately, the deep purple solution turns brown. The mixture was stirred for one hour. The pyridine was removed under vacuum, the brown solid was extracted with THF, filtered and the filtrate was evaporated under vacuum. The brown solid was recrystallized from a pyridine/hexane mixture to afford brown needles of [U(bis-H_2salophen)] **9** suitable for X-ray diffraction (21 mg, 50 % yield). ^{1}H NMR (200 MHz, pyridine-d_5, 298 K): δ = 24.0 (s, 2H), 20.1 (s, 2H), 18.6 (s, 2H), 16.8 (s, 2H), 15.9 (s, 2H), 13.1 (s, 2H), 12.4 (s, 2H), 11.6 (s, 2H), 10.8 (s, 2H), 8.6 (s, 2H), 8.3 (s, 2H), 8.1 (s, 2H), 2.9 (s, 2H), 0.1 (s, 2H), -3.1 (s, 2H), -17.6 (s, 2H). ESI-MS : m/z = 869.3 ([M+H]$^+$) Anal. Calcd for **9**: $C_{40}H_{30}N_4O_4U$: C, 55.50; H, 3.48; N, 6.47. Found: C: 55.88; H, 3.35; N, 6.67.

Reduction of Na_2[U(bis-salophen)] 7, isolation of Na_6[U_2(bis-(bis-salophen))] 10

A purple THF solution (2 mL) of complex Na_2[U(bis-salophen)] (100.0 mg, 0,109 mmol, 1 equiv) was added to a sodium dispersion (3.0 mg, 0.131 mmol, 1.2 equiv) in 3 mL hexane. The mixture was stirred

for 12 hours, affording a deep bluish-brown suspension. The ^{1}H NMR (200 MHz, THF-d_8, 298 K) spectrum recorded for the crude mixture showed that several species have formed. The suspension was centrifuged, the supernatant was removed and the solid was washed with 3 x 2 mL THF. Blue single crystals of $Na_6[U_2$(bis-(bis-salophen))] **10** suitable for X-ray diffraction were grown upon recrystallisation of this solid by slow diffusion of hexane into a pyridine solution of the complex in presence of dibenzo18c6. ESI-MS : m/z = 1847.2 ([M-Na]$^-$).

[U_2(bis-salophen)]I_2 11-I

A deep purple solution of Na_2[U(bis-salophen)] **7** (98.2 mg, 0.107 mmol, 1 equiv) in THF (1 mL) was added dropwise to a red solution of [$UI_4(OEt_2)_2$)] (96.2 mg, 0.107 mmol, 1 equiv) in THF (1 mL). The reaction mixture was stirred for 12 hours at room temperature, affording a deep orange/brown suspension. The reaction mixture was filtered to remove NaI and 2 mL of hexane were added to the brown filtrate. The resulting solid was collected and dried *in vacuo* to give [U_2(bis-salophen)]I_2 **11-I** as a brown powder (107.0 mg). Attempts to further purify this solid from NaI impurities were unsuccessful. ESI-MS : m/z = 1231.1 ([U_2(bis-salophen)I]$^+$). ^{1}H NMR (200 MHz, THF-d_8, 298 K): δ = 91.2 (brs, 2H), 74.1 (brs, 2H), 70.6 (brs, 2H), 52.2 (brs, 2H), 50.8 (brs, 2H), 39.0 (s, 2H), 36.8 (s, 2H), 35.8 (brs, 2H), 26.6 (s, 2H), 17.9 (brs, 2H), -12.8 (s, 2H), -18.3 (s, 2H), -24.5 (s, 2H), -40.4 (s, 2H). Redissolution of the complex into pyridine results in a strong color change from orange to dark green-brown. Single crystals suitable for X-ray diffraction where obtained by slow diffusion of hexane into a pyridine solution of the complex. ^{1}H NMR (200 MHz, pyridine-d_5, 298 K): δ = 86.0 (brs, 4H), 83.6 (s, 2H), 72.7 (s, 2H), 68.6 (s, 2H), 55.0 (s, 2H), 50.0 (s, 2H), 43.4 (s, 2H), 41.1 (s, 2H), 32.1 (s, 2H), -19.6 (s, 2H), -21.3 (s, 2H), -24.0 (s, 2H), -27.6 (s, 2H).

[U_2(bis-salophen)]Cl_2 11-Cl

A deep purple solution of Na_2[U(bis-salophen)] **7** (10.0 mg, 0.011 mmol, 1 equiv) in THF (1 mL) was added onto UCl_4 (4.2 mg, 0.011 mmol, 1 equiv). The reaction mixture was stirred for 15 minutes at room temperature, affording an orange suspension. The reaction mixture was filtered to remove NaCl and the resulting orange filtrate was taken to dryness. Attempts to further purify this solid from NaCl impurities were unsuccessful. ^{1}H NMR (200 MHz, THF-d_8, 298 K): δ = 83.7 (brs, 2H), 67.7 (brs, 2H), 64.7 (brs, 2H), 46.0 (brs, 4H), 35.9 (s, 2H), 33.0 (s, 2H), 32.4 (brs, 2H), 24.5 (s, 2H), 7.3 (brs, 2H), -10.4 (s, 2H), -15.5 (s, 2H), -20.7 (s, 2H), -38.7 (s, 2H).

Reaction of [U_2(bis-salophen)]I_2 with I_2

A solution of [U_2(bis-salophen)]I_2 **11-I** (10.0 mg, ~0.007 mmol, 1 equiv) in pyridine (0.5 mL) was added onto I_2 (3.7 mg, 0.015 mmol, 2 equiv). The mixture was stirred at room temperature for 12 hours,

affording a red-orange solution. The ^{1}H NMR spectrum (200 MHz, pyridine-d_5, 298 K) recorded for the crude reaction mixture showed that complex $[UI_2(salophen)(py)_2]$ **3** was quantitatively formed.

$[U_2(cyclo\text{-}salophen)(THF)_4]$ 4-THF from $Na_2[U(bis\text{-}salophen)]$ 7

A deep purple solution of $Na_2[U(bis\text{-}salophen)]$ **7** (20.0 mg, 0.022 mmol, 1 equiv) in THF (1 mL) was added dropwise to a red solution of $[UI_4(OEt_2)_2]$ (19.6 mg, 0.022 mmol, 1 equiv) in THF (2 mL). The THF volume was adjusted to 4 mL and the reaction mixture was stirred for 12 hours, affording a deep orange/brown suspension. A potassium chunk (1.7 mg, 0.043 mmol, 2 equiv) was added and the mixture was stirred for another 12 hours giving a dark brown suspension. The reaction mixture was filtered and the resulting dark brown solution was taken to dryness to give $[U_2(cyclo\text{-}salophen)(THF)_4]$ **4-THF** as a brown solid (25.8 mg, 0.019 mmol, 85 % yield). The ^{1}H NMR spectrum of this solid (200 MHz, THF-d_8) was in agreement with the formation of $[U_2(cyclo\text{-}salophen)(THF)_4]$.

Synthesis of $[U(salfen)_2]$ 12

A solution of K_2salfen (50.0 mg, 0.099 mmol, 2 equiv) in THF (4 mL) was added to a red solution of $[UI_4(OEt_2)_2]$ (44.1 mg, 0.049 mmol, 1 equiv) in THF (4 mL). The resulting red suspension was stirred for 12 hours at room temperature before filtration. The resulting red filtrate was evaporated to dryness to give $[U(salfen)_2].0.2(KI)$ as a red powder (40.8 mg, 0.037 mmol, 75 % yield). The ^{1}H NMR spectrum recorded for this solid was identical to those obtained from the synthesis with $[UI_3(THF)_4]$. Single crystals suitable for X-ray diffraction were obtained by slow diffusion of diisopropyl ether into a THF solution of **12**. ^{1}H NMR (200 MHz, THF-d_8, 298 K): δ = 23.5 (s, 4H), 17.6 (t, 4H), 12.8 (d, 4H), 12.2 (t, 4H), 10.6 (s, 4H), 3.6 (s, 4H), -2.9 (s, 4H), -7.6 (s, 4H), -19.0 (s, 4H). ^{1}H NMR (200 MHz, pyridine-d_5, 298 K): δ = 23.9 (s, 4H), 17.8 (t, 4H), 12.9 (d, 4H), 12.3 (t, 4H), 10.7 (s, 4H), 4.1 (s, 4H), -2.6 (s, 4H), -7.6 (s, 4H), -19.0 (s, 4H). Anal. Calcd for $[U(salfen)_2].0.2(KI)$ $C_{48}H_{36}Fe_2N_4O_4UK_{0.2}I_{0.2}$: C, 51.67; H, 3.25; N, 5.02. Found: C, 51.70; H, 3.48; N, 4.96.

Reaction of K_2salfen with $[UI_3(THF)_4]$

A solution of K_2salfen (7.5 mg, 0.010 mmol, 1 equiv) in THF-d_8 (0.5 mL) was added to a blue solution of $[UI_3(THF)_4]$ (5.0 mg, 0.010 mmol, 1 equiv) in THF-d_8 (0.5 mL). The resulting brown suspension was stirred for 1 hour at room temperature and the solids were removed by filtration. The ^{1}H NMR (200 MHz, THF-d_8, 298 K) spectrum of this solution shows that $[U(salfen)_2]$ **12** is obtained as the unique salfen-containing species.

Reduction of [U(salfen)$_2$]

A solution of K_2salfen (50.0 mg, 0.099 mmol, 2 equiv) in THF (4 mL) was added to a red solution of [$UI_4(OEt_2)_2$] (44.1 mg, 0.049 mmol, 1 equiv) in THF (4 mL). The resulting red suspension was stirred for 30 minutes at room temperature. To the resulting red-orange suspension was added KC_8 (26.5 mg, 0.196 mmol, 4.0 equiv) and the mixture was stirred at room temperature for 2 hours. This afforded a dark brown suspension. The solid residues were removed by centrifugation. The ^{1}H NMR spectrum recorded for the supernatant fraction showed the formation of mixture of K_3[U(bis-salfen)(bis-Hsalfen)] **13-H** and K_2[U(bis-Hsalfen)$_2$] **13-H$_2$**. Single crystals of **13-H** suitable for X-ray diffraction were grown by slow diffusion of diisopropyl ether into this solution. While the quality of the structure is not sufficient for a discussion of the metrical parameters, the connectivity clearly shows the presence of a complex of formula K_3[U(bis-salfen)(bis-Hsalfen)] ; space group $P2_1/a$; a = 20.5937(13) Å, b = 31.3962(15) Å, c = 25.6297(12) Å, α = β = 90, γ = 108.864(6) Å. Spectroscopic data for K_3[U(bis-salfen)(bis-Hsalfen)] **13-H**: ESI-MS : m/z = 1201.0 $[M + H]^+$. ^{1}H NMR (200 MHz, THF-d_8, 298 K): δ = 36.4 (d, 1H), 32.3 (d, 1H), 30.5 (d, 1H), 27.5 (d, 1H), 21.0 (t, 1H), 17.3 (d, 1H), 16.2 (d, 1H), 15.7 (d, 1H), 13.6 (d, 1H), 12.1 (s, 1H), 10.4 (s, 1H), 10.1 (s, 1H), 9.6 (t, 1H), 9.3 (t, 1H), 9.1 (t, 1H), 9.0 (t, 1H), 7.0 (t, 1H), 6.8 (t, 1H), 6.4 (t, 1H), 6.1 (t, 1H), 4.5 (s, 1H), 3.4 (s, 1H), 3.3 (s, 1H), 2.5 (s, 1H), 2.1 (s, 1H), 2.0 (d, 1H), 1.5 (s, 1H), 0.9 (d, 1H), 0.4 (s, 1H), 0.3 (d, 1H), -1.5 (d, 1H), -1.7 (s, 1H), -2.6 (s, 1H), -3.0 (s, 1H), -23.2 (s, 1H), -26.6 (s, 1H), -27.5 (s, 1H).

Single crystals of K_2[U(bis-H_2salfen)] **13-H$_2$** suitable for X-ray diffraction were grown by slow diffusion of hexane into a pyridine solution of the complex in presence of excess dibenzo18c6. Spectroscopic data for K_2[(bis-Hsalfen)$_2$] **13-H$_2$**: ^{1}H NMR (200 MHz, THF-d_8, 298 K): δ = 19.7 (d, 2H), 13.5 (t, 2H), 13.0 (d, 2H), 11.7 (t, 2H), 10.4 (t, 2H), 9.6 (t, 2H), 9.2 (d, 2H), 8.0 (d, 2H), -2.7 (s, 2H), -3.1 (s, 2H), -3.3 (s, 2H), -5.3 (s, 2H), -6.1 (s, 2H), -6.9 (s, 2H), -12.0 (s, 2H), -13.1 (s, 2H), -16.8 (s, 2H), -19.1 (brs, 2H).

When a larger excess (up to 8.0 equiv) of KC_8 was used, intractable mixtures were obtained. The ^{1}H NMR spectra recorded for the crude mixtures were displaying numerous resonances corresponding to the formation of several unidentified complexes in addition of K_3[U(bis-salfen)(bis-Hsalfen)] and K_2[U(bis-H_2salfen)].

[UCl$_2$(^{Me}naphtquinolen)$_2$] 14-Cl

A solution of K-^{Me}naphtquinolen (92.3 mg, 0.263 mmol, 2 equiv) in THF (10 mL) was added to UCl_4 (50.0 mg, 0.132 mmol, 1 equiv) and the reaction mixture was stirred at room temperature overnight, affording an orange suspension. The mixture was filtered to remove KCl, the THF volume of the filtrate was reduced to 2 mL and the solution was layered with hexane. The resulting orange precipitate was filtered and dried under vacuum to afford **14-Cl** as an orange solid. (89.0 mg, 0.096

mmol, 72% yield). ^{1}H NMR (200 MHz, THF-d_8, 298 K): δ = 25.7 (s, 2H), 19.4 (d, 2H), 13.0 (d, 2H), 11.8 (d, 2H), 10.1 (t, 2H), 9.7 (t, 2H), 9.5 (m, 2H), 5.6 (s, 6H), 1.0 (d, 2H)-0.4 (t, 2H), -0.8 (m, 2H), -3.0 (d, 2H), -6.1 (s, 2H). Anal. Calcd for [UCl_2(^{Me}naphtquinolen)$_2$] **14-Cl** : $C_{42}H_{30}Cl_2N_4O_2U$: C, 54.15; H, 3.25; N, 6.01. Found: C, 54.03; H, 3.41; N, 6.06. Single crystals suitable for X-ray diffraction were obtained by slow diffusion of hexane into a pyridine solution of **14-Cl**.

[U(μ-bis-^{Me}naphtquinolen)]$_2$ 15

A solution of K^{Me}naphtquinolen (150.0 mg, 0.428 mmol, 2 equiv) in THF (8 mL) was added to [$UI_4(OEt_2)_2$] (191.3 mg, 0.214 mmol, 1 equiv) and the reaction mixture was stirred at room temperature overnight, affording a yellowish-brown suspension. Intermediate data for [UI_2(^{Me}naphtquinolen)$_2$] **14-I**: ^{1}H NMR (200 MHz, pyridine-d_5, 298 K): δ = 108.9 (br s, 2H), 37.9 (s, 2H), 37.3 (s, 6H), 31.1 (s, 2H), 29.7 (br s, 2H), 22.1 (s, 2H), 21.6 (s, 2H), 18.0 (br s, 6H), 16.9 (s, 2H), 4.3 (s, 4H), 0.6 (s, 2H), -3.2 (s, 2H) -7.4 (s, 2H). This mixture was added onto potassium chunks and then stirred at room temperature for 12 hours. The reaction mixture gradually turned dark olive brown. The mixture was filtered to remove KI and the filtrate evaporated to dryness. The resulting brown solid was extracted with toluene (12 mL) to give a brown suspension that was filtered. The filtrate was taken to dryness to give [U(μ-bis-^{Me}naphtquinolen)]$_2$ **15** as a brown solid (122.9 mg, 0.071 mmol, 67% yield). ^{1}H NMR (200 MHz, toluene-d8, 298 K): δ = 88.0 (s, 2H), 46.2 (s, 2H), 41.7 (m, 4H), 33.1 (d, 2H), 31.2 (d, 2H), 30.9 (d, 2H), 20.0 (t, 2H), 17.8 (d, 2H), 15.1 (d, 2H), 14.9 (m, 2H), 13.2 (t, 2H), 12.3 (t, 2H), 10.4 (t, 2H), 8.9 (dt, 2H), 7.2 (d, 2H), 5.6 (d, 2H), 5.2 (d, 2H), 2.5 (d, 2H), -3.9 (d, 2H), -5.1 (d, 2H), -5.9 (t, 2H), -7.7 (s, 6H, CH_3), -9.0 (d, 2H), -13.8 (d, 2H), -25.8 (s, 6H, CH_3). Anal. Calcd for **15** $C_{84}H_{60}N_8O_4U_2$: C, 58.61; H, 3.51; N, 6.51. Found: C, 58.37; H, 3.73; N, 6.38. Single crystals suitable for X-ray diffraction were obtained by slow diffusion of hexane into a toluene solution of **15**.

Upon dissolution of **15** into pyridine, 2 sets of proton signals are observed in solution assigned to the dimeric complex **15** and the monomeric analogue **15-b** : ^{1}H NMR (500 MHz, pyridine-d_5, 298 K): Ratio of complexes **15** : **15-b**: 3:1 after 30 minutes, 0,5:1 after 4 days. Complex **15**: δ = 85.7 (s, 2H), 47.4 (d, 2H), 41.1 (d, 2H), 35.2 (d, 2H), 32.3 (d, 2H), 28.9 (s, 2H), 28.1 (d, 2H), 18.4 (t, 2H), 16.7 (d, 2H), 15.2 (t, 2H), 11.3 (t, 2H), 11.2 (t, 2H), 11.1 (t, 2H), 10.9 (d, 2H), 9.8 (d, 2H), 8.9 (d, 2H), 8.1 (d, 2H), 6.3 (d, 2H), 5.2 (d, 2H), 0.9 (s, 6H, CH_3), -0.7 (d, 2H), -3.8 (t, 2H), -6.7 (d, 2H), -9.5 (d, 2H), -10.0 (d, 2H), -13.9 (s, 6H, CH_3). Complex **15-b** : δ = 91.3 (s, 2H), 47.6 (d, 2H), 45.9 (d, 2H), 44.1 (s, 2H), 35.6 (d, 2H), 32.1 (d, 2H), 20.2 (d, 2H), 19.3 (d, 2H), 19.1 (t, 2H), 17.5 (m, 2H), 14.3 (t, 2H), 13.9 (t, 2H), 13.7 (d, 2H), 13.4 (t, 2H), 13.3 (d, 2H), 6.5 (s, 6H, CH_3), 5.7 (d, 2H), 4.6 (d, 2H), 3.7 (t, 2H), 2.2 (s, 2H), 1.6 (d, 2H), -5.3 (t, 2H), -5.7 (d, 2H), -7.0 (d, 2H), -11.8 (d, 2H), -15.0 (s, 6H, CH_3).

Reduction of [UCl_2(^{Me}naphtquinolen)$_2$] 14-Cl

To a solution of **14-Cl** (24.5 mg, 0.026 mmol, 1 equiv) in THF (2 mL) was added a suspension of potassium graphite (7.1 mg, 0.053 mmol, 2 equiv) in THF (2 mL) and the reaction mixture was stirred at room temperature for 15 minutes, affording a deep brown suspension. Graphite was removed by centrifugation. The ^{1}H NMR spectrum (200 MHz, THF-d_8, 298 K) recorded for the crude reaction mixture showed the formation of **15** and **15-b** as the only ^{Me}naphtquinolen-containing species.

To a solution of **14-Cl** (24.5 mg, 0.026 mmol, 1 equiv) in THF (4 mL) was added a potassium chunk (2.1 mg, 0.053 mmol, 2 equiv) and the reaction mixture was stirred at room temperature overnight, affording a deep brown suspension. The ^{1}H NMR spectrum (200 MHz, THF-d_8, 298 K) recorded for the crude reaction mixture showed that a complex mixture of compounds had formed, among which the resonances of **15** and **15b** could be identified.

[U(9,10-phenanthrenediol)(^{Me}naphtquinolen)$_2$] 16

A toluene (6 mL) 9,10-phenanthrenequinone (12.2 mg, 0.059 mmol, 2 equiv) solution was prepared and added to a toluene (4 mL) solution of complex **15** (50.6 mg, 0.029 mmol, 1 equiv). Immediately the deep brown solution turned yellowish green. The mixture was stirred 3 hours before filtration. The brown solid was washed with 2 x 0.5 mL toluene and dried *in vacuo* to give [U(9,10-phenanthrenediol)(^{Me}naphtquinolen)$_2$] **16** as a brown-gold solid (33.8 mg, 0.032 mmol, 54% yield). Similar results were obtained when performing the reaction in pyridine. Single crystals suitable for X-ray diffraction were obtained by slow evaporation of a saturated pyridine solution of the complex. ^{1}H NMR (200 MHz, toluene-d_8, 298 K): δ = 27.6 (s, 2H), 19.9 (s, 2H), 19.1 (s, 2H), 18.6 (s, 2H), 16.2 (d, 2H), 13.0 (t, 2H), 12.5 (d, 2H), 11.7 (t, 2H), 9.4 (t, 2H), 9.3 (t, 2H), 8.0 (d, 2H), 0.7 (t, 2H), 0.6 (d, 2H), -1.1 (d, 2H), -2.4 (d, 2H), -5.2 (d, 2H), -10.5 (s, 6H). Anal. Calcd for **16**.(toluene$_{0.2}$) $C_{57.2}H_{39.6}N_4O_4U$: C, 63.32; H, 3.68; N, 5.16. Found: C, 63.54; H, 3.85; N, 5.25.

Reaction of 15 with I_2

To a stirring solution of **15** (9.7 mg, 0.006 mmol, 1 equiv) in toluene (0.5 mL) was added dropwise a solution of iodine (2.9 mg, 0.011 mmol, 2 equiv) in toluene (1 mL). Immediately, the dark brown solution turned pale brown and a yellowish-brown precipitate formed. After 10 minutes stirring, the crude reaction was taken to dryness and dissolved back into pyridine. The ^{1}H NMR spectrum (200 MHz, pyridine-d_5, 298 K) recorded for the crude reaction mixture showed that complex **14-I** was restored.

Reaction of 15 with dry O_2, isolation of $[UO_2(^{Me}naphtquinolen)_2]$ 17

A pyridine (6 mL) solution of complex **15** (58.0 mg, 0.034 mmol, 1 equiv) was transferred into a reaction vessel. The suspension was degassed using a freeze-pump-thaw procedure. Then 1 atmosphere of dry dioxygen was introduced into the flask. Immediately, a color change from dark brown to dark red/orange was observed. The reaction was stirred for 12 hours at room temperature before the solvent was removed *in vacuo*. The solid was washed with toluene (3 x 2 mL), recovered and dried in vacuo to afford $[UO_2(^{Me}naphtquinolen)_2]$ **17** as a bright orange solid (42.0 mg, 0.047 mmol, 69% yield). ^{1}H NMR (200 MHz, THF-d_8, 298 K): δ = 10.3 (s, 2H, N=CH), 8.5 (d, 2H, H_{aro}), 8.2 (d, 2H, H_{aro}), 7.9-7.8 (m, 6H, H_{aro}), 7.7-7.5 (m, 6H, H_{aro}), 7.4 (t, 2H, H_{aro}), 7.2 (t, 2H, H_{aro}), 6.2 (d, 2H, H_{aro}), 3.4 (s, 6H, CH_3). Anal. Calcd for **17**.($KI_{0.25}$) $C_{42}H_{30}N_4O_4UK_{0.25}I_{0.25}$: C, 54.00; H, 3.24; N, 6.00. Found: C, 53.88; H, 3.49; N, 5.98. The presence of KI arises from the residual presence of KI in the batch of complex **15** used in this reaction.

$[U(OSi(O^tBu)_3)_2(\mu\text{-}OSi(O^tBu)_3)]_2$ 18

A cold solution of $(^tBuO)_3SiOH$ (1.174 g, 4.44 mmol, 3 equiv) in hexane (3 mL, -40 °C) was added dropwise to a cold slurry of $[U\{N(SiMe_3)_2\}_3]$ (1.070 g, 1.48 mmol, 1 equiv) in hexane (4 mL, -40 °C), resulting in a color change from violet to dark brown. The solution was stirred at -40 °C for 20 minutes, and the solution was filtered on a cold frit. The brown crystals collected, suitable for XRD studies, were washed with cold hexane (2 x 0.5 mL) and dried *in* vacuum to yield 730 mg of a brown crystalline powder of $[U(OSi(O^tBu)_3)_2(\mu\text{-}OSi(O^tBu)_3)]_2$ **18**. The dark filtrate was left standing at -40°C for one week, resulting in the isolation of another crop of brown crystals. (517 mg collected). Combined yield: 1.247 g, 0.61 mmol, 82%. ESI-MS: m/z = 1027.3 ($[U(OSi(O^tBu)_3)_3]^+$). ^{1}H NMR (400 MHz, THF-d_8, 298 K): δ = 2.62 (s, 162H, CH_3). ^{1}H NMR (200 MHz, hexane-d_{14}, 298 K): δ = 5.13 (s, 108H, $CH_{3\ terminal\ silanol}$). -9.55 (s, 54H, $CH_{3\ bridging\ silanol}$). ^{1}H NMR (200 MHz, toluene-d_8, 298 K): δ = 5.25 (s, 108H, $CH_{3\ terminal\ silanol}$). -9.57 (s, 54H, $CH_{3\ bridging\ silanol}$). Anal. Calcd for **18**: $C_{72}H_{162}O_{24}Si_6U_2$: C 42.05; H 7.94; N 0.00; U, 23.14; Found C 41.31; H 7.85; N, <0.2. The lower value found for carbon is probably due to the partial decomposition of the complex.

$[U(OSi(O^tBu)_3)_3(THF)_2]$ 18-THF

Cold THF (4 mL) was added onto a refrigerated (- 40°C) pure sample of **1** (70.0 mg, 0.034 mmol) inside the fridge (- 40°C) and the resulting purple/brown solution was stirred at - 40°C for 10 minutes. THF was removed *in vacuo*, and the resulting purple/brown powder was dried under vacuum for 15 min to give the solvate analogue of **18** $[U(OSi(O^tBu)_3)_3(THF)_2]$ **18-THF** (75.0 mg, 0.064 mmol, 94% yield). Elemental analysis confirmed the presence of two molecule of THF solvent. Anal. Calcd for **18-THF**: $C_{44}H_{97}O_{14}Si_3U$: C 45.07; H 8.34; N 0.00; Found : C 44.71; H 8.16; N 0.20. Purple hexagonal plates

suitable for X-ray diffraction were obtained upon letting stand at -40°C a hexane solution of **18** in presence of 0.05 mL of THF. While the quality of the structure is not sufficient for a discussion of the metrical parameters, the connectivity clearly shows the presence of a complex of formula $[U(OSi(O^tBu)_3)_3(THF)2]$; space group P_{63}, a = b = 13.9953(1) Å, c = 17.3289(8) Å, α = β = 90, γ = 120, Z = 2. ^{1}H NMR (400 MHz, THF-d_8, 298 K): δ = 2.6 (s, 81H, CH_3). This complex decomposes in 5 days at room temperature in THF solution to give a new unidentified species as seen by ^{1}H NMR (200 MHz, THF-d_8, 298 K): δ = 10.5 (brs, 81H, CH_3).

Decomposition studies of 18

The brown/orange powder of **18** fades slowly to pale brown in 3 days at r.t., and then to pale blue/green in 1 week to give $[U(OSi(O^tBu)_3)_2(\mu\text{-}O_2Si(O^tBu)_2)]_2$ **19** that can be recrystallized from hexane. The formation of **19** from **18** is also occurring in solution. Proton NMR studies in deuterated hexane show that decomposition of **18** to yield **19** occurs at room temperature over 7 days.

When the decomposition reaction is stopped earlier a decomposition intermediate is isolated. Notably when the hexane decomposition reaction mixture is filtered after 24 hours and the resulting pale brown filtrate is taken to dryness, extracted with toluene and cooled to -40°C, few pale brown crystals of $[U_2(OSi(O^tBu)_3)_4(\mu\text{-}O_2Si(O^tBu)_2)(\mu\text{-}OSi(O^tBu)_3)]$ **20** suitable for XRD studies were obtained in one week. This complex could not be isolated analytically pure as **18**, **19** and **20** cocrystallized in the same conditions, and their separation by recrystallization was unsuccessful as these species exhibit similar solubility.

$[U(OSi(O^tBu)_3)_2(\mu\text{-}O_2Si(O^tBu)_2)]_2$ 19

A vial was charged with $[U(OSi(O^tBu)_3)_2(\mu\text{-}OSi(O^tBu)_3)]_2$ **18** (160.0 mg, 0.077 mmol) and the compound was heated in the solid state at 80°C for 30 minutes during which time the color of the solid turned from brown/orange to pale blue. The volatiles were distilled in a NMR tube containing frozen deuterated toluene in liquid nitrogen. ^{13}C and ^{1}H NMR spectra from this tube reveal the formation of isobutene ^{1}H NMR (200 MHz, toluene-d_8, 298 K): δ = 4.70 (s, 2H, C=CH_2), 2.60 (s, 6H, CH_3). ^{13}C NMR (50 MHz, toluene-d_8, 298 K): δ = 141.81 (Me_2C=CH_2), 111.10 (Me_2C=CH_2), 23.14 (CH_3). ^{1}H NMR (200 MHz, THF-d_8, 298 K): δ = 4.62 (m, 2H, C=CH_2), 1.69 (t, 6H, CH_3). The ^{1}H NMR spectra also reveal the formation of alkane volatile products that could correspond to isobutane. Analysis of the volatile fraction by GC indicated the absence of H_2. The blue/green solid was recrystallized in hexane (1 mL) to afford after 12 hours at -40°C turquoise hexagonal plates suitable for XRD studies. The crystals were collected and dried *in vacuo* to give **19** as a pure crystalline solid (121.7 mg, 0.063 mmol, 81% yield). Complex **19** is stable for weeks in hexane and toluene at room temperature. Alternatively pale blue single crystals of **19-THF** were grown upon letting stand at -40°C a saturated hexane

solution of **19** in presence of 10% THF. ESI-MS: m/z = 1677.5 ([2-OSi(O^tBu)$_3$]$^+$). ^{1}H NMR (200 MHz, toluene-d_8, 298 K): δ = 3.5 (s, 108H, $CH_{3\ terminal\ silanol}$); -7.1 (s, 36H, $CH_{3\ bridging\ silanol}$). ^{1}H NMR (200 MHz, hexane-d_{14}, 298 K): δ = 3.5 (s, 108H, $CH_{3\ terminal\ silanol}$); -7.5 (s, 36H, $CH_{3\ bridging\ silanol}$). ^{1}H NMR (200 MHz, THF-d_8, 298 K): δ = 7.8 (s, 108H, $CH_{3\ terminal\ silanol}$); -9.3 (s, 36H, $CH_{3\ bridging\ silanol}$). Anal. Calcd for **19**: $C_{64}H_{144}O_{24}Si_6U_2$: C 39.57; H 7.47; N 0.00; Found C 39.51; H 7.48; N <0.2.

Thermal decomposition of [U(OSi(O^tBu)$_3$)$_2$(μ-O_2Si(O^tBu)$_2$)]$_2$ 19

A vial was charged with turquoise crystals of [U(OSi(O^tBu)$_3$)$_2$(μ-O_2Si(O^tBu)$_2$)]$_2$ **19** and the compound was heated in the solid state at 200°C for 2 hours during which time the color of the solid turned khaki green. This material is insoluble in THF. Addition of deuterated THF into the vial followed by filtration gave a colorless solution. The ^{1}H NMR spectrum recorded for this solution showed the resonances of H_2O, HOSi(O^tBu)$_3$ and isobutene. The resonances of **19** were not detected.

[KU(OSi(O^tBu)$_3$)$_2$(μ-O_2Si(O^tBu)$_2$)]$_2$ 21

A 8 mL THF solution of **19** (41.2 mg, 0.021 mmol, 1 equiv) was added onto KC_8 (7.2 mg, 0.053 mmol, 2.5 equiv). The mixture was stirred at room temperature for 2 hours, affording a dark brown suspension. The mixture was centrifuged, the THF supernatant was collected and THF was removed *in vacuo*. The resulting purple-brown solid was washed with 0.5 mL hexane and dried *in vacuo* to afford [KU(OSi(O^tBu)$_3$)$_2$(μ-O_2Si(O^tBu)$_2$)]$_2$ **21** as a brown powder (36.2 mg, 0.018 mmol, 85% yield). Brown single crystals suitable for X-ray diffraction were obtained upon letting stand at -40°C a saturated THF/DIPE solution of **21** for 12 hours. ESI-MS: m/z = 1659.3 ([**21** -KOSi(O^tBu)$_3$ –^{t}Bu]$^+$). ^{1}H NMR (200 MHz, THF-d_8, 298 K): δ = 2.7 (s, 108H, $CH_{3\ terminal\ silanol}$); -11.8 (s, 36H, $CH_{3\ bridging\ silanol}$). Anal. Calcd for **21**: $C_{64}H_{144}O_{24}Si_6U_2K_2$: C 38.04; H 7.18; N 0.00; Found C 37.80; H 7.04; N <0.1. ^{1}H NMR studies of a THF solution of **21** stored at r.t. showed that **21** is completely converted after 7 days into **22** and other unidentified decomposition products.

[K_2U_2(OSi(O^tBu)$_3$)$_4$(O_2Si(O^tBu)$_2$)(O_3Si(O^tBu))]$_2$ 22

A vial was charged with [KU(OSi(O^tBu)$_3$)$_2$(μ-O_2Si(O^tBu)$_2$)]$_2$ **21** (23.0 mg, 0.011 mmol) and the compound was heated in the solid state at 80°C for 120 minutes during which time the color of the solid turned from brown/purple to greenish grey. The solid was recrystallized in hexane (0.4 mL) to afford after 12 hours at -40°C green single crystals suitable for XRD studies. The crystals were collected and dried *in vacuo* to give **22** as a pure crystalline solid (14.4 mg, 0.073 mmol, 69% yield). ^{1}H NMR (200 MHz, THF-d_8, 298 K): δ = 23.4 (s, 9H); 22.0 (s, 9H); 14.5 (s, 9H); -5.8 (s, 54H); -5.9 (s, 54H). Anal. Calcd for **22**: $C_{120}H_{270}O_{48}Si_{12}U_4K_4$: C 36.70; H 6.93; N 0.00; Found C 36.80; H 6.94; N <0.2.

$[U(OSi(O^tBu)_3)_4]$ 23

A solution of $[UI_4(OEt_2)_2]$ (227.5 mg, 0.25 mmol, 1 equiv) in THF (2 mL) was added to a solution of $KOSi(O^tBu)_3$ (308.0 mg, 1.02 mmol, 4 equiv) in THF (2 mL). The reaction mixture was stirred at room temperature for 4 hours. The resulting light blue suspension was filtered to remove KI and the green filtrate was evaporated to dryness to give a microcrystalline pale green solid. This solid was dissolved twice in 3 mL of hexane, triturated, and evaporated to dryness. The resulting solid was dissolved in 1 mL of hexane and cooled to -40°C. After 12 hours, blue crystals were recovered and dried *in vacuo* for 4 hours giving $[U(OSi(O^tBu)_3)_4]$ **23** as a light lilac powder (289.0 mg, 0.22 mmol, 88% yield). Single crystals suitable for X-ray diffraction analysis were obtained upon cooling a concentrated toluene solution of $[U(OSi(O^tBu)_3)_4]$ to -40°C. Recrystallization of this complex in pyridine afforded green single crystals of $[U(OSi(O^tBu)_3)_4(py)_2]$, **23-py**. ^{1}H NMR (200 MHz, hexane-d_{14}, 298 K): δ = 0.98 (s, 108H, CH_3). ^{1}H NMR (200 MHz, toluene-d_8, 298 K): δ = 1.06 (s, 108H, CH_3). ^{1}H NMR (200 MHz, THF-d_8, 298 K): δ = 1.9 (br s, 108H, CH_3). ^{1}H NMR (200 MHz, pyridine-d_5, 298 K): δ = 1.90 (s, 54H, CH_3) ; 1.90 (s, 54H, CH_3). ^{1}H NMR (200 MHz, pyridine-d_5, 263 K): δ = 9.7 (br s, 54H, CH_3) ; -2.7 (br s, 54H, CH_3). ^{1}H NMR (200 MHz, pyridine-d_5, 353 K): δ = 3.1 (br s, 108H, CH_3). ^{13}C NMR (50 MHz, hexane-d_{14}, 298 K): δ = 28.99 (s, CH_3), 68.33 (s, $OC(CH_3)_3$). ^{13}C NMR (50 MHz, toluene-d_8, 298 K): δ = 31.29 (s, CH_3), 67.74 (s, $OC(CH_3)_3$). Anal. Calcd for $[U(OSi(O^tBu)_3)_4]$ **23**: $C_{48}H_{108}O_{16}Si_4U$: C 44.6; H 8.4; N 0.0; Found: C 44.3; H 8.3; N <0.2. ESI-MS: m/z = 1313.5 ($[M+Na]^+$); 1329.5 ($[M+K]^+$).

$[K(18c6)][U(OSi(O^tBu)_3)_4]$ 24

KC_8 (25.3 mg, 0.187 mmol, 1.5 equiv) was added to a cold (- 40°C) solution of $[U(OSi(O^tBu)_3)_4]$ **23** (161.0 mg, 0.125 mmol, 1 equiv) and 18-crown-6 (32.9 mg, 0.125 mmol, 1 equiv) in THF (2 mL). The resulting dark orange suspension was stirred for 1 hour at -40°C. The suspension was centrifuged, the supernatant was collected and the solvent was removed *in vacuo*. The resulting solid was washed with 1 mL of hexane and 6 x 1 mL of toluene and dried *in vacuo* to give $[K(18c6)][U(OSi(O^tBu)_3)_4]$ **24** as an orange solid in 69% yield (138 mg, 0.087 mmol). Recrystallisation of this orange solid in toluene produced X-ray quality crystals of **24**. ^{1}H NMR (400 MHz, toluene-d_8, 298 K): δ 3.40 (s, 24H, 18c6), -0.15 (brs, 108H, $OC(CH_3)_3$). ^{1}H NMR (400 MHz, THF-d_8, 298 K): δ 3.64 (s, 24H, 18c6), 1.18 (brs, 108H, $OC(CH_3)_3$). Anal. Calcd for $[K(18c6)][U(OSi(O^tBu)_3)_4]$ **24**: $C_{60}H_{132}O_{22}Si_4KU$: C 45.2; H 8.3; N 0.00; Found: C 45.0; H 8.3; N <0.1. ESI-MS: m/z= 1290.4 $[U(OSi(O^tBu)_3)_4]^-$.

$[\{U(OSi(O^tBu)_3)_3\}_2(\mu\text{-}\eta^2\text{:}\eta^2\text{-}CS_2)]$ 25

Carbon disulfide (11.2 µL, 0.117 mmol, 2 equiv, i.e. 1 equiv per U center) dissolved in hexane (1 mL) was added to a suspension of **18** (120.0 mg, 0.058 mmol, 1 equiv) in hexane (1 mL). Within seconds, the brown precipitate disappeared and the hexane solution faded to yellow. The solution was stirred at

room temperature for 30 min, filtered and then cooled to -40 °C. After 12 hours, dark brown crystals were collected and dried *in vacuo*. Reduction of the solvent volume and cooling to -40°C produced a second crop of crystals. Combined yield: 53% (66.1mg, 0.031 mmol). The relatively low yield is due to the high solubility of the complex and could be increased by performing the reaction on larger scale. ^{1}H NMR (400 MHz, hexane-d_{14}, 298 K): δ = 0.61 (s, 81H, CH_3), 0.02(s, 81H, CH_3). ^{13}C NMR (100 MHz, hexane-d_{14}, 298 K): δ = 70.37 (s, $OC(CH_3)_3$), 68.61 (s, $OC(CH_3)_3$), 28.65 (s, CH_3), 28.25 (s, CH_3). Anal. Calcd for **25**: $C_{73}H_{162}O_{24}Si_6S_2U_2$: C 41.11; H 7.66; N 0.00; Found: C 40.51; H 7.49; N <0.2. The same procedure was followed to produce the^{13}C carbon disulfide analogue of **25**. The ^{1}H NMR and ^{13}C NMR (100 MHz, hexane-d_{14}, 298 K) spectra were identical those of **25**.

[{U(OSi(O^{t}Bu)$_3$)$_3$}$_2$(μ-η^1:η^2-CO$_3$)] 26

Two equivalents of CO_2 (0.108 mmol, 2 equiv, i.e. 1 equiv per U center) were condensed on a liquid nitrogen frozen suspension of **18** (111.2 mg, 0.054 mmol, 1 equiv) in toluene (8 mL). The brown suspension was allowed to warm up at room temperature under stirring, during which time continuous bubbling was observed. The reaction was stirred at room temperature over 5 h resulting in a color fading of the solution to pale green. The solvent was evaporated to dryness, and the resulting solid was recrystallized in 1 mL toluene at -40 °C. Pale green crystals of **26** suitable for XRD studies were grown in one night, collected and dried *in vacuo* (38.2 mg, 0.018 mmol, 33% yield). Concomitant generation of CO during the reaction was observed, and was characterized by ^{13}CNMR and by reaction with vanadocene affording $V(Cp)_2(CO)$ (see below). ESI-MS: m/z = 2155.0 ([**26**+K]$^+$) ; 1173.5 ([U(CO$_3$)(OSi(O^{t}Bu)$_3$)$_3$].hexane$^+$) ; 1027.3 ([U(OSi(O^{t}Bu)$_3$)$_3$]$^+$). ^{1}H NMR (200 MHz, hexane-d_{14}, 298 K): δ = 0.492 (s, 162H, CH_3). Anal. Calcd for **26**: $C_{73}H_{162}O_{27}Si_6U_2$: C 41.42; H 7.71; N, 0.00; Found: C 40.97; H 7.88; N, <0.2. The same procedure was followed to produce the ^{13}C carbon dioxide analogue of **26** and the reaction was followed by ^{13}C-NMR. This analysis revealed that ^{13}CO was formed during the reaction. ^{1}H NMR studies showed that **26** is not stable in solution and evolves in a few hours to give a pale blue toluene solution containing [U(OSi(O^{t}Bu)$_3$)$_4$] **23** as the single siloxide species. Pale blue crystals of **23** suitable for XRD studies were grown from this concentrated solution at -40°C confirming the presence of [U(OSi(O^{t}Bu)$_3$)$_4$].

Characterisation of CO generated during the course of the reaction using V(Cp)$_2$

Condensation of the gases generated during the reaction on a frozen violet solution of $V(Cp)_2$ (3 mg, 0.016 mmol, 0.66 equiv) afforded, after allowing the solution to warm up at room temperature, a dark brown solution. This solution was cooled down at -40°C to afford dark brown micro-crystals of $V(Cp)_2(CO)$, presenting identical IR spectra than the published compound, with a strong band at 1881 cm^{-1} attributed to the CO stretches.[488]

Reaction of 18 with AdN_3, isolation of $[U_2(NAd)_4(OSi(O^tBu)_3)_4]$ 27

A vial was charged with $[U(OSi(O^tBu)_3)_2(\mu\text{-}OSi(O^tBu)_3)]_2$ **18** (123.5 mg, 0.060 mmol, 1 equiv) and the compound was dissolved in 5 mL of toluene. To this brown solution was added a 5 mL toluene solution of AdN_3 (21.3 mg, 0.120 mmol, 2 equiv) and the reaction mixture was vigorously stirred for 4 hours at room temperature. A strong N_2 bubbling was observed. Analysis of the crude reaction mixture by ^{1}H NMR (200 MHz, toluene-d_8, 298 K) showed the formation of $[U_2(NAd)_4(OSi(O^tBu)_3)_4]$ **27** and $[U(OSi(O^tBu)_3)_4]$ **23** in a 1:2 ratio. The resulting dark brown solution was taken to dryness and the residue was extracted with 0.5 mL hexane, filtered and the filtrate was cooled to -40°C. Crystals were grown from this solution in 2 days. The crystals were collected and dried *in vacuo* to give **27** as a brown crystalline solid (22.2 mg, 0.010 mmol, 35 % yield). The presence of small amounts (~ 6%) of the second reaction product (**23**) in this solid prevented the obtention of a satisfactory elemental analysis. Brown crystals of **27** suitable for XRD were grown similarly. ESI-MS: m/z = 2141.7 ($[M+OH]^-$). ^{1}H NMR (200 MHz, toluene-d_8, 298 K): δ 2.29 (brs, 3H, $H_{adamantyl}$), 1.91 (brs, 9H, $H_{adamantyl}$), 1.83 (brs, 108H, $OC(CH_3)_3$), 1.54 (brs, 3H, $H_{adamantyl}$), 1.23 (brs, 6H, $H_{adamantyl}$), 1.12 (brs, 18H, $H_{adamantyl}$), 0.67 (brs, 18H, $H_{adamantyl}$).

$[K(18c6)][U(NSiMe_3)(OSi(O^tBu)_3)_4]$ 28-TMS

A 100 µL portion of a 0.94 M THF solution of trimethylsilyl azide (0.094 mmol, 1 equiv) was added to a cold (-40°C) 2 mL THF solution of $[K(18c6)][U(OSi(O^tBu)_3)_4]$ **24** (150.0 mg, 0.094 mmol, 1 equiv). An immediate color change from dark orange to brown was observed together with N_2 evolution. The resulting solution was stirred for 30 minutes before the solvent was removed *in vacuo*. The resulting brown oil was extracted with 2 mL toluene, filtered and the filtrate was stored 48 hours at -40° C to afford $[K(18c6)][U(NSiMe_3)(OSi(O^tBu)_3)_4]$ **28-TMS** as a brown crystalline solid in 48% yield (75.5 mg, 0.045 mmol). Similar procedure was followed to produce brown triangular shaped single crystals suitable for X-ray diffraction. ^{1}H NMR (400 MHz, toluene-d_8, 298 K): δ 10.98 (s, 9H, $SiMe_3$), 3.51 (s, 24H, 18c6), -0.25 (brs, 108H, $OC(CH_3)_3$). Anal. Calcd for **28-TMS**: $C_{63}H_{141}O_{22}Si_4NKU$: C 45.0; H 8.5; N 0.8; Found: 44.5; H 8.2; N 0.9. ESI-MS: Due to the extreme reactivity of this compound towards dioxygen, it was not possible to acquire a mass spectrum for this compound. Indeed, even when taking all the usual precautions, the only compound observed in the spectra was the uranyl(VI) tris-siloxy $[UO_2(OSi(O^tBu)_3)_3]^-$ complex (m/z = 1059.5). The remaining pale brown filtrate was cooled down to -40°C. This afforded pale blue single crystals of $[K(18c6)][U(N_3)\{N(SiMe_3)\}_2\{OSi(O^tBu)_3\}_3]$ **29** suitable for X-ray diffraction. The reaction of **24** with TMS-N_3 was also performed in toluene but the outcome of the reaction was similar to those observed in THF.

[K(18c6)][U(NAd)(OSi(O^{t}Bu)$_3$)$_4$] 28-Ad

A toluene solution (2 mL) of adamantylazide (11.1 mg, 0.063 mmol, 1 equiv) was added to a 4 mL toluene suspension of [K(18c6)][U(OSi(O^{t}Bu)$_3$)$_4$] **24** (100.0 mg, 0.063 mmol, 1 equiv). Immediately, the orange suspension turned dark brown, all the solid solubilized and a strong N_2 bubbling was observed. The resulting solution was stirred for 2 hours before filtration. The filtrate was taken to dryness and extracted with 2 mL hexane. The brown suspension was filtered and the brown filtrate was cooled to -40°C for 24 hours to afford [K(18c6)][U(Nad)(OSi(O^{t}Bu)$_3$)$_4$] **28-Ad** as a brown crystalline solid (72.1 mg, 0.041 mmol, 66% yield). Single crystals suitable for X-ray diffraction were grown by slow evaporation of a hexane solution of the complex. This complex is highly soluble in toluene. ^{1}H NMR (400 MHz, toluene-d_8, 298 K): δ 21.83 (brs, 6H, $H_{adamantyl}$), 14.93 (s, 3H, $H_{adamantyl}$), 10.61 (d, 3H, $H_{adamantyl}$), 8.45 (d, 3H, $H_{adamantyl}$), 3.48 (s, 24H, 18c6), -0.73 (brs, 108H, OC(CH_3)$_3$). Anal. Calcd for **28-Ad**: $C_{70}H_{147}O_{22}N_1Si_4K_1U_1$: C 48.2; H 8.5; N 0.8; Found C 48.0; H 8.3; N 0.9. ESI-MS: Due to the extreme reactivity of this compound towards dioxygen, it was not possible to acquire a mass spectrum for this compound. Indeed, even when taking all the usual precautions, the only compound observed in the spectra was the uranyl(VI) tris-siloxy [UO$_2$(OSi(O^{t}Bu)$_3$)$_3$]$^-$ complex (m/z = 1059.5).

Reaction of [K(18c6)][U(OSi(O^{t}Bu)$_3$)$_4$] 18 with CsN_3

A vial was charged with [K(18c6)][U(OSi(O^{t}Bu)$_3$)$_4$] **18** (50.0 mg, 0.031 mmol, 1 equiv) and the compound was dissolved in 2 mL of THF at -40°C. This solution was added onto CsN_3 (5.5 mg, 0.031 mmol, 1 equiv) and the reaction mixture was vigorously stirred with a glass-coated stir bar for 24 hours at -40°C. The resulting brownish red solution was taken to dryness, and the residue was extracted with 2 mL of toluene, filtered and the filtrate was cooled at -40°C. Two types of crystals suitable for XRD were grown from this solution: pale blue rectangular parallelepipeds of [K(18c6)][U(N$_3$)(OSi(O^{t}Bu)$_3$)$_4$] **30** and brown rhombus-faced parallelepipeds of [KU(μ-N)$_2$(OSi(O^{t}Bu)$_3$)$_3$]$_2$ **31**. ^{1}H NMR (400 MHz, toluene-d_8, 298 K) of crystals of **31** shows only one peak at -1.76 ppm.

[Cs(μ-N){U(OSi(O^{t}Bu)$_3$)$_3$}$_2$] 32

A vial was charged with [U(OSi(O^{t}Bu)$_3$)$_2$(μ-OSi(O^{t}Bu)$_3$)]$_2$ **18** (124.9 mg, 0.061 mmol, 1 equiv) and the compound was dissolved in 2 mL of THF and cooled to -40°C. This cold solution was added onto cold CsN_3 (10.7 mg, 0.061 mmol, 1 equiv) and the reaction mixture was vigorously stirred with a glass-coated stir bar for 24 hours at -40°C. The resulting brownish red solution was taken to dryness, and the residue was extracted with 2 mL of hexane, filtered and the filtrate was cooled to -40°C. Crystals were grown from this solution in 10 days. The crystals were collected and dried *in vacuo* to give **32** as a pure crystalline solid (63.6 mg, 0.029 mmol, 47% yield). Brown-red crystals of **32** suitable for XRD

were grown by slow evaporation of a hexane solution of **32**. ESI-MS: m/z = 1957.8 ([**32** – $Si(O^tBu)_3$ + 2H]$^+$), 1027.6 ([$U(OSi(O^tBu)_3)_3]^+$). ^{1}H NMR (200 MHz, toluene-d_8, 298 K): δ = -1.16 (s, 108H, CH_3), -2.49 (s, 54H, CH_3). Anal. Calcd for **32**: $C_{72}H_{162}CsNO_{24}Si_6U_2$: C 39.2; H 7.4; N 0.6; Found C 38.9; H 7.5; N, 0.8.

$[U(OSi(O^tBu)_3)_3(\mu\text{-}\eta^6\text{:}\eta^6\text{-}C_7H_8)]_2$ 33

To a light orange suspension of **18** (30 mg, 0.0145 mmol) in hexane (2 mL) 0.1 mL of toluene were added and the mixture was left standing for two days resulting in the formation of large dark brown crystals. The crystals were filtered, rinsed with toluene (2 x 1 mL) and dried in vacuo to afford 28 mg of complex **33** (0.013 mmol, 89% yield). It should be noted that due to the long reaction time and to the low stability of the precursor **18**, the yield for the preparation of **33** can vary depending on the scale of the reaction from 50 to 89%. ESI-MS: m/z = 2146.1 ([**33**-H]$^-$). ^{1}H NMR (200 MHz, THF-d_8, 298 K): δ = 82.94 (s, 3H, $CH_{3\ toluene}$), 1.19 (s, 162H, $CH_{3\ silanol}$), -112.68 (s, 2H, *o*/*m*-$CH_{\ toluene}$), -122.41 (s, 2H, *o*/*m*-$CH_{\ toluene}$), -137.88 (s, 1H, *p*-$CH_{\ toluene}$). Crystals suitable for X-ray diffraction were obtained with the same procedure.

$[K\{U(OSi(O^tBu)_3)_3\}_2(\mu\text{-}\eta^6\text{:}\eta^6\text{-}C_7H_8)]$ 34

Black crystals of **33** (42.8 mg, 0.020 mmol, 1 equiv) were added to a suspension of KC_8 (2.4 mg, 0.018 mmol, 0.9 equiv) in THF (2 mL). The reaction mixture was stirred vigorously at room temperature for 2 hours, affording a dark brown suspension. The suspension was centrifuged and the supernatant was collected. The solid residue was extracted with 2 x 1 mL THF and the supernatant was collected after centrifugation. The organic fractions were combined and THF was evaporated to dryness. The resulting brown residue was extracted with 4 mL toluene to give a brown suspension that was filtered. The brown filtrate was let standing at -40°C for 3 days affording black crystals of **34** (36.0 mg, 0.016 mmol, 81 % yield). Single crystals suitable for X-ray diffraction were obtained similarly. ^{1}H NMR (400 MHz, THF-d_8, 298 K): δ = 63.2 (s, 3H, $CH_{3\ toluene}$), 2.1 (s, 81H, $CH_{3\ silanol}$), -0.6 (s, 81H, $CH_{3\ silanol}$), -83.5 (s, 2H, *o*/*m*-$CH_{\ toluene}$), -93.7 (s, 2H, *o*/*m*-$CH_{\ toluene}$), -98.4 (s, 1H, *p*-$CH_{\ toluene}$). ^{1}H NMR (200 MHz, toluene-d_8, 298 K): δ = 62.9 (s, 3H, $CH_{3\ toluene}$), 3.4 (s, 81H, $CH_{3\ silanol}$), 0.5 (s, 81H, $CH_{3\ silanol}$), -80.0 (s, 2H, *o*/*m*-$CH_{\ toluene}$), -90.0 (s, 2H, *o*/*m*-$CH_{\ toluene}$), -94.3 (s, 1H, *p*-$CH_{\ toluene}$). Anal. Calcd for **34**: $C_{79}H_{170}O_{24}Si_6KU_2$: C 43.37; H 7.83; N 0.00; Found : C 42.65; H 8.04; N <0.1.

$[K_2\{U(OSi(O^tBu)_3)_3\}_2(\mu\text{-}\eta^6\text{:}\eta^6\text{-}C_7H_8)]$ 35

Black crystals of **33** (17.0 mg, 0.008 mmol, 1 equiv) were added to a KC_8 (2.4 mg, 0.017 mmol, 2.2 equiv) suspension in 1 mL THF. The reaction mixture was stirred vigorously at room temperature for 1.5 hours, affording a dark brown suspension. The suspension was centrifuged and the supernatant was collected. The solid residue was washed with 1 mL THF and the supernatant was collected after

centrifugation. This step was repeated 5 times until the organic phase was colorless. The organic fractions were combined and THF was removed *in vacuo*. The resulting brown solid was recovered, washed with 1 mL hexane and dried *in vacuo* affording **35** as a brown powder (12.4 mg, 0.007 mmol, 70 % yield). Single crystals of **35** were grown letting stand a toluene solution (0,5 mL) of the complex (10.0 mg) at -40°C. ESI-MS: m/z = 2225.0 ([**35**]$^+$). ^{1}H NMR (400 MHz, THF-d_8, 298 K): δ = 16.8 (s, 3H, $CH_{3\ toluene}$), 0.7 (s, 162H, $CH_{3\ silanol}$), -72.8 (s, 1H, *p*-$CH_{toluene}$), -77.1 (s, 2H, *o*/*m*-$CH_{toluene}$), -77.5 (s, 2H, *o*/*m*-$CH_{toluene}$). ^{1}H NMR (200 MHz, toluene-d_8, 298 K): δ = 18.0 (s, 3H, $CH_{3\ toluene}$), 0.9 (s, 162H, $CH_{3\ silanol}$), -70.7 (s, 1H, *p*-$CH_{toluene}$), -74.9 (s, 2H, *o*/*m*-$CH_{toluene}$), -75.8 (s, 2H, *o*/*m*-$CH_{toluene}$). Anal. Calcd for **35**: $C_{79}H_{170}O_{24}Si_6K_2U_2$: C 42.61; H 7.69; N 0.00; Found : C 42.19; H 7.35; N <0.2. The addition of an excess (40 equiv) 18c6 on a THF solution of $[K_2\{U(OSi(O^tBu)_3)_3\}_2\{\mu\text{-}\eta^6\text{:}\eta^6\text{-}C_7H_8\}]$ affords a brown solution. The ^{1}H NMR spectrum shows a new set of signals assigned to $[K(K18c6)\{U(OSi(O^tBu)_3)_3\}_2\{\mu\text{-}\eta^6\text{:}\eta^6\text{-}C_7H_8\}]$, **35-18c6** : ^{1}H NMR (200 MHz, THF-d_8, 298 K): δ = 19.8 (s, 3H, $CH_{3\ toluene}$), 1.4 (s, 81H, $CH_{3\ silanol}$), 0.2 (s, 81H, $CH_{3\ silanol}$), -74.5 (s, 1H, *p*-$CH_{toluene}$), -80.4 (s, 2H, *o*/*m*-$CH_{toluene}$), -80.6 (s, 2H, *o*/*m*-$CH_{toluene}$).

Reduction of $[U(OSi(O^tBu)_3)_2(\mu\text{-}OSi(O^tBu)_3)]_2$ 18 with KC_8 in toluene

$[U(OSi(O^tBu)_3)_2(\mu\text{-}OSi(O^tBu)_3)]_2$ **18** (100.0 mg, 0.049 mmol) was added to a suspension of KC_8 (14.5 mg, 0.107 mmol, 2.2 equiv) in toluene (4 mL). The reaction mixture was stirred vigorously at room temperature for 3 days, affording a dark brown suspension. The ^{1}H NMR spectrum recorded for the reaction mixture showed the characteristic resonances of **35** together with another set of resonances that we attribute to the formation of an unidentified toluene-uranium adduct. The suspension was centrifuged and the supernatant was removed. The black residue was extracted with 8 x 2 mL THF and the brown supernatant was collected after centrifugation. The organic fractions were evaporated to dryness. The resulting brown solid was washed with toluene (3 x 2 mL) and dried *in vacuo*. The powder was dissolved in 6 mL THF and let standing at -40°C. After 3 days, a microcristalline black solid of **35** (confirmed by NMR spectroscopy) was collected by filtration. (43.0 mg, 0.019 mmol, 40% yield). NMR data for the unidentified toluene-uranium adduct: ^{1}H NMR (200 MHz, toluene-d_8, 298 K): δ = 2.2 (s, 162H, $CH_{3\ silanol}$), -11.1 (brs, 3H, $CH_{3\ toluene}$), -27.1 (brs, 1H, *p*-$CH_{toluene}$), -54.5 (brs, 2H, *o*/*m*-$CH_{toluene}$), -55.2 (brs, 2H, *o*/*m*-$CH_{toluene}$). ^{1}H NMR (200 MHz, THF-d_8, 298 K): δ = 2.2 (s, 162H, $CH_{3\ silanol}$), -14.7 (s, 3H, $CH_{3\ toluene}$), -24.7 (s, 1H, *p*-$CH_{toluene}$), -53.1 (s, 2H, *o*/*m*-$CH_{toluene}$), -54.2 (s, 2H, *o*/*m*-$CH_{toluene}$).

Reaction of $[U(OSi(O^tBu)_3)_3(\mu\text{-}\eta^6\text{:}\eta^6\text{-toluene})]_2$ 33 with KOTf

Ratio KOTF:2 ≤1.6. A THF (0.5 mL) solution of KOTf (2.0 mg, 0.011 mmol, 1.6 equiv) was added onto $[U(OSi(O^tBu)_3)_3(\mu\text{-}\eta^6\text{:}\eta^6\text{-toluene})]$ **33** (14.2 mg, 0.007 mmol, 1 equiv). The resulting suspension was stirred for 1 hour to yield a dark black solution. The ^{1}H NMR spectrum recorded for the reaction

mixture showed the characteristic resonances of $[K\{U(OSi(O^tBu)_3)_3\}_2(\mu\text{-}\eta^6\text{:}\eta^6\text{-}C_7H_8)]$ **34** together with another resonance at 1.6 ppm assigned to the U(IV) complex $[U(OSi(O^tBu)_3)_3(OTf)(THF)_2]$ **36**. The THF was removed *in vacuo* and the residue was dissolved in toluene (0.4 mL). After letting the resulting solution stand at -40°C for 12 hours black crystals of $K[(\mu\text{-}\eta^6,\eta^6\text{-toluene})\{U(OSi(O^tBu)_3)_3\}_2]$ **34** formed (5.8 mg, 0.003 mmol, 80% yield). The cell parameters for these crystals were checked and were identical to thoses of **34**. Pale blue single crystals of $[U(OSi(O^tBu)_3)_3(OTf)(THF)_2]$ **36** suitable for X-ray diffraction were obtained by letting stand at -40°C the toluene filtrate.

Ratio KOTF:2 ≥ 2. A THF (0.5 mL) solution of KOTf (2.2 mg, 0.012 mmol, 2 equiv) was added onto $[U(OSi(O^tBu)_3)_3(\mu\text{-}\eta^6\text{:}\eta^6\text{-toluene})]_2$ **33** (12.6 mg, 0.006 mmol, 1 equiv). The resulting suspension was stirred for 1 hour to yield a dark black solution. The ^{1}H NMR spectrum recorded for the reaction mixture showed the characteristic resonances of $[K\{U(OSi(O^tBu)_3)_3\}_2(\mu\text{-}\eta^6\text{:}\eta^6\text{-}C_7H_8)]$ **34** together with another resonance at 1.6 ppm assigned to $[U(OSi(O^tBu)_3)_3(OTf)(THF)_2]$ **36**. After letting the reaction mixture stand at room temperature for several days, the resonances assigned to $[K_2\{U(OSi(O^tBu)_3)_3\}_2(\mu\text{-}\eta^6\text{:}\eta^6\text{-}C_7H_8)]$ **35** appeared in the ^{1}H NMR spectrum. The reaction is kinetically slow and takes more than 1 month to go to completion. After one month, large black crystals of $[K\{U(OSi(O^tBu)_3)_3\}_2(\mu\text{-}\eta^6\text{:}\eta^6\text{-}C_7H_8)].(THF)_2$ **35**.$(THF)_2$ formed in the tube. The reaction was not faster when a large excess (20 equiv) of KOTf was employed.

Reaction of $[U(OSi(O^tBu)_3)_3(\mu\text{-}\eta^6,\eta^6\text{-toluene})]_2$ 33 with Bu_4NOTf

A THF (0.5 mL) solution of Bu_4NOTf (2.9 mg, 0.008 mmol, 2 equiv) was added onto **33** (8.0 mg, 0.004 mmol, 1 equiv). The resulting suspension was vigorously stirred for 2 hours, affording a dark brown solution. The ^{1}H NMR spectrum (400 MHz, THF-d_8, 298 K) recorded for the crude mixture showed the characteristic resonances of **33** as well as four resonances for the Bu_4N^+ protons (δ = 3.3 (t, 2H, NCH_2), 1.7 (m, 2H, CH_2), 1.4 (m, 2H, CH_2), 1.0 (t, 3H, CH_3).) and a singlet at 2.6 ppm related to the formation of $[U(OSi(O^tBu)_3)_3(THF)_2]$ **18-THF**. After 36 hours, **33** was entirely converted into **18-THF**, and no toluene-adduct complex was present in solution, as observed by ^{1}H NMR spectroscopy.

CHAPTER VI
References

1. Tolman, W. B., *Activation of small molecules*. Wiley VCH: Weinheim, Germany, 2006.
2. Sakakura, T.; Choi, J.-C.; Yasuda, H., *Chem. Rev.* **2007,** *107*, 2365-2387.
3. Cokoja, M.; Bruckmeier, C.; Rieger, B.; Herrmann, W. A.; Kuhn, F. E., *Angew. Chem.-Int. Edit.* **2011,** *50*, 8510-8537.
4. Appel, A. M.; Bercaw, J. E.; Bocarsly, A. B.; Dobbek, H.; DuBois, D. L.; Dupuis, M.; Ferry, J. G.; Fujita, E.; Hille, R.; Kenis, P. J. A.; Kerfeld, C. A.; Morris, R. H.; Peden, C. H. F.; Portis, A. R.; Ragsdale, S. W.; Rauchfuss, T. B.; Reek, J. N. H.; Seefeldt, L. C.; Thauer, R. K.; Waldrop, G. L., *Chem. Rev.* **2013,** *in press*.
5. Costentin, C.; Drouet, S.; Robert, M.; Saveant, J. M., *Science* **2012,** *338*, 90-94.
6. Yandulov, D. V.; Schrock, R. R., *Science* **2003,** *301*, 76-78.
7. MacLeod, K. C.; Holland, P. L., *Nat. Chem.* **2013,** *5*, 559-565.
8. Evans, W. J.; Zucchi, G.; Ziller, J. W., *J. Am. Chem. Soc.* **2003,** *125*, 10-11.
9. Lu, C. C.; Saouma, C. T.; Day, M. W.; Peters, J. C., *J. Am. Chem. Soc.* **2007,** *129*, 4-5.
10. Davies, N. W.; Frey, A. S. P.; Gardiner, M. G.; Wang, J., *Chem. Commun.* **2006**, 4853-4855.
11. Thammayongsy, Z.; Seda, T.; Zakharov, L. N.; Kaminsky, W.; Gilbertson, J. D., *Inorg. Chem.* **2012,** *51*, 9168-9170.
12. Vidyaratne, I.; Scott, J.; Gambarotta, S.; Budzelaar, P. H. M., *Inorg. Chem.* **2007,** *46*, 7040-7049.
13. Ohki, Y.; Fryzuk, M. D., *Angew. Chem.-Int. Edit.* **2007,** *46*, 3180-3183.
14. Gambarotta, S.; Scott, J., *Angew. Chem.-Int. Edit.* **2004,** *43*, 5298-5308.
15. Hui, S.; Yi, Y.; James, A. J.; Sharp, P. S., *Science* **1997,** *275*, 1460-1462.
16. Krogman, J. P.; Foxman, B. M.; Thomas, C. M., *J. Am. Chem. Soc.* **2011,** *133*, 14582-14585.
17. Akagi, F.; Matsuo, T.; Kawaguchi, H., *Angew. Chem.-Int. Edit.* **2007,** *46*, 8778-8781.
18. Ballmann, J.; Pick, F.; Castro, L.; Fryzuk, M. D.; Maron, L., *Inorg. Chem.* **2013,** *52*, 1685-1687.
19. Li, J.; Hermann, M.; Frenking, G.; Jones, C., *Angew. Chem.-Int. Edit.* **2012,** *51*, 8611-8614.
20. Monreal, M. J.; Diaconescu, P. L., *Nat. Chem.* **2010,** *2*, 423-423.
21. Gardner, B. M.; Liddle, S. T., *Eur. J. Inorg. Chem.* **2013,** *in press*.
22. Korobkov, I.; Sandro, G., *Progress in Inorganic Chemistry* **2005,** *54*, 321-349.
23. Fox, A. R.; Bart, S. C.; Meyer, K.; Cummins, C. C., *Nature* **2008,** *455*, 341-349.
24. Evans, W. J.; Kozimor, S. A., *Coord. Chem. Rev.* **2006,** *250*, 911-935.
25. Arnold, P. L., *Chem.Commun.* **2011,** *47*, 9005-9010.
26. Castro-Rodriguez, I.; Meyer, K., *Chem. Commun.* **2006**, 1353-1368.
27. Tsoureas, N.; Summerscales, O. T.; Cloke, F. G. N.; Roe, S. M., *Organometallics* **2012,** *32*, 1353-1362.
28. Lam, O. P.; Meyer, K., *Polyhedron* **2012,** *32*, 1-9.
29. Franceschi, F.; Solari, E.; Floriani, C.; Rosi, M.; Chiesi-Villa, A.; Rizzoli, C., *Chem.-Eur. J.* **1999,** *5*, 708-721.
30. Gambarotta, S.; Urso, F.; Floriani, C.; Chiesivilla, A.; Guastini, C., *Inorg. Chem.* **1983,** *22*, 3966-3972.
31. Floriani, C.; Solari, E.; Franceschi, F.; Scopelliti, R.; Belanzoni, P.; Rosi, M., *Chem.-Eur. J.* **2001,** *7*, 3052-3061.
32. Solari, E.; Maltese, C.; Franceschi, F.; Floriani, C.; ChiesiVilla, A.; Rizzoli, C., *J. Chem. Soc.-Dalton Trans.* **1997**, 2903-2910.
33. Gallo, E.; Solari, E.; Re, N.; Floriani, C.; ChiesiVilla, A.; Rizzoli, C., *J. Am. Chem. Soc.* **1997,** *119*, 5144-5154.
34. DeAngelis, S.; Solari, E.; Gallo, E.; Floriani, C.; ChiesiVilla, A.; Rizzoli, C., *Inorg. Chem.* **1996,** *35*, 5995-6003.
35. Van Hoecke, M.-P.; Leroy, M., *L'Actualité Chimique* **2011,** *358*, 24-29.
36. Kaltsoyannis, N.; Scott, P., *The f elements*. Oxford University Press: Oxford, 1999.
37. Cotton, A. F.; Wilkinson, G., *Advanced inorganic chemistry*. fifth edition ed.; Wiley-Interscience: 1988.

38. Burns, C. J.; Neu, M. P.; Boukhalfa, H.; Gutowski, K. E.; Bridges, N. J.; Rogers, R. D., *Comprehensive Coordination Chemistry II*. Elsevier ltd: Oxford, UK, 2004; Vol. 3.
39. Kettle, S., F., A., *Physical Inorganic Chemistry : A Coordination Chemistry Approach*. Oxford University Press: Oxford, 1998.
40. Clark, D. L.; Hecker, S. S.; Jarvinen, G. D.; Neu, M. P., *The Chemistry of the Actinide and Transactinide Elements*. Springer: Dordrecht, 2006.
41. Sastri, V., S.; Bünzli, J.-C., G.; Rao, V. R.; Rayudu, G. V. S.; Perrumaredi, J. R., *Modern Aspects of Rare Earths and Their Complexes*. Elsevier: Amsterdam, 2003.
42. Neidig, M. L.; Clark, D. L.; Martin, R. L., *Coord. Chem. Rev.* **2013,** *257*, 394-406.
43. Rinehart, J. D.; Harris, T. D.; Kozimor, S. A.; Bartlett, B. M.; Long, J. R., *Inorg. Chem.***2009,** *48*, 3382-3395.
44. Panak, P. J.; Geist, A., *Chem. Rev.* **2013,** *113*, 1199-1236.
45. Hudson, M. J.; Harwood, L. M.; Laventine, D. M.; Lewis, F. W., *Inorg. Chem.***2013,** *52*, 3414-3428.
46. Denecke, M. A.; Panak, P. J.; Burdet, F.; Weigl, M.; Geist, A.; Klenze, R.; Mazzanti, M.; Gompper, K., *C. R. Chim.* **2007,** *10*, 872-882.
47. Ephritikhine, M., *Dalton Trans.* **2006**, 2501-2516.
48. Marks, T. J., *Science* **1982,** *217*, 989-997.
49. Greenwood, N., N.; Earnshaw, A., *Chemistry of The Elements*. Elsevier: Amsterdam, 1997.
50. Settle, F. A., *J. Chem. Educ.* **2009,** *86*, 316-323.
51. Jones, M. B.; Gaunt, A. J., *Chem. Rev.* **2013,** *113*, 1137-1198.
52. Bart, S. C.; Meyer, K., Highlights in uranium coordination chemistry. In *Organometallic and Coordination Chemistry of the Actinides*, 2008; Vol. 127, pp 119-176.
53. Albrecht-Schmitt, T. E., *Angew. Chem.-Int. Edit.* **2005,** *44*, 4836-4838.
54. Sessler, J. L.; Melfi, P. J.; Pantos, G. D., *Coord. Chem. Rev.* **2006,** *250*, 816-843.
55. Fortier, S.; Hayton, T. W., *Coord. Chem. Rev.* **2010,** *254*, 197-214.
56. Nyman, M.; Burns, P. C., *Chem. Soc. Rev.* **2012,** *41*, 7354-7367.
57. Qiu, J.; Burns, P. C., *Chem. Rev.* **2013,** *113*, 1097-1120.
58. Fortier, S.; Walensky, J. R.; Wu, G.; Hayton, T. W., *J. Am. Chem. Soc.* **2011,** *133*, 11732-11743.
59. Fortier, S.; Wu, G.; Hayton, T. W., *Inorg. Chem.* **2009,** *48*, 3000-3011.
60. Graves, C. R.; Kiplinger, J. L., *Chem.Commun.* **2009**, 3831-3853.
61. Arnold, P. L.; Love, J. B.; Patel, D., *Coord. Chem. Rev.* **2009,** *253*, 1973-1978.
62. Arnold, P. L.; Jones, G. M.; Odoh, S. O.; Schreckenbach, G.; Magnani, N.; Love, J. B., *Nat. Chem.* **2012,** *4*, 221–22.
63. Nocton, G.; Horeglad, P.; Vetere, V.; Pecaut, J.; Dubois, L.; Maldivi, P.; Edelstein, N. M.; Mazzanti, M., *J. Am. Chem. Soc.* **2010,** *132*, 495-508.
64. Mougel, V.; Horeglad, P.; Nocton, G.; Pecaut, J.; Mazzanti, M., *Chem.-Eur. J.* **2010,** *16*, 14365-14377.
65. Chatelain, L.; Mougel, V.; Pecaut, J.; Mazzanti, M., *Chem. Sci.* **2012,** *3*, 1075-1079.
66. Mougel, V.; Chatelain, L.; Pecaut, J.; Caciuffo, R.; Colineau, E.; Griveau, J.-C.; Mazzanti, M., *Nat. Chem.* **2012,** *4*, 1011-1017.
67. Karmazin, L.; Mazzanti, M.; Pecaut, J., *Inorg. Chem.* **2003,** *42*, 5900-5908.
68. Sonnenberger, D. C.; Gaudiello, J. G., *Inorg. Chem.* **1988,** *27*, 2747-2748.
69. Morris, D. E.; Da Re, R. E.; Jantunen, K. C.; Castro-Rodriguez, I.; Kiplinger, J. L., *Organometallics* **2004,** *23*, 5142-5153.
70. Schelter, E. J.; Yang, P.; Scott, B. L.; Thompson, J. D.; Martin, R. L.; Hay, P. J.; Morris, D. E.; Kiplinger, J. L., *Inorg. Chem.* **2007,** *46*, 7477-7488.
71. Avens, L. R.; Barnhart, D. M.; Burns, C. J.; McKee, S. D.; Smith, W. H., *Inorg. Chem.* **1994,** *33*, 4245-4254.
72. Amoroso, A. J.; Jeffery, J. C.; Jones, P. L.; McCleverty, J. C.; Rees, L.; Rheingold, A. L.; Sun, Y.; Takats, J.; Trofimenko, S.; Ward, M. D.; Yap, G. P. A., *J. Chem. Soc., Chem. Commun.* **1995**, 1881-1882.
73. Stewart, J. L.; Andersen, R. A., *Polyhedron* **1998,** *17*, 953-958.
74. Diaconescu, P. L.; Arnold, P. L.; Baker, T. A.; Mindiola, D. J.; Cummins, C. C., *J. Am. Chem. Soc.* **2000,** *122*, 6108-6109.
75. Korobkov, I.; Gorelsky, S.; Gambarotta, S., *J. Am. Chem. Soc.* **2009,** *131*, 10406-10420.
76. Baker, R. J., *Coord. Chem. Rev.* **2012,** *256*, 2843-2871.
77. Clark, D. L.; Sattelberger, A. P.; Bott, S. G.; Vrtis, R. N., *Inorg. Chem.* **1989,** *28*, 1771-1773.
78. Avens, L. R.; Bott, S. G.; Clark, D. L.; Sattelberger, A. P.; Watkin, J. G.; Zwick, B. D., *Inorg. Chem.* **1994,** *33*, 2248-2256.
79. Monreal, M. J.; Thomson, R. K.; Cantat, T.; Travia, N. E.; Scott, B. L.; Kiplinger, J. L., *Organometallics* **2011,** *30*, 2031-2038.

80. Carmichael, C. D.; Jones, N. A.; Arnold, P. L., *Inorg. Chem.* **2008,** *47*, 8577-8579.
81. Avens, L. R.; Barnhart, D. M.; Burns, C. J.; McKee, S. D., *Inorg. Chem.* **1996,** *35*, 537-539.
82. Boisson, C.; Berthet, J. C.; Lance, M.; Nierlich, M.; Ephritikhine, M., *Chem. Commun.* **1996**, 2129-2130.
83. Larch, C. P.; Cloke, F. G. N.; Hitchcock, P. B., *Chem. Commun.* **2008**, 82-84.
84. Korobkov, I.; Gambarotta, S.; Yap, G. P. A., *Organometallics* **2001,** *20*, 2552-2559.
85. Drozdzynski, J., *Coord. Chem. Rev.* **2005,** *249*, 2351-2373.
86. Moody, D. C.; Zozulin, A. J.; Salazar, K. V., *Inorg. Chem.* **1982,** *21*, 3856-3857.
87. Maury, O.; Ephritikhine, M.; Nierlich, M.; Lance, M.; Samuel, E., *Inorg. Chim. Acta* **1998,** *279*, 210-216.
88. Natrajan, L.; Mazzanti, M.; Bezombes, J. P.; Pecaut, J., *Inorg. Chem.* **2005,** *44*, 6115-6121.
89. Berthet, J. C.; Nierlich, M.; Miquel, Y.; Madic, C.; Ephritikhine, M., *Dalton Trans.* **2005**, 369-379.
90. Nocton, G.; Burdet, F.; Pecaut, J.; Mazzanti, M., *Angew. Chem.-Int. Edit.* **2007,** *46*, 7574-7578.
91. Andersen, R. A., *Inorg. Chem.* **1979,** *18*, 1507-1509.
92. Vandersluys, W. G.; Burns, C. J.; Huffman, J. C.; Sattelberger, A. P., *J. Am. Chem. Soc.* **1988,** *110*, 5924-5925.
93. Mansell, S. M.; Kaltsoyannis, N.; Arnold, P. L., *J. Am. Chem. Soc.* **2011,** *133*, 9036-9051.
94. Ephritikhine, M., *Chem. Rev.* **1997,** *97*, 2193-2242.
95. Odom, A. L.; Arnold, P. L.; Cummins, C. C., *J. Am. Chem. Soc.* **1998,** *120*, 5836-5837.
96. Duhovic, S.; Khan, S.; Diaconescu, P. L., *Chem. Commun.* **2010,** *46*, 3390-3392.
97. Monreal, M. J.; Diaconescu, P. L., *Organometallics* **2008,** *27*, 1702-1706.
98. Lewis, A. J.; Williams, U. J.; Kikkawa, J. M.; Carroll, P. J.; Schelter, E. J., *Inorg. Chem.* **2012,** *51*, 37-39.
99. Yin, H.; Lewis, A. J.; Williams, U. J.; Carroll, P. J.; Schelter, E. J., *Chem.l Sci.* **2013,** *4*, 798-805.
100. Mora, E.; Maria, L.; Biswas, B.; Camp, C.; Santos, I. C.; Pecaut, J.; Cruz, A.; Carretas, J. M.; Marcalo, J.; Mazzanti, M., *Organometallics* **2013,** *32*, 1409-1422.
101. Chomitz, W. A.; Minasian, S. G.; Sutton, A. D.; Arnold, J., *Inorg. Chem.* **2007,** *46*, 7199-7209.
102. Arnold, P. L.; Blake, A. L.; Wilson, C., *Chem.-Eur. J.* **2005,** *11*, 6095-6099.
103. Cooper, O. J.; McMaster, J.; Lewis, W.; Blake, A. J.; Liddle, S. T., *Dalton Trans.* **2010,** *39*, 5074-5076.
104. Kiplinger, J. L.; Morris, D. E.; Scott, B. L.; Burns, C. J., *Organometallics* **2002,** *21*, 5978-5982.
105. Enriquez, A. E.; Scott, B. L.; Neu, M. P., *Inorg. Chem.* **2005,** *44*, 7403-7413.
106. Roussel, P.; Tinker, N. D.; Scott, P., *J. Alloy. Compd.* **1998,** *271*, 150-153.
107. Reynolds, L. T.; Wilkinson, G., *J. Inorg. Nucl. Chem.* **1956,** *2*, 246-253.
108. Ephritikhine, M., *Organometallics* **2013,** *32*, 2464-2488.
109. Rabinovich, D.; Haswell, C. M.; Scott, B. L.; Miller, R. L.; Nielsen, J. B.; Abney, K. D., *Inorg. Chem.* **1996,** *35*, 1425-1426.
110. Sun, Y.; McDonald, R.; Takats, J.; Day, V., W.; Eperspacher, T. A., *Inorg. Chem.* **1994,** *33*, 4433-4434.
111. Carvalho, A.; Domingos, A.; Gaspar, P.; Marques, N.; Pires de Matos, A.; Santos, I., *Polyhedron* **1992,** *11*, 1481-1488.
112. Maria, L.; Domingos, A.; Santos, I., *Inorg. Chem.* **2001,** *40*, 6863-6864.
113. Daly, S. R.; Girolami, G. S., *Inorg. Chem.* **2010,** *49*, 5157-5166.
114. Schelter, E. J.; Wu, R. L.; Scott, B. L.; Thompson, J. D.; Cantat, T.; John, K. D.; Batista, E. R.; Morris, D. E.; Kiplinger, J. L., *Inorg. Chem.* **2010,** *49*, 924-933.
115. Wright, R. J.; Power, P. P.; Scott, B. L.; Kiplinger, J. L., *Organometallics* **2004,** *23*, 4801-4803.
116. Villiers, C.; Thuery, P.; Ephritikhine, M., *Eur. J. Inorg. Chem.* **2004**, 4624-4632.
117. Gaunt, A. J.; Scott, B. L.; Neu, M. P., *Chem. Commun.* **2005**, 3215-3217.
118. Mills, D. P.; Moro, F.; McMaster, J.; van Slageren, J.; Lewis, W.; Blake, A. J.; Liddle, S. T., *Nat. Chem.* **2011,** *3*, 454-460.
119. Vidjayacoumar, B.; Ilango, S.; Ray, M. J.; Chu, T.; Kolpin, K. B.; Andreychuk, N. R.; Cruz, C. A.; Emslie, D. J. H.; Jenkins, H. A.; Britten, J. F., *Dalton Trans.* **2012,** *41*, 8175-8189.
120. Cantat, T.; Graves, C. R.; Scott, B. L.; Kiplinger, J. L., *Angew. Chem.-Int. Edit.* **2009,** *48*, 3681-3684.
121. Fox, A. R.; Silvia, J. S.; Townsend, E. M.; Cummins, C. C., *C. R. Chim.* **2010,** *13*, 781-789.
122. Turner, Z. R.; Bellabarba, R.; Tooze, R. P.; Arnold, P. L., *J. Am. Chem. Soc.* **2010,** *132*, 4050-4051.
123. Roger, M.; Arliguie, T.; Thuery, P.; Ephritikhine, M., *Inorg. Chem.* **2008,** *47*, 3863-3868.
124. Roussel, P.; Scott, P., *J. Am. Chem. Soc.* **1998,** *120*, 1070-1071.
125. Monteiro, B.; Roitershtein, D.; Ferreira, H.; Ascenso, J. R.; Martins, A. M.; Domingos, A.; Marques, N., *Inorg. Chem.* **2003,** *42*, 4223-4231.
126. Lam, O. P.; Bart, S. C.; Kameo, H.; Heinemann, F. W.; Meyer, K., *Chem. Commun.* **2010,** *46*, 3137-3139.
127. Bart, S. C.; Heinemann, F. W.; Anthon, C.; Hauser, C.; Meyer, K., *Inorg. Chem.* **2009,** *48*, 9419-9426.
128. Castro-Rodriguez, I.; Olsen, K.; Gantzel, P.; Meyer, K., *Chem.l Commun.* **2002**, 2764-2765.

129. Arnold, P. L.; Potter, N. A.; Magnani, N.; Apostolidis, C.; Griveau, J. C.; Colineau, E.; Morgenstern, A.; Caciuffo, R.; Love, J. B., *Inorg. Chem.* **2010,** *49*, 5341-5343.
130. Riviere, C.; Nierlich, M.; Ephritikhine, M.; Madic, C., *Inorg. Chem.* **2001,** *40*, 4428-4435.
131. Berthet, J.-C.; Rivière, C.; Miquel, Y.; Nierlich, M.; Madic, C.; Ephritikhine, M., *Eur. J. Inorg. Chem.* **2002**, 1439-1446.
132. Iveson, P. B.; Riviere, C.; Guillaneux, D.; Nierlich, M.; Thuery, P.; Ephritikhine, M.; Madic, C., *Chem. Commun.* **2001**, 1512-1513.
133. Karmazin, L.; Mazzanti, M.; Bezombes, J. P.; Gateau, C.; Pecaut, J., *Inorg. Chem.* **2004,** *43*, 5147-5158.
134. Wietzke, R.; Mazzanti, M.; Latour, J.-M.; Pécaut, J., *J. Chem. Soc., Dalton Trans.* **1998**, 4087-4088.
135. Wietzke, R.; Mazzanti, M.; Latour, J. M.; Pecaut, J., *J. Chem. Soc., Dalton Trans.* **2000**, 4167-4173.
136. Mazzanti, M.; Wietzke, R. L.; Pecaut, J.; Latour, J. M.; Maldivi, P.; Remy, M., *Inorg. Chem.* **2002,** *41*, 2389-2399.
137. Carretas, J. M.; Cui, J.; Santos, I. C.; Cruz, A.; Maria, L.; MarÃ§alo, J., *Inorg. Chim. Acta* **2012,** *385*, 53-57.
138. Matson, E. M.; Forrest, W. P.; Fanwick, P. E.; Bart, S. C., *J. Am. Chem. Soc.* **2011,** *133*, 4948-4954.
139. Fortier, S.; Walensky, J. R.; Wu, G.; Hayton, T. W., *J. Am. Chem. Soc.* **2011,** *133*, 6894-6897.
140. King, D. M.; Tuna, F.; McInnes, E. J. L.; McMaster, J.; Lewis, W.; Blake, A. J.; Liddle, S. T., *Science* **2012,** *337*, 717-720.
141. Castro-Rodriguez, I.; Nakai, H.; Zakharov, L. N.; Rheingold, A. L.; Meyer, K., *Science* **2004,** *305*, 1757-1759.
142. Arney, D. S.; Burns, C. J., *J. Am. Chem. Soc.* **1993,** *115*, 9840-9841.
143. Fortier, S.; Kaltsoyannis, N.; Wu, G.; Hayton, T. W., *J. Am. Chem. Soc.* **2011,** *133*, 14224-14227.
144. Fortier, S.; Brown, J. L.; Kaltsoyannis, N.; Wu, G.; Hayton, T. W., *Inorg. Chem.* **2012,** *51*, 1625-1633.
145. Duval, P. B.; Burns, C. J.; Clark, D. L.; Morris, D. E.; Scott, B. L.; Thompson, J. D.; Werkema, E. L.; Jia, L.; Andersen, R. A., *Angew. Chem.-Int. Edit.* **2001,** *40*, 3357-3361.
146. Lam, C. P.; Anthon, C.; Heinemann, F. W.; O'Connor, J. M.; Meyer, K., *J. Am. Chem. Soc.* **2008,** *130*, 6567-6576.
147. Arnold, P. L.; Turner, Z. R.; Bellabarba, R. M.; Tooze, R. P., *Chem. Sci.* **2011,** *2*, 77-79.
148. McKay, D.; Frey, A. S. P.; Green, J. C.; Cloke, F. G. N.; Maron, L., *Chem. Commun.* **2012,** *48*, 4118-4120.
149. Frey, A. S. P.; Cloke, F. G. N.; Coles, M. P.; Maron, L.; Davin, T., *Angew. Chem.-Int. Edit.* **2011,** *50*, 6881-6883.
150. Frey, A. S.; Cloke, F. G. N.; Hitchcock, P. B.; Day, I. J.; Green, J. C.; Aitken, G., *J. Am. Chem. Soc.* **2008,** *130*, 13816-13817.
151. Summerscales, O. T.; Cloke, F. G. N.; Hitchcock, P. B.; Green, J. C.; Hazari, N., *J. Am. Chem. Soc.* **2006,** *128*, 9602-9603.
152. Summerscales, O. T.; Cloke, F. G. N.; Hitchcock, P. B.; Green, J. C.; Hazari, N., *Science* **2006,** *311*, 829-831.
153. Frey, A. S. P.; Cloke, F. G. N.; Coles, M. P.; Hitchcock, P. B., *Chem.-Eur. J.* **2010,** *16*, 9446-9448.
154. Gardner, B. M.; Stewart, J. C.; Davis, A. L.; McMaster, J.; Lewis, W.; Blake, A. J.; Liddle, S. T., *Proc. Nat. Acad. Sci.* **2012,** *109*, 9265-9270.
155. Castro-Rodriguez, I.; Meyer, K., *J. Am. Chem. Soc.* **2005,** *127*, 11242-11243.
156. Parry, J.; Carmona, E.; Coles, S.; Hursthouse, M., *J. Am. Chem. Soc.* **1995,** *117*, 2649-2650.
157. Korobkov, I.; Gambarotta, S.; Yap, G. P. A., *Angew. Chem.-Int. Edit.* **2002,** *41*, 3433-3436.
158. Cloke, F. G. N.; Hitchcock, P. B., *J. Am. Chem. Soc.* **2002,** *124*, 9352-9353.
159. Evans, W. J.; Kozimor, S. A.; Ziller, J. W., *J. Am. Chem. Soc.* **2003,** *125*, 14264-14265.
160. Todorova, T. K.; Gagliardi, L.; Walensky, J. R.; Miller, K. A.; Evans, W. J., *J. Am. Chem. Soc.* **2010,** *132*, 12397-12403.
161. Mansell, S. M.; Farnaby, J. H.; Germeroth, A. I.; Arnold, P. L., *Organometallics* **2013**.
162. Siladke, N. A.; Meihaus, K. R.; Ziller, J. W.; Fang, M.; Furche, F.; Long, J. R.; Evans, W. J., *J. Am. Chem. Soc.* **2012,** *134*, 1243-1249.
163. Castro-Rodriguez, I.; Nakai, H.; Gantzel, P.; Zakharov, L. N.; Rheingold, A. L.; Meyer, K., *J. Am. Chem. Soc.* **2003,** *125*, 15734-15735.
164. Hayton, T. W., *Dalton Trans.* **2010,** *39*, 1145-1158.
165. Hayton, T. W., *Chem. Commun.* **2013,** *49*, 2956-2973.
166. Roussel, P.; Boaretto, R.; Kingsley, A. J.; Alcock, N. W.; Scott, P., *J. Chem. Soc., Dalton Trans.* **2002**, 1423-1428.
167. Brown, J. L.; Fortier, S.; Lewis, R. A.; Wu, G.; Hayton, T. W., *J. Am. Chem. Soc.* **2012,** *134*, 15468-15475.
168. King, D. M.; Tuna, F.; McInnes, E. J. L.; McMaster, J.; Lewis, W.; Blake, A. J.; Liddle, S. T., *Nat. Chem.* **2013,** *5*, 482-488.

169. Hayton, T. W.; Boncella, J. M.; Scott, B. L.; Batista, E. R.; Hay, P. J., *J. Am. Chem. Soc.* **2006,** *128*, 10549-10559.
170. Hayton, T. W.; Boncella, J. M.; Scott, B. L.; Palmer, P. D.; Batista, E. R.; Hay, P. J., *Science* **2005,** *310*, 1941-1943.
171. Lukens, J., Wayne W.; Beshouri, S. M.; Blosh, L. L.; Andersen, R. A., *J. Am. Chem. Soc.* **1996,** *118*, 901-902.
172. Biswas, B.; Mougel, V.; Pecaut, J.; Mazzanti, M., *Angew. Chem.-Int. Edit.* **2011,** *50*, 5744-5747.
173. Aresta, M.; Dibenedetto, A., *Dalton Trans.* **2007**, 2975-2992.
174. Finn, C.; Schnittger, S.; Yellowlees, L. J.; Love, J. B., *Chem. Commun.s* **2011,** *48*, 1392-1399.
175. Benson, E. E.; Kubiak, C. P.; Sathrum, A. J.; Smieja, J. M., *Chem. Soc. Rev.* **2009,** *38*, 89-99.
176. Castro-Rodriguez, I.; Olsen, K.; Gantzel, P.; Meyer, K., *J. Am. Chem. Soc.* **2003,** *125*, 4565-4571.
177. Berthet, J. C.; Lemarechal, J. F.; Nierlich, M.; Lance, M.; Vigner, J.; Ephritikhine, M., *J. Organomet. Chem.* **1991,** *408*, 335-341.
178. Summerscales, O. T.; Frey, A. S. P.; Geoffrey, F.; Cloke, N.; Hitchcock, P. B., *Chem. Commun.***2009**, 198-200.
179. Castro, L.; Lam, O. P.; Bart, S. C.; Meyer, K.; Maron, L., *Organometallics* **2010,** *29*, 5504-5510.
180. Schmidt, A.-C.; Nizovtsev, A. V.; Scheurer, A.; Heinemann, F. W.; Meyer, K., *Chem. Commun.* **2012,** *48*, 8634-8636.
181. Webster, C. L.; Ziller, J. W.; Evans, W. J., *Organometallics* **2012,** *31*, 7191–7197.
182. Zuend, S. J.; Lam, O. P.; Heinemann, F. W.; Meyer, K., *Angew. Chem.-Int. Edit.* **2011,** *50*, 10626-10630.
183. Evans, W. J.; Walensky, J. R.; Ziller, J. W., *Organometallics* **2010,** *29*, 945-950.
184. Bart, S. C.; Anthon, C.; Heinemann, F. W.; Bill, E.; Edelstein, N. M.; Meyer, K., *J. Am. Chem. Soc.* **2008,** *130*, 12536-12546.
185. Korobkov, I.; Gambarotta, S., *Organometallics* **2004,** *23*, 5379-5381.
186. Lescop, C.; Arliguie, T.; Lance, M.; Nierlich, M.; Ephritikhine, M., *J. Organomet. Chem.* **1999,** *580*, 137-144.
187. Lam, O. P.; Franke, S. M.; Heinemann, F. W.; Meyer, K., *J. Am. Chem. Soc.* **2012,** *134*, 16877-16881.
188. Matson, E. M.; Fanwick, P. E.; Bart, S. C., *Organometallics* **2011,** *30*, 5753-5762.
189. Arnold, P. L.; Turner, Z. R.; Germeroth, A. I.; Casely, I. J.; Nichol, G. S.; Bellabarba, R.; Tooze, R. P., *Dalton Trans.* **2013,** *42*, 1333-1337.
190. Brennan, J. G.; Andersen, R. A.; Zalkin, A., *Inorg. Chem.* **1986,** *25*, 1756-1760.
191. Castro, L.; Maron, L., *Chem.-Eur. J.* **2012,** *18*, 6610-6615.
192. Lam, O. P.; Castro, L.; Kosog, B.; Heinemann, F. W.; Maron, L.; Meyer, K., *Inorg. Chem.* **2012,** *51*, 781-783.
193. Lam, O. P.; Heinemann, F. W.; Meyer, K., *Angew. Chem.-Int. Edit.* **2011,** *50*, 5965-5968.
194. Eikey, R. A.; Abu-Omar, M. M., *Coord. Chem. Rev.* **2003,** *243*, 83-124.
195. Nugent, W. A.; Mayer, J. M., *Metal-Ligand Multiple Bonds*. John Wiley & Sons: New York, 1988.
196. Cramer, R. E.; Panchanatheswaran, K.; Gilje, J. W., *J. Am. Chem. Soc.* **1984,** *106*, 1853-1854.
197. Brennan, J. G.; Andersen, R. A., *J. Am. Chem. Soc.* **1985,** *107*, 514-516.
198. Andrea, T.; Eisen, M. S., *Chem. Soc. Rev.* **2008,** *37*, 550-567.
199. Ren, W.; Zi, G.; Walter, M. D., *Organometallics* **2012,** *31*, 672-679.
200. Belkhiri, L.; Lissillour, R.; Boucekkine, A., *Theochem-J. Mol. Struct.* **2005,** *757*, 155-164.
201. Spencer, L. P.; Yang, P.; Minasian, S. G.; Jilek, R. E.; Batista, E. R.; Boland, K. S.; Boncella, J. M.; Conradson, S. D.; Clark, D. L.; Hayton, T. W.; Kozimor, S. A.; Martin, R. L.; MacInnes, M. M.; Olson, A. C.; Scott, B. L.; Shuh, D. K.; Wilkerson, M. P., *J. Am. Chem. Soc.* **2013,** *135*, 2279-2290.
202. Spencer, L. P.; Yang, P.; Scott, B. L.; Batista, E. R.; Boncella, J. M., *Inorg. Chem.* **2009,** *48*, 2693-2700.
203. Graves, C. R.; Yang, P.; Kozimor, S. A.; Vaughn, A. E.; Clark, D. L.; Conradson, S. D.; Schelter, E. J.; Scott, B. L.; Thompson, J. D.; Hay, P. J.; Morris, D. E.; Kiplinger, J. L., *J. Am. Chem. Soc.* **2008,** *130*, 5272-5285.
204. Lam, O. P.; Franke, S. M.; Nakai, H.; Heinemann, F. W.; Hieringer, W.; Meyer, K., *Inorg. Chem.* **2012,** *51*, 6190-6199.
205. Wietzke, R.; Mazzanti, M.; Latour, J. M.; Pecaut, J.; Cordier, P. Y.; Madic, C., *Inorg. Chem.* **1998,** *37*, 6690-6697.
206. Streit, M.; Ingold, F., *J. Europ. Ceram. Soc.* **2005,** *25*, 2687-2692.
207. Silva, G. W. C.; Yeamans, C. B.; Ma, L. Z.; Cerefice, G. S.; Czerwinski, K. R.; Sattelberger, A. P., *Chem. Mat.* **2008,** *20*, 3076-3084.
208. Thomson, R. K.; Cantat, T.; Scott, B. L.; Morris, D. E.; Batista, E. R.; Kiplinger, J. L., *Nat. Chem.* **2010,** *2*, 723-729.
209. Nocton, G.; Pecaut, J.; Mazzanti, M., *Angew. Chem.-Int. Edit.* **2008,** *47*, 3040-3042.
210. Evans, W. J.; Miller, K. A.; Ziller, J. W.; Greaves, J., *Inorg. Chem.* **2007,** *46*, 8008-8018.
211. Evans, W. J.; Kozimor, S. A.; Ziller, J. W., *Science* **2005,** *309*, 1835-1838.

212. Fox, A. R.; Arnold, P. L.; Cummins, C. C., *J. Am. Chem. Soc.* **2010,** *132*, 3250-3251.
213. Fox, A. R.; Cummins, C. C., *J. Am. Chem. Soc.* **2009,** *131*, 5716-5717.
214. Fortier, S.; Wu, G.; Hayton, T. W., *J. Am. Chem. Soc.* **2010,** *132*, 6888-6889.
215. Simpson, S. J.; Turner, H. W.; Andersen, R. A., *Inorg. Chem.* **1981,** *20*, 2991-2995.
216. Benaud, O.; Berthet, J.-C.; Thuery, P.; Ephritikhine, M., *Inorg. Chem.* **2011,** *50*, 12204-12214.
217. Johnson, K. R. D.; Hayes, P. G., *Chem. Soc. Rev.* **2013,** *42*, 1947-1960.
218. Thomson, R. K.; Graves, C. R.; Scott, B. L.; Kiplinger, J. L., *Eur. J. Inorg. Chem.* **2009**, 1451-1455.
219. Rosen, R. K.; Andersen, R. A.; Edelstein, N. M., *J. Am. Chem. Soc.* **1990,** *112*, 4588-4590.
220. Zalkin, A.; Brennan, J. G.; Andersen, R. A., *Acta Cryst. Sec. C* **1988,** *44*, 1553-1554.
221. Castro-Rodriguez, I.; Nakai, H.; Meyer, K., *Angew. Chem.-Int. Edit.* **2006,** *45*, 2389-2392.
222. Lam, O. P.; Heinemann, F. W.; Meyer, K., *C. R. Chim.* **2010,** *13*, 803-811.
223. La Pierre, H. S.; Meyer, K., *Inorg. Chem.* **2013,** *52*, 529-539.
224. Matson, E. M.; Crestani, M. G.; Fanwick, P. E.; Bart, S. C., *Dalton Trans.* **2012,** *41*, 7952-7958.
225. Matson, E. M.; Forrest, W. P.; Fanwick, P. E.; Bart, S. C., *Organometallics* **2013,** *32*, 1484-1492.
226. Warner, B. P.; Scott, B. L.; Burns, C. J., *Angew. Chem.-Int. Edit.* **1998,** *37*, 959-960.
227. Brennan, J. G.; Andersen, R. A.; Zalkin, A., *J. Am. Chem. Soc.* **1988,** *110*, 4554-4558.
228. Jilek, R. E.; Spencer, L. P.; Lewis, R. A.; Scott, B. L.; Hayton, T. W.; Boncella, J. M., *J. Am. Chem. Soc.* **2012,** *134*, 9876-9878.
229. Cesari, M.; Pedretti, U.; Zazzetta, Z.; Lugli, g.; Marconi, W., *Inorganica Chimica Acta* **1971,** *5*, 439-444.
230. Cotton, F. A.; Schwotzer, W., *Organometallics* **1987,** *6*, 1275-1280.
231. Baudry, D.; Bulot, E.; Charpin, P.; Ephritikhine, M.; Lance, M.; Nierlich, M.; Vigner, J., *Journal of Organometallic Chemistry* **1989,** *371*, 155-162.
232. Cotton, F. A.; Schwotzer, W., *Organometallics* **1985,** *4*, 942-943.
233. Campbell, G. C.; Cotton, F. A.; Haw, J. F.; Schwotzer, W., *Organometallics* **1986,** *5*, 274-279.
234. Cotton, F. A.; Schwotzer, W.; Simpson, C. Q., *Angew. Chem.-Int. Edit.* **1986,** *25*, 637-639.
235. Krieck, S.; Goerls, H.; Yu, L.; Reiher, M.; Westerhausen, M., *J. Am. Chem. Soc.* **2009,** *131*, 2977-2985.
236. Tsai, Y.-C.; Wang, P.-Y.; Lin, K.-M.; Chen, S.-A.; Chen, J.-M., *Chem. Commun.* **2008**, 205-207.
237. Ni, C.; Ellis, B. D.; Fettinger, J. C.; Long, G. J.; Power, P. P., *Chem. Commun.* **2008**, 1014-1016.
238. Tsai, Y.-C.; Wang, P.-Y.; Chen, S.-A.; Chen, J.-M., *J. Am. Chem. Soc.* **2007,** *129*, 8066-8067.
239. Nikiforov, G. B.; Crewdson, P.; Gambarotta, S.; Korobkov, I.; Budzelaar, P. H. M., *Organometallics* **2007,** *26*, 48-55.
240. Monillas, W. H.; Yap, G. P. A.; Theopold, K. H., *Angew. Chem.-Int. Edit.* **2007,** *46*, 6692-6694.
241. Turner, L. E.; Davidson, M. G.; Jones, M. D.; Ott, H.; Schulz, V. S.; Wilson, P. J., *Inorg. Chem.* **2006,** *45*, 6123-6125.
242. Bochkarev, M. N., *Chem. Rev.* **2002,** *102*, 2089-2117.
243. Hitchcock, P. B.; Lappert, M. F.; Protchenko, A. V., *J. Am. Chem. Soc.* **2001,** *123*, 189-190.
244. Gun'ko, Y. K.; Hitchcock, P. B.; Lappert, M. F., *Organometallics* **2000,** *19*, 2832-2834.
245. Frank, W.; Reiland, V.; Reiss, G. J., *Angew. Chem.-Int. Edit.* **1998,** *37*, 2984-2985.
246. Cassani, M. C.; Duncalf, D. J.; Lappert, M. F., *J. Am. Chem. Soc.* **1998,** *120*, 12958-12959.
247. Cotton, F. A.; Kibala, P. A.; Wojtczak, W. A., *J. Am. Chem. Soc.* **1991,** *113*, 1462-1463.
248. Muetterties, E. L.; Bleeke, J. R.; Wucherer, E. J.; Albright, T. A., *Chem. Rev.* **1982,** *82*, 499-525.
249. Huang, W.; Khan, S. I.; Diaconescu, P. L., *J. Am. Chem. Soc.* **2011,** *133*, 10410-10413.
250. Huang, W.; Dulong, F.; Wu, T.; Khan, S. I.; Miller, J. T.; Cantat, T.; Diaconescu, P. L., *Nature Communications* **2013,** *4*.
251. Gianetti, T. L.; Nocton, G.; Minasian, S. G.; Tomson, N. C.; Kilcoyne, A. L. D.; Kozimor, S. A.; Shuh, D. K.; Tyliszczak, T.; Bergman, R. G.; Arnold, J., *J. Am. Chem. Soc.* **2013,** *135*, 3224-3236.
252. Evans, W. J.; Kozimor, S. A.; Ziller, J. W.; Kaltsoyannis, N., *J. Am. Chem. Soc.* **2004,** *126*, 14533-14547.
253. Patel, D.; Moro, F.; McMaster, J.; Lewis, W.; Blake, A. J.; Liddle, S. T., *Angew. Chem.-Int. Edit.* **2011,** *50*, 10388-10392.
254. Diaconescu, P. L.; Cummins, C. C., *J. Am. Chem. Soc.* **2002,** *124*, 7660-7661.
255. Diaconescu, P. L.; Cummins, C. C., *Inorg. Chem.***2012,** *51*, 2902-2916.
256. Monreal, M. J.; Khan, S. I.; Kiplinger, J. L.; Diaconescu, P. L., *Chem. Commun.* **2011,** *47*, 9119-9121.
257. Arnold, P. L.; Mansell, S. M.; Maron, L.; McKay, D., *Nat. Chem.* **2012,** *4*, 668-674.
258. Vlaisavljevich, B.; Diaconescu, P. L.; Lukens, W. L.; Gagliardi, L.; Cummins, C. C., *Organometallics* **2013,** *32*, 1341-1352.
259. Patel, D.; Tuna, F.; McInnes, E. J. L.; McMaster, J.; Lewis, W.; Blake, A. J.; Liddle, S. T., *Dalton Trans.* **2013,** *42*, 5224-5227.

260. Diefenbach, M.; Schwarz, H., *Chem.-Eur. J.* **2005,** *11*, 3058-3063.
261. Mazzanti, M., *Nat. Chem.* **2011,** *3*, 426-427.
262. Chirik, P. J., *Inorg. Chem.* **2011,** *50*, 9737-9740.
263. Chirik, P. J.; Wieghardt, K., *Science* **2010,** *327*, 794-795.
264. Eisenberg, R.; Gray, H. B., *Inorg. Chem.* **2011,** *50*, 9741-9751.
265. Wang, Y. D.; DuBois, J. L.; Hedman, B.; Hodgson, K. O.; Stack, T. D. P., *Science* **1998,** *279*, 537-540.
266. Muller, J.; Weyhermuller, T.; Bill, E.; Hildebrandt, P.; Ould-Moussa, L.; Glaser, T.; Wieghardt, K., *Angew. Chem.-Int. Edit.* **1998,** *37*, 616-619.
267. Jazdzewski, B. A.; Tolman, W. B., *Coord. Chem. Rev.* **2000,** *200*, 633-685.
268. Luca, O. R.; Crabtree, R. H., *Chem. Soc. Rev.* **2013,** *42*, 1440-1459.
269. Praneeth, V. K. K.; Ringenberg, M. R.; Ward, T. R., *Angew. Chem.-Int. Edit.* **2012,** *51*, 10228-10234.
270. Bouwkamp, M. W.; Bowman, A. C.; Lobkovsky, E.; Chirik, P. J., *J. Am. Chem. Soc.* **2006,** *128*, 13340-13341.
271. Smith, A. L.; Hardcastle, K. I.; Soper, J. D., *J. Am. Chem. Soc.* **2010,** *132*, 14358-14360.
272. Sylvester, K. T.; Chirik, P. J., *J. Am. Chem. Soc.* **2009,** *131*, 8772-8774.
273. Jaroschik, F.; Momin, A.; Nief, F.; Le Goff, X. F.; Deacon, G. B.; Junk, P. C., *Angew. Chem.-Int. Edit.* **2009,** *48*, 1117-1121.
274. Blackmore, K. J.; Sly, M. B.; Haneline, M. R.; Ziller, J. W.; Heyduk, A. F., *Inorg. Chem.* **2008,** *47*, 10522-10532.
275. Dzik, W. I.; van der Vlugt, J. I.; Reek, J. N. H.; de Bruin, B., *Angew. Chem.-Int. Edit.* **2011,** *50*, 3356-3358.
276. Huang, W. L.; Khan, S. I.; Diaconescu, P. L., *J. Am. Chem. Soc.* **2011,** *133*, 10410-10413.
277. Ringenberg, M. R.; Kokatam, S. L.; Heiden, Z. M.; Rauchfuss, T. B., *J. Am. Chem. Soc.* **2008,** *130*, 788-789.
278. Bart, S. C.; Lobkovsky, E.; Chirik, P. J., *J. Am. Chem. Soc.* **2004,** *126*, 13794-13807.
279. Myers, T. W.; Berben, L. A., *Chem. Commun.* **2012,** *49*, 4175-4177.
280. Tondreau, A. M.; Atienza, C. C. H.; Weller, K. J.; Nye, S. A.; Lewis, K. M.; Delis, J. G. P.; Chirik, P. J., *Science* **2012,** *335*, 567-570.
281. Myers, T. W.; Kazem, N.; Stoll, S.; Britt, R. D.; Shanmugam, M.; Berben, L. A., *J. Am. Chem. Soc.* **2011,** *133*, 8662-8672.
282. Bachmann, J.; Nocera, D. G., *J. Am. Chem. Soc.* **2004,** *126*, 2829-2837.
283. Bachmann, J.; Nocera, D. G., *Inorg. Chem.* **2005,** *44*, 6930-6932.
284. Haneline, M. R.; Heyduk, A. F., *J. Am. Chem. Soc.* **2006,** *128*, 8410-8411.
285. Zarkesh, R. A.; Ziller, J. W.; Heyduk, A. F., *Angew. Chem.-Int. Edit.* **2008,** *47*, 4715-4718.
286. Blackmore, K. J.; Lal, N.; Ziller, J. W.; Heyduk, A. F., *J. Am. Chem. Soc.* **2008,** *130*, 2728-2729.
287. Stanciu, C.; Jones, M. E.; Fanwick, P. E.; Abu-Omar, M. M., *J. Am. Chem. Soc.* **2007,** *129*, 12400-12401.
288. Khusniyarov, M. M.; Bill, E.; Weyhermueller, T.; Bothe, E.; Harms, K.; Sundermeyer, J.; Wieghardt, K., *Chem.-Eur. J.* **2008,** *14*, 7608-7622.
289. Kraft, S. J.; Williams, U. J.; Daly, S. R.; Schelter, E. J.; Kozimor, S. A.; Boland, K. S.; Kikkawa, J. M.; Forrest, W. P.; Christensen, C. N.; Schwarz, D. E.; Fanwick, P. E.; Clark, D. L.; Conradson, S. D.; Bart, S. C., *Inorg. Chem.* **2011,** *50*, 9838-9848.
290. Kraft, S. J.; Fanwick, P. E.; Bart, S. C., *J. Am. Chem. Soc.* **2012,** *134*, 6160-6168.
291. Cladis, D. P.; Kiernicki, J. J.; Fanwick, P. E.; Bart, S. C., *Chem. Commun.* **2013,** *49*, 4169-4171.
292. Matson, E. M.; Opperwall, S. R.; Fanwick, P. E.; Bart, S. C., *Inorg. Chem.* **2013,** *52*, 7295-304.
293. Blackmore, K. J.; Ziller, J. W.; Heyduk, A. F., *Inorg. Chem.***2005,** *44*, 5559-5561.
294. Kraft, S. J.; Fanwick, P. E.; Bart, S. C., *Inorg. Chem.* **2010,** *49*, 1103-1110.
295. Rivière, C.; Berthet, J.-C.; Nierlich, M.; Ephritikhine, M.; Madic, C., *Inorg. Chem.* **2001,** *40*, 4428-4435.
296. Mehdoui, T.; Berthet, J. C.; Thuery, P.; Salmon, L.; Riviere, E.; Ephritikhine, M., *Chem.-Eur. J.* **2005,** *11*, 6994-7006.
297. Zi, G. F.; Jia, L.; Werkema, E. L.; Walter, M. D.; Gottfriedsen, J. P.; Andersen, R. A., *Organometallics* **2005,** *24*, 4251-4264.
298. Kraft, S. J.; Walensky, J.; Fanwick, P. E.; Hall, M. B.; Bart, S. C., *Inorg. Chem.* **2010,** *49*, 7620-7622.
299. Schelter, E. J.; Wu, R. L.; Scott, B. L.; Thompson, J. D.; Morris, D. E.; Kiplinger, J. L., *Angew. Chem.-Int. Edit.* **2008,** *47*, 2993-2996.
300. Schelter, E. J.; Wu, R. L.; Veauthier, J. M.; Bauer, E. D.; Booth, C. H.; Thomson, R. K.; Graves, C. R.; John, K. D.; Scott, B. L.; Thompson, J. D.; Morris, D. E.; Kiplinger, J. L., *Inorg. Chem.* **2010,** *49*, 1995-2007.
301. Berthet, J. C.; Thuery, P.; Baudin, C.; Boizot, B.; Ephritikhine, M., *Dalton Trans.* **2009**, 7613-7616.
302. Evans, W. J.; Nyce, G. W.; Johnston, M. A.; Ziller, J. W., *J. Am. Chem. Soc.* **2000,** *122*, 12019-12020.
303. Evans, W. J.; Nyce, G. W.; Ziller, J. W., *Angew. Chem.-Int. Edit.* **2000,** *39*, 240-242.
304. Evans, W. J.; Kozimor, S. A.; Ziller, J. W., *Chem. Commun.* **2005**, 4681-4683.

305. Evans, W. J.; Traina, C. A.; Ziller, J. W., *J. Am. Chem. Soc.* **2009,** *131*, 17473-17481.
306. Atwood, D. A., *Coord. Chem. Rev.* **1997,** *165*, 267-296.
307. Hobday, M. D.; Smith, T. D., *Coord. Chem. Rev.* **1973,** *9*, 311-337.
308. Yoon, T. P.; Jacobsen, E. N., *Science* **2003,** *299*, 1691-1693.
309. Matsumoto, K.; Saito, B.; Katsuki, T., *Chem. Commun.* **2007**, 3619-3627.
310. Mihara, H.; Xu, Y.; Shepherd, N. E.; Matsunaga, S.; Shibasaki, M., *J. Am. Chem. Soc.* **2009,** *131*, 8384-8385.
311. Kato, Y.; Furutachi, M.; Chen, Z.; Mitsunuma, H.; Matsunaga, S.; Shibasaki, M., *J. Am. Chem. Soc.* **2009,** *131*, 9168-9169.
312. Yoshino, T.; Morimoto, H.; Lu, G.; Matsunaga, S.; Shibasaki, M., *J. Am. Chem. Soc.* **2009,** *131*, 17082-17083.
313. Arnold, P. L.; Pecharman, A. F.; Hollis, E.; Yahia, A.; Maron, L.; Parsons, S.; Love, J. B., *Nat. Chem.* **2010,** *2*, 1056-1061.
314. Arnold, P. L.; Pecharman, A. F.; Love, J. B., *Angew. Chem.-Int. Edit.* **2011,** *50*, 9456-9458.
315. Arnold, P. L.; Hollis, E.; White, F. J.; Magnani, N.; Caciuffo, R.; Love, J. B., *Angew. Chem.-Int. Edit.* **2011,** *50*, 887-890.
316. Takao, K.; Kato, M.; Takao, S.; Nagasawa, A.; Bernhard, G.; Hennig, C.; Ikeda, Y., *Inorg. Chem.* **2010,** *49*, 2349-2359.
317. Mougel, V.; Horeglad, P.; Nocton, G.; Pecaut, J.; Mazzanti, M., *Angew. Chem.-Int. Edit.* **2009,** *48*, 8477-8480.
318. Selbin, J.; Ortego, J. D., *J. Inorg. Nucl.Chem.* **1967,** *29*, 1449-1456.
319. Calderazzo, F.; Floriani, C.; Pasquali, M.; Cesari, M.; Perego, G., *Gazz. Chim. Ital.* **1976,** *106*, 127-137.
320. Salmon, L.; Thuery, P.; Ephritikhine, M., *Dalton Trans.* **2004**, 1635-1643.
321. Salmon, L.; Thuery, P.; Ephritikhine, M., *Dalton Trans.* **2004**, 4139-4145.
322. Le Borgne, T.; Riviere, E.; Marrot, J.; Thuery, P.; Girerd, J. J.; Ephritikhine, M., *Chem.-Eur. J.* **2002,** *8*, 774-783.
323. Le Borgne, T.; Riviere, E.; Marrot, J.; Girerd, J. J.; Ephritikhine, M., *Angew. Chem.-Int. Edit.* **2000,** *39*, 1647-1649.
324. Salmon, L.; Thuery, P.; Ephritikhine, M., *Polyhedron* **2003,** *22*, 2683-2688.
325. Salmon, L.; Thuery, P.; Ephritikhine, M., *Polyhedron* **2004,** *23*, 623-627.
326. Salmon, L.; Thuery, P.; Ephritikhine, M., *Polyhedron* **2006,** *25*, 1537-1542.
327. Arnold, P. L.; Potter, N. A.; Carmichael, C. D.; Slawin, A. M. Z.; Roussel, P.; Love, J. B., *Chem. Commun.* **2010,** *46*, 1833-1835.
328. Calderazzo, F.; Pasquali, M.; Corsi, N., *J. Chem. Soc.-Chem. Commun.* **1973**, 784-785.
329. Monreal, M. J.; Wright, R. J.; Morris, D. E.; Scott, B. L.; Golden, J. T.; Power, P. P.; Kiplinger, J. L., *Organometallics* **2013,** *32*, 1423-1434.
330. Bandoli, G.; Clemente, D. A.; Croatto, U.; Vidali, M.; Vigato, P. A., *J. Chem. Soc.-Dalton Trans.* **1973**, 2331-2335.
331. Roussel, P.; Alcock, N. W.; Boaretto, R.; Kingsley, A. J.; Munslow, I. J.; Sanders, C. J.; Scott, P., *Inorg. Chem.* **1999,** *38*, 3651-3656.
332. Kahr, B.; Van Engen, D.; Mislow, K., *J. Am. Chem. Soc.* **1986,** *108*, 8305-8307.
333. Baldridge, K. K.; Kasahara, Y.; Ogawa, K.; Siegel, J. S.; Tanaka, K.; Toda, F., *J. Am. Chem. Soc.* **1998,** *120*, 6167-6168.
334. Fokin, A. A.; Chernish, L. V.; Gunchenko, P. A.; Tikhonchuk, E. Y.; Hausmann, H.; Serafin, M.; Dahl, J. E. P.; Carlson, R. M. K.; Schreiner, P. R., *J. Am. Chem. Soc.* **2012,** *134*, 13641-13650.
335. Maury, O.; Villiers, C.; Ephritikhine, M., *Angew. Chem.-Int. Edit.* **1996,** *35*, 1129-1130.
336. Maury, O.; Villiers, C.; Ephritikhine, M., *New J. Chem.* **1997,** *21*, 137-139.
337. Kosog, B.; Kefalidis, C. E.; Heinemann, F. W.; Maron, L.; Meyer, K., *J. Am. Chem. Soc.* **2012,** *134*, 12792-12797.
338. Monreal, M. J.; Khan, S.; Diaconescu, P. L., *Angew. Chem.-Int. Edit.* **2009,** *48*, 8352-8355.
339. Monreal, M. J.; Diaconescu, P. L., *J. Am. Chem. Soc.* **2010,** *132*, 7676-7683.
340. Morss, L. R.; Edelstein, N. M.; Fuger, J., *The Chemistry of the Actinide and Transactinide Elements*. Springer: Dordrecht, 2006.
341. Edelstein, N. M.; Lander, G. H., *The Chemistry of the Actinide and Transactinide Elements*. Springer: Dordrecht, 2006.
342. Schelter, E. J.; Veauthier, J. M.; Graves, C. R.; John, K. D.; Scott, B. L.; Thompson, J. D.; Pool-Davis-Tournear, J. A.; Morris, D. E.; Kiplinger, J. L., *Chem.-Eur. J.* **2008,** *14*, 7782-7790.

343. McCullough, L. G.; Turner, H. W.; Andersen, R. A.; Zalkin, A.; Templeton, D. H., *Inorg. Chem.* **1981,** *20*, 2869-2871.
344. Antunes, M. A.; Dias, M.; Monteiro, B.; Domingos, A.; Santos, I. C.; Marques, N., *Dalton Trans.* **2006**, 3368-3374.
345. Clark, D. L.; Sattelberger, A. P.; Vandersluys, W. G.; Watkin, J. G., *J. Alloys Compd.* **1992,** *180*, 303-315.
346. Mayer, J. M., *Acc. Chem. Res.* **2011,** *44*, 36-46.
347. Lam, O. P.; Feng, P. L.; Heinemann, F. W.; O'Connor, J. M.; Meyer, K., *J. Am. Chem. Soc.* **2008,** *130*, 2806-2816.
348. Terzis, A.; Mentzafos, D.; Tajmirriahi, H. A., *Inorg. Chim. Acta* **1984,** *84*, 187-193.
349. Hill, R. J.; Rickard, C. E. F., *J. Inorg. Nucl. Chem.* **1978,** *40*, 793-797.
350. Hou, Z. M.; Fujita, A.; Koizumi, T.; Yamazaki, H.; Wakatsuki, Y., *Organometallics* **1999,** *18*, 1979-1985.
351. Hou, Z. M.; Fujita, A.; Zhang, Y. G.; Miyano, T.; Yamazaki, H.; Wakatsuki, Y., *J. Am. Chem. Soc.* **1998,** *120*, 754-766.
352. Covert, K. J.; Wolczanski, P. T., *Inorg. Chem.* **1989,** *28*, 4565-4567.
353. Hirota, N.; Weissman, S. I., *J. Am. Chem. Soc.* **1964,** *86*, 2538-2545.
354. Kawai, A.; Hirakawa, M.; Abe, T.; Obi, K.; Shibuya, K., *J. Phys. Chem. A* **2001,** *105*, 9628-9636.
355. Gomberg, M., *J. Am. Chem. Soc.* **1900,** *22*, 757-771.
356. Lankamp, H.; Nauta, W. T.; Maclean, C., *Tet. Lett.* **1968**, 249-254.
357. Covert, K. J.; Wolczanski, P. T.; Hill, S. A.; Krusic, P. J., *Inorg. Chem.* **1992,** *31*, 66-78.
358. Ephritikhine, M.; Maury, O.; Villiers, C.; Lance, M.; Nierlich, M., *J. Chem. Soc.-Dalton Trans.* **1998**, 3021-3027.
359. Camp, C.; Guidal, V.; Biswas, B.; Pecaut, J.; Dubois, L.; Mazzanti, M., *Chem. Sci.* **2012,** *3*, 2433-2448.
360. Isse, A. A.; Gennaro, A.; Vianello, E., *Electrochim. Acta* **1997,** *42*, 2065-2071.
361. Lewis, A. J.; Williams, U. J.; Carroll, P. J.; Schelter, E. J., *Inorg. Chem.* **2013,** *52*, 7326-7328.
362. Shannon, R. D., *Acta Cryst. Sect. A* **1976,** *32*, 751-767.
363. Evans, W. J.; Davis, B. L., *Chem. Rev.* **2002,** *102*, 2119-2136.
364. Morss, L. R., *Chem. Rev.* **1976,** *76*, 827-841.
365. MacDonald, M. R.; Bates, J. E.; Ziller, J. W.; Furche, F.; Evans, W. J., *J. Am. Chem. Soc.* **2013,** *135*, 9857-9868.
366. Seibig, S.; Toth, E.; Merbach, A. E., *J. Am. Chem. Soc.* **2000,** *122*, 5822-5830.
367. Veauthier, J. M.; Schelter, E. J.; Carlson, C. N.; Scott, B. L.; Da Re, R. E.; Thompson, J. D.; Kiplinger, J. L.; Morris, D. E.; John, K. D., *Inorg. Chem.* **2008,** *47*, 5841-5849.
368. Connelly, N. G.; Geiger, W. E., *Chem. Rev.* **1996,** *96*, 877-910.
369. Berthet, J. C.; Nierlich, M.; Ephritikhine, M., *C. R. Chim.* **2002,** *5*, 81-87.
370. Gladysz, J. A.; Ball, Z. T.; Bertrand, G.; Blum, S. A.; Dong, V. M.; Dorta, R.; Hahn, F. E.; Humphrey, M. G.; Jones, W. D.; Klosin, J.; Manners, I.; Marks, T. J.; Mayer, J. M.; Rieger, B.; Ritter, J. C.; Sattelberger, A. P.; Schomaker, J. M.; Yam, V. W.-W., *Organometallics* **2011,** *31*, 1-18.
371. Fachinetti, G.; Floriani, C.; Zanazzi, P. F., *J. Am. Chem. Soc.* **1978,** *100*, 7405-7407.
372. Gambarotta, S.; Arena, F.; Floriani, C.; Zanazzi, P. F., *J. Am. Chem. Soc.* **1982,** *104*, 5082-5092.
373. Hammouche, M.; Lexa, D.; Momenteau, M.; Saveant, J. M., *J. Am. Chem. Soc.* **1991,** *113*, 8455-8466.
374. Pinkes, J. R.; Steffey, B. D.; Vites, J. C.; Cutler, A. R., *Organometallics* **1994,** *13*, 21-23.
375. Hanna, T. A.; Baranger, A. M.; Bergman, R. G., *J. Am. Chem. Soc.* **1995,** *117*, 11363-11364.
376. Memmler, H.; Kauper, U.; Gade, L. H.; Scowen, I. J.; McPartlin, M., *Chem. Commun.* **1996**, 1751-1752.
377. Jeoung, J. H.; Dobbek, H., *Science* **2007,** *318*, 1461-1464.
378. Cozzi, P. G., *Chem. Soc. Rev.* **2004,** *33*, 410-421.
379. Shafir, A.; Fiedler, D.; Arnold, J., *J. Chem. Soc.-Dalton Trans.* **2002**, 555-560.
380. Broderick, E. M.; Thuy-Boun, P. S.; Guo, N.; Vogel, C. S.; Sutter, J.; Miller, J. T.; Meyer, K.; Diaconescu, P. L., *Inorg. Chem.* **2011,** *50*, 2870-2877.
381. Broderick, E. M.; Diaconescu, P. L., *Inorg. Chem.* **2009,** *48*, 4701-4706.
382. Monreal, M. J.; Carver, C. T.; Diaconescu, P. L., *Inorg. Chem.* **2007,** *46*, 7226-7228.
383. Dunitz, J. D.; Orgel, L. E.; Rich, A., *Acta Cryst.* **1956,** *9*, 373-375.
384. Westmoreland, I.; Arnold, J., *Acta Cryst. Sect. E* **2006,** *62*, M2303-M2304.
385. Graves, C. R.; Vaughn, A. E.; Schelter, E. J.; Scott, B. L.; Thompson, J. D.; Morris, D. E.; Kiplinger, J. L., *Inorg. Chem.* **2008,** *47*, 11879-11891.
386. Xu, G.-L.; Crutchley, R. J.; DeRosa, M. C.; Pan, Q.-J.; Zhang, H.-X.; Wang, X.; Ren, T., *J. Am. Chem. Soc.* **2005,** *127*, 13354-13363.

387. Kaufmann, L.; Breunig, J.-M.; Vitze, H.; Schodel, F.; Nowik, I.; Pichlmaier, M.; Bolte, M.; Lerner, H.-W.; Winter, R. F.; Herber, R. H.; Wagner, M., *Dalton Trans.* **2009,** *38*, 2940-2950.
388. Han, F.; Li, B.; Zhang, Y.; Wang, Y.; Shen, Q., *Organometallics* **2011,** *29*, 3467-3470.
389. Bozoklu, G.; Gateau, C.; Imbert, D.; Pecaut, J.; Robeyns, K.; Filinchuk, Y.; Memon, F.; Muller, G.; Mazzanti, M., *J. Am. Chem. Soc.* **2012,** *134*, 8372-8375.
390. Allouche, L.; Marquis, A.; Lehn, J.-M., *Chem.-Eur. J.* **2006**, 7520–7525.
391. Mougel, V.; Pecaut, J.; Mazzanti, M., *Chem. Commun.* **2012,** *48*, 868-870.
392. Kay, E. R.; Leigh, D. A.; Zerbetto, F., *Angew. Chem.-Int. Edit.* **2007,** *46*, 72-191.
393. Guillemot, G.; Castellano, B.; Prange, T.; Solari, E.; Floriani, C., *Inorg. Chem.* **2007,** *46*, 5152-5154.
394. Albright, T. A.; Burdett, J. K.; Whangbo, M. H., *Orbital Interactions in Chemistry*. Wiley: New York, 1985.
395. Wolczanski, P. T., *Polyhedron* **1995,** *14*, 3335-3362.
396. Marciniec, B.; Maciejewski, H., *Coord. Chem. Rev.* **2001,** *223*, 301-335.
397. Tolman, C. A., *Chem. Rev.* **1977,** *77*, 313-348.
398. Muller, T. E.; Mingos, D. M. P., *Transition Metal Chemistry* **1995,** *20*, 533-539.
399. Poater, A.; Cosenza, B.; Correa, A.; Giudice, S.; Ragone, F.; Scarano, V.; Cavallo, L., *Eur. J. Inorg. Chem.* **2009,** *2009*, 1759-1766.
400. *https://www.molnac.unisa.it/OMtools/sambvca.php*.
401. Clavier, H.; Nolan, S. P., *Chem. Commun.* **2010,** *46*, 841-861.
402. King, L.; Sullivan, A. C., *Coord. Chem. Rev.* **1999,** *189*, 19-57.
403. Murugavel, R.; Voigt, A.; Walawalkar, M. G.; Roesky, H. W., *Chem. Rev.* **1996,** *96*, 2205-2236.
404. Lorenz, V.; Fischer, A.; Giessmann, S.; Gilje, J. W.; Gun'ko, Y.; Jacob, K.; Edelmann, F. T., *Coord. Chem. Rev.* **2000,** *206*, 321-368.
405. Boyle, T. J.; Ottley, L. A. M., *Chem. Rev.* **2008,** *108*, 1896-1917.
406. Lorenz, V.; Fischer, A.; Jacob, K.; Bruser, W.; Edelmann, F. T., *Chem.-Eur. J.* **2001,** *7*, 848-857.
407. Heppekausen, J.; Stade, R.; Goddard, R.; Fuerstner, A., *J. Am. Chem. Soc.* **2010,** *132*, 11045-11057.
408. Lysenko, S.; Volbeda, J.; Jones, P. G.; Tamm, M., *Angew. Chem.-Int. Edit.* **2012,** *51*, 6757-6761.
409. Jarupatrakorn, J.; Tilley, J. D., *J. Am. Chem. Soc.* **2002,** *124*, 8380-8388.
410. Fujdala, K. L.; Tilley, T. D., *Chem. Mat.* **2004,** *16*, 1035-1047.
411. Brutchey, R. L.; Lugmair, C. G.; Schebaum, L. O.; Tilley, T. D., *J. Catal.* **2005,** *229*, 72-81.
412. Terry, K. W.; Tilley, T. D., *Chem. Mat.* **1991,** *3*, 1001-1003.
413. Su, K.; Tilley, T. D.; Sailor, M. J., *J. Am. Chem. Soc.* **1996,** *118*, 3459-3468.
414. Terry, K. W.; Lugmair, C. G.; Tilley, T. D., *J. Am. Chem. Soc.* **1997,** *119*, 9745-9756.
415. Lee, C.-S.; Lin, C.-H.; Wang, S.-L.; Lii, K.-H., *Angew. Chem.-Int. Edit.* **2010,** *49*, 4254-4256.
416. Burns, P. C.; Olson, R. A.; Finch, R. J.; Hanchar, J. M.; Thibault, Y., *J. Nucl. Mater.* **2000,** *278*, 290-300.
417. Porchia, M.; Brianese, N.; Casellato, U.; Ossola, F.; Rossetto, G.; Zanella, P.; Graziani, R., *J. Chem.Soc.-Dalton Trans.* **1989**, 677-681.
418. Lorenz, V.; Fischer, A.; Jacob, K.; Brüser, W.; Gelbrich, T.; Jones, P. G.; Edelmann, F. T., *Chem. Commun.* **1998**, 2217-2218.
419. Nishiura, M.; Hou, Z. M.; Wakatsuki, Y., *Organometallics* **2004,** *23*, 1359-1368.
420. Evans, W. J.; Golden, R. E.; Ziller, J. W., *Inorg. Chem.* **1991,** *30*, 4963-4968.
421. Chadwick, F. M.; Ashley, A.; Wildgoose, G.; Goicoechea, J. M.; Randall, S.; O'Hare, D., *Dalton Trans.* **2010,** *39*, 6789-6793.
422. Antunes, M. A.; Pereira, L. C. J.; Santos, I. C.; Mazzanti, M.; Marcalo, J.; Almeida, M., *Inorg. Chem.* **2011,** *50*, 9915-9917.
423. Moro, F.; Mills, D. P.; Liddle, S. T.; van Slageren, J., *Angew. Chem.-Int. Edit.* **2013,** *52*, 3430-3433.
424. Korobkov, I.; Gambarotta, S.; Yap, G. P. A.; Thompson, L.; Hay, P. J., *Organometallics* **2001,** *20*, 5440-5445.
425. Roussel, P.; Hitchcock, P. B.; Tinker, N.; Scott, P., *Chem. Commun.* **1996**, 2053-2054.
426. Fujdala, K. L.; Tilley, T. D., *J. Catal.* **2003,** *216*, 265-275.
427. Rulkens, R.; Male, J. L.; Terry, K. W.; Olthof, B.; Khodakov, A.; Bell, A. T.; Iglesia, E.; Tilley, T. D., *Chem. Mat.* **1999,** *11*, 2966-2973.
428. Su, K.; Tilley, T. D., *Chem. Mat.* **1997,** *9*, 588-595.
429. Uvarova, Y. A.; Sokolova, E.; Hawthorne, F. C.; Agakhanov, A. A.; Pautov, L. A., *Canad. Miner.* **2004,** *42*, 1005-1011.
430. Stieff, L. R.; Stern, T. W.; Sherwood, A. M., *Science* **1955,** *121*, 608-609.
431. Chen, C. S.; Lee, S. F.; Lii, K. H., *J. Am. Chem. Soc.* **2005,** *127*, 12208-12209.
432. Liu, H.-K.; Lii, K.-H., *Inorg. Chem.* **2011,** *50*, 5870-5872.

433. Kulyukhin, S. A.; Mikheev, N. B.; Kamenskaya, A. N.; Konovalova, N. A.; Rumer, I. A., *Radiochemistry* **2006,** *48*, 535-551.
434. Berg, J. M.; Clark, D. L.; Huffmann, J. C.; Morris, D. E.; Sattelberger, A. P.; Streib, W. E.; Van Der Sluys, W. G.; G., W. J., *J. Am. Chem. Soc.* **1992,** *114*, 10811-10821.
435. Van Der Sluys, W. G.; Sattelberger, A. P., *Chem. Rev.* **1990,** *90*, 1027-1040.
436. Nakai, H.; Hu, X. L.; Zakharov, L. N.; Rheingold, A. L.; Meyer, K., *Inorg. Chem.* **2004,** *43*, 855-857.
437. Fagan, P. J.; Manriquez, J. M.; Marks, T. J.; Day, C. S.; Vollmer, S. H.; Day, V. W., *Organometallics* **1982,** *1*, 170-180.
438. Evans, W. J.; Lee, D. S.; Rego, D. B.; Perotti, J. M.; Kozimor, S. A.; Moore, E. K.; Ziller, J. W., *J. Am. Chem. Soc.* **2004,** *126*, 14574-14582.
439. Bianchini, C.; Mealli, C.; Meli, A.; Orlandini, A.; Sacconi, L., *Angew. Chem.-Int. Edit.* **1979,** *18*, 673-674.
440. Baenziger, N. C.; Duax, W. L., *J. Chem. Phys.* **1968,** *48*, 2974-2981.
441. Moltzen, E. K.; Klabunde, K. J.; Senning, A., *Chem. Rev.* **1988,** *88*, 391-406.
442. Castro, L.; Labouille, S.; Kindra, D. R.; Ziller, J. W.; Nief, F.; Evans, W. J.; Maron, L., *Chem.-Eur. J.* **2012,** *18*, 7886-7895.
443. Spencer, L. P.; Gdula, R. L.; Hayton, T. W.; Scott, B. L.; Boncella, J. M., *Chem. Commun.* **2008**, 4986-4988.
444. Krot, N. N.; Grigoriev, M. S., *Russ. Chem.Rev.* **2004,** *73*, 89-100.
445. Arney, D. S. J.; Burns, C. J.; Smith, D. C., *J. Am. Chem. Soc.* **1992,** *114*, 10068-10069.
446. Arney, D. S. J.; Burns, C. J., *J. Am. Chem. Soc.* **1995,** *117*, 9448-9460.
447. Spencer, L. P.; Yang, P.; Scott, B. L.; Batista, E. R.; Boncella, J. M., *Inorg. Chem.* **2009,** *48*, 11615-11623.
448. Seaman, L. A.; Fortier, S.; Wu, G.; Hayton, T. W., *Inorg. Chem.* **2011,** *50*, 636-646.
449. Swartz, D. L., II; Spencer, L. P.; Scott, B. L.; Odom, A. L.; Boncella, J. M., *Dalton Trans.* **2010,** *39*, 6841-6846.
450. Spencer, L. P.; Schelter, E. J.; Yang, P.; Gdula, R. L.; Scott, B. L.; Thompson, J. D.; Kiplinger, J. L.; Batista, E. R.; Boncella, J. M., *Angew. Chem.-Int. Edit.* **2009,** *48*, 3795-3798.
451. Nocton, G.; Horeglad, P.; Pecaut, J.; Mazzanti, M., *J. Am. Chem. Soc.* **2008,** *130*, 16633-16645.
452. Brown, D. R.; Denning, R. G., *Inorg. Chem.***1996,** *35*, 6158-6163.
453. Hayton, T. W.; Boncella, J. M.; Scott, B. L.; Batista, E. R., *J. Am. Chem. Soc.* **2006,** *128*, 12622-12623.
454. Sullens, T. A.; Jensen, R. A.; Shvareva, T. Y.; Albrecht-Schmitt, T. E., *J. Am. Chem. Soc.* **2004,** *126*, 2676-2677.
455. Alekseev, E. V.; Krivovichev, S. V.; Depmeier, W.; Siidra, O. I.; Knorr, K.; Suleimanov, E. V.; Chuprunov, E. V., *Angew. Chem.-Int. Edit.* **2006,** *45*, 7233-7235.
456. Newton, T. W.; Baker, F. B., *Inorg. Chem.* **1965,** *4*, 1166-1170.
457. Ekstrom, A., *Inorg. Chem.***1974,** *13*, 2237-2241.
458. Steele, H.; Taylor, R. J., *Inorg. Chem.* **2007,** *46*, 6311-6318.
459. Kovacs, A.; Konings, R. J. M., *Chemphyschem* **2006,** *7*, 455-462.
460. Fortier, S.; Wu, G.; Hayton, T. W., *Inorg. Chem.* **2008,** *47*, 4752-4761.
461. Meyer, K.; Mindiola, D. J.; Baker, T. A.; Davis, W. M.; Cummins, C. C., *Angew. Chem.-Int. Edit.* **2000,** *39*, 3063-3066.
462. Seaman, L. A.; Wu, G.; Edelstein, N.; Lukens, W. W.; Magnani, N.; Hayton, T. W., *J. Am. Chem. Soc.* **2012,** *134*, 4931-4940.
463. Cloke, G., F. N.; Hitchcock, P. B., *J. Am. Chem. Soc.* **2002,** *124*, 9352-9353.
464. Fortier, S.; Wu, G.; Hayton, T. W., *Dalton Trans.* **2010,** *39*, 352-354.
465. Kiplinger, J. L.; Pool, J. A.; Schelter, E. J.; Thompson, J. D.; Scott, B. L.; Morris, D. E., *Angew. Chem.-Int. Edit.* **2006,** *45*, 2036-2041.
466. Cotton, A. F.; Marler, O. D.; Schwotzer, W., *Inorg. Chem.* **1984,** *23*, 4211-4215.
467. Salmon, L.; Thuery, P.; Miyamoto, S.; Yamato, T.; Ephritikhine, M., *Polyhedron* **2006,** *25*, 2439-2446.
468. Duval, P. B.; Burns, C. J.; Buschmann, W. E.; Clark, D. L.; Morris, D. E.; Scott, B. L., *Inorg. Chem.* **2001,** *40*, 5491-5496.
469. Madelung, O., *Landolt-Börnstein : Numerical Data and Functional Relashionship in Science and Technology*. Springer: Berlin, 1987; Vol. 15.
470. Arliguie, T.; Lance, M.; Nierlich, M.; Vigner, J.; Ephritikhine, M., *J. Chem. Soc.-Chem. Commun.* **1995**, 183-184.
471. Lam, O. P.; Heinemann, F. W.; Meyer, K., *Chem. Sci.* **2011,** *2*, 1538-1547.
472. Rinehart, J. D.; Long, J. R., *J. Am. Chem. Soc.* **2009,** *131*, 12558-12559.

473. King, D. M.; Tuna, F.; McMaster, J.; Lewis, W.; Blake, A. J.; McInnes, E. J. L.; Liddle, S. T., *Angew. Chem.-Int. Edit.* **2013,** *52*, 4921-4924.
474. Rinehart, J. D.; Meihaus, K. R.; Long, J. R., *J. Am. Chem. Soc.* **2010,** *132*, 7572-7573.
475. Coutinho, J. T.; Antunes, M. A.; Pereira, L. C. J.; Bolvin, H.; Marcalo, J.; Mazzanti, M.; Almeida, M., *Dalton Trans.* **2012,** *41*, 13568-13571.
476. Tanner, J. E., *J. Chem. Phys.* **1970,** *52*, 2523-2527.
477. Johnson, C. S., *Progress in Nuclear Magnetic Resonance Spectroscopy* **1999,** *34*, 203-256.
478. Wu, D. H.; Chen, A. D.; Johnson, C. S., *J. Magnet. Res., Series A* **1995,** *115*, 260-264.
479. Bain, G. A.; Berry, J. F., *J. Chem. Educ.* **2008,** *85*, 532-536.
480. Evans, D. F., *J. Am. Chem. Soc.* **1959**, 2003-2005.
481. Palatinus, L.; Chapuis, G., *J. Appl. Cryst.* **2007,** *40*, 786-790.
482. Dolomanov, O. V.; Bourhis, L. J.; Gildea, R. J.; Howard, J. A. K.; Puschmann, H., *J. Appl. Cryst.* **2009,** *42*, 339-341.
483. *CCDC : http://www.ccdc.cam.ac.uk/pages/Home.aspx*. Cambridge, U.K., 2004-2009.
484. Chen, H. Y.; Cronin, J. A.; Archer, R. D., *Inorg. Chem.* **1995,** *34*, 2306-2315.
485. Cameron, P. A.; Gibson, V. C.; Redshaw, C.; Segal, J. A.; White, A. J. P.; Williams, D. J., *J. Chem. Soc.-Dalton Trans.* **2002**, 415-422.
486. Takano, K.; Takahashi, M.; Fukushima, T.; Takezaki, M.; Tominaga, T.; Akashi, H.; Takagi, H.; Shibahara, T., *Bull. Chem. Soc. Japan* **2012,** *85*, 1210-1221.
487. Mazzanti, M.; Gambarotta, S.; Floriani, C.; Chiesivilla, A.; Guastini, C., *Inorg. Chem.* **1986,** *25*, 2308-2314.
488. Calderazzo, F.; Fachinetti, G.; Floriani, C., *J. Am. Chem. Soc.* **1974,** *96*, 3695-3696.
489. MacDonald, M.; Fieser, M.; Bates, J.; Ziller, J.; Furche, F.; Evans, W., *J. Am. Chem. Soc.* **2013**, *135*, 13310-13313.

APPENDIX

Crystallographic data

Table VII.1. **X-ray crystallographic data.**

Compound	**[3]**	**[4-py].py$_4$**	**[5-a]**	**[5-b]**
Formula	C25 H22.5 N3.5 O2.5 I2 U	C70 H58 N10 O4 U2	C50 H105 N7 O2 Si10 U2	C50 H105 N7 O2 Si10 U2
Crystal size [mm]	0.44 x 0.36 x 0.14	0.15 x 0.15 x 0.05	0.20 x 0.09 x 0.02	0.32 x 0.06 x 0.04
Crystal system	Monoclinic	Triclinic	Triclinic	Triclinic
Space group	P $2_1/c$	P -1	P -1	P -1
Volume [Å^3]	2737.2(4)	2960.99(9)	3568.0(2)	3555.5(2)
a [Å]	17.6636(18)	11.6556(2)	10.9766(4)	12.3235(4)
b [Å]	10.7960(7)	12.0214(2)	16.2207(7)	15.6292(5)
c [Å]	15.9829(15)	22.0847(4)	21.4478(9)	19.8856(8)
α [°]	90	103.1296(14)	74.424(4)	95.444(3)
β [°]	116.096(13)	99.9454(15)	75.995(3)	104.832(3)
γ [°]	90	91.5909(14)	87.630(3)	103.254(3)
Z	4	2	2	2
Absorption coefficient [mm^{-1}]	8.215	5.523	4.739	4.756
F (000)	1660	1528	1588	1588
T [K]	150(2)	150(2)	150(2)	150(2)
Exposure time [s]	10	15	60	20
Narrow data	165	1310	420	377
Total no. reflexions	7818	94669	32250	24821
Unique reflexions [R(int)]	5035 [R(int) = 0.0545]	18076 [R(int) = 0.0499]	17652 [R(int) = 0.0763]	14496 [R(int) = 0.0544]
Final R indices [I>2σ(I)]	R1 = 0.0767, wR2 = 0.1786	R1 = 0.0456, wR2 = 0.1030	R1 = 0.0533, wR2 = 0.0660	R1 = 0.0554, wR2 = 0.1115
Largest diff. peak and hole [eA^{-3}]	3.105 and -1.676	2.916 and -0.632	1.555 and -1.342	2.223 and -0.724
GOF	0.869	0.846	0.927	0.752

Table VII.2. **X-ray crystallographic data (continued).**

Compound	**[6].THF**	**[6-^{t}Bu].py$_3$**	**[7-18c6].py$_{0.65}$**
Formula	C40 H28 N4 O4 U	C87 H107 N7 O4 U	C87.27 H99.27 N8.65 Na2 O16 U
Crystal size [mm]	0.15 x 0.08 x 0.04	0.20 x 0.10 x 0.01	0.47 x 0.20 x 0.02
Crystal system	Monoclinic	Monoclinic	Monoclinic
Space group	P 2_1/n	P 2_1/n	P 2_1/n
Volume [Å^3]	3162.04(18)	8031.1(6)	8440(3)
a [Å]	11.0533(4)	13.7278(6)	14.019(3)
b [Å]	16.1590(5)	23.1999(7)	45.018(9)
c [Å]	18.3135(6)	25.8473(13)	14.960(3)
α [°]	90	90	90
β [°]	104.828(4)	102.681(5)	116.62(3)
γ [°]	90	90	90
Z	4	4	4
Absorption coefficient [mm^{-1}]	5.185	2.074	2.004
F (000)	1680	3208	3698
T [K]	150(2)	150(2)	150(2)
Exposure time [s]	15	300	60
Narrow data	431	215	399
Total no. reflexions	28635	33653	18423
Unique reflexions [R(int)]	7842 [R(int) = 0.0654]	16242 [R(int) = 0.1029]	18423 [R(int) = 0.0526]
Final R indices [I>2σ(I)]	R1 = 0.0464, wR2 = 0.0907	R1 = 0.00755, wR2 = 0.0845	R1 = 0.0589, wR2 = 0.0985
Largest diff. peak and hole [eA^{-3}]	2.254 and -0.695	1.557 and -1.539	1.279 and -2.355
GOF	0.784	1.020	0.890

***Table VII.3. X*-ray crystallographic data (continued).**

Compound	**[7-Me-dibenzo18c6]**	**[7-^{t}Bu]THF.DIPE**	**[8].THF**	**[9].THF**
Formula	C84 H84 N4 O16 K2 U	C82 H114 N4 O6 K2 U	C34 H38 F6 N2 O11 S2 U	C44 H38 N4 O5 U
Crystal size [mm]	0.31 x 0.13 x 0.02	0.23 x 0.13 x 0.02	0.36 x 0.09 x 0.05	0.51 x 0.17 x 0.05
Crystal system	Monoclinic	Monoclinic	Monoclinic	Monoclinic
Space group	P 2_1/n	C 2/c	P 2_1/c	C 2/c
Volume [Å^3]	7474.6(5)	7613.8(5)	3892.9(5)	7166.5(6)
a [Å]	14.6016(5)	21.6841(9)	15.2090(13)	32.0371(18)
b [Å]	22.5205(7)	30.4275(10)	17.2523(14)	12.7827(4)
c [Å]	22.9060(9)	11.8633(4)	15.0510(10)	19.3828(9)
α [°]	90	90	90	90
β [°]	97.096(4)	103.413(4)	99.689(7)	115.465(6)
γ [°]	90	90	90	90
Z	4	4	4	8
Absorption coefficient [mm^{-1}]	2.356	2.295	4.365	4.585
F (000)	3496	3248	2088	3696
T [K]	150(2)	150(2)	150(2)	150(2)
Exposure time [s]	200	120	80	10
Narrow data	221	200	383	109
Total no. reflexions	34324	16076	26300	17849
Unique reflexions [R(int)]	18381 [R(int) = 0.0876]	9401 [R(int) = 0.0569]	9767 [R(int) = 0.0570]	10810 [R(int) = 0.0456]
Final R indices [I>2σ(I)]	R1 = 0.0796, wR2 = 0.1435	R1 = 0.0526, wR2 = 0.0877	R1 = 0.0790, wR2 = 0.1862	R1 = 0.0522, wR2 = 0.0903
Largest diff. peak and hole [eA^{-3}]	5.071 and -2.451	1.330 and -1.636	7.728 and -1.286	2.209 and -1.158
GOF	1.026	1.007	0.899	1.000

Table VII.4. **X-ray crystallographic data (continued).**

Compound	**[10].py$_2$**	**[11-I].py$_3$**	**[12].THF**	**[13-H$_2$].py$_5$**
Formula	C150 H129 N18 O14 Na6 U2	C85 H73 N13 O4 I2 U2	C52 H44 Fe2 N4 O5 U	C123 H121 Fe2 K2 N11 O16 U
Crystal size [mm]	0.31 x 0.07 x 0.03	0.43 x 0.34 x 0.06	0.75 x 0.39 x 0.20	0.91 x 0.59 x 0.10
Crystal system	Triclinic	Monoclinic	Monoclinic	Triclinic
Space group	P -1	P 2$_1$/c	P 2$_1$/n	P -1
Volume [Å^3]	6757.6(3)	7864.2(8)	4362.62(19)	2727.99(15)
a [Å]	17.2006(4)	13.3578(11)	13.6625(4)	14.5470(5)
b [Å]	18.7274(4)	15.3976(7)	14.8238(3)	15.1229(5)
c [Å]	22.0526(5)	38.2404(17)	22.5571(5)	15.6904(5)
α [°]	76.424(2)	90	90	111.275(3)
β [°]	87.154(2)	90.910(5)	107.265(3)	109.039(3)
γ [°]	78.135(2)	90	90	105.703(3)
Z	2	4	4	1
Absorption coefficient [mm^{-1}]	2.483	4.958	4.414	1.892
F (000)	3034	3984	2272	1246
T [K]	150(2)	150(2)	150	150
Exposure time [s]	90	20	10	4
Narrow data	420	228	964	908
Total no. reflexions	55868	31445	30553	65344
Unique reflexions [R(int)]	27372 [R(int) = 0.0598]	16050 [R(int) = 0.0671]	13159 [R(int) = 0.0241]	16651 [R(int) = 0.0763]
Final R indices [I>2σ(I)]	R1 = 0.0513, wR2 = 0.0818	R1 = 0.0799, wR2 = 0.1342	R1 = 0.0355, wR2 = 0.0763	R1 = 0.0633, wR2 = 0.1285
Largest diff. peak and hole [eA^{-3}]	1.811 and -1.136	2.363 and -2.295	2.524 and -1.536	2.109 and -1.086
GOF	0.995	1.108	1.083	1.040

Table VII.5. **X-ray crystallographic data (continued).**

Compound	**[14-Cl].py**	**[15].toluene$_2$**	**[16].py$_{4.5}$**	**[17]**
Formula	C47 H35 N5 O2 Cl2 U	C98 H76 N8 O4 U2	C78.5 H60.5 N8.5 O4 U	C84 H60 N8 O8 U
Crystal size [mm]	0.28 x 0.22 x 0.15	0.32 x 0.19 x 0.02	0.25 x 0.10 x 0.02	0.27 x 0.14 x 0.03
Crystal system	Triclinic	Triclinic	Monoclinic	Monoclinic
Space group	P -1	P -1	C 2/c	P 2_1/c
Volume [Å^3]	1977.10(13)	1897.75(15)	12586.6(13)	3319.99(15)
a [Å]	10.0338(4)	11.1583(6)	45.625(2)	16.2723(5)
b [Å]	12.7361(5)	13.4999(7)	15.8387(9)	11.8342(3)
c [Å]	16.6880(7)	13.5383(5)	18.5959(13)	18.1568(5)
α [°]	101.098(3)	97.421(3)	90	90
β [°]	101.394(3)	107.177(4)	110.506(5)	108.281(3)
γ [°]	102.627(3)	98.029(4)	90	90
Z	2	1	8	2
Absorption coefficient [mm^{-1}]	4.287	4.324	2.640	4.941
F (000)	988	936	5720	1736
T [K]	150(2)	150(2)	150(2)	150(2)
Exposure time [s]	15	100	200	80
Narrow data	866	430	377	498
Total no. reflexions	41283	14739	31319	39686
Unique reflexions [R(int)]	12067 [R(int) = 0.0592]	7739 [R(int) = 0.0961]	9013 [R(int) = 0.1193]	10126 [R(int) = 0.0740]
Final R indices [I>2σ(I)]	R1 = 0.0511, wR2 = 0.1229	R1 = 0.0780, wR2 = 0.1140	R1 = 0.0623, wR2 = 0.1318	R1 = 0.0450, wR2 = 0.0736
Largest diff. peak and hole [eA^{-3}]	5.549 and -2.664	2.983 and -1.895	2.465 and -1.712	1.340 and -1.248
GOF	1.155	0.939	1.063	1.012

Table VII.6. **X-ray crystallographic data (continued).**

Compound	**[18]**	**[19].hexane**	**[19-THF]**	**[20].toluene$_{0.25}$**
Formula	$C_{72}H_{162}O_{24}Si_6U_2$	$C_{70}H_{158}O_{24}Si_6U_2$	$C_{72}H_{160}O_{26}Si_6U_2$	$C_{69.75}H_{155}O_{24}Si_6U_2$
Crystal size [mm]	0.17 x 0.12 x 0.07	0.64 x 0.55 x 0.27	0.35 x 0.20 x 0.08	0.22 x 0.09 x 0.02
Crystal system	Monoclinic	Triclinic	Monoclinic	Triclinic
Space group	C 2/c	P -1	C 2/c	P -1
Volume [Å^3]	10155.7(4)	2417.7(3)	9952(5)	4800.6(2)
a [Å]	26.0861(6)	13.1952(5)	19.212(9)	13.4586(4)
b [Å]	14.2528(3)	13.3870(12)	21.2876(10)	14.5229(4)
c [Å]	27.5816(6)	16.4078(8)	26.332(4)	25.5217(7)
α [°]	90	99.881(6)	90	94.991(2)
β [°]	97.974(2)	103.361(4)	112.47(4)	90.903(2)
γ [°]	90	115.622(6)	90	104.812(3)
Z	4	1	4	2
Absorption coefficient [mm^{-1}]	3.315	3.480	3.386	3.505
F (000)	4216	1038	4272	2067
T [K]	150(2)	150(2)	150(2)	150(2)
Exposure time [s]	40	100	40	150
Narrow data	433	430	504	496
Total no. reflexions	53081	19000	60187	42991
Unique reflexions [R(int)]	15502 [R(int) = 0.0599]	9878 [R(int) = 0.0186]	15186 [R(int) = 0.0698]	19571 [R(int) = 0.0775]
Final R indices [I>2σ(I)]	R1 = 0.0552, wR2 = 0.1062	R1 = 0.0223, wR2 = 0.0526	R1 = 0.0542, wR2 = 0.1142	R1 = 0.0570, wR2 = 0.0982
Largest diff. peak and hole [eA^{-3}]	2.424 and -0.664	1.191 and -0.682	5.122 and -1.305	2.839 and -1.380
GOF	1.053	1.051	1.067	1.015

Table VII.7. **X-ray crystallographic data (continued).**

Compound	**[21].THF**	**[22]**	**[23]**	**[23-py]**
Formula	$C_{76}H_{168}O_{27}Si_6K_2U_2$	$C_{60}H_{135}O_{24}Si_6K_2U_2$	$C_{48}H_{108}O_{16}Si_4U$	$C_{58}H_{118}N_2O_{16}Si_4U_2$
Crystal size [mm]	0.21 x 0.05 x 0.01	0.25 x 0.10 x 0.01	0.64 x 0.53 x 0.24	0.25 x 0.15 x 0.09
Crystal system	Monoclinic	Triclinic	Monoclinic	Monoclinic
Space group	C c	P -1	C 2/m	C 2/c
Volume [$Å^3$]	10592.7(9)	4446.7(4)	6607.2(5)	7426.0(4)
a [Å]	34.5194(19)	13.8604(6)	24.1332(9)	24.5649(8)
b [Å]	14.0159(5)	16.9261(8)	13.5042(6)	13.2630(3)
c [Å]	22.5154(11)	21.5762(15)	20.4034(9)	25.9619(8)
α [°]	90	105.960(5)	90	90
β [°]	103.494(6)	102.604(6)	96.462(4)	118.606(4)
γ [°]	90	105.642(4)	90	90
Z	4	2	4	4
Absorption coefficient [mm^{-1}]	3.263	3.873	2.584	2.308
F (000)	4584	1986	2688	3024
T [K]	150(2)	150(2)	150(2)	150(2)
Exposure time [s]	240	250	2	20
Narrow data	492	435	289	662
Total no. reflexions	49805	37698	20116	33275
Unique reflexions [R(int)]	21521 [R(int) = 0.1346]	18032 [R(int) = 0.0771]	8461 [R(int) = 0.0462]	7590 [R(int) = 0.0351]
Final R indices [I>2σ(I)]	R1 = 0.0767, wR2 = 0.0838	R1 = 0.0586, wR2 = 0.0874	R1 = 0.0459, wR2 = 0.1007	R1 = 0.0234, wR2 = 0.0529
Largest diff. peak and hole [eA^{-3}]	1.484 and -0.936	2.745 and -1.479	2.798 and -1.553	0.990 and -0.288
GOF	0.937	0.972	1.098	1.049

Table VII.8. **X-ray crystallographic data (continued).**

Compound	**[24].toluene**	**[25].toluene**	**[26]**
Formula	$C_{67}H_{140}O_{22}Si_4U$	$C_{80}H_{170}O_{24}S_2Si_6U_2$	$C_{73}H_{162}O_{27}Si_6U_2$
Crystal size [mm]	0.24 x 0.06 x 0.02	0.95 x 0.78 x 0.55	0.49 x 0.21 x 0.16
Crystal system	Orthorhombic	Triclinic	Triclinic
Space group	P b c a	P -1	P -1
Volume [$Å^3$]	17420.0(16)	2860.6(4)	5211.8(2)
a [Å]	18.2032(12)	13.5950(8)	14.0102(4))
b [Å]	25.9028(11)	13.6700(11)	17.1746(4)
c [Å]	36.9447(18)	18.2122(14)	23.3721(6)
α [°]	90	77.159(7)	82.8748(9)
β [°]	90	72.602(6)	84.870(2)
γ [°]	90	62.906(7)	69.240(2)
Z	8	1	2
Absorption coefficient [mm^{-1}]	2.028	2.983	3.234
F (000)	7080	1142	2168
T [K]	150(2)	150(2)	150(2)
Exposure time [s]	300	1,5	5
Narrow data	141	509	494
Total no. reflexions	37095	30373	63372
Unique reflexions [R(int)]	14742 [R(int) = 0.1529]	14146 [R(int) = 0.0451]	31567 [R(int) = 0.0352]
Final R indices [I>2σ(I)]	R1 = 0.0729, wR2 = 0.1034	R1 = 0.0601, wR2 = 0.1509	R1 = 0.0423, wR2 = 0.0857
Largest diff. peak and hole [eA^{-3}]	1.744 and -1.191	2.762 and -1.077	2.945 and -1.250
GOF	0.980	1.072	1.028

Table VII.9. **X-ray crystallographic data (continued).**

Compound	**[27]**	**[28-Ad].hexane$_{0.5}$**	**[28-TMS].toluene$_2$**
Formula	$C_{88}H_{168}N_4O_{16}Si_4U_2$	$C_{71.5}H_{150.5}O_{22}KNSi_4U$	$C_{77}H_{157}O_{22}KNSi_5U$
Crystal size [mm]	0.10 x 0.09 x 0.02	0.11 x 0.08 x 0.03	0.57 x 0.25 x 0.08
Crystal system	Monoclinic	Triclinic	Hexagonal
Space group	P 2_1/n	P 1	P 3_2
Volume [Å^3]	10900.6(8)	4651.9(4)	7365.7(8)
a [Å]	15.5600(7)	14.4543(8)	14.0470(8)
b [Å]	28.0501(11)	14.5344(8)	14.0470(8)
c [Å]	25.1711(11)	25.4464(12)	43.104(3)
α [°]	90	94.358(4)	90
β [°]	97.154(5)	91.810(4)	90
γ [°]	90	118.909(5)	120
Z	4	2	3
Absorption coefficient [mm^{-1}]	3.066	1.902	1.817
F (000)	4368	1859	2949
T [K]	150(2)	150(2)	150(2)
Exposure time [s]	150	98	90
Narrow data	252	384	221
Total no. reflexions	49524	35721	26095
Unique reflexions [R(int)]	22210 [R(int) = 0.1588]	18800 [R(int) = 0.0979]	15296 [R(int) = 0.0693]
Final R indices [I>2σ(I)]	R1 = 0.0822, wR2 = 0.1722	R1 = 0.0785, wR2 = 0.1100	R1 = 0.0640, wR2 = 0.1083
Largest diff. peak and hole [eA^{-3}]	3.150 and -2.063	1.648 and -1.013	1.887 and -1.474
GOF	0.983	0.986	1.022

Table VII.10. **X-ray crystallographic data (continued).**

Compound	**[29].toluene$_2$**	**[30].toluene**	**[31].toluene$_2$**	**[32]**
Formula	$C_{68}H_{139}O_{18}N_4Si_5KU$	$C_{67}H_{140}N_3O_{22}Si_4KU$	$C_{86}H_{178}O_{24}K_2N_2Si_6U_2$	$C_{72}H_{162}O_{24}CsNSi_6U_2$
Crystal size [mm]	0.75 x 0.36 x 0.12	0.87 x 0.62 x 0.42	0.60 x 0.41 x 0.09	0.24 x 0.21 x 0.07
Crystal system	Monoclinic	Monoclinic	Triclinic	Triclinic
Space group	P 2_1/n	C c	P -1	P -1
Volume [Å^3]	9025.9(4)	9037.0(5)	2831.69(17)	5158.6(3)
a [Å]	13.7947(3)	14.0305(5)	13.3139(4)	15.3369(5)
b [Å]	26.1912(7)	24.7215(7)	13.6374(4)	17.9607(7)
c [Å]	25.0278(5)	26.3108(9)	18.3661(7)	19.2055(6)
α [°]	90	90	90.824(3)	78.456(3)
β [°]	93.479(2)	98.009(3)	106.789(3)	84.822(3)
γ [°]	90	90	115.962(3)	86.879(3)
Z	4	4	1	2
Absorption coefficient [mm^{-1}]	1.969	1.957	3.054	3.612
F (000)	3596	3608	1206	2232
T [K]	150(2)	150(2)	150(2)	150(2)
Exposure time [s]	15	4	110	10
Narrow data	509	492	444	1019
Total no. reflexions	95622	44869	67850	48524
Unique reflexions [R(int)]	22368 [R(int) = 0.0564]	21805 [R(int) = 0.0454]	17272 [R(int) = 0.0842]	25447 [R(int) = 0.0536]
Final R indices [I>2σ(I)]	R1 = 0.0449, wR2 = 0.0941	R1 = 0.0580, wR2 = 0.1200	R1 = 0.0739, wR2 = 0.1549	R1 = 0.0456, wR2 = 0.0912
Largest diff. peak and hole [eA^{-3}]	1.395 and -0.953	2.530 and -1.285	11.179 and -3.932	2.337 and -1.164
GOF	1.052	1.070	1.137	0.929

Table VII.11. **X-ray crystallographic data (continued).**

Compound	**[33]**	**[34]**.toluene$_2$	**[35]**.toluene$_2$	**[36]**.toluene$_{0.5}$
Formula	$C_{48}H_{108}O_{16}Si_4U$	$C_{93}H_{186}O_{24}K_1Si_6U_2$	$C_{93}H_{186}O_{24}K_2Si_6U_2$	$C_{48.5}H_{101}O_{17}SF_3Si_3U$
Crystal size [mm]	0.20 x 0.17 x 0.05	0.66 x 0.28 x 0.08	0.39 x 0.28 x 0.09	0.29 x 0.17 x 0.03
Crystal system	Monoclinic	Triclinic	Triclinic	Triclinic
Space group	C 2	P 1	P -1	P -1
Volume [Å^3]	6643.2(4)	2928.67(7)	2956.7(3)	6612.3(6)
a [Å]	24.1880(8)	13.4665(2)	13.3414(9)	13.7142(7)
b [Å]	13.5267(4)	13.62912(19)	13.4816(9)	22.5380(13)
c [Å]	20.4395(6)	18.7780(3)	19.0912(8)	24.3589(9)
α [°]	90	79.9012(11)	80.367(5)	112.780(5)
β [°]	96.595(3)	70.3501(13)	71.774(5)	106.259(4)
γ [°]	90	64.5426(14)	65.136(6)	90.107(4)
Z	4	1	1	4
Absorption coefficient [mm^{-1}]	2.570	2.919	2.926	2.607
F (000)	2688	1223	1241	2820
T [K]	150(2)	150(2)	150(2)	150(2)
Exposure time [s]	70	10	20	170
Narrow data	194	1971	504	493
Total no. reflexions	15508	121106	27018	59781
Unique reflexions [R(int)]	11374 [R(int) = 0.0360]	28982 [R(int) = 0.0534]	12063 [R(int) = 0.0322]	26995 [R(int) = 0.0834]
Final R indices [I>2σ(I)]	R1 = 0.0473 wR2 = 0.1062	R1 = 0.0426 wR2 = 0.0955	R1 = 0.0333 wR2 = 0.0755	R1 = 0.0602 wR2 = 0.1258
Largest diff. peak and hole [eA^{-3}]	1.563 and -0.861	3.495 and -1.219	1.163 and -0.590	5.646 and -2.408
GOF	1.076	1.092	1.055	1.008

Diffusion coefficient data

The values measured in pyridine are in agreement with the presence of a dinuclear and mononuclear complexes as the ratio of the molecular weights is equal to the reciprocal cube of the ratio of diffusion coefficients measured.

Table VII.12. Diffusion coefficient values and estimated spherical radii (solvent = pyridine, η = 0.879 mPa.s (298K)).

Compound	M [g.mol^{-1}]	D [m^2.s^{-1}]
[U(μ-bis-^{Me}naphtquinolen)]$_2$ **15**	1721.5	7.36 10^{-10}
[U(bis-^{Me}naphtquinolen)(py)$_2$] **15-b**	1019.9	6.26 10^{-10}

$$\mathbf{M_A/M_B = 1.69 \;\; ; \;\; (D_A/D_B)^3 = 1.63}$$

UV-visible spectra

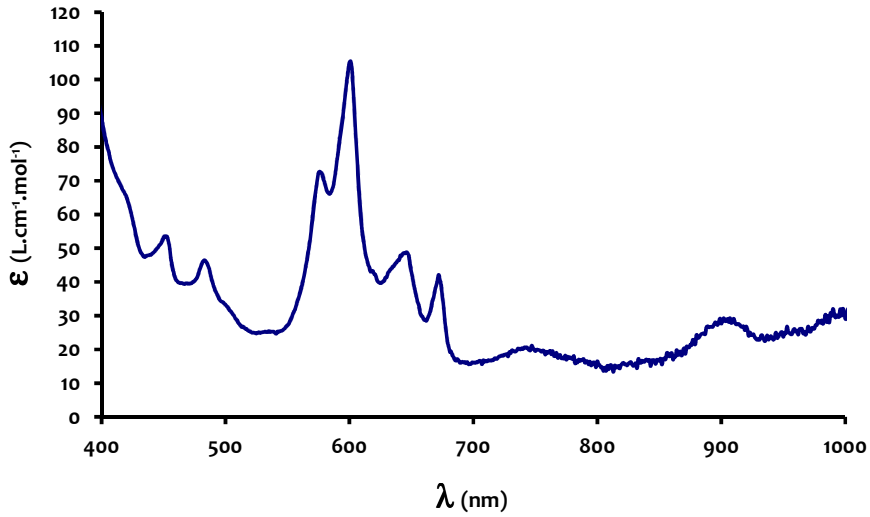

Figure VII.1. Visible absorption spectrum of **22** in THF solution.

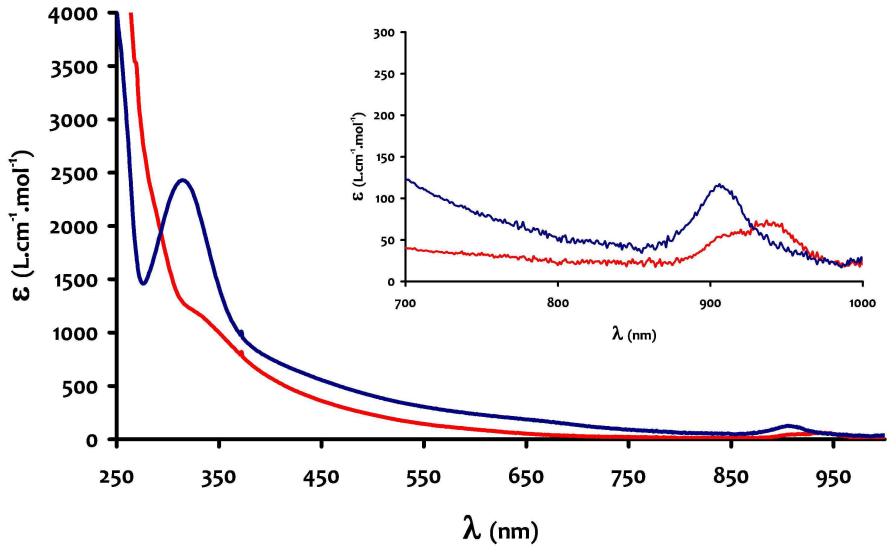

Figure VII.2. UV/visible spectrum (298 K) of a THF solution of complex **28-Ad** (blue line) and of complex **28-TMS** (red line).

Magnetic data

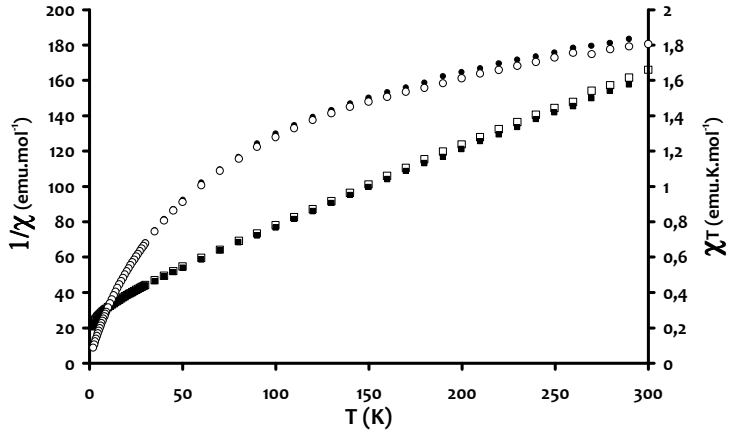

Figure VII.3. Temperature-dependant SQUID magnetization data (0.5 T) for complexes **4-py** (black) and **4-THF** (white) (data per U center) plotted as 1/χ (squares) and χT (circles) versus temperature.

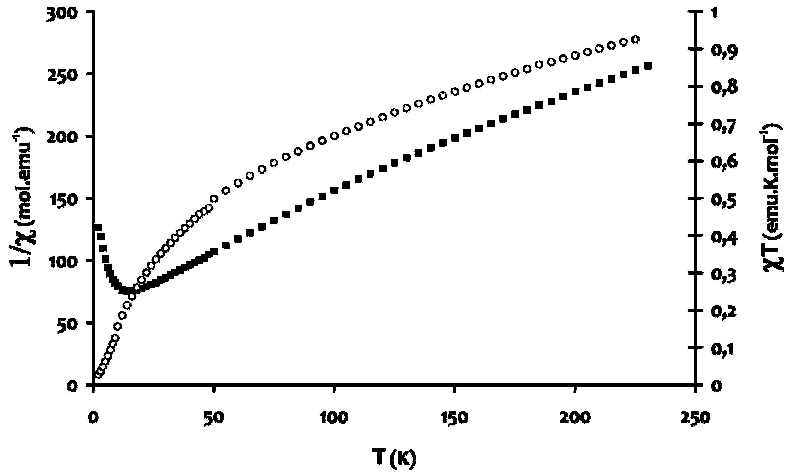

Figure VII.4. Temperature-dependant SQUID magnetization data (0.5 T) for complex **18** (data per U center) plotted as χT (open circles) and 1/χ (black squares) versus temperature.

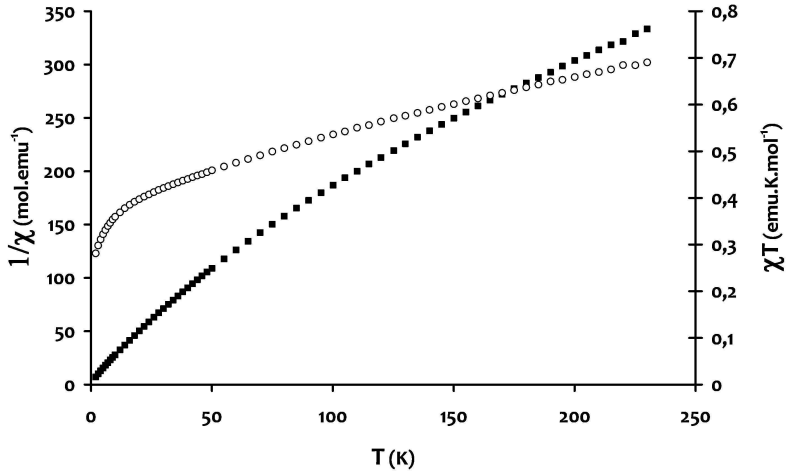

Figure VII.5. Temperature-dependant SQUID magnetization data (0.5 T) for complex **24** plotted as χT (open circles) and 1/χ (black squares) versus temperature.

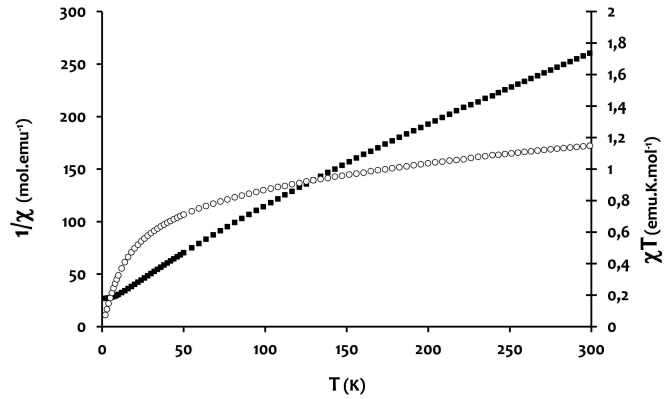

Figure VII.6. Temperature-dependant SQUID magnetization data (0.5 T) for complex **32** (data per U center) plotted as χT (open circles) and 1/χ (black squares) versus temperature.

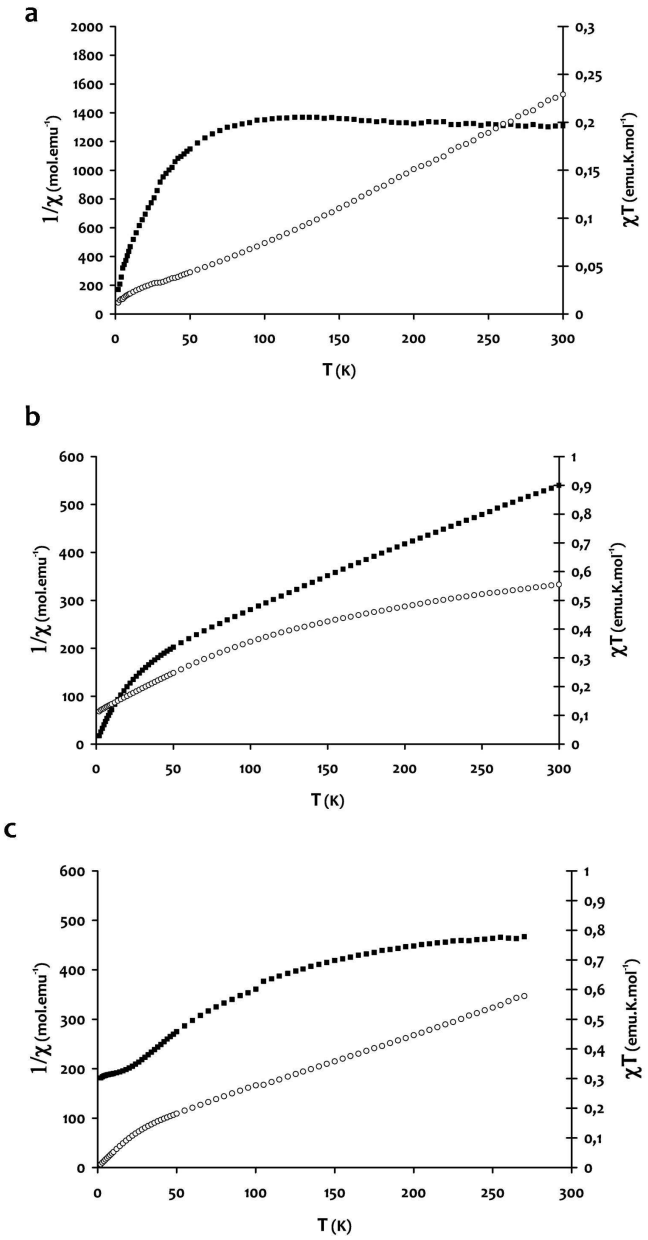

Figure VII.7. Temperature-dependant SQUID magnetization data (0.5 T) for complexes **33** (a), **34** (b) and **35** (d) (data per U center) plotted as χT (open circles) and 1/χ (black squares) versus temperature.

Computational profiles

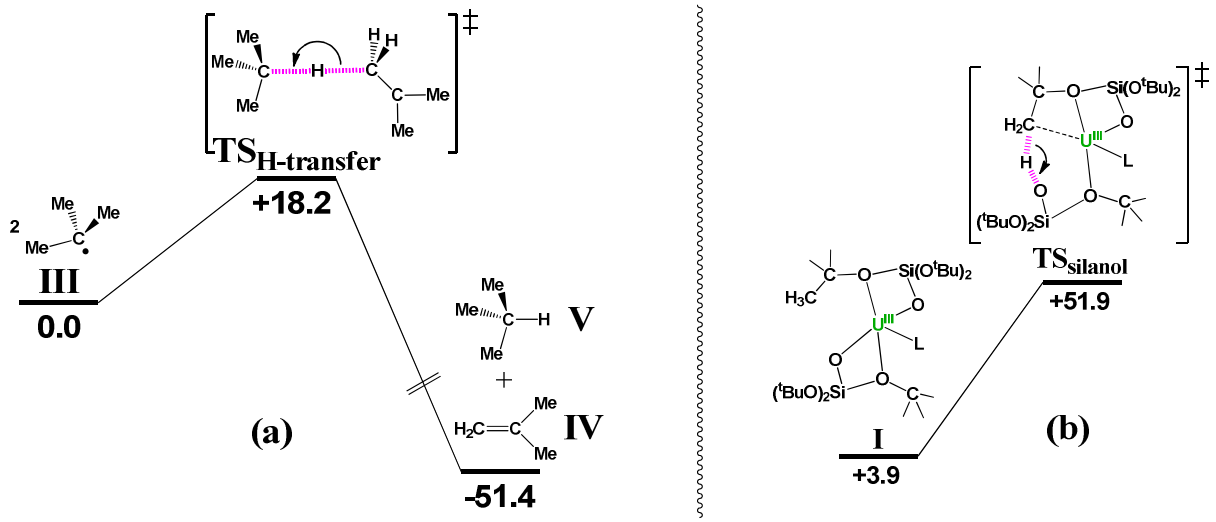

Figure VII.8. Enthalpy energy computed profiles (a) for the proton transfer between trityl radicals, and (b) for the possible formation of $HOSi(O^tBu)_3$.

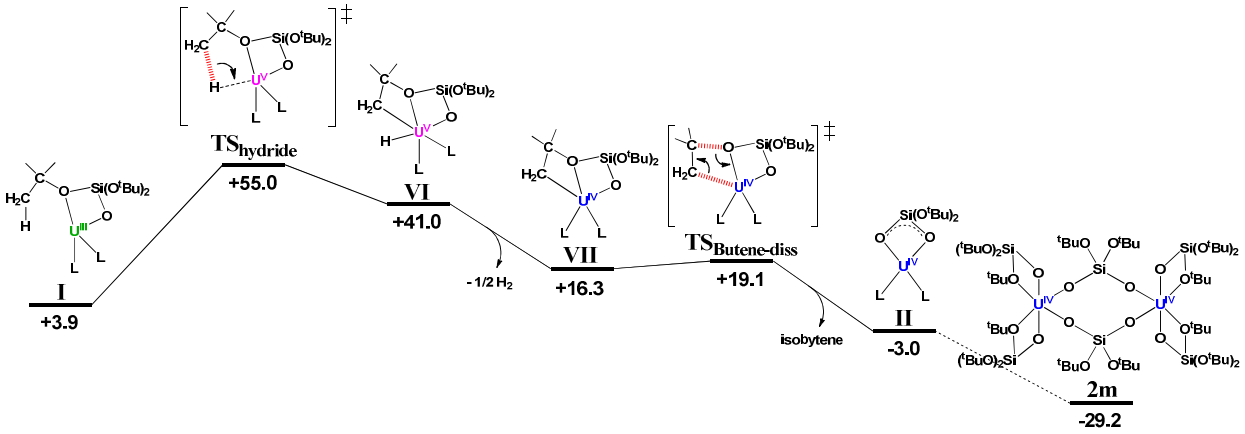

Figure VII.9. Enthalpy energy computed profile for the decomposition of model complex **18** into **19** via γ-H involving the formation of a U(V) hydride intermediate.

Abbreviations

Acac	acetylacetonate
Ad	adamantyl
bipy	bipyridine
Bu	butyl
COT	cyclooctatetraene
Cp	cyclopentadienyl
Cp*	pentamethylcyclopentadienyl
d	doublet
deg	degree
DFT	density functional theory
DIPE	diisopropylether
DME	dimetoxyethane
eqn	equation
equiv	equivalents
ESI-MS	electro-spray ionization mass spectrometry
Et	ethyl
Hz	hertz
HBBN	9-bora-9-bicyclononane
^{i}Pr	isopropyl
Ln	lanthanide
m	multiplet
Me	methyl
Mes	mesityl (1,3,5-trimethylbenzyl)
NMR	nuclear magnetic resonance
OTf	triflate : $CF_3SO_3^-$
Ph	phenyl
ppm	parts per million
py	pyridine
r.t.	room temperature
s	singlet
salen	N,N'-bis(salicyldiene)-ethylenediamine
salophen	N,N'-bis(salicyldiene)-*o*-phenylenediamine
SET	single electron transfer
SCIB	service de chimie inorganique et biologique
SQUID	superconducting quantum interference device
t	triplet
tacn	triazacyclononane
^{t}Bu	tertiobutyl
TEMPO	(2,2,6,6-tetramethylpiperidin-1-yl)oxyl
THF	tetrahydrofuran
TIP	temperature independant paramagnetism
TMEDA	tetramethylethylenediamine
TMS	trimethylsilyl
UV	ultra-violet
Vis	visible
vs	versus
XANES	X-ray absorption near edge structure spectroscopy

List of Compounds

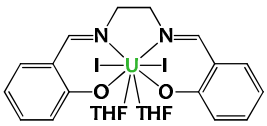

$[UI_2(salen)(THF)_2]$
1

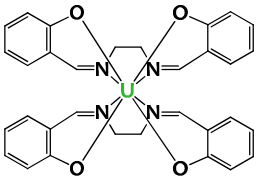

$[U(salen)_2]$
2

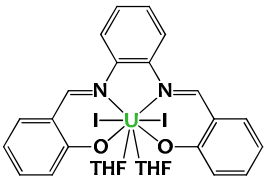

$[UI_2(salophen)(THF)_2]$
3

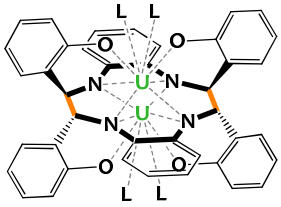

$[U_2(cyclo\text{-}salophen)(L)_4]$
4-THF (L = THF)
4-py (L = pyridine)

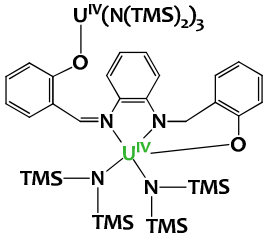

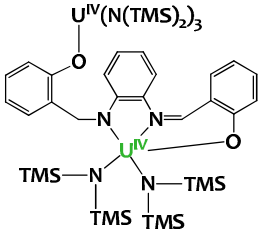

$[U_2(\mu\text{-}salophean)\{N(SiMe_3)_2\}_5]$
5-a 5-b

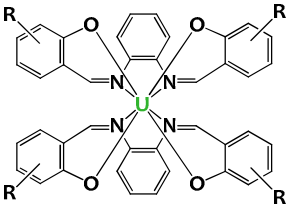

$[U(^{R}salophen)_2]$
R = H, Me, ^{t}Bu
6-R

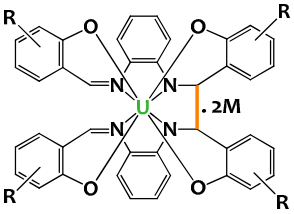

$M_2[U(bis\text{-}salophen)]$
R , M = H , Na ; Me , K ; ^{t}Bu , K
7-R

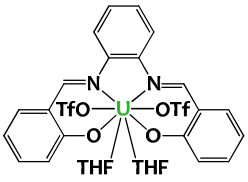

$[U(salophen)(OTf)_2(THF)_2]$
8

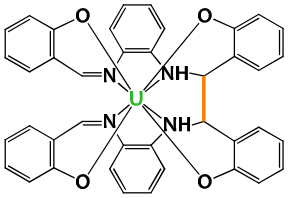

$[U(bis\text{-}H_2salophen)]$
9

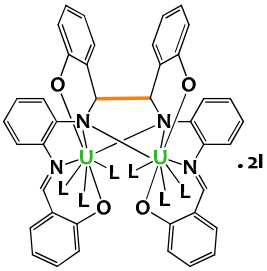

$[U_2(bis\text{-}salophen)(py)_6]I_2$ L = py
11

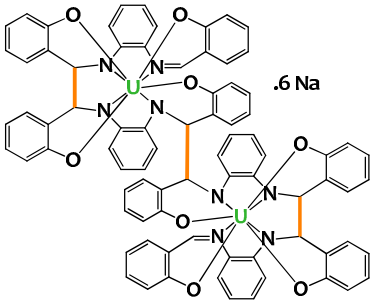

$Na_6[U_2(bis\text{-}(bis\text{-}salophen))]$
10

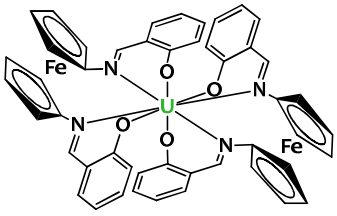

$[U(salfen)_2]$
12

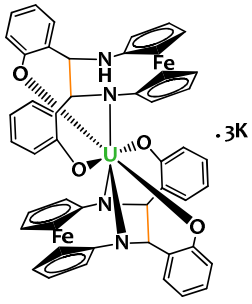

$K_3[U(bis\text{-}salfen)(bis\text{-}Hsalfen)]$
13-H

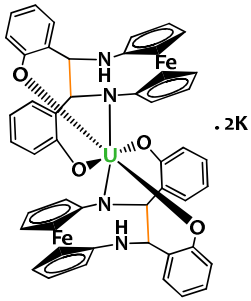

$K_2[U(bis\text{-}Hsalfen)_2]$
13-H_2

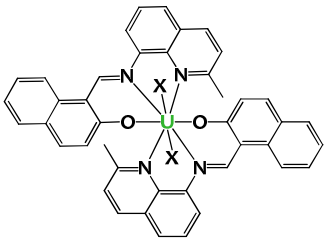

[UX_2(^{Me}naphtquinolen)$_2$] X = Cl, I
14-X

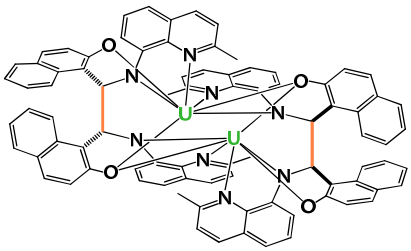

[U(μ-bis-^{Me}naphtquinolen)]$_2$
15

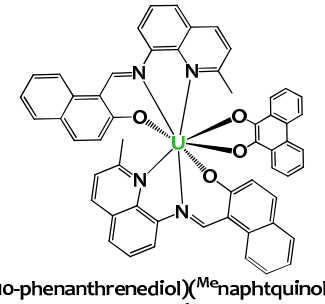

[U(9,10-phenanthrenediol)(^{Me}naphtquinolen)$_2$]
16

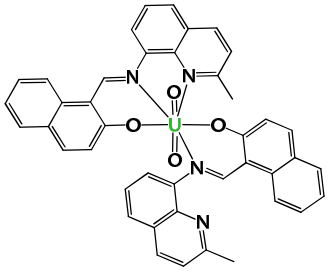

[UO_2(^{Me}naphtquinolen)$_2$]
17

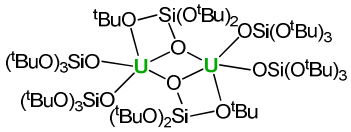

[U(OSi(O^{t}Bu)$_3$)$_2$(μ-OSi(O^{t}Bu)$_3$)]$_2$
18

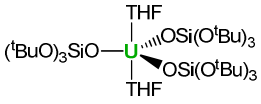

[U(OSi(O^{t}Bu)$_3$)$_3$(THF)$_2$]
18-THF

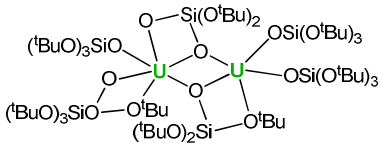

[U_2(μ-O_2Si(O^{t}Bu)$_2$)(μ-OSi(O^{t}Bu)$_3$)(OSi(O^{t}Bu)$_3$)$_4$]
20

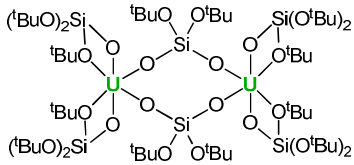

[U(OSi(O^{t}Bu)$_3$)$_2$(μ-O_2Si(O^{t}Bu)$_2$)]$_2$
19

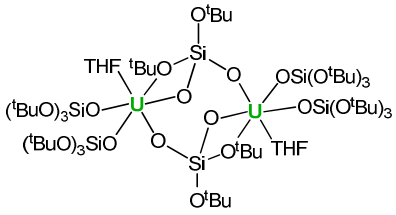

[U(OSi(O^{t}Bu)$_3$)$_2$(μ-O_2Si(O^{t}Bu)$_2$)(THF)]$_2$
19-THF

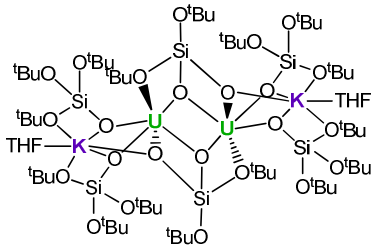

[K(THF)U(OSi(O^{t}Bu)$_3$)$_2$(μ-O_2Si(O^{t}Bu)$_2$)]$_2$
21

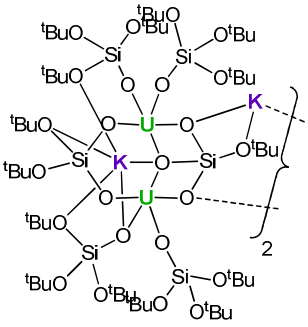

[K_2U_2(OSi(O^{t}Bu)$_3$)$_4$(O_2Si(O^{t}Bu)$_2$)(O_3Si(O^{t}Bu))]$_2$
22

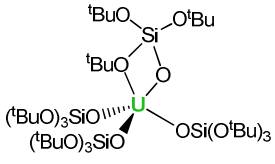

[U(OSi(O^{t}Bu)$_3$)$_4$]
23

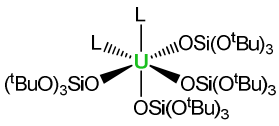

[U(OSi(O^{t}Bu)$_3$)$_4$(L)$_2$]
23-py L = pyridine
23-THF L = THF

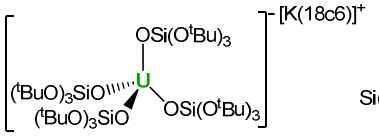

[K18c6][U(OSi(O^{t}Bu)$_3$)$_4$]

24

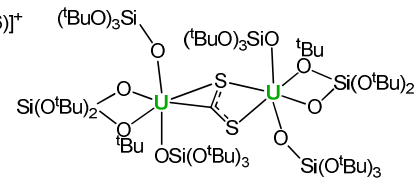

[{U(OSi(O^{t}Bu)$_3$)$_3$}$_2$(μ-η^2:η^2-CS$_2$)]

25

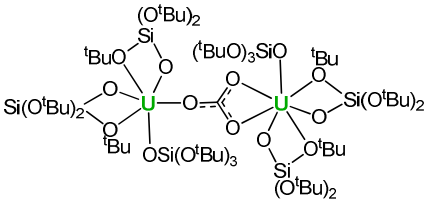

[{U(OSi(O^{t}Bu)$_3$)$_3$}$_2$(μ-η^1:η^2-CO$_3$)]

26

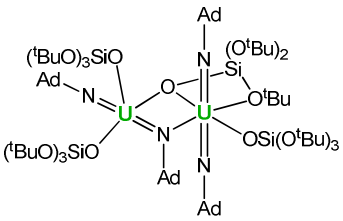

[U$_2$(NAd)$_4$(OSi(O^{t}Bu)$_3$)$_4$]

27

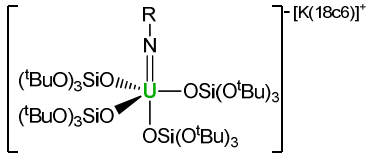

[K18c6][U(NR)(OSi(O^{t}Bu)$_3$)$_4$]

28-R R = Ad, TMS

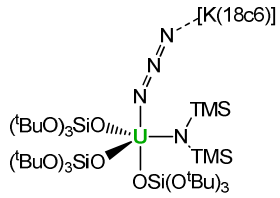

[K18c6][U(N$_3$){N(SiMe$_3$)$_2$}{OSi(O^{t}Bu)$_3$}$_3$]

29

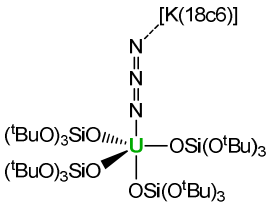

[K18c6][U(N$_3$)(OSi(O^{t}Bu)$_3$)$_4$]

30

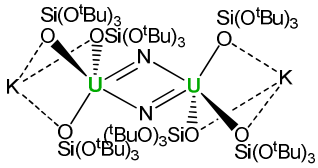

[KU(μ-N)(OSi(O^{t}Bu)$_3$)$_3$]$_2$

31

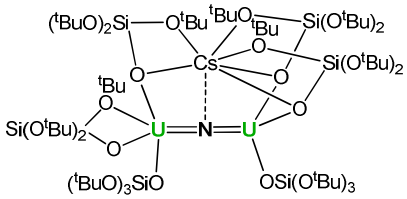

[Cs(μ-N){U(OSi(O^{t}Bu)$_3$)$_3$}$_2$]

32

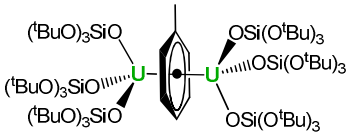

[{U(OSi(O^{t}Bu)$_3$)$_3$}$_2$(μ-η^6:η^6-C$_7$H$_8$)]

33

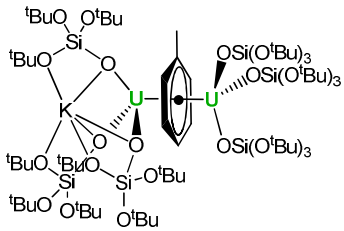

[K{U(OSi(O^{t}Bu)$_3$)$_3$}$_2$(μ-η^6:η^6-C$_7$H$_8$)]

34

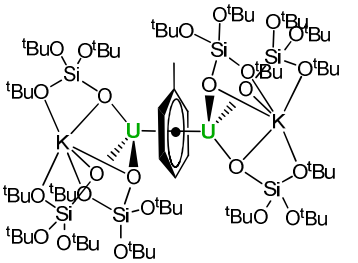

[K$_2${U(OSi(O^{t}Bu)$_3$)$_3$}$_2$(μ-η^6:η^6-C$_7$H$_8$)]

35

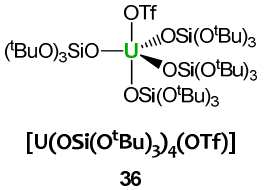

[U(OSi(O^{t}Bu)$_3$)$_4$(OTf)]

36

List of Publications

- 8. C. Camp; C. E. Kefalidis; J. Pecaut; L. Maron and M. Mazzanti "Comtrolled thermolysis of uranium (alcoxy)siloxy complexes: a route to polymetallic complexes of low-valent uranium" *Angew. Chem. Int. Ed.* **2013**, *In Press* **DOI:** 10.1002/anie.201307291.

- 7. C. Camp; V. Mougel; J. Pecaut; L. Maron and M. Mazzanti "Cation mediated conversion of the state of charge in uranium arene inverted-sandwich complexes" *Chem. Eur. J.* **2013**, *In Press* **DOI:** 10.1002/chem.201302752.

- 6. C. Camp; J. Pecaut and M. Mazzanti "Tuning uranium-nitrogen multiple bond formation with ancillary siloxide ligands" *J. Am. Chem. Soc.* **2013**, 135(*32*), 12101-12111.

- 5. C. Camp; J. Andrez; J. Pecaut and M. Mazzanti "Synthesis of electron-rich uranium(IV) complexes supported by tridentate Schiff base ligands and their multi-electron redox chemistry" *Inorg. Chem.* **2013**, 52(*12*), 7078-7086. ***Highlighted Article.***

- 4. E. Mora; L. Maria; B. Biswas; C. Camp; I. C. Santos; J. Pecaut; A. Cruz; J. M. Carretas; J. Marçalo and M. Mazzanti "Diamine bis(phenolate) as supporting ligands in organoactinide (IV) chemistry" *Organometallics* **2013**, 32(*5*), 1409--1422.

- 3. V. Mougel; C. Camp; J. Pecaut; C. Copéret; L. Maron; C. E. Kefalidis and M. Mazzanti "Siloxide as a supporting ligand in U(III)-mediated small molecule activation" *Angew. Chem. Int. Ed.* **2012**, 51(*49*), 12280-12284.

- 2. C. Camp; V. Guidal; B. Biswas; J. Pecaut; L. Dubois and M. Mazzanti "Multielectron redox chemistry of lanthanide Schiff base complexes" *Chem. Science* **2012**, 3(*8*), 2433-2448. ***Cover Article.***

- 1. C. Camp; V. Mougel; P. Horeglad; J. Pecaut and M. Mazzanti "Multielectron redox reactions involving C-C coupling and cleavage in uranium Schiff base complexes" *J. Am. Chem. Soc.* **2010**, 132(*49*), 17374-17377.

Résumé

Au-delà de son importance dans l'industrie nucléaire, la chimie d'oxydoréduction de l'uranium retient de plus en plus l'attention des chercheurs. En effet, la capacité toute particulière des complexes d'uranium à bas degré d'oxydation à promouvoir des réductions originales par des voies inhabituelles suscite actuellement un grand intérêt, tout particulièrement leur aptitude à activer dans des conditions douces des petites molécules telles CO, CO_2, N_2, ou encore des composés aromatiques et des azotures. Les composés d'uranium, de part leurs propriétés de coordination tout à fait uniques pourraient offrir une alternative aux métaux de transition classiques pour la conception de catalyseurs. Cependant, comparativement aux métaux du bloc d, les processus polyélectroniques sont rares dans la chimie de l'uranium à bas degré d'oxidation qui est dominée par les transferts monoélectroniques. C'est pourquoi le développement de nouveaux complexes d'uranium capables de réaliser des réductions poly-électroniques est particulièrement intéressant. Le premier objectif de ce travail était d'associer à l'uranium des ligands non-innocents servant de réservoir d'électrons. Ainsi nous avons utilisé des bases de Schiff π-conjuguées pour explorer la chimie de cet élément à bas degree d'oxydation. Cela nous a permis d'isoler des complexes riches en électrons dans lesquels des électrons sont stockés sur le ligand via la formation de liaisons C-C. Ces mêmes liaisons sont rompues en présence d'agent oxydant, et les électrons sont libérés pour réaliser des transformations polyélectroniques. Ce procédé a été observé pour plusieurs bases de Schiff, permettant de moduler les propriétés des composés. Dans une seconde approche, nous nous sommes intéressés à la synthèse et à l'étude de la réactivité de nouveaux complexes d'uranium trivalent supportés par des ligands silanolates. De nouveaux composés dinucléaires d'uranium à basse valence ont été obtenus. Ces composés très réactifs décomposent spontanément en clivant des groupements tertiobutyls des ligands, conduisant à la formation de complexes d'uranium(IV). En parallèle, un complexe monoanionique mononucléaire d'U(III) a été isolé, nous permettant de comparer la réactivité de l'uranium trivalent dans différents environnements stériques et électroniques. Ces études de réactivité ont permis de stabiliser un exemple rare de dimère d'uranium ponté par un groupement CS_2^{2-} et ont mis en évidence la capacité de l'uranium trivalent à promouvoir la dismutation de CO_2 en carbonate et CO. La réaction de ces composés d'uranium trivalent vis-à-vis d'azotures organiques et inorganiques a produit de nouveaux nitrures et nitrènes d'uranium originaux. Enfin, la capacité de ces agents réducteurs puissants à transférer des électrons au toluène a permis d'isoler une famille de complexes sandwiches inversés où deux cations uranium sont liés de part et d'autre d'un cycle aromatique.

Mots-clés
uranium, réduction, bases de Schiff, ligand redox-actif, silanol, petites molécules, CO_2, azotures

Discipline
Chimie Inorganique

Laboratoire
Laboratoire de Reconnaissance Ionique et Chimie de Coordination
Service de Chimie Inorganique et Biologique, UMR-E3 CEA-UJF
Institut Nanosciences et Cryogénie, CEA Grenoble
17 Rue des Martyrs, 38054 Grenoble Cedex, France